Faculty of Textile Engineering
Technical University of Liberec

STRUTEX

Structure and Structural Mechanics of Textile Fabrics

Struktura a strukturní mechanika textilií

21st international conference
21. mezinárodní konference

2016

CONFERENCE BOOK

SBORNÍK TEXTŮ

PARTNERS / SPONSORS

Faculty of Textile Engineering
Technical University of Liberec

21st international conference
21. mezinárodní konference

STRUTEX

Structure and Structural Mechanics of Textile Fabrics

Struktura a strukturní mechanika textilií

CONFERENCE BOOK

SBORNÍK TEXTŮ

December / Prosinec 2016
Faculty of Textile Engineering
Technical University of Liberec

President of the conference

Prof. Ing.Bohuslav Neckář, DrSc.
Technical University of Liberec

Scientific committee

S. M. ISHTIAQUE, IIT Delhi, India
Y. KYOSEV, HS Niederrhein, Germany
J. MASAJTIS, IAT, Poland
M. KING, NCSU, USA
J. MILITKÝ, TUL, Czech Republic
B. NECKÁŘ, TUL, Czech Republic
J.WIENER, TUL, Czech Republic
L. HES, TUL, Czech Republic
O. JIRSÁK, TUL, Czech Republic

ISBN 978-80-7494-269-3

Nový obor – OMS!

Pohony EPCO – přímočarý pohyb

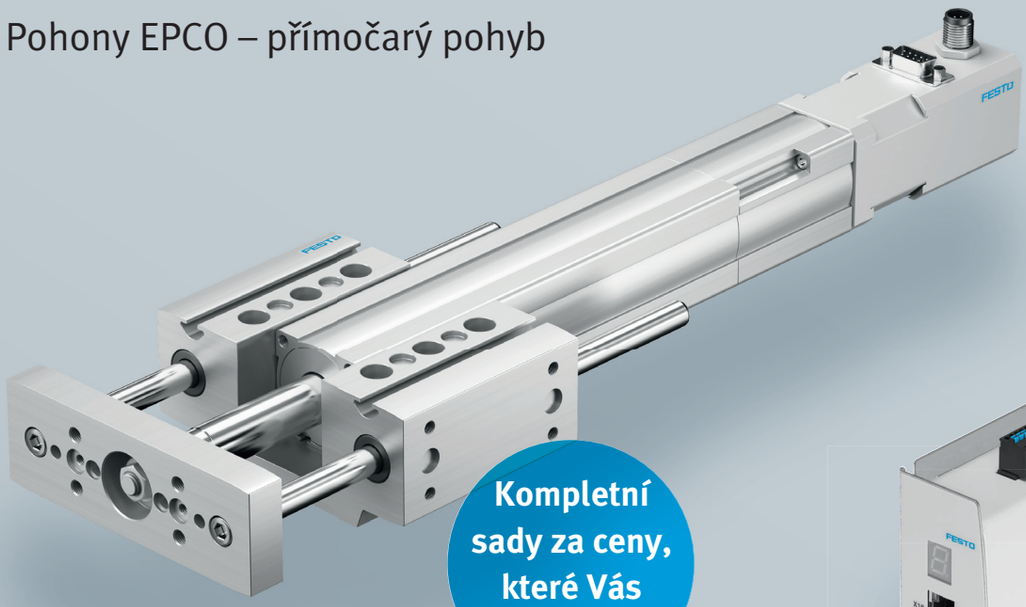

FESTO

Kompletní sady za ceny, které Vás překvapí!

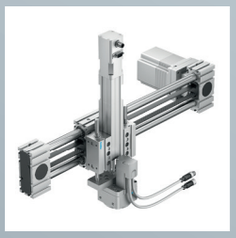

IO-Link Modbus PROFINET EtherNet/IP EtherCAT

Hledáte jednoduché řešení pro Vaší aplikaci? Potřebujete snadno a levně polohovat nebo manipulovat? Vyberte si svoji sadu z OMS, nové skupiny elektrických pohonů!

→ WE ARE THE ENGINEERS OF PRODUCTIVITY.

- Polohování ještě nikdy nebylo tak snadné – několik základních údajů o potřebném pohybu postačí k výběru sestavy pohonu s namontovaným motorem, se správným ovladačem i kabely.
- Ušetříte v konstrukci, nákupu i logistice – vše je za velmi nízkou cenu a pod jediným objednacím číslem.
- Oživení zvládne každý – po vyplnění tabulky na webové stránce ovladače je pohon připraven pracovat.

www.festo.cz/OMS
prodej@festo.com
tel.: 261 099 611

Rieter CZ s.r.o.

Ústí nad Orlicí

Rieter CZ s.r.o. is part of the Swiss Group, Rieter, that is a leading world producer of textile machinery and complete textile systems. Rieter CZ s.r.o. is characterised by a strong emphasis on innovations that are developed in the company development centre. Other features include precision production of textile machines and components for modern technologies and processes.

Rieter – The Comfort of Competence.
http://www.rieter.cz, http://rieter.jobs.cz

RIETER

Innovative solution of surface treatment - **laboratory** development process/**MASS PRODUCTION**

ENVIRONMENTAL FRIENDLY TECHNOLOGY

Plasma discharge+working gas = ACTIVE PARTICLES

New functional groups on the polymeric chain

Hydrophilisation/adhesion enhancement

PLASMA SURFACE TREATMENT

- **POWDERS**(LDPE, HDPE, UHMWPE, PP)
- excellent dispersion - additives for paints and plastics
- treatment effect stays also on the sintered surface from the treated powder - rotomolding

- **PLASTIC PARTS** - plain or complex shapes
- activation prior to gluing, printing, etc.
- no chemical/flame pretreatment
- process without altering the bulk material

- **atmospheric/vacuum systems**
- **toll service or machine delivery**
- testing and development processes
- production of special equipments for plasma surface treatment
- adjustment of current plasma devices
- R&D in the area of plasma surface treatment

www.surface-treat.cz

www.surface-treat.cz
SurfaceTreat
PLASMA TECHNOLOGY - SYSTEMS - CONSULTING

Production plant: Na Lukách 669, 511 01 Turnov
T.: +420 481 322 223, E: info@surface-treat.cz

Company Driga Group s.r.o. represents on the Czech and Slovak markets the following manufacturers of a textile machinery and equipments:

1/ Bonas Textile Machinery NV (Belgium) is trendsetter in design and manufacture of electronic jacquards for weaving machines.
Principally located in Belgium Bonas Textile Machinery is a brand of VANDEWIELE consisting of several textile machine companies all synonymous within their field of textile machinery expertise: **Van de Wiele**, carpet and velvet looms, **IRO** & **ROJ**, yarn feeders for weaving, **Memminger-IRO**, advanced knitting technology, **Protechna**, quality assurance for textiles and **Titan**, sewing/finishing machines, to name but a few.Throughout the history of Bonas our philosophy remains unchanged, continual investment in R&D. This resulted in the invention of the electronic jacquard years ago.
To our valued customers we have the technology and expertise to consistently offer the very best in speed, reliability, robustness and efficiency within the global marketplace of Jacquard weaving.Manufacturing excellence from our hub in Kortrijk, Belgium enables us to supply the most technologically advanced electronic Jacquards whilst professional dedicated and disciplined sales and service departments, operating throughout the world, ensure that Bonas customers remain continually satisfied with our products of past, present and for the future.,

2/ CCI TECH INC. (Thaiwan) commit ourselves to the development of sampling solutions for the weaving industries. We provide the markets with the most innovative tools for fabric sampling, new designs development as well as small quantity production. This is a brand new dimension to sampling which will give you unexceptional experiences in the most efficient and economical way!

3/ **ICOMATEX** (Spain) has continued to broaden its program of machinery, and are today producing a wide range of machinery from continous washing/bleaching, relax dryers, stenter to specialized machinery, for many different industrial segments across the globe.

4/ **Salvadè S.r.l.** (Italy) was founded in 1967 by brothers Alberto and Luigi. In the ensuing years it grew as a maintenance company for textile plant of all types and brands ranging from rameuse to printing machines, steaming plant and dryers, and gradually becoming a machine constructor itself.Thanks to the vast experience it acquired in maintenance, and fielding an extremely broad range of machinery for textile dyeing, printing and finishing, Salvadè is now one of the leading companies in the sector, at international level.The company is aware that the production evolves continuously with research and updating, development and innovation; constant monitoring of technological evolution and customer requirements therefore represent a fundamental point of passage towards the objectives that Salvadè has set itself for the near future, such as the expansion of the manufacturing range and the continuous improvement of products. The new solution are in fact seen as a means to improve the customer's production cycles, in terms of space and time.

5/ **Pentek Textile Machinery, Srl (** Italy) Design and manufacture of *machinery* for discontinuous washing, scouring, steaming, drying and continuous tumbling in *textile* processing and finishing.

Veba

Czech producer
of first class
clothing fabrics

life is fashion

Head Office

VEBA, textilní závody a.s.
Přadlácká 89, 550 01 Broumov
Czech republic

Sale Offices

Přadlácká 89, 550 01 **Broumov**
Czech republic

U Elektry 830/2b, 190 00 **Prague** 9
Czech republic

Call Centre

Tel.: +420 491 502 300
E-mail: callcentrum@veba.cz
www.veba.cz

CLINITEX CZ s.r.o.

CLINITEX CZ s.r.o., 1. máje 3236/103, CZ 703 00 Ostrava
tel.: +421 597 578 688, fax: +421 597 579 005
e-mail: info@clinitex.cz
www.clinitex.cz

CONTACTS

CLINITEX CZ s.r.o. (Ltd. company) was established in 2005 and then it was focussed purely on medical textile manufacture. The company was certified with ISO 9001:2009 and ISO 14385:2012 and nowadays, it is a major supplier of CLINITEX brand products both to medical facilities of various types and especially to laundries oriented to provide services for them, i.e. renting linens and textiles in health care industry.

In the sector of medical aids' production the company is manufacturing and developing **surgical gowns, clothing and drapes for clean areas** under the CLINITEX brand; the parameters comply with EN 13795:2011+A1:2013 European standard. New products include production and supply of incontinence products in standard version as well as in special custom-made version.

If you choose CLINITEX medical wear, you will always get verified quality, appropriate materials and components as well as perfect design an ergonomic cut. We are anxious to listen carefully to our customers and combine their feedback with our extensive experience as well as hard work of the whole CLINITEX team. We feel this is the only way for our workshops to make professional and high quality wear.

Our manufacturing programme consists of these main product ranges:

- Outfits for doctors
- Outfits for nurses
- Outfits for patients
- Outfits for surgery personnel
- Surgery protection and drapes
- Bed linens and flat textile products
- Incontinence products

ADFORS
glass fibre fabrics producer

2 production plants - in Litomyšl and Hodonice

1 770 employees

6,86 bn CZK turnover

110 k tons of glass fibre per year

6 brands of unique glass fibre products

Vertex®
Glass fibre mesh fabrics designed for insulation systems and wall or façade reinforcement.

Vertex® Grid
Glass fibre meshes for floor reinforcement, excellent alternative of heavy metal meshes.

Fibatape®
Self-adhesive tapes for drywall joints and crack repair.

Novelio®
Glass fibre wall coverings used for decoration and wall protection in both public spaces and households.

GlasGrid®
Glass fibre grids used as asphalt concrete overlays reinforcement and cracks prevention.

TWINFAB® and glass fibre non-woven fabrics
Protective top layer for gypsum boards wall protection (as paintable wall coverings) and water resistant membrane and separating layers for roof reinforcement.

www.adfors.cz
SAINT-GOBAIN ADFORS CZ s.r.o.
Sokolovská 106
570 21 Litomyšl
teL: 461 651 110
e-mail: adfors-cz@saint-gobain.com

ADFORS SAINT-GOBAIN

Your Partner for Innovative Textiles

Fehrer AUTOMOTIVE

Fehrer Bohemia s.r.o. is a supplier of interior parts for the automotive industry.

Plant Liberec produces armrests, center and rear consoles for customers :

- AUDI
- BMW
- Daimler
- Nissan
- Seat
- Škoda
- VW

Interior Modules

multifunctional armrests

center armrests

center consoles

side bolsters

console covers

seat-mounted-armrests

www.fehrer.com

BORGERS

MAJOR SUPPLIER FOR GLOBAL CAR MANUFACTURERS

- tradition since 1866
- parts and moulded components from non-woven textiles for vehicle interiors and luggage compartments
- manufacture mostly from recycled raw materials
- 4 plants, more than 3000 employees in the Rokycany region

BORGERS

Borgers CS spol. s r.o.
Stehlíkova 1111,
337 01 Rokycany - Nové Město
Tel.: 727 810 977
www.borgers-group.com

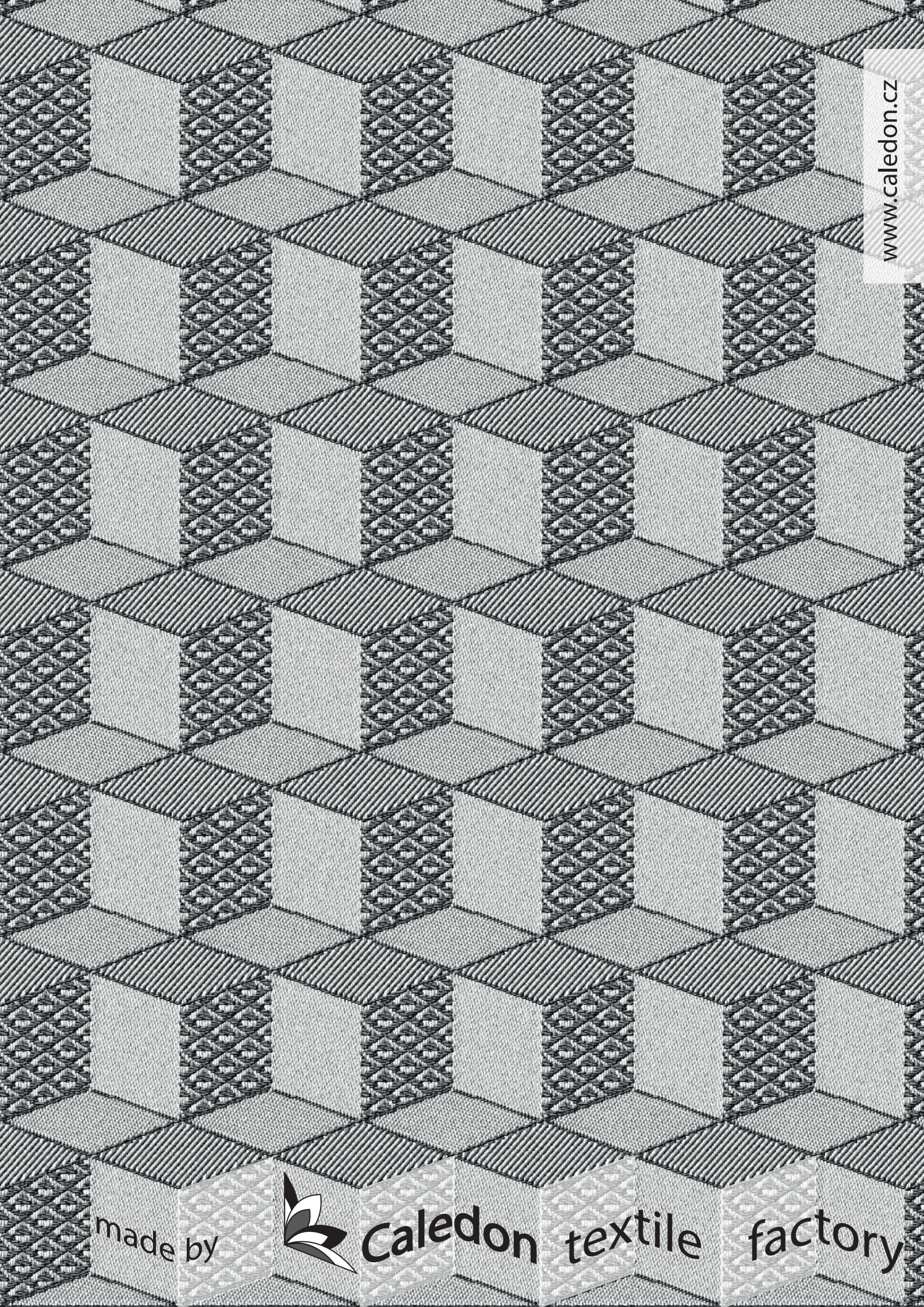
www.caledon.cz
made by
Caledon textile factory

SHIMA SEIKI ITALIA S.P.A.

PITTI IMMAGINE FILATI
25-27 January 2017
Florence

ISPO
5-8 February 2017
Munich

TECHTEXTIL
9-12 May 2017
Frankfurt am Main

SHIMA SEIKI ITALIA S.p.A.
Via Redecesio,11
20090 Segrate -MI-
Tel: +039 02/216621
Fax: +039 02/2139410
www.shimaseiki.eu
info@shimaseiki.eu

Become a fan on Facebook
Shima Seiki Italia Spa

Official agent for Czechia
and Slovakia
KNIT-TEX CS, s.r.o.
Hlavni 227
CZ-251 66 Mirosovice u Prahy
Tel: +420 602 461 722
www.shimaseiki.cz

Follow us on Instagram
@shimaseikiitalia

CONTENTS

GEOMETRICAL AND MECHANICAL MODELLING OF TEXTILE STRUCTURES AT FIBER AND YARN LEVEL - SOFTWARE AND DATA STRUCTURES

Yordan Kyosev

Hochschule Niederrhein - University of Applied Sciences, Faculty of Textile and Clothing Technology, Research Institution of Textile and Clothing, Mönchengladbach, Webschulstr. 31, Germany
yordan.kyosev@hs-niederrhein.de

Abstract:

This paper presents the common strategies for multiscale modelling of textiles, concentrating on the yarn and filament level. The advantages and disadvantages of the both used ways of creation of geometrical models are discussed. Reference to works, related to the generation of the coordinates of the filaments within the yarns and example results for warp knitted and braided structures are given. Overview of the common software solution of textile generators is included. After analysis of the configuration of a braided structure one recursive structure definition for the data storage is proposed. This allows modelling of fabrics with unlimited number of grouping levels of the fibers.

Key words:

Modelling, geometry, fibers, filaments, data structures, multiscale models

1. Introduction

The mathematical modelling of textile structures allows the computer aided investigation of their behavior without their production. Many textile engineers expect to have tools similar to those of the machine engineers for calculation and evaluation of textiles. Indeed in the last decades the modelling of textiles has been developed significantly, but the complexity of the fibrous structures does not allow the same efficiency and accuracy of the computations as for metal parts. This work presents some methods and problems, related to the multiscale modelling of fibrous structures and represents an overview of some commonly used preprocessors/geometrical generators and simulation programs for textiles.

2. Strategies for multiscale modelling of textiles

The modelling of the textiles multiple scales - for instance yarn and fiber/filament level requires separate algorithms and methods for each scale. The knitted, woven and braided structures are yarn based and require certain description of the yarn geometry. There are three popular methods for retrieving the yarn geometry:

- By using image processing of 2D or 3D images, for instance by X-ray micro-computer tomography [1, 2]. This method can produce very accurate data about the geometry of the fibrous structure and the orientation of the fibers, but is applicable only over already produced structures. Because of this it is not going to be a point of interest in this paper.

- Simulating the complete production process [3–5]. This method is connected with many computations and a lot of simulation time at current. Nevertheless, considering the rapid development of the computer technic and methods for parallel processing, it is going to become soon more popular.

- Generating the topology of the structure parametrically and refining it by using some mechanical methods. This approach is the common one and allows generation of textile geometry in a very short time. One of the first works regarding woven structures are the ones of Peirce and Kemp [6, 7]. Several geometrical methods are summarized by Behera and Hari in [8]. The modern methods considering the mechanical properties of the yarns are based usually on minimization of the potential energy of the yarns, as described in the book of Ron Postle, Carnaby and Jong [9]. In the software Wisetex [10–12] are implemented the mechanical models for woven and braided structures. The geometry of the loops in knitted structures is investigated by researchers as for instance Leaf [13], Postle and Munden [14, 15], Hart et al [16, 17], Goktepe and Harlock [18], Wu [19]. Software, useful for 3D modelling of knitted structures is the WeftKnit (part of Wisetex) by M. Moesen [20] and the different computer realisations of Kyosev and Renkens [21–23]. Very good photorealistic simulations of knitted fabrics at yarn level are reported by Kaldor et al. [24]. They are extended for complete clothing by Yuksel et al. [25].

Both the techniques, that are able to create virtual product without using an existing one - the simulation of the complete production process and generating topology of the structure - require normally the use of the yarns as a main object at the first step. As second step the created yarns are filled with filaments and eventually refined by consideration of the contact between the filaments. The distribution of the fibers or filaments in the yarns can be based on statistical distribution, based on some of the methods used by Neckar and Das [26], Grishanov and Lomov [27], using complete FEM calculation where the fibers are represented as beams as done by Durville in his Multifil package [28, 29] or arbitrary arrangement of the single filaments in circular or parallel layers as implemented in the packages of the TexMind software and described by Kyosev in [30].

3. Yarn level topology

The main principle for the creation of the yarn topology is based on the definition of several points of the yarn axis, whose coordinates can be calculated parametrically. One part of the models use not only the points, but defines the curves and lines between these points explicitly. Figure 1a presents a well-known model for woven fabrics produced of yarns with circular cross section, where each yarn axis can be presented by a connected circle arcs and straight lines. Extended version of such models is implemented very successfully in both commercially and academically used software Wisetex [11, 12] for woven structures. The large number of reported such models for weft knitted structures by Kurbak [31–37] demonstrate nice geometries rendered within 3DS studio. If these models can be applied in the general case within textile CAD software depends on the sensibility of the models on the input data, which should be tested in the future. Less accurate, but more flexible for implementation in computer applications are the models, based on the sequence of the key-points only, where the connecting curve is computed at a next step. Drawing for development of such model for woven structure is presented in Fig. 1b and for knitted structures in Fig. 2. The flexibility of these models is in the less relations, which have to be programmed, which allow the extension of such models for larger number of different structural elements to be done in more clear way. For instance for woven structures one algorithm can be used for complete class of pattern or for knitted structures the programming of loops, tucks, missed and transferred stitches can be done with less steps. Actually this simplicity has its price – during the interpolation the curve between the key-points at some positions the yarn volume can intersect the neighbor yarns, as visualized on the Fig 3. This defect happens, because the distance between the yarns is defined only at the places between the key-points and what happens between these key-points is not controlled during the generation of the interpolating curves.

Which of these approaches is more suitable for modelling should be decided case by case from the modeler. For the cases, where more generality is required and with one algorithm several classes of

structures have to be covered, the definition of the key-points only has its advantage; for models, created to investigate one type of structures (during Master or PhD thesis or some specific product) the analytical description of the curves can be preferable.

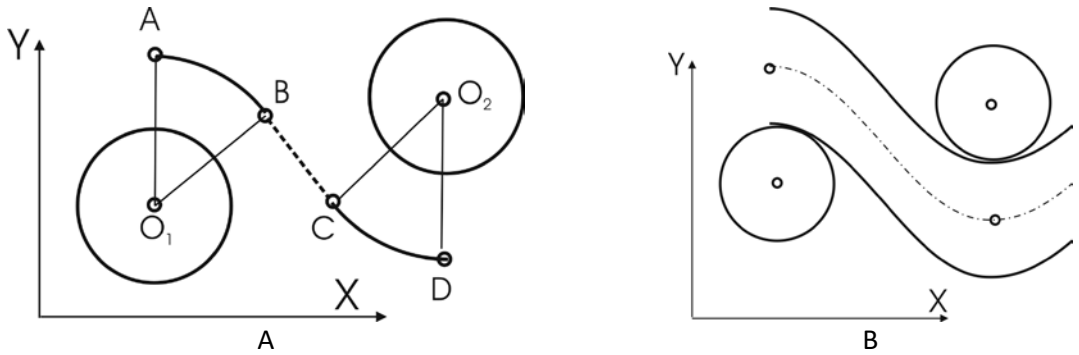

Figure 1. Idealized geometrical model of the yarn path of a woven structure a) based on circular arcs and lines b) based on spline interpolation between key points [38].

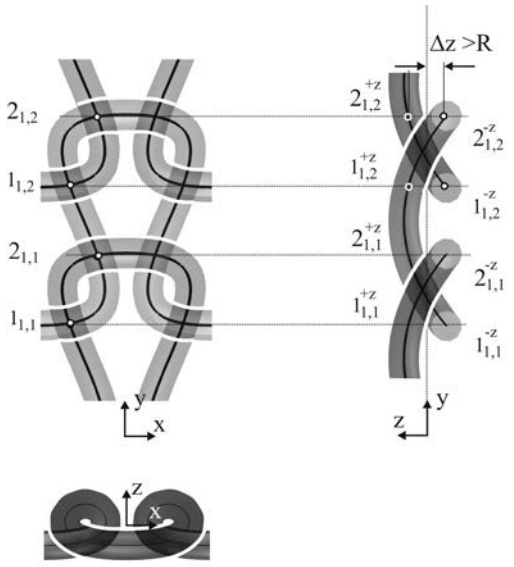

Figure 2. Idealized geometry of weft knitted loop and common points there for creation of geometrical model of these [23]

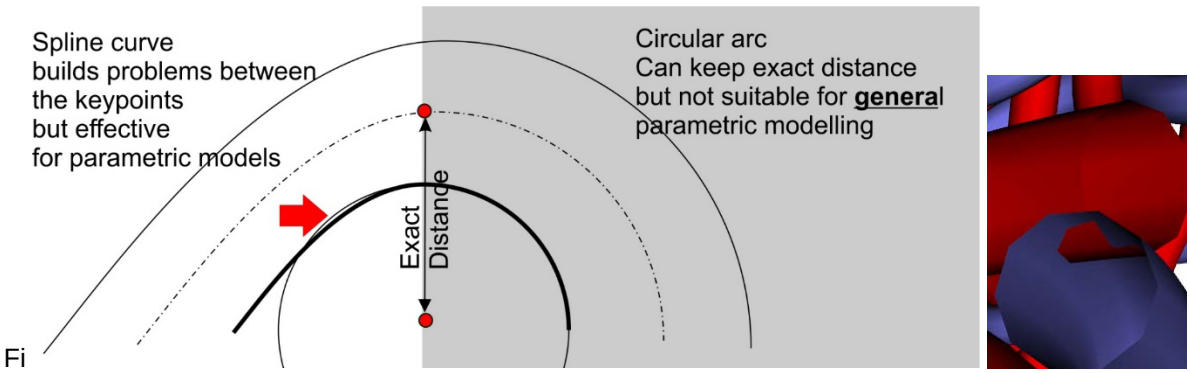

Figure 3. Defects of the interpolation between key points only.

4. Filament level

The generation of the filaments within the yarns can be done in different ways. Duville [28, 29] creates the filaments with some regular initial arrangement and moves these later to their final position applying artificial forces in order to create the topology of the structure. Checking and adjusting the contact between the filaments generates the filament distribution “automatically”. Kyosev [30] defines the local coordinates of the filaments in one cross section (Fig. 4) and then moves this cross section with the set of all coordinates along the yarn axis, considering the orientation of the curve. The yarn cross section is located in the plane of the normal ***n*** and binormal ***b*** vectors, but rotated to some angle γ to these, so the main coordinate axes of the local plain are ***p*** and ***q***. Each filament center ***ci*** can be then defined in local coordinates and placed in the 3D space after simple coordinate transformation. This approach allows controlled creation of twisted structures or structures with flat (for composites) or circular arrangement (for ropes) of the filaments, but requires refining step after the generation in order the structure to be compacted.

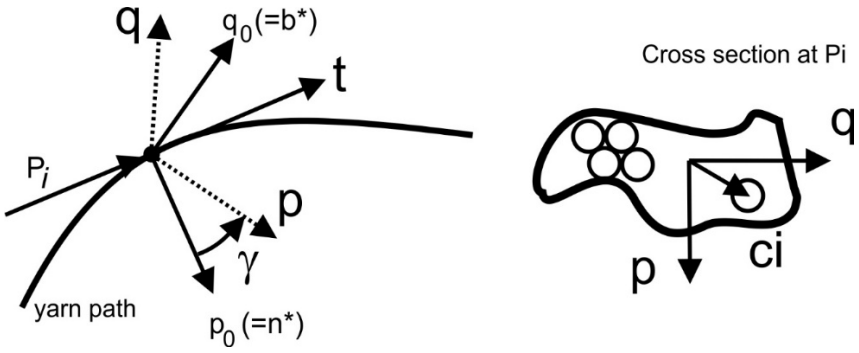

Figure 4. Yarn axis as a curve and the yarn cross section in local coordinates [30].

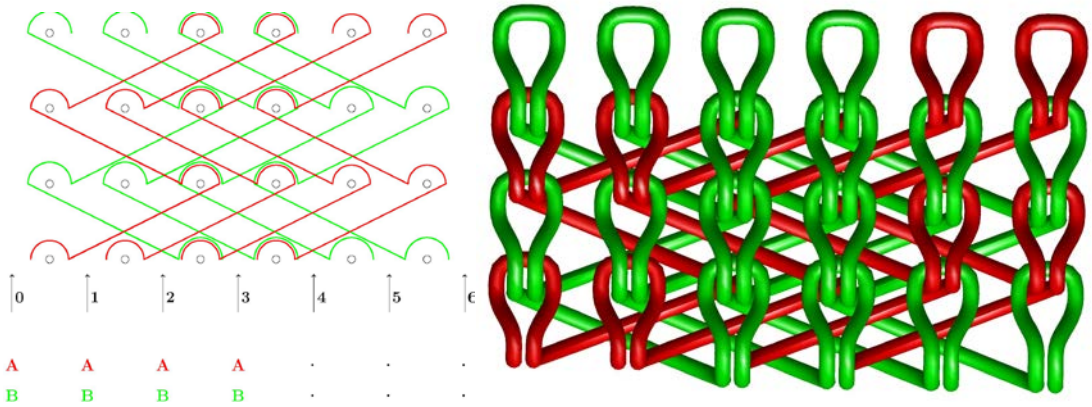

Figure 5. Starting pattern for warp knitted structure and generated yarn level geometrical 3D model [39].

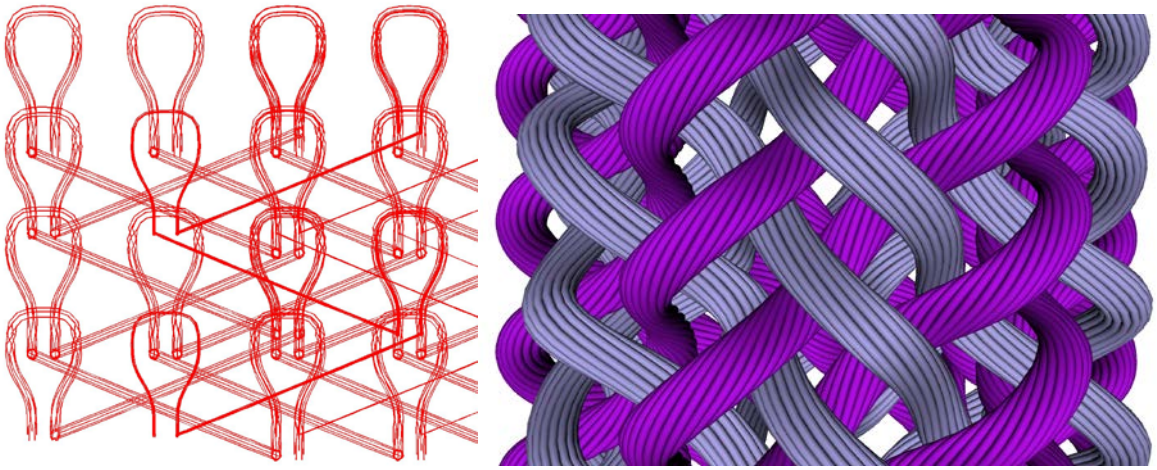

Figure 6. Multifilament model, generated on the basis of the yarn model from Figure 5 and multifilament model of a tubular braided structure [30, 40].

Figure 5 demonstrates the starting data for warp knitted structure and the created 3D geometry at yarn level. It is used at the next step for generation of the filament axes, presented in Figure 6. Multifilament model of a tubular braid is presents as well in Figure 6.

5. Software overview

The following table visualizes some of the packages known or used by the author for creation of models of textile structures. It presents a moment view of the capabilities of these programs, as all these are continuously being developed and extended. The Multiscale Designer of Altair, acquired of Multiscale Design Systems, LLC, proves, that the commercial FEM Software producers try already to integrate textile generators for calculation of composites in their software.

Table 1. Overview of ***some*** software packages for modelling of textiles, used or known by the author

Generators	**Wisetex Suite**	**TexGen**	**TexMind Suite**	**VTMS** Virtual Textile Manufacturing Suite	**Multifil**	**Multiscale Designer**
Some sources	[11, 12, 41, 42]	[43][44]	[30, 40]	[45]	[28, 29]	[46]
Developer	KU Leuven	Univ. Nottingham	TexMind UG	The University of Dayton	Laboratoire MSSMat - Centrale Paris	Altair, Multiscale Design Systems
License	Proprietary	GPL	Proprietary	Proprietary	Proprietary	Proprietary
Source	Closed	Open	Closed	Closed	Closed	Closed
Structure Type						
Woven	Single- and Multilayer woven each yarn individually defined	Single layer, orthogonal, angle interlock, layer to layer, yarn group properties	Basic structures, Each yarn individually defined	Single layer, orthogonal, angle interlock, layer to layer, yarn group properties	Basic structures, (manual generator)	5 Basic structures
Weft Knitted	Loop based fine, Tucks need improvement	- Scripting or import from	Plain Loops in flat and tubular structure	- (import possible)	- (import possible	-

		TexMind or Wisetex				
Warp Knitted	Needle stitched only	- Scripting or import	Loop3D - several classes structures on single and double needle bed machines	- (import possible)	- (import possible)	-
Braided	Unit Cell of biaxial and triaxial braids	- Scripting or import from TexMind or WiseTex	Braider - tubular and flat; Configurator - custom (Geometry)	Unit cell of biaxial and triaxial, Tubular briads	Manual generation (import possible)	-
Yarn Level						
Yarn Level - Mechanics	Beam - Energy minimization	- (scripting possible)	-	Digital Chain	Beam	-
Yarn Contact	Algorithmically included	-	(*)Local Sections	Mesh	Beam-Beam	Surface-Surface
Scripting	-	Python	-	-		-
Imports		WiseTex Weave Pattern	WiseTex,			Abaqus inp File
Exports	Abaqus, Ansys, WiseTex XML (TexGen)	Step, STL, Abaqus, Voxel Grid, (WiseTex)	Abaqus, Ansys, VTMS, WiseTex, TexGen, ImpactFEM, X3D, STL			
Yarn definition	Initially constant cross section	Variable cross section	Constant Cross section	Constant Cross section		Constant Cross section
Filament level						
Filament Visualization	-	-	Yes	yes	Yes	-
Filament Data Stored	Yes	-	Yes	Yes	Yes	
Filament Data Used for computations	Yes	-	Yes	Yes	Yes	-
Initial filament Distribution in the yarn cross section	-	-	Circular layers, flat layers and arbitrary distribution possible	Number of filaments	Program dependent	-
Structural levels	2(3): Fabrics-Yarn-(Fiber data); In LamTex: 3	3: Layered textile - Textiles - Yarn	4: Textile-4: Yarn Groups-Yarns-Fibers	3: Fabrics-Yarn-Fibers	3 Fabrics-Yarns-Fibers	1: Yarn volume mesh

4. Levels in textile structures

Table 1 shows that the filament level is presented at three of the packages currently. The TexMind packages can cover 4 level of grouping of filaments, common are three levels. The actual situation for modelling of textiles at fiber or filament level require several levels, as presented in figure 7 for the case of a rope – normally several houndert of filaments build one yarn, this build a ply yarn toghether with another yarns, commonly twisted toghether. Then often several twisted yarns are again twisted, in order

to get required thickness and strength and after the twisting several yarns are braided together. Figure 8 shows this information and makes clear the similarity between the levels. It is well visible, that only two main types of virtual objects are required for storage of the data for simulation of textile structures – fibers (fialments) and “groups of fibers”. Each “group of fibers” can be yarn, ply yarn, twisted yarn or braided structure. It is a linear product and it can be characterised from the programming and modelling point of view as a larger and thicker fiber or “micro-fiber”. In order the properties of this macro-fiber to be visualised at the current level, all its properties – diameter, fineness, color and mechanical properties should be defined or calculated. In such recursive definition, where the main object is “group of fibers”, consisting another “groups of fibers” there is no limitation of the number of the levels of groupping and all kind of fabrics can be modelled and represented.

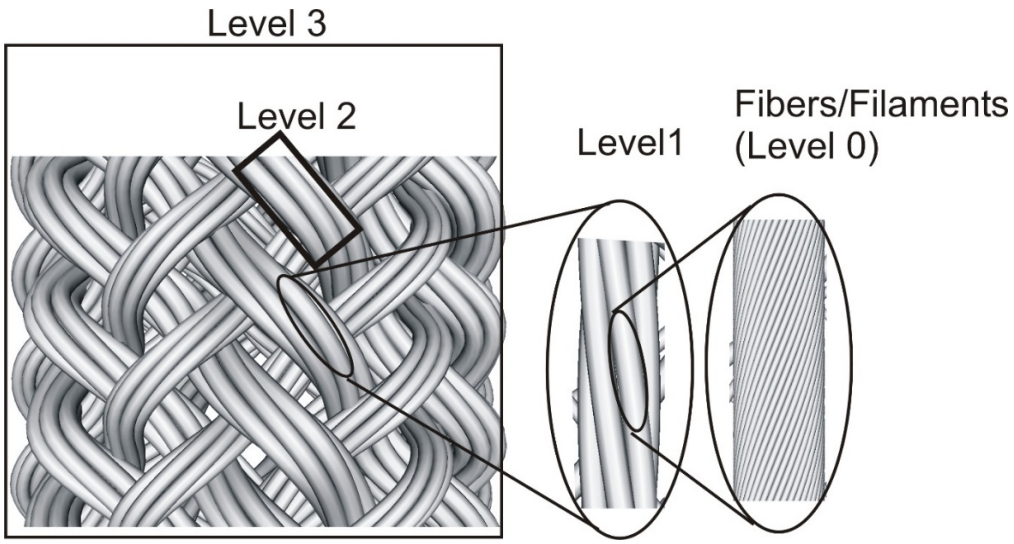

Figure 7. Example of the basic element (Filament) and levels of grouping of the fibrous assemblies in this case for a braided structure.

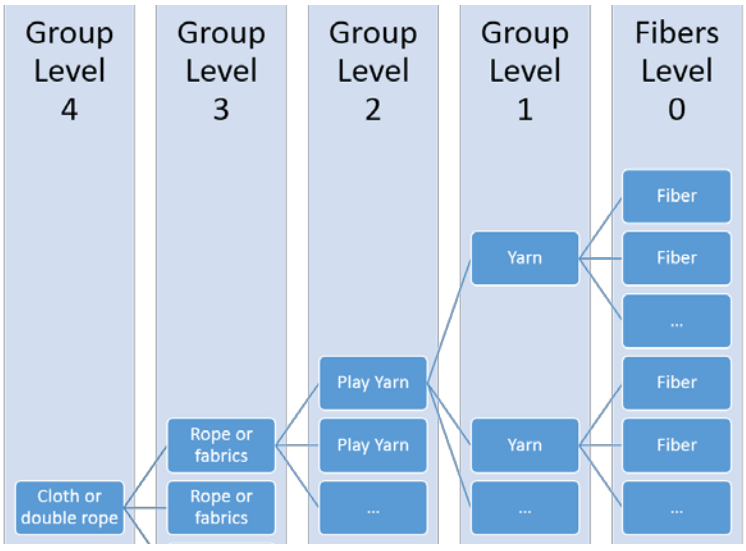

Figure 8. Fibers (or filaments) are basic object of fibrous structures. All higher levels consists of groups of another groups.

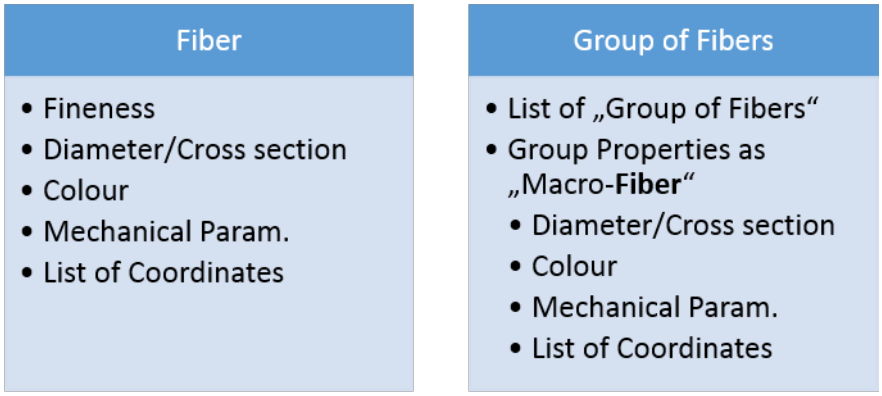

Figure 9. Two required types of objects (classes) – fibers and “group of fibers” and their principle properties. Each group of fibers can be represented as well as a macro-fiber (yarn, ply yarn) and because of this the definition of fiber-similar properties as resulting color, diameter and mechanical properties can be useful.

6. CONCLUSIONS

This paper gives an overview of the methods for geometrical modelling of textile structures. It points out the advantages and disadvantages of the both popular methods for the description of the yarn geometry – using key-points only or using key-points and explicitly defined curves between these points. Overview of the common used software packages for modelling demonstrates their capabilities at the current time. It shows, that the programs cover two, three and up to four levels of grouping of fibrous objects today. During the analysis of one rope structure is found, that only two classes of objects are required for multiscale modelling of textile structures, if recursive definition is used. These are the “fiber/filament” and “group of fibers”, which can consists list of another “groups of fibers”. Using such objects, structures with unlimited number of levels of grouping can be modeled.

References

1. *Harjkova, G., Barburski, M., Lomov, S.V., Kononova, O., Verpoest, I.: Weft knitted loop geometry of glass and steel fiber fabrics measured with X-ray micro-computer tomography. Textile Research Journal **84**(5), 500–512 (2014). doi: 10.1177/0040517513503730*
2. *Naouar, A., Vidal-Salle, E., Boisse, P.: Meso-FE forming of a non-crimp 3D orthogonal weave E-glass composite reinforcement based on X-ray computed tomography. In: Boussu, F., Chen, X. (eds.) 3D Fabrics & Their applicattions. Proceedings of the 7th World Conference. 7th World Conference 3D Fabrics and their applications, Roubaix, 8-9.9, pp. 285–293 (2016)*
3. *Finckh, H.: Textile micromodels as a result of idealized simulation of production processes. In: Finite Element Modeling of Textiles and Textile Composites. 22nd BEM-FEM Conference, Saint-Petersburg, Russia, 26-28 September 2007. Katholieke Universiteit Leuven & St-Petersburg State University of Technology and Design, Saint-Petersburg, Russia (2007)*
4. *Akkerman, R.a.R.B.H.V.: Braiding simulation for rtm preforms. In: TexComp 8 (2006)*
5. *Kyosev, Y.K.: Machine configurator for braided composite profiles with arbitrary cross section. In: 16th European conference on composite materials ECCM 16. 16th European conference on composite materials ECCM 16, 22-26.06.2014, Seville-Spain (2014)*
6. *Peirce, F.T.: 5—THE GEOMETRY OF CLOTH STRUCTURE. Journal of the Textile Institute Transactions. Journal of the Textile Institute Transactions **28**(3), T45-T96 (1937). doi: 10.1080/19447023708658809*

7. *Kemp, A.: An Extension of Peirce's Cloth Geometry to the Treatment of Non-circular Threads. Journal of the Textile Institute Transactions. Journal of the Textile Institute Transactions **49**(1), T44-T48 (1958). doi: 10.1080/19447025808660119*
8. *Behera, B., Hari, B.K.: Woven textile structure. Theory and application. Woodhead Publishing Ltd, Cambridge (2010)*
9. *Postle, R., Carnaby, G., Jong, S. de: The mechanics of wool structures. Ellis Horwood Limited (1988)*
10. *Lomov, S., Bernal, E., Koissin, V., Peeters, T.: Integrated textile preprocessor WiseTex, Version 2.5. Computational models, methods and algorithms. KU Leuven, Department MTM, Leuven (2006)*
11. *Lomov, S., et al.: WiseTex. KU Leuven, Leuven (2011)*
12. *Verpoest, I., Lomov, S.V.: Virtual textile composites software Wisetex: integration with micro-mechanical, permeability and structural analysis. Composites Science and Technology **65(15-16)**, 2563–2574 (2005)*
13. *Leaf, G.G.A.: The Geometry of a plain Knitted Loop. Journal of the Textile Institute **45**, 605 (1955)*
14. *Postle, R., Munden, D.: Analysis of the dry-relaxed knitted-loop configuration Part 1: Two-Dimensional Analysis. Journal of the Textile Institute **58(8)**, 329–351 (1967)*
15. *Postle, R., Munden, D.: Analysis of the dry-relaxed knitted-loop configuration Part 2: Three-dimensional analyses. Journal of the Textile Institute **58(8)**, 352–365 (1967)*
16. *Hart, K., Jong, S. de, Postle, R.: Analysis of the Single Bar Warp Knitted Structure Using an Energy Minimization Technique: Part I: Theoretical Development. Textile Research Journal **55**(8), 489–498 (1985). doi: 10.1177/004051758505500807*
17. *Hart, K., Jong, S. de, Postle, R.: Analysis of the Single Bar Warp Knitted Structure Using an Energy Minimization Technique: Part II: Results and Comparison with Woven and Weft Knitted Analysis. Textile Research Journal **55**(9), 530–539 (1985). doi: 10.1177/004051758505500903*
18. *Goktepe, O., Harlock, S.: Three-Dimensional Computer Modeling of Warp Knitted Structures. Textile Research Journal **72**, 266–272 (2002)*
19. *Wu, W., Hamada, H., Maekawa, Z.: Computer Simulation of the deformation of weft knitted fabtrics for composite materials. Journal of the Textile Institute **85(2)**, 198–214 (1994)*
20. *Moesen, M.: Modelleren van de vlakke vervorming van gladde inslagbreisels. http://liegebeest.studentenweb.org/weftknitEN.html*
21. *Kyosev, Y.: Computational Model of Loops of a Weft Knitted Fabric. In: Dragčević, Z. (ed.) Magic world of textiles. Book of proceedings ; ITC&DC, 3rd International Textile Clothing & Design Conference, October 8th to October 11th, 2006, Dubrovnik, Croatia, Zagreb (2006)*
22. *Kyosev, Y., Renkens, W.: 3D-CAD für die Gestaltung von gewirkten Strukturen. In: 11-Chemnitzer Textiltagung, 24-25 Oktober 2007, pp. 110–117 (2007)*
23. *Kyosev, Y., Renkens, W.: Modelling and visualization of knitted fabrics. In: Chen, X. (ed.) Modelling and predicting textile behaviour, pp. 225–262. Woodhead Publishing; In association with the Textile Institute; CRC Press, Cambridge, Boca Raton, Fla (2010)*
24. *Kaldor, J., James, D.L., Marschner, S.: Simulating Knitted Cloth at the Yarn Level. In: Proceedings of SIGGRAPH 2008. Held in Los Angeles, California, August 2008 (2008)*
25. *Yuksel, C., Kaldor, J.M., James, D.L., Marschner, S.: Stitch Meshes for Modeling Knitted Clothing with Yarn-level Detail. ACM Transactions on Graphics (Proceedings of SIGGRAPH 2012) **31**(3), 37:1-37:12 (2012). doi: 10.1145/2185520.2185533*
26. *Neckar, B., Das, D.: Theory of Structure and Mechanics of Fibrous Assemblies and Yarns. Woodhead Publishing India Ser. Woodhead Publishing Limited; Ingram Publisher Services [distributor], Sawston, LaVergne (2012)*
27. *Grishanov, S., Lomov, S.e.a.: The Simulation of the Geometry of Two-component Yarns. Part I: The Mechanics of Strange Compression: Simulating Yarn Cross-section Shape. Journal of Textile Institute **88, Part 1**(2) (1997)*
28. *Durville, D.: Finite element simulation of textile materials at mesoscopic scale. In: Finite element modelling of textiles and textile composites - St-Petersburg – 26-28 September (2007)*

29. *Durville, D.: Simulation of the mechanical behaviour of woven fabrics at the scale of fibers. Int J Mater Form **3**(S2), 1241–1251 (2010). doi: 10.1007/s12289-009-0674-7*
30. *Kyosev, Y.: Generalized geometric modeling of tubular and flat braided structures with arbitrary floating length and multiple filaments. Textile Research Journal **86**(12), 1270–1279 (2016). doi: 10.1177/0040517515609261*
31. *Kurbak, A.: Geometrical and mechanical modelings of dry relaxed slack plain-knitted fabrics for the benefit of technical textile applications Part I. A geometrical model. Textile Research Journal (2016). doi: 10.1177/0040517516641358*
32. *Kurbak, A., Amreeva, G.: Creation of a Geometrical Model for Milano Rib Fabric. Textile Research Journal **76**(11), 847–852 (2006). doi: 10.1177/0040517507071968*
33. *Kurbak, A., Ekmen, O.: Basic Studies for Modeling Complex Weft Knitted Fabric Structures Part I: A Geometrical Model for Widthwise Curlings of Plain Knitted Fabrics. Textile Research Journal **78**(3), 198–208 (2008). doi: 10.1177/0040517507082352*
34. *Kurbak, A., Soydan, A.S.: Basic Studies for Modeling Complex Weft Knitted Fabric Structures Part III. A Geometrical Model for 1 x 1 Purl Fabrics. Textile Research Journal **78**(5), 377–381 (2008). doi: 10.1177/0040517507082465*
35. *Kurbak, A.: Geometrical models for weft-knitted spacer fabrics. Textile Research Journal, 0040517516631320. doi: 10.1177/0040517516631320*
36. *Kurbak, A.: Geometrical Models for Balanced Rib Knitted Fabrics Part I: Conventionally Knitted 1 × 1 Rib Fabrics. Textile Research Journal **79**(5), 418–435 (2009). doi: 10.1177/0040517508095598*
37. *Kurbak, A., Kayacan, O.: Basic Studies for Modeling Complex Weft Knitted Fabric Structures Part V: Geometrical Modeling of Tuck Stitches. Textile Research Journal **78**(7), 577–582 (2008). doi: 10.1177/0040517507087672*
38. *Kyosev, Y.K.: Simulation of wound packages, woven, braided and knitted structures. In: Veit, D. (ed.) Simulation in textile technology, pp. 266–309. Woodhead Publishing Limited (2012)*
39. *Renkens, W., Kyosev, Y.: Geometry modelling of warp knitted fabrics with 3D form. Textile Research Journal **81**(4), 437–443 (2011). doi: 10.1177/0040517510385171*
40. *Kyosev, Y.K.: TexMind Braider, www.texmind.com, Mönchengladbach (2012)*
41. *Moesen, M., Lomov, S.V.: WeftKnit (2011)*
42. *Moesen, M., Lomov, S., Verpoest, I.: Modelling of the geometry of weft-knit fabrics. In: Techtextil (Hg.) 2003 – TechTextil Symposium 7-10 April 2003 (2003)*
43. *Sherburn, M.: Geometric and Mechanical Modelling of Textiles. PhD, University of Nottingham. http://etheses.nottingham.ac.uk/303/1/thesis-final.pdf (2007)*
44. *University of Nottingham: TexGen. University of Nottingham (2011)*
45. *Zhou, G., Sun, X., Wang, Y.: Multi-chain digital element analysis in textile mechanics. Composites Science and Technology **64**(2), 239–244 (2004). doi: 10.1016/S0266-3538(03)00258-6*
46. *Altair: Multiscale Design. http://www.altair.com/ (2016)*

GEOMETRICAL MODEL OF A KNITTED FABRIC MADE FROM HYALURONAN BASED FIBERS

Tomáš Pitucha

Contipro a.s., R&D department, Dolní Dobrouč, Czech Republic,
Technical University of Liberec, Faculty of Textile Engineering, Liberec, Czech Republic,
pitucha@contipro.com, +420 467 070 361

Abstract:

Hyaluronan is a linear polysaccharide that can be manufactured by wet spinning to the form of monofilament fibers. The natural hyaluronan is soluble in water; the solubility can be eliminated by chemical modification (acylation). Nevertheless fibers made from acylated hyaluronan significantly swell when dipped in water. Fabrics made from such fibers are substantially influenced by this swelling: as the fiber thickness increases the textile structure gets closer and tighter and the fabric dimensions change.

A geometrical model of a warp knitted fabric has been created and relations between geometrical and structural characteristics of fibers, yarns and fabric have been determined via mathematical formulas. A set of knitted fabrics of different loop density have been manufactured from acylated hyaluronan fibers. Geometry of hyaluronan based fibers, yarns and fabrics in dry and wet state have been analyzed using various optical methods (optical microscopy, SEM, laser scanning). Experimental data have been compared with the results calculated using the geometrical model.

The geometrical model enables to explain some causes of the dimensional changes of knitted fabrics due to swelling. Moreover the model seems to be a useful tool for description and prediction of the behavior of knitted fabrics made from fibers of high level of swelling.

Key words:

Geometrical model, knitted fabric, hyaluronan fibers, swelling

1. Introduction

Hyaluronan is a natural polymer that is widely used in cosmetics and pharmacy. A wet spinning process has been adapted to create monofilaments both from the native hyaluronan and its derivatives [1,2,6]. Fibers from hyaluronan modified by fatty acids are insoluble in water but they strongly swell. Fabrics made from these fibers significantly shrink when dipped in water. It is known that the most important factors responsible for shrinkage of knitted fabrics are just swelling of yarn and the relaxation of internal stress imposed during the knitting process. Shrinkage of weft knitted fabrics was studied by Suh [7] who created a geometrical model that explains shrinkage principles of cotton jersey fabric. Structure of warp knitted fabrics has been intensively studied in the last decade and sophisticated 3D models have been developed [3,5,8] but influence of fiber swelling is out of their scope. The objective of this study has been to create a simple 2D geometrical model of the tricot-patterned warp knitted fabric that would respect an influence of fiber and yarn swelling and shrinkage.

Each level of the textile structure hierarchy can participate on the total dimensional changes of a fabric so that the total shrinkage/extension results from structural and geometrical changes of fibers, yarns and fabric. Swelling and shrinkage of fibers are connected with the rearrangement of the polymer chains that interact with water and with the consequent relaxation of the stress imposed during fiber processing. Shrinkage on the yarn structure level relates mainly to the increase of the fiber diameter within the twisted yarn. Neckář [4] created a helical model of the yarn that explains dimensional changes of yarns based on the knowledge of fiber swelling and shrinkage.

Geometrical model of tricot

Inputs of the proposed model include a dry yarn diameter D, wet yarn diameter D', and yarn shrinkage. Geometry of yarn axis in the model is composed by combination of line segments and circular arcs as shown in Fig 1. The following formulas have been derived for the course distance a and wale distance b:

$$a = [L - 2R(\tan\gamma + \pi - \gamma)] \cdot \frac{\cos\gamma}{3} \quad (1)$$

$$b = 2a \cdot \tan\gamma + \frac{R}{\cos\gamma}, \quad (2)$$

where L is the yarn length in the loop, R is the radius of loop arcs (both needle and sinker) and γ is the angle between loop legs and the machine (wale) direction.

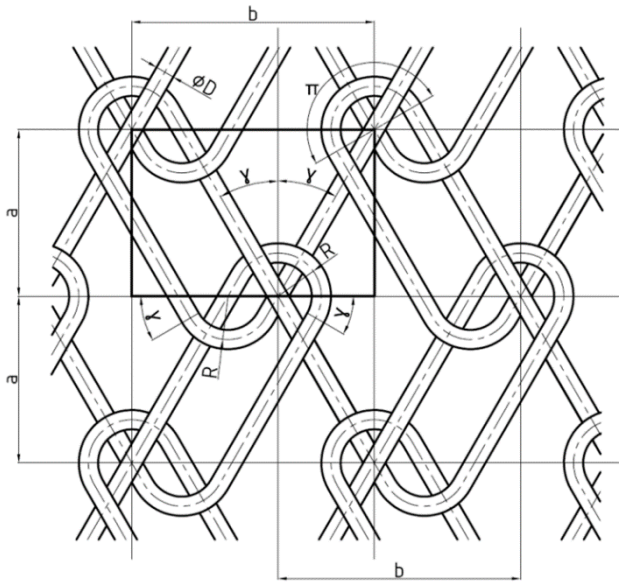

Figure 1. 2D geometrical model of the tricot-patterned warp knitted fabric.

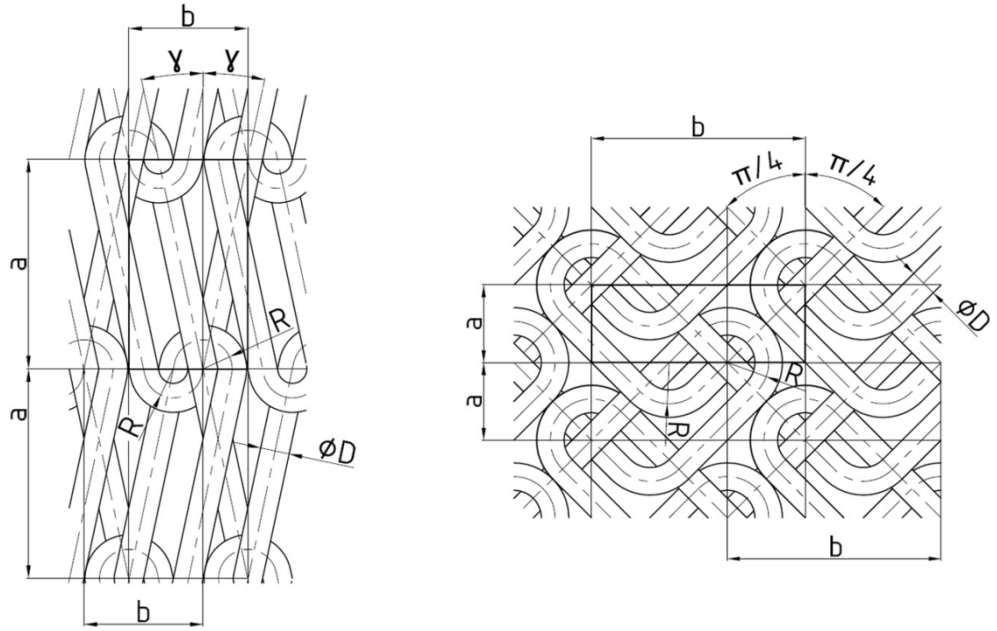

Figure 2. Special cases of the tricot-patterned warp knitted fabric: a) (left): Geometrical model of the fabric stretched lengthwise. b) (right): Geometrical model of the relaxed fabric.

Based on this general model it is possible to determine 2 special cases, depicted on the Fig. 2:

a) If the fabric is stretched lengthwise the needle loop arcs touch the adjacent loop legs and the radius R match the value of the yarn diameter D ($R = D$);
b) if the fabric is maximally relaxed the angle γ between loop legs and the wale direction match the value 45° ($\pi/4$) and the radius R tend to be as large as possible so that loops touch adjacent loops and the following formula is valid:

$$R = R_{\max} = \frac{L-3D}{8+\frac{3}{2}\pi} \quad (5)$$

A fabric during knitting on a raschel machine is stretched between the needles and take-down rollers so that the loops are stretched lengthwise and the adjacent wales tend to get closer to each other (see the Fig 3a). It is expected that this state can be approximated by the geometrical model on the Fig 2a.

As soon as the fabric is taken off the machine it can partially relax which results in shrinkage in the wale direction and extension in the course direction. When such fabric from modified hyaluronan is dipped in water (see the Fig 3b) the dimensional changes continue intensively: the fibers significantly swell and the loops become shorter, wider and round. This state of the fabric should correspond to the geometrical model on the Fig 2b.

If the fabric is consequently freeze-dried it keeps the loop geometry that is similar to the density of the fabric in the wet swollen state. So if we are able to determine the relation between the stretched state and the swollen state we should be able to set up the knitting process parameters (warp feeding and take-down speed) according to the desired loop density of the final freeze-dried fabric.

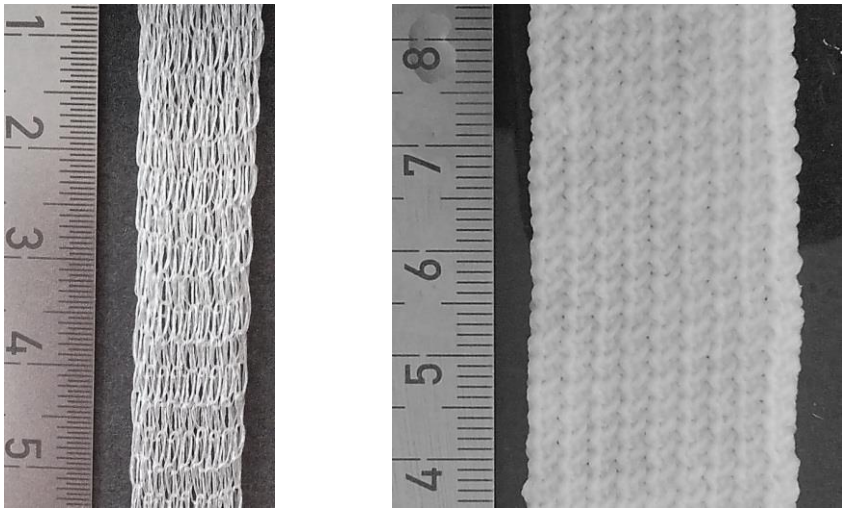

Figure 3. Photos of the fabric made from the hyaluronan based fibers: a) (left): On the knitting machine - stretched between needles and take-down rollers, b) (right) In the swollen state - after wetting in demineralized water.

2. Experimental

2.1. Materials

Fibers (monofilaments) of 11 tex fineness made from palmitoyl hyaluronan of molecular weight 320 kDa and degree of substitution 55% were employed (product of Contipro a.s.). Yarns composed from 3 monofilaments (300 twists/meter) were used for the knitting trials. The geometrical characteristics of the fibers and yarns are listed in the table 1.

Table 1. Geometrical characteristics of the fibers and yarns.

	Average value	Standard deviation	Koeficient of variation [%]
Fiber fineness [tex]	10,8	0,5	4
Dry fiber diameter [μm]	109	9	8,5
Wet fiber diameter [μm]	530	72	14
Fiber shrinkage [%]	12,4	2,2	18
Dry yarn diameter [μm]	207	7	3,3
Wet yarn diameter [μm]	733	64	8,8
Yarn shrinkage [%]	17,0	1,6	9,2

2.2. Methods

The fabric samples were made on the double needle bed warp knitting machine Comez DNB-80, gauge 12. All the samples had the same tricot pattern composed from two layers knitted simultaneously on the front and back needle bar and locked together by underlaps. Various loop densities of individual samples were reached by changing feeding and take-down speeds. Fabrics were washed in ethanol at 40°C for 2 x 20 min and dried at room temperature. Then the samples were immersed in demineralized water for 20 min, frozen at -20°C for 5 hours and freeze-dried for 16 hours (Lyophilizator Christ Alpha).

Diameter of dry fibers and yarns were determined using 4-direction laser scanning during rewinding of the fibers/yarns (Accuscan 6012). Diameters of the wet (swollen) fibers and yarns were measured using optical microscopy (Nikon Eclipse Ci-L). Course and wale distances in the knitted fabric were determined as a reciprocal value of the corresponding loop densities; the loop densities were determined for the fabric at the machine (stretched between needles and taken-down rollers), for the relaxed fabric (without external stress) and for the wet fabric in the swollen state.

3. Results and discussion

3.1. Dimensional changes of the knitted fabric

Both the experimental and the theoretical values of the course distances are shown on the Fig. 4. For each sample the course distance is maximal when the fabric is on the machine (the stretched state), after relaxation the distance decreases and after swelling is minimal. The curves calculated using the geometrical model shows the trend of the course distance in dependence on the yarn length in the loop. Experimental values of the fabric on the machine are near the corresponding model values of the stretched fabric and the experimental values of the wet fabric are near the corresponding model values of the swollen fabric.

The divergence between the theoretical and experimental values results mainly from the simplified loop shape geometry used in the model. The real fabric fixed on the machine during knitting is not so stretched in order that the loop legs would be perfectly straighten and the yarn arc would curve tightly over the yarn segments of the next loop. In case of the swollen state the important factors is the yarn shrinkage and especially increase of the yarn diameter. These changes result in considerable three-dimensional character of the knitted structure and the consumption of the yarn increases because the yarn has to crimp over and under the other yarn segments.

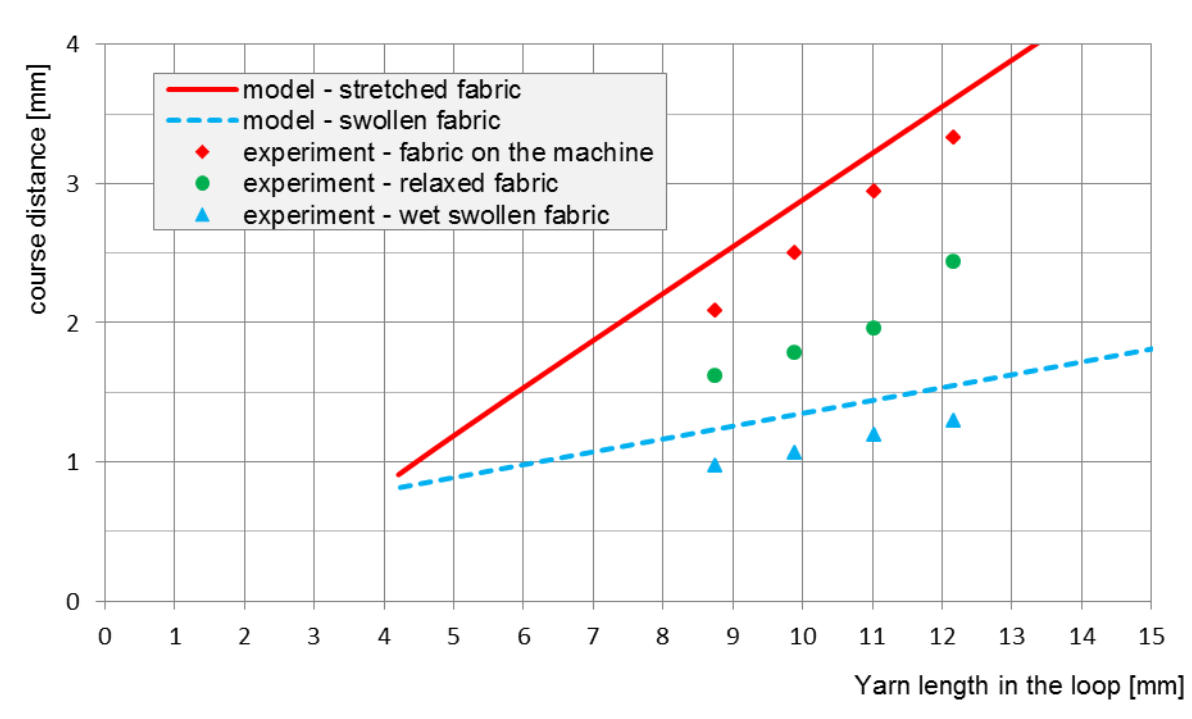

Figure 4. Dependence of the course distance on the yarn length in the loop - comparison of the model and experimental data.

When we calculate dimensional changes of the fabric samples between the swollen state and the stretched state (see Table 2) we find out that the fabric shrinkage in the wale direction is not constant but increases with the yarn length in the loop. This result is logical because the larger loops have longer legs that can get round and transform themselves into parts of loop arc segments of higher diameter which results in decrease of the course distance.

Table 2. Fabric shrinkage in the machine direction – dimensional changes between the stretched and swollen states. Comparison of the theoretical and experimental results.

Sample	Yarn lenght in the loop [mm]	Shrinkage in the wale direction [%]	
		model	experimental
A	8,74	50	53
B	9,88	53	57
C	11,02	55	60
D	12,16	57	61

3.2. Participation of individual structural levels

The experimental results prove that all three levels of the textile structure (fiber, yarn and fabric) participate markedly on the total shrinkage of the knitted fabric (see the tables 1 and 2). Anyway the most important share pertains to the dimensional changes caused by the rearrangement of the knitted structure that lies in the change of the loop shape and size. Calculation of the dimensional changes using the geometrical model can be helpful to predict shrinkage of other variants of fabrics, e.g. made from fibers of different fineness or swelling rate.

4. CONCLUSIONS

A simple geometrical model of a warp knitted fabric has been developed and employed to explain shrinkage of fabrics made from hyaluronan based fibers. The fabric shrinkage is caused not only by the fiber and yarn shrinkage but mainly by changing of the loop geometry, esp. by increase of loop leg angle and the loop arc radius which is significantly supported by huge swelling of the used fibers. Both the model and experimental results show a similar dependence of the course distances on the yarn length in the loop. The model can be utilized for designing of fabrics that are made from fibers of high level of swelling.

References

1. *Betak, J., Buffa, R., Nemcova, M,; Pitucha, T. et. al.: Endless fibres on the basis of hyaluronan selectively oxidized in the position 6 of the n-acetyl-d-glucosamine group, preparation and use thereof, threads, staples, yarns, fabrics made thereof and method for modifying the same. Patent. PCT/CZ2013/000157, WO2014082610 A1.*
2. *Burgert, L., Hrdina, R., Masek, D., Velebny, V.: Hyaluronan fibres, method of preparation thereof and use thereof. Patent. PCT/CZ2011/000126. WO 2012089179 A1.*
3. *Honglian, C., Mingqiao, G., Gaoming, J. (2009). Three-Dimensional Simulation of Warp-knitted Fabric. Fibres and Textiles in Eastern Europe, 3(74), 66-69.*
4. *Neckář, B. (1990). Příze (1st ed.). SNTL (Praha).*
5. *Renkens, W., Kyosev, Y. (2011). Geometry modelling of warp knitted fabrics with 3D form. Textile Research Journal, 81(4), 437-443.*
6. *Scudlová, J., Betak, J., Wolfova, L., Buffa, R., et. al.: Fibres based on hydrophobized derivatives of hyaluronan, method of their preparation and use, textiles on base thereof and use thereof. Patent. PCT/CZ2013/000158, WO2014082611 A1.*
7. *Suh, M. W., (1967). A study of the Shrinkage of Plain Knitted Cotton Fabric, Based on the Structural Changes of the Loop Geometry Due to Yarn Swelling and Deswelling. Textile Research Journal, 37(5), 417-431.*
8. *Xu, H.-Y., Chen, N.-L., Jiang, J.-H., Jin, L.-X., Wang, Z.-X. (2015). 3D Simulation of Warp Knitted Structures with a New Algorithm Based on NURBS. Fibres and Textiles in Eastern Europe, 1(109), 57-60.*

IMAGE ANALYSIS AND DESCRIPTION OF SINGLE JERSEY LOOP GEOMETRY

Monika Vysanska

Technical University of Liberec, Department of Textile Technologies, Liberec, Czech Republic, monika.vysanska@tul.cz, +420485353215

Abstract

Many geometrical models of single jersey loop and various approaches to its image analysis exist there. The contribution presents original approach to the image analysis of deformed loop and to the consequent substitution by polynomial functions. The loop is defined by the set of parameters, their changes are observed and evaluated during the NiTi knitted fabric deformation.

Key words

Single jersey loop, image analysis, polynomial function, MatLab, superelastic material

1. Introduction

Investigation into the dimensional properties of knitted structures began with experimental works. Doyle [1], Munden [2], Knapton et al. [3, 4] and Kurbak [5, 6] gave some empirical formulas by conducting experimental works. At the same time researches also tried to create some geometrical and physical models for knitted fabric structures. Previously created geometrical models for plain knitted fabric include those of Chamberlain [7], Peirce [8], Leaf and Glaskin [9], Leaf [10], Munden [11], Postle [12], Kurbak [13, 14] and Demiroz [15].

To overcome the problem for plain-knitted fabrics, a numerical model consisting of a system of rectangular cells is proposed, and a finite-element method (FEM) has been chosen as the basis for model evaluation [16, 17]. The FEM has been used successfully to solve a wide variety of problems. Originating from the study of structural mechanics in the 1950s the FEM is now well documented by thousands of publications [18], the majority being specialized papers. More general textbooks [19 – 23] have appeared during recent decades. The method was successfully employed in the area of the mechanics of textiles by Lloyd [24] and then developed in the mechanics of yarns [25 – 30].

The presented paper focuses on the problems of image analysis of chosen (marked) loop in NiTi knitted fabric. Further it pursues the change of defined parameters of the loop during the knitted fabric deformation. At the same time it deals with the possibility of substitution of loop shape by the mathematical functions differently from mentioned sources. The outputs are graphical illustrations of loop parameters changes in dependence on knitted fabric deformation. The observed knitted fabric was made from Nitinol with the superelastic properties. Thanks to these properties the behavior of this material is precisely defined during the deformation. This fact should theoretically reflect also in changes in knitted fabric, loop respectively. The results of the measurement will show whether it really works.

2. Notes to NiTi Material Properties

In this work the thin superelastic Nitinol (NiTi) filaments of diameter 100 microns as the material providing the functional properties to be projected onto the weft knitted textiles. The filaments were delivered in so called straight-annealed state i.e. they exhibited functional properties in as received state and no further heat treatment had to be applied. The selected NiTi alloy is called superelastic as the stable microstructure phase at room temperature is cubic austenite, which can be transformed into monoclinic martensite, stable at lower temperatures, by applying external loads. Such so called stress induced martensitic transformation gives rise to nonlinear hysteretic tensile behavior shown in Fig. 1, which depicts all peculiar features of superelastic NiTi filaments such as large recoverable strain (8%), occurrence of plateaus, different Young module of austenite (~50 GPa) and martensite (~20 GPa),

stress hysteresis and strong thermomechanical coupling shifting the transformation plateaus by 5.5 MPa per degree of temperature change [31].

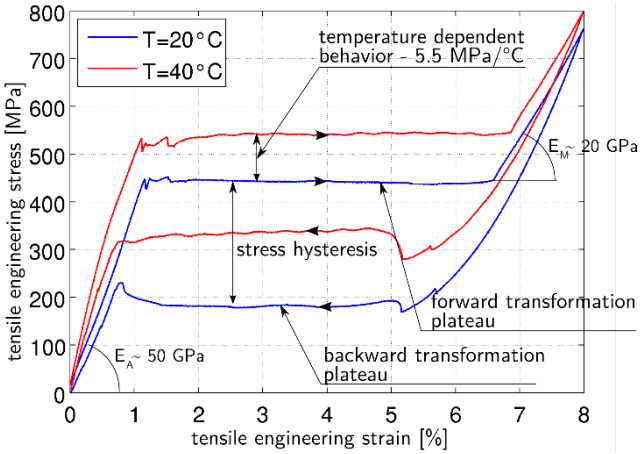

Figure 1. Tensile behavior of the used superelastic NiTi filaments of diameter 0.1mm at two temperatures.

3. Notes to the adjustment of the image of the knitted fabric loop

The procedure is determined for previously colored knitted fabric loop (the colored loop is contrast in relation to the rest of fabric and also to the background), see Fig. 2. The image (the sequence of the images) is then adjusted in the system of the image analysis.

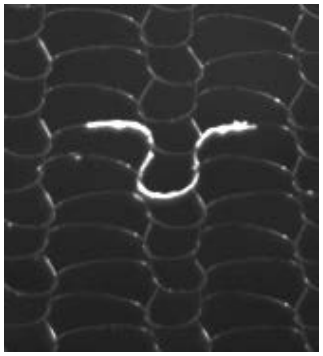

Figure 2. Colored loop in the knitted fabric

3.1 Usage of the system of image analysis

The image sequence is adjusted in the system of image analysis NIS Elements semi-automatically by the macro with the possibility of user intervention. The presented procedure is not probably totally universal, because of image analysis high sensitivity on the reflections of non-colored knitted loops during the threshold, see Fig. 2.

The following operations are executed through the macro on each image of the image sequence. The image sequence consists of the set of images of deformed knitted fabric captured once every second:

1. Open of the image, of the image sequence respectively.
2. The change of the contrast of the color image – recommended is exponential transformation.
3. Possible image rotation, if the knitted fabric is not oriented like on Fig. 2.
4. Crop of all images in the sequence on the same size (the reducing of the image size – procedure speeding).
5. Interactive threshold of all images in the sequence at the same time.

6. Binary image cleaning by the optional structural element with one or more iterations to clear all binary objects except the loop.
7. Dilation of the binary image by octagon structural element, four time.
8. The function of the medial line is applied. It finds the object axis.
9. Object (loop axis).
10. Binary image is overlaid over the color one and single images are exported to the format *.tif for further processing in MatLab.

3.2 Usage of the programming language MatLab

Each image of previous sequence of image analysis NIS Elements are processed separately as follows:

1. Image segmentation first, when the threshold is determined according to the method of Otsu own MatLab [32].
2. Set the basic parameters of the loop, see Fig. 3. Unfortunately not yet be utilized commonly used basic Dalidovic loop description [33] because of missing information on interlacing with other loops.

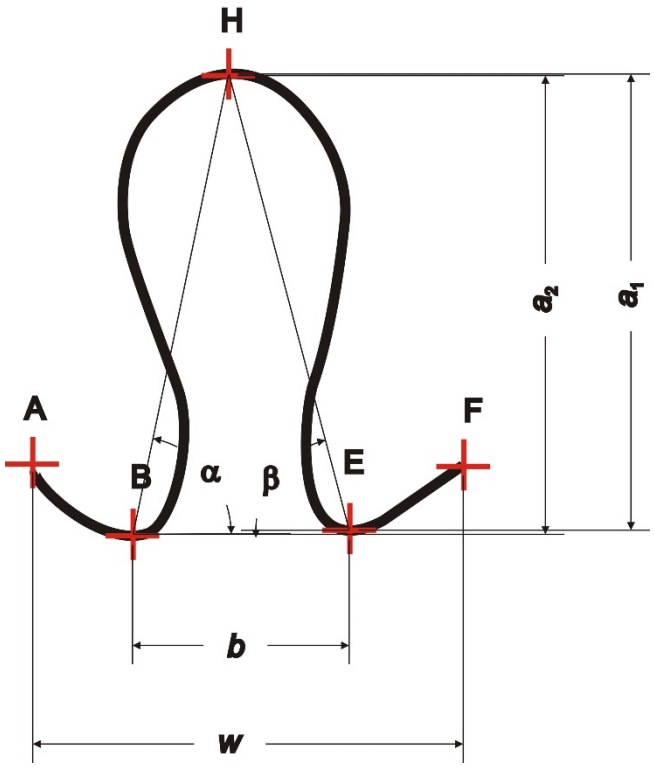

Fig.
Figure 3. The shape of the loops with marked parameters measured

First are found points A, B, H, E, F according to the criteria:

A ... the point with the smallest x-coordinate of the existing points of the loop
H ... point with the biggest y-coordinate from existing points of the loop (if found more such points the middle is determined as the point H)
F ... point with the biggest x-coordinate of the existing points of the loop
B ... point with minimum y-coordinate of the left of the point x-coordinate of the point H
E ... point with minimum y-coordinate of the right of point x-coordinate of the point H

Then follows the calculation of the loop actual parameter:

$$a_1 = y_H - y_E \quad (1a)$$

$$a_2 = y_H - y_B \quad (1b)$$

$$w = x_F - x_A$$

$$b = x_E - x_B$$

Because of the possibility of $y_B \neq y_E$ the parameter *a* is counted both ways (see equations (1a), (1b) for the a_1 and a_2 above) and calculated the angle γ, which, if previous equality y-coordinate equal to 0:

$$\gamma = \arctan \frac{y_E - y_B}{x_E - x_B}, \quad (2)$$

then the following angles α and β are expressed by:

$$\alpha = \arctan \frac{y_H - y_E}{x_H - x_B} \quad (3)$$

$$\beta = \arctan \frac{y_H - y_E}{x_H - x_E}$$

3. Furthermore, the loop is vertically bisected by the x-coordinate of the point H and rotated by 90 °, see Fig. 3. The resulting upper and lower half of the loop is separately interspersed with a polynomial function of third degree together with 95% confidence intervals (Fig. 4 - red curve - less accurate polynomial).
4. Next, the data are excluded from those that have the same x-coordinate and fit process of a polynomial function of the third degree with 95% confidence intervals is repeated (Fig. 4 - black curve - more accurate polynomial).

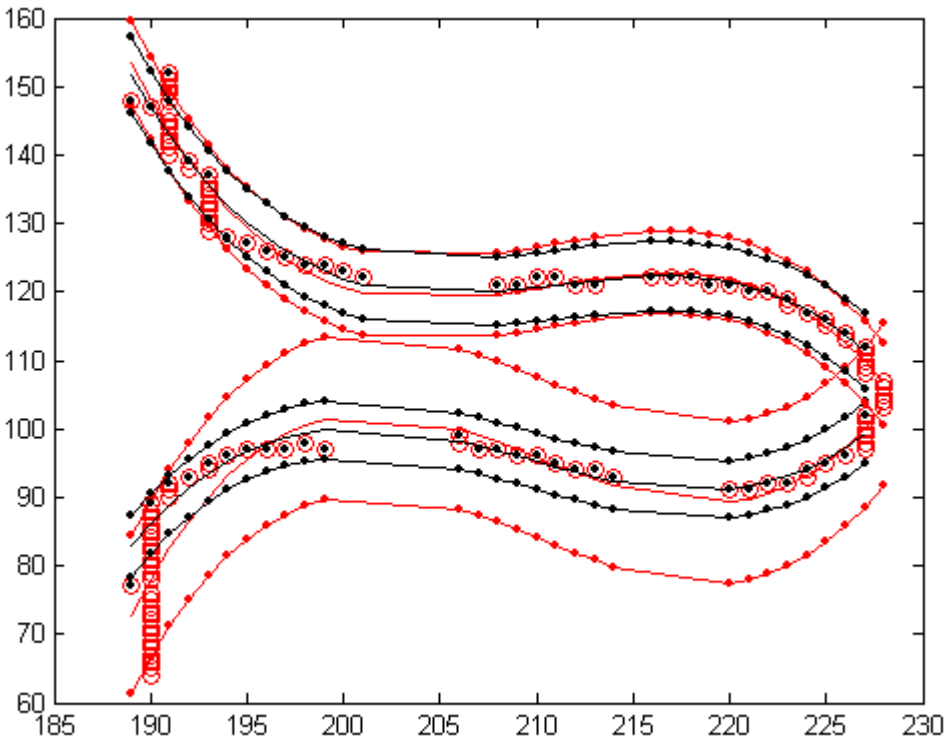

Figure 4. The fit of loop points with two (resp. four) polynomial function of third degree + indicated 95% confidence intervals

5. The inflection points are calculated for all four of the polynomial functions.
6. Searched for x-coordinates 90 ° rotated halves of the loop ≥ x-coordinate of the inflection points for every polynomial function separately of course.
7. The respective parts of the polynomial function are again rotated to its original position and according to the following relationship (4) (see Fig. 5) approximate circle radius *r* is calculated [34]. This corresponds to the shape of the head of the loop (again for both options fit round points). Consequently, the curvature of the head of the loop as the inverse of radius *r* is calculated:

$$D = x_2 - x_1$$
$$L = y_H - y_{1,2} \qquad (4)$$
$$r = \frac{\left(\frac{L}{2}\right)^2 + D^2}{2D}$$

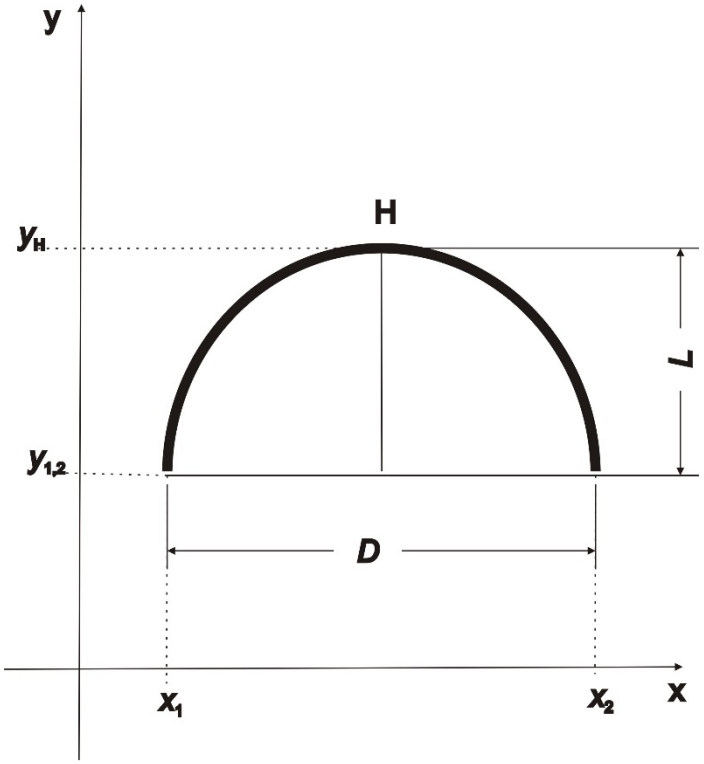

Figure 5. Schematic representation of a distances L, D to calculate the radius of the circle r[1]

4. Outputs and Discussion

NiTi jersey weft knitted fabric was cyclically loaded in the direction of columns, see Fig. 1, chap. 2. One marked loop was observed, see Fig. 2. The following graphic reports show the change in the basic parameters of the loop during cyclic loading of the knitted NiTi in the direction of the columns.

Changes of parameters a_1 and a_2 (see Fig. 3) practically correspond to deformation of knitting in the direction of columns, therefore, are shown depending on the other parameters just to them. Proof of this is Fig. 8, on which, inter alia, to see the dependence of a_1, respectively a_2 on the number of the image with observed loop. Relevant dependencies are linear with breakthrough curve, which indicates the second (return) half-cycle distortion.

[1] The bigger y-coordinate of the point of inflexion is set like smaller y-coordinate of the second point of inflexion.

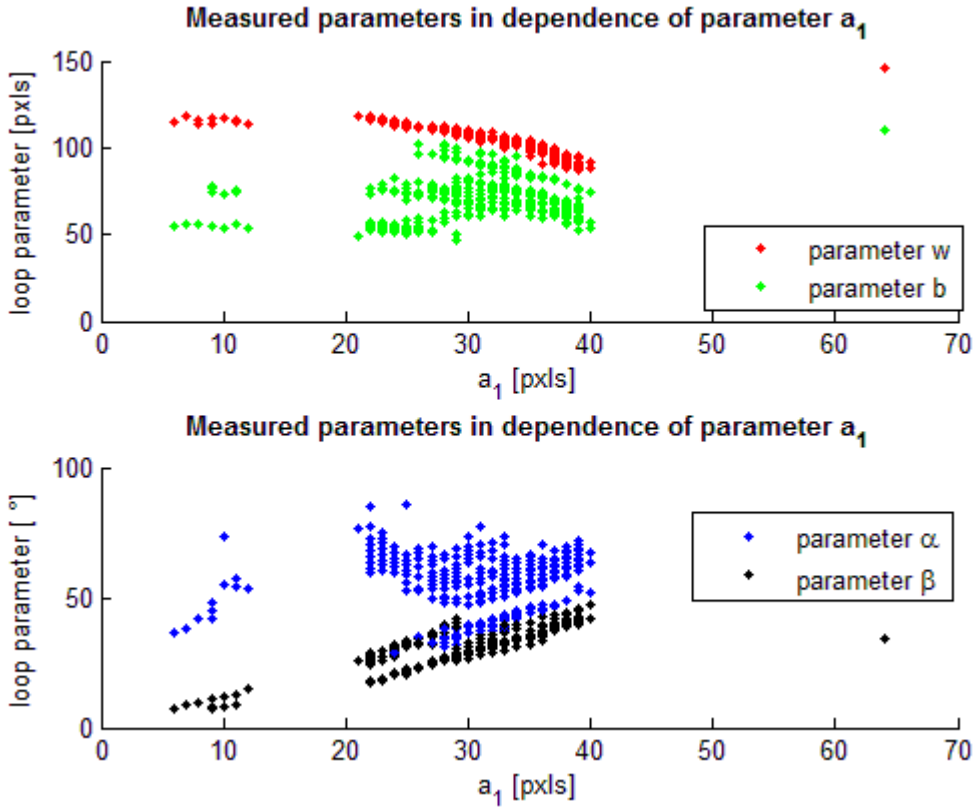

Figure 6. Measured parameters in dependence of parameter a_1

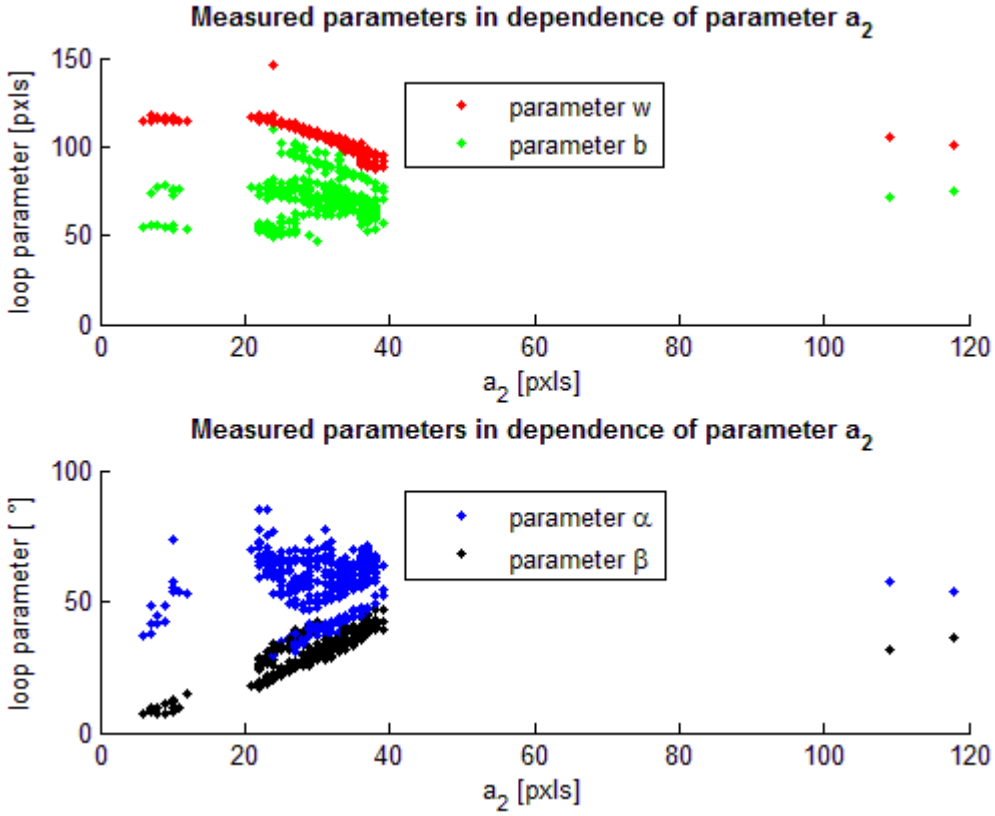

Figure 7. Measured parameters in dependence of parameter a_2

Graphical representation of dependencies of parameters of the loop clearly illustrates the narrowing of the loop and at the same time enlarging the inclination angle of the walls of the loop, Figs. 6 and 7. The effect of cyclic stress is unfortunately not legible on the graphs in Figs. 6, 7. It is a superelastic material, where the values of the loop parameters return to the same position as at the beginning of the test.

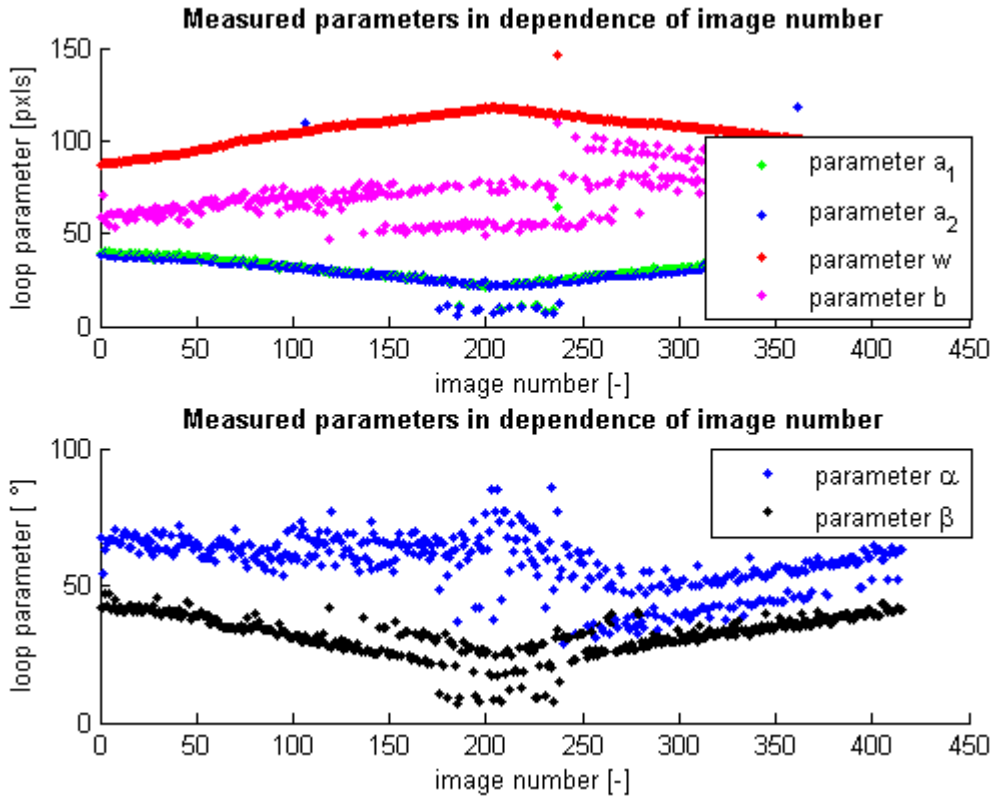

Figure 8. Measured parameters in dependence of image number

Hysteresis during cyclic loading is clearly evident from Fig. 8. It is the image numbers of about 200 to 250, where the values of the parameters are substantially constant.

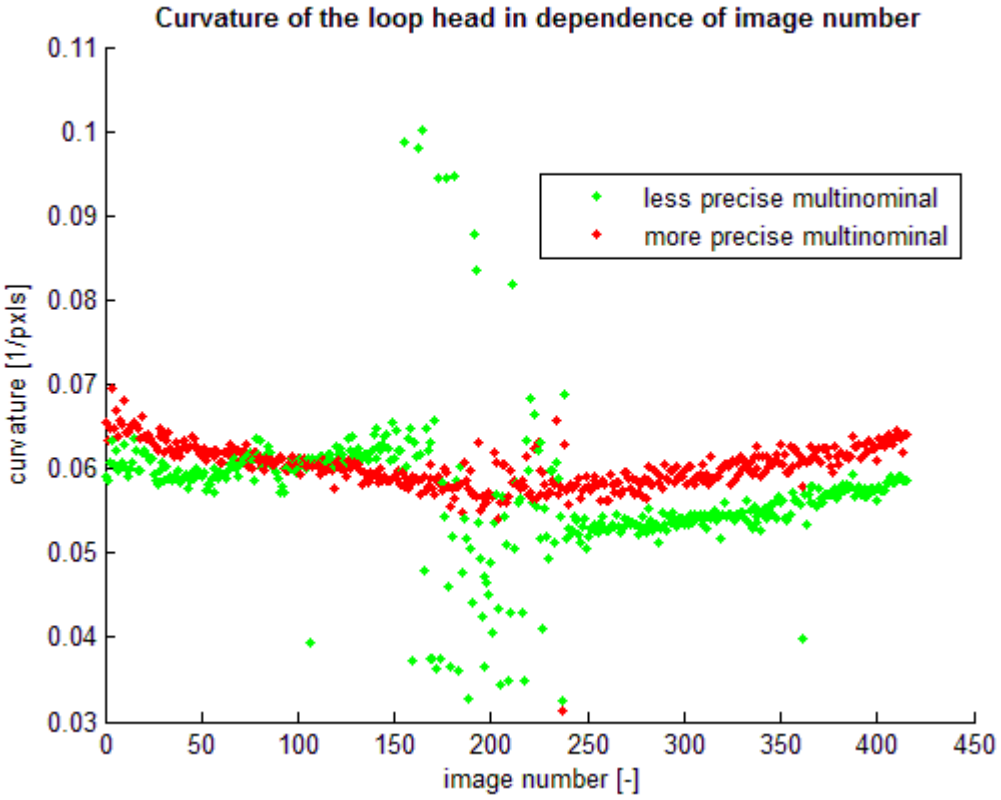

Figure 9. Curvature of the loop head in dependence of image number

The final endpoint was the change of curvature of the head of the loop again depending on the applied deformation. Both methods of the fitting by polynomial functions show a similar results, no significant difference in the change of radius of curvature due to deformation of the knitting in the direction of columns. This fact is most likely due to high stiffness of NiTi wire bending, which prevents deformation of the head of the loop. At the same time Fig. 9 shows areas of the NiTi material hysteresis between the numbers of images 200-250, where values of curvature suddenly show higher values of dispersion identically to the previous parameters on the previous graphs, Figs. 6 to 8.

5. Conclusion

The presented article provides an overview of existing geometrical and physical models of the loop of jersey knitted fabric. Infinitely then followed by the actual parameters defining loop and original image processing of marked loop in the image analysis. It is presented the possibility of fitting of the loop shape by the polynomial functions and define the curvature of the head of the loop. The final outcome of this work there are dependences of the loop parameter changes on the knitting deformation in the direction of the columns. Specific knitted fabric monitored in the work is made of special NiTi material, which is characterized by the superelastic properties. Superelastic properties of NiTi wire are also reflected in the parameters of the loop of knitting, which proves the correctness of the approach to image processing of the loop and a description of its parameters.

References

1. *Doyle, P. J.: Fundamental Aspects of the Design of Knitted Fabrics, J. Textile Inst., 44, 561, 1953*
2. *Munden, D. I.: Geometry and Dimensional Properties of Plain Knit Fabrics, J. Text. Inst., 50, T448, 1959*
3. *Knapton, J. J. F., Ahrens, F. J., Ingenthorn, W. W. and Fong, W.: The Dimensional Properties of Knitted Wool Fabrics Part I: The Plain Knitted Structure, Textile Res. J., 38, 999, 1968*

4. *Knapton, J. J. F., Ahrens, F. J., Ingenthorn, W. W. and Fong, W.: The Dimensional Properties of Knitted Wool Fabrics Part II: 1x1, 2x2 Rib and Half Cardigan Structures, Textile Res. J., 38, 1013, 1968*
5. *Kurbak, A.: Relaxation Lines for Weft Knits, Tekstil ve Makine, 2(9), 125-132, 1988*
6. *Kurbak, A.: Plain Knitted Fabric Dimensions (Part I), Textile Asia, March, 34-36, 41-44, 1998*
7. *Chamberlain, J.: Hosiery Yarn and Fabrics, Vol. II, Leicester College of Technology and Commerce, Leicester, 1926*
8. *Peirce, F. T.: Geometrical Principles Applicable to the Design of Functional Fabrics, Textile Res. J., 17, 123, 1947*
9. *Leaf, G. A. V., Glaskin, A.: Geometry of a Plain Knitted Loop, J. Textile Inst., 46, T587, 1955*
10. *Leaf, G. A. V.: Models of the Plain Knitted Loop, J. Textile Inst., 51, T49, 1960*
11. *Munden, D. L.: The Geometry of Knitted Fabric in its Relaxed Condition, Hosiery Times, April, 43, 1961*
12. *Postle, R.: Structure Shape and Dimensions of Wool Knitted Fabrics, Applied Polymer Symposium, No. 18, John Wiley and Sons, New York, p. 149, 1971*
13. *Kurbak, A,: Some Investigations on the Geometric Properties of Plain Knitted Fabrics, Tekstil ve Makine, 2(11), 238, 1988*
14. *Kurbak, A.: Plain Knitted Fabric Dimensions (Part II), Textile Asia, April, 34-36, 41-44, 1998*
15. *Demiroz, A.: A Study of Graphical Representation of Knitted Structures, PhD Thesis, UMIST, Manchester, 1998*
16. *Loginov, A. U., Grishanov, S. A., Harwood, R. J.: Modelling the Load-Extension Behavior of Plain-knitted Fabric, Part I: A Unit-cell Approach towards Knitted-fabric Mechanics, J. Text. Inst., 93, 218-238, 2002*
17. *Loginov, A. U., Grishanov, S. A., Harwood, R. J.: Modelling the Load-Extension Behavior of Plain-knitted Fabric, Part II: Energy Relationships in the Unit Cell, J. Text. Inst., 93, 239-250, 2002*
18. *Norrie, D. H., Vries, G.: Finite Element Bibliography, Plenum Press, New York, NY, USA, 1976*
19. *Postnov, V. A., Harhurim, I.: The Finite Element Method: Application to Naval Architecture Mechanics, Sudostroenie, Leningrad, USSR, 1974*
20. *Shabrov, N. N.: The Finite Element Method: Application to Heat-engine Mechanics, Machinery Society, Leningrad, USSR, 1983*
21. *Obraszov, L. F., Savelev, L. M., Hazanov, H. S.: The Finite Element Method: Application to Aircraft Mechanics, High School Press, Moscow, USSR, 1986*
22. *Matthews, F. I.: Finite Element Modelling of Composite Materials and Structures, Woodhead, Cambridge, UK, 2000*
23. *Zienkiewicz, O. C., Taylor, R. I.: Finite Element Method, Butterworth-Heinemunn, Oxford, UK, 2000*
24. *Lloyd, D. W.: The Analysis of Complex Fabric Deformations, In Mechanics of Flexiible Fibre Assemblies, Sijthoff and Noordhoff, Alpen aan den Rijn, The Netherlands, pp. 311-342, 1980*
25. *Van Luijk, C. J.: Structural Analysisof Wool Yarns, PhD Thesis, University of Canterbury, New Zealand, 1981*
26. *Van Luijk, C. J., Carr, A. J., Carnaby, G. A.: Finite-element Analysis of Yarns, Parts I and II, J. Text. Inst., 75, 342-353, 354-362, 1984*
27. *Carr, A. J., Moss, P., Carnaby, G. A.: The Tangent Compliance Matrix of Wool Fibre Assemblies, In The Application of Mathematics and Physics in the Wool Industry, Wool Research Organization of New Zealand and The Textile Institute New Zealand Section, Christchurch, New Zealand, pp. 193-203, 1988*
28. *Djaja, R. G., Moss P. P., Carr, A., Carnaby, G. A., Lee, D. H.: Finite Element Modelling of an Oriented Assembly of Continuous Fibres, Text. Res. J., 62, 445-457, 1992*
29. *Munro, W. A., Carnaby, G. A., Carr, A. J., Moss, P. J.: Some Textile Applications of Finite-element Analysis, Part I: Finite Elements for Aligned Fibre Assemblies, J. Text. Inst., 88, 325-338, 1997*
30. *Munro, W. A., Carnaby, G. A., Carr, A. J., Moss, P. J.: Some Textile Applications of Finite-element Analysis, Part II: Finite Elements for Yarn Mechanics, J. Text. Inst., 88, 339-351, 1997*
31. *Heller, L et al.; E-MRS2007, European Physical Journal: Special Topics 158 (1).*

32. *Otsu, N.: "A Threshold Selection Method from Gray-Level Histograms," IEEE Transactions on Systems, Man, and Cybernetics, vol. 9, no. 1, pp. 62-66, 1979*
33. *Kovář, R.: Struktura a vlastnosti plošných textilií, skriptum TUL, Liberec, 2006*
34. *http://cs.wikipedia.org/wiki/Kru%C5%BEnice*

WOVEN FABRIC STRUCTURAL PORE MODELS ANALYSIS

Brigita Kolčavová Sirková, Iva Mertová

Technical University of Liberec, Faculty of Textile Engineering, Department of Textile Technologies, Liberec, Czech Republic brigita.kolcavova@tul.cz, iva.mertova@tul.cz

Abstract:

This paper is focused on description of woven structural pore models and their basic geometrical, forces and deformation ratios in woven structure. Necessary regularities about the balance of variable forces, the transformation of binding element (cell), the achievable densities, stability weaving can be deduced from the description of relationships between the stress and the geometric changes in the binding cell. Study of geometric, strength and deformation ratios in woven fabric are based on definition of the basic binding element in a plain weave. The element of binding point in plain weave is part of the four basic structural pores of woven fabric. Definitions of individual pores is based on the mutual interlacing of two neighbouring threads in the warp and in the weft direction. Dobby as well as jacquard pattern is possible to create by the various combinations of these structural pores in repeat.

Key words:

Structure, pore, models, interlacing, warp, weft, force, deformation

1. Introduction

Woven fabric structure and its mechanical and end-use properties are given by planar and spatial geometry. Based on the geometry, it is possible to analyse the external and internal relations in woven fabric resulting by mutual relations entering thread systems. Planar geometry defines the basic structure of woven fabric, and is determined by the input parameters of the yarn as well as parameters of woven fabrics [1]. Among the priority parameters of the planar geometry we classify material fineness, thread density and weave. Spatial geometry is defined by the internal arrangement of threads in woven fabric relative to axis of the fabric, by force and deformation ratios in the binding element of woven fabrics, the transverse deformation of the threads, etc. Structural change of woven fabric given by mutual interlacing is based on four basic pores - structural pore models: pore type 1 (P1) - full interlacing, pore type 2 (P2) - partial interlacing, pore type 3 (P3) - doubling interlacing and pore type 4 (P4) - full float. Definitions of individual pores is based on the mutual interlacing of two neighbouring threads in both the warp and in the weft direction [2]. On the basis of these pores it is possible to create all design solutions for dobby as well as jacquard woven fabrics.

2. Geometrical disposition, forces and deformations in the binding element of woven fabric

The whole process of weaving is the process of creating of binding points. Their dimensions and the tension gradually changes from the cloth fell in the forming zone as far as some place of the steady state inside of fabric. The structure of the formed fabric is determined by a) the quantity of weft, which is inserted into the binding point, b) tension which is formed in weft during insertion, c) the tension of warp [3].
Study of geometric, strength and deformation ratio in the fabric is based on description of the basic binding element in a plain weave. Plain interlacing is formed only mutual crossing of warp and weft

threads, thereby is limiting structure of woven fabric. All other weaves are looser weaves with specific float part. Float part is non-interlacing length of threads, where the position of float is given by the effect of woven fabric (warp and weft effect). Study of basic element of the plain weave can be used for clarification and explanation of action during weaving and forming of woven fabric. During weaving, the warp threads are under tension Q (we can analyse the tensile strength So in centreline of warp threads) and weft threads under tension U (we can analyse the tensile strength Su in centreline of weft threads) and waviness ratio of warp and weft systems is given by the ratio of these two forces [3].

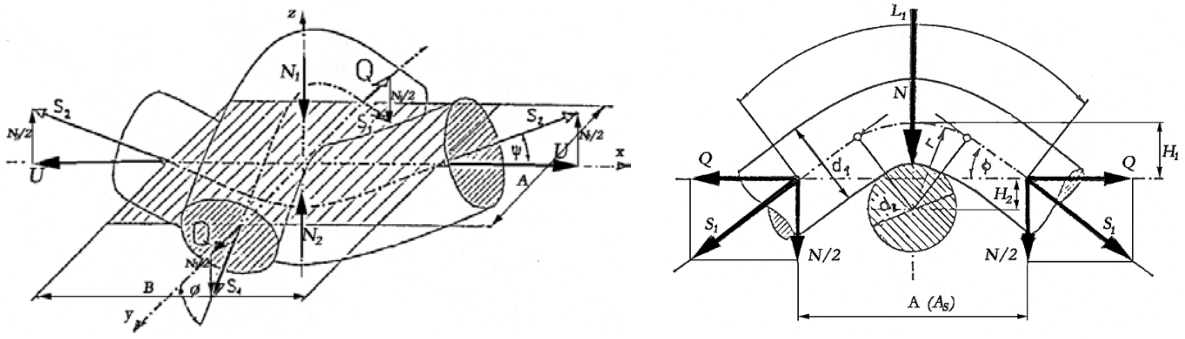

Figure 1. Geometrical and forces ratios in binding element of woven fabric

Basic element of binding point in woven fabric will be evaluated in the steady state, which is assumed symmetrical steady element, see FIG. 1, apart from the forming zone (on the fell of woven fabric), where the binding point is asymmetrical in the warp direction. For simplicity, the evaluated element of binding point, due to the shape of the input yarn, based on the circular cross section.

$$GE = \begin{bmatrix} d_s = \dfrac{d_1 + d_2}{2} \\ A = \dfrac{1}{D_1} \\ B = \dfrac{1}{D_2} \\ H_1 = e_1 . d_s \\ H_2 = e_2 . d_s \\ e_2 = 1 - e_1 \\ \varphi = arctg\left(\dfrac{dy}{dx}\right) \\ \psi = arctg\left(\dfrac{dy}{dx}\right) \end{bmatrix} \begin{pmatrix} d_s = mean\ diameter\ of\ thread;\ d_1 = diameter\ of\ end \\ d_2 = diameter\ of\ pick \\ A = distance\ of\ ends;\quad D_1 = density\ of\ ends \\ B = distance\ of\ picks;\ D_1 = density\ of\ picks \\ H_1 = height\ of\ binding\ wave\ of\ warp;\ e_1 = warp\ waviness \\ H_2 = height\ of\ binding\ wave\ of\ weft;\ e_2 = weft\ waviness \\ \varphi = angle\ of\ ends\ interlacing\ is\ given\ by\ shape\ of\ binding\ wave \\ \psi = angle\ of\ picks\ interlacing\ is\ given\ by\ shape\ of\ binding\ wave \end{pmatrix} \quad (1)$$

Geometric ratios (*GE*) in woven fabric are determined by the areas of one interlacing point, its dimension is given by distances *AxB*. Warp and weft are in binding point defined by waviness having a height of binding wave $H_{1,2}$ by the shape of the binding wave as well as the resulting rake angle of binding waves, see Fig. 1. Individual parameters of geometric ratios are possible to write as vector of geometric parameters *GE*, see equations (1).

Force ratios (*FO*) are described by force equations for a given geometrical ratios of binding point, see Fig.1. Ratios in threads interlacing of woven fabric are determined by tension *Q* in the plane of warp treads, and the tensile force S_2 in the centreline of the weft thread. From the tension of warp thread interlacing *Q* and interlacing angle φ, which is known from the vector of structures can be calculated tensile force in the centreline of the warp threads S_1 and the normal force N_1 warp to weft. From the reaction of weft (where is valid $N_2 = -N_1$) can be expressed tensile force in the weft S_2.

$$FO = \begin{bmatrix} Q \\ S_1 = \dfrac{Q}{\cos\varphi} \\ S_2 = \dfrac{U}{\cos\psi} \\ N_1 = 2.Q.tg\varphi \\ N_1 = -N_2 \\ U = \dfrac{N_2}{2.tg\psi} \end{bmatrix} \begin{pmatrix} Q = \text{force (tensile stress) in warp threads} \\ S_1 = \text{final force in end on interface of binding elements} \\ S_2 = \text{final force in pick on interface of binding elements} \\ N_1 = \text{the normal force of warp thread} \\ N_2 = \text{the normal force of weft thread} \\ U = \text{force (tensile stress) in weft direction} \end{pmatrix} \quad (2)$$

$$DF = \begin{bmatrix} L_1 = \int_0^{T_1} \sqrt{1 + \left(\dfrac{dy}{dx}\right)^2}\, dx \\ L_1 = A + l\Delta_1 + \Delta l_1 \\ l_1 = A + l\Delta_1 \\ L_2 = \int_0^{T_2} \sqrt{1 + \left(\dfrac{dy}{dx}\right)^2}\, dx \\ L2 = B + l\Delta_2 + \Delta l_2 \\ l_2 = B + l\Delta_2 \\ \Delta l_1 = L_1 - l_1 \text{(respectively)} \\ \Delta l_1 = \dfrac{S_1}{E_1.F_1}.l_1 \\ \Delta l_2 = L_2 - l_2 \text{(respectively)} \\ \Delta l_2 = \dfrac{S_2}{E_2.F_2}.l_2 \\ \varepsilon_1 = \dfrac{\Delta l_1}{l_1} \\ \varepsilon_2 = \dfrac{\Delta l_2}{l_2} \\ S_1 = E_1.F_1.\varepsilon_1 \\ S_2 = E_2.F_2.\varepsilon_2 \end{bmatrix} \begin{pmatrix} L_1 = \text{lenght of warp thread in binding wave with elongation of end } \Delta l_1 \\ l_1 = \text{inserted length of pick during weft insertion with over supply of weft } l\Delta_1 \\ L2 = \text{lenght of weft thread in binding wave with elongation of end } \Delta l_2 \\ l_2 = \text{inserted length of pick during weft insertion with over supply of weft } l\Delta\Delta \\ \Delta l_1 = \text{elongation of end,} \\ E_1.F_1 = \text{rigidity of warp thread in tension where} \\ E_1 = \text{Young' s modulus of thread,} \\ F_1 = \text{cross - section thread} \\ \Delta l_2 = \text{elongation of pick,} \\ E_2.F_2 = \text{rigidity of weft thread in tension where} \\ E_2 = \text{Young' s modulus of thread,} \\ F_2 = \text{cross - section of thread} \\ \varepsilon_1 = \text{elongation of end after interlacing of threads} \\ \varepsilon_2 = \text{elongation of pick after interlacing of threads} \\ S_1 = \text{final force in end on interface of binding elements} \\ S_2 = \text{final force in pick on interface of binding elements} \end{pmatrix} \quad (3)$$

From the force S_2 and the known angle ψ can be expressed tensile force in the direction of the temples U. At the same, can be expressed from tensile force S_2 elongation of the weft ε_2 in the binding element. Based ε_2 and extension of the length of the thread L_2 in binding wave may be expressed crimp of threads, which means expressing consumption of weft converted to un-tensioned state [3]. Force ratios is given by vector or forces parameters in structure of woven fabric, see equations (2).

Deformation - Force ratios (*DF*) based on the fundamental relation between the tensile force on the border of the binding element and the arising extension of the thread, see Figure 1. Deformation - Force ratios is given by vector of deformation parameters in structure of woven fabric, see equations (3).

3. Definition and analysis of structural pore models of woven fabric interlacing

The method of mutual interlacing of the two sets of threads in woven fabric gives the weave. The correct choice of weave in woven fabric is important not only for the construction of the fabric, but it adds additional necessary mechanical and end-use properties (strength, elongation, permeability, roughness, feel, flexibility, etc.). Weave in woven fabric are usually illustrates by patterns, which show the fabric design and way of interlacing. Patterns are usually drawn on squared paper as a sequence of dark and light pixels (show the position of the warp threads relative to the median plane of the fabric) [4]. Structural change in woven fabric formed by weave is based on definition of four basic pores - structural models in the weave repeat. In terms of structural pores are distinguished: Pore type 1 - full interlacing, Pore Type 2 - partial interlacing, Pore type 3 - doubling and Pore Type 4 - full float.

In the description of the planar geometry of woven fabric weave, besides writing of weave in pattern paper, it is possible to use a weave pattern depiction based on the matrix of structural pore models. The size of the matrix is based on the size of the pattern repeat. The number of warp threads in a pattern repeat no determines the number of rows and the number of weft threads nu number of columns. Definitions of individual pores is based on mutual interlacing of two neighbouring threads in the warp direction and in the weft direction. On the basis of these pores it is possible to create all structural binding solutions as dobby so jacquard fabrics. Repeat of dobby weave, jacquard repeat of the pattern is based on the distribution of the individual pores in the area of pattern. The relative frequency of each RP1-4 pores in the area of the pattern (weave repeat) influences the behaviour of woven fabric during weaving as well as the resulting end-use and mechanical properties.

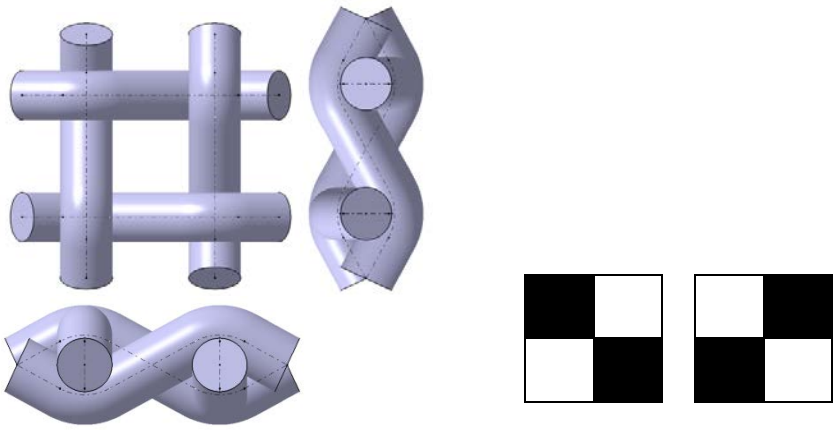

Figure 2. Woven fabric structural pore model “type 1 (P1)“ – full interlacing pore
Spatial structure of pore model “type 1” (left side), positive and negative areal depiction of pore model “type 1” (right side)

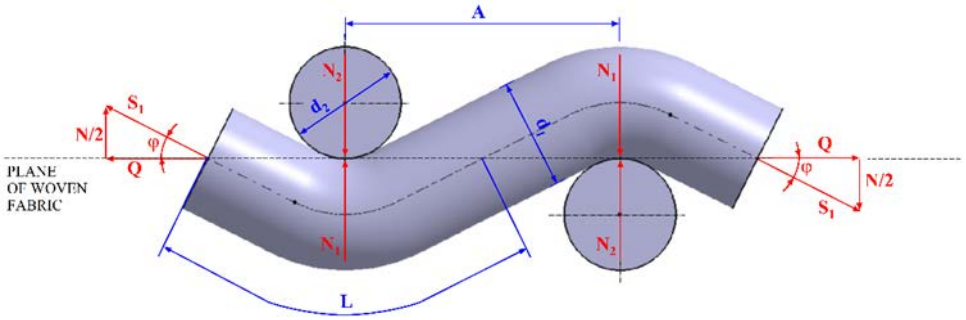

Figure 3. Geometrical and forces depiction of woven fabric structural pore model P1, (definition is identical for longitudinal and transversal cross section of woven fabric)

Definition of woven fabric structure of the binding element of structural pores in terms of geometric, strength and deformation ratios is identical with the abovementioned general relationships defined for the binding element in a steady state, see equation fabric structures (1-3). Expressing the relative frequency of each structural pores in the pattern repeat is given by equations (4).

$$RP1 = \frac{\sum P1}{n_o.n_u} \qquad RP2 = \frac{\sum P2}{n_o.n_u} \qquad RP3 = \frac{\sum P3}{n_o.n_u} \qquad RP4 = \frac{\sum P4}{n_o.n_u} \tag{4}$$

Full interlacing structural pore model is illustrated in Figure 2-3. It is only one pore which is given by crossing point only. The final length of binding weave is higher the input length of inserts threads. The final forces in threads we obtain for each threads in repeat. Full interlacing pore has maximal compactness of fabric. Plain weave is created only with this pore.

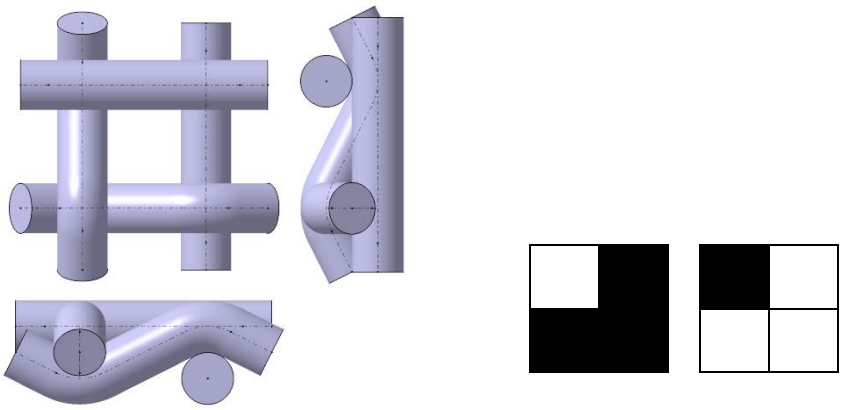

Figure 4. Woven fabric structural pore model "type 2 (P2)" – partial interlacing pore
Spatial structure of pore model "type 2" (left side), positive and negative areal depiction of pore model "type 2" (right side)

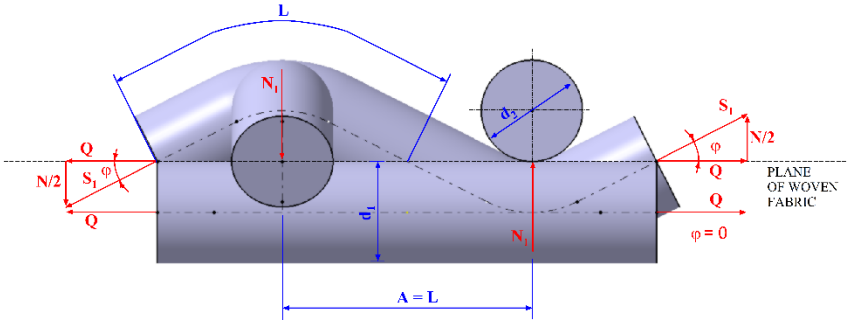

Figure 5. Geometrical and forces depiction of woven fabric structural pore model P2, (definition is identical for longitudinal and transversal cross section of woven fabric)

Partial interlacing structural pore model is described in Figure 4-5. One threads in same cross section is created by interlacing of threads and one in the same direction is full float. Woven fabric structure compactness is increasing in comparison with pore 3, 4. Forces and deformations vector is possible to write identical for both cross section of woven fabric (only with definition for weft, warp). This pore in woven fabric structure is possible to use only with combination with the others pores.

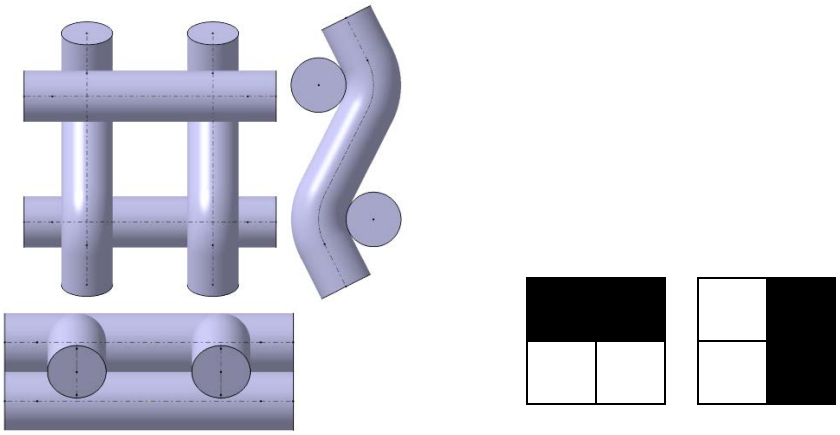

Figure 6. Woven fabric structural pore model "type 3" – double effect pore
Spatial structure of pore model "type 3" (left side), positive and negative areal depiction of pore model "type 3" (right side)

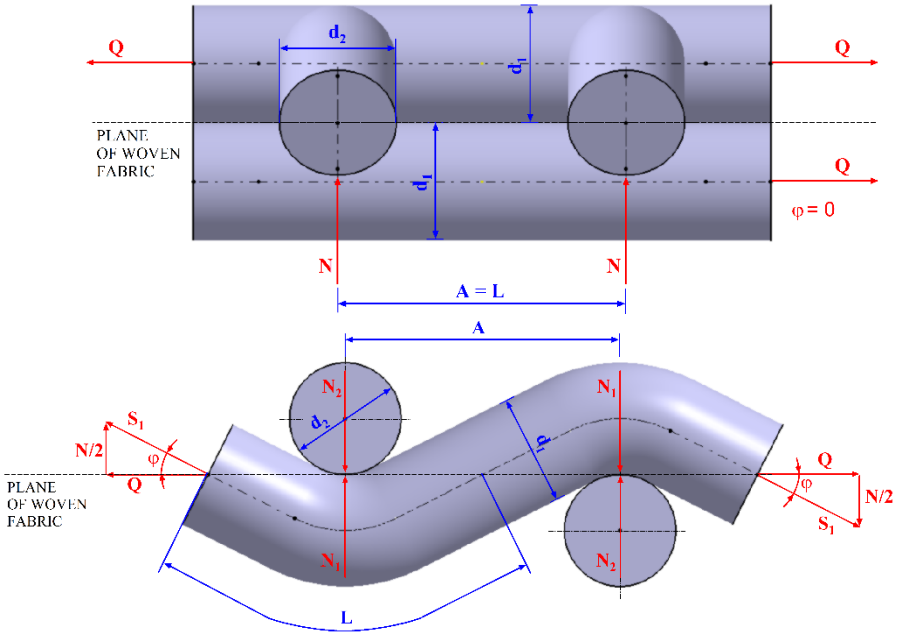

Figure 7. Geometrical and forces depiction of woven fabric structural pore model P2

Double effect structural pore model is described in Figure 6-7. Woven fabric structure has the compactness in one direction only. The other direction is given by interlacing of threads. The forces reaction is possible to see in the Figure 7. First figure illustrates one direction of cross section of woven fabric a second figure illustrates the other direction of cross section of woven fabric. Final force in threads is created only in second case. This pore in woven fabric structure is possible to use only with combination with the others pores.

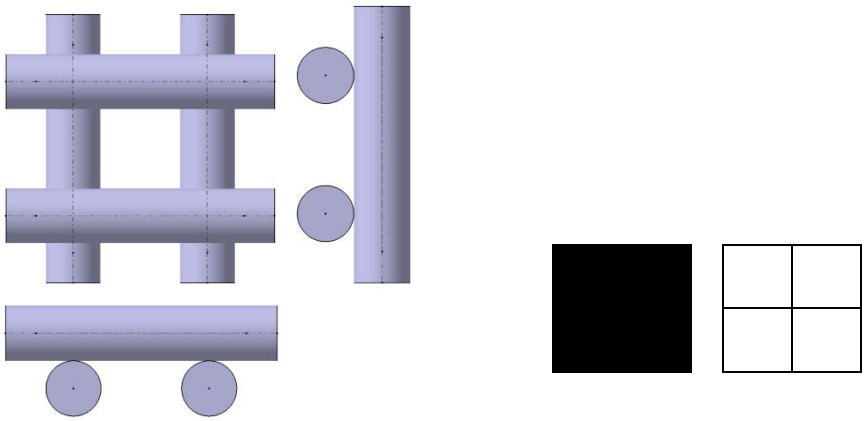

Figure 8. Woven fabric structural pore model "type 2 (P2)" – partial interlacing pore
Spatial structure of pore model "type 2" (left side), positive and negative areal depiction of pore model "type 2" (right side)

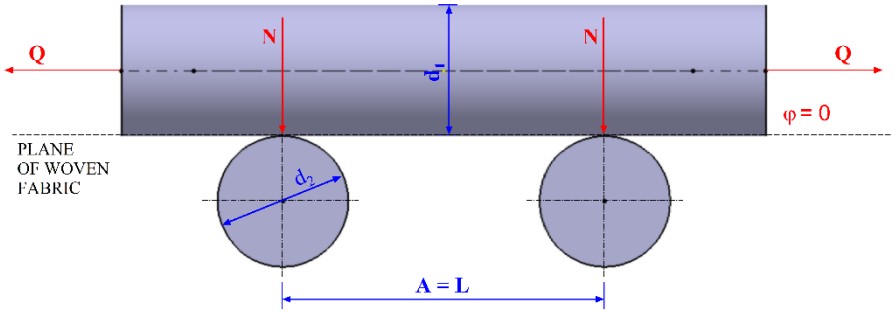

Figure 9. Geometrical and forces depiction of woven fabric structural pore model P1, (definition is identical for longitudinal and transversal cross section of woven fabric)

Full float structural pore model is described in Figure 8-9. It is only one pore where we do not have interlacing of threads. Woven fabric structure has not compactness. On the basis of forces vectors view point the compactness is given by angel of interlacing and input tension of warp threads Q. On the basis these parameters create the final force in thread. This pore in woven fabric structure is possible to use only with combination with the others pores. When the weave repeat is increasing then is increasing the number of pore 4.

4. Evaluation of the impact of structural pore models on warp and weft crimp

By mutual interlacing of warp and weft threads arises waviness of threads. Subsequently, threads have a greater length of yarn than the threads dimension of the final fabric in the appropriate direction. This difference in length of yarn is expressing the threads crimp. The thread crimp is expressed in a percentage from the dimension of the fabric. The length of yarn in cross section is given of position of yarn in interlacing. Pore 1, full interlacing pore, has maximal length of yarn in repeat which is possible to create in weave. Pore 4, full float pore, it is opposite pore with minimal length of yarn in repeat.

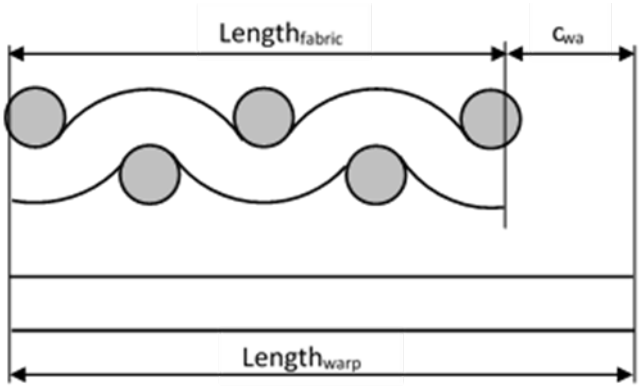

Figure 10. Depiction of threads interlacing - expression of thread crimp

Warp crimp c_{wa} and weft crimp c_{we} is given by equation (5):

$$c_{wa} = \frac{Length_{warp} - Length_{fabric}}{Length_{fabric}}.10^2 \;,\; c_{we} = \frac{Length_{weft} - Width_{fabric}}{Width_{fabric}}.10^2 \qquad (5)$$

Basic parameters of woven fabric structure and weaving process with influence on crimp threads in the fabric are: input parameters of yarn (yarn fineness), mutual interlacing of threads, weave – distribution of structural pores in repeat, the relative frequency of each RP1-4 pores in the area of the pattern, sett threads in fabric, thread waviness in the fabric, tension of warp, etc.

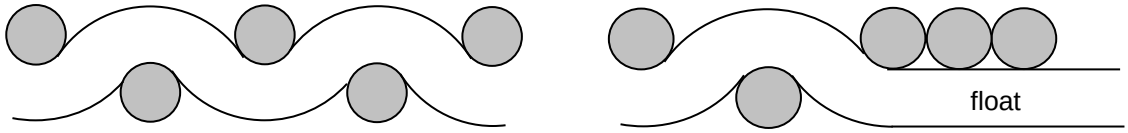

Figure 11. Influence of weave on warp and weft crimp
Depiction of plain weave (max crimp of weave) (left side), depiction of looser float weave (float = min crimp) (right side)

Parameters of experimental polyester samples for evoluation of structural pore models influence on warp and weft crimp are given in Table 1. Spatial structure of individual samples weaves and areal depiction of weaves with pores definition in area are demonstrated by Figure 12-14.

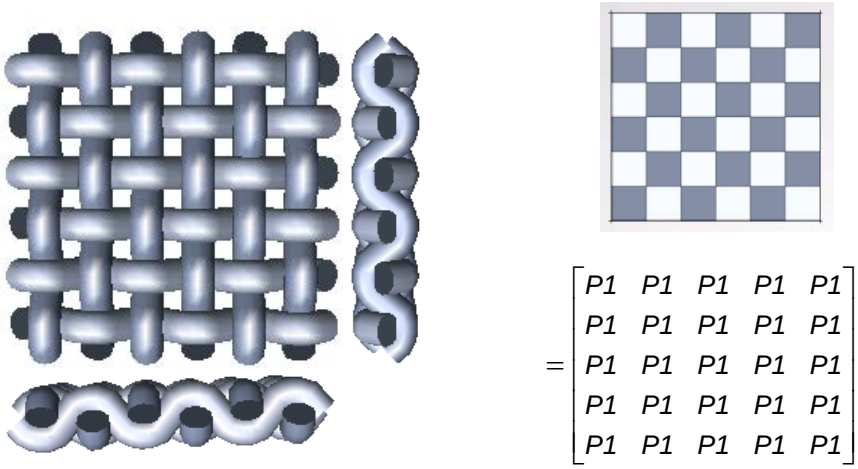

$$= \begin{bmatrix} P1 & P1 & P1 & P1 & P1 \\ P1 & P1 & P1 & P1 & P1 \\ P1 & P1 & P1 & P1 & P1 \\ P1 & P1 & P1 & P1 & P1 \\ P1 & P1 & P1 & P1 & P1 \end{bmatrix}$$

Figure 12. Analysis of structural pore models in plain weave
Spatial structure of plain weave (left side), areal depiction of plain weave with pores definition in area (right side)

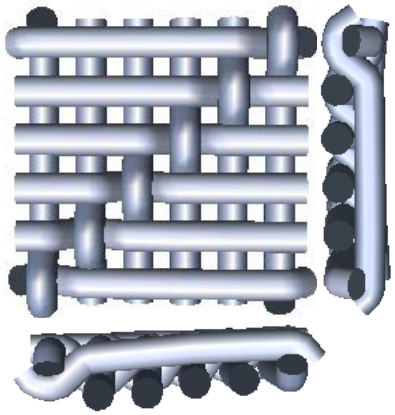

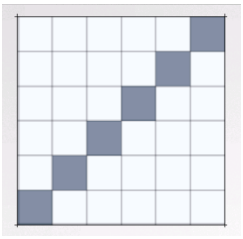

$$= \begin{bmatrix} P2 & P4 & P4 & P2 & P1 \\ P4 & P4 & P2 & P1 & P2 \\ P4 & P2 & P1 & P2 & P4 \\ P2 & P1 & P2 & P4 & P4 \\ P1 & P2 & P4 & P4 & P2 \end{bmatrix}$$

Figure 13. Analysis of structural pore models in twill weave
Spatial structure of plain weave (left side), areal structure of plain weave with pores definition in area (right side)

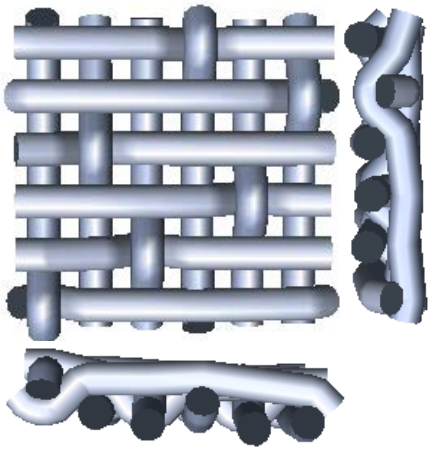

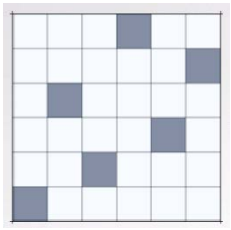

$$= \begin{bmatrix} P2 & P2 & P4 & P2 & P2 \\ P2 & P4 & P2 & P2 & P2 \\ P4 & P2 & P2 & P2 & P2 \\ P2 & P2 & P2 & P2 & P4 \\ P2 & P2 & P2 & P4 & P2 \end{bmatrix}$$

Figure 14. Analysis of structural pore models in satin weave
Spatial structure of plain weave (left side), areal structure of plain weave with pores definition in area (right side), weave was created in CAD system EAT at FT TUL

Table 1 Basic parameters of experimental woven fabric samples

Fabric number	Woven fabric weave	Yarn count [tex]		Thread sett[1/cm]	
		warp	weft	warp	weft
1	Plain weave	25	25	19	19
2	Twill 1/5 Z	25	25	19	19
3	Sateen 1/5	25	25	19	19
4	Plain	25	25	22,4	22,4
5	Twill 1/5 Z	25	25	22,4	22,4
6	Sateen 1/5	25	25	22,4	22,4
7	Plain weave	25	25	26	26
8	Twill 1/5 Z	25	25	26	26
9	Sateen 1/5	25	25	26	26

Table 2 shows the relative frequencies of pores and warp and weft crimp. The number of pores in a pattern repeat of the individual interlacing is shown in Figures 9 to 11. Relative frequency were

calculated according to equation (3). Crimp of threads is shown in Table 2. The resulting values of thread crimp are obtained by evaluation of tensile operating curves of yarn before weaving and yarns removed from the fabric. The experiment is described in detail in [5]. The Table 2 presents only mean values of threads crimp.

In the graph of Figure 15 shows the growing dependence of warp and weft crimp on the relative frequency of the pore type P1. This trend was anticipated. Pore type 1 is a full interlacing pore where the waviness of warp and weft threads is greatest. Conversely, pore type 4 contains only from float sections this is full float pore, see Figure 8. We can therefore assume that number of pore type 4 is increasing then the final threads crimp is decreasing. Also is decreasing the compactness of woven fabrics. The relationship between the threads crimp and the relative frequency of the pores of type 4 can be seen in Figure 16.

Table 2 Relative frequency of pores and yarn crimp

Fabric number	Woven fabric weave	Relative frequency of pores (pore P3=0)			Yarn crimp, %	
		P1	P2	P4	warp	weft
1	Plain 1/1	1,00	0,00	0,00	4,89	6,72
2	Twill 1/5	0,17	0,33	0,50	0,79	3,79
3	Sateen 1/5	0,00	0,67	0,33	1,16	4,30
4	Plain 1/1	1,00	0,00	0,00	5,87	7,13
5	Twill 1/5	0,17	0,33	0,50	1,84	6,75
6	Sateen 1/5	0,00	0,67	0,33	1,35	5,61
7	Plain 1/1	1,00	0,00	0,00	6,00	9,15
8	Twill 1/5	0,17	0,33	0,50	2,81	5,39
9	Sateen 1/5	0,00	0,67	0,33	1,71	5,46

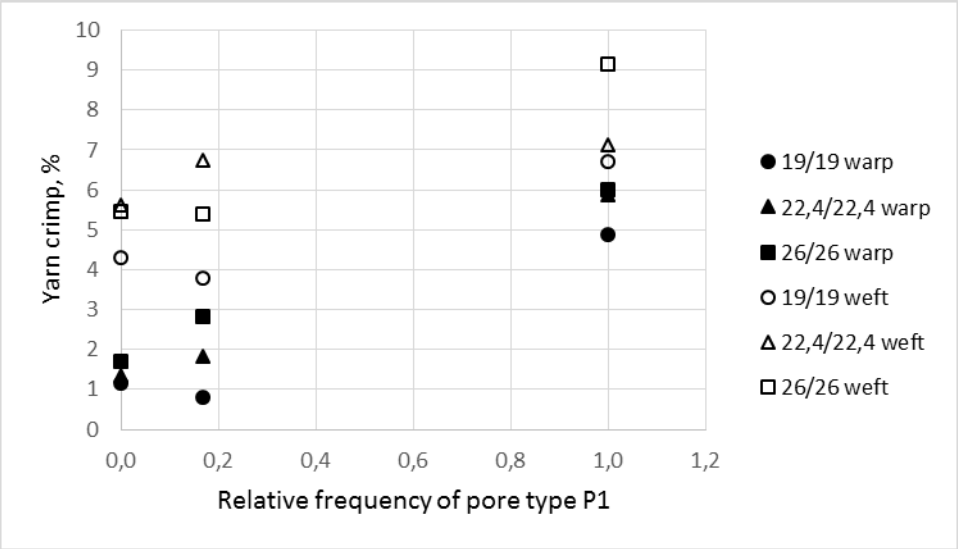

Figure 15. Dependence between yarn crimp and relative frequency of pore type P1

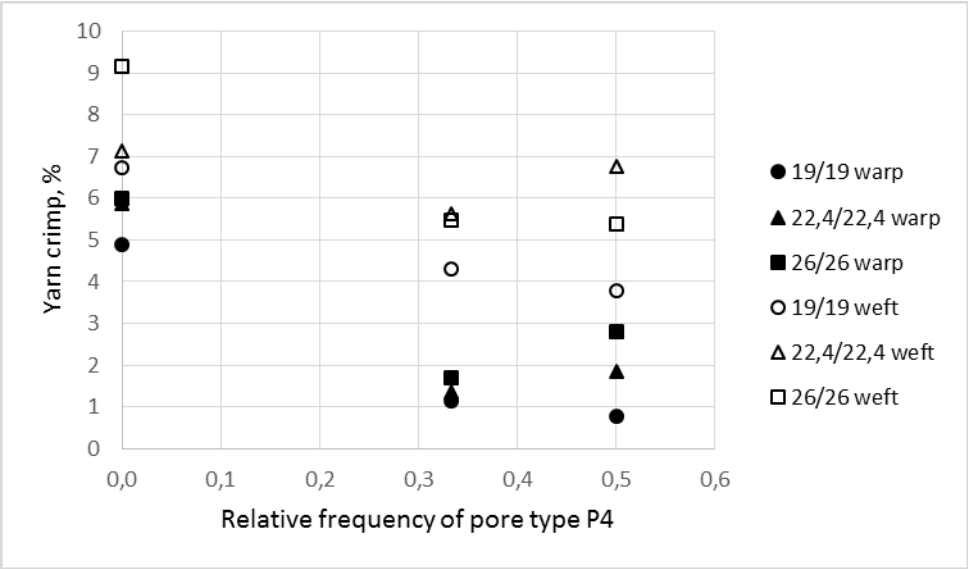

Figure 16. Dependence between yarn crimp and relative frequency of pore type P4

5. CONCLUSIONS

Mutual interlacing of woven structure is given by weave. Is possible to select only four structural pore models for creation of each type of woven fabric design. As is possible to see from above mentioned description of structural, forces and deformation vectors the mutual interlacing and yarn elongation in binding point is given by structural pore type 1. When the number of structural pore model 1 in repeat is increasing then is increasing elongation of the yarn in binding point, final yarn crimp is increasing too). The compactness of woven fabrics is increasing too. If we want to keep the compactness of woven fabric, at reducing the pore 1, it is necessary to increase the thread density. This is a case of float weave. In the repeat of float weave the number of pore 1 is decreasing. The length of yarn in cross section of woven fabric is a sum of individual lengths of yarn parts in individual pores. Theoretically the length of yarn in cross section is increasing on the basic of the shape of binding wave. Theoretical pore models use for calculation and modelling the linear part for substitution of float part. From the Figure 17 is possible to see the construction of woven fabric can influence the final shape as well as the yarn length in binding wave in float part.

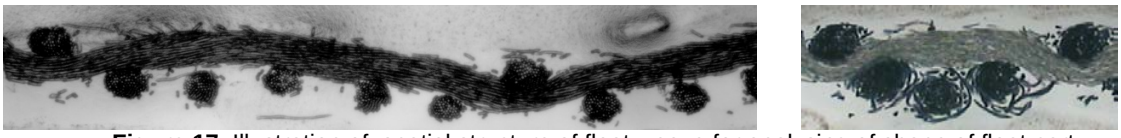

Figure 17. Illustration of spatial structure of float weave for analysing of shape of float part

References

1. *Nosek, S.: The theory of weaving process, part I., Dům techniky ČSVTS, 1988*
2. *Kolcavová Sirková, B., Mertová, I.: Prediction of woven fabric properties using software protkatex, Autex Research Journal, Volume: 13(1), Pages: 11-16, 2013*
3. *Nosek, S.: The structure and geometry of the woven fabrics, Liberec 1996*
4. *Backer, S.: The relationship between the structural geometry of textile fabric and its physical properties, Part IV: Interstice geometry and air permeability, Textile Research Journal 1951, Vol. 17 (10) 703-714*
5. *Mertová, I., Neckář, B., Ishtiaque, S.M.: New method to measure yarn crimp in woven fabric, Textile Research Journal 2016, Vol. 86(10) 1084–1096. [TRJ].*

STRUCTURAL AND THERMAL-MECHANIC PROPERTIES OF FILAMENTS PRODUCED FROM SHAPE MEMORY POLYMERS

Selcuk Aslan, Sibel Kaplan

Suleyman Demirel University, Textile Engineering Dept., Isparta, Turkey
selcukaslan0444@gmail.com

Abstract:

In this study, shape memory polyurethane (SMPU) fiber was spun by wet spinning process and chemical/mechanical characterization was carried out. SMPU solutions were prepared with two different concentrations (20% and 25%) and three different coagulation bath concentrations (0%, 1% and 3%).Influences of solvent and coagulation bath concentrations on mechanical, thermal and shape memory performances of fibers were investigated. For this aim, differential scanning calorimetry (DSC), dynamic mechanical analysis (DMA) and mechanical tests were conducted. DSC and DMA analysis results show that shape memory polyurethane filaments have a glass transition temperature about 35-40°C and solvent concentrations in coagulation bath did not have a remarkable effect on glass transition temperature of filaments. SMPU fibers showed good tensile performance with an average tenacity of 1.74 cN/tex and elongation at break of 1343 %. Thermo mechanical test results showed that, all shape memory filaments have good shape memory effect with recovery and fixity ratios up to 91% and 71% respectively.

Key words:

shape memory polyurethane, wet spinning, characterization, glass transition temperature, shape memory behavior.

1. Introduction

Shape memory polymer (SMP) have gained much popularity because of their special capability to return their original (permanent) shapes from a temporary shape under appropriate external stimulus such as heat, light, pH, moisture etc. [1,2,3,4]. When compared to other shape memory materials, SMPs have been widely studied and used in academic researches and industrial applications owing to its lightweight, good processing ability, high shape recoverability and large range of shape recovery temperature [5,6]. Nowadays, most studies of SMPs focus on thermal induced SMPs because of their wide possible applications in different fields such as textile, engineering and biomedical devices [7,8,9].

Shape memory polyurethanes (SMPU) are the most notable kind of SMPs and they have the advantage of broad switch temperature (glass transition or melting transition) by changing soft segment and hard segment type and contents [3,10]. SMPUs are phase separated due to the thermodynamic incompability between hard and soft segments. Thus, they exhibit remarkable shape memory effect. Various applications of shape memory polymers with different forms such as fiber, yarn, film have been used in textile field. In recent years, many researchers have focused on development of functional fibers and smart textile products with shape memory effects [1, 2, 4, 6, 7, 8, 11, 12 ,13].

In this study, shape memory fibers were spun from SMPUs by wet spinning and their mechanical, thermal and shape memory behaviors were investigated.

2. Experimental

2.1. Materials

Pellet-type MM-3520 SMPU (SMP Technologies Inc. Japan) was used for production of shape memory fibers (SMF). Shape memory polymer solution was prepared with N, N-dimethylformamide (DMF) [1] as solvent and shape memory fibers were spun by wet spinning.

2.1.1. Preparation of SMPU fibers

Shape memory fibers were spun by wet spinning method with DMF as solvent of polymer solutions. After some pre-trials, solid concentrations of the SMPU solution in DMF were adjusted to 20% and 25% to meet the viscosity requirements for wet spinning process. For investigating the effects of solvent concentration of coagulation bath on mechanical and shape memory effect of SMPU fiber, 0%, 1% and 3% concentrations were applied. SMPU solution is extruded through single spinneret capillary hole horizontally through a coagulation bath with arranged concentrations to diffuse out the solvent with a spinning speed of 3.2 m/min. Mono-filament which is formed in coagulation bath are taken up to a second bath including water for removal of residual DMF. Then, the SMPU filament was wound with 90 rpm on a cylindrical bobbin. Totally, six type of SMPU fibers with different parameters were produced (Table 1).

2.2. Methods

Thermal properties of the prepared SMPU filaments were determined using a differential scanning calorimeter (DSC) device with nitrogen as purge gas. First, SMPU sample was cooled to -30^{o}C at the cooling rate 10 ^{o}C/min, then the polymer was heated from -30^{o}C to 240^{o}C at 10 ^{o}C/min heating rate. Pellet type SMPU polymer was also investigated by DSC. The heat flow change with increasing temperature was recorded. The dynamic mechanical properties of the shape memory filaments were determined by using dynamic mechanical analysis (DMA) device at a frequency of 2 Hz. The gauge length for each filament between the clamps was 15 mm and temperature was scanned from -120^{o}C to 200^{o}C with 2^{o}C/min heating rate.

Tensile tests of the SMPU fibers was carried out with a Lloyd Tensile Testing Machine (LR5K) according to ASTM D2236. All tests were conducted under standard atmospheric conditions (20^{o}C and 65RH%).

Table 1. Production details and mechanical characteristics of SMPU filaments

Yarn code	Polymer concentration in solution (%)	Coagulation bath concentration (%)	Linear Density (tex)
SMPU200	20	0	55
SMPU201	20	1	45
SMPU203	20	3	68
SMPU250	25	0	74
SMPU251	25	1	71
SMPU253	25	3	81

The thermo-mechanical cyclic tensile test was conducted to investigate the shape memory behavior of shape memory filaments. Test was performed on Lloyd tensile tester (AMETEK Test&Calibration Instruments, UK) within a temperature controlled chamber. The fiber gauge length was 25,4 mm. Steps of a typical thermo-mechanical cycle test procedure for shape memory filaments are as follows: I) The fiber was initially stretched to 100% elongation ratio at 40^{o}C with a speed of 100 mm/min, which is above the glass transition temperature (switch temperature) of filaments. II) The sample is cooled

down to 22°C and temperature was maintained for 15 minutes to fix temporary elongation. III) The upper clamp was returned to original position and the filament shrank from 100% strain (ε_m) to strain after unloading at 22°C (ε_u) because of instant elastic recovery. IV) Sample was heated to 40 °C again to allow shape memory recovery enabling the filament elongation returning to residual strain (ε_p) [10]. After the cycle was completed, another cycle began and a total of three cycles were carried out in order to investigate the shape memory effect of filaments.

3. Results and Discussion

3.1. Thermal Property Analysis of Shape Memory Filaments

The glass transition temperature of the shape memory polyurethane was determined by using differential scanning calorimetry (DSC) and results are shown in Table 2. Generally, glass transition temperature is determined from the second heating cycle to provide T_g value independent of the thermal history during processing. In the second heating scan, glass transition of soft segment of shape memory polyurethane filaments can be found between the range 36.43-37.37°C. This glass transition is used as the switch temperature to fix the shape of the filament (below and above the thermal transition temperature).

Table 2. DSC analyses results for shape memory samples

Sample code	1. Heating glass transition temp. (T_g)(°C)	1. Heating heat capacitity (ΔC_p)(J/g)	Cooling glass transition temp.(T_g)(°C)	Cooling heat capacity (ΔC_p) (J/g)	2. Heating glass transition temp.(T_g)(°C)	2. Heating heat capacity (ΔC_p)(J/g)
SMPU200	29.26	0.645	35.26	0.395	37.37	0.440
SMPU201	22.10	0.305	33.45	0.433	37.03	0.493
SMPU203	20.97	0.313	34.09	0.396	36.43	0.434
SMPU250	20.80	0.251	35.26	0.287	36.58	0.415
SMPU251	22.24	0.253	34.70	0.415	36.95	0.390
SMPU253	21.79	0.268	32.33	0.444	36.81	0.375
SMPU polymer	26.17	0.297	33.96	0.315	37.69	0.338

3.2. Dynamic Mechanical Analysis of Shape Memory Filaments

The storage modules, loss modules and phase angle results of shape memory filaments are shown in Figure 1 and Figure 2 respectively. Elasticity of shape memory filaments is directly related to density of crosslinks contained in the structure and elasticity properties are reduced with increasing crosslink density. According to storage modulus curves, increasing difference storage modulus between plateau regions obtained on before and after T_g value means a reduction in the amount of crosslinking. In this case, storage modulus of SMPU251 and SMPU250 which are spun with 25% polymer concentration in solution and 1% and 0% concentration of coagulation bath, respectively, has a sharp decrease at 27°C and highest storage modulus were obtained for these filaments. As shown in Figure 1, SMPU251 and SMPU250 have the lowest crosslink density, accordingly, these filaments have been found to have the highest elasticity value.

Loss modulus is related to the hysteresial energy dissipation and it shows mobility of polymer chains. High and wide loss modulus relate with mechanical properties of material such as impact resistance. It means that, material have better mechanical properties with increasing width of loss modulus curve [14]. According to loss modulus curve of shape memory filaments, SMPU250 and SMPU251 which are spun with 25% polymer concentration in solution, 0% and 1% concentration in coagulation bath, respectively, have better loss modulus and consequently mechanical properties.

Moreover, SMPU201 which is spun 20% polymer concentration in solution and 1% concentration in coagulation bath has lowest loss modulus. This result is in harmony with the tensile test results of filaments. Besides, the loss modulus peak locating at 38-40ºC is due to glass transition of soft segment phase. The loss modulus has a sharp decrease at highest temperature than T_g. This means that, filaments can be easily deformed at temperatures above T_g and shape can be fixed at temperature below T_g.

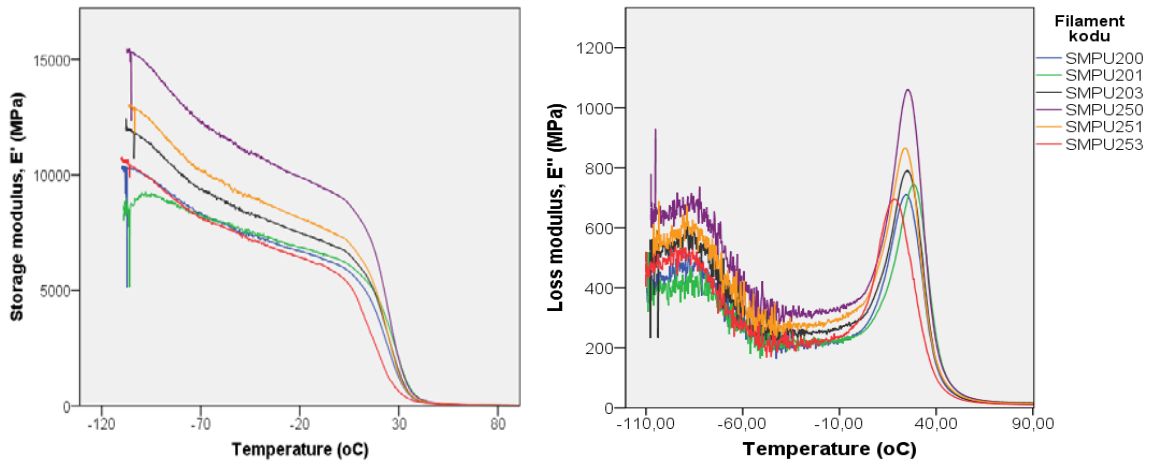

Figure 1. Storage and loss modulus of shape memory filaments

Figure 2 shows that the tanδ peak of the shape memory filaments range between 35.7-40.5 ºC, which is associated with the glass transition temperature of shape memory filaments. It is generally accepted that the transition temperature measured by DMA is slightly higher than that obtained from DSC as the working principles of DSC and DMA are different [12]. Confirming literature there is a difference of 2-3 ºC between glass transition temperatures measured by DSC and DMA. The peak height of Tan(δ) provides information about the mobility of molecule chains of the materials and Tan(δ) peak width give information about homogenity of crosslinking. The mobility of molecular chains in the material structure rises with increasing peak height of Tan(δ). The width of Tan(δ) gives idea about heterogenity of material crosslinking.

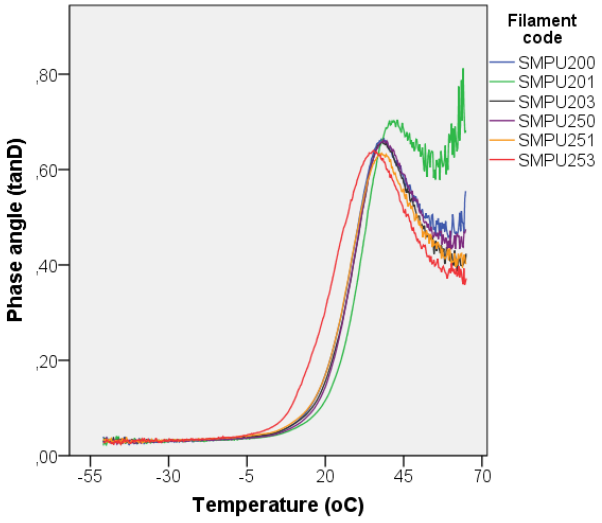

Figure 2. Phase angle curve of shape memory filaments

When phase angle curves (tan δ) of shape memory filaments obtained by DMA analyses are analyzed (Figure 2), SMPU201 filament which is spun with 20% polymer concentration in solution and 1% concentration of coagulation bath has the highest peak value. Consequently, its chain mobility is more

than the other filaments. Moreover, SMPU251 filament which is spun with 25% polymer concentration in solution and 1% concentration of coagulation bath has the lowest chain mobility. Besides, SMPU251 and SMPU253 filaments which are spun with 25% polymer concentration in solution, 1% and 3% concentration of coagulation bath, respectively, has a more heterogeneous structure than the others.

3.3. Mechanical properties of shape memory filaments

According to test results, there are not significant differences between breaking tenacity performances of shape memory fibers. However, as shown in Figure 3, SMPU200 and SMPU250 fibers which are produced with 0% solvent concentration in coagulation bath showed the highest breaking tenacity among other shape memory fibers. Strain test results showed that, high polymer concentration increased significantly elongation performance of filaments. SMPU251 and SMPU253 which are spun with 25% polymer concentration in solution, 1% and 3% concentration of coagulation bath, respectively, had the highest strain performance while SMPU203 and SMPU251 fibers had lower values. According to the statistical analysis results of strain, polymer content in solution had a positive effect on the elongation values of fibers. As a general result, it can be said that all fibers showed acceptable tensile and elongation performances.

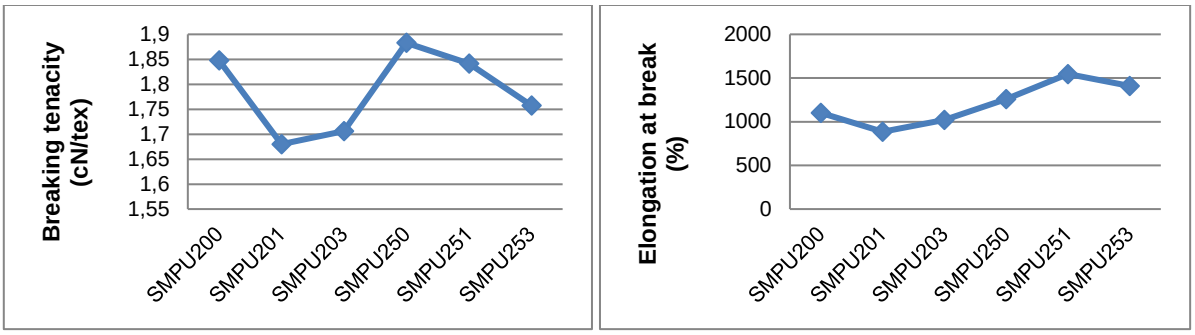

Figure 3. Tensile properties of SMPU fibers

3.4. Shape memory effect of fibers

The results of thermo-mechanical cyclic tensile test are summarized in Table 3. The shape memory filaments have a fixity ratio about 72.5% and recovery ratio of up to 91.5% in the first cycle. The filaments show up to 95% recovery ratio and 71% fixity ratio in the other two cycles. This results show that, prepared filaments have good shape memory effect. Because of molecule orientation and crystallization, there were differences between the first cycle and others. The shape memory effect and stress-strain behavior of filaments were very similar except for the first cycle. Beside this, shape memory filaments were not completely fixed to temporary shapes due to instant elastic recovery after releasing external stress.

Table 3. Thermomechanical properties of shape memory filaments under drawing temperature

Cycle code	Shape recovery ratio (%)	Shape fixity ratio (%)
1	91.5	72.5
2	95.2	71.3
3	95.9	71.6
4	97.3	71.3

The results of thermomechanical cyclic tensile test of shape memory filaments are shown in Figure 4. According to thermomechanical test results, all shape memory filaments showed similar shape memory performances. However, SMPU251 fiber which is spun with 25% polymer concentration in

solution and 1% concentration of coagulation bath has slightly higher recovery and fixity ratio values, demonstrating a better shape memory effect than other filaments.

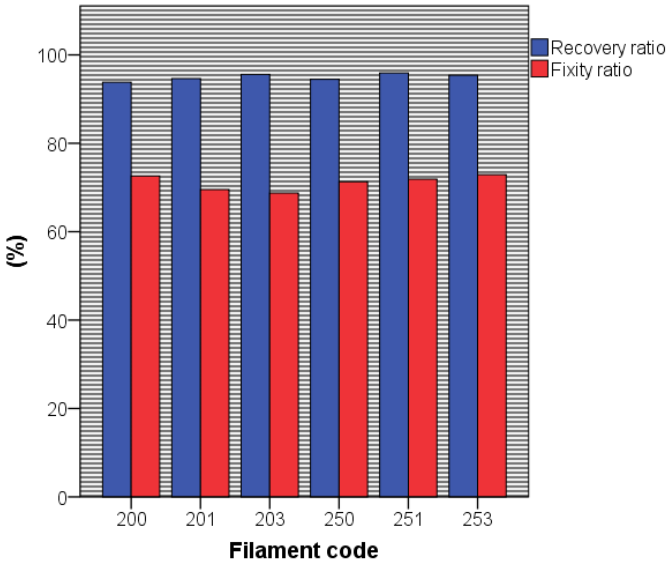

Figure 4. *Shape recovery and shape fixity of shape memory filaments*

4. CONCLUSIONS

Summing up, it can be concluded that, glass transition of soft segment of shape memory polyurethane filaments spun by wet spinning method were found between the range 36-40°C by DSC and DMA analyses. Shape memory polyurethane filaments showed good tensile performances, especially the fibers spun with high polymer solution concentration and without solvent in coagulation bath. Similarly, shape memory filaments have remarkable shape memory performances. They have a fixity ratio about 72.5% and recovery ratio of up to 91.5% in the first cycle. The filaments show up to 95% recovery ratio and 71% fixity ratio in the other cycles. Shape memory polymers have great potential for developing functional and smart textile products such as breathable, waterproof, modified structures.

ACKNOWLEDGEMENTS

This study was funded by a project of Suleyman Demirel University Scientific Research Projects Coordination Unit *(*4393-D2-15*). We want to thank for their support.*

References

1. *Meng, Q., (2010). Studies of Functional Shape Memory Fibers. Institute of Textiles & Clothing, The Hong Kong Polytechnic University.*
2. *Zhuo, H., Hu, J., Chen, S., (2011). Study of Water Vapor Permeability of Shape Memory Polyurethane Nanofibrous Nonwoven,* Textile Research Journal*, 81(9), 883-891.*
3. *Ahmad, M., Xu, B., Purnawali, H., Fu, Y., Huang, W., Miraftab, M., Luo, J., (2012). High Performance Shape Memory Polyurethane Synthesized with High Molecular Weight Polyol as the Soft Segment, Applied Sciences, 2(2), 535-548.*
4. *Han, H.R., Chung, S.E., Park, C.H., (2013). Shape memory and breathable waterproof properties of polyurethane nanowebs, 83(1), 76-82.*
5. *Zhu, Y., Hu, J., Yeung, L.Y., Liu, Y., Ji, F., Yeung, K., 2006. Development of shape memory polyurethane fiber with complete shape recoverability, Smart Materials and Structures, 15 (2006) 1385–1394.*
6. *Meng, Q., Hu, J., Zhu, Y., Lu, J., Liu, Y., (2007). Polycaprolactone-Based Shape Memory Segmented Polyurethane Fiber, Journal of Applied Polymer Science, 106(4), 2515–2523.*

7. *Yan, L., Aggie, C., JinLian, H., Jing, L., (2007). Shape memory behavior of SMPU knitted fabric, Journal of Zhejiang University Science A, 8(5):830-834.*
8. *Liu, Y., Lu, J., Hu, J., Chung, A., (2013). Study on the bagging behavior of knitted fabrics by shape memory polyurethane fiber, The Journal of The Textile Institute, 104(11), 1230–1236.*
9. *Jing, L., Hu, J., 2010. Study on the Properties of Core Spun Yarn and Fabrics of Shape Memory Polyurethane, FIBRES & TEXTILES in Eastern Europe, Vol. 18, No. 4 (81) pp. 39-42.*
10. *Meng, Q., Hu, J., Zhu, Y., Lu, J., Liu, B., (2009). Biological Evaluations of a Smart Shape Memory Fabric, Textile Research Journal Vol 79(16): 1522–1533.*
11. *Mondal, S., Hu, J.L., (2006). Temperature Stimulating Shape Memory Polyurethane for Smart Clothing. Indian Journal of Fibre&Textile Research, 31(1); 66-71.*
12. *Yan, Y.L., (2009). Structure and Thermal-Mechanical Properties of Shape Memory Polyurethanes and Textiles, Institute of Textiles & Clothing, The Hong Kong Polytechnic University.*
13. *Zhu, Y., Hu, J., Yeung, L.Y., Lu, J., Meng, Q., et al. (2007). Effect of steaming on shape memory polyurethane fibers with various hard segment contents, Smart Materials and Structures, 16(4), 969–981.*
14. *Gultekin, G., (2006). Production of Fatty Acid Based Polyurethane Films for Application of Wound Dressing Materials. The Istanbul Technical University.*

INVESTIGATING POSSIBILITIES OF THREE-STRAND YARN PRODUCTION

Murat Demir[1], **Musa Kilic**[1]

Dokuz Eylül University, Department of Textile Engineering, Tinaztepe Campus, 35397, İzmir, TURKEY
Phone: +902323017730 Fax: +902323017750
E-mail: murat.demir@deu.edu.tr , musa.kilic@deu.edu.tr

Abstract

Conventional ring spinning system is used for the largest proportion of total yarn production today and has kept same principle since 19th century. Analyzing new spinning systems shows that some modifications on conventional systems aid to produce yarn in better quality. Siro-spun spinning can be counted amongst one of the modern systems that enable to produce yarn in better quality and more economical way with help of some modifications. In this study, it was aimed to produce three-strand yarn in single process inspiring from siro-spun spinning. For this purpose, some modifications developed on siro-spun system and three-strand yarns were produced. Physical and mechanical properties of yarns that produced from different materials were measured and compared with three-plied yarns. Results showed that three-strand yarns are superior in terms of hairiness and elongation, but inferior in terms of unevenness. Moreover, there is no statistically significant difference between strengths of three-strand and three-plied yarns.

Keywords:

Yarn technology, twist spinning, siro-spun spinning

1. Introduction

Twist spinning has been known many years and has an increasing popularity within the recent years. Twist spinning is also known as two-strand spinning. Currently, two systems are used for two strand spinning: Duospun (designed by Ems Sa and Huber and Suhner) and Sirospun (designed by Zinser Textilmaschinen GmbH).

During the production process of twist spinning, two fibre strands are given into the drafting area of conventional ring spinning machine and leave drafting area together. At the same time, single yarn is produced by twisting individual fibre strand on themselves with aid of spindle, ring and traveler and then two individual single yarns are twisted for production of two-plied yarn.

In siro-spun spinning, elimination of plying and twisting machines provide economic superiority against conventional plied yarns and related with economic advantages and less production process siro-spun has become a big competitor against conventional two-fold yarns [1]. However, because of the variety of twists, siro-spun yarns cannot take all market from two-plied yarns [2]. Production of siro-spun yarns is provided by some modifications on conventional ring spinning machine. Two rovings are fed individually through slightly modified but generally conventional ring drafting area. After drafting area, the fibre strands leave front cylinder separately and they become single yarn with the help of common spindle and spinning triangle. These two yarns bound together to form of composite yarn [3].

Inside the literature, there are many studies that compare two-strand yarns and two-plied yarns in terms of physical, mechanical and structural properties. Siro-spun yarns have more strength and abrasion resistance and less hairiness when compared to single fold yarns [4]. Comparing compact and siro-spun yarns showed that, siro-spun yarns are superior in terms of hairiness, degrees of imperfections and strength [5]. At same twist level, siro-spun yarns have less hairiness and degrees of imperfections while more elongation compared with two fold yarns [6].

Strand space and spinning triangle are important production parameters that affects properties of siro-spun yarns. During the production of siro-spun three spinning triangles are occurred and structure of those triangles are directly related with strand space [7]. There is a positive influence between strand space and cohesion forces between fibres that affect yarn strength [8].

Inside the literature, it can be seen that many researchers attempt to modify conventional and modern systems in order to obtain superior yarn properties. Yılmaz and Usal [9], applied air nozzle and yarn guide on compact spinning machine and it is called compact-jet. With this new spinning system, it is possible to produce yarn with less hairiness. Moreover, it is also possible to produce yarns in better quality by combining siro and compact spinning systems [10].

Moreover, some researchers investigate the possibilities of production of multi-spun yarns. These studies mostly focused on yarn structure or mathematically analysed spinning conditions [11,12].

In the scope of this study, possibilities for the production of three-strand yarn will be investigated. For this purpose, some modifications on conventional ring spinning machine is planned. It is predicted that these modifications will provide great impacts on physical, mechanical and structural properties of three-strand yarns.

2. Experimental

In the study, three-strand and three-plied yarns were produced from cotton, PES, Tencel and %50 cotton-%50 nylon 6.6 based on given structural properties in Table 1.

Table 1. Structural properties of three-strand and three-plied yarns

Yarn	Number of single yarn	Number of produced yarn	Twist of single yarn	Twist of produced yarn
Three-strand yarn	Ne 60	Ne 60/3	650 T/m (Z)	650 T/m (Z)
Three-plied yarn	Ne 60	Ne 60/3	*1300 T/m (Z)* ➔ before plying 650 T/m (Z) ➔ after plying	650 T/m (S)

Investigating literature and analyzing some practical experiences are showed that better guiding strands during production have positive influence on yarn properties. Therefore, it is thought that some modifications should be made on siro-spun spinning machine to produce better quality yarns (Figure 1). In this study, only an extra funnel for the third roving was placed on the machine for better guiding. Future studies might be focused on improving strand delivery by using additional attachments such as three-grooved delivery cylinder.

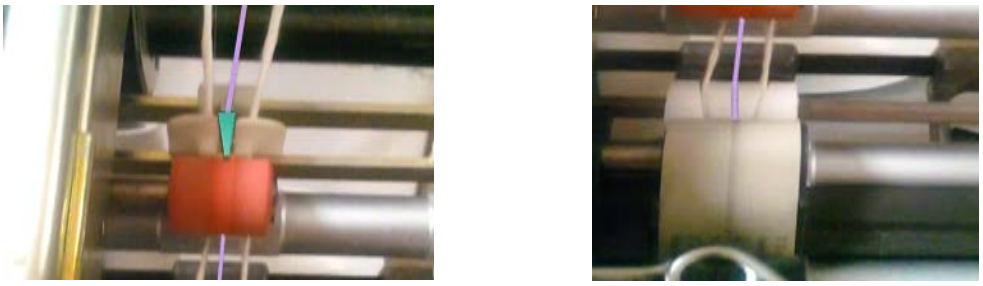

a. **b.**

Figure 1. Modifications on drafting zone (a. Embedding third roving funnel, b. Third groove on delivery cylinder)

In the study, physical, structural and mechanical properties such as unevenness, imperfections, hairiness, strength and elongation were measured by using Uster Tester and Uster Tensorapid.

Results and Discussion

Properties of three-strand and three-plied yarns that produced from different materials were statistically analyzed. For this purpose, ANOVA analysis at α = 0.05 were performed and graphs for confidence intervals at 95% were illustrated.

Hairiness

Result of eliminating plying and twisting machine, hairiness values (H) of three-strand yarns were found lower than three-plied yarns (Figure 2). As it seen from Table 2, differences between three-strand and three-plied yarns in terms of hairiness is statistically significant for all raw material types.

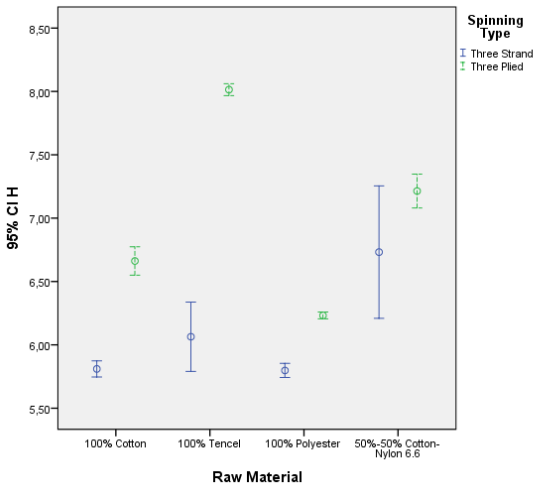

Figure 2. Hairiness (H) values of three-strand and three-plied yarns

Table 2. ANOVA table for *H* values

	Type III Sum of Squares	df	Mean Square	F	Sig.
100% Cotton	1,815	1	1,815	335,445	,000
100% Tencel	9,506	1	9,506	381,700	,000
100% Polyester	,471	1	,471	378,225	,000
50%-50% Cotton-Nylon 6.6	,581	1	,581	6,148	,038

Mechanical Properties

Comparing mechanical properties of three-plied yarns and three-strand yarns show that part from cotton yarns, there is no statistically significant difference between strength values of three-strand and three-plied yarns. Moreover, elongation properties of three-strand yarns are higher than three-plied yarns. As it seen from Table 3 and Table 4, differences between three-strand and three-plied yarns in terms of breaking force and breaking elongation are not statistically significant in general.

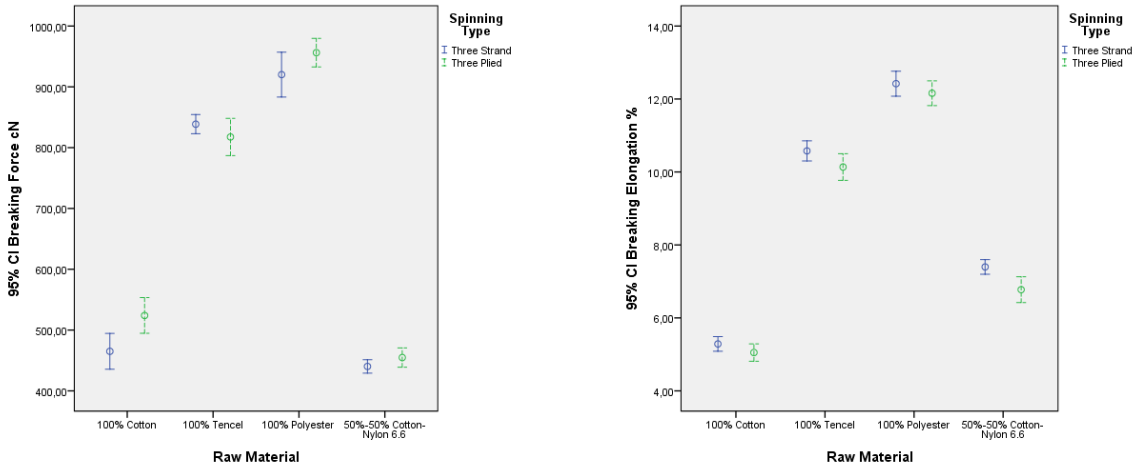

Figure 3. Breaking force (cN) and breaking elongation (%) values of three-strand and three-plied yarns

Table 3. ANOVA table for breaking force (cN) values

	Type III Sum of Squares	df	Mean Square	F	Sig.
100% Cotton	8702,500	1	8702,500	15,499	,004
100% Tencel	1102,500	1	1102,500	2,867	,129
100% Polyester	3261,636	1	3261,636	5,257	,051
50%-50% Cotton-Nylon 6.6	532,900	1	532,900	4,370	,070

Table 4. ANOVA table for breaking elongation (%) values

	Type III Sum of Squares	df	Mean Square	F	Sig.
100% Cotton	,139	1	,139	4,401	,069
100% Tencel	,488	1	,488	7,164	,028
100% Polyester	,172	1	,172	2,284	,169
50%-50% Cotton-Nylon 6.6	,973	1	,973	18,018	,003

Unevenness

Results showed that unevenness values of three-strand yarns are higher than three-plied yarns in general. It is assumed that this situation might be the result of lack of control on strand delivery. In the present work, strand delivery is only tried to be controlled by using third sliver funnel. As it seen from Figure 4a, strand spaces can be changed when the strands are fed into the drafting zone. As a result of this situation, irregularity between strand spaces are seen on spinning triangle (Figure 4b).

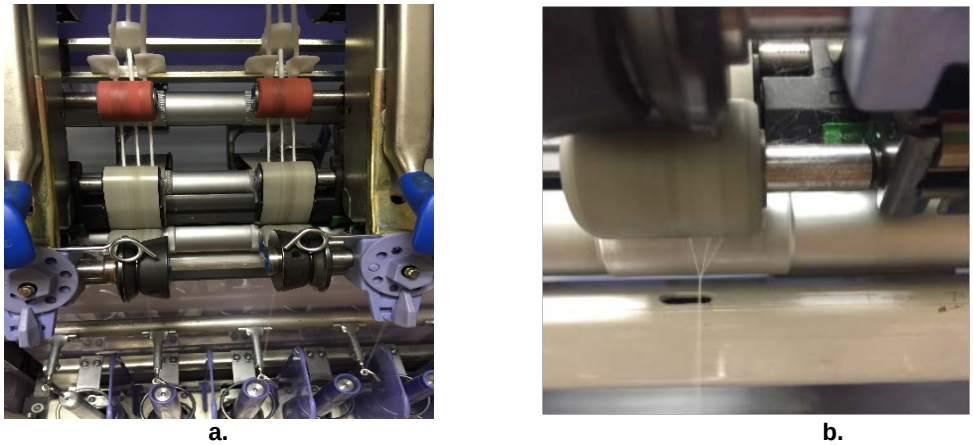

a. **b.**

Figure 4. Modifications on drafting zone (a. Strand delivery, b. Three-strand yarn spinning triangle)

This situation which has direct influence on yarn properties is assumed to be fixed with the better controlled strand delivery. Moreover, it is also seen from Table 5, there is significantly statistical difference in unevenness values for all raw materials.

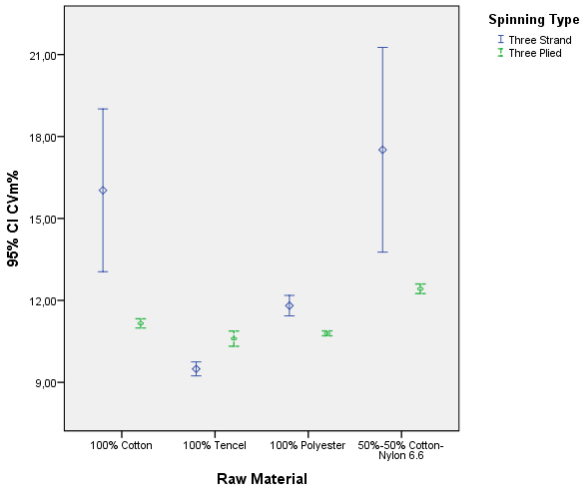

Figure 5. Unevenness (CVm%) values of three-strand and three-plied yarns

Table 5. ANOVA table for Unevenness (CVm%) values

	Type III Sum of Squares	df	Mean Square	F	Sig.
100% Cotton	59,341	1	59,341	20,538	,002
100% Tencel	3,069	1	3,069	65,918	,000
100% Polyester	2,570	1	2,570	53,413	,000
50%-50% Cotton-Nylon 6.6	64,770	1	64,770	14,200	,005

Imperfections

Due to lack of strand guiding, thick place values of three strand yarns are higher than three-plies yarn, as it similar with unevenness values. Comparing thin places (+%50 /km) and neps (+200p /km) values of three-strand and three-plied yarns show that there are no statistically significant differences in general. Due to the fact that neps values are mostly related with spinning preparations, results are obtained independent of spinning type.

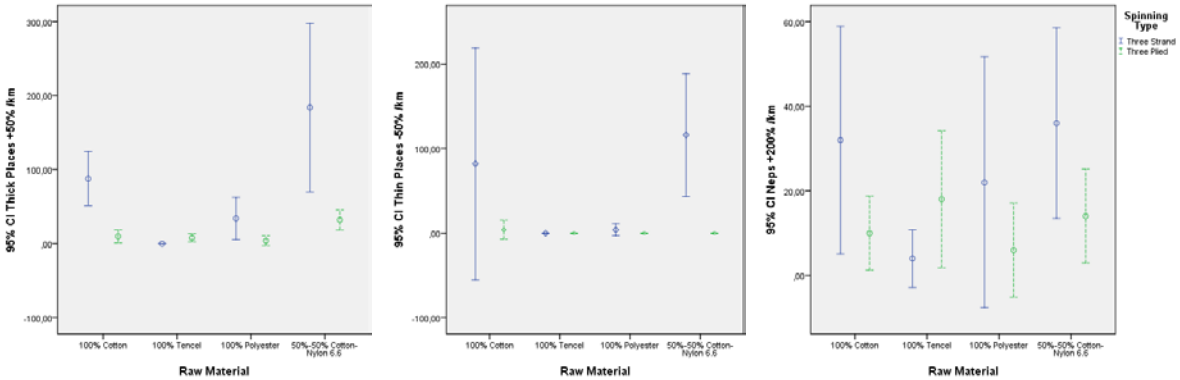

Figure 6. Imperfections values of three-strand and three-plied yarns

Table 6. ANOVA table for thick places (+50% /km) values

	Type III Sum of Squares	df	Mean Square	F	Sig.
100% Cotton	15210,000	1	15210,000	33,065	,000
100% Tencel	160,000	1	160,000	16,000	,004
100% Polyester	2250,000	1	2250,000	8,036	,022
50%-50% Cotton-Nylon 6.6	57760,000	1	57760,000	13,511	,006

Table 7. ANOVA table for thin places (+50% /km) values

	Type III Sum of Squares	df	Mean Square	F	Sig.
100% Cotton	15210,000	1	15210,000	2,483	,154
100% Tencel	,000	1	,000	.	.
100% Polyester	40,000	1	40,000	2,667	,141
50%-50% Cotton-Nylon 6.6	33640,000	1	33640,000	19,615	,002

Table 8. ANOVA table for neps (+200% /km) values

	Type III Sum of Squares	df	Mean Square	F	Sig.
100% Cotton	1210,000	1	1210,000	4,654	,063
100% Tencel	490,000	1	490,000	4,900	,058
100% Polyester	640,000	1	640,000	1,969	,198
50%-50% Cotton-Nylon 6.6	1210,000	1	1210,000	5,902	,041

Conclusions

In this study, it was aimed to investigate the production possibilities of three-strand yarns with the same principle of siro-spun spinning. For production of three-strand yarns, third funnel was attached on laboratory type siro-spun spinning machine and 100% Cotton, 100% Tencel, 100% polyester and 50%-50% cotton-Nylon 6.6 yarns were produced. Properties of three-strand yarns were compared with three plied yarns.

Hairiness values of yarns are mostly related with production processes. Eliminating twisting and doubling machines from production flow, three-strands yarns have better hairiness value than three-plied yarns for all material types. It is also seen from the results that there is no statistically significant difference between mechanical properties of three-strand and three plied yarns.

Investigating literature and experimental results showed that strand delivery and strand spacing have significant impact on unevenness. When the strands leave drafting zone, spaces between strands have direct influence on geometry of spinning triangle. It is expected that controlling strands from strand feeding to condensing zone of yarn will provide to produce yarns in better quality.

Siro-spun spinning has been placed in market and has become a strong rival against two-plied yarns. It is believed that, three-strand yarn spinning with the same production principle of siro-spun spinning will be placed in market as a big competitor of three-plied yarns with the economic benefit of eliminating plying and twisting process.

Acknowledgements

This study is carried out in cooperation with KİPAŞ Mensucat A.Ş., Kahramanmaraş, TURKEY.

References

1. Mansour, S. & Tawfik, M., 1985. *Production of Siro-spun Yarns from Short-staple Fibers.* Indian Journal of Textile Research, vol.11, pp.70-72.
2. Stalder, H., 2014. *Rieter Manuel of Spining, Issue 6: Modern Spining Systems.* Winterthur: Rieter Machine Works.
3. Kılıç, M., Balcı Kılıç, G. and Okur, A., 2011. *Eğirme Sisteminin İplik Özelliklerine Etkileri.* Tekstil ve Mühendis, 18(81), pp.22-34.
4. Salhotra, K., 1987. *Some Quality Aspetcs of Ply-Spun Yarn*. Indian Journal of Fibre and Textile Research, Issue 12, pp.197-200.
5. Örtlek, H., Kılıç, G. and Bilgin, S., 2011. *Comparative Study on the Properties of Yarns Produced by Modified Ring Spining Method.* Industria Textila, 3(62), pp.129-133.
6. Sun, M. and Cheng, K., 2000. *Structure and Properties of Cotton Sirospun Yarns.* Textile Research Journal, vol.70, pp.261-265.
7. Lawrence, Carl.A., 2003. *Fundamentals of Spun Yarn Technology*. CRC Press New York Document
8. Gokarneshan, N., Anbumani, N. and Subramaniam, V., 2006. *Influence of Strand Spacing on the Interfibre Cohesion in Siro Yarns*. The Journal of the Textile Institute, 3(98), pp.289-292.
9. Yılmaz, D. and Usal, M.R., 2010. *Comparision of Compact-Jet, Compact and Conventional Ring Spun Yarns*. Textile Research Journal, 81(5), pp.459-470.
10. Han, C., Wei, M., Xue, W. and Cheng, L., 2015. *Numerical Simulation and Analysis of Airflow in the Condensing Zone of Compact-siro Spining*. Textile Research Journal, 85(14), pp.1506-1511.
11. Matsumoto, Y., Kimura, H., Yamamoto, T., Matsuoko, T. and Fukushima, K., 2009. *Charecteristics of Novel Triplet Spun Yarns Made from Fibers of Differing Fineness*. Textile Research Journal, 79(10), pp. 947-952.
12. Xu, W., Xia, Z., Wang, X., Chen, J., Cui, W., Ye, W., Ding, C. and Wang, X., 2011. *Embeddable and Locatable Spining*. Textile Research Journal, 81(3), pp.223-229.

PARAMETERS AFFECTING SPORTS SOCKS PRESSURE AND PRESSURE PREDICTION FROM TENSILE CHARACTERISTICS

Sertaç Güney, Betül Akgünoğlu, Sibel Kaplan

Süleyman Demirel University, Engineering Faculty, Textile Engineering Department, Isparta, Turkey
sertacguney@sdu.edu.tr

Abstract:

The interaction between lower leg and the lower leg part of socks is an important factor affecting sports performance and wearing comfort. Garment fit, garment slip and fabric stretch are three essential components effecting comfort of the wearer's dynamic movement: 'Garment slip' is mostly determined by the coefficient of friction between skin and fabric and between different layers of garments. 'Fabric stretch', an important factor in pressure comfort, depends largely on elastic characteristics of fabrics. Sports socks were designed to give necessary pressure on leg muscles and enable comfort for not to decrease the performance of the sports people. If a fabric has high friction and stretching resistance, high clothing pressure is likely to be exerted on the body, which could result in discomfort feeling. This study aims to investigate the effects of structural mechanics of knitted fabrics on the amount of pressure generated on the underlying body. Five sports socks made of polyamide, polyester and cotton including different amounts of elastane fibers and having different knits on different parts of leg regions according to the necessities of sports were selected from the market. We carried out friction and tensile tests on different parts of sports socks. We also measured the pressure generated by socks' fabrics by pressure sensors and then discuss a method of validating the reliability of Laplace law for calculating pressure applied to a cylindrical body of known radius and compare the predicted and objectively measured pressure values. Results show that the fabrics having high tensions exerted high pressure values on body and the factor of tension given in Laplace Law is very important in pressure evaluation. But the fabric weight and friction coefficient are also important for the pressure applied on body. We can see these influences when comparing the predictive and objective pressure results. The Laplace Law was not clear and acceptable for all the results.

Key words:

Pressure comfort, sports socks, material, fabric structure.

1. Introduction

Socks play an important role in maintaining foot comfort. Therefore, designers cannot ignore pressure comfort parameters while producing functional socks, especially the top part of socks [1]. Nowadays, various functional socks are available in the market; necessary compression support is provided in sports socks to help increasing movement performance and in compression stockings and pantyhose for patients suffering some diseases such as varicose vein. The pressure value of the top part of sock is an important factor to consider when designing and developing socks. Degree of pressure produced by a garment is determined by complex interrelations between the following principle factors: the construction and fit of the garment, structure and physical properties of its materials, the size and shape of the body parts to which it is applied and the nature of the sports activity undertaken [2]. Dan et al. (2013) investigated the relationships between pressure and material properties of the top part of socks and established four indices which closely relate to pressure level; these are elastic coefficient of top part of socks, Poisson's ratio, elastic elongation and width of top part of socks [3]. Matsumoto et

al. (2004) measured leg size, tensile properties and pressure values of the top of socks and found comfortable pressure values as 2.02+/- 0.29 kPa and investigated the feeling of pressure changes depending on wearing period. They pointed out that for accurate estimations of pressure feelings, it is necessary to measure the pressure approximately 2 hours after putting on the socks [5]. Kirk and Ibrahim (1966) explained that the garment slip which is mostly related to the friction coefficient of fabric is an important factor effective on the garment pressure [4].

Existing research in the area of compression garments indicates that, application of the Laplace law formula is a suitable method to predict the magnitude of the pressure that can be applied to a cylindrical body of known radius by applying specific amounts of tension to an external fabric covering [6].

2. Experimental

2.1. Materials

Five men's sports socks having different compositions and knit structures (Figure 1) were selected from the market.

Code	A	B	C
Knit Structure		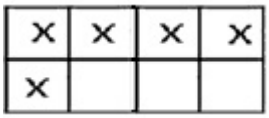	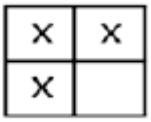

Figure 1. Sock knit structures

Their physical and structural parameters were given in Table 1.

Table 1. Physical parameters of fabric samples

Fabric	Fiber Composition (%)	Course /Wale density stitch/cm	Mass per unit area (g/m^2)	Knit Structures
1	87/12/1% PA/PES/Elastane	9/7	A: 264 B: 338 C: 160	
2	99/1% PA/Elastane	9/7	A: 325 B: 398 C:279	
3	96/3/1% PES/ Elastane/PA	10/7	A: 240 B: 280	
4	82/15/2/1 % Cotton/PES/Elastane/PA	12/8	A: 425 B: 479 C:472	
5	81/17/1/1% Cotton/PES/PA/Elastane	12/9	A:422 B:500 C:552	

2.2. Methods

Each section having different structures on the lower leg part of socks were separated and the tensile characteristics under different extension rates (30-40-50%) were tested according to ASTM D 4964-96. Friction coefficients (static and dynamic) were tested and calculated from the force-displacement graphics for each section for course direction according to ASTM D-1894 by using a Lloyd Tensile Tester (LR5K plus). Dimensions of the cradle was 4.5 x 4.0 cm and test was carried out on the sample placed on a horizontal platform by movement of the cradle with a speed of 50 mm/min. Extra weights were used to obtain a normal force of 1,2 g/cm^2 by the cradle. The objective pressure was measured by flexible pressure sensor system (Tekscan, USA). A plastic cylinder of 23.5 cm circumference was adopted in this test. The cylinder surface was covered by extended knitted fabrics. The interfacial pressure between fabric and cylinder was recorded at the center marked location of the circumferential line [7]. Laplace law formula can explain the relation between the pressure (P) and the tension on a curved surface and is expressed by the following equation:

$$P=T/r \quad (1)$$

where T is the tension of the shell (N/m), r is the radius of curvature (m) and P is the pressure (Pa). The ratio of the tensile force *T* to radius *R* represents a quantitative measure of the relevant structural properties of that particular fabric. A high *T/r* ratio represents a tight fitting fabric, and a low ratio represents a looser fitting fabric. This single quantitative measure may provide approximation of many fabric properties that are relevant in the design of compression and general sport garments and may provide insight for the development of a predictive model for the behavior of garments under tension. It is important to note however, that due to the nonlinear dynamics of stretching and deformation in fabrics and garments, the ratio *T/r* may not be constant over a whole garment over time [2]. In the pressure prediction part, the following assumptions were made; the relationship between the pressure *P* generated by the sock, circumferential tension force in the fabric *T* and the cylinder radius r *(m)* is described by the Laplace formula *(1)*; the longitudinal stretch of the fabrics in the garment is not considered and value of predictive pressure only applies at the time of application.

3. Results and Discussion

Tension characteristics of knit structures of the socks parts at different extension levels were tested. Figure 2 shows that knit structures exhibited different tension characteristics for each fabric because of their different material compositions and constructions (stitch density, weight).

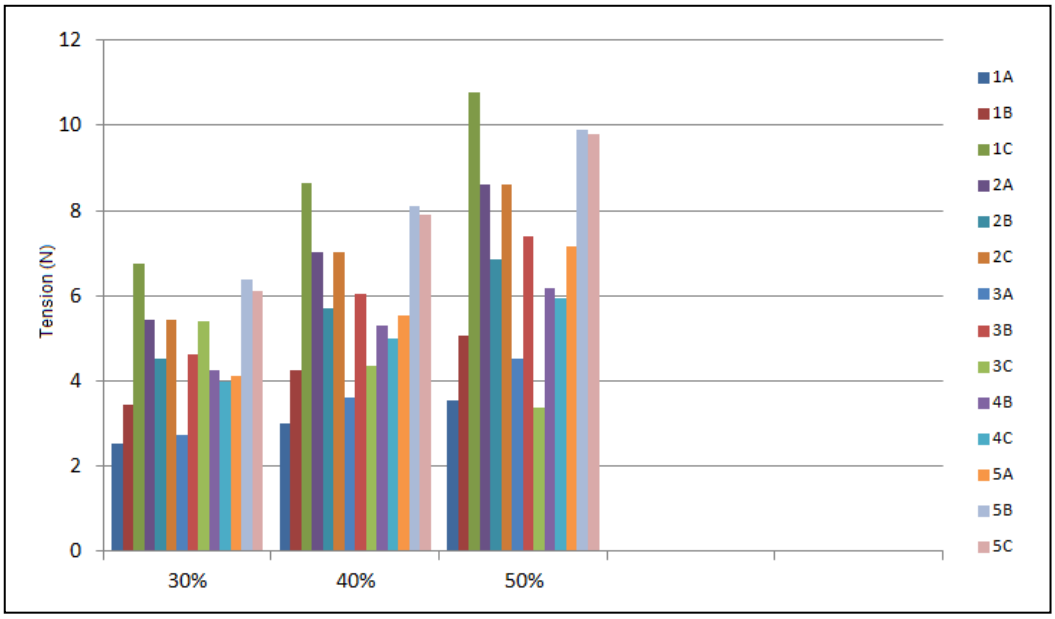

Figure 2. Tension characteristics of fabrics at different extension level (30-40-50 %)

Fabrics in knit structure C showed higher tension values. Knit structures in all fabrics showed different friction and elastic characteristics (Table 2). The values for Fabric 4A could not be measured because of inadequate fabric dimensions for the test.

Table 2. Friction and elastic characteristics of different socks parts

Fabric Code/ Knit Structure	Static Friction Coefficient (S.D.)	Kinetic Friction Coefficient (S.D.)	Tension (N)			Objective Pressure (gr/cm²)		
			30% Extension	40% Extension	50% Extension	30% Extension	40% Extension	50% Extension
1.A	0.493[b] (0.074)	0.482[b] (0.062)	2.54 (0.635)	3.01 (0.752)	3.53 (0.882)	6,50 (1,33)	9,76 (1,33)	29,30 (2,31)
1.B	0.569[bc] (0.104)	0.472[bc] (0.088)	3.44 (0.86)	4.25 (1.062)	5.08 (1.27)	32,56 (1,33)	39,07 (2,31)	42,33 (2,66)
1.C	0.241 (0.048)	0.208[a] (0.042)	6.74 (1.685)	8.66 (2.165)	10.77 (2.692)	3,25 (0)	6,50 (1,33)	22,78 (2,31)
2.A	0.225[a] (0.129)	0.312[a] (0.136)	5.44 (1.152)	7.04 (1.465)	8.61 (1.79)	6,50 (0)	9,76 (1,33)	13,01 (2,31)
2.B	0.648[c] (0.073)	0.557[c] (0.108)	4.54 (1.135)	5.7 (1.425)	6.87 (1.717)	9,76 (1,33)	19,53 (0)	29,30 (2,31)
2.C	0.372 (0.151)	0.368[b] (0.108)	5.44 (1.36)	7.04 (1.76)	8.61 (2.152)	6,50 (1,33)	16,25 (1,33)	26,04 (2,31)
3.A	0.302[a] (0.072)	0.293[a] (0.700)	2.73 (0.682)	3.62 (0.905)	4.54 (1.135)	-	3,25 (0)	9,76 (1,33)
3.B	0.447[ab] (0.090)	0.425[ab] (1.105)	4.62 (1.155)	6.03 (1.507)	7.4 (1.85)	3,25 (0)	13,01 (1,33)	29,30 (2,31)
4.A	-	-	5.39 (0.847)	4.36 (1.09)	3.39 (1.347)	3,25 (0)	6,50 (1,33)	9,76 (1,33)
4.B	0.406[a] (0.123)	0.311[a] (0.118)	-	-	-	6,50 (1,33)	16,28 (0)	22,78 (1,33)
4.C	0.302 (0.063)	0.246[a] (0.062)	4.27 (1.067)	5.29 (1.322)	6.18 (1.545)	6,50 (1,33)	9,76 (1,33)	13,01 (0)
5.A	0.297[a] (0.038)	0.227[a] (0.052)	3.97 (0.992)	5 (1.25)	5.94 (1.485)	6,50 (1,33)	13,01 (0)	19,53 (1,33)
5.B	0.463[ab] (0.118)	0.368[ab] (0.211)	4.12 (1.03)	5.55 (1.387)	7.15 (1.787)	16,28 (1,33)	29,30 (1,33)	45,59 (2,66)
5.C	0.354 (0.057)	0.264[ab] (0.063)	6.38 (1.595)	8.11 (2.027)	9.89 (2.472)	16,28 (1,33)	32,56 (2,66)	42,33 (2,66)

According to the results, kinetic friction coefficients can be ranked as B>C>A for all fabric types. Float stitches have negative effects on friction characteristics. So the knit structures B and C have higher kinetic friction coefficients (except for fabric code 1).The knit structure C has more repeated pattern and it gives an irregular fabric surface. As can be seen in Table 2, all sock parts and types have significantly different friction coefficient values. Statistically identical parts were coded with the same labels in Table 2. Objective pressure measurements taken on the cylinder surface are also given in Table 2. The fabrics having high tensions exert high pressure values. Results show that tension calculated by Laplace Law is valuable in pressure evaluation. But the fabric weight and friction coefficients are also important. We can see this effect when the predictive and objective pressure results are compared (Table 3). The Laplace Law is not clear and acceptable for all the results. As it was mentioned in some studies [8-9], fabric is assumed to be a shell, but the fabrics have dynamic behaviours under tension. So in pressure comfort evaluation, tension is not the only factor, the parameters friction coefficient, fabric weight, knit structures, materials etc. should also be taken into consideration. In this study, also fabrics having the same structures gave different pressure values under same tension values because of their physical differences (surface, weight, etc.). Tension values of fabric 1C are higher than the value of fabric 1B. But the objective pressure values are not in

harmony with tension values. It can be explained by higher friction coefficients and higher weights. In Laplace law, the tension is very important factor so according to the predictive pressures, it seems that fabric 1C exerts higher pressure than fabric 1B.

Table 3. Objectively measured,pressure values, predicted pressure values and deviations

Fabric Code/ Knit Structure	Objective Pressure (gr/cm²)			Predictive Pressure (gr/cm²)			Deviation (%)		
	30% Extension	40% Extension	50% Extension	30% Extension	40% Extension	50% Extension	30% Extension	40% Extension	50% Extension
1.A	6,50	9,76	29,30	6,84	8,10	9,50	4,88	-20,39	-208,28
1.B	32,56	39,07	42,33	9,26	11,44	13,68	-251,46	-241,32	-209,44-
1.C	3,25	6,50	22,78	18,15	23,32	29	82,07	72,10	21,43
2.A	6,50	9,76	13,01	14,65	18,96	23,18	55,58	48,52	43,87
2.B	976	19,53	29,30	12,22	15,35	18,50	20,17	-27,24	-58,40
2.C	6,50	16,25	26,04	14,16	18,88	23,18	55,58	13,76	-12,30
3.A	-	3,25	9,76	-	9,74	12,22	-	66,63	20,17
3.B	3,25	13,01	29,30	12,44	16,24	19,93	73,85	19,86	-47,05
4.A	3,25	6,50	9,76	-	-	-	-	-	-
4.B	6,50	16,28	22,78	11,50	14,24	16,64	43,41	-14,27	-36,91
4.C	6,50	9,76	13,01	10,69	13,46	15,99	39-14	27,52	18,65
5.A	6,50	13,01	19,53	11,09	14,94	19,25	11,09	14,94	19,25
5.B	16,28	29,30	45,59	17,18	21,84	21,33	17,18	21,87	26,63
5.C	16,28	32,56	42,33	16,51	21,33	26,39	16,51	21,33	26,39

Objective pressures of the top part of socks at different extension levels were measured on cylinder surface and the pressure levels of socks at 50% extension level can be ranked as 5>3>2>1>4 respectively. Fabric code 5C has generally high friction coefficient, tension and weight so it generated higher pressure. Predictive pressures in cuff parts were calculated according to the Laplace law formula at extension level of 50% and the values matched to the objective pressure measurement in 10-25% deviation (except for 3B and 4C). But the deviation is not generally uniform for all parts of socks. The fabrics at 50% extension level flattened and get a shell form. This may be the reason of differences between predicted and objectively measured results (10-25% deviation for some parts of socks) (1C, 2C, 3A, 4C, 5A). In this study, it is not clear to see the influences of materials on pressure values but PA and Cotton materials are smoother than PES. It is expected that socks with PES may exert much more pressure on body.

4. CONCLUSIONS

According the friction and pressure measurement results carried out on sports socks produced from different materials; tensile, friction characteristics and weight of fabrics have important effect on pressure generated on body. If a fabric has high friction and stretching resistance, high clothing pressure is likely to be exerted on the body, which could result in discomfort feeling. During designing and developing the pressure comfort of the socks, we should take account of these characteristics. This research also focused on the evaluation of the accuracy of Laplace law for sock fabrics. The results of this study show that Laplace law was not able to predict the measured pressure values in all parts of socks. The fabrics at extension level of 50% flattens and gets a shell form. Therefore the predicted pressure values matched objective pressure values with 10-25% deviation for some parts of socks.

References

1. *Li, J., (2007). Study on the pressure comfort of the top part of socks, Shanghai, Donghua University.*

2. *Troynikov, O., Ashayeri, E., Burton, M., Subic, A., Alam., F. and Marteau,S., (2010). Factors influencing the effectiveness of compression garments used in sports,* Procedia Engineering 2, 2823-2829
3. *Dan, R., Fan, X., Xu, L. and Zhang, M., (2013). Numerical simulation of the relationship between pressure and material properties of the top part of socks, The Jounal of The Textile Institute, 104(8), 844-851.*
4. *Kirk, W.J., ve İbrahim S.M., (1996). Fundamental Relationship of Fabric Extensibility to Antropometric Requirements and Garment Performance, Textile Research Journal, 57:p.37-47.*
5. *Matsumoto, Y. and Morooka, H., (2004). Comfort Pressure pf the Top Part of Men's Socks, Textile Research Journal, 74(7), 598-602.*
6. *Chatard J.C., Atlaoui D., Farjanel J., louisy F., Rastel D., Guezennec C.Y., (2004). Elastic stokings, performance and leg pain recovery in the 63-yearold sportsmen. European Journal of Applied Physiology, Vol 93(3): 347-352*
7. *Sang, J.S, Lee, M.S. and Park, M.J., (2015). Structural effect of polyester SCY knitted fabric on fabric size, strecth properties and clothing pressure, Fashion and Textiles, 2:22.*
8. *Aghajani, M., Jeddi, A. ve Tehran, M.A., (2011). Investigating the Accuracy of Prediction Pressure by Laplace Law in Pressure Garment Applicaitons, Journal of Applied Polymer Science, Vol.121:2699-2704.*
9. *Aghajani, M., Tehran, M.A. and Jeddi, A.A.A., (2013). Precise Measurement of Tension on Curvature Elastic Shells, Journal of Engineered Fibers and Fabrics, Vol.8(1), 82-87.*

TENSILE PROPERTIES OF SYNTHETIC BLOOD VESSEL REPLACEMENT

Karolina Čermáková, Michal Ackermann, Lukáš Čapek, Jana Horáková

Technical University of Liberec, Studentská 2, Liberec, Czech Republic, lukas.capek@tul.cz, +420485352949

Abstract:

Determination of tensile properties of synthetic blood vessel is an essential knowledge for researchers so that the biomechanical behavior of natural physiological vessel can be easily substituted. In this contribution, tensile tests of electrospun double layered vascular grafts made from polyesters were done. In order to analyze the developed vessel replacement in virtual simulations, a phenomenological material model was fitted to measured data.

Key words:

Synthetic graft, uniaxial test, finite element method

1. Introduction

Heart attack is worldwide one of the most risky health accident which frequently leads to death of the patient [1]. The consequence of the heart attack is usually a surgery of the heart during which so called bypasses are placed. Nowadays, the autograft veins are used in clinical practice [2]. This solution brings several complications, among all the long term surgery that might be risky for the patients. The state of the art in this domain is the synthetic vascular graft development.

Much effort was put into biocompatibility tests and material research in development of synthetic blood vessel replacements [3,4]. Only few studies are dealing with mechanical behavior and none of them with finite element modelling. The aim of this study is to present the uniaxial experiments of selected synthetic tubular grafts followed by finite element modelling.

2. Experimental

Experimental samples are electrospun double layered vascular grafts made from polyesters. Inner layer of the graft is made from copolymer of polylactide and polycaprolactone (70/30, PURASORB) and the outer layer is made from polycaprolactone (Mn 80,000, Sigma Aldrich). The thickness of the final graft is 200 µm (100 µm inner layer + 100 µm outer layer) as depicted in figure 1. The samples were sorted into two groups, one of which was not sterilized. The second one was sterilized by ethylene oxide (37°C).

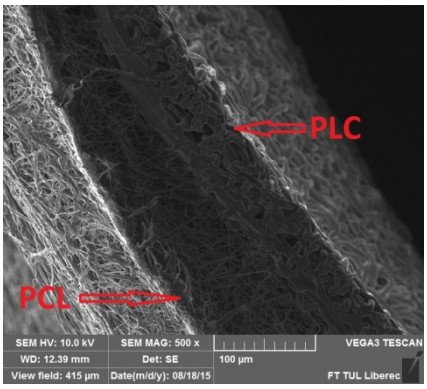

Figure 1: Scanning electron microscopy picture of cross section of double-layered vascular graft made from electrospun copolymer PLC in the inner layer and from electrospun polycaprolactone in the outer layer.

2.1. Uniaxial structural tests

The uniaxial tests were done on universal one column traction machine. The loading speed was 5 mm/min for all samples. The samples were loaded up to the rupture of the specimen. The initial length of samples was 50 mm. In the following step, the stress-strain curves were built on the basis of the measured data

2.2 Finite element simulation

The engineering stress strain curves were calculated by true strain and true stress by following equations

$$\sigma_{true} = \sigma \cdot (1 + \varepsilon) \quad (1)$$

$$\varepsilon_{true} = \ln(1 + \varepsilon) \quad (2)$$

The true data were imported into the software MSC.MARC were experimental data fitting was done, fig. 2.

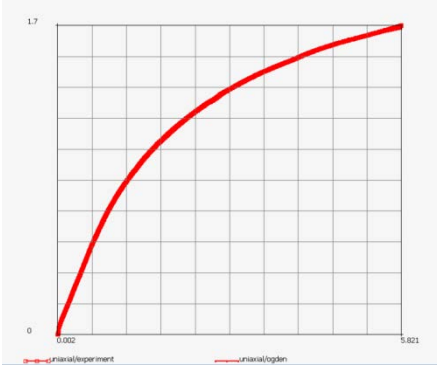

Figure 2. Experimental data fitting

The material model used for simulation is two-parametric Ogden model. The calculated material parameters are in Tab. 1.

$$W = \sum_{n=1}^{N} \frac{\mu_n}{\alpha_n}\left[J^{\frac{-\alpha_n}{3}}\left(\lambda_1^{\alpha_n} + \lambda_2^{\alpha_n} + \lambda_3^{\alpha_n}\right) - 3\right] \quad (3)$$

Table 1. Material parameters of the Ogden model

μ_1[MPa]	α_1[-]	μ_2[MPa]	α_2[-]
4.05	0.84	10.45	- 0.26

The finite element model of the sample consists of eight node shell elements (1600). The nodes of the left free edge are constrained via control node in all direction of movement. The nodes of the right free edge are constrained via control node and axial displacement of 8 mm is prescribed.

3. Results

3.1 Experiment

The measured data from uniaxial tensile tests of sterilized and non-sterilized samples are seen on figure 3.

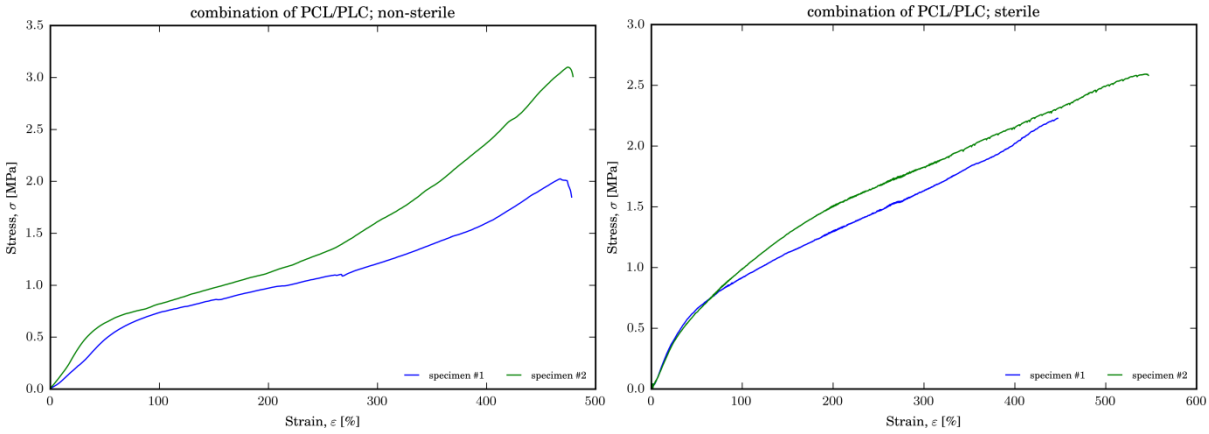

Figure 3. Force strain curve for non-sterilized samples (left) and sterilized samples (right)

The true strain and stress distribution along the axis of the model can be seen on figure 4 and 5.

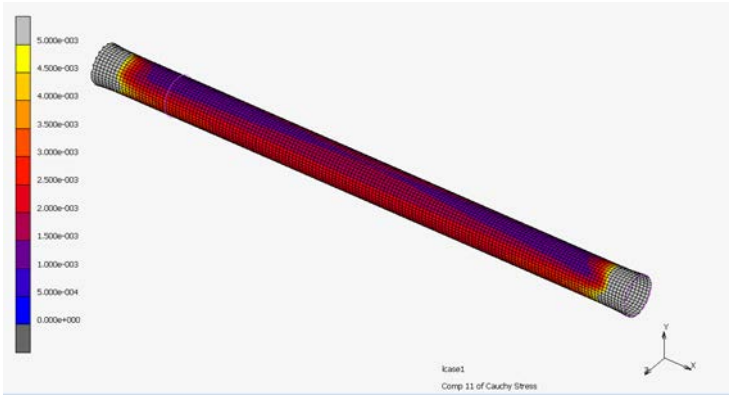

Figure 4. Cauchy stress distribution in sample axis [MPa]

4. CONCLUSIONS

Development of synthetic veins used for bypass surgery is of a great interest in the field of cardiovascular surgery. To our knowledge, none of them was applied yet. The research in this field cannot be done without understanding mechanical behavior of these artificial vascular replacements. The goal is to approximate its mechanical properties to the biologic ones.

The loading the samples up to the failure showed that extreme strains can be observed. There is no physiological meaning for loading veins up to 500 % that is why the FEM analysis was provided only up to 160 % strain. Phenomenological Ogden material model was used for finite element simulation.

In spite of favorable agreement between experimental data curves and results gained by finite element method, it should be noted that the future of FEM modelling of electrospun vein replacement must be in multiscale modelling. Using this method, the real morphology of the structure can be captured.

ACKNOWLEDGEMENTS

The authors are thankful to the grant of the Ministry of Health of the Czech Republic: NV15-29241A (Nanofibrous Biodegradable Small-Diameter Vascular Bypass Graft).

References

1. *http://ec.europa.eu/eurostat/statistics-explained/index.php/Cardiovascular_diseases_statistics*
2. *Prim DA,, Zhou B., Hartstone-Rose A., Uline MJ., Shazly T., Eberth JF. A mechanical argument for the differential performance of coronary artery grafts. J Mech Behav Biomed Mater. 2016;54:93-105.*
3. *Tan Z., Wang H., Gao X., Liu T., Tan Y. Composite vascular grafts with high cell infiltration by co-electrospinning. Mater Sci Eng C Mater Biol Appl. 2016 Oct 1;67:369-77.*
4. *Xie Y., Guan Y., Kim SH., King MW.. The mechanical performance of weft-knitted/electrospun bilayer small diameter vascular prostheses. J Mech Behav Biomed Mater. 2016;;61:410-418.*

HOW FIBERS ARE BOREN

M. Sivan[1], P. Mikeš[1,2], J Chaloupek[1], K. Strnadová[1], J. Horáková, M. Tunák[1], J. Chvojka[1,2], D. Lukas[1,2]

[1]Faculty of Textile Engineering, Technical University of Liberec, Studentska 2, Liberec 1, Czech Republic, 461 17. [2]Centre for Nanomaterials, Advanced Technologies and Innovation of Technical university of Liberec, Studentská 2, Liberec 1, Czech Republic, 461 17. David.lukas@tul.cz

Abstract:

This work analyses the hydrodynamic stability of viscose polymeric solution jets created by drawing technology concentrating on the liquid-solid transitions. The analysis starts with estimations predicting the fastest growing rate and the assigned wavelength of the Plateau-Rayleigh instability. The results show that creation of the thread from a polymer solution droplet has a character of an immediate liquid-solid transition, where the solid has a form of a gel. A method of video records of the fiber drawing process aided by image analysis is employed to obtain capillary pressure distribution along the jet axis. These results confirm the quick creation of a solid-liquid coexistence due to a violation of constant mean curvature on the equilibrium liquid surface. The analysis follows with introduction of an evaporative model from the jet including the physical reason for enhanced evaporation with decreasing jet diameter. A flow of the solvent inside the jet is supposed to be at its surface only. It results in creation of a solid gel film as a skin of the jet. The film provides the system with both instant and sufficient hydrodynamic stability. The existence of such films are thereafter experimentally evidenced.

Key words:

Justified Fiber, Hydrodynamics and Hydrodynamics Stability, diffusion

1. Introduction

Drawing a single fiber is a fascinating technique to produce polymeric (nano) fibers in diameter range from tens of nanometers to hundreds of micrometers [1]. The process itself is rather simple and versatile. A drawing lab-device is generally based on a micromanipulator that moves with a needle, micropipette or AFM tip, i.e., drawing element in general. When the polymeric solution has a suitable composition, a solid jet, called here as a thread of fiber, is withdrawn from the polymer solution droplet and is moved away rapidly. The drawing element pulls the fiber that should attain in a length from one millimeter up to tens of centimeters. The pulled fiber is as a rule deposited by touching the surface with the extremity of the drawing element. This method is unique, since it allows the deposition of fibers in predetermined patterns.

The small diameter of nanofibers resembling an extracellular matrix makes them extremely attractive in wound dressing and tissue engineering applications. For each specific application, a narrow range of fiber diameters is required to optimize their performance. Therefore, fiber diameter control based on a detailed knowledge of the drawing process is essential.

The stability of a liquid jet is affected by a variety of physical phenomena such as capillary driven hydrodynamics, variation in the temperature, viscosity or surface tension [2,3]. The jet stability is also heavily influenced by the interaction between the evaporating solvent and surrounding air. A liquid jet has in instances of nanofiber spinning a tiny diameter, resulting in significant evaporation rates. In spite of the importance of the topic in question, they are very limited studies addressing the instability of

evaporating jets [4,5]. We hypothesize here that the solvent evaporation from polymer solution jets decisively influences their hydrodynamic stability during fiber drawing process by immediate creation of a thin polymeric film on the jet surface.

One of the models of hydrodynamic stability of drawn individual viscous jets and cylinders is the Chandrasekhar approach [3]. Using the poloidal-toroidal decomposition he found an analytical relationship between the growing rate σ and the wave number *k* in an implicit form.

$$2x^2\left(x^2+y^2\right)\frac{I_1'(x)}{I_0(x)}\left[1-\frac{2xy}{x^2+y^2}\frac{I_1(x)}{I_1(y)}\frac{I_1'(y)}{I_1'(x)}\right]-\left(x^4-y^4\right)=J\frac{x\,I_1(x)}{I_0(x)}\left(1-x^2\right),$$

where $x=kr$, $y=\kappa r$, $\kappa^2=k^2+\sigma/\nu$, and $J=\gamma R/\left(\rho\nu^2\right)$. The jet radius is denoted here as *R*. Physicochemical parameters of the liquid are: kinematic viscosity ν, surface tension and γ and density ρ. The wave growth parameter is denoted as σ, Symbols $I_i(x)$ represent modified Bessel functions of the 1st kind and the bar denotes the derivative. Note that *J* is the reciprocal of the square of the Ohnesorge number.

2. Numerical analysis

The dependence of the dimensionless growth parameter $\sigma R^2/\nu$ on the dimensionless wavenumber, $x=kr$, according to equation (3) is plotted in Figure 1. The curves are shown sequentially for the following values of the *J* parameter, *J* = 1·10^{-5}, 5·10^{-5}, 10·10^{-5}, 15·10^{-5} and 20·10^{-5}. The most bottom curve corresponds to the smallest value of the parameter *J*.

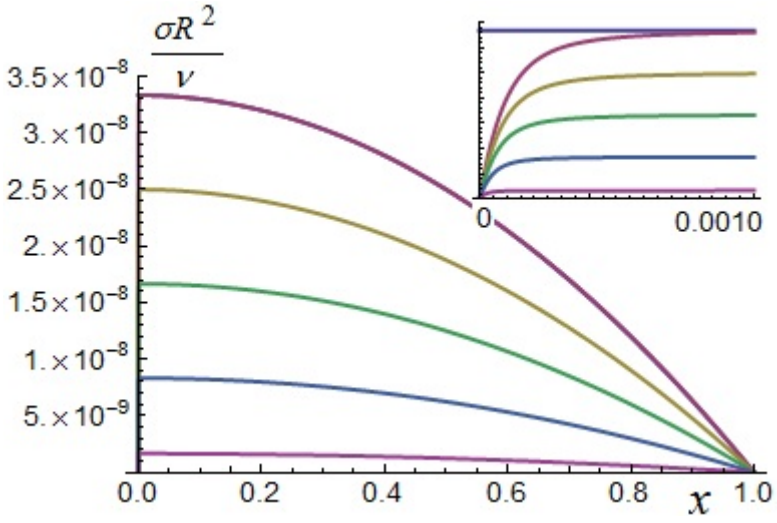

Figure 1. The dependence of the dimensionless growth parameter $\sigma R^2/\nu$ on the dimensionless wavenumber, kR. The curves are plotted sequentially for the following values of the parameter J = 1·10^{-5}, 5·10^{-5}, 10·10^{-5}, 15·10^{-5} and 20·10^{-5}. The lowest value of J corresponds to the most bottom curve. The inserted figure shows details of the curves in the vicinity of the x axes origin.

The numerical evaluation of the wavelength and corresponding relaxation time is carried out for the original 15%wt PVA aqueous solution, from which the liquid jet is drawn. Poly(vinyl alcohol) PVA with predominant molecular weight 30 000 g/mol. Fresh 16% w/w solutions were prepared by dissolving the Poly-vinyl-alcohol in distilled water. This solution has the following physico-chemical parameters: the

specific gravity $\rho = 1.0091 \cdot 10^3$ kg/m^3, kinematic viscosity $\nu = 5.0109 \cdot 10^{-4}$ m^2/s and a surface tension $\gamma = 44.3 \cdot 10^{-3}$ N/m. It is well-known, that a pooling a fiber requires a material with an appropriate viscoelastic behavior to undergo strong deformations, while being stable enough to sustain the Plateau-Rayleigh instability support and the stresses developed during the drawing. One have to highlight that the physicochemical data indicated in the last row of Tab. 1 of the original solution does not provide the jet having the radius R of 75 μm with sufficient stability. These admit the liquid thread existence for five microseconds only as opposed to the experimental experience. This contradiction leads to the conclusion that the jet has to have four orders higher viscosity than the polymeric solution from which it is created. Therefore, the drawn jet form the liquid polymeric droplet has to consist of some form of a solid phase.

3. Experiment

The experimental measurements of a distribution of the Laplace pressure p_c provides with a direct evidence of the liquid-solid transition between the liquid droplet and the tough gel, from which the thread has to be at least partly formed. For the Laplace pressure holds, $p_c = 2\gamma\vec{\nabla}\vec{n}$. Here the divergence of the normal $\vec{\nabla}\vec{n}$ has the meaning of twice the mean curvature. For the axisymmetric surface, which boundary is given by a dependence of its radius on z-axis position, $r = r(z)$, takes force the following relation.

$$\vec{\nabla}\vec{n} = \frac{1}{r\sqrt{1+r'^2}} - \frac{r''}{\left(1+r'^2\right)^{3/2}} \ ,$$

where the primes denote the space derivatives d/dz.

An experimental setup is composed of two metallic capillaries connected to syringes that supply them with the polymeric solution. Each of the capillaries has its outer radius is of 1 mm. Capillaries are laterally adjusted in the grooves of a cylindrical pedestal that ensures their axial alignment. One of the capillaries is firmly fixed to the pedestal while the latter is connected to the device providing it with a linear movement. This assembly is placed under a microscope that enables video-recording of the drawing process from the upper view.

Figure 1. A fibre is drawn from the 16%wt water solution of PVA. The metallic capillary diameter is 1 mm.

The Figure 2 depicts the basic drawing steps of the aqueous solution of PVA. At first, droplets are created at the rims of both capillaries by pooling the polymer solution from them using syringes. Than the moveable capillary, i.e. the drawing element, is shifted until both droplets come into contact. Next, the movable capillary is displaced horizontally with a constant velocity and stopped at a predetermined distance. The polymeric solution is deformed using the movement of the drawing element into a relatively stable jet/thread bridging the two droplets. The threat is evidently longer than the Plateau limit, $\lambda > 2\pi r$. This exhibits an apparent violation of liquid behavior.

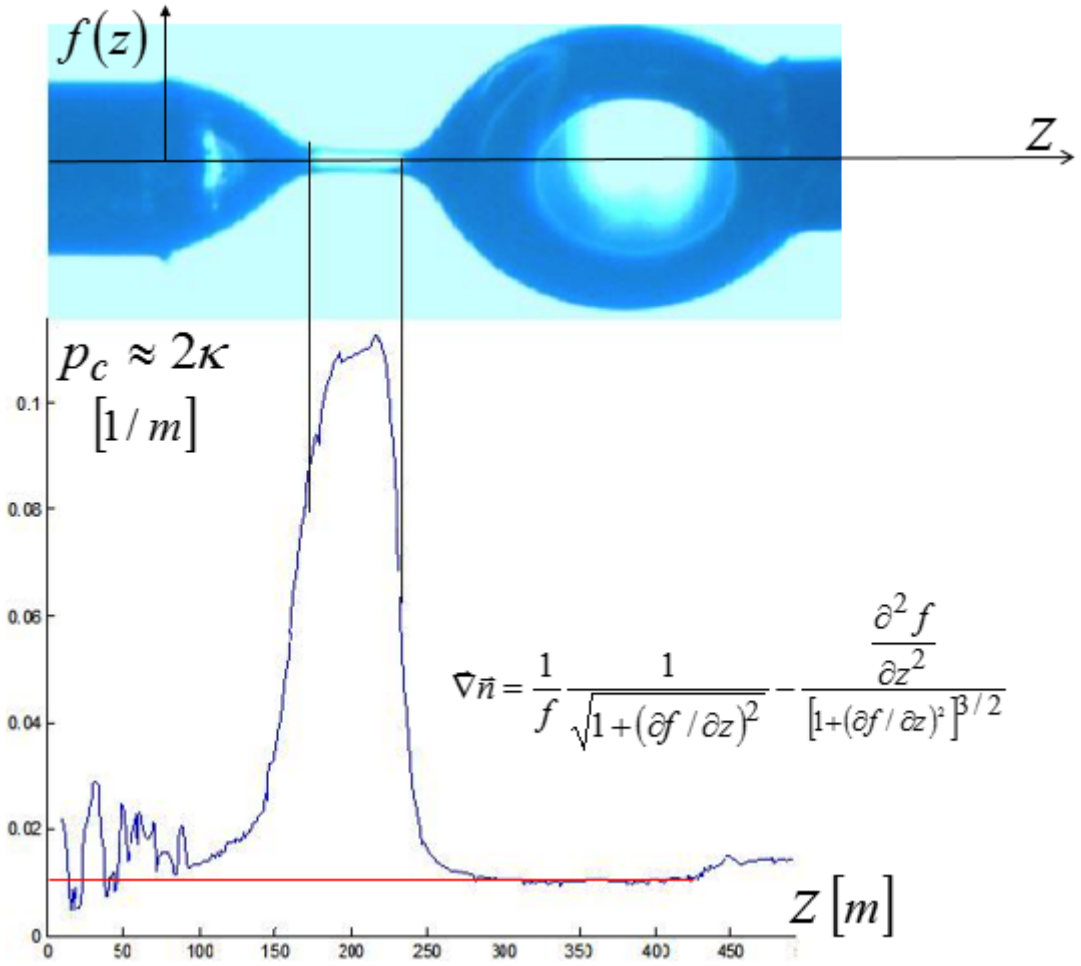

Figure 1. A nonuniform distribution of the capillary pressure p_c inside the threat is obtained using the calculation of twice the mean curvature.

Moreover, liquid bodies that are close to their mechanical equilibrium have to have constant Laplace pressure anywhere. A highly nonuniform capillary pressure distribution inside the threat is depicted in Figure 3. The capillary pressures are constant inside each of the droplets and both these pressures are nearly equal. However the pressure inside the jet/thread is much higher than the one inside a droplet. The transition between these unequal pressure areas has an abrupt character.

4. Jet thermodynamics

We hypothesize that the solid phase formation inside the creating polymeric jets/threads is a consequence of a rapid solvent evaporation. Evaporation of a solvent is a diffusion controlled process and hence a gaseous region above a polymer jet is immediately saturated with solvent vapor and the vapor concentration profile is formed [6,7,8]. Consequently the problem of an evaporating polymeric jet and the vapor concentration spatial distribution is considered here as a quasi-static problem into stagnant air. It means that the local solvent vapor concentration ϕ in mol·m^{-2}s^{-1} given by a solution of the diffusion equation, $\partial\phi/\partial t = D\Delta\phi$, reduces to the Laplace equation $\Delta\phi = 0$. An evaporative flux $\vec{j}$ at the jet surface is given by the gradient in the vapor pressure, $\vec{j} = -D\vec{\nabla}\phi$. Symbols Δ and $\vec{\nabla}$ are Laplace and Hamilton operators respectively and D is diffusivity.

The Laplace equation is solved here regarding to two main following boundary conditions. The first boundary condition prescribes the solvent concentration on the jet surface, and the latter defines this concentration at the infinite distance from the jet surface. Cylindrical symmetry of the problem is

supposed in the area close to the jet, while a spherical one is used at distances greater a length *L* of the jet/thread. The solvent vapor concentration belonging to the Laplace equation with the cylindrical symmetry has the assigned general solution, ${}^{c}\phi(r) = A\ln(r) + B$. The spherically symmetric field of vapor concentration has the general solution, ${}^{s}\phi(r) = C/r + F$.

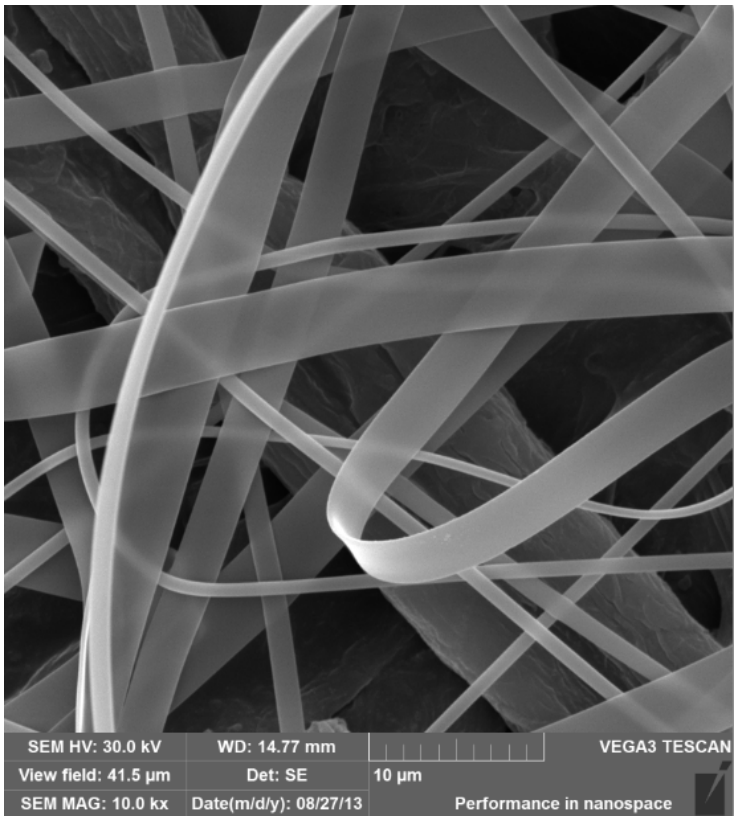

Figure 1. Representative SEM image of PVP/AMT fibers prepared from a 15% PVP/AMT 1 : 1 precursor solution by capillary needle electrospinning method.

Solutions of both Laplace equations have to be smooth at the boundary between them, where $r = L$. Therefore, four boundary conditions for four unknown constants *A*, *B*, *C* and *F* are required.

$${}^{c}\phi = \phi_s, \quad \text{for } r = a; \qquad {}^{c}\phi = {}^{s}\phi, \quad \text{for } r = L;$$

$$\frac{\partial {}^{c}\phi}{\partial r} = \frac{\partial {}^{s}\phi}{\partial r}, \quad \text{for } r = L; \qquad {}^{s}\phi = \phi_\infty, \quad \text{for } r \to \infty.$$

The evaporative flux $\vec{j}$ at the jet surface is determined by the constant *A* only,

$$\vec{j} = -D\vec{\nabla}\,{}^{c}\phi(a) = \frac{D(\phi_s - \phi_\infty)}{[1 + \ln(L/a)]a}.$$

The diffusion coefficient of water vapor in air at 20°C is D=24.2·10^{-6} m^{2}s^{-1}. The molar concentration of the saturated water vapor has the value ϕ_s = 0.9587 mol/m^3 and at 50% of relative humidity its value is ϕ_∞ =0.4974 mol/m^3. The evaporative flux $\vec{j}$ at these conditions and for the jet radius a = 75 μm and the jet length L = 1 cm has the value of $\vec{j}$ =0.4792 $mol \cdot m^{-2}s^{-1}$. The molar volume of liquid water at the temperature of 277 K is V_{mol} = 18.016·10^{-6} m^3. The surface area S [m^2] of the unitary jet length of the

radius 75 μm is $S = 2\pi \cdot 75 \cdot 10^{-6} = 4.71239 \cdot 10^{-4} m^2$. The volume of liquid water that evaporates from this jet unitary length surface per one second is $V = S \cdot j \cdot V_{mol} = 4.067 \cdot 10^{-9}$ m^3. The thickness h of the evaporated water from the jet is $h = V/(2\pi r) = 8.63 \cdot 10^{-6}$ m. The original PVA concentration is 16%, hence one can conclude that during one second a sheath of about 1 μm of PVA gel is formed on the jet surface that stops the development of the Plateau-Rayleigh instability. This results supports the hypothesis about an abrupt change of rheological parameters of the drawn polymeric solution. A circumstantial evidence of the gel formation on jet surfaces during a fibre spinning process is a formation of so-called ribbon-like fibres.

5. CONCLUSION

In summary, based on the experimental evidence, one can conclude that the model presented here adequately describes the fiber formation process during drawing. Our model emphasizes the hydrodynamics and thermodynamic nature of the mechanism controlling the jet stability. The two relevant time scales corresponding to each of these processes, characteristic hydrodynamic σ and evaporation τ_e times, are identified. Moreover, the model allows achieving quantitative agreement to the experimental data.

ACKNOWLEDGEMENTS

The authors thank Associated Professor M. Brzezina for useful remarks. Authors acknowledge financial support from the project MZ ČR: NV15-29241A. 2015-2018. Nanovlákenná biodegradabilní maloprůměrová cévní náhrada.

References

1. *D. H. Reneker, A. L. Yarin, E. Zussman, and H. Xu, Adv. Appl. Mech.* ***41****, 43 (2007). VZOR*
2. *M. Doi and S. Edwards, The Theory of Polymer Dynamics (Clarendon Press, Oxford, 1986), p. 391.*
3. *T. Ondarçuhu and C. Joachim, Europhys. Lett.,* ***42*** *(2), 215-220 (1998).*
4. *M. Saroka,Y. Guo, and N. Ashgriz, AIAA Journal,* ***39*** *(9), 1728 (2001).*
5. *S. Chandrasekhar, Hydrodynamics and Hydromagnetic Stability (Dover Publications, New York, 1982) p. 540.*
6. *Z. W. Lian and Reitz, R. D., The Effect of Vaporization and Gas Compressibility on Liquid Jet Atomization, Atomization and Sprays,* ***3****, 249 (1993).*
7. *X.-F. Wu, Y. Salkovskiy and Y. A. Dzenis, Modeling of solvent evaporation from polymer jets in electrospinning, Applied Physics Letters,* ***98****, 223108 (2011).*
8. *A. F. Routh, Drying of thin colloidal films, Rep. Prog. Phys.* ***76,*** *046603 (2013).*
9. *Y. O. Popov, Evaporative deposition patterns: spatial dimension of the deposit, Phys. Rev. E* ***71,*** *036313 (2005).*
10. *H. Hu and R. G. Larson, Evaporation of a sessile droplet on a substrate J. Phy. Chem. B* ***106,*** *1334 (2002).*

ELECTROSPUN POLYESTERS: COMPARISON OF POLYMERIC FIBROUS STRUCTURE AND ITS INFLUENCE ON FIBROBLAST PROLIFERATION

AlešŠaman[1], Lucie Vejsadová[1], Jana Horáková[1], Věra Jenčová[1], Petr Mikeš[1]

[1]Technical university of Liberec, Department of Nonwovens and Nanofibrous Materials, Studentska 2, 461 17 Liberec, Czech Republic, +420 485 353 230
ales.saman@tul.cz

Abstract

Polyesters have been recognized as promising polymers for use in tissue engineering applications due to their biocompatibility and biodegradability. The main advantage of synthetic polymers is its reproducibility of fabrication process due to a controllable narrow molecular weight distribution in comparison with natural polymers. Fibrous materials were prepared by needleless electrospinning. Planar layers from polycaprolactone and polylactic acid with various molecular weights were fabricated. Resulting fibrous mats were seeded with fibroblasts and cell viability was compared using metabolic MTT test.

Key words:

Polylactide, polycaprolactone, electrospinning, in vitro testing.

1. Introduction

Electrostatic spinning (electrospinning) is a method for production of sub-micron fibers with highly potential applications in tissue engineering and regenerative medicine. Nanofibrous structures are characterized by large specific surface area, high porosity with a small pore size that makes these materials tremendous interest for various applications. Electrospinning uses high electric field intensity which is affecting surface of polymeric solution. Electric forces create instabilities on the polymeric solution surface and when it reaches its critical values, the polymeric jet appears. During the process, the most of the solvent is being evaporated and dry nanofibers are collected on the counter electrode [4].

Electrospun fibers mimic extracellular matrix of native tissue therefore they are extensively investigated for various types of scaffolds [3]. An idea of tissue engineering and regenerative medicine is based on designing of an optimal scaffold that degrades during the time of cell infiltration and proliferation that could by enhanced by releasing of supporting factors [2]. This demands a list of requirements on material properties. An appropriate scaffold possesses slightly hydrophilic surface, adequate mechanical properties and degradation rate. Usage of natural polymers is limited due to their broad distribution of molecular weights that is one of the main parameters affecting electrospinnability. To the contrary, synthetic polymers benefit of relatively narrow molecular weight distribution. Aliphatic polyesters such as polyglycolic acid (PGA), polylactic acid (PLA) and polycaprolactone (PCL) belong among the most investigated synthetic polymers in the field of tissue engineering nowadays [6]. These materials have already been approved in a variety of biomedical applications such as bioresorbable sutures used in a surgery [5].

In this work, polycaprolactone and polylactic acid with different molecular weights were electrospun and the influence of molecular weight and resulting fibers were discussed. Further *in vitro* testing investigated the influence of fibrous scaffold composition on fibroblast proliferation rate.

2. Experiment

The work was focused on the preparation of nano/microfibrous layers made from aliphatic polyesters using electrospinning. Polycaprolactone and polylactic acid electrospinning conditions were firstly optimized using needle electrospinning. Then, the method was transferred to high production needleless electrospinning where planar samples for further *in vitro* testing were obtained.

2.1. Materials

Biodegradable polyesters, namely polycaprolactone (PCL, Sigma Aldrich) and poly(L-lactic) acid (PLA, Polysciences) were selected for preparation of fibrous samples. Two different molecular weights were used for further fabrication of fibrous mats. Lower molecular weight was approximately 45,000 g/mol (samples marked as PCL45 and PLA45), higher molecular weight was around 80,000 g/mol (samples marked as PCL80 and PLA80). Polycaprolactone **PCL45** had the average number molecular weight (M_n) of 45,000 g/mol (M_n 40,000-50,000 g/mol) and polydispersity index (PDI) between 1.2 and 1.8 with the mass average molecular weight (M_w) of 48,000-90,000 g/mol. Polycaprolactone with average M_n 80,000 g/mol (**PCL80**) had polydispersity index lower than 2. Poly(L-lactic) acid **PLA45** molecular weight was in range of 45,000 and 55,000 g/mol with polydispersity index of 1.94 and **PLA80** had molecular weight of 80,000 -100,000 g/mol.

2.2. Electrospinning

At first, needle electrospinning was performed in order to optimize polymeric concentration for further experiments. The electrospinning apparatus consisted of a syringe filled with electrospinning solution, a needle, a syringe pump, a high-voltage power supply and a flat collector covered with an aluminum foil. Electrospinning solutions were prepared 24 hours before the spinning. Aliphatic polyesters were dissolved in solvent system composed of chloroform, ethanol and acetic acid in ratio 8/1/1 (v/v/v).

Optimized electrospinning solutions were transferred for the spinning using strings within the device Nanospider™ NS 1W500U (Elmarco). Electrospinning conditions of each tested polymer are depicted in Table 1. The positive voltage (35-45 kV) was applied to the wire that served as a spinning electrode and the negative voltage of 25 kV was applied to the collector. The distance between the spinner and the collector was kept between 160 and 185 mm. The temperature during the experiments was kept at 21 ± 1 °C and the relative humidity 40 ± 5 %.

Resulting fibrous mats were analyzed using scanning electron microscopy (SEM) Tescan Vega 3SB. Fiber diameters were measured using NIS Elements software (n=100). The data were expressed as median ± standard deviation.

Table 1. Spinning parameters of PCL45, PCL80, PLA45, PLA 80 using needleless electrospinning.

Sample name	Mass concentration [wt %]	Distance [mm]	Voltage		Speed of EWM (Endless Motion Wire) [mm /sec]	Fiber diameter [nm]
			Positive source [+kV]	Negative source [-kV]		
PCL45	16	180	35	25	220	319.8 ± 575.7
PCL80	10	170	40	25	140	487.6 ± 407.3
PLA45	10	175	40	25	190	921.2 ± 617.3
PLA80	6	185	45	25	140	1161.0 ± 666.3

2.3. Cell Sources and Seeding

Prior to cell seeding, scaffolds were cut into round patches of 6 mm in diameter and sterilized by immersion in 70% ethanol for 30 minutes followed by double washing in phosphated buffer saline (PBS, Lonza).

Mouse 3T3 fibroblasts (ATCC) were cultivated in Dulbecco´s Modified Eagle Medium (DMEM, Lonza) supplemented by 10% fetal bovine serum (FBS, Lonza), 1% glutamine (Biosera) and 1% penicilin/streptomycin/amfotericin B (Lonza). The cells were placed in humidified incubator at an atmosphere of 5% CO2 at 37°C. When cells became confluent, they were suspended using trypsin-EDTA (Lonza). Fibroblasts (passage 10) were seeded on the scaffolds placed in 96well plate at density of $5x10^3$ per well plate. Medium was changed twice a week during the experiment (11 days). Materials incubated in the complete medium without cells served as negative controls for MTT test (n=2 per each testing day).

2.4. Metabolic MTT assay

Viability of the cells seeded on the scaffolds was analyzed by MTT test after 3, 7 and 11 days of culture period. MTT [3-(4,5-dimethylthiazol-2-yl)-2,5-diphenyl-2H-tetrazolium bromide] has been reduced to purple formazan by mitochondrial dehydrogenase in cells indicating normal metabolism. 50 µl of MTT solution was added to 150 µl of complete medium and samples were incubated at 37°C for 4 hours. Formed violet crystals of formazan were dissolved with acidic isopropanol. Optical density of suspension was measured (λ_{sample} 570 nm, $\lambda_{reference}$ 690 nm). Each testing day, 8 samples of each material were incubated with MTT solution and final absorbance was calculated as the difference between absorbance measured by 570 nm and by reference wavelength 690 nm. The absorbance of negative controls was subtracted from measured values of absorbance of tested samples and placed into the graph comparing viability of cells cultured on tested materials. The data were expressed as mean of measured absorbance ± standard error of the mean.

3. Results and discussion

3.1. Electrospinnability of aliphatic polyesters

Polycaprolactone and polylactic acid in both tested molecular weight were spinnable using needle electrospinning as well as in needleless setup. The electrospinning parameters using needle were optimized as follows: voltage 15-20 kV, distance 180 mm, needle diameter 0.9 mm, feed rate of 1-1.5 ml/h, temperature 20-23°C and relative humidity 35-40%. Conditions of needleless electrospinning are summarized in Table 1. Resulting fibrous structures are depicted by scanning electrone microscopy in Figure 1. Spinnability of higher molecular weight polymers (PCL80 and PLA80) was strongly dependent on process parameters such as distance between the string and collector and speed of EWM (Endless Motion Wire). If the processing conditions were not kept precisely, resulting fibers were pulled out during the deposition on the collector. Lower molecular polymers (PCL45 and PLA45) were spinnable in more robust conditions.

Optimal concentration of polymer mass was found as: 16 wt% for PCL45, 10 wt% for PCL80 and PLA45 and 6 wt% for PLA80. Polylactic acid was electrospun from more concentrated solutions than polycaprolactone of corresponding molecular weights. Other properties such as viscosity or polymer crystallinity can influence the optimal amount of polymer in the electrospinning solution.

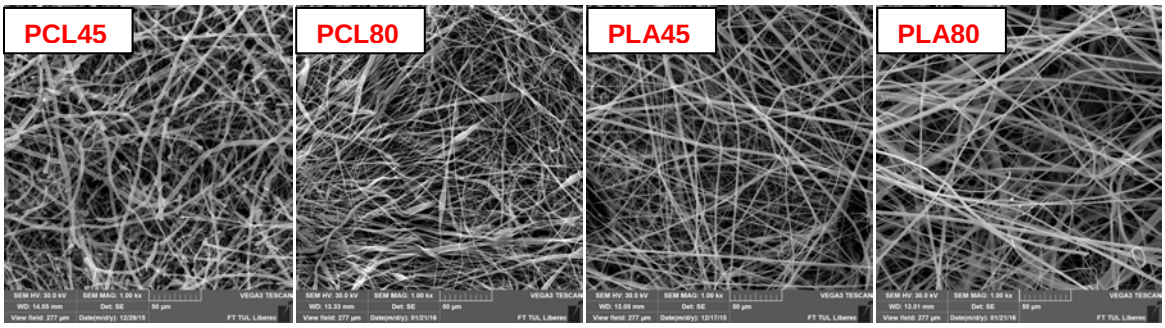

Figure 1. Scanning electron microscopy pictures of electrospun PCL45, PCL80, PLA45 and PLA80.

3.2. Fiber diameter characterization

Fiber diameter of resulting planar fibrous mats was compared using image analysis software. Electrospun polycaprolactone mat formed uniform fibers with fiber diameter median ± standard deviation of 319.8 ± 575.7 nm in case of PCL45 and 487.6 ± 407.3 nm in case of PCL80. Similarly polylactic acid with lower molecular weight (PLA45) resulted in fiber diameter of 921.2 ± 617.3 nm and with higher molecular weight (PLA80) of 1161.0 ± 666.3 nm. The fiber diameter distribution was wider in PLA samples as seen from fiber diameter characterization that is depicted in figure 2. Fiber distribution could be influenced by polydispersity index of polymer. Polycaproloactone PCL45 with lower PDI than PLA45 possessed narrow fiber distribution compared to PLA45. PCL80 with PDI less than 2 showed also wider fiber diameter distribution compared to PCL45 with PDI between 1.2 and 1.8. No data of PLA80 polydispersity index were available from the supplier. However, based on the fiber diameter characterization it could be assumed that polydispersity index will be around 2 or even higher.

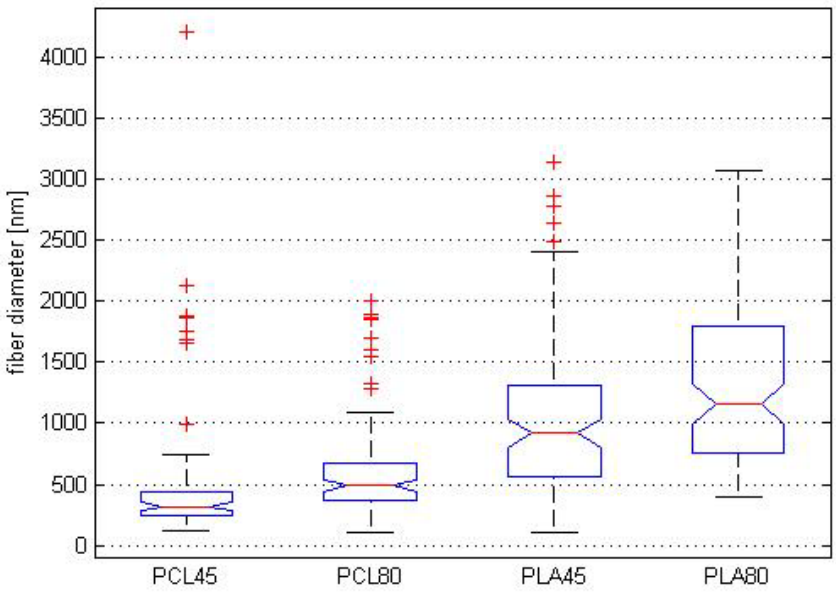

Figure 2. Box plot of fiber diameter distribution of electrospun PCL45, PCL80, PLA45 and PLA80 with standard settings including 50% percentile for the box with median, maximum and minimum values and the extremes.

3.3. Metabolic activity of fibroblasts

Fibroblasts were seeded on prepared electrospun layers made from PCL45, PCL80, PLA 45 and PLA 80. During the cell culturing, fibroblast metabolic activity was measured using MTT test after 3, 7 and 11 days. The results showed that electrospun polylactide in both molecular weights supported fibroblast proliferation since their metabolic activity was continuously increasing during the culture period as depicted in graph in Figure 3. Electrospun polycaprolactone supported cell adhesion (cell viability in day 3 was comparable to electrospun PLA) but the proliferation was delayed compared to electrospun PLA. It is assumed that PCL did not possess ideal surface properties because of its hydrophobicity [1].

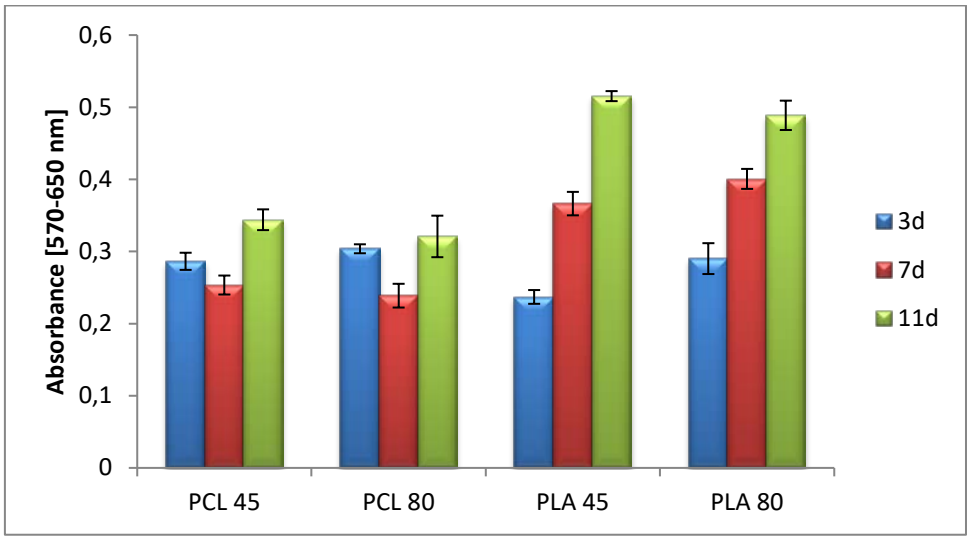

Figure 3. Metabolic MTT test of fibroblasts seeded on electrospun PCL45, PCL80, PLA45 and PLA80 after 3, 7 and 11 days of culturing.

4. CONCLUSIONS

Aliphatic polyesters in different molecular weights were successfully electrospun. Polycaprolactone formed fiber diameters in range of hundreds of nm (300-500 nm) whereas polylactide created mostly microfibers with wide range distribution. Lower molecular weight of 45,000 led to thinner fiber diameter compared to higher molecular weight of 80,000 in both tested polymers. *In vitro* tests showed that electrospun layers support fibroblast adhesion. However, cell proliferation was accelerated on electrospun PLA compared to PCL.

ACKNOWLEDGEMENTS

The authors are thankful to the grant of the Ministry of Health of the Czech Republic: NV15-29241A (Nanofibrous Biodegradable Small-Diameter Vascular Bypass Graft) and to the Department of Nonwovens and Nanofibrous materials, Faculty of Textile Engineering, Technical University of Liberec. Aleš Šaman, Lucie Vejsadová and Jana Horáková thank the Student's Grant Competition of Technical University of Liberec: 21150 (Development and modification of nanofibrous drainage implant for use in the treatment of glaucoma).

References

1. *Bacakova, L., Filova, E., Parizek, M., Ruml, T., Svorcik, V. (2011). Modulation of cell adhesion, proliferation and differentiation on materials designed for body implants. Biotechnology, 58, 739-767.*
2. *Hu, X., Lui, S., Zhou, G., Huang, Y., Xie, Z., Jing, X. (2014). Electrospinning of polymeric nanofibers for drug delivery applications. Journal of Controlled Release, 165, 12-21.*
3. *Lanza, R., Langer, R., Vacanti,J.P. (2000) Principles of Tissue Engineering (2nd edition), Academic Press (Cambidge).*
4. *Lukáš, D., Sarkar, A., Martinová, L., Vodsed'álková, K., Lubasová. D., Chaloupek, J., Pokorný P., Mikeš, P., Chvojka,J., Komárek, M. (2009). Physical principles of electrospinning (Electrospinning as a nano-scale technology of the twenty-first century). Textile Progress, 41(2), 59-140.*
5. *Middleton, J.C., Tipton, A.J. (2000). Synthetic biodegradable polymers as orthopedic device, Biomaterials, 21, 2335-2346.*
6. *Zhan, J., Singh, A., Zhang, Z., Huang, L., Elisseeff, J.H. (2012). Multifunctional aliphatic polyester nanofibers for tissue engineering. Biomaterials, 2(2), 202–212.*

COMPARISON OF THE WELL KNOWN SPINNING AND ELECTROSPINNING METHODS FOR POLYVINYL ALCOHOL

Blažková Lenka, Hlavatá Jana, Horáková Jana, Kalous Tomáš, Novák Patrik, Pelcl Martin, Strnadová Kateřina, Šaman Aleš, Chvojka Jiří

Technical University of Liberec, Studentská 2, Department of Nonwovens and Nanofibrous Materials, Liberec, Czech Republic, jiri.chvojka@tul.cz

Abstract:

The electrospinning is known for more than 100 years. Since then, many spinning and electrospinning techniques have been developed. This article aims to introduce and compare spinning methods which are used to create nanofibers and nanofibrous mats. Polyvinyl alcohol (PVA) has been chosen as a polymeric model. Different concentrations of PVA were spun using various techniques. Depending on the spinning method, different fibrous morphologies have been created. Spinnability of PVA as well as fiber diameter measurement was evaluated showing that spinning techniques provide large tool for various applications.

Key words:

Electrospinning, polyvinyl alcohol, spinning techniques, spinnability

1. Introduction

A method of using electrostatic forces for creating very fine fibers has been known for more than 100 years. Electrospinning has proved relatively simple method for forming submicron fibers, typically from 100 nm to 1μm. The exception is not the fibers reaching of few micrometers. Nanofiber structures are characterized by large specific surface area, high porosity, but with a small pore size, these materials are built foreground interest for various applications. This method can prepare fibers of different polymers, natural, synthetic polymers and containing various additives depending on the use and desired properties. (Lukáš 2009) Depending on the final application, various requirements on nanofibrous layers are demanded. Therefore, the novel techniques are being discovered leading to new properties of fibrous mats, higher fibrous production or improved spinnability of some polymers.

This article aims to describe and compare various spinning techniques which are investigated at the Technical university of Liberec, Department of nonwovens and nanofibrous materials. The description of used spinning methods is introduced in experimental part and results with chosen model polymer polyvinyl alcohol (PVA) are shown. Polyvinyl alcohols are water soluble polymers manufactured by alcoholysis of polyvinyl acetate. The properties of the various grades are mainly governed by the molecular weight and the remaining content of acetyl groups.

Nowadays it is possible to develop novel spinning techniques based on the older ones that are known for many years. The electrospinning process could be transformed to new ways of spinning techniques such as bubble spinning, drawing technique and centrifugal spinning. Some of them use the high voltage for production of fibers, the others use capillary forces or their combination. Here, we present the results of spinning of various concentration of PVA ranging from 8% to 28% using centrifugal spinning, drawing, electrospinning from the rod, from the needle, bubble spinning, needle-less spinning and alternative current spinning, Spinnability of these solutions is evaluated and the fibrous morphology is characterized by fiber diameter measurement.

2. Experimental

2.1. Materials

The experiments were carried out with a chosen polymer polyvinyl alcohol (PVA), Mowiol grade 18-88 (Kuraray) supplied in granule form.

The polymeric solutions were prepared from the PVA granules that were dissolved in the distilled water. The experimentally tested concentrations of polymeric solutions were set as 8%, 12%, 16%, 20%, 24% and 28% (w/w). The volume of polymer solution (each concentration) was 100 ml that was further divided into smaller amount of volume and distributed to individual spinning technologies. All these solutions were spun by spinning technologies, namely centrifugal spinning, drawing, electrospinning from the rod, from the needle, bubble spinning, needle-less spinning and alternative current spinning that are described in the following subchapter.

Polymeric solution were characterized by dynamic surface tension and viscosity measurement since these parameters are useful for prediction of spinnability of polymeric solutions. Dynamic surface tension of PVA solutions was measured by the maximum pressure in a bubble using the bubble pressure tensiometer PocketDyne (Krüss). Surface tension values are presented as the average of five measurements (n=5). Viscosity measurement was carried out on the rotational viscometer Haake Rotovisco 1 (Thermo Scientific) with a rotary nozzle C35 / 1 ° TIL. Each sample was measured 5 times at a constant speed of 300 s-1 and 5X at increasing speeds from 10 to 300 s-1 (8%, 12%, 16%, 20%), respectively, from 10 to 1000 s-1 (8%, 12%) according to the density of the polymer. The viscosities were averaged and plotted (n=5).

2.2. Methods

2.2.1 The centrifugal spinning technology is based on a relatively simple idea. Spinning fluid is placed into spinneret unit [2]. When the rotating speed reaches critical value, the centrifugal force overcomes the surface tension of spinning fluid, and liquid jets are ejected from the nozzles of the spinneret unit (Fig. 1). The centrifugal force, together with the air frictional force, elongates the jets and leads to the formation of nanofibers. In addition to the centrifugal force and air friction force, other forces such as rheological force, surface tension, and gravitational force, might also influence the nanofiber formation (Zhang 2014).

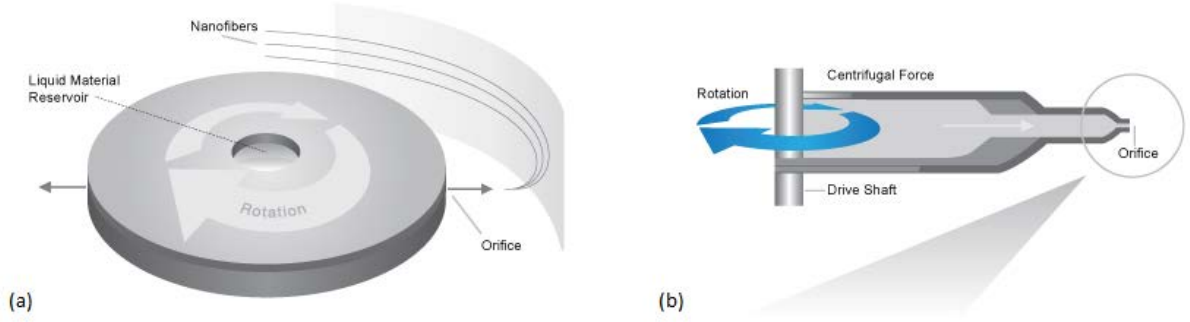

Figure 1. Detail of the spinneret for needle force spinning and fiber formation developed by FibeRio: a) diagonal view, b) side view [3].

2.2.2 The drawing technique has been known for centuries. Nevertheless, our team is focused on its innovation and application. Polymer solution in a forms of a droplet is placed on a workbench. The droplet is eroded with drawing element which retracts from it, pulling a bridge of material as depicted in Fig.2. The bridge stretches, solidifies, and finally forms a single fiber which is accurately positioned. If the parameters are optimized, the fiber diameter reaches hundreds of nanometers (Amrinder 2006).

Periodical repeatition of this process will give rise to a defined structure. The technique enables drawing of fibers made from polyvinyl alcohol, polyvinyl butyral (PVB), polycaprolactone (PCL) and polystyrene (PS) where single nanofibers are precisely arranged on a holder. To accomplish such goals, a micro manipulating machine has been developed and used for parameter tuning, due to its repeatable accuracy.

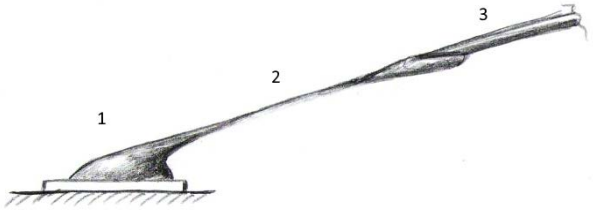

Figure 2. Detail of the drawing setup: 1 polymer droplet on the workbench, 2 polymeric fiber, 3 drawing element.

2.2.3 Electrospinning from the rod, respectively from a conductive cylinder, is technology particularly suitable for verification of polymeric solution spinnability in a laboratory conditions rather than for large scale fibrous production. The basic setup of electrospinning from the rod is described in Fig. 3. Small amount of polymer solution (about 3 g) can be used for testing the spinnability of polymer solution that makes the technology useful in laboratory conditions since the polymers could be very expensive. The rod is made from integrated conductive roller having a diameter of approximately 5 -15 mm which is placed in vertical position on the non-conductive frame. High voltage is supplied on the body of the rod. Polymer solution is manually applied on said the top of the where the action of the electrostatic field produces nanofibers. Nanofibers dropped on the collector that can be in a various forms such as coated backing fabric with black paper or aluminum foil. It is possible to influence the morphology of the resultant fibers changing a few parameters. At first, there are technological parameter settings such as the diameter of the rod or distance between the peak of the rod and the collector, value of the used electric voltage. Secondly, parameters of the polymer solution, especially concentration that is directly proportional to the viscosity of the solution, composition of used solvent system, the molecular weight of the entering polymer, play an important role in the characteristics of resulting fibrous mats. (Sill 2008), (Hu 2014)

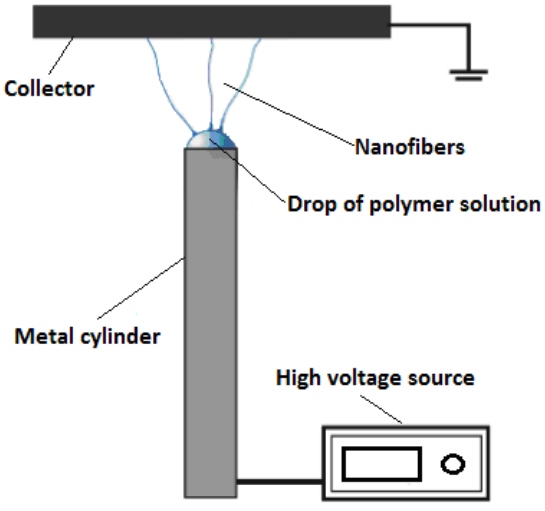

Figure 3. Schematic representation of electrostatic spinning from rod

2.2.4 Another electrospinning technique is spinning from the needle where polymeric solution is ejected from the needle as depicted in Fig.4. The needle is connected to a syringe which serves as a reservoir for the polymer solution and simultaneously applying a pressure in induced dosage. Linear pump acts on the syringe set speed and thus leads to a controlled flow polymer solution from needle. Formation of the fibers depends on the high voltage which is supplied across the wire to the body of the needle and

thereby into the solution. At the end of the needle is formed Taylor cone by applying a high voltage where the fibers are drawn from. . Electrospinning from the needle, as well as from the rod mentioned in the previous paragraph, is from the perspective of production very inefficient. The methods are more suitable for laboratory use where large scale production is not required. These techniques are mainly used for the testing of new polymers, solvents or additives, optimizing of solution parameters and spinning conditions. Their main advantage is simple construction and rapid response to change of various parameters settings. The resulting morphology can unlike rods also affect needle diameter, shape and type of the collector etc. (Bhardwaj 2010)

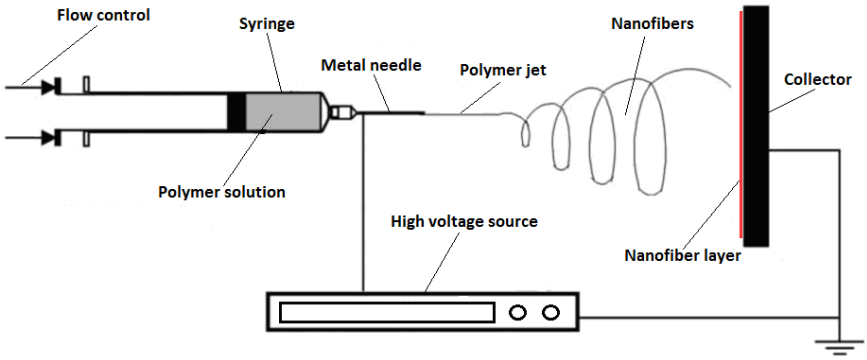

Figure 4. Schematic representation of electrospinning from the needle.

2.2.5 Bubble electrospinning was firstly mentioned in the year of 2007.Recently, the technology belongs to novel technology of electrospinning (see Fig.5) capable of large scale fiber production (Chen 2014). This method utilizes the electrostatic force to overcome the surface tension of the bubbles, instead of classical electrospinning, where a Taylor´s cones occurs. The main part of this device is electro conductively round container which serves as a reservoir of polymer solution. On the bottom part of this round container, a hole is drilled for air supply which provides the bubble effect. The container is fixed to the electrically conductive tube through the air flows and is connected to a high voltage. Electrospinning process takes place in an optional distance on a flat collector.

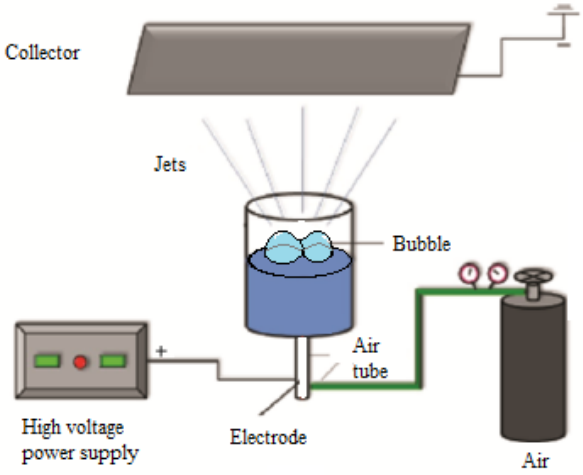

Figure 5. Bubble spinning technology.

2.2.6 Nanospider technology is needle-less technology using high voltage where fibers are created directly from free liquid surface. The principle of the Nanospider is based on the possibility of producing nanofibers from a thin layer of polymer solution. In this case, Taylor cones are created on the surface of a rotating roller or wire immersed in a polymer solution. Because the Taylor streams are formed next to each other throughout the entire length of spinning electrode, this revolutionary idea produced many advantages such as high production rate. This commercial method for production of polymeric

nanofibers is used in industry (Mohamed 2012). This is a simple and versatile method for production of nanofibers from a variety of polymeric materials. In the experiment, the laboratory scale machine Nanospider Production Line NS 1WS500U (Elmarco) was used (see Fig. 6).

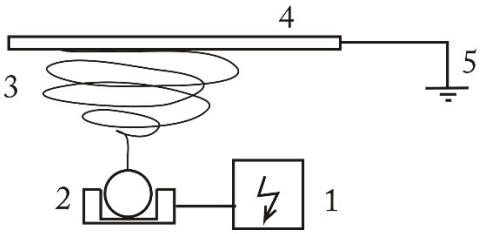

Figure 6. Scheme of Nanospider, (1) High voltage supplies (2) roller in polymer solution (3) nanofibers (4) collector, (5) grounding,

2.2.7 The technology alternating current spinning is currently being developed at Technical university of Liberec as a novel method that uses alternating current (AC) power sources for the creation of nanofibrous materials through the phenomenon of electrospinning. This technology requires a high voltage transformer for step up conversion of standard voltages to high voltages (Pokorny 2014). There is no need for frequency control therefore it is possible to use the standard 50 Hz source. This technology is much more productive than standard direct current (DC) setups employed in previously introduced technologies but does not produce materials with the same degree of homogeneity. The use of collector, powered or grounded, is merely a matter of convenience for AC electrospinning because it typically creates a rising smoke-like column of electrically neutral nanofibers as shown in Fig. 7. This is of great interest for numerous potential applications because it simplifies the required engineering solutions for operations with nanofibrous material. Materials produced by this technology have potential to be used for filtration and absorption of harmful substances (bacteria, gasses) or in medical products.

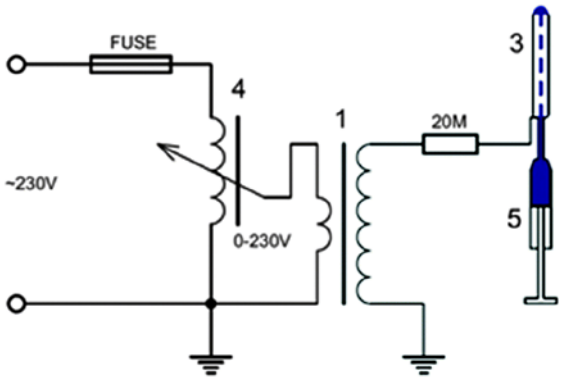

Figure 7. Schematic AC – spinning setup and the spinning electrode , 1 high voltage supply, connected on 4 variable transformer, 3 spinning electrode, 5- controlled infusion pump

All above mentioned techniques were used for spinning of PVA in different concentrations from 8% to 28%. Spinnability and fiber diameter was evaluated for each technology. Morphology of fibrous samples was assessed by scanning electron microscopy (SEM) and image analysis software to characterize fiber diameter. Samples for SEM analyses were sputter coated with gold and analyzed using TESCAN Vega 3SB Easy probe (Czech Republic). All specimens were recorded in appropriate magnification to enable image analysis of fibrous morphology. Image analysis of fibers was evaluated from SEM pictures using software NIS Elements (LIM s.r.o., Czech Republic). Fiber diameter characteristics were assessed from 100 measurements (n=100) and showed in a box plot.

Centrifugal spinning technology O = force spinning diameter of spinneret 50mm, speed of spinneret 3000rpm, distance between spinneret and collector 100mm, t=23°C, RH=35%.OT = force spinning jets diameter of spinneret 100mm,speed of spinneret 2500rpm, diameter of jets 1,2mm,distance between spinneret and collector 100mm, t=22°C, RH=40%. EO = force electrospinning diameter of spinneret 50mm,speed of spinneret 2500rpm, distance between spinneret and collector 100mm, t=21°C, RH=41%. Drawing technique the fibers were pulled onto micromanipulator second generation (MMP II) at 1000 m / s with an acceleration of 500 m / s and 0.3 radios. The fibers were pulled in the length of 18 cm at an air temperature of 19.6 ° C and humidity 30%. On the campaign was used 20G peak (OKI International, Taper Tip 20G x 1-1 / 4 "). The concentration of 8%, 12% and 15% percent were not suitable to form fibers. At a concentration of 20% PVA has been possible fiber winding. Dosing pump was used with a pressure piston of 0.25 bar for 0.8 seconds. The polymer was dosed approximately every two stretch fiber. SEM analysis of the samples were prepared of fibers fixed in the fixation rings having about 400 fibers per sample. Samples were prepared a total of five levels from this one. For further experiments with drawing fibers were prepared two higher concentrations of PVA. Drawing of the 28% PVA was at a temperature of 19.8 ° C and humidity 35% (1 February 2016). For drawing was used pressure of 0.25 bar for 1.5 seconds. Again we gave 5 samples for SEM. Electrospinning ROD the voltage +40-55kV, distance 150mm and needle the voltage +25-36kV, distance 150mm, feeding 6-7ml/h, temperature 21°C humidity 31%, bubble spinning the voltage +23kV, set distance 150mm, t=22°C, RH=40%, Nanospider voltage+50kV and -10kV, distance 150mm,t=22°C, RH=35% AC spinning 37-38kV, spinning without collector, t=23°C, RH=42%

3. Results and discussion

Polyvinyl alcohol granules were dissolved in water in concentrations ranging between 8% and 28 %. The various concentrations and technologies lead to different diameters of resulting nanofibers that was assessed after the spinning. The value of fibers diameters is connected with boundary condition surface tension summarized in Tab 1 that also records the average temperature of the solutions during measurement.

Table 1. Surface tension, incl. standard deviations, and the temperature of the PVA solutions in different concentrations.

	concentration [w/w %]	**Surface tension [mN/m]**	**Temperature of polymer solution [°C]**
PVA	8	59.38 ± 0.30	25.1
	12	61.96 ± 0.49	25.0
	16	81.46 ± 0.31	25.1
	20	115.46 ± 1.06	25.3
	24	182.70 ± 1.85	23.7
	28	209.42 ± 3.62	24.1

The Table showed that with increasing concentrations of PVA solutions, surface tension was growing. However, this increase was not linear and the values were influenced by varying solution viscosity. The surface tension of PVA solutions with a concentration of 24 wt% and higher was very difficult to measure because of the formation of bubbles spans approximately one thousand ms. In contrast, in the case of solutions having lower concentrations, respectively. Viscosities, the emergence of bubbles ranged from tens to hundreds of milliseconds.

The polymer concentration of 20wt% was not possible to measure at higher speed than 300 sec-1. The measurement of viscosity of each sample is shown in the Fig 8 and Fig 9. The concentration of 24wt% and 28wt% are not mentioned in Fig. 8; 9 due to their higher viscosity. The electrospinning with this higher concentration was not able, these high viscosity solutions were suitable only for drawing technique as described later.

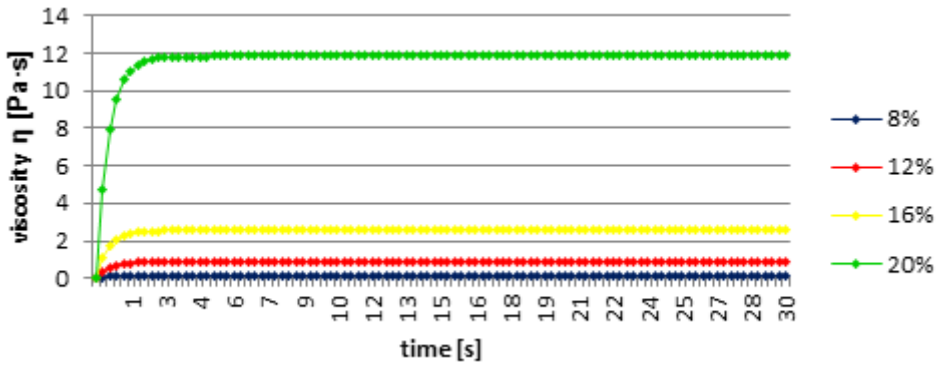

Figure 8. Viscosity of PVA at constant shear rate 300 s^{-1}

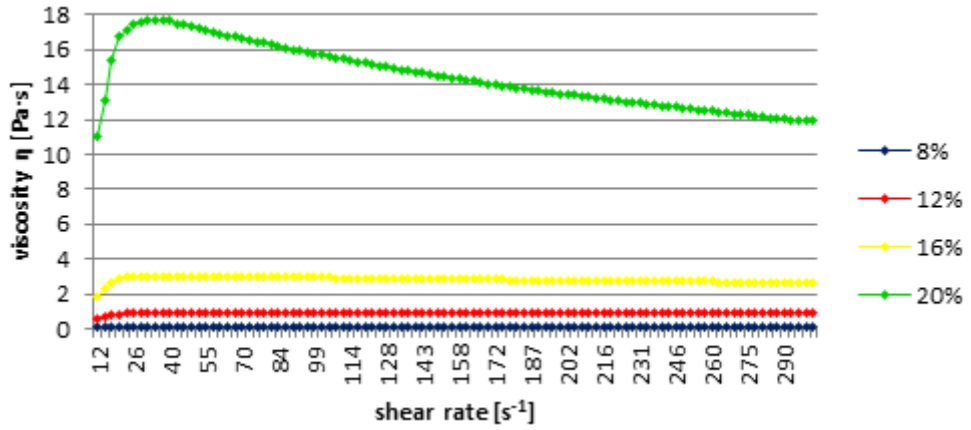

Figure 9. Viscosity of PVA at linearly increasing shear rate 10-300 s^{-1}

Table 2. Spinnability of PVA solutions using spinning technologies and their corresponding fiber diameter median ± standard deviation.

	8 wt%	12 wt%	16 wt%	20 wt%	24 wt%	28 wt%
Centrifugal spinning	x	409 ± 168 nm	338 ± 139 nm	474 ± 411 nm	4670 ± 4265 nm	X
Electro-centrifugal spinning	391 ± 194 nm	361 ± 177 nm	519 ± 221 nm	1002 ± 697 nm	2275 ± 2482 nm	2804 ± 2483 nm
Centrifugal spinning - Rod	393 ± 150 nm	572 ± 211 nm	915 ± 258 nm	2212 ± 1069 nm	X	X
Drawing	x	x	X	1093 ± 236 nm	1777 ± 648 nm	1895 ± 763 nm
Electrospinning from the rod	145 ± 57 nm	279 ± 63 nm	321 ± 102 nm	725 ± 256 nm	X	X
Electrospinning from the needle	155 ± 45 nm	318 ± 68 nm	442 ± 71 nm	795 ± 151 nm	X	X
Bubble spinning	177 ± 42 nm	302 ± 74 nm	413 ± 75 nm	692 ± 107 nm	962 ± 254 nm	X
Needle-less electrospinning	239 ± 79 nm	423 ± 75 nm	450 ± 155 nm	X	X	X
AC spinning	174 ± 73 nm	310 ± 168 nm	502 ± 126 nm	878 ± 470 nm	2734 ± 1109 nm	X

Spinnability of the polymers is summarized in the Table 2, where resulting fiber diameter characteristics are displayed. It is seen that fiber diameter is increasing with polymeric content within the spinning solution. Different technologies require various parameters of solution properties. For example drawing is able to create fibers from highly viscose solution of 20 wt% and higher. On the other hand, needle less electrospinning was possible to carry out from low viscose solution ranging from 8 to 16 wt%. Electro centrifugal spinning was the most versatile technique since all tested concentrations were electro spun.

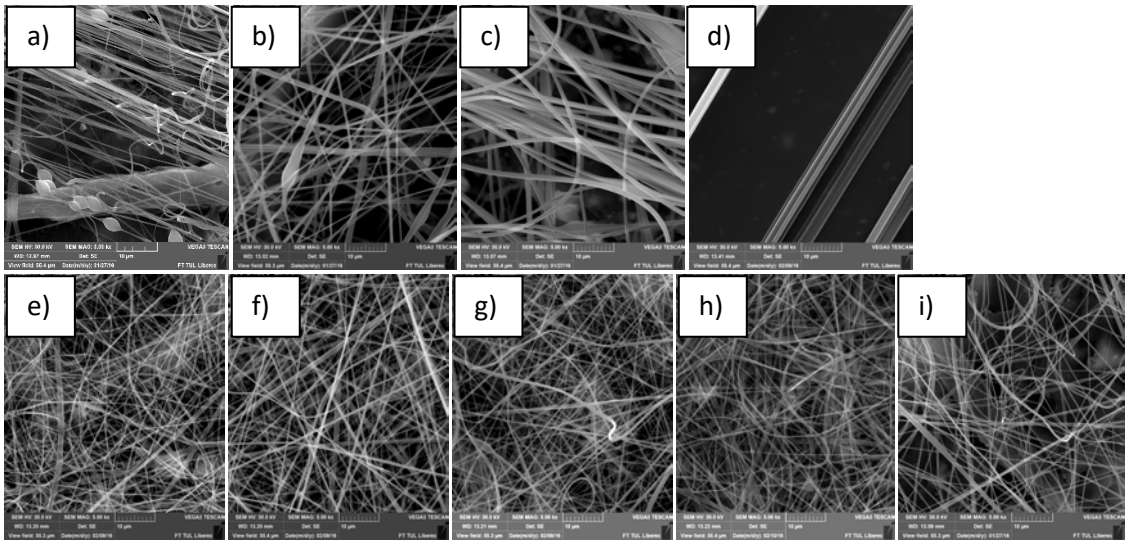

Figure 10: Morphology of the PVA fibers spun from 16 wt% solution (except of drawing technology where 24 wt% solution was used) using centrifugal spinning (a), electro-centrifugal spinning (b), centrifugal spinning with rod collector (c), drawing (d), electrospinning from the rod (e), electrospinning from the needle (f), bubble spinning (g), needle-less electrospinning (h) an AC spinning (i), scale bars 10 µm.

The resulting fibers were analyzed by SEM followed by fiber diameter measurement. Box plot of fiber diameter distribution of 16 wt% is depicted in Figure 11 showing that centrifugal spinning led to the fibers with high range distribution of fiber diameters whereas electrospinning from the rod, needle or bubble spinning possess homogeneous fibrous mats as seen also from SEM pictures in Figure 10.

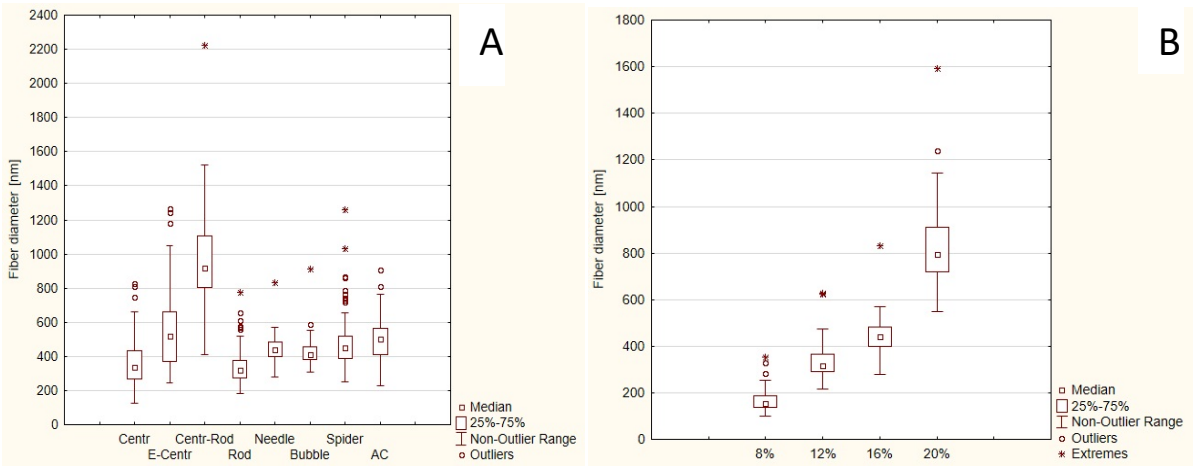

Figure 11: Box plot of fiber diameters obtained by spinning of 16 wt% PVA (A) using centrifugal spinning (Centr), electro-centrifugal spinning (E-Centr), centrifugal spinning with rod collector (Centr-Rod), electrospinning from the rod (Rod), electrospinning from the needle (Needle), bubble spinning (Bubble), needle-less electrospinning (Spider) an AC spinning (AC); box plot of fiber diameter distribution of increasing PVA concentrations and their respective fiber diameter obtained by needle electrospinning (B).

The voltage used during electrospinning process play a crucial role for fibers formation and their diameter. The most important factor that has to be considered is the electric intensity which is connected with geometry of spinnerets. This article compares various spinning processes therefore it is not possible to set common spinneret and stable voltage or distance. Considering these facts, spinning parameters were described for each spinning technology separately.

4. CONCLUSIONS

The polymer concentration and spinning conditions play important role in formation of fibrous mats and their morphology. The article was focused on introduction of variety of accessible spinning technologies that allow production of micro- and nanofibers. The concentrations of 12 wt%, 16 wt% and 20 wt% are the most common for electrospinning and spinning in general. The highest concentration of PVA (28 wt%) was capable of sinning using only electro centrifugal spinning and drawing. These methods are using mechanical capillary forces for elongation the polymer solution therefore highly viscose polymer solutions were able to spin. On the other hand, low concentration of 8 wt% was not spin able by centrifugal and drawing techniques. The low viscosity polymer solutions don not allow creation of fibrous structures using these methods. The concentrations of 12 wt%, 16 wt%, and 20 wt% were spinned by majority of technologies except drawing and needleless electrospinning.

ACKNOWLEDGEMENTS

This research was supported by the project "Nanofiber materials for tissue engineering", reg. No. CZ.1.05/3.1.00/14.0308, which is co-financed by the European Social Fund and the state budget of the Czech Republic.

References

1. *Amrinder S. Nain, Joanna C. Wong, etc.: Drawing suspended polymer Micro/nanofibers using glass micropipettes, Applied Physics Letters, vol.89, no.18, pp.183105-7, (2006)*
2. *Bhardwaj,N., Kundu, S., C., Electrospinning: A fascinating fiber fabrication technique, Biotechnology Advances, Vol. 28, No. 3, s. 325–347.(2010)*
3. *Chen, Rou-Xi; LI, Ya and He, J. Mini-review on Bubbfil spinning process for mass-production of nanofibers. Matéria (Rio J.) [online]. 2014, vol.19, n.4 [cited 2016-06-14], pp.325-343.Availablefrom: <http://www.scielo.br/scielo.php?script=sci_arttext&pid=S1517-70762014000400325&lng=en&nrm=iso>.ISSN1517-076. http://dx.doi.org/10.1590/S1517-70762014000400002.*
4. *Hu, X., Lui, S., Zhou, G., Huang, Y., Xie, Z., Jing, X., Electrospinning of polymeric nanofibers for drug delivery applications. Journal of Controlled Release. Vol. 165, s. 12-21.(2014)*
5. *Lukáš, D., Sarkar, A., Martinova, L., Vodseďalkova, K., Lubasová. D., at.al Physical principles of electrospinning (Electrospinning as a nano-scale technology of the twenty-first century), Textile Progress, Vol. 41, No. 2, s. 59-140., (2009),*
6. *Mohamed H. El-Newehy, Salem S. Al-Deyab, El-Refaie Kenawy, and Ahmed Abdel-Megeed, "Fabrication of Electrospun Antimicrobial Nanofibers Containing Metronidazole Using Nanospider Technology," Fibers And Polymers, vol. 13, no. 6, pp. 709–717, (2012).*
7. *Pokorny, P.; Kostakova, E.; Sanetrnik, F.; et al.:Effective AC needleless and collectorless electrospinning for yarn production,PHYSICAL CHEMISTRY CHEMICAL PHYSICS, Volume: 16 Issue: 48 Pages: 26816-26822 Published: (2014)*
8. *Sill, T., Recum, H. A., Electrospinning: Applictions in Drug Delivery and Tissue Engineering. Biomaterials. Vol. 29, No 13, s. 1989-2006.(2008)*

9. *Zhang, X., Yao L.: Centrifugal Spinning: An Alternative Approach to Fabricate Nanofibers at High Speed and Low Cost. Polymer Reviews [online]. (2014),* ***54****(4): 677-701 [cit. 2015-09-18]. DOI: 10.1080/15583724.2014.935858. ISSN 1558-3724. Dostupné z: http://www.tandfonline.com/doi/abs/10.1080/15583724.2014.935858*

FUNCTIONAL CHARACTERISTIC EVALUATION OF 3-DIMENSIONAL KNITTED SPACER FABRICS

Veerakumar Arumugam*, Rajesh Mishra, Jana Salacova, Mohanapriya Venkatraman, Dana Kremenakova, Hafsa Jamshaid, Tao Yang, Xiaoman Xiong, Kasthuri Venkatesh, Jiri Militky

Dept. of Materials Engineering, Technical University of Liberec, Liberec, Czech Republic 461 17
(Email: veerakumar27@gmail.com, arumugam.veerakumar@gmail.com)

Abstract:

Nowadays, the utilization of 3-Dimensional (3D) porous textile materials by the civil and mechanical engineers for improved acoustical environment and shear behavior during composite forming has widened the research scope. Since spacer textile fabrics have superior functional characteristics such as acoustical, thermal and shear characteristics compared to conventional woven/knitted structures or nonwovens due to their wonderful 3D sandwich pattern and porous nature. Hence this research paper presents an experimental evaluation on the sound absorption behavior and in-plane properties of 3D knitted spacer fabrics. The Sound absorption coefficient (SAC) was measured using two microphone impedance tube. Moreover, tortuosity of the spacer fabrics was carefully calculated analytically and compared with experimental results. This study deeply discusses the influence of material parameters and characteristics on acoustical properties of 3D spacer knitted fabrics. The results show that the fabric surface property, porosity, flow resistivity and tortuosity have significant effects on the sound absorbability. Also, a fixture was designed to analyze the intra-ply shear properties of these fabrics. The nonlinear behavior of shear force versus shear angle and the deformation mechanism were analyzed. The curves for shear force versus shear angle and position of buckling for intra-ply shear test are recorded. Load–displacement curves of intra-ply shear tests are also analyzed. In addition to this, a program was developed in MATLAB using Hough transform to analyze the shear angle in the real-time image taken during displacement of specimen at various positions. These findings are important requirement for the further improvements in designing of picture frame fixture and to study the in-plane shear properties of 3D fabrics.

Key words:

Sound Absorption, 3D Spacer knitted fabrics, Shear, Tortuosity, Porosity, Acoustic property.

1. Introduction

Due to new emerging textile material of this decade, only very few researchers are evaluated and analyzed the advance characteristics of spacer fabrics. Here those literatures are presented with advantages and limitations of spacer fabrics. Spacers knitted fabrics are known to possess excellent comfort properties. They not only allow for stretching and ease of movement, but they also have relatively good hand related characteristics and facilitate the easy transmission of water vapor from the body. These attributes make knitted fabrics the commonly preferred choice for sportswear, casual wear and underwear. Due to technological development and increases in demand of 3D knitted fabrics, many researchers carry out work on various technical applications. 3D knitted spacer fabrics are like a sandwich, consisting of two complementary fabrics with a third layer tucked in between [8]. These fabrics are produced with different thicknesses and can be used in thermal insulation applications because of their higher thickness compared to woven and knitted fabrics. These are lightweight and breathable structures. They have good physiological and thermal comfort. They transport moisture easily; their air permeability and water vapor permeability values are high. Their compression characteristic is also better than conventional textile structures. Compression resilience is an important attribute of spacer fabrics, which is related to sensation of mechanical comfort. Modern

consumers consider compression as one of the most important attributes in the comfort sensation such as hand of clothing material. Fabric thickness and compressibility have a linear relationship with thermal conductivity. Compression characteristic of knitted fabrics has been studied by various researchers [1]. Postle indicated that bulk density or compression property of knitted structures is related to the effective diameter of the yarn inside of the fabric and also to the fabric thickness [2]. Xu-hong and Ming-qiao analyzed the stress-strain behavior of warp knitted spacer fabrics when compressed [3]. Mecit Armakan and Roye investigated the compression characteristic of warp knitted spacer fabrics on the basis of spacer yarns in their structure. They noted that, the material, pattern and threading of the spacer yarns have significant effect on compression characteristic of the fabrics. It was also observed that the location angle and the amount of the spacer yarns influence the compression behaviour of fabrics [4]. Yip and Ng found that warp knit spacer fabrics have a lower thermal conductivity rating than the weft knit fabrics, which means the excess heat from the body would not be quickly transferred if a warp knit spacer fabric is being utilized as compared to a weft knit fabric [5].

Shear properties influence draping, flexibility and also the handle of fabric. Shear properties are important not only for standard fabrics but for textile reinforced composites preforming as well. Automated manufacturing of textile composite shell-like products typically requires draping of dry or pre-impregnated textile sheets. Large local deformations occur in the textile sheet in order to adapt to the curved shape [6]. These deformations affect the local fiber directions, volume fractions, and thickness. Several factors together with the consolidation level and the occurrence of flaws (e.g. wrinkling and tearing) determine the product quality. Simulation tools that link product quality to material, mold and process parameters are being developed to support design and process optimization [7]. Three dimensional (3D) textile structural composites provide excellent strength through thickness, outstanding damage tolerance and good impact and fatigue resistance. As one type of the 3D textile structural reinforcements for composites, the 3D spacer fabric has been widely used in engineering field owing to its easy and efficient processing in warp and weft knitting. In addition, the most attractive advantage of spacer fabric is the three dimensional shape forming capacity to manufacture composites. The 3D spacer fabric preforms have excellent mechanical properties and good formability. With the development of the preforming technology, complex shape and different size of the structural parts can be produced. In the structure integrated manufacture of composites, the 3D spacer fabric is preformed according to the shape of the final composite that can be complex [8]. The in-plane behavior and the inter-laminar behavior are the most important deformations in 3D fabrics, and also shear behavior predominates the deformation mode of the material [9]. It is necessary to study the inter/intra-ply shear behavior of 3D fabric because of their wide application in production especially in the case of forming process. Dial et al. introduced fabric with spacer structure to improve sound absorption performances. Their studies analyzed and reported that acoustic performance of plain weft knitted spacer is good in middle and high frequency range . Liu and Hu analyzed and compared the effects of different fabric layers and arrangement sequences of both warp and weft knitted spacer fabrics on the noise absorption coefficient. They suggested that sound absorption behavior of spacer fabrics are effective with multilayer arrangements backed up with air cavity. There is only few research studies conducted on acoustic performance of spacer fabrics. The lack of comprehensive studies on the functional characteristics especially on thermo-physiological, mechanical and properties of weft knitted 3D spacer fabrics are sound basis for this research. So, this paper deeply discusses the advance characteristics of knitted spacer fabrics such as thermal, in-plane shear and sound absorption behavior.

2. Experimental

2.1. Materials

The six spacer fabric samples were classified into two groups for convenient analysis of results, the first group has been developed using Polyester/Polypropylene blend with three different proportions and second group with Polyester/Polypropylene/Lycra blend having another 3 different compositions.

Table 1. Fabric particulars.

Fabric sample No.	Fabric layers	Technical face	Spacer yarn	Technical back	Fiber composition (%)
Group 1 - Without Lycra					
S1	Type of yarns and linear density	Polypropylene (PP) - 14.5 tex	Polyester monofilament (PES) - 88 dtex	Polypropylene (PP) -14.5 tex	58% PP, 42% PES monofilament
S2		Polypropylene (PP)- 14.5 tex	Polyester (PES) - 14.5 tex	Polypropylene (PP) -14.5 tex	45% PP, 55% PES
S3		Polypropylene (PP) - 14.5 tex	Polyester (PES) - 167 dtex	Polypropylene (PP) -14.5 tex	41%PP, 59% PES
Group 2- With Lycra					
S4	Type of yarns and linear density	Polypropylene (PP)- 14.5 tex Lycra - 44dtex	Polyester monofilament (PES) - 88 dtex	Polypropylene (PP) -14.5 tex	55%PP, 39%PES monofilament, 6% Lycra
S5		Polypropylene (PP)- 14.5 tex Lycra - 44dtex	Polyester (PES) - 14.5 tex	Polypropylene (PP) -14.5 tex	42% PP, 52% PES, 6% Lycra
S6		Polypropylene (PP)- 14.5 tex and Lycra - 44dtex	Polyester (PES) - 167 dtex	Polypropylene (PP) -14.5 tex	39% PP, 55% PES, 6% Lycra

As a spacer yarn, three different types of 88 dtex Polyester monofilament yarn and Polyester multifilament yarns (167 dtex and 14.5 tex) were used. 14.5 tex Polypropylene and 44 dtex multifilament yarns with Lycra were also used for the face and back side of the spacer fabrics.

2.2. Methods

The Structural properties including the yarn linear density and fabric weights per unit area were determined according to ASTM D1059 standard using electronic weighing scales. The thickness of the fabrics was measured according to ASTM D1777-96 standard with the SDL digital thickness gauge at a pressure of 100 Pa. Air flow resistance of spacer fabric was calculated from air permeability value obtained from Textest FX-3300 air permeability tester. The Stitch density was calculated from wales per centimeter (WPC) and course per centimeter (CPC) with the help of optical microscope. Porosity, H, was calculated with bulk density of spacer fabrics and weighted average absolute density of fibres in the spacer fabric, expressed in kg/m^3. These results are shown in Table 2.

2.2.1. In-plane shear

The picture frame is an effective way for characterizing intra-ply (in-plane) shear property of fabrics. The 3D spacer fabrics for shear tests were prepared according to the size of the picture frame and the characteristics of samples. Shear tests were conducted on a TIRA - universal tensile testing machine with a crosshead speed of 10 mm/min. The test was conducted for 5 samples of each type under the same conditions [5].

Direct measurement of axial load and shear angle is possible through this following relationship.

$$F_s = \frac{F_x}{2cos\varphi} \qquad (1)$$

Shear force (F_s) is determined by the axial force (F_x) frame rig length (L) and the frame angle (φ). Meanwhile frame angle can be determined directly from cross head displacement (d). Shear angle (γ) can be obtained from frame angle by using the following equations 2 and 3.

$$\varphi = \cos^{-1}\left[\frac{L\sqrt{2}+d}{2L}\right] \quad (2)$$

$$\gamma = \frac{\pi}{2} - 2\varphi \quad (3)$$

In this research, the impedance tube method was used to determine the normal incident sound absorption coefficient, SAC (α). A minimum of three specimens for each sample were tested according to ASTM E 1050-07. Standard test method for impedance and absorption of acoustic materials using a tube with two microphones and a digital frequency analysis system was used.

Table 2. Spacer Fabric characteristics

Samples	Areal Density (g.m^{-2})				Thickness (mm)				Density (kg.m^{-3})	Stitch Density (Stitches/cm^2)			
	Mean	ME	LL	UL	Mean	ME	LL	UL		Mean	ME	LL	UL
S1	493.00	0.16	492.84	493.16	4.40	0.88	3.52	5.28	112.00	200.00	0.10	199.90	200.10
S2	443.00	0.12	442.88	443.12	2.62	1.10	1.52	3.72	169.10	150.00	0.04	149.96	150.04
S3	477.00	0.20	476.80	477.20	2.74	0.61	2.13	3.35	174.10	150.00	0.12	149.88	150.12
S4	632.00	0.10	631.90	632.10	4.40	0.55	3.85	4.95	144.80	350.00	0.06	349.94	350.06
S5	657.00	0.12	656.88	657.12	3.50	0.86	2.64	4.36	187.70	280.00	0.10	279.90	280.10
S6	695.00	0.22	694.78	695.22	3.40	0.45	2.95	3.85	205.40	280.00	0.10	279.90	280.10

2.2.2. Thermal properties

Air permeability tests were performed according to standard ISO 9237 using a Textest FX-3300 air permeability tester. Thermal conductivity measurements were performed using C-Therm Thermal Conductivity Analyzer Tci. The standard test method EN 61326-2-4:2006 was used for this testing using TCi. This test was performed under room temperature. The results are reported in figures.

2.2.3. Measurement of sound absorption coefficient

In this research, the impedance tube method was used to determine the normal incident sound absorption coefficient, SAC (α). A minimum of three specimens for each sample were tested according to ASTM E 1050-07. Standard test method for impedance and absorption of acoustic materials using a tube with two microphones and a digital frequency analysis system was used (Figure 6).

2.2.4. Calculation of NRC (noise reduction coefficient)

The "Noise Reduction Coefficient" (NRC) is a measure of how much sound is absorbed by a particular material, and is derived from the measured Sound Absorption Coefficients. The NRC was determined using the following formula (eqn. 4) [10].

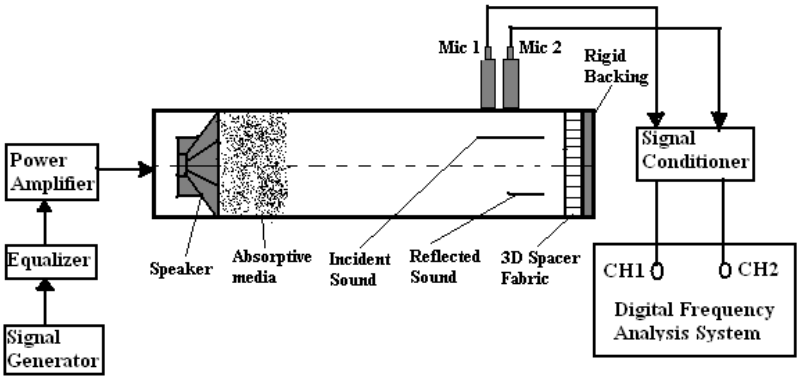

Figure 6. Impedance tube method (ASTM E 1050-08 and Bruel & Kjaer, 2009)

$$NRC = \frac{\alpha_{250Hz} + \alpha_{500Hz} + \alpha_{1000Hz} + \alpha_{2000Hz}}{4} \quad (4)$$

3. Results and discussion

3.1. In-plane shear properties-comparitive discussion

The shear angles are calculated by considering sample length as a substitute for L in Equation 2 and it is further used for calculation of shear force. Figure 1 shows the comparison of shear angles between image analysis and experimental measurements for all six specimens. The differences between image analysis and calculated shear angle using sample length at the chosen points are relatively small. Less than 8% CV was obtained in all measurements. It does not show any significant difference until pre-buckling occurs (upto 20 mm displacement) but significant difference is observed after 20 mm displacement. It is also believed that during image processing in MATLAB, detection of X and Y coordinates on the image is not accurate due to wrinkling in the central zone of samples. Also, it is noted that dimension of the frame and rig length can cause big difference in shear angle. Further study is required on the effect of different frame rig length and ratio of frame length to specimen size on in-plane shear behavior of 3D spacer fabrics.

3.2. Effect of density and air permeability on thermal properties

This study found that spacer fabrics with lower density and higher air permeability exhibit relatively lower thermal conductivity for both the group of samples As shown in Figure 2. Also denser fabric has better thermal conductivity. It is also found that the spacer fabrics composed of monofilament spacer yarn (S1 & S4) have higher capacity to resist conduction of heat as compared to fabrics with multifilament spacer yarn (S2, S3 & S5, S6). It is mainly because monofilament spacer yarns make the fabric more bulky with lower density which offers more space to entrap air between the face and back layer. A remarkable difference between the heat transfer rates of group 1 and 2 fabrics are also justified here. It is also observed that fabrics made up of 6% of lycra yarn in the face layers (S4, S5 & S6) have lower thermal conductivity value than group 1 samples without lycra (S1, S2 & S3). The air trapped within the fabric structure starts to circulate and that's why the heat transfer rate of Group 2 is lower than that of Group 1. Due to higher stitch density and lycra based filament yarns on the surface

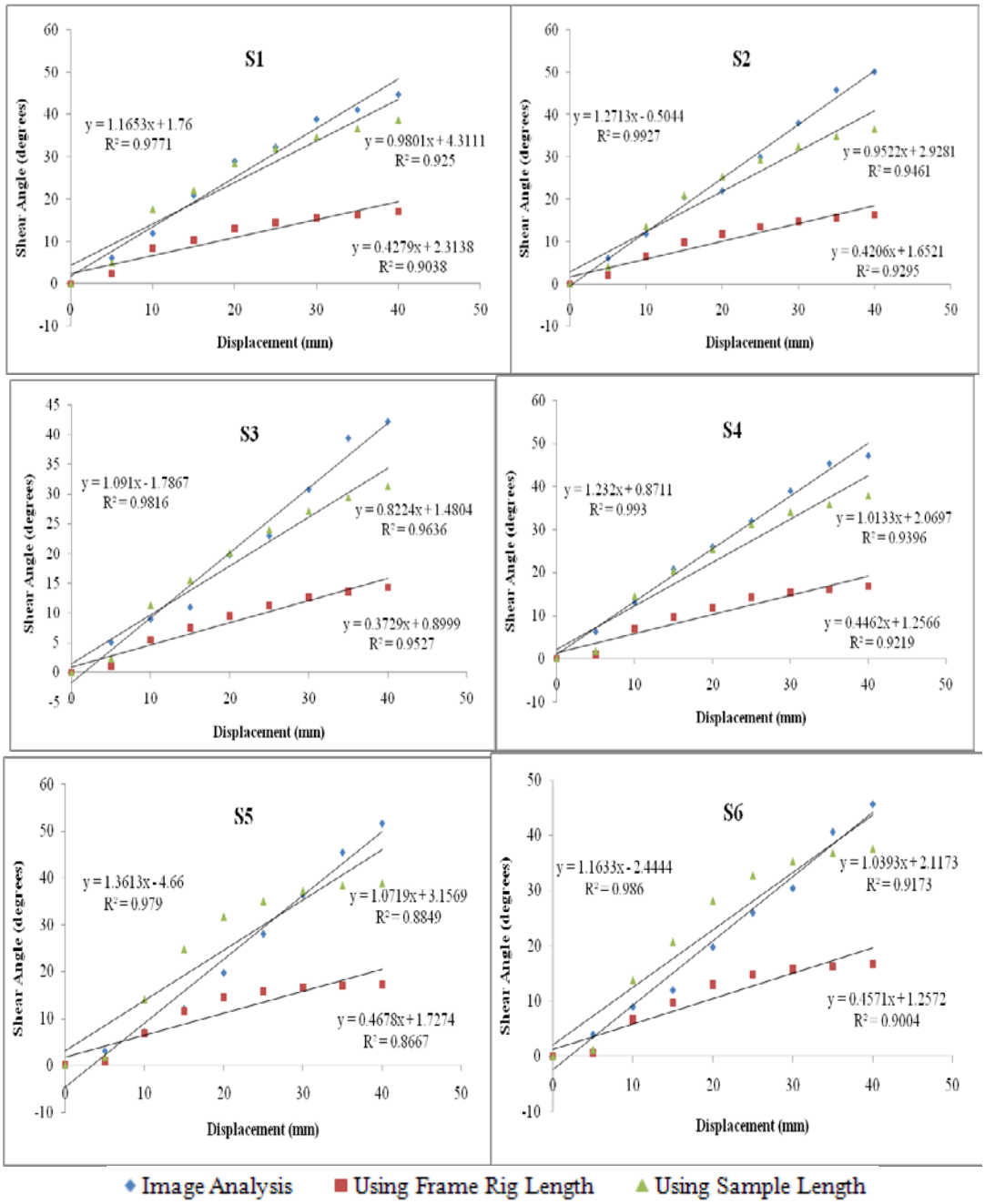

Figure 1. Comparison of shear behavior of samples using different methods.

layers, these spacer fabrics have lower air permeability value and consequently a lower thermal conductivity. The thickness is also a significant factor which influences the thermal resistance of spacer fabrics, higher thickness leads to higher thermal resistance.

Fabrics with a lower value of thermal effusivity give us a ‘‘warm’’ feeling as shown in Figure 2. 3D spacer fabrics have a much lower value of thermal absorption, so they give us warmer feeling than other commercial 2D fabrics, which are not ideal for summer clothes [8]. Thermal effusivity is a very important parameter from the point of view of thermal insulation; it is directly proportional to the fabric density and inversely proportional to air permeability. Due to increase in density between the samples S1 to S3 and S4 to S6, one can observe the increase in thermal effusivity value (Figure 2), and in contrast effusivity decreases as air permeability increases. So spacer fabrics with lower thermal conductivity and effusivity is perfect option for some special climate sportswear.

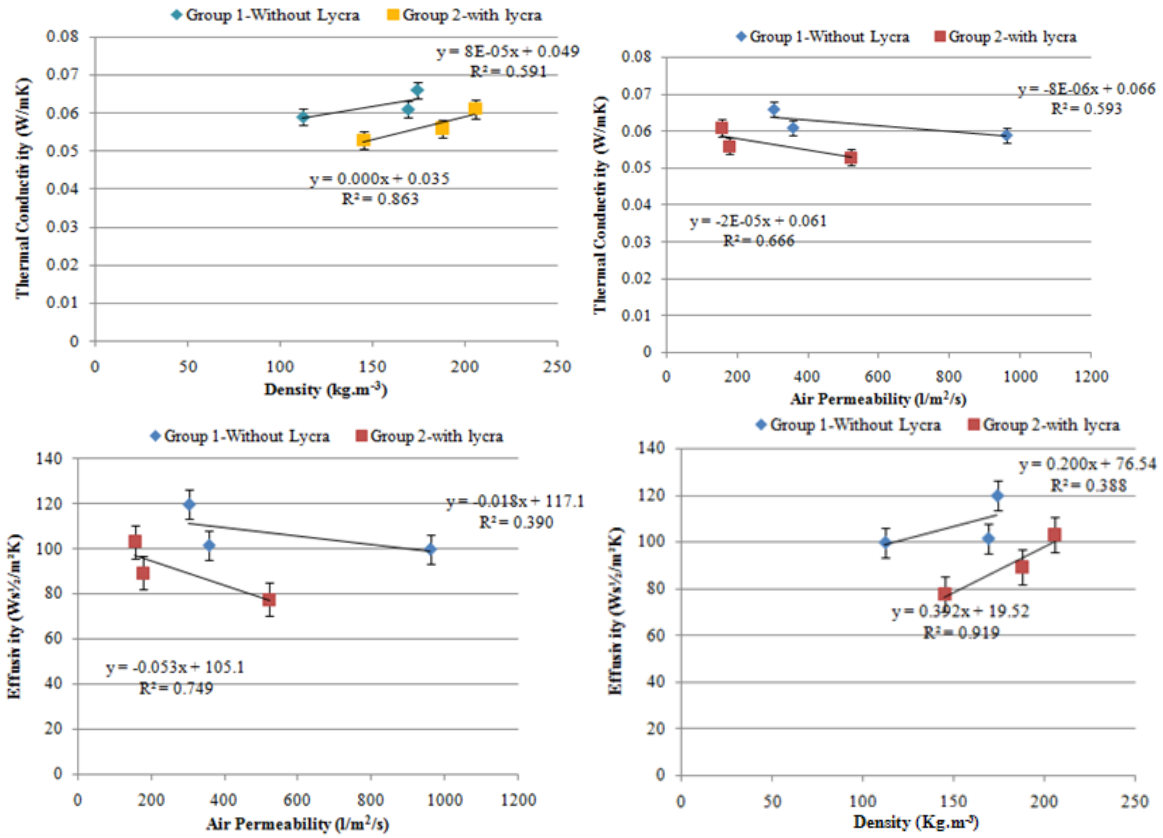

Figure 2. Influence of density and air permeability on thermal conductivity and thermal effusivity

3.3 Influence of material characteristics on sound absorption coefficient

For the range of considered porosity, the influence on the sound absorption is complicated. When porosity increases from 85 to 90 % for group 1 samples, the changes on sound absorption is insignificant for low freqency range (50 Hz to 2000 Hz). But for frequency range above 2000 Hz, the absorption coefficient decreases drastically when the porosity increases to 90%. This is mainly because of too much space between the two layers in spacer fabrics which entraps excess of air, hence, the sound energy dissipation is substantially weaken, especially when the porosity is higher than 90%. In case of group 2 samples with porosity (83 to 87%), there is signicant sound absorption both in low and high frequency ranges. In case of spacer fabric samples with monofilament (S1), the sound absorption is comparitively lower than samples with multifilaments (S2 and S3) because of higher porosity. In contrast, the trend is reversed for group 2 samples, S4 shows higher sound absorption than S5 and S6, though the porosity is higer (87%) for S4. This is mainly because of surface roughness and stitch density of the spacer fabrics which causes sound waves to reflect more on the surface itself. Variations of porosity in the range of 2 or 3 % have minor influence on the acoustic behavior of spacer fabrics (Figure 3).

As can be seen, sound absorption coefficient increases with decrease in the tortuosity values for both the group of samples (S1 to S6) for middle and high frequency ranges. At higher values of the tortuosity, the behavior shifts towards lower values of sound absorption. The thickness of the porous material layer has a great influence on the position of the peak value in the frequency spectrum. The sound absorbency of spacer fabrics increases with the reduction in its porosity for group 1 samples (S1 to S3) but the trend is reversed in case of group 2 samples (S4 to S6). This may be because of tortuous path in the middle layer and closeness of surface yarns in case of 3-dimensional knitted spacer fabrics.

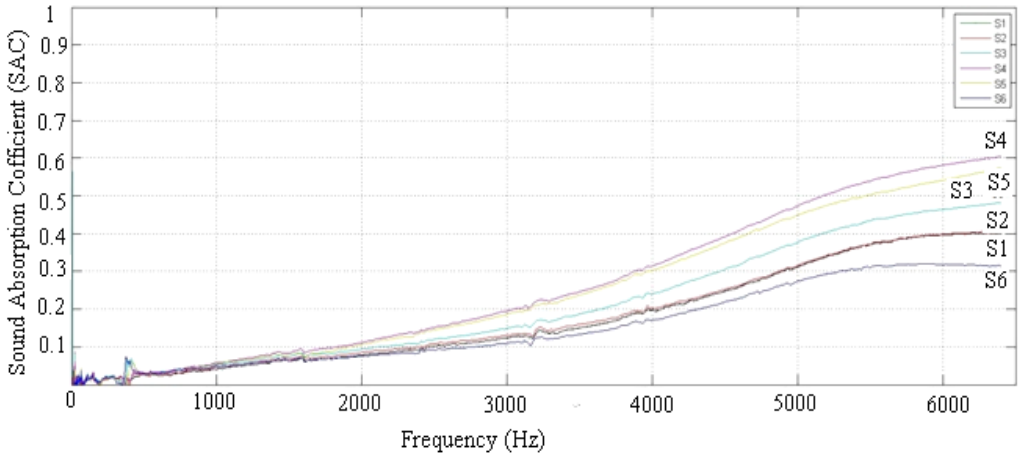

Figure 3. Sound absorption coefficient of spacer knitted fabrics.

4. CONCLUSIONS

In knitted spacer fabrics, It is found that shear deformations depend very much on the type of spacer yarn and the fabric stitch density The shear angles of samples using different methods are almost identical to each other before shear locking (buckling) effect takes place. The non-linearity of shear deformation increases after limiting locking angle which initiates the buckling of the sample. The 3D spacer fabrics have more tortuous path but still lower sound absorption because incident sound energy may get reflected away from the top layer and does not penetrate in to the fabric. The thickness of the porous material layer has also a great influence on the position of the peak value in the frequency spectrum. But the effect of density is more predominant in terms of sound absorbency as compared to effect of thickness.

References

1. *Liu, Y., Hu, H., (2011). Compression Property and Air Permeability of Weft-Knitted Spacer Fabrics. Journal of the Textile Institute, 102(4), 366-372.*
2. *Postle, R., (1974). A geometrical assessment of the thickness and bulk density of weft knitted fabrics, Journal of the Textile Institute, 65 (4), 155-163.*
3. *Xu-hong, M., and Ming-qiao, G, (2009). The compression behaviour of warp knitted spacer fabric, Fibers and Textiles in Eastern Europe, 16 (1), 90-92.*
4. *Mecit Armakan, D., and Roye, A., (2009). A study on the compression behaviour of spacer fabrics designed for concrete applications, Fibers and Polymers, 10 (1), 116-123.*
5. *Yip, J., and Ng, S., (2008). Study of three-dimensional spacer fabrics: Physical and mechanical properties. Journal of Material Processing Technology, 206 (1-3), 359-64.*
6. *Liu, Y. et al. (2006). Dynamic Response of 3D Biaxial Spacer Weft-Knitted Composite Under Transverse Impact. Journal of Reinforced Plastics and Composites, 25(15), 1629-1641.*
7. *Liu, Y. et al. (2008) Compression Behavior of Warp-Knitted Spacer Fabrics for Cushioning Applications. Textile Research Journal, 82(1), 11-20.*
8. *Walker, K. et al. (2008). Active Protection System. In: Advanced materials and processes, 166(9), 36-37.*
9. *Charmetant, A. et al. (2012). Hyper elastic Model for Large Deformation Analyses Of 3D Interlock Composite Preforms. Composite Science and Technology, 72, 1352–1360.*
10. *Arumugam, V. et al. (2015). Thermo - acoustic Behavior of 3D Knitted Spacer Fabrics. Fibers and Polymers, 16(11), 2467-2476.*

PERFORMANCE CHARACTERIZATION OF BASALT HYBRID WOVEN FABRIC REINFORCED CONCERETE

Hafsa Jamshaid [a,b], Rajesh Mishra[a], Jiri Militky[a] , Muhammad Tayyab Noman[a], Mohanapriya Venkataraman[a], Veerakumar Arumugam[a], Tao Yang[a], Xiaoman Xiong[a]

a. Department of Material Engineering, Faculty of Textile Engineering Liberec, Technical University of Liberec, Czech Republic

b. Department of Fabric Manufacturing, Faculty of Textile Engineering, National Textile University, Faisalabad, Pakistan

Abstract:

In this work structural performance and durability of Textile reinforced concrete (TRC) is investigated. The aim of this work is to understand the bonding charetrictics between different yarns and concrete that was studied by yarn pull out test. Impact of accelerated ageing under alkaline environment on basalt, polypropylene, polyester and jute are studied. The present study provides information about durability of different fiber-reinforced cement composites which can be forecast by fiber/cement bonds and accelerated aging conditions. It helps in better insight into the specific material behavior of the concrete with textile reinforcement

Key words:

TRC, basalt yarn pull out, durability, textile reinforcement, woven structures

1. Introduction

The structural materials most often used in civil engineering are concrete and steel. It is noteworthy that concrete material is more brittle than other materials and have inherent disadvantages including low tensile strength and weakness in impact resistance. Besides, this the concrete materials are easy to crack because of the shrinkage of the materials and the concentration of stress [1–5]. Thus, plain concrete is not applicable if significant tensile loading cannot be ruled out in advance, as it is the case in arch structures or short columns where predominantly compressive loading comes into picture. Usage with steel, it has also some limitations in terms of weight, thick concrete convers and more importantly resistance against corrosion of reinforcement.As a result, the structures begin to suffer degradation after a period of using time. How to use structures safely has become a major concerned issue in the development of sustainable engineering structures

In the 1950s, textile -reinforced concrete gained the interest due to evolution of the concept of composite materials. There are many researches about the properties of TRC. A number of previous studies have shown that the introduction of fibers increases the mechanical strength of the concrete[6-8] A combination of non-corrosive fiber grid along with finely grained concrete formulates Textile reinforced concrete (TRC). It can be catagorically defined as a combination of fiber/yarn structure, cementitious matrix and fiber/matrix interface. The presence of fibers also lowers the number and the width of cracks in the concrete due to the bridge action of them[6].As soon as the health risks associated with asbestos were found, an urge to find a replacement for building materials was raised and generated. By the 1960s, materials for reinforcement of concrete were Glass, Steel and Synthetic fibers such as Polypropylene. Extensive research work is carried out to find out new fiber-reinforced concretes [9-10]. Variety of fibers were used to increase toughness and prevent cracking of cement. Sustainable, energy efficient and eco-friendly construction material is

sought around the world. Sustainable, green construction material, natural fiber based reinforcement in a cement matrix is a feasible approach.

If fibers are exposed to aggressive environments, durability could become an issue. High concentration of alkali ions present in civil applications of concrete can be main reason of fiber damage. Reduction in mechanical properties and weight loss can be consequent outcomes of exposure to alkali ions. Different studies are quoted in the technical literature, yet the results reported show a contrast in them. As a matter of fact, TRC-based research reveals multi-promising attributes, recognition of them still needs to reach a conclusion due to absence of standard & long term behavior and lack of availability of design tools.

Basalt fibers are very promising materials due to their fire resistance ,superior mechanical properties and relatively low cost. On the other hand, being a relatively new kind of fiber, its in depth study is yet to be done. There are very few indications in technical papers about their behavior after aging treatments. The current study investigates the possibility of using basalt with other types of yarns on load bearing capacity and durability. In the present work, the load-bearing behavior of Textile Reinforced Concrete (TRC), which is a composite of a fine-grained concrete matrix and a reinforcement of high-performance fibers processed to textiles, when exposed to uniaxial tensile loading was investigated. When textile yarns are embedded in concrete, they are not entirely impregnated with cementitious matrix, which leads to associated heterogeneity of the concrete and the yarns to a complex load-bearing and failure behavior of the composite system. The main objective of the work is the investigation of hybridization effects in the load-bearing behavior of TRC. The scope and target of this work was to investigate durability and structural performance of TRC in order to evaluate its usage for civil applications

2. Experimental

2.1. Materials

The materials used are polyester(PET),Polypropylene PP and jute(J) yarns used in this study were available commercially. The basalt(B) yarn was used as received from company Kamenny Vek (KV) (Russia).

A commercial ordinary Portland cement (OPC) was used and green cement (GEOPOLYMER BAUCIS L110) produced by České lupkové závody, a.s was taken.The alkalis used for accelerated aging treatment are analytical grade NaOH (sodium hydroxide, Lach:ner.s.r.o) and $Ca(OH)_2$ (Calcium hydroxide LACHMEMA.N.P.Brno)

2.2. Methods

2.21 Preparation of Cement Matrix

The OPC pastes were prepared by mixing the cement with distilled water, in water to cement ratio of water/cement (w/c) ratio of 0.4. The samples were thoroughly mixed using glass rod for two minutes and then samples were subsequently cast in the molds with yarn in it. After 1 day, the samples were removed from the molds and after 2 days testing was done.Preparation of geopolymer(GPC) mixture is typically done with 5 parts by weight of cement and 4 parts by weight of alkali (NaOH).

2.22 Yarn pull out test

The pull-out test primarily gives information on the compatibility/interfacial behavior between the yarns selected for the reinforcement and the cement matrix. From this test, estimates can be derived for the failure behavior, and thus for the durability and load bearing capacity The pull-out tests encompassed the evaluation of both pull-out and rupture of the textile material as failure modes.

So strand/yarn in cement test, is used to quantitatively analyze this test. The yarn specimens were embedded into cement slab of 40x40x10 mm. The yarn is precisely placed in the center of the

specimen. The yarn lengths have to be set so as to ensure protruding ends, for mounting in a tensile tester. It is important to protect the protruding yarn ends from the exposure to avoid strength losses. The specimens were demolded after 48 h and then dried again for 48 h at room temperature. Five specimens were produced for each yarn in order to obtain a representative trend of the pull-out behavior.

The yarn was pulled out from the cement by an *TIRA 2300 (LaborTech s.r.o., Opava,Czech Republic)universal tensile testing machine* at the rate of 2.0 mm/min. The experimental setup developed to conduct the pull-out tests is illustrated in Fig. 1. In the standard pull-out test, load applied to the yarn end is recorded as a function of the displacement of this end with respect to a ‘‘stationary’’ point in the specimen.

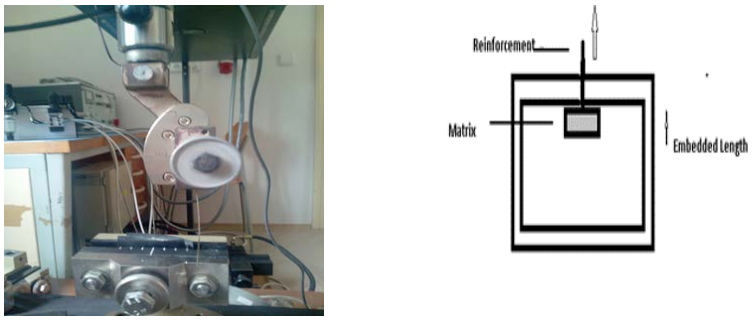

(a) TIRA Tester *(b)Experimental set up*

Figure 1: Pull out test method

2.23 Accelerated aging in alkaline solution

The action of aqueous sodium hydroxide and calcium hydroxide solutions 10 g/L (w/V) on basalt, PET, PP and jute yarns were investigated under a variety of conditions of pH. For this purpose, loss in weight (W), breaking load, % elongation to break and scanning electron micrographs of the yarn surfaces were studied. Tensile tests were conducted on specimens before and after ageing treatment, given that the materials could be tested based on their level of degradation. Furthermore, the interpretation of the experimental results involved the documentation of visual observations before and after testing.

2.24 Scanning Electron Microscope (SEM) for characterizing surface degradation

SEM was used for morphological analysis and for investigating the surface degradation of alkali treated samples. SEM images were prepared with different magnifications ranging from 2.5 KX to 50 KX. The microstructures of yarns were prepared on a Vegas-Tescan Scanning Electron Microscope (SEM) with accelerating voltage of 20 kV.

2.25 Tensile measurement to evaluate loss of mechanical properties

Textile materials are exposed to an alkaline environment in the cement matrix, which makes them susceptible to damage. A comparison of the measured breaking strength to the breaking strength of undamaged yarns allows an assessment of the selected reinforcement. Tensile properties of all alkali treated and control samples were measured on a TIRA 2300 (LaborTech s.r.o., Opava,Czech Republic) universal testing machine according to standard ASTM E 2098-00.

3. Results and discussion

3.1. Yarn pull out

The interaction between the concrete matrix and reinforcement is characterized by the bond behavior. It is very important that there is good adhesion between the reinforcing fibers and the concrete or cement matrix, otherwise deboning may take place. If bond strength at the interface between the fiber and the matrix is too high, the reinforcement ruptures after the first crack initiates.

On the other hand, the reinforcement is easily pulled out if the bond strength is too low. Bond strength may dominate the mechanical properties of fiber-reinforced concrete. Pull out test is most general test for this purpose. This tests is useful to get information about the load transfer behavior between matrix and reinforcement. The pull-out tests characterize both pull-out and rupture of the textile yarn as failure modes. The breaking point does not designate the definitive breaking point of the yarn in itself, but rather the location of crack initiation.
The yarn pull out was carried by testing machine. From the experiment, the average maximum force and the respective average crack-opening displacement, i.e. total slip, were calculated.
In case of basalt, very small slippage (displacement) is observed, as they have good adhesion with cement matrix. Maximum stress recorded as tensile stress of yarn is highest in case of basalt yarn. Similar situation is observed in case of jute yarn, but in this case Force recorded is much lower as jute yarn has overall lower strength value.
In case of PP and PET, adhesion is not good and it can be viewed by high slippage/displacement/deformation. Such large displacement prior to material failure are crucial with regard to structural safety as well as energy dissipation, in particular in the case of dynamic loading. However, the fact that high strength levels can be only reached at high deformations means that for the service state, where only small deformations are acceptable, and the design load-bearing capacity of TRC must be considerably lower than its tensile strength. Moreover, relatively wide cracks observed at high deformations are undesirable.
It can be seen that performance of highly twisted yarn e.g. PP is higher than less twisted PET yarn. This can be explained on the basic of mechanical anchoring which is the result of waviness. Also if density of crimped yarn increased effect is more prominent. The experimental findings are given in Table 1.

Table 1: Experimental findings of the pull out study.

Reinforcement type	**Max force N**		**Crack opening displacement at max force (mm)**		**Failure mechanism**
	OPC	**GPC**	**OPC**	**GPC**	
B	82.90	33.24	2.56	1.46	Telescopic
PP	53.54	17.87	21.19	9.30	Pull out
PET	52.61	10.14	10.84	7.28	Pull out
J	5.68	3.21	2.30	4.24	Rupture

Photographic investigation shows that overall, the force is transmitted by adhesion and friction between the reinforcement and the concrete. The load transfer between the filaments enclosed in the yarn/roving will however occur either based on adhesion or friction depending on the quality of the bond. The bond quality differs across the depth of yarn/roving which causes a complex failure mechanism involving the partial rupture and pull-out of singular filaments. The failure mechanism denoted as pull-out, was often observed to be a telescopic failure (i.e. partial rupture and pull-out) a common failure phenomenon.

3.2. Accelerated aging in alkaline solution

The degradation of fiber due to the alkaline pore solution in the cement matrix seriously decreases the durability and may cause premature failure of the concrete composite. Calcium hydroxide is the primary cause of alkaline environment in cement. In this case, the high concentration of alkali ions is the main cause of fiber damage. Particularly, weight loss and reduction in mechanical properties could appear. In the technical literature different studies are present, but the reported results appear somewhat contrasting.
After a careful scientific research, accelerated aging tests were made to evaluate the weight loss and the loss of mechanical properties of basalt, PP, PET and Jute fibers, in order to quantify their performance limits. 5 samples for each category were tested and their averages is reported.

3.2.1 Visual observations

The external appearance of the yarns specimens was examined pre- and post-alkali treatment, for comparison of color, surface degradation and change in shape. In Basalt yarn, no significant visible change of color or surface texture were observed after 7 days of immersion in pH=10, pH=11 and pH=12 of two types of alkali namely NaOH and $CaOH_2$. The Jute samples degradation was marked by color change. These samples lost a great deal of stiffness to the point that they broke prior to removal from the solution. For those exposed to pH 12, the observed degradation was similar to the pH 11 samples, yet these could be further tested in tension. The PP and PET specimens also lost a significant amount of physical stiffness. Effect of sodium hydroxide is stronger in all samples as compared to calcium hydroxide.

3.2.2 % Weight loss

The specimen's weight was measured both before and after the aging in order to evaluate weight loss. These results reflect the conditions for a range of pH of alkali treatment in aqueous sodium hydroxide and calcium hydroxide solution. The weight loss increases with increasing pH and use of stronger alkali (NaOH). The weight loss of basalt fiber is minimum as it is least affected by alkali followed by PP fiber

3.2.3 Tensile test of alkali treated yarns

After the aging in alkali solution, tensile tests were made in order to evaluate the maximum load F_{max} and the ultimate tensile elongation % of all the yarns before and after the aging, comparing the values obtained from controlled sample. ASTM E 2098-00 standard test method was used for this test. The graphical representation of strength loss is given in Fig. 2.

The tensile test results for the controlled samples are compared to the alkali treated samples in terms of applied maximum load versus elongation %. It can be noticed that ultimate tensile strain decreases in all the fiber types along with decrease in F_{max}. Reduction in mechanical properties in basalt yarn is minimum.

Table 2: % Weight loss.

Reinforcement Type	Weight loss [%] (1 week)					
	NaOH			$Ca(OH)_2$		
	pH 10	pH 11	pH 12	pH10	pH11	pH12
B	0.4	0.8	1.0	0.3	0.5	0.7
PP	1.4	1.6	1.7	0.9	1.0	1.1
PET	2.8	3.2	3.5	2.0	2.5	3.0
J	4.7	6.2	7.2	4.1	5.0	5.2

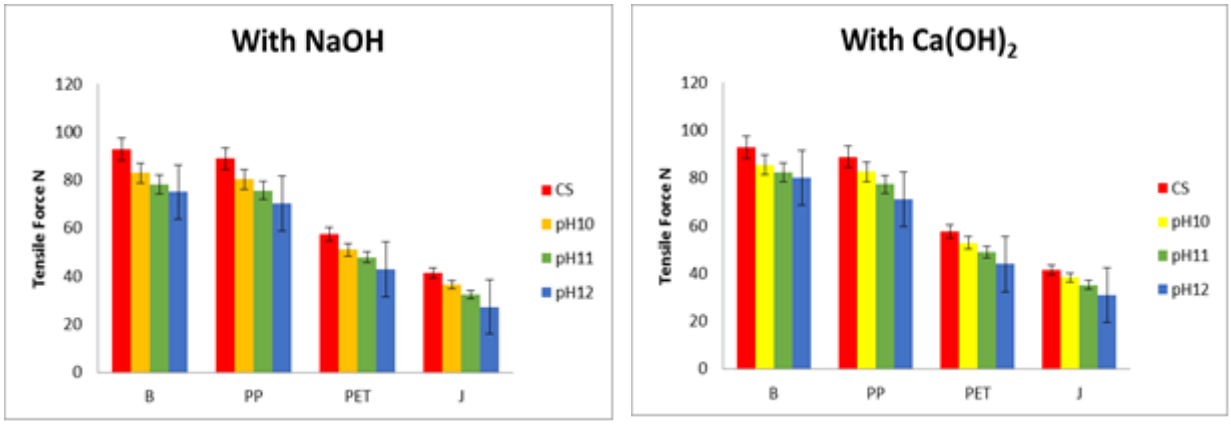

1 week treatment with NaOH 1 weeks treatment with $Ca(OH)_2$

Figure 2: Effect of pH on degradation of yarn after alkali treatment.

These results reflect the conditions for a range of pH and duration of alkali treatment in aqueous sodium hydroxide and calcium hydroxide solution. The weight loss increases with increasing treatment pH and use of stronger alkali (NaOH). The weight loss of basalt fiber is minimum as it is least affected by alkali followed by PP fiber.

The tensile test results for the controlled samples are compared to the alkali treated samples in terms of applied maximum load versus elongation %. It can be noticed that ultimate tensile strain decreases in all the fiber types along with decrease in F_{max}. Reduction in mechanical properties in basalt yarn is minimum. Basalt yarn mechanical properties are decreased probably due to the crystallographic structure of basalt, which is made by olivine (single tetrahedron), pyroxenes (linear chain) and plagioclase (tetrahedral space structure). In fact, alkaline aggressive environment can break some bonds of the linear tetrahedral chain of pyroxenes, so that a strength reduction can be seen. Jute is a ligno-cellulosic fiber with hemicellulose (22-24%), α - cellulose (58-60%) and lignin (12-14%) as the main constituents with other minor constituents as well. Among the three main organic components, hemicellulose and lignin are amorphous with relatively low polymerization degree, so they have a higher hydrolysis rate and solubility in alkaline medium than cellulose, which is the main reason for the degradation. The alkaline pore water dissolves the lignin and hemicellulose of fiber, which are sensitive to $Ca(OH)_2$ and high alkalinity causes hydrolysis of cellulose molecules, which leads to degradation of molecular chains and then a reduction in degree of polymerization and lower tensile strength. The crystallization of lime in the lumen of the fibers and middle lamellae leads to a decrease in the technical fiber flexibility and strength and relatively lower durability of jute fiber in cement matrix.

The alkali treatment produced a drop in both tensile strength and Young's modulus of the fibers. This was attributed to the damage induced in the cell walls and the excessive extraction of lignin and hemicellulose, which play a cementing role in the structure of the fibers. SEM images showed that some of the fibers were split, had ramifications and presented a tape form rather than cylindrical.

Although PET can offer good mechanical properties and is suitable for some applications; however it is susceptible to hydrolysis under strong alkaline conditions, when hydroxyl anion attacks the electron deficient carbonyl carbon atom of the ester group (The polar C=O bond provides an active site for chemical reaction) and, in turn, results with a scission of the bond in the polymer chain. PET can also be susceptible to heightened degradation where there is concrete or cement present. The PET material loses its weight when the polymer chains break down and dissolve in the alkaline bath. The attack of highly ionized aqueous sodium hydroxide is limited essentially to the surface of the PET material as the nonpolar PET disfavors diffusion of ionic bodies inside the polymer phase. Thus the diameter of PET filaments decreases with the loss of polymer on the surface. However, the molecular weight and tenacity of the slimmed filaments remain essentially unchanged.

Polypropylene can be considered as inert to acid and alkali attack. Polypropylene fibers have a high resistance to acids and alkalis in all concentrations, and up to comparatively high temperatures. Although PP has not very good bond with the cement matrix, this fiber is considered as attractive for the reinforcement of cement matrices, because of their high resistance to the alkaline environment of cement matrix and of low cost.

SEM morphology analysis

The time-dependent degradation of fiber surface is additionally investigated using an electron-microscope.

Surface morphology of fiber samples was analyzed by using a scanning electron microscope. The microstructure of yarn surfaces indicated that the jute fiber encountered the most severe alkali attack and precipitation of hydration products in the cement matrix. Fibrillation and diameter reduction is evident in the jute fiber. Fig. 3 also shows the damage in the cell walls and a rougher fiber surface. Also, the collapse of fiber lumen can be seen. This is responsible for the decrease in capillary pressure and therefore decreases in permeability.

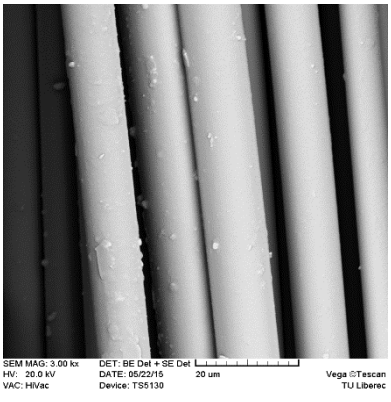

Control Basalt

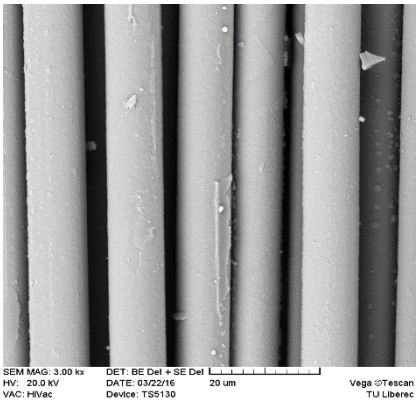

Basalt after NaOH treatment

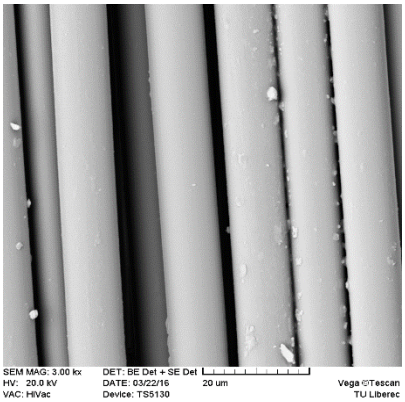

Basalt after $Ca(OH)_2$ treatment

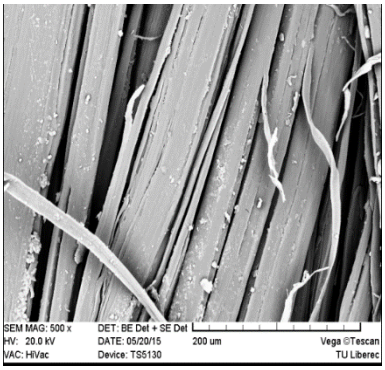

Control Jute

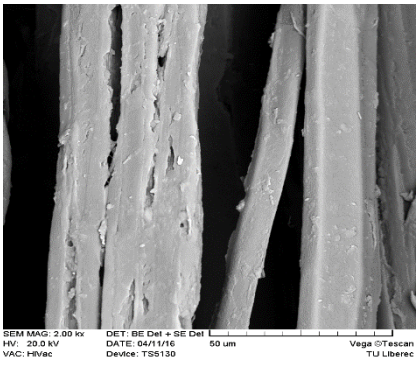

Jute after NaOH treatment

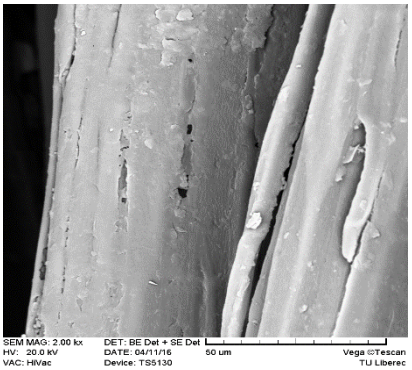

Jute after $Ca(OH)_2$ treatment

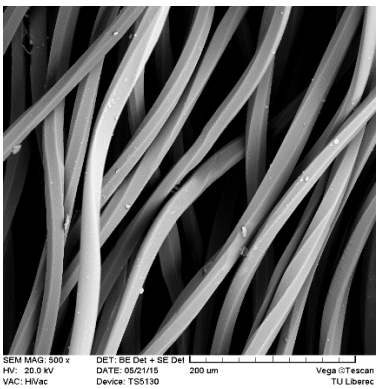

Control PET

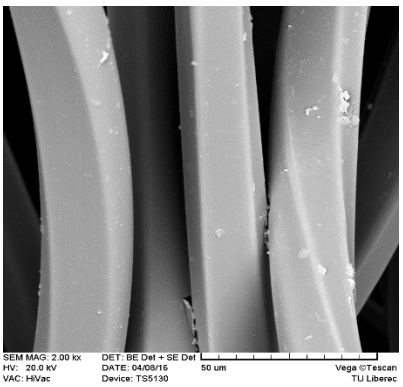

PET after NaOH treatment

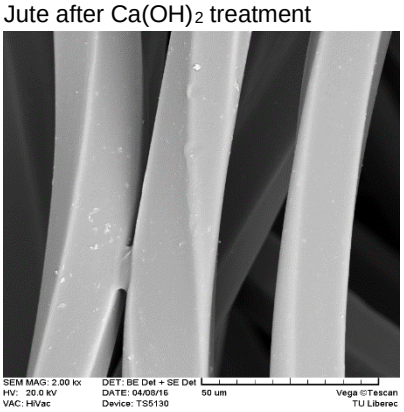

PET after $Ca(OH)_2$ treatment

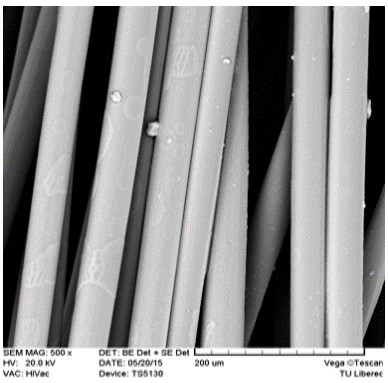

Control PP

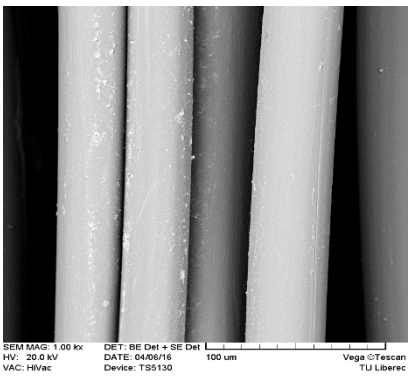

PP after NaOH treatment

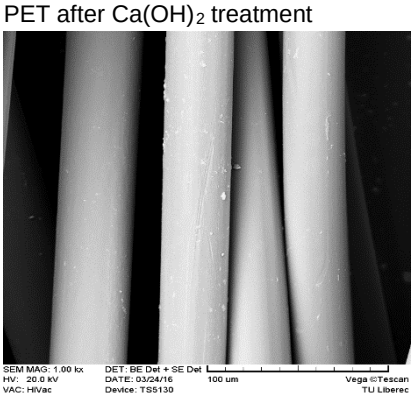

PP after $Ca(OH)_2$ treatment

Figure 3: SEM images of fibers after alkali treatment.

On the contrary, the controlled jute fiber (Fig. 3) shows open lumens. Besides, SEM images showed the presence of diffused micro-cracks on fiber surface and evidenced a variation in surface morphology before and after aging.

4. CONCLUSIONS

Textile -reinforced composites are gaining popularity within the construction sector. This study investigated the effect of using different yarns on load bearing capacity and durability in cement composite.

It has been discussed that the interfacial bond between textile reinforcement and the concrete matrix is greatly heterogeneous. The bond behavior of textile reinforcement embedded in a concrete matrix was experimentally investigated in this work. All tests results reveal that addition of fibers to the cement can significantly enhance the interfacial bonding is significant. The increase in the bond strength can be attributed to this fact that, on one hand, the use of fiber in the cement reduces shrinkage cracking in the interfacial transition zone and bleeding at the interface.

The results obtained from tensile tests demonstrated clearly the positive influence of basalt yarn on the mechanical performance of TRC. In general the use of high strength fibers like basalt increases the strength and toughness of the cement composites providing strain-hardening behavior. Low modulus fiber such as PP and PET enhance mainly the ductility of the cement composites, but not its strength in a strain softening behavior. The PP/PET structure did not bond strongly with the cement matrix, resulting in relatively low composite performance. The B/PP, B/J or B/PET yarn combination in a hybrid fabric should be considered as reinforcement for cement composites. The hybridization of PP/PET yarn with basalt during weaving can solve this problem

According to the results, it can be concluded that the accelerated ageing test was too aggressive for textiles made of jute and PET, leading to extensive degradation; however, basalt and PP textiles were found to be promising alternative as they have superior durability properties in an alkaline environment without undergoing much strength loss. Despite the hydrophobic characteristics of PP fibers and their poor bond with the cement matrix, these fibers are considered as attractive for the reinforcement of cement matrices because of their high resistance to the alkaline environment of the cement matrix and their low cost.

References

1. *N. Banthia, C. Zanotti, and M. Sappakittipakorn, "Sustainable fiber reinforced concrete for repair applications," Construction and Building Materials, vol. 67, pp. 405–412, 2014.*
2. *O. Karahan and C. D. Atis ¸, "The durability properties of polypropylene fiber reinforced fly ash concrete," Materials & Design, vol. 32, no. 2, pp. 1044–1049, 2011.*
3. *S. B. Kim, N. H. Yi, H. Y. Kim, J.-H. J. Kim, and Y.-C. Song, "Material and structural performance evaluation of recycled PET fiber reinforced concrete," Cement and Concrete Composites, vol. 32, no. 3, pp. 232–240, 2010.*
4. *.E. T. Dawood and M. Ramli, "The effect of using high strength flowable system as repair material," Composites Part B: Engineering, vol. 57, pp. 91–95, 2014.*
5. *M. Hsie, C. Tu, and P. S. Song, "Mechanical properties of polypropylene hybrid fiber-reinforced concrete," Materials Science and Engineering A, vol. 494, no. 1-2, pp. 153–157, 2008.*
6. *P. S. Song and S. Hwang, "Mechanical properties of high strength steel fiber-reinforced concrete," Construction and Building Materials, vol. 18, no. 9, pp. 669–673, 2004.*
7. *A.Izaguirre,J.Lanas,andJ.I.Alvarez,"Effect of a polypropylene fibre on the behaviour of aerial lime-based mortars," Construction and Building Materials, vol. 25, no. 2, pp. 992–1000, 2011.*
8. *Wang, Y.; Wu, HC.; Li, V. (November 2000). Concrete Reinforcement With Recycled Fibers. Journal Of Materials In Civil Engineering, 12:4(314).314-319.*
9. *Jump Up,Ochia, T.; Okubob, S.; Fukuib, K. (July 2007). Development Of Recycled PET Fiber And Its Application As Concrete-Reinforcing Fiber.. Cement And Concrete Composites, 29(6), 448–455.*
10. *Liu Q, Giffard HS, Shaw MT, McDonnell AM, Parnas RS. Preliminaryinvestigation of basalt fiber composite properties for applications intransportation.The Official Newsletter of the International Institute for FRP in Construction 2005; 2. 6– 8.*

BENDING BEHAVIOUR OF SPORTS BRA FABRICS: EXPERIMENTAL AND FINITE ELEMENT SIMULATION OF ASTM D1388 CANTILEVER TEST

Michaela Hassmann[1], Seraphina Stöger[1], Natalie Mentel[1], Wolfgang Krach[2]

[1]University of Vienna, Institute of Sport Science, Vienna, Austria, +43-1-4277-48883, michaela.hassmann@univie.ac.at
[2]CAE Simulation & Solutions GmbH, Vienna, Austria, +43-1-9748991-11

Abstract:

Finite Element (FE) simulation of sports bra fabrics requires knowledge of textile material properties. Bending behaviour of textiles is determined according to ASTM D1388. Standard procedure of ASTM D1388 Cantilever test has been criticized in literature due to the fixed bending angle θ = 41.5°. Following extensive pre-tests, overhang length was defined to L = 70 mm for stiff textiles and L = 20 mm for flexible textiles in this investigation. From the bending lines of eight specimens of an ODLO High Padded sports bra, flexural rigidity G and bending modulus E_f were calculated. Formulae given in literature other than ASTM D1388 had to be used due to an unexplained factor and a different unit introduced in the 2008 issue. Experimental results were compared to nonlinear FE analysis in MSC Nastran using CQUAD4 shells with calculated material parameters. Separate trends of mostly overestimating vertical tip displacement f for stiff and flexible textiles were found. This leads to the conclusion that the assumption of pure bending in the Cantilever test is not valid especially for flexible sports bra fabrics. For their FE simulation, shell elements with decoupled membrane and bending stiffness must be used and Young's modulus has to be determined from tensile testing.

Key words:

knitted fabrics, preformed foam, flexural rigidity, decoupled shell elements, membrane stiffness

1. Introduction

Sports bras consist of one or more layers of knitted textiles, an elastic underbust band and straps. Padded sports bras additionally incorporate preformed foam to provide stability to cups and comfort to straps. Besides sewing pattern, Finite Element (FE) simulation requires material properties to model the sports bra's efficacy in reducing breast movement during sports activities [5]. If these properties are not known to the manufacturer, they have to be found out using standardized procedures.

Characterization of stiffness according to ASTM D1388 proposes the Cantilever test (Option A) as the preferred procedure, whereas very limp textiles with an overhang length of less than 4 cm at a bending angle of 43° [7] or those that show a marked tendency to curl or twist should rather be tested by Heart Loop test (Option B) [1]. Both these procedures go back to Peirce [7]. Peirce [7] himself as well as other authors [4; 10] propose further modifications of Cantilever test, indicating dissatisfaction with standardized procedures. Bending rigidity is not directly measured but calculated by approximated formulae [3; 2]. Peirce admitted that his formulae were only applicable for small deflections, while the ASTM D1388 standard specifies a bending angle of 41.5° which indicates large deflections [4].

This paper describes stiffness testing for all relevant fabrics of a sports bra using experimental Cantilever test and comparing the results with FE simulation. The primary aim is to find the needed material properties, for which the Cantilever test is the easiest to perform for the wide range of fabrics used in sports bras. Moreover, the implications and limitations of this procedure will be pointed out.

2. Experimental

2.1. Specimens

One set of specimens was taken from one manufactured ODLO High Padded sports bra (size 95E), as fabric samples were not available. Specimens were cut according to ASTM D1388 guidelines [1], weight was measured using a precision scale, thickness and other dimensions were determined using sliding calliper. Density ρ [t/mm³] was calculated as weight per unit area M divided by thickness T in modified SI units for FE. For the strap foam (1), underbust elastic band (2), piping (3) and elastic strap (4) no specimen in cross-machine direction could be cut due to limited size. For the cup foam (5), warp knit stretch mesh (6), single knit mesh (7) and single jersey (8) one specimen was cut along machine direction (A) and one along cross-machine direction (B). The base layer of the foam padded strap was excluded, as it was too limp to be considered relevant for mechanical analysis. Numbering and location of specimens can be seen in Figure 1, their specifications are given in Table 1.

Figure 1. Numbering and locations of sports bra specimens.

Difficulties in cutting specimens occurred due to the preformed cups, especially as thickness was not constant and had to be averaged. Specimen size was limited, for which 25 by 200 mm is recommended [1]. Yet bending length is not dependent on the width, and none of the specimens reaches an overhang length higher than 100 mm before bending to an angle of 90° which is the maximum amount of bending in Cantilever test.

Table 1. Specifications of sports bra specimens.

specimen		length l [mm]	width b [mm]	weight per unit area M [g/m²]	thickness T [mm]	density ρ [t/mm³]	description
1		150	25	298.7	3.50	$8.533 \cdot 10^{-11}$	strap foam
2		150	30	844.4	2.10	$4.021 \cdot 10^{-10}$	underbust elastic band
3		150	16	350.0	1.10	$3.182 \cdot 10^{-10}$	piping
4		150	19	491.2	1.45	$3.388 \cdot 10^{-10}$	elastic strap
5	A	150	25	632.0	4.80	$1.317 \cdot 10^{-10}$	cup foam
	B	150	25	624.0	3.35	$1.863 \cdot 10^{-10}$	
6	A	150	25	160.0	0.45	$3.556 \cdot 10^{-10}$	warp knit stretch mesh
	B	105	25	160.0		$3.556 \cdot 10^{-10}$	
7	A	150	25	114.7	0.40	$2.867 \cdot 10^{-10}$	single knit mesh
	B	120	25	123.3		$3.083 \cdot 10^{-10}$	
8	A	150	25	208.0	0.50	$4.160 \cdot 10^{-10}$	single jersey
	B	150	25	178.7		$3.573 \cdot 10^{-10}$	

2.2. Experimental Cantilever test

Extensive pre-tests concerning optimum overhang length L were carried out, for L = 10 mm to 100 mm increasing by every 10 mm. They showed that the highest feasible overhang length was L = 70 mm for stiff textiles (specimens 1 to 5) and L = 20 mm for flexible textiles (specimens 6 to 8). Bending lines for all four directions (face and back of both ends) were photographed with a millimetre scale in the front plane. Bending angle θ [°] and vertical displacement of tip f [mm] were measured using Kinovea 0.8.22 (Figure 2).

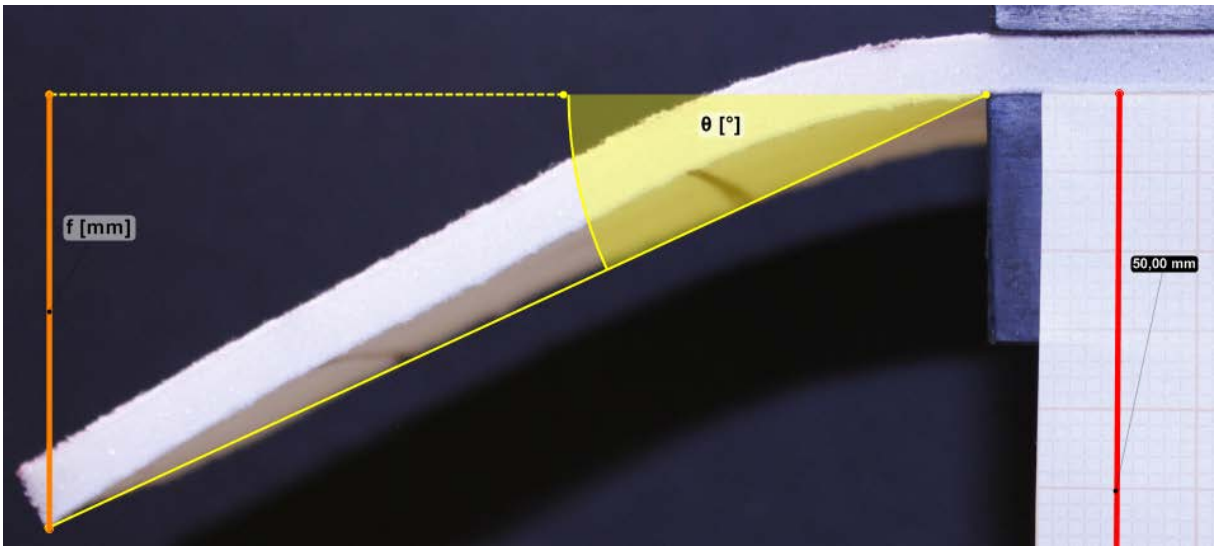

Figure 2. Analysis of experimental Cantilever test in Kinovea.

Calculation of flexural rigidity G relied on formulae and variables given in [9]. First, a so-called bending length C was calculated from overhang L and bending angle θ (1), from which flexural rigidity G (2) was computed and averaged according to ASTM D1388 [1]. In a linear isotropic material, bending modulus E_f (3) and tensile Young's modulus E are identical [7]. For pure bending problems, this assumption can also be adopted for non-isotropic materials like textiles.

$C = L\left(\frac{\cos^{\frac{1}{2}}\theta}{8\ \tan\theta}\right)$ [mm] with L [mm] (1)

$G = M \cdot C^3 \cdot 9.807 \cdot 10^{-6}$ [µNm] with M [g/m²] (2)

$E_f = \frac{12 \cdot G}{T^3 \cdot 10^3}$ [N/mm²] with T [mm] (3)

ASTM D1388 introduced an unexplained factor of $1.421 \cdot 10^{-5}$ for flexural rigidity G in the 2008 issue [4] that is still used in the 2014 issue [1] (4). Furthermore, the unit of flexural rigidity G has been changed from former [mg·cm] to [µjoule/m] in [1], which seems to be inconsistent in terms of units for the given formula and inconsistent with multiples of [Nm] in most other literature [8; 9] (5).

$G = 1.421 \cdot 10^{-5} \cdot W \cdot c^3$ [µjoule/m] with factor [m/s²], W [g/m²] and c [mm] (4)

$$[G] = \left[1.421 \cdot 10^{-5} \cdot \frac{m}{s^2}\right] \cdot \left[\frac{g}{m^2}\right] \cdot [mm^3] = 1.421 \cdot 10^{-5} \cdot 10^{-12} \left[\frac{kg \cdot m^2}{s^2}\right] = 1.421 \cdot 10^{-5} \cdot 10^{-12}\ [Nm] \quad (5)$$

2.3. FE modelling

In [4] ABAQUS quadratic shell elements were used and material parameters of the specimen (density ρ, Young's modulus E, Poisson's ratio v) were known. FE models in this paper were pre-processed in MSC Patran 2014.1. Standard PSHELL shell formulation with linear CQUAD4 elements and an average element size of 3 mm for L = 70 mm and 1.5 mm for L = 20 mm. Linear elastic material MAT1 with measured density, calculated bending modulus E_f and assuming v = 0.32 [5] was defined. Inertial loading with the appropriate boundary conditions restraining displacements and rotations at the upper end simulated specimens hanging under their own weight.

3. Results and discussion

Table 2 summarizes the results of experimental and FE Cantilever test.

Table 2. Results of Cantilever test of sports bra specimens.

specimen		overhang L [mm]	bending angle θ [°]	bending modulus E_f [N/mm²]	vertical tip displacement		
					experimental f [mm]	FE f [mm]	difference [%]
1		70	29.5	0.06151	32.688	32.682	0.0
2			47.3	0.40164	47.733	47.900	0.4
3			71.9	0.38309	62.314	60.621	-2.7
4			70.4	0.23703	59.639	60.576	1.6
5	A		19.0	0.09809	21.300	19.336	-9.2
	B		41.4	0.09435	44.063	43.446	-1.4
6	A	20	53.7	0.15338	14.650	15.554	6.2
	B		50.7	0.15543	13.099	15.510	18.4
7	A		44.8	0.19871	12.870	14.604	13.5
	B		69.3	0.07390	16.356	17.399	6.4
8	A		50.9	0.15140	12.913	15.462	19.7
	B		61.6	0.07892	15.405	16.797	9.0

Resulting bending lines from MSC Nastran Implicit Nonlinear analysis (SOL 400) are shown in Figure 3 for stiff (left) and flexible (right) textiles separately.

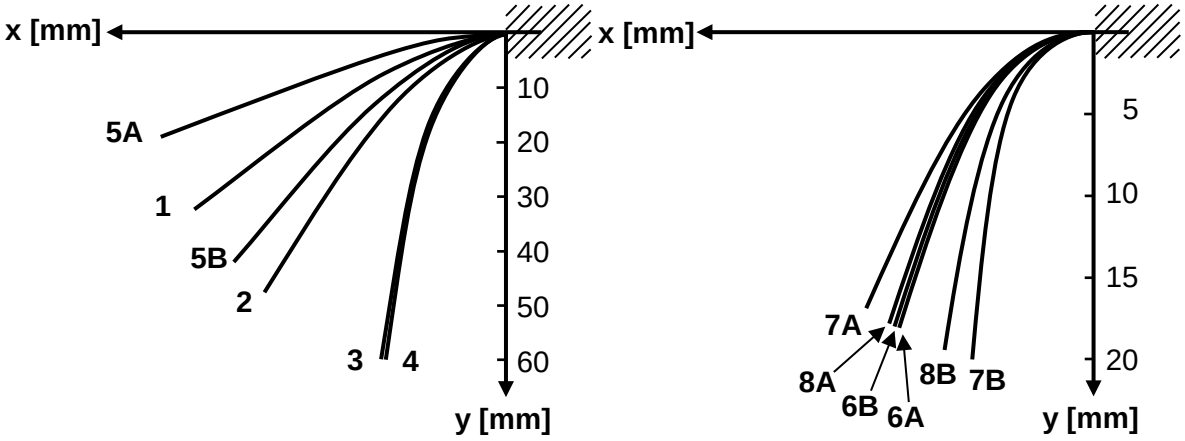

Figure 3. Bending lines of all stiff (left) and flexible (right) specimens with vertical tip displacement f [mm]

Difference of vertical tip displacement f between FE result and experimental Cantilever test in percent of Cantilever result over bending angle θ is shown in Figure 4. Comparison showed good accordance for stiff textiles with a maximum difference of -9.2 % for specimen 5A. Spearman correlation calculated in IBM SPSS 23 revealed a slightly positive trend between difference and bending angle θ ($p = 0.234$, $\rho = 0.371$). For the flexible specimens, overestimation of vertical tip displacement was collectively larger (up to 19.7 % for specimen 8A) and strongly negatively correlated to bending angle θ ($p = 0.104$, $\rho = -0.600$). Although strap foam (1) and cup foam (5A, 5B) had lower bending moduli than knitted textiles, they behaved like stiff textiles due to their thickness T = 3.50 / 4.80 / 3.35 mm.

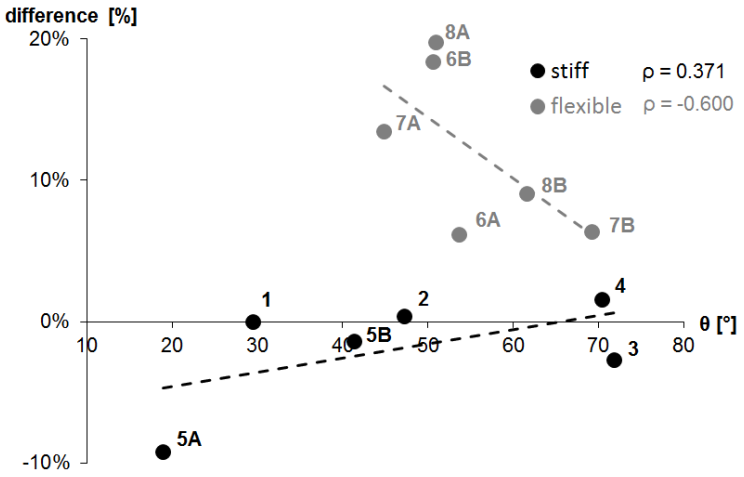

Figure 4. Difference of vertical tip displacement f [mm] between FE result and experimental Cantilever test, dashed lines indicate linear correlations for stiff and flexible specimens separately

4. CONCLUSIONS

The main point of criticism for Cantilever test is the fixed bending angle θ = 41.5°, which is neither optimal for very flexible nor for very stiff textiles. Especially flexible sports bra fabrics yield a very low overhang making this test specification impracticable. We therefore suggest revising ASTM D1388 Cantilever test procedure by either allowing a variable bending angle θ or by giving suitable ranges of overhang length L for different types of textiles. In accordance with [4], formulae given in the current issue could not be used due to an unexplained factor and inconsistent units.

Therefore, the intention was to invert fixed value and measured variable. Bending line photography can be assumed to achieve comparable accuracy in the order of (sub)millimetres to commercially available Cantilever test apparatus when manually setting a variable bending angle. The standard

requires five specimens in each direction, which would not increase accuracy compared to measuring only one specimen in this investigation, where experimental and FE results were compared.

For stiff textiles, low differences between FE simulation and experimental Cantilever test occur, and a detailed stress tensor analysis exhibits only one nonzero value for σ_{xx} component. Values of bending modulus E_f calculated by approximated formulae can be regarded as accurate enough for bending problems, following Peirce's statement [7]. For larger bending angles and displacements occurring in flexible textiles, the Cantilever procedure is no longer a pure bending problem. Flexible specimens are also exposed to tensile stress when extension increases to about 3 to 5 % as in this investigation or even higher in sports bra simulation. MSC Nastran's PSHELL property card offers decoupling of Young's modulus E for the membrane stiffness and bending modulus E_f for the bending stiffness. Decoupling in-plane and out-of-plane properties is supposed to yield more comparable results for flexible textiles, as proposed by [6] using a different modelling approach. Determination of Young's modulus E is done by tensile testing gaining the load-extension curve of the specimen [9]. Gaining a comparable plot for bending behaviour requires KES pure bending test [2].

Most textiles show different bending behaviour on face and back side which is taken into account by Note 8 in ASTM D1388 [1]. This differentiation might be necessary for FE simulation of sports bras where the orientation of bending is known. In contrast, curl and twist effects can be neglected in FE simulation of sports bras, as they are not expected to occur to a large extent compared to when fabrics are hanging under their own weight.

ACKNOWLEDGEMENTS

The project "Sports bra optimization by Finite Element simulation of interaction between breast tissue and textile" is funded by Vienna Business Agency (Call FemPower 2015).

References

1. *ASTM D1388-14 (2014). Standard Test Method for Stiffness of Fabrics.*
2. *Ghosh, T. K., Zhou, N. (2003). Characterization of fabric bending behavior: A review of measurement principles. Indian Journal of Fibre & Textile Research, 28, 471–476.*
3. *Hummel, F. H., Morton, W. B. (1927). XXXII. On the large bending of thin flexible strips and the measurement of their elasticity. The London, Edinburgh, and Dublin Philosophical Magazine and Journal of Science, 4(21), 348–357.*
4. *Lammens, N., Kersemans, M., Luyckx, G., van Paepegem, W., Degrieck, J. (2014). Improved accuracy in the determination of flexural rigidity of textile fabrics by the Peirce cantilever test (ASTM D1388). Textile Research Journal, 84(12), 1307–1314.*
5. *Li, Y., Zhang, X., Yeung, K. (2003). A 3D Biomechanical Model for Numerical Simulation of Dynamic Mechanical Interactions of Bra and Breast during Wear. FIBER, 59(1), 12–21.*
6. *Pabst, S., Krzywinski, S., Schenk, A., Thomaszewski, B. (2008). Seams and Bending in Cloth Simulation. In F. Faure, M. Teschner (Eds.), VRIPHYS 08. 5th Workshop on Virtual Reality Interactions and Physical Simulations.*
7. *Peirce, F. T. (1930). 26 – The "handle" of cloth as a measurable quantity. Journal of the Textile Institute Transactions, 21(9), T377–T416.*
8. *Plaut, R. H. (2015). Formulas to determine fabric bending rigidity from simple tests. Textile Research Journal, 85(8), 884–894.*
9. *Saville, B. P. (1999). Physical testing of textiles. Woodhead (Cambridge).*
10. *Szablewski, P., Kobza, W. (2003). Numerical Analysis of Peirce's Cantilever Test for the Bending Rigidity of Textiles. FIBRES & TEXTILES in Eastern Europe, 11(4), 54–57.*

A HYDROGEL PHANTOM FOR TESTING BIOSIGNALS FROM A TEXTRONICS T-SHIRT

Emilia Frydrysiak[1], Michał Frydrysiak[2], Łukasz Tęsiorowski[2]

[1]Lodz University of Technology, Institute of General Chemistry, Lodz, Poland, Stefanowskiego 4/10 90-924, em.frydrysiak@gmail.com, tel. +48 42 631-34-10, fax +48 42 631-28-42

[2]Lodz University of Technology, Faculty of Material Technologies and Textile Design, Lodz, Poland, St. Zeromskiego 116, 90-924

Abstract:

A textronics system in the form of T-shirt was designed for elders for controlling their life parameters. For testing in a phantom with proper filling is required. That filling should be hydrogel: made of agar mixed with an electrolyte or polyacrylamide which maintain their 'jelly-like' properties at temperatures between 36-40° C (human body temperature). The resistance of agar gel with sodium chloride in concentrations of 0, 1, 2, 3, 4 and 10% was obtained and also there were obtained gels made of polyacrylamide in concentrations of 5, 10 and 15%. The best results were for 3, 4 and 10% sodium chloride-agar gel and for 10% PAM gel. As a phantom filling the 10% PAM gel and 3% agar hydrogel were chosen because of their electrical conductive properties and durability under certain temperature over a long period of time.

Key words:

Hydrogels, phantom, biosignals, textronics, T-shirt, elders

1. Introduction

A textronics system in the form of T-shirt was designed for elders for controlling their life parameters. The system allows to measure pulse, frequency of breathing, temperature of a body and also can show a patient's electrocardiogram. However such systems cannot be tested in humans in the first place, because a medical bioethics commission agreement is required. That is why phantoms are designed – for testing such systems on them. The best phantom fulfillment are hydrogels.

Hydrogels are crosslinked polymeric structures, absorbing significant quantities of water. According to the type of hydrogels, they can be divided into two groups: chemical or physical cross-linking hydrogels. Chemical ones are crosslinkable permanently, and physical ones - temporary (e.g. Agar, gelatin), which is a result of the entanglements of their chains or physical interactions, e.g. ionic or hydrogen bonds. Hydrogels can also be divided based on their origin: natural or synthetic. Natural polymers include collagen or gelatin which are proteins and polysaccharides: agarose and alginate. Synthetic hydrogel-forming polymers are prepared with the use of polymerization reactions [1, 2].

2. Experimental

Presented research concerns execution of the phantom chest which allows for testing of physiological parameters of a man. Substance which is a filling of the phantom must have similar properties to

physiological properties of human tissue. The perfect fulfillment of this type of application are hydrogels which have 'jelly-like' consistency at temperatures between 36-40° C, which is the temperature range of the human body.

2.1. Materials

Agar and polyacrylamide were chosen as testing substances which could be good as a phantom fulfillment. Agar (Figure 1. a) is a polysaccharide which consists of two linear heterogeneous fractions: agarose and agaropectin combined with glycoside binds. Agarose has gelling properties and agaropectin hinders the formation of gels. However if gel is formed, agaropectin increases its flexibility. Polyacrylamide (PAM) (Figure 1. b), is a polymer which is obtained by the acrylamide polymerization. It is important that in contrast to mentioned acrylamide, polymer is not toxic.

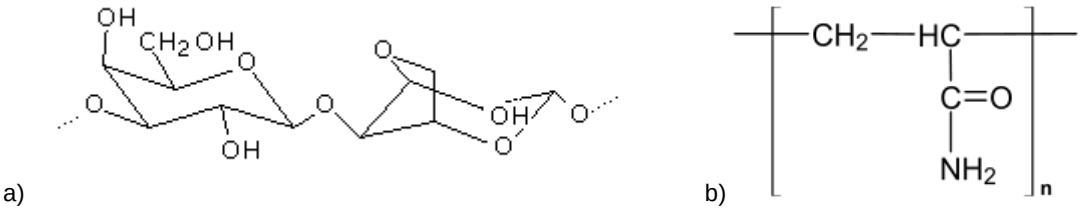

Figure 1. Chemical structures of: a) agar; b) polyacrylamide

Agar was mixed with cold water and heated up. After heating agar solution it was mixed with an electrolyte in forms in order to reduce the resistance of the gel. The electrolyte used in samples was sodium chloride in concentrations: 1, 2, 3, 4 and 10%.

There were prepared three probes of the acrylamide/bisacrylamide gels in their concentrations of 5%, 10% and 15%. An acrylamide/bisacrylamide solution (30% of acrylamide and 0,8% of bisacrylamide), buffer, tetramethylen diamine (TEMED) and distilled water were mixed. Then a prepared 10% solution of ammonlumpersulphate (APS) in distilled water was added to the solution in an amount of 0.1 ml to 15 ml sample. APS was added slowly with stirring. The polymerization last for approximately 30 minutes.

2.2. Methods

In both kinds of gels there was resistance measured. In agar gel the measurement was done with the use of indirectly method, and in polyacrylamide gel – with directly method (Figure 2). The aim of those measurements was to obtain the resistance gels similar to resistance of human skin which was approximately 200 Ω. The construction of phantom for testing the textronics system for elders requires the choice of the proper fulfillment.

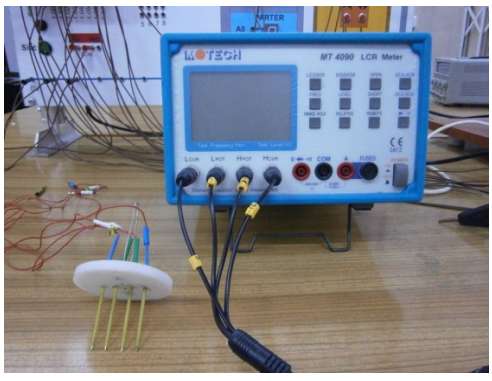

Figure 2. Measuring bridge for testing the resistance of the agar gel and the polyacrylamide gel

3. Results and discussion

A concentration of 3, 4, 10% of electrolyte in agar gel allowed to obtain the gel characteristics of the electrical conductive properties which is the closest to human skin (approx. 200 Ω/1 cm) (Table 1). Agar gel maintained its consistency after staying in the oven at 40° C, but had cracked due to drying.

The best properties of electrical conductivity in the interesting range was gel concentration of 10% (Table 2). The obtained gel well maintain its consistency in the temperature range of 36-40° C. The measurements scheme of resistance distribution in gels' samples is presented in Figure 3.

Table 1. The averaged results of the resistance of the agar gels depending on the electrolyte concentration

The electrolyte concentration [%]	**0**	**1**	**2**	**3**	**4**	**10**
Resistance [Ω] series I	4214	307	300	253	214	264
Resistance [Ω] series II	5040	837	320	793	660	685

Table 2. The averaged results of the resistance of the PAM gels

Diameter, φ [cm]	**Resistance [Ω]**					
	Distance [cm]					
	0	1	2	1	2	0
	PAM 5%					
3	307,10	115,70	94,90	132,80	89,46	305,40
2	202,30	114,31	63,29	110,75	83,64	174,50
1	189,20	97,73	52,99	80,14	47,19	224,00
Diameter, φ [cm]	**PAM 10%**					
3	367,00	178,10	93,23	164,50	117,25	428,90
2	361,60	131,51	81,75	139,11	92,78	349,50
1	345,40	109,42	72,90	108,34	66,18	315,10
Diameter, φ [cm]	**PAM 15%**					
4,5	590,30	312,60	-	333,10	-	603,50
3	683,20	230,20	-	216,14	-	666,40
2	376,50	181,70	-	168,30	-	584,70
1	440,00	138,70	-	149,37	-	423,00

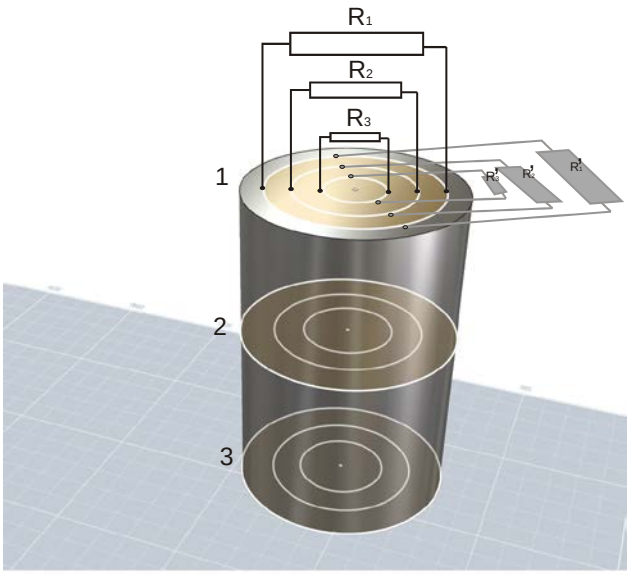

Figure 3. The measurements scheme of resistance distribution in gels' samples

The chosen PAM fulfillment of phantom was presented in Figure 4. a, and the phantom fulfilled with agar hydrogel is presented in the Figure 4. b. Silver-colored stripes painted on the phantom are made with electroconductive paint in both sides: outside and inside. Thanks to that the textronics system in the form of the T-shirt can be tested – because the agar hydrogel and the paint conducts current and so that biosignals can be measured.

a)  b) 

Figure 4. a) The phantom filling PAM gel in the form of a cylinder; b) Phantom filled with agar hydrogel

For phantom verification, an arbitral generator was connected to it. The generator contained a reference pulse signal. A textronics measurement system was put on the phantom and it recorded pulse signal from the phantom. Measurement results are presented in the Figure 5.

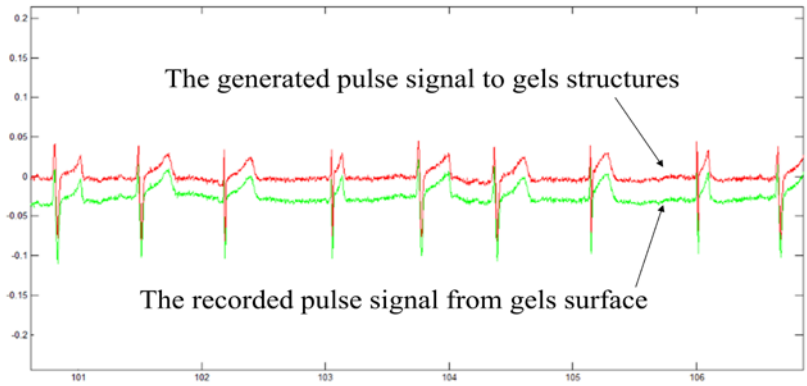

Figure 5. Measurement results of recorded pulse signal

4. CONCLUSIONS

Presented solution of the gel phantom is useful for non-conventional measurement systems. Textronics biomeasurement systems are the types of applications which should be tested on phantoms. For the construction these kinds of phantoms different kinds of electroconductive gels can be used, such as polysaccharides or polyacrylamide. Very important of gels features are their electroconductive and mechanical stability parameters at higher temperatures equal to the body temperature. That makes tests possible to carry out under conditions similar to real measurement conditions.

Based on the study of the different concentrations of agar gel with the addition of electrolyte and PAM gels there were chosen the best fillings of the phantom which are the polyacrylamide hydrogel in the concentration of 10% and agar hydrogel in the concentration of 0,5% and the electrolyte concentration of 3%. These gels were selected because of their electrical conductive properties and durability under certain temperature over a long period of time.

ACKNOWLEDGEMENTS

Presented research is financed by The National Centre for Research and Development in Lider IV program, based on decision number 035/657/L-4/12/NCBR/2013.

References

1. *http://thesis.library.caltech.edu/1774/1/Chapter1.pdf, 1-2, access: June 2016*
2. *Tyliszczak B., Pielichowski K. (2007). Charakterystyka matryc hydrożelowych - zastosowania biomedyczne superabsorbentów polimerowych. Czasopismo techniczne, 1, 1-9.*
3. *Frydrysiak, M., Tęsiorowski, Ł., Adamowicz, E. Fantom do testowania systemów pomiarowych przetwarzających sygnały bioelektryczne [Phantom for testing measurement systems processing bioelectric signals] Patent Application (P. 409096). August 4, 2014.*
4. *Frydrysiak, M., Tęsiorowski, Ł., Adamowicz, E., Zięba, J. (2014). Pulse-human phantom to testing textronic measurement system, IEEE - Institute of Electrical and Electronics Engineers.*

ANALYSIS OF WATER VAPOUR TRANSFER IN SKIN MODEL TEXTILE TESTERS

Lubos Hes[1], Monika Boguslawska – Baczek[2]

[1]Technical University of Liberec, Faculty of Textiles, 460 15 Liberec, Czech Republic
[2]University of Technology, Faculty of Materials and Environmental Sciences, 43-309 Bielsko Biala, Poland
e-mail: lubos.hes@gmail.cz

Abstract

Measuring of water vapour resistance of fabrics in a Skin model must be an isothermic process, in order to avoid the heat transfer by convection. However, improper design of the measuring hotplate of the Skin model may cause a negative temperature drop, resulting in unwanted heat transfer by radiation. In the paper, the effect of the emissivity level of internal walls of the measuring chamber on the measurement presision is theoretically analyzed and experimentally verified.

Key words:

Textile fabrics, water vapor permeability, Skin model, measurement precision, emissivity.

1. Introduction

The most important standard for testing of thermo-physiological comfort of fabrics presents the ISO 11092. This very complex standard became the basic one for the manufacturers of special performance fabrics or garments with high added value. That is why increased attention is paid to the application of this standard in recent decades.

The related instrument called “Skin Model” consists of heated metallic plate surrounded on most of its surface by a thermal insulation layer kept electronically at the same temperature. Due to this isothermal arrangement, no heat is transferred out of this plate, except the heat passing through the only free surface. Free surface of this measuring plate covered by the porous layer is exposed to parallel air flow of 1 m/s velocity moving in the special wind channel.

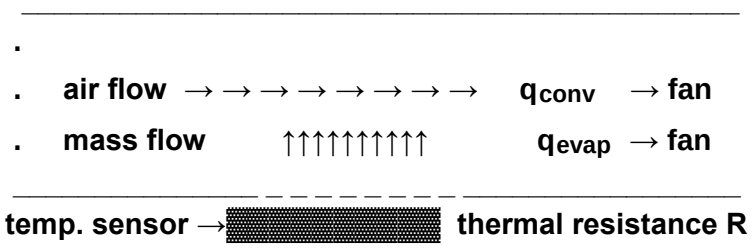

Figure 1. Heat and mass transfer in a Skin model [1]

When measuring the fabric thermal resistance R_{ct}, the air temperature in the channel is kept at 20 °C, and the measuring plate is dry. First, the power H supplied to the hotplate in order to heat the measuring system to temperature 35 °C is measured. Then, the tested fabric is placed on the porous layer of the measuring plate and the electric power representing the heat passing through the system to the outer air is measured again.

When evaluating the water vapour resistance R_{et}, both the measuring plate and the air temperature are kept at 35°C (to achieve the isothermal conditions) and the porous layer is continuously filled with water. Then, again the heating power H without and with the specimen is

measured and saved. All the power values then serve for the calculation of thermal and water vapour resistance values according to the simple formulas presented in the ISO 11092.

During the measurement of thermal resistance, heat is transferred from the hotplate and the fabric surface into the environment by convection and radiation, as this way of measurement requires certain temperature gradient. The portion of heat transferred by radiation depends on surface emission coefficients of the tested fabric ε_1, of the hotplate porous surface ε_O and that of the surrounding walls ε_2. Nevertheless, the ISO 11092 Standard does not inform about the required surface emission coefficient of these walls. Thus, the heat flow transferred by radiation in two Skin models with different emissivity levels of the interior walls can differ.

Moisture from the wet porous plate through the dry tested fabric to the parallel air flow in the instrument air channel is transfered by convection. From the declared isothermal conditions at the water vapour resistance measurement should follow, that no heat is simultaneously transferred. However, in the praxis, the hotplate surface cooling may cause some negative temperature gradient Δt against the place inside the hotplate (close to the bottom of the hotplate) where the temperature sensor is placed. This temperature drop even the sophisticated temperature controlling system cannot compensate this negative effect caused by unwanted thermal resistance R_s between ther temperature sensor and the cooled plate surface. Let us suppose that the central part of the hotplate is kept at the same temperature t_b as the surrounding air t_a. The effective heat flow q_{evap}(eff) passing through the porous plate generates the mentioned negative temperature gradient Δt as follows [2]:

$$\Delta t = q_{evap}\ (\text{eff})\ R_s \qquad (1)$$

When measuring thin fabrics, this temperature gradient should appear at the fabrics outer surface, thus causing the following fabric heating (not cooling as the evaporation) by convection, characterized by the heat transfer coefficient α.

$$q_{conv} = \alpha\Delta t, \quad \Delta t = q_{evap}\ R_s, \qquad q_{conv} = \alpha\ q_{evap}\ (\text{eff})\ R_s \qquad (2)$$

Thus unwanted convection then heats both the porous layer of the tester and the tested fabric (when the fabric is placed on the porous layer), thus reducing the measurement precision:

$$q_{evap}\ (\text{eff}) = q_{evap}(\text{theor}) - q_{conv} = q_{evap}\ (\text{theor}) - \alpha\ R_s\ q_{evap}\ (\text{eff}) \qquad (3)$$

To reduce the effect of the $q_{conv,}$ thermal resistance R_s in the plate must be as low as possible. Unfortunately, the explained temperature drop Δt influences also heat transfer between the tested fabric and the walls surrounding the measuring space by radiation. This effect characterize the next equations (here the σ means the radiation constant), where the first one applies for the porous surface (when determining the R_{eto} of the boundary layer):

$$q_{evap,o,eff} = (\Delta p / R_{eto}) - \Delta t\ .\alpha - \Delta t\ .4\sigma(t_1 + 273)^3/[(1/\varepsilon_o)+(1/\varepsilon_1)-1] \qquad (4)$$

$$q_{evap,o,eff} = (\Delta p/R_{eto}) - q_{evap,o,eff}\ .R_s.\alpha - q_{evap,o,eff}\ .R_s.4\sigma(t_1 + 273)^3/[(1/\varepsilon_o)+(1/\varepsilon_1)-1] \qquad (5)$$

For the fabric surface (when determining the $R_{eto\ +\ Ret}$), the final equation will be similar:

$$q_{evap,s,eff} = (\Delta p/R_{et} + R_{eto}) - q_{evap,s,eff}\ .R_s.\alpha - q_{evap,s}\ .R_s\ .4\sigma(t_1 +273)^3/[(1/\varepsilon_o)+(1/\varepsilon_1)-1] \qquad (6)$$

Then, both Eq. ( ) and Eq. ( ) then serve for calcullation of R_{eto} and (R_{eto} + R_{eto}) and finally for the determination of the required evaporation resistance Ret. For ideal isothermal conditions, the Ret is given by the relationship

$$R_{et} = \Delta p\ /[\ (1/q_{evap,s,teor)} - \ 1/q_{evap,o,teor)}\ ] \qquad (7)$$

For real quasi - isothermal (non - isothermal) conditions, the terms qevap,s,teor and qevap,o,teor will be replaced by the relationships for qevap,s,eff and qevap,s,eff, which will confirm the negative effect of the unwanted thermal resistance Rs and hence relatively high emissivity levels of the surrounding walls ε2 on the measurement precision. Similar relationships can be derived fo the effect of the above parameters Rs and ε2 on the precision of measurement of thermal resistance of fabrics Rct.

2. Experimental results

In order to confirm the above findings, Ret values of 3 polyester and 3 cotton plain woven fabrics differing in their square mass (from 106 to 260/439 g/m^2) were determined in two different testing instruments – Skin models. The first one was designed according to the ISO 11092, having relatively thick porous plate (more then 5 mm), and the second one was the PERMETEST [1], where the thickness of its porous plate is 0,1 mm only. Emissivity levels of the walls surrounding the measured sample were 0,1 and 0,7 mm (approximately).

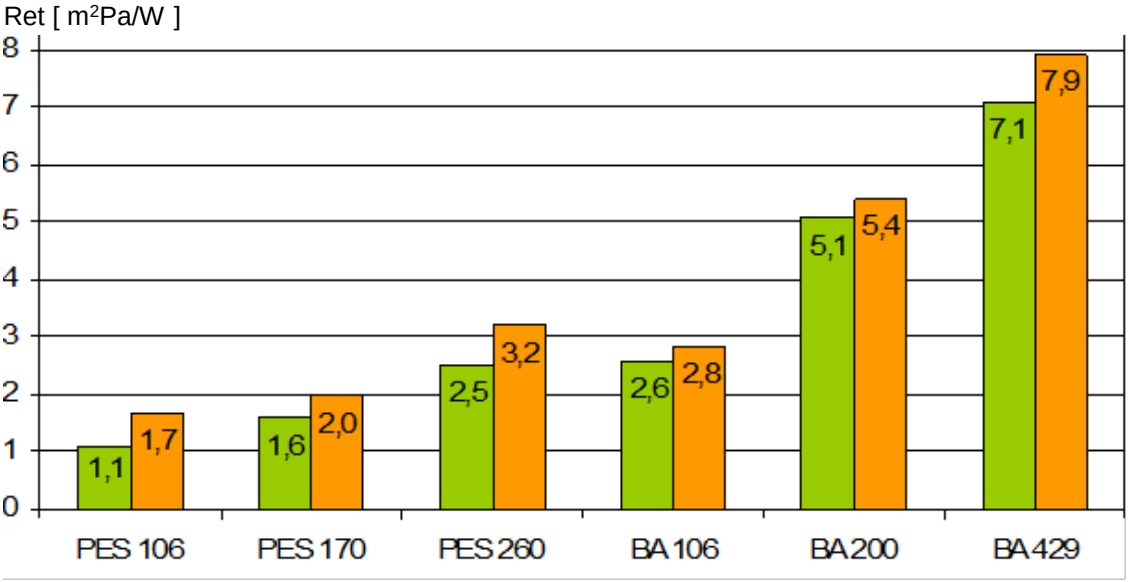

Figure 2. Values of the evaporation resistance Ret [m^{2}Pa/W] of PES and cotton (BA) fabrics with **varying square mass** (from 106 to 260/429 g/m^2) determined on a Skin model (according to the ISO 11092) with thick porous measuring plate (5 mm), **where the green columns present values for the grey surface** (emissivity approx. 0,7) of the inner walls of the measuring surface, whereas the **orange levels were found for the polished surfaces** (emissivity approx. 0,1).

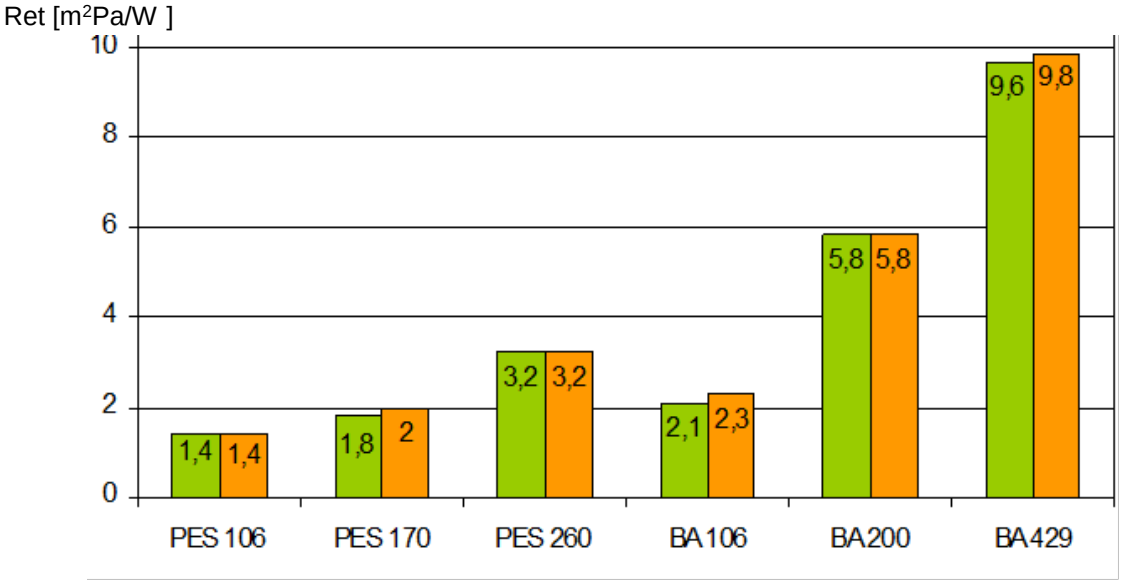

Figure 3. Values of the evaporation resistance Ret [m^{2}Pa/W] of PES and cotton (BA) fabrics with **varying square mass** (from 106 to 260/429 g/m^2) determined on a small PERMETEST Skin model (according to the modified ISO 11092) with thin porous measuring plate (0,1 mm), **where the green columns present values for the black surface** (emissivity approx. 0,9) of the inner walls of the measuring surface, whereas the **orange levels were found for the polished surfaces (emissivity approx. 0,1).**

Figure 4. The PERMETEST non-destructive water vapour permeability tester (Skin model)

3. Evaluation of results

It was found, that in the first instrument with the thick measuring plate, the dark (grey) channel walls caused the reduction of the Ret values from 6 to 20%, both for the PES and cotton fabrics, whereas in the second instrument with ultrathin porous plate, smaller reduction effects (2 to 5%) of the emissivity of the channel walls on the measured Ret values were observed.

4. CONCLUSIONS

The objective of the presented study was to verify whether the different mechanical design of two different Skin model testers may influence the measurement precision of these important textile comfort testing instruments. The presented experiments confirmed the predicted imperfections of the Skin model with higher thermal resistance of the measuring plate. However, the observed relatively low inaccuracy still do not limit the practical use of these devices [3], unless more systematic study provide other negative results.

References

1. *Hes, L. and Dolezal, I., A New Computer-Controlled Skin Model for the measurement of water vapour resistance (2003). In: 7th Asian Textile Conference, New Delhi.*
2. *Hes, L. (2008): Comments to the use of skin models for determination of water vapour resistance of fabrics. In: Fiber Society Internat. Conference, ENSITM Mulhouse.*
3. *Baczek-Boguslawska M., Hes, L.(2013). The Effective Water Vapour Permeability of Wet Wool Fabric and Blended Fabrics. Fibres & Textiles in Eastern Europe 21, 1(97),67-71.*

EXPERIMENTAL AND PREDICTED SPECIFIC STRESS STRAIN CURVES OF WORSTED STAPLE YARNS

[1]Muhammad Zubair[1], Bohuslav Neckar[1], Hafiz Shahzad Maqsood[2]

[1]Department of Textile Technology, Faculty of Textile Engineering, Technical University of Liberec, Liberec, Czech Republic

[2]Department of Material and Technics, Faculty of Textile Engineering, Technical University of Liberec, Liberec, Czech Republic
Corresponding author:zubair_fmd@yahoo.com

Abstract

In this paper, specific stress strain curves were predicted for worsted staple spun yarns. The experimental fiber specific stress strain and predicted coefficient of fiber stress utilization curves were used to predict the yarn specific stress strain curves before break. Experimental fiber specific stress strain curve, twist angle, contraction ratio and fiber angular preference C were used to evaluate the coefficient of fiber stress utilization before the process of break. The predicted coefficient of fiber stress utilization and yarn specific stress strain curves captured well the experimental coefficient of fiber stress utilization and yarn specific stress strain curves both in shape and position for the studied worsted yarn types.

Keywords:

Worsted *fiber specific stress, worsted yarn specific stress, coefficient of fiber stress utilization, fiber average curves, yarn average curves.*

1. Introduction

The mechanical properties of yarn have considerable effect on processing behavior and performance characteristics of both yarn and fabric. The strength of staple spun yarn is one of the most important mechanical properties. So, yarn theoretical analysis is essential for understanding factors contributing to yarn strength. Theoretical analysis of tensile behavior of staple spun yarns is very complex because of discontinuities at fiber ends, fibers can slip, break or both phenomena can occur during yarn extension.

he frequent attempts were made by Hearle et al. [1] to establish fundamental theories for staple spun yarns. The yarn strength in terms of yarn structure was analysed by Gegauff [2] in 1907. Gregory [3] established a relationship between fiber properties and geometrical arrangement for strength of spun yarns. Gurney [4] developed a relationship by taking into account frictional properties and fiber length to evaluate stress developed in individual fibers. Sullivan [5] derived a relation for maximum strength at optimum twist. He assumed that all fibers are parallel, helical and arbitrary tension is developed in fibre in outer layers of yarn. Some other studies predicted spun yarn tenacity [6, 7, 8, 9, 10, 11]. Dang, M. et al. [12] predicted the stress strain curves of wool spandex core spun yarns using finite element analysis. They used the concept of Luijk et al. [13, 14] and Hearle's theory [1]. Sriprateep, K. et al. presensed a method to model the whole stress strain curves for multifilament twisted yarns using finite element analysis [15]. The present authors have presented mathematical model considering real stress strain

relation for fiber and yarn and its validation for coefficient of fiber stress utilization for viscose ring and rotor staple spun yarns [16] [17].

Yet, no mathematical model has been reported that is able to calculate the yarn specific stress before break from the concept of coefficient of fiber stress utilization and fiber stress strain curves for worsted staple spun yarns. In the current study, the same mathematical model has enabled to calculate the yarn specific stress before break from the concept of coefficient of fiber stress utilization and experimental fiber stress strain curves for worsted staple spun yarns.

2. Experimental

Experiments were carried out to verify the theoretical model that predicts coefficient of fiber stress utilization and yarn specific stress [16] . Two different linear densities of worsted staple spun yarns were used for validation of the proposed mathematical model.

2.1. Material and method

Worsted fiber was used for the model validation. Tenacity and fineness of the worsted fiber was measured on Lenzing Vibrodyn-400 according to the standard test method EN ISO 1973. Fibre specifications are shown in Table 1.

Table1. Fiber specifications

Parameters	Worsted
Fineness (dtex)	3.81
Tenacity (cN/tex)	15.43
Breaking force (N)	5.90
Breaking strain (%)	31.7

The yarns tensile properties were tested using Instron-4411 in accordance with standard test method EN ISO 2060. The stress-strain curves data before break of fifty fiber samples was obtained from the software of the instruments used. Then the average curves for fiber and yarn were obtained by using Matlab software. Yarn diameter was determined by image analysis technique according to the standard test method [18]. The physical characteristics of worsted yarns are presented in the Table 2.

Table 2 Worsted yarn specifications

Yarn linear densities		Yarn twist	Yarn dia.	Twist angle
Nominal[tex]	Actual[tex]	Z [m-1]	D[mm]	$\beta_D[\mathrm{deg.}]$
20	20.03	790	0.177	23.7
23	23.25	640	0.190	21.0

3. Results and discussions

Based on the average worsted fiber stress strain curves and fiber stress utilization coefficient predicted from our mathematical model we have obtained yarn specific stress strain curves before break. We have compared predicted and experimental coefficient of fiber stress utilization and yarn specific stress strain curves in order to verify the accuracy level of the proposed model.

3.1 Average fiber and yarn stress strain curves

Figure 1 displays the average experimental stress-strain curves for worsted fiber and yarns. It can be noticed that the shape of the fiber stress-strain curve is very similar to that of the yarn stress-strain curve, but, as expected, the former is lying above the latter.

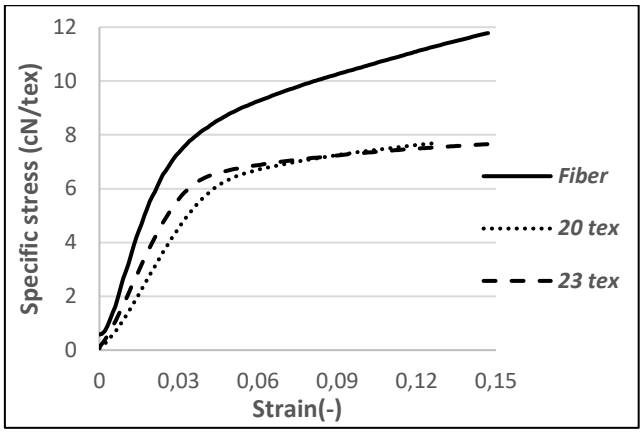

Figure 1. Average specific stress strain curves for worsted fiber and yarns

3.2 Coefficient of fiber stress utilization in yarn

Coefficient of fiber strength utilization in yarn is "in fact" the ratio of yarn tenacity and fiber tenacity and it is an indication of the contribution for the mechanical properties of the fiber to the mechanical properties of the yarn spun from it." Using fiber and yarn curves in Figure 1 the coefficient of fibre stress utilization in yarn was calculated from the following formula

$$\varphi\,(\varepsilon_Y) = \frac{\sigma_Y\,(\varepsilon_Y)}{\sigma_f\,(\varepsilon_Y = \varepsilon_f)} = \frac{\sigma_Y\,(\varepsilon_Y)}{\sigma_f\,(\varepsilon_Y)} \qquad (1)$$

where φ denotes coefficient of fibre stress utilization in yarn, σ_f indicates specific fiber stress, refers to fiber strain ε_f, σ_Y represents specific yarn stress, and ε_Y expresses yarn strain. The calculation for fiber stress utilization was performed for a range of strains started from $\varepsilon_Y = \varepsilon_f = 0.02$ and ended to strain of yarn before the process of break. Based on our experience, a very small value of strain was not chosen mainly as a consequence of relative uncertainty of measurement and/or fiber crimp. Liu et al. [19] reported a similar conclusion for measurement of fiber and yarn strains and they studied the stress-strain relationship beyond a strain of 2 %. We, therefore, decided to analyze the mutual stress-strain relation between fibre and yarn for a strain value ε_Y and/or σ_f of 0.05 (5 %) and beyond due to higher crimp and variability in worsted fiber. The fibre stress and yarn stresses for a given strain were found out from the corresponding stress-strain curves and then coefficient of fibre stress utilization φ_e in yarn was evaluated experimentally using Eq. (1).

The experimentally obtained numerical values for the coefficient of fibre stress utilization in yarns were compared with those obtained from the theoretical models. The simplest of all models is Gégauff's

model. According to this model, the coefficient of fiber stress utilization in yarn φ_G is expressed as follows

$$\varphi_G = (1+\eta)(\cos^2\beta_D) + \eta \ln\cos^2\beta_D/\tan^2\beta_D \quad (2)$$

Here, η denotes yarn lateral contraction ratio and β_D indicates twist angle of surface fibres in yarn. The other model, considering real fiber stress-strain relation, expressed the coefficient of fiber stress utilization in yarn φ_{C1} as follows

$$\varphi_{c1} = \frac{2}{\sigma_f(\varepsilon_Y)\ \tan^2\beta_D} \int_0^{\beta_D} \sigma_f(\varepsilon_f)\ \tan\beta d\beta \quad (3)$$

Here, δ_f (ε_f) refers to fiber stress-strain function, ε_f represents fiber axial strain and is written as $\varepsilon_f = \varepsilon_Y\ (\cos^2\beta - \eta \sin^2\beta)$, ε_Y shows yarn axial strain, β is general twist angle of fibre and β_D is maximum twist angle. Considering real fiber stress-strain relation and fiber orientation distribution in yarn, coefficient of fiber stress utilization in yarn φ_{c2} can be expressed as follow,

$$\varphi_{c2}(\varepsilon_Y) = \frac{2}{\sigma_f(\varepsilon_Y)\tan^2\beta_D} \int_0^{\beta_D} [\int_0^{\vartheta_u} \sigma_f(\varepsilon_f) \cos^2\vartheta\ u(\vartheta) d\vartheta]\ \frac{\sin\beta}{\cos^3\beta}\ d\beta \quad (4)$$

Where ε_Y is yarn axial strain, β is general twist angle of fibre, $\sigma_f(\varepsilon_f)$ is fiber specific stress σ_f as a function of fibre strain ε_f, $u(\vartheta)$ denotes probability density function of fiber inclination angle ϑ, and ϑ_u indicates upper limit of fibre inclination angle. The unimodal probability density function, $u(\vartheta)$ of non-oriented angles $\vartheta \in (0, \frac{\pi}{2})$ was derived earlier by Neckar et al. [20]. Fibers with angles ϑ approaching $\frac{\pi}{2}$ are being found in yarn structure only very seldom, however, they were identified by experimental analysis of internal structure of yarns derived by Neckář et al. [21, 22].

$$u(\vartheta) = \frac{1}{\pi} \frac{C}{C^2 - (C^2-1)\cos^2(\vartheta+\beta)} + \frac{1}{\pi} \frac{C}{C^2 - (C^2-1)\cos^2(\vartheta-\beta)} \quad (5)$$

Where *C* is parameter depends on angular preference of fibers in yarn, and it varies according to fibre type and spinning technology. The value of parameter *C* = 4.9 for worsted staple spun yarns was used. Furthermore, the following expressions are required for calculations.

$$\tan\beta_D = \pi DZ \quad (6)$$

ε_f and ϑ_u can be obtained as follows,

$$\varepsilon_f = \varepsilon_Y\ (\cos^2\vartheta\ -\ \eta\sin^2\vartheta) \quad (7)$$

$$\vartheta_u = \sin^{-1}\frac{1}{\sqrt{(1+\eta)}} \quad (8)$$

Where η is yarn lateral contraction ratio and it can be taken as 0.5 for textile materials. The coefficients of fiber stress utilization in yarns was calculated using data from Table 2, equations (4-8) and Matlab software. The predicted and experimental coefficient of fiber stress utilization at each strain value before break for worsted staple spun yarns from three different mathematical models as function of strain are shown in Figure 2 (a) and (b).

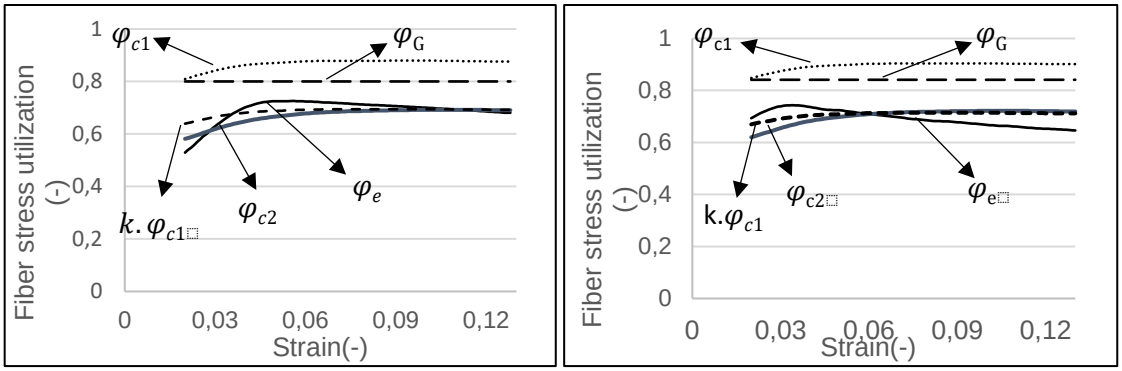

(a) 20 tex (b) 23 tex

Figure 2. Fiber stress utilization in worsted staple yarn(φ_e: fully experimental, : φ_G calculated according to Eq.(2) φ_{c1}, & $k.\varphi_{c1}$:calculated according to Eq. (3), φ_{c2} : calculated according to Eq. (4-8))

3.3 Yarn specific stress

The theoretical coefficient of fiber specific stress utilization, $\varphi_{c2}(\varepsilon_Y)$ and the average fiber specific stress strain curve data was used to predict the worsted yarn specific stress, $\delta_Y(\varepsilon_Y)$ as follows,

$$\sigma_Y(\varepsilon_Y) = \sigma_f(\varepsilon_Y).\varphi_{c2}(\varepsilon_Y) \quad (9)$$

Where $\sigma_f(\varepsilon_Y)$ is fiber specific stress σ_f as a function of yarn strain ε_Y. Theoretical and experimental yarn specific stress strain curves for both worsted yarns are shown in the Figure 3. Comparing results, it can be observed that the theoretical worsted yarn specific stress strain curves agree well with the experimental yarn specific stress strain curves both in shape and position before process of yarn break.

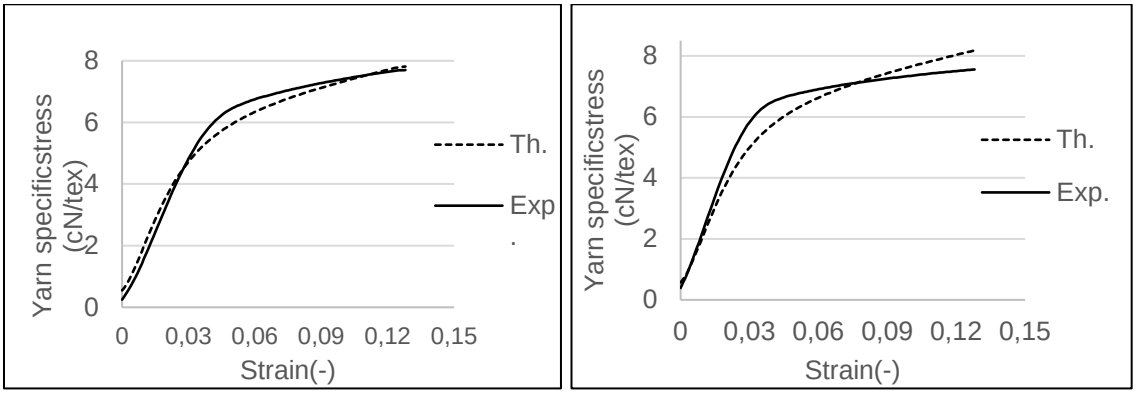

(a) (b)

Figure 3. Specific stress strain curves for worsted yarns; (a) 20 tex, and (b) 23 tex.

The slight difference between predicted and experimental curves in 23 tex yarn might be the result of higher crimp and variability in worsted fiber in that yarn.

4. CONCLUSION

The fiber specific stress strain curves are at higher position when compared with yarn specific stress strain curves for both yarns used in this study. The individual coefficient of fiber stress utilization and yarn specific stress strain curves predicted from theoretical model coincided well with the experimental coefficient of fiber stress utilization and specific stress strain curves for both worsted yarns before the process of break. However, for 23 tex worsted yarn, the prediction was not very accurate because of higher crimp and variability in worsted fiber.

ACKNOWLEDGEMENTS

The author is indebted to Ing. Petra Jiraskove from Department of Textile Technology who provide worsted yarn for this research.

References

1. *J. W. Hearle, P. Grosberg and S. Backer, Structural Mechanics of Fibers, Yarns, and Fabrics, NY: Wiley-Interscience, 1969.*
2. *M. C. Gégauff , "Strength and Elasticity of Cotton Threads," Bull. Soc. Ind. Mulhouse, vol. 77, pp. 153-176, 1907.*
3. *J. Gregory, "The Strength of Twisted Yarn Elements in Relation to The Properties of The Constituent Fibers," Journal of Textile Institute, vol. 41, p. T499–T512, 1953.*
4. *H. P. Gurney, "The Distribution of Stress in Cotton Products," Journal of Textile Institute, vol. 16, pp. T269-289, 1925.*
5. *R. R. Sullivan, "A Theoretical Approach to The Problem of Yarn Strength," Journal of Applied Physics, vol. 13, 1942.*
6. *N. Pan, "Development of a Constitutive Theory for Short Fiber Yarns: Mechanics of Staple Yarn Without Slippage Effect," Textile Research Journal, vol. 62, no. 12, pp. 749-765, 1992.*
7. *N. Pan, "Development of a Constitutive Theory for Short Fiber Yarns. Part II: Mechanics of Staple Yarn with Slippage Effect," Textile Research Journal, vol. 63, no. 9, pp. 504-514, 1993.*
8. *N. Pan, "Prediction of Statistical Strengths of Twisted Fibre Structures," Journal of Materials Science, vol. 28, no. 22, pp. 6107-6114, 1993.*
9. *N. Pan , T. Hua and Y. Qui, "Relationships Between Fiber and Yarn Strengths," Textile Research Journal, vol. 71, pp. 960-964, 2001.*

A. *Ghosh, S. M. Ishtiaque and R. S. Rengasamy, "A Generalized Mathematical Approach to Predict the Strength of Different Spun Yarns," in Proceedings of The 5th International Conference: TEXTILE SCIENCE 03, Technical University of Liberec, Czech Republic, 2003.*

10. *H. W. Krause and H. A. Soliman, "Theoretical Study of The Strength of Single Jet False Twist Spun Yarns," Textile Research Journal, vol. 60, pp. 309-318, 1990.*
11. *M. Dang and S. Wang, "Theoretical Prediction on Tensile Model of Wool/Spandex Core Spun Yarn," Journal of Industrial Textiles, vol. 37, no. 4, pp. 301-313, 2008.*
12. *C. J. Luijk, A. J. Carr and G. A. Carnaby, "Finite-element Analysis of Yarns Part I: Yarn Model and Energy Formulation," Journal of Textile Institute, vol. 75, no. 5, pp. 342-353, 2008.*
13. *C. J. Luijk, A. J. Carr and G. A. Carnaby, "Finite-element Analysis of Yarns Part II: Stress Analysis," Journal of Textile Institute, vol. 75, no. 5, pp. 354-362, 2008.*
14. *K. Sriprateep and L. J. Bohez, "Cad/Cae for Stress–Strain Properties of Multifilament Twisted Yarns," Textile Research Journal, vol. 0, no. 0, pp. 1-12, 2016.*
15. *B. Neckář and D. Das, "Tensile behavior of staple fiber yarns part I: theoretical models," Journal of textile institute, vol. 0, no. 0, pp. 1-9, 2016.*
16. *M. Zubair and B. Neckar, "Tensile behavior of staple fiber yarns part II: model validation," Journal of textile institute, vol. 0, no. 0, pp. 1-4, 2016. Faculty of Textiles, Textile Research Center, Internal Standards, Section B – Textile Materials and Design of Textile Products.IS 22-103-01/01, Technical University of Liberec, 2004.*
17. *T. Liu , K. Choi and Y. Li , "Mechanical modeling of single yarns," Textile research journal, vol. 77, pp. 123-130, 2007.*
18. *B. Neckář and D. Das, Theory of Structure and Mechanics of Fibrous Assemblies, New Delhi: Woodhead Publishing India, 2012.*
19. *B. Neckář and M. K. Soni, "Modeling of Radial Fiber Migration in Yarn," Textile Research Journal, vol. 76, pp. 486-491, 2006.*
20. *B. Neckář and M. K. Soni, "Physical Model of Internal Yarn Structure, Part VI. Research Report PT 2 – XI/79," State Textile Research Institute, Liberec, 1979.*

THEORETICAL ANALYSES OF AIR JET YARN STRENGTH

Moaz Eldeeb

Department of Textile Technology, Faculty of Textiles
Technical University of Liberec, Liberec, Czech Republic
Correspondence author: eldeeb.moaaz@gmail.com
Telephone: +420 776 714 456

Abstract:

In this article, a mathematical model that predicts Viscose and Tencel air jet spun yarn strength on short gauge length has been presented. The method is based on calculating the core fibre strength as a parallel bundle of fibres, wrapper fibre strength as a bundle of fibres in the form of helical path and considering the interaction effect between wrapper and core fibres. Fibre parameters in addition to yarn structural parameters were used to obtain theoretical yarn strength at short gauge length. Results showed that the accuracy of proposed model is satisfactory.

Keywords:

air jet yarn, prediction, strength, structure, core fibres, wrapper fibres

1. Introduction

Air jet spun yarns consist of untwisted parallel core fibres and covered with twisted surface wrapping fibers that incline on yarn axis by different angles. To engineer such yarns aiming better quality, this requires to know the relationship between fibre properties, yarn structure and yarn properties. The mathematical models are usually used to describe and explain such relationships. Numerous researchers presented a good contribution in this topic. Many of them presented mathematical models for ring spun [1][2][3][4] and rotor yarns [5]. Nevertheless, mathematical models of air jet spun yarns are limited [6][7][8][9]. Rajamanickam et al. presented mathematical models that predict air jet yarn strength. They obtained a mathematical relationship between yarn breaking load and its structure. The model also classified the modes of yarn failure into noncatastrophic, catastrophic, and failure due to complete slippage [10][11]. However, they obtained a prediction error which was quite high. In this article, their model has been modified targeting better prediction accuracy.

To achieve this goal, we have divided the air jet yarn into core which is almost parallel fibers and wrapper which is in a helical form. We have calculated the core strand strength as a parallel bundle of fibres. This strand is also subjected to normal forces of the wrapper fibres. Therefore, the frictional forces applied on the core fibres strand have been calculated. In addition, we have calculated the strength of the wrapper fibre strand. It is worth mentioning that the predicted core fibre strand was calculated based on the assumption that the fibers are griped between two jaws and the gauge length of the yarn tensile tester is less than fibre length. Consequently, to verify our model, the air jet yarn strength was measured at a gauge length shorter than the fibre length. The yarn structure is assumed to be ideal as shown in Figure 1. Where we assumed that wraps width and height are constant and distributed regularly along yarn axis, helix angle is constant, and core fibres are straight and parallel to yarn axis.

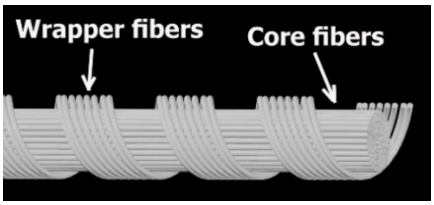

Figure 1. Ideal structure of air jet yarn.

2. Model for the failure of air jet yarn:

2.1 Failure of core fibre strand:

There are two components that contribute to core yarn strength; the strength of a parallel bundle of fibres griped between two jaws of the tensile testing instrument and the strength of that bundle originated from a fiber-to-fiber frictional force caused by the normal forces from the wrapper fiber strand during extension process. Assuming that the yarn cross section is circular and remains circular till break. To obtain the normal forces on core fibres, Krause et al. model was used. By analyzing the forces acting on an elemnet of a wrapper fiber as shown in Figure 2 and following the same derivation steps, equations (1-6) have been used to calculate average strained wrapper fibre helix angle α, average strained pitch of wrapper fibers p, strained yarn radius r, and normal forces exerted by wrapper fibers per unit length N. [6][7][8][9].

$$e_y = 2(sin\,\alpha_o)^2 - 1 + \sqrt{(2(sin\,\alpha_o)^2 - 1)^2} + e_f\left(2 + e_f\right) \quad (1)$$

$$e_r = -e_y \quad (2)$$

$$sin\,\alpha = \left(\frac{1 + e_r}{1 + e_f}\right) sin\,\alpha_o \quad (3)$$

$$p = p_o\left(1 + e_y\right) \quad (4)$$

$$r = r_o(1 + e_r) \quad (5)$$

$$N = \frac{\sigma_f(\sin\alpha)^2}{r} \quad (6)$$

Where e_y expresses yarn longitudinal strain, α_o is average unstarained wrapper fibre helix angle, e_f is fibre breaking elongation, e_r indicates yarn lateral strain, p_o is average unstrained pitch of wrapper fibers, and r_o is unstrained yarn radius.

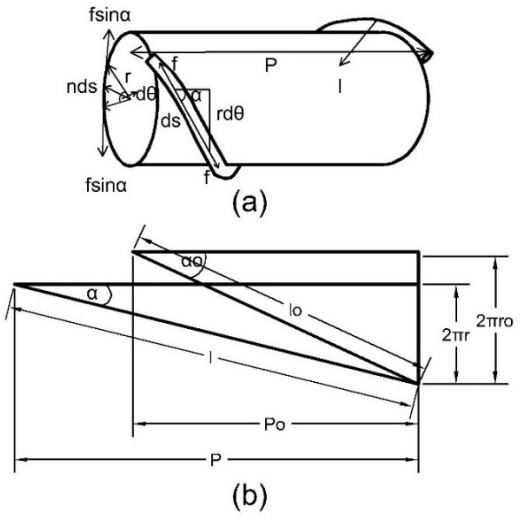

Figure 2. Air jet yarn (a) Stress analyses. (b) Unstrained and strained yarn geometry [6].

We can then obtain the total frictional forces on core fibres σ_2 as a result of the total normal forces exerted by wrappers fiber strand σ_2 as follows,

$$\sigma_2 = \mu \frac{\sigma_f (\sin\alpha)^2}{r} \frac{W}{100} \frac{T_y}{T_f} p \tag{7}$$

Where μ is the fibre friction coefficient.

Assume a yarn has linear density T_y is gripped between tensile tester gauges with a gauge length less than fibre length. The yarn was spun using short staple fibres with linear density T_f. And let us assume that these fibres are straight, parallel to yarn axis, have equal circular diameters, no slippage occurs between core fibres due to the usage of short gauge length, inter-fibre friction is so small that can be ignored and individual fibre position in the yarn is random. Therefore, using Neckář theory of parallel fibre bundle [12], fibre length utilization factor η can be calculated using the following formula,

$$\eta = \begin{cases} \int_0^{l_{max}} \left(1 - \frac{h}{l}\right) \gamma(l)\, dl \,, h < l_{max} \\ 0 \qquad\qquad\qquad\qquad\quad , h \geq l_{max} \end{cases} \tag{8}$$

And h denotes the gauge length, l is fibre length, and $\gamma(l)$ is mass fraction function which is the summation of the partial mass fractions of each fiber in the yarn and can be calculated using equation (9)

$$\gamma(l) = \sum_{j=1}^{k} \frac{m_j}{m} \tag{9}$$

And m_j is the mass of jth fiber and m is the mass of the yarn calculated at the maximum fiber length. The value of $\gamma(l)$ is from 0 to 1. If all fibres in the yarn have the same fibre length and equal to the maximum fibre length, then $\gamma(l)$ will be equal to 1 and the parallel bundle strength will be a function of gauge length only. Thus, we can obtain the core fibres strength as a parallel bundle griped between two jaws σ_1 using equation (8) and (9) as follows,

$$\sigma_1 = \sigma_f \frac{100 - W}{100} \frac{T_y}{T_f} \eta \tag{10}$$

And σ_f denotes fibre breaking load and W denotes wrapper fibres percentage

2.2 Failure of wrapper fibre strand:

If we hypothesized the existence of uniform normal pressure on core fibers due to the wrapping effect, constant wrapping angle and fibers are breaking simultaneously due to extension at a gauge length less than fibre length. Total wrapper fibres strength σ_3 can be obtained using the following relation [6].

$$\sigma_3 = \sigma_f \cos\alpha \frac{W}{100}\frac{T_y}{T_f} \tag{11}$$

According to equations (1-11), it is possible to obtain yarn strength σ_Y using the following equation.

$$\sigma_Y = \sigma_1 + \sigma_2 + \sigma_3 \tag{12}$$

3. Experimental verification

Air jet yarns were spun from 38 mm Viscose and Tencel fibres using Rieter air jet spinning machine J20 with different linear densities. Tenacity and fineness of fibers were measured on Lenzing Vibrodyn-400 according to ENISO1973. Fibre length distribution was obtained using Sinus instrument according to ASTMD1447. Yarn number of wraps per meter and average helix angle were measured using microscope. Yarn wrapper ratio W was calculated according to the formula,

$$W = \frac{c(b^2 - a^2)}{c(b^2 - a^2) + a^2 d}.100 \tag{13}$$

Figure 3 shows the 23 Tex yarn longitudinal view under the microscope for 1000 random yarn section were analyzed and parameters a, b, c and d were obtained. Yarn diameter was measured using Uster tester according to ASTM1425. Yarn strength was measured at short gauge length (30 mm) using Labortech instrument.

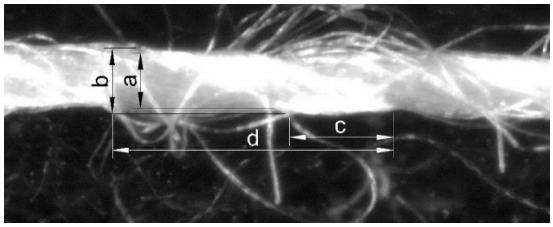

Figure 3. 23 Tex viscose yarn longitudinal view under microscope.

4. Results and discussion

Table 1 shows the fibre parameters that were used as an input for the calculation. It also shows the measured yarn parameters under microscope along with predicted and experimental values of yarn tenacity are shown in Table 1. Results show that the proposed model exhibited good agreement with the experimental results of yarn breaking load where the prediction error varies from -8.58% to 11.85%. The higher values of prediction error could be ascribed to the variation in the measured values of wrapper fibre helix angle, wrapper fibre ratio and number of wraps per unit length. By comparing the breaking load of 23 Tex viscose and tencel yarns in the table, it can be seen that the tencel yarn is stronger than viscose yarn. The fibre length utilization factor of viscose fibre is greater than tencel fibres, nevertheless, the fibre breaking load of tencel (5.14) is greater that viscose fibre (3.9). This difference influenced more the core and wrapper fibre strength, σ_1, σ_2 and σ_3, and consequently the final yarn strength. It can be observed that the theoretical strength of core fibres

(σ_1+σ_2) is bigger than the wrapper fibres strength σ_3. This is because the number of core fibres in yarn cross section is bigger than wrapper fibers, in addition, these core fibres are subjected to the normal forces from the wrapper fibers.

Table 1. Spun fibres parameters along with the theoretical and experimental values of yarn breaking load.

Parameters	Viscose					Tencel
Fibre length utilization factor η (-)	0.199	0.199	0.199	0.199	0.199	0.188
Fibre friction coefficient μ (-)	0.35	0.35	0.35	0.35	0.35	0.35
Fibre breaking elongation e_f (%)	13.00	13.00	13.00	13.00	13.00	8.20
Fibre fineness T_f (tex)	0.13	0.13	0.13	0.13	0.13	0.13
Fibre breaking load σ_f (cN)	3.90	3.90	3.90	3.90	3.90	5.14
Actual yarn count T_y (tex)	15.90	20.00	22.40	25.00	29.4	22.6
Wrapper fibre ratio W (%)	31.70	31.50	30.90	30.10	29.20	31.00
Yarn diameter d (mm)	0.20	0.23	0.25	0.28	0.27	0.25
Average unstrained wrapper fibre helix angle α_o (deg)	30.37	28.65	29.22	27.50	26.36	28.65
Average yarn wraps per meter (1/m)	958.00	948.00	817.00	807.00	709.00	795.00
Average unstrained pitch of wrapper fibers p_o (mm)	1.04	1.05	1.22	1.24	1.41	1.26
Yarn lateral strain e_r (%)	-13.48	-13.43	-13.45	-13.40	-13.37	-8.62
Average strained wrapper fibre helix angle α (deg)	22.92	21.77	21.77	20.63	20.05	24.06
Strained yarn radius r (mm)	0.09	0.10	0.11	0.12	0.12	0.11
Average strained pitch of wrapper fibers p (mm)	1.18	1.20	1.39	1.41	1.60	1.37
Predicted core pressure σ_2 (cN)	108.02	107.25	131.47	114.69	141.19	189.94
Predicted wrapper strand breaking load σ_3 (cN)	139.42	175.79	192.59	211.14	242.17	253.04
Predicted core strand breaking load σ_1 (cN)	64.83	81.79	92.41	104.33	124.27	115.80
Predicted yarn breaking load σ_Y (cN)	312.27	364.83	416.46	430.16	507.63	558.77
Experimental yarn breaking load (cN)	287.60	361.60	415.40	453.20	575.90	612.50
Prediction error (%)	-8.58	-0.89	-0.26	5.08	11.85	8.77

5. CONCLUSIONS

Based on fibre parameters, namely friction coefficient, mean fibre length, fibre length distribution, breaking load, breaking elongation, fineness and air jet spun yarn structural parameters, namely wrapper fibre helix angle, wrapper fibre ratio and number of warps per unit length, it is possible to predict air jet yarn strength at short gauge length using the presented model in this article. The model calculated three component of strength, core strength as a parallel bundle of fibers, wrapper fibers pressure on core fibres and wrapper fibre strength. The experimental result agreed with the proposed model. The model may be developed to calculate the yarn strength at longer gauge length (500 mm).

ACKNOWLEDGEMENTS

The author acknowledge Prof. Sayed Ibrahim for giving the basic notion to develop the proposed model.

References

1. *E. Önder and G. Baser, "A comprehensive stress and breakage analysis of staple fiber yarns Part I: Stress analysis of a staple yarn based on a yarn geometry of conical helix fiber paths," Text. Res. J., vol. 66, no. 9, pp. 562–575, 1996.*
2. *W. Zurek, I. Frydrych, and S. Zakrzewski, "A method of predicting the strength and breaking strain of cotton yarn," Text. Res. J., vol. 57, no. 8, pp. 439–444, 1987.*
3. *N. Pan, "Development of a constitutive theory for short fiber yarns: Mechanics of staple yarn without slippage effect," Text. Res. J., vol. 62, no. 12, pp. 749–765, 1992.*
4. *S. K. Aggarwal, "A model to estimate the breaking elongation of high twist ring spun cotton yarns part I: Derivation of the model for yarns from single cotton varieties," Text. Res. J., vol. 59, no. 11, pp. 691–695, 1989.*
5. *X. Y. Jiang, J. L. Hu, and R. Postle, "A new tensile model for rotor spun yarns," Text. Res. J., vol. 72, no. 10, pp. 892–898, 2002.*
6. *H. W. Krause and H. A. Soliman, "Theoretical study of the strength of single jet false twist spun yarns," Text. Res. J., vol. 60, no. 6, pp. 309–318, 1990.*
7. *Y. Xie, W. Oxenham, and P. Grosberg, "24—A study of the strength of wrapped yarns part I: The theoretical model," J. Text. Inst., vol. 77, no. 5, pp. 295–304, 1986.*
8. *Y. Xie, W. Oxenham, and P. Grosberg, "25—A study of the strength of wrapped yarns part II: Computation and experimental," J. Text. Inst., vol. 77, no. 5, pp. 305–313, 1986.*
9. *Y. Xie, W. Oxenham, and P. Grosberg, "26—A study of the strength of wrapped yarns part III: The relationship between structural parameters and strength," J. Text. Inst., vol. 77, no. 5, pp. 314–326, 1986.*
10. *R. Rajamanickam, S. M. Hansen, and S. Jayaraman, "Analysis of the modeling methodologies for predicting the strength of air-jet spun yarns," Text. Res. J., vol. 67, no. 1, pp. 39–44, 1997.*
11. *R. Rajamanickam, S. M. Hansen, and S. Jayaraman, "A model for the tensile fracture behavior of air-jet spun yarns," Text. Res. J., vol. 68, no. 9, pp. 654–662, 1998.*
12. *B. Neckář and D. Das, Theory of structure and mechanics of fibrous assemblies. Woodhead Publishing India, 2012.*

THE EFFECT OF MOISTURE CONTAINED IN WOVEN FABRIC ON ITS AIR PERMEABILITY AND POROSITY

Marie Havlová[1], Jana Špánková[2]

[1]Technical University of Liberec, Department of textile evaluation, Liberec, Czech Republic
e-mail: marie.havlova@tul.cz; telephone number: 420 485 353 234
[2]Technical University of Liberec, Department of textile technology, Liberec, Czech Republic
e-mail: jana.spankova@tul.cz; telephone number: 420 485 353 831

Abstract:

Air permeability and porosity are very important properties of textile fabrics and these properties are strongly related to each other. Another very important property of fabrics is their ability to moisture absorption. During normal use, the textile materials are moisturized due to the sweating. Moisture contained in the fabric reduces its porosity and therefore, it can be expected that it will also reduce its air permeability. This paper presents the results of an experiment which was carried out on a set of fabrics – cotton, polypropylene and cotton/polypropylene blends. Changes in the porosity and air permeability of these fabrics were investigated depending on the portion of the moisture contained in the fabric and also on the portion of the cotton fibres contained in the fabric. It was found that the changes in polypropylene fabrics are only little, conversely the most pronounced changes are in cotton fabrics. The change of the air permeability depending on the percentage of moisture content it is possible to approximate by a second-order polynomial model.

Key words:

Air permeability, porosity, woven fabric, moisture content, material composition

1. Introduction

Air permeability is one of the fundamental textile properties and it is an important factor in the comfort of a fabric. [1] This parameter is generally understood as the ability of air-permeable fabric to transmit air under the given well specified conditions – especially pressure difference Δp [Pa] and clamping area of the test sample S [m^2]. Air permeability depends on the structural parameters of the fabric – porosity plays the crucial role among them. Therefore, a number of authors research the relationship between the structure and permeability of a woven fabric [e.g. 1 – 5]. The property usually given by the description of the structure of the fabric is the porosity. The results of a number of earlier papers show that these two characteristics of the textile material – air permeability and porosity – are strongly related to each other [e.g. 1 – 3, 5].

Textile materials are generally porous materials. They are therefore composed from textile fibres and from air. Porosity P [-] expresses the proportion of air voids contained in the textile. It is therefore dimensionless quantity that is complementary to the filling. Conversely, filling F [-] expresses the portion of fibre material contained in the textile. Thus, the following applies:

$$P + F = 1 \qquad (1).$$

To determine the porosity or filling of textile material there are a number of theoretical models [6] (e.g. density based porosity models, area filling based porosity or volume filling based porosity) and experimental methods (e.g. method used an image analysis).

The porosity inside textile materials can be divided into [7, 8]:

- Inter-yarn porosity – includes pores between the yarns from which the fabric is made (see Figure 1),
- Intra-yarn porosity – includes pores inside the yarns, which are formed between the fibres,
- Intra-fiber porosity – includes spaces in the fiber substances.

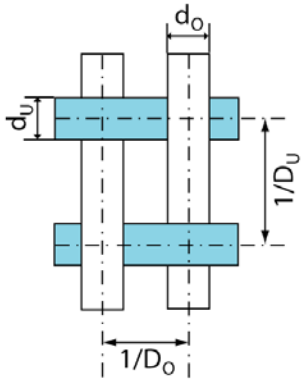

Figure 1. 2-D model of one inter-yarn pore

The ability of moisture absorption is also one of the fundamental properties of textile materials. The moisture in textiles may be placed in the spaces between fibres – in the intra-yarn and in the inter-yarn pores and in the case of moisture absorbing fibres (e.g. cotton, wool, viscose etc.) also within the structure of textile fibres. Moisture content can significantly affect the properties of textile material including air permeability. Moisture contained in the fabric reduces its porosity. Therefore, it can be expected that it will also reduce its air permeability. During normal use, the textile materials are moisturized due to the sweating. Therefore it seems very important to investigate the comfort properties of fabrics not only in a dry state but also in a wet state.

For example, the aspect of changes in the effective water vapour permeability of wool fabric and blended fabric due to the moisture content were discussed in paper [9]. It was shown that an increasing of moisture content in fabrics significantly worsens their ability to transport water vapour. For wool fabrics and wool/viscose blended fabrics the value decreases by over 70-80%.

In paper [8] the thermal resistance models of fleece fabrics in wet state were investigated. The contributions of fibres, air and moisture in textile material were used to predict the total thermal resistance of fabric. It was also shown that more than a 70% reduction in thermal resistance occurs between a 0.03 to 0.30 water ratio in wet fabric and therefore a small amount of moisture present in a fabric has a significant impact on its thermal resistance.

Wehner at al. in [10] investigated moisture induced changes in fabric structure and the air permeability measurement was used for evidence these changes. Their experiments have indicated that the air permeability of textile structures decreases as relative humidity is increased and the dimensional swelling of the fiber caused by moisture absorption leads to changes in fabric thickness and porosity. Rapid changes are already reflected when the relative humidity is increased from 0 to 40%.

Our contribution is aimed at evaluation of the impact of moisture contained in the fabric to the fabric porosity and to the air permeability. The fabrics used are made of cotton fibres, polypropylene fibres and cotton/polypropylene blends. These two fibrous materials have vastly different properties – e.g.

sorption of cotton fibres is 8.5% (under conditions 65% r. h., 22°C) and sorption of polypropylene fibres is 0%, density of cotton fibres is 1520 kg/m^3 and density of polypropylene fibres is 910 kg/m^3.

2. Experimental part

Cotton, polypropylene and cotton/polypropylene blended woven fabrics were used for the experiment. Air permeability and porosity of these fabrics were measured in the conditioned state and in the states when the samples are moistened to a certain percentage of moisture.

2.1. Materials

In this research two sets of woven fabrics were used for the experiment. All fabrics were made of yarns 45 tex linear density, in plain weave. The yarns used were produced by ring spinning technology. All fabrics in one set were produced with the same sett of warp yarns D_O [1/cm] – 18 yarns per cm for both sets and with the same sett of weft yarns D_U [1/cm] – 7.2 respective 10.8 yarns per cm. Only the material compositions of yarns were different. The fiber material was mixed by the mass method, which means that the yarn diameter varied depending on the proportion of cotton and polypropylene fibers. The yarn diameters were determined experimentally using USTER apparatus and are listed in Table 1.

Table 1. Yarn diameters [mm]

Material composition	100% CO	65%CO/35%PP	50%CO/50%PP	35%CO/65%PP	100%PP
Yarn diameter	0.262	0.313	0.297	0.321	0.339

For each fabric the D_O and D_U values were determined experimentally according to the standard ČSN EN 1049-2 and weight of the fabrics according to the standard ČSN EN 12127. A summary of the fabric parameters is shown in Table 2.

Table 2. Parameters of fabrics used (conditioned samples)

Sample No.	Count of yarns [tex]	D_O [1/cm]	D_U [1/cm]	Material composition	Weight [g/m^2]	AP [dm^3/m^{2}s]	P_{IA} [-]
1	45	18.1	7.5	100% cotton	155	1085	0.332
2		17.9	8.0	65% cotton/35% polypropylene	157	772	0.259
3		18.0	7.4	50% cotton/50% polypropylene	154	781	0.261
4		18.1	7.3	35% cotton/65% polypropylene	154	709	0.237
5		18.3	8.7	100% polypropylene	164	657	0.189
6		18.5	11.4	100% cotton	181	930	0.285
7		18.4	12.4	65% cotton/35% polypropylene	187	640	0.218
8		18.5	11.2	50% cotton/50% polypropylene	180	645	0.220
9		18.4	11.5	35% cotton/65% polypropylene	181	641	0.196
10		18.4	13.6	100% polypropylene	194	590	0.159

2.2. Methods

First of all, the air permeability of conditioned samples AP [dm^3/dm^{2}s] was measured using a digital tester – FX 3300 according to the Standard ČSN EN ISO 9237 (20 cm^2, 100 Pa) – these measured values are shown in Table 2.

Then, using an image analysis (software Nis Elements from Laboratory Imaging) the surface porosity P_{IA} [-] of fabrics was determined as a ratio between the number of pixels belonging to pores and the total number of pixels in the image. Some examples of images of fabrics are shown in Figure 2. This

method of porosity determination corresponds to the two dimensional theoretical model of porosity very well [5]:

$$P_S = 1 - (D_O d_O + D_U d_U - D_O d_O D_U d_U) \quad (2),$$

where d_O, d_U [m] are the diameters of a warp and weft yarn, respectively, and D_O, D_U [1/m] are setts of warp and weft yarns, respectively. The measurement P_{IA} [-] values was carried out in accordance with internal standard TU in Liberec (No. IN 23-107-01/01: Porosity and covering of fabrics). Images of fabrics were captured using microscope Nicon ECLIPSE E200 and camera Progres CT3 JENOPTIK. The measured porosity values of conditioned samples P_{IA} [-] are shown in Table 2. Due to the changing yarn diameter values (see Table 1) the porosity values P_{IA} [-] of fabrics in one set are also changed (see Table 2).

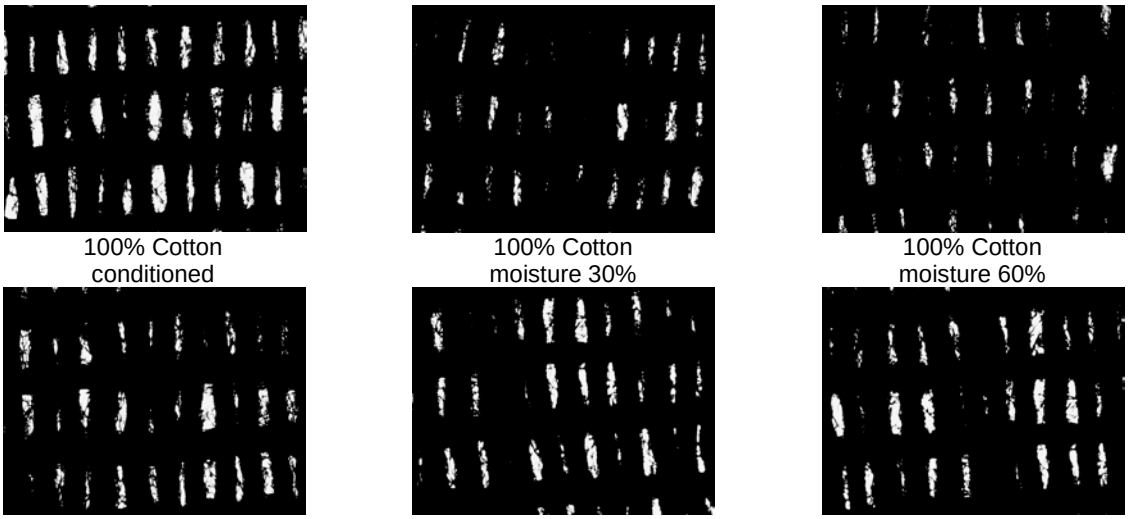

100% Cotton conditioned | 100% Cotton moisture 30% | 100% Cotton moisture 60%

100% Polypropylene conditioned | 100% Polypropylene Moisture 30% | 100% Polypropylene moisture 60%

Figure 2. Examples of images of woven fabrics, which were used for porosity determination (sample No. 1 and sample No. 5)

Furthermore, each sample of fabric was first completely wetted (20 min in 1l water containing 1 ml nonionic detergent) and then drying to a pre-defined moisture content in the sample (30%, 60%, 80% and 110%). Moisture percentage U [%] was determined as:

$$U = \frac{(m_m - m_c)}{m_c} * 100 \quad (3),$$

where m_m [g] is weight of a moistened sample and m_c [g] is weight of a conditioned sample. Drying was carried out on the basis of drying curves that have been previously determined for each sample.

Air permeability and surface porosity were measured also for these moistened samples of woven fabrics. All values of air permeability introduced in Table 2 and in the graphs below are average values obtained from 10 measurements. All introduced values of porosity are average values obtained from 75 measurements.

3. Results and discussion

Figure 3 shows the air permeability values of evaluated fabrics depending on the portion of cotton contained in fabric. Average values for conditioned and moistened samples are plotted. Similarly, Figure 4 shows the porosity values for conditioned and moistened samples. It is evident that in

conditioned state porosity and air permeability increase depending on the portion of cotton content. This is due to the mass method of mixture mentioned above.

In Figure 3 and Figure 4, there it is also evident that air permeability and porosity of polypropylene sample is changed due to the moisture content only little (up to 110% moisture content). Changes of air permeability and porosity due to moisture content in the fabric increase depending on the cotton content in the fabric, but in the cases of cotton/polypropylene blended fabrics the changes are quite similar. The most significant change is in the case of 100% cotton fabric. The most significant changes of porosity and permeability occur when fabric is moistened on the 30%. In further moistening the further changes are relatively small. The porosity of the fabrics decreases due to swelling of cotton fibres. The water molecules to get inside the fibres, and consequently increases the length and thickness of the cotton fiber. Assuming that the fabric structure has pores enough – i.e. spaces filled with air, due to the swelling of cotton fibres the yarn diameter gets larger and thus the inter-yarn pores are reduced. In contrast, the polypropylene fiber does not receive water molecules into its structure, and therefore does not swell. Figure 4 shows that the decrease of the inter-yarn porosity of fabric increases with increasing proportion of cotton fibres. The changes in the inter-yarn porosity are also evident in the Figure 2:

- In the case of 100% polypropylene fabric the changes in the inter-yarn porosity are only very small, the moisture is placed in the intra-yarn pores, the fibres do not swell.
- In the case of 100% cotton fabric the changes in the inter-yarn porosity are evident even when fabric is wetted to 30%. It is due to the swelling of cotton fibres. When further increases moisture content (e.g. to 60%), moisture gets into the intra-yarn pores primarily and other changes in inter-yarn porosity are already relatively small.

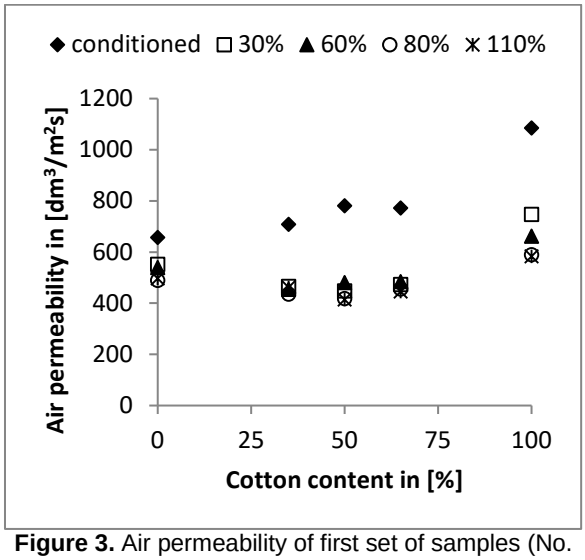

Figure 3. Air permeability of first set of samples (No. 1-5) – conditioned and moistened samples

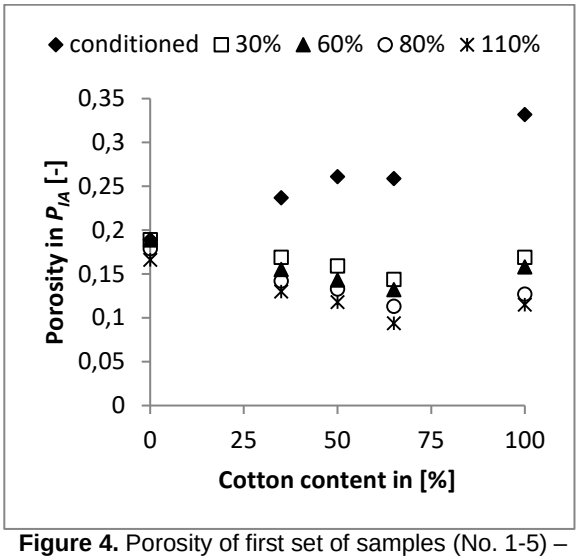

Figure 4. Porosity of first set of samples (No. 1-5) – conditioned and moistened samples

The inter-yarn porosity is crucial parameter for air permeability of fabric. Therefore, when the inter-yarn porosity of a fabric decreases, its air permeability will also decrease. Figure 5 shows the changes in the air permeability values depending on the moisture content in fabric. The values for the cotton, polypropylene and cotton/polypropylene blended fabrics are plotted. It is shown (in the case of 100% cotton fabric) that this dependence can be well approximate by a second-order polynomial model. It is evident that the highest drop in air permeability occurs when fabric is wetted to 30% moisture content.

Figure 6 shows relationship between air permeability and porosity of conditioned and moistened samples – 50% cotton/50% polypropylene, i.e. sample No. 3 and sample No. 8. This data indicate that

relationship between these parameters – porosity and air permeability – is still linear, even when there is moisture in the fabrics.

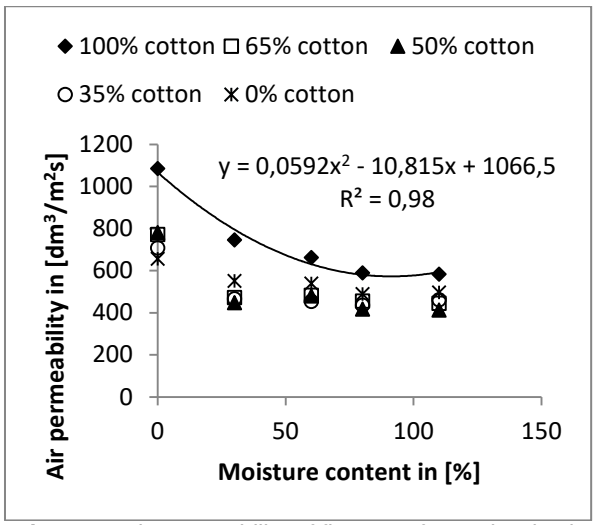

Figure 5. Air permeability of first set of samples (1-5) depending on the moisture content

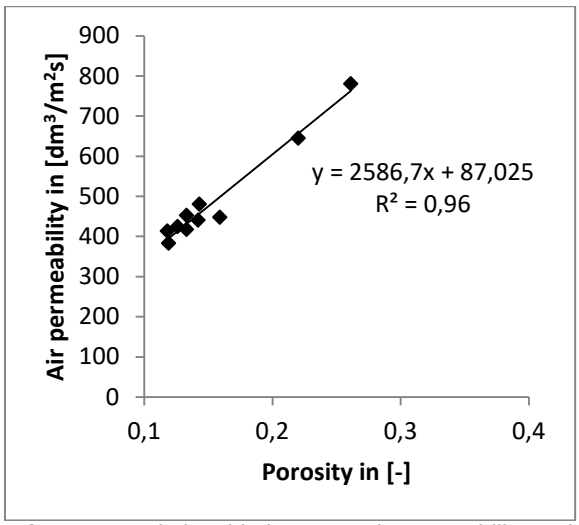

Figure 6. Relationship between air permeability and porosity conditioned and moistened 50%cotton/50%polypropylene samples (3 and 8)

4. CONCLUSIONS

The main aim of our contribution was investigation of the changes in the porosity and in the air permeability of woven fabrics depending on the portion of the moisture contained in the fabric. Cotton, polypropylene and cotton/polypropylene blended fabrics were used for the experiment. The results showed that:

- Air permeability and inter-yarn porosity of polypropylene woven fabrics are changed due to the moisture content only little. The moisture gets only into the intra-yarn pores, polypropylene fibres do not swell and therefore the yarn diameter remain approximately the same.
- The yarn diameter is increased, due to the moisture content, when the cotton fibres are contained in the yarn. The moisture gets inside the cotton fibres themselves, causing the fibres swelling. Therefore the inter-yarn porosity and air permeability decrease. This decrease is greater when the cotton fibres content is higher. The greatest changes occur in the 100% cotton fabrics.
- The most significant changes of porosity and air permeability already occur when the fabric is moistened to 30% moisture content. Dependence of the air permeability value on the percentage of moisture content in the fabric may be approximated by a second-order polynomial model.

In further research will be very interesting to investigate in more detail the area just up to 30% moisture content in the fabric.

References

1. *Zupin, Ž., HLadnik, A., Dimitrovski, K.(2011). Prediction of one-layer woven fabrics air permeability using porosity parameters. Textile Research Journal, 82 (2), 117-128.*
2. *Ogulata, R. T., Mavruz, S.(2010). Investigation of Porosity and Air Permeability Values of Plain Knitted Fabrics. FIBRES & TEXTILES in Eastern Europe, 18 (5), 71-75.*
3. *Havlová, M. (2014). Model of Vertical Porosity Occuring in Woven Fabrics and its Effect on Air Permeability. FIBRES & TEXTILES in Eastern Europe, 22 (4), 58-63.*
4. *Fatahi, I., Yazdi, A. (2012). Predicting Air Permeability from the Parameters of Weave Structure. FIBRES & TEXTILES in Eastern Europe, 20 (3), 78-81.*
5. *Militký, J., Trávníčková, M., Bajzík, V. (1999). Air permeability and light transmission of weaves. Internationsl Journal of Clothing Science and Technology, 11 (2/3), 116-124.*
6. *Militký, J., Havrdová, M. (2001). Porosity and air permeability of composite clean room textiles. International Journal of Clothing Science and Technology, 13 (3/4), 280-288.*
7. *Turan, R. B., Okur, A., Deveci, R. (2011). Predicting the intra-yarn porosity by image analysis method. Textile Research Journal, 82(16), 1720-1728.*
8. *Mangat, M., M., Hes, L., Bajzík, V. (2015). Thermal resistance models of selected fabrics in wet state and their experimental verification. Textile Research Journal, 85(2),200-210.*
9. *Boguslawska-Baczek, M., Hes, L. (2013). Effective Water Vapour Permeability of Wet Wool Fabric and Blended Fabrics. FIBRES & TEXTILES in Eastern Europe, 1 (97), 41-45.*
10. *Wehner, J., A., Miller, B., Rebenfeld, L. (1987). Moisture Induced Changes in Fabric Structure as Evidenced by Air Permeability Measurements. Textile Research Journal, 57(5), 247-256.*

INFLUENCE OF SELECTED PROCESS VARIABLES ON WORSTED COMPACT YARN PROPERTIES

Eva Moučková, Petra Jirásková

Technical University of Liberec, Faculty of Textile Engineering, Department of Textile Technologies, Liberec, Czech Republic, Studentská 2, 461 17 Liberec 1, The Czech Republic,
Telephone: +420 48 535 3274; Fax: +420 48 535 3542, eva.mouckova@tul.cz

Abstract:

In the work the influence of small change of draft and negative air pressure in condensation zone of drafting unit of compact spinning machine on selected worsted yarn properties is studied. Yarns (80% WO, 20% PA) were produced on a compact spinning machine equipped with the compression zone type Suessen EliTe from three rovings of various fineness using two levels of air negative pressure. Main draft ratio on the compact spinning machine was changed to the yarn of the same count be produced. To eliminate influence of roving irregularity on final yarn mass irregularity, machine irregularity was calculated and evaluated. Results confirmed that higher negative air pressure positively influences all observed properties of tested yarn (mass irregularity, number of faults, yarn hairiness, tenacity and breaking elongation) whereas increasing draft ratio up 20 % has statistically significant effect on thin places, number of neps as well as on yarn mass irregularity, but in this case from the point of practice, the difference is insignificant. On the other hand, draft has positive effect on yarn breaking elongation and, in much lesser extent on yarn tenacity. According to results, the level of negative air pressure is more significant factor which affects yarn property compared to observed range of draft ratio.

Key words:

Worsted yarn, compact spinning, draft, negative air pressure, hairiness, mass irregularity, yarn fault, tenacity, elongation.

1. Introduction

At present, compact spinning ranks among more widespread methods of spinning (staple spun yarn production). This spinning system is a modification of a conventional ring spinning system. A compression zone is added there and placed immediately after the three-roller two-apron drafting system on the compact spinning system. The reason of this is to create technological conditions for reduction of the spinning triangle and to create fibrous ribbon with an improved structure of fibers arrangement with respect to subsequent twisting. Narrowing of the fiber assembly in the compression zone, can be realized either mechanically or by the action of vacuum air.

The consequence is:

- Twisting fibrous band with more circular cross-section, i.e. elimination of different stress of fibres.
- Higher degree of orientation and arrangement of fibres and their uniform distribution, i.e. it is possible to better create yarn with structure closer to helical arrangement of fibres. All fibres are better tied with yarn body and contribute more on yarn tenacity. Overall, it leads to higher breaking strength and breaking elongation [6], [8].

- Higher condensation of fibres leads to a smaller yarn diameter, lower number of imperfectly spin-in fibres and thus to lower yarn hairiness and number of neps [6].
- Compact yarn has better yarn mass irregularity and lower number of yarn faults compared with conventional ring spun yarns [1], [3].

As manufacturers of compact spinning machines as well as yarn processors report, process of fibre condensation is also beneficial during subsequent processing of yarns and it significantly influences the properties of fabrics. Today, the compact spinning is used for both the cotton and the worsted spinning systems, where it is applied for spinning of conventional textile fibres as well as special fibres (for example aramid fibres) during production of technical yarns.

In an area of compact spinning a series of works were published. These works deal with comparison of the properties of compact and conventional ring spun yarns [1 - 8] or comparing properties of yarns produced employing various systems of a compression device [9], [10]. Most of the published works is focused on the cotton type of yarns. The works where authors evaluated worsted compact yarns are less frequent. As example we can mention work [8] where authors concluded that compact 100% WO, 100% PAN yarns and blended yarns (45% WO/55% PET, 50% WO/50% PAN) showed statistically significant lower yarn hairiness, higher tenacity and breaking elongation compared to conventional yarns; number of faults and mass irregularity of these compact yarns were also lower compared to conventional yarns, but the differences were not statistically significant for whole tested yarns. Other published works deal with comparing the properties of knitted and woven fabrics made of compact and conventional ring spun yarns (e.g.[11]), modelling and simulation of fibre behaviour in condensing zone (e.g. [12]). Not only the method of spinning, but also the adjustment of technological and technical parameters of machines affects yarn properties. Within the basic technological settings, in the case of compact spinning machines, the draft ratio, number of twist through spindle revolutions and delivery roller speed, and the negative pressure level is usually adjusted. The effect of these variables on the quality of the resulting yarn is generally known from the literature as well as practical experience. Authors in the work [13] observed the influence of negative pressure level and the distance of rovings on the Eli - Twist yarn properties. They experimentally demonstrated a beneficial effect of higher negative pressure and greater distance of rovings in the drawing mechanism on reduction of yarn hairiness and reduction the number of small faults (-30%, + 35%, neps + 140%).

The aim of this work is to study the influence of small changes of draft of drafting device and level of negative air pressure in the compression zone of compact spinning machine on selected properties of worsted yarn (mass irregularity, number of faults, yarn hairiness, tenacity and elongation). Negative pressure in condension zone of compact spinning frame is important for fibre strand compacting, but it increases production cost. Draft is necessary for supply roving attenuation but it increases mass irregularity. We assume that small change of draft (in total range of ca 20%) will not affect yarn mass irregularity significantly but on the other hand, using higher draft ratio (up to 20%) for production of yarn of the same count should brings significantly time saving during roving manufacturing. Also narroving the scale of roving fineness used for production of yarn of different fineness could lead to higher production flexibility.

2. Experiment

For experiment we used compact worsted yarns 80% WO/20% PA of count 10 tex, produced from rovings of three various fineness. To obtain yarns with the same count, they were spun using three levels of main draft ratio, break draft ratio was constant. Observed levels of total draft ratio was: 19.8; 22; 24.2. Yarns were spun with maximum possible negative air pressure (3.9 kPa) in compression zone of compact spinning machine and minimum negative air pressure under which the yarn spinning was technologically possible (2.4 kPa). Yarn twist was constant (nominal value 850 tpm). Compact spinning machine Suessen Fiomax 2000 was employed for yarn production. Selected parameters of used fibres are shown in the table 1.

Table 1: Main selected parameters of fibres

Material	Average fibre length	Average fibre fineness
WO	65 mm	16.5 μm
PA	65 mm	2.2 dtex

Within the experiment, yarn mass irregularity and yarn faults (thin places -50%, thick places +50%, and neps +200%), yarn hairiness (S12 and S3), yarn tenacity and breaking elongation were observed. Yarn mass irregularity and yarn faults were measured employing the Uster Tester IV instrument. Measuring conditions: speed 400m/min, time: 1 min. Yarn hairiness was measured using the Zweigle hairiness tester G567. Measuring conditions: speed: 50 m/min, time: 2 min. The Instron tensile tester was used for measuring tenacity and elongation. The clamping length of 500 mm was set during measurement, speed of crosshead: 370 mm/min. Obtained data were statistically treated using two-way analysis of variance (ANOVA). The significance level of 5% was applied.

2.1 Results and discussion

Mass irregularity and yarn faults

Average values and corresponding 95% confidence intervals of yarn mass irregularity and yarn faults are presented in Figure 1 – 4. Selected results of two-way analysis of variance are mentioned in the table 2.

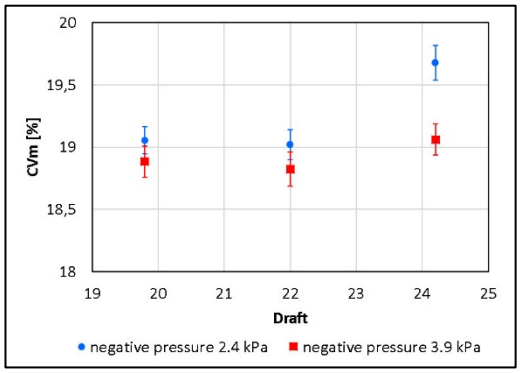

Figure 1: Yarn mass irregularity versus draft and negative air pressure

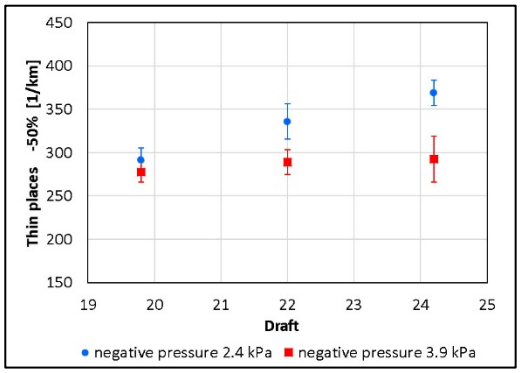

Figure 2: Yarn thin places (-50%) versus draft and negative air pressure

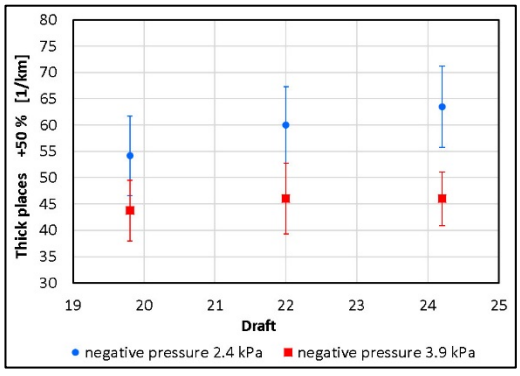

Figure 3: Yarn thick places (+50%) versus draft and negative air pressure

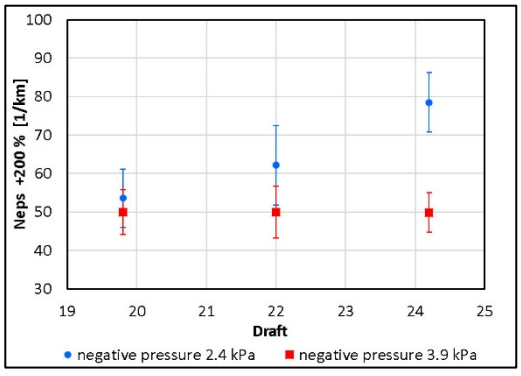

Figure 4: Yarn neps (+200 %) versus draft and negative air pressure

Table 2: Results of 2-way ANOVA - yarn irregularity and yarn faults

Property	Source of variance	Sum of squares	Mean square	F-ratio	Critical quantile	p-value	Results
Yarn mass irregularity	**Draft**	1.753	0.876	**14.941**	**3.091**	$2.24 .10^{-6}$	**significant**
	Neg. press.	1.35	1.350	**23.0176**	**3.94**	$5.88.10^{-6}$	**significant**
	Interaction	0.109	0.054	0.931	3.091	0.397665	insignificant
Yarn thin places (-50%)	**Draft**	28111.49	14055.75	**11.692**	**3.089**	$2.79 .10^{-5}$	**significant**
	Neg. press.	43147.21	43147.21	**35.891**	**3.938**	$3.46 . 10^{-8}$	**significant**
	Interaction	10360.77	5180.387	**4.309**	**3.089**	0.016081	**significant**
Yarn thick places (+50%)	**Draft**	441.136	220.568	1.275	3.089	0.284056	insignificant
	Neg. press.	4517.315	4517.315	**26.110**	**3.938**	$1.59 . 10^{-6}$	**significant**
	Interaction	108.798	54.399	0.314	3.089	0.73094	insignificant
Yarn neps (+200 %)	**Draft**	2745.717	1372.858	**6.567**	**3.088**	0.002099	**significant**
	Neg. press.	5720.439	5720.439	**27.363**	**3.937**	$9.43 .10^{-7}$	**significant**
	Interaction	2812.115	1406.057	**6.725**	**3.088**	0.001824	**significant**

From the results (see Fig. 1and Table 2) can be seen that yarn mass irregularity is not significantly changed when using draft ratio 19.8 and 22 as both in the case of negative air pressure 2.4 kPa and 3.9 kPa. The value of CVm is significantly increased when increasing draft ratio on 24.2. Although in the case of negative air pressure 3.9 kPa the value CVm is for this draft ratio (24.2) statistically significantly higher compared to other, from the technological point of view this growth of CVm is insignificant and is only 0,95 %. Mass irregularity of yarns produced using lower negative air pressure is higher compared to yarn produced using higher negative pressure, but the differences are statistically insignificant except the total draft ratio 24.2. However, roving irregularity must be taken into account during yarn mass irregularity evaluation. For this reason the roving mass irregularity was measured too and machine irregularity CV_{ma} were calculated according to formula (1).

$$CV_{ma} = \sqrt{(CV_{yarn}^2 - CV_{\lim yarn}^2)^2 - (CV_{roving}^2 - CV_{\lim roving}^2)^2} \quad (1)$$

Where CV_{yarn}, CV_{roving} is mass irregularity of yarn, roving [%], $CV_{\lim yarn}$, $CV_{\lim roving}$ is limiting irregularity of yarn (roving) [%], for the case of blended fibrous product calculated acording to formula (2):

$$CV_{\lim} = \frac{\sqrt{\sum_{i=1}^{k}(CV_{\lim i} \cdot T_i)^2}}{T} \quad (2)$$

where CV_{limi} is limiting mass irregularity of component [%] defined by Martindale [14] as:

$$CV_{\lim i} = \frac{100}{\sqrt{n_i}} \cdot \sqrt{1 + \left[\frac{v_{pi}}{100}\right]^2} \quad (2a)$$

v_{pi} is variation coefficient of cross-section of fibre of i–th component [%], T_i is mean fineness of i-th proportion of components in the yarn [tex], determined as:

$$T_i = \frac{T.p_i}{100} \quad (2b)$$

k is number of component, p_i is component representation in product (blending ratio) [%], n_i is mean number of fibres in the cross-section of i-th component.

For calculation of limiting irregularity of WO component in yarn the variation coefficient of fibres diameter v_{pi} = 21 % was used. Calculated values of machine irregularity are presented in table 3.

Table 3: Machine irregularity

Negative air pressure	Draft	$CV_{limroving}$ [%]	CV_{roving} [%]	$CV_{lim\ yarn}$ [%]	CV_{yarn} [%]	Machine irregularity CVma [%]
2,4	19,8	3,88	5,91	17,54	19,05	5,96
	22	3,7	5,39		19,02	6,23
	24,2	3,51	5,27		19,38	7,25
3,9	19,8	3,88	5,91		18,88	5,38
	22	3,7	5,39		18,82	5,6
	24,2	3,51	5,27		19,06	6,35

Comparing machine irregularity values (CVma) we can confirm generally known theory that higher draft ratio leads to higher yarn irregularity. These facts were confirmed for both applied level of negative air pressure. Values of CVma of yarns spun using higher negative air pressure were significantly reduced.

Such trends can be seen also in the case of number of thin places (-50%) of the yarn, which increases with increasing main draft ratio. This growth is statistically significant in the case of lower negative air pressure. Higher negative air pressure has also statistically significant positive influence on number of thin places (-50%) of the yarn compared to lower negative air pressure. According to two-way Anova the interaction between draft and negative air pressure is significant at significance level of 5%, lowest number of thin places has yarn produced with higher air negative pressure and lowest draft ratio. Negative air pressure also significantly influences number of thick places in the yarn. Higher negative pressure keeps number of thick places nearly constant when draft ratio is increased, while in the case of lower negative air pressure, number of thick places (+50%) shows increasing tendency with increasing draft ratio, but the growth is not statically significant within the range of observed draft ratio. The similar results can be seen in the case of yarn neps (+200%), where difference between number of neps, when setting the lowest and the highest observed draft ratio, is statistically significant.

The reason of decreasing yarn irregularity and yarn faults when setting higher negative air pressure can be probably attributed to the compression zone. Due to higher negative air pressure the fibrous strand is more compressed and spinning triangle is more eliminated. Thus probably fibres strand behaves more compactly, fibres are more bounded among each other so they probably could not so much migrate in the zone between a nip line of delivery roller and a twisting point. Thus, in the case of fine yarn with small number of fibre in cross-section, it results in significant decreasing of mass variability on short section as well as number of yarn faults. From the results it can be seen that small (tension) draft in the compression zone has not probably any negative influence on number of yarn faults.

Yarn hairiness

Average values of yarn hairiness in the length categories S3 and S12 and their corresponding 95% confidence intervals are presented in Figure 5 and Figure 6. Selected results of two-way analysis of variance are mentioned in the table 4. The length category S12 expresses total number of fiber ends protruding from the yarn body into the length of 2 mm per 100 m and length category *S3* shows total number of protruding fiber ends equal of 3 mm and longer than 3 mm per 100 m.

From the results it is evident that draft ratio (in observed range) has not any influence on hairiness in the cumulative length categories *S12* and *S3.* Yarn hairiness in the length category *S3* is significantly lower when yarn is spun with setting higher negative air pressure with comparison to lower negative pressure. Higher negative pressure causes higher compression of drawn fibrous strand, ends of fibers are then more twisted-in to the yarn body and thus less protrude from yarn body.

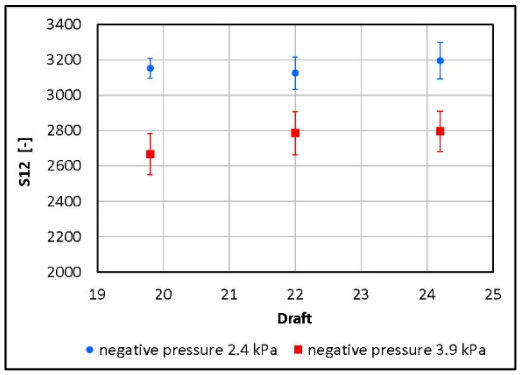

Figure 5: Yarn hairiness S12 versus draft and negative air pressure

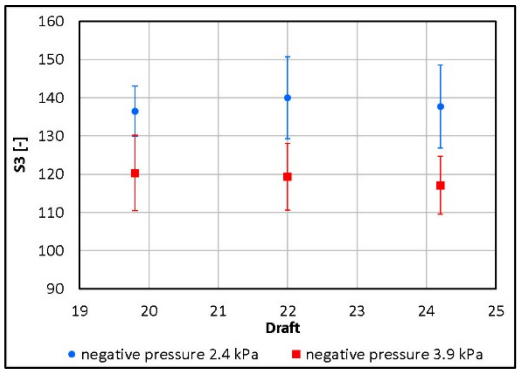

Figure 6: Yarn hairiness S3 versus draft and negative air pressure

Table 4: Results of 2-way ANOVA – yarn hairiness

Property	Source of variance	Sum of squares	Mean square	F-ratio	Critical quantile	p-value	Results
Yarn hairiness S12	**Draft**	221426.9	110713.4	1.341	3.048	0.264274	insignificant
	Neg. press.	7528587	7528587	**91.189**	**3.895**	$1.22 .10^{-17}$	**significant**
	Interaction	165639.6	82819.8	1.003	3.048	0.368837	insignificant
Yarn hairiness S3	**Draft**	153.641	76.82	0.126	3.048	0.847383	insignificant
	Neg. press.	16537.9	16537.898	**27.234**	**3.895**	$3.02.10^{-8}$	**significant**
	Interaction	198.641	99.321	0.163	3.048	0.437594	insignificant

Yarn tenacity and elongation

Results of yarn tenacity and elongation are shown in Figure 7 and Figure 8. Selected results of two-way analysis of variance are mentioned in the table 5.

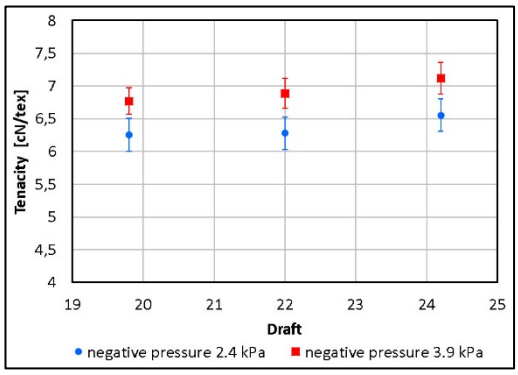

Figure 7: Yarn tenacity versus draft and negative air pressure

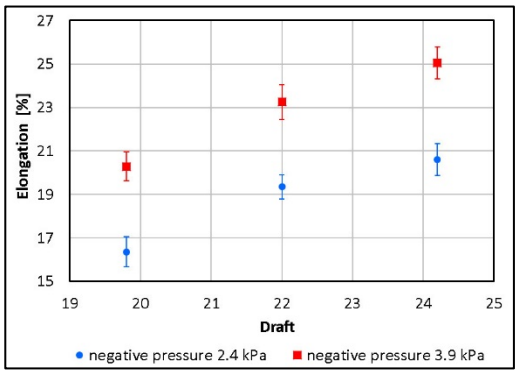

Figure 8: Yarn elongation versus draft and negative air pressure

The yarn spun at maximum negative air pressure and the highest observed draft ratio shows the highest value of tenacity. The values of tenacity show slightly decreasing tendency with decreasing draft. This fact could be probably caused by lower straightening and parallelizing of fibres during lower draft ratio and this causes lower utilization of fibres in the yarn. Level of negative air pressure has more significant effect on yarn tenacity compared to observed range of draft ratio. Yarn tenacity significantly increased using higher negative air pressure. This growth can be attributed to higher compression of fibres strand and thus their higher twisted-in into yarn body. The two-way variance analysis confirmed the statistical significant effect of negative air pressure and surprisingly draft ratio

on yarn elongation. Compared to lower observed level of negative air pressure, yarn spun at maximum negative air pressure has higher elongation. This results confirmed the fact that compact yarn has higher elongation in comparison with conventional yarn.

Table 5: Results of 2-way ANOVA - yarn tenacity and elongation

Property	Source of variance	Sum of squares	Mean square	F-ratio	Critical quantile	p-value	Results
Yarn tenacity	Draft	13.926	6.963	**4.034**	**3.008**	0.018113	**significant**
	Neg. press.	56.641	56.641	**32.813**	**3.854**	$1.50 .10^{-8}$	**significant**
	Interaction	0.271	0.136	0.078	3.008	0.924439	insignificant
Yarn elongation	Draft	538.354	269.177	**18.054**	**3.008**	$2.25.10^{-8}$	**significant**
	Neg. press.	2996.484	2996.484	**200.977**	**3.854**	$2.33.10^{-40}$	**significant**
	Interaction	1977.863	988.931	**66.329**	**3.008**	$3.87.10^{-27}$	**significant**

3. CONCLUSION

In this experimental work the effect of small changes of draft ratio (namely main draft) and level of negative air pressure of the compact spinning machine Fiomax Suessen Elite on selected properties (yarn irregularity, number of faults (-50%, +50%, neps +200%), hairiness S12 and S3, elongation and tenacity) of blended worsted yarn (80% WO/20% PA of count 10 tex). The results showed that setting the highest possible level of negative air pressure brought positive statistical significant influence on all observed properties of tested yarns compared to yarns spun at technologically possible lowest values of negative pressure. The number of yarn faults decreases in a range of (17-30)%, yarn hairiness in 15%. Yarn tenacity increases up to 8.5 % and breaking elongation up to 20 %. In the case of yarn mass irregularity, the decrease was up to ca 1.6 %, which is from the technological point of view insignificant, but when we compare machine irregularity, we can see a decrease in a range of (10-13%.) Increasing total draft ratio of about 20 % showed statistically significant negative influence on mass irregularity in the short length sections, number of thin places (-50 %) and neps (+200 %) of yarn. Mass irregularity of tested yarn increased up to 1.7 %, number of observed faults increased in the range of (5 – 46) %. Also statistically significant positive effect on tested yarn elongation and yarn tenacity (but with the smallest significance for the last mentioned property) was recorded. Tenacity increases up to 5 % whereas elongation up to 26 %.
Interaction of negative air pressure and draft ratio has statistically significant influence on number of thin places, neps and elongation of tested yarn. Using higher draft ratio (from the observed range) in combination of low negative air pressure leads to the highest number of thin places, nep and value of yarn irregularity but on the other hand higher draft ratio in combination of the highest negative air pressure leads to the highest value of yarn breaking elongation. According to two-way ANOVA, negative air pressure is more significant factor compared to observe range of draft ratio.

This work confirmed generally known theory that draft has negative influence of yarn mass irregularity and number of faults. The draft occurs in the drawing mechanism due to differential speed of pairs of roller. In a drafting zone fibers move with respect to one another and thus they are distributed over a relatively large length, which is proportional to the draft ratio. The smallest mass irregularity is achieved in the case of so called ideal draft. The ideal draft may occur only when certain conditions [15] are ensured. However, these conditions are not kept when real fibrous product is drawn because of variable staple length of fibers. Given that the distance of the rollers in the drafting zone is adjusted according to longer fibers, it is possible to divide fibers in the drawing zone into long or longer than the nipping line and fibers shorter than rollers setting. The speed of the fibers of the same length or longer is determined by the speed of the roller which gripped the fibers at the moment (i.e. controlled fiber). Shorter fibers after leaving the nip line of feeding rollers, do not reach its front end into the nip line of delivery rollers and their motion and speed is uncontrolled until they reach this nip line (i.e. floating

fibers). These fibers are the cause of the increasing mass irregularity of yarn and number of faults, which increase with increasing draft ratio. This effect was confirmed in a series of papers, e.g. [15]. Unlike the mass irregularity, draft ratio has a positive effect on the yarn tenacity because due to a higher draft fibers are more straightened and parallelized in the longitudinal direction. This results in better utilization of fiber length and tensile strength of fibers in the yarn. Due to higher negative air pressure in the condensing zone the fibrous strand is more compressed and spinning triangle is more eliminated, fibres strand behaves more compactly, fibres are more bounded among each other and utilized in yarn body, thus yarn tenacity and breaking elongation is higher, yarn hairiness is lower compared to yarn spun with lower negative air pressure. Due to higher compression fibres probably could not so much migrate in the zone between a nip line of delivery roller and a twisting point as well as fibre loss from yarn body is reduced, which positively influences yarn mass irregularity and number of yarn faults.

Due to lack of work focused on the compact worsted yarns it is not possible to compare the results presented in this paper. In the future, it is necessary to verify the acquired knowledge both for a set of yarns of different count and other materials. This work could open new possibilities for scientific research, particularly as regards the impact of the draft on the elongation of blended worsted compact yarns.

References:

1. *Jackowski, T., Cyniak, D., Czekalski, J.(2004). Compact cotton yarn. Fibres & Textiles in Eastern Europe, Vol. 12, No. 4 (48), pp. 22-26.*
2. *Atlas, S., Kadoglu, H. (2012). Comparison of conventional Ring, mechanical Compact and Pneumatic compact yarn spinning systems. Journal of Engineered Fibers and Fabrics, Volume 7, Issue 1-2012, pp. 87-100.*
3. *Rajaney, J.P. (2015). Comparative Analysis of Compact Spun Yarns and Ring Spun Yarns. Indian Jounal of Fibre & Textile Research, Vol.40, March 2015, pp. 43-50.*
4. *Khurshid, M.F., Nadeem, K., Asad, M., Chaudhry, M.A., Amanullah, M. (2013). Comparative Analysis of Cotton Yarn Properties Spun on Pneumatic Compact Spinning Systems. Fibres & Textiles in Eastern Europe, 21, 5(101), pp. 30-34.*
5. *Guldemet Basal, G., Oxenham, W. (2006). Comparison of Properties and Structures of Compact and Conventional Spun Yarns. Textile Research Journal, 76 (7), pp. 567 – 575.*
6. *Nikolič, M., Stjepanovič Z., Lesjak,F., Štritof, A. (2003). Compact Spinning for Improved Quality of Ring-Spun Yarn, Fibres & Textiles in Eastern Europe. Vol. 11, No. 4 (43), pp.30-35.*
7. *Rashid, M. R., Ahmed, E., Azad, A.K., Ullah, A.N.M.A. (2011). Comparative Study On Cotton Yarn Quality Made From Compact And Conventional Ring Frame. Journal of Innovation & Development Strategy, Vol. 5, Issue 3.*
8. *Çelik, P., Kadoğlu, H. (2004). A Research on the Compact Spinning for Long Staple Yarns, Fibres & Textiles in Eastern Europe. Vol. 12, No. 4 (48), pp. 27-41.*
9. *Göktepe, F., Yilmaz, D., Göktepe, O. (2006). A Comparison of Compact Yarn Properties Produced on Different Systems. Textile Research Journal, Vol. 76(3), pp. 226 – 234.*
10. *Altmatwally, A. A., Mourad, M. M., Hebeish, A. A., Ramadan, M.A. (2015). Comparison between physical properties of ring-spun yarn and compact yarns spun from different pneumatic compacting systems. Indian Journal of Fibre & Textile Research, Vol. 40, March 2015, pp. 43-50.*
11. *Hassan, N.A.E.M. (2013). An Investigation about Spirality Angle of Cotton Single Jersey Knitted Fabrics Made from Conventional Ring and Compact Spun Yarn. Journal of American Science 9(11), pp. 402- 4016.*
12. *Han, Ch., Wei, M., Xue, W., Cheng, L. (2014).Numerical simulation of fiber strands on Condensing Effect of Suction Slot in Compact Spinning with Lattice Apron. Fibers and Polymers Vol.15, No.5, pp. 1084-1091.*
13. *Mageshkumar, P., Ramachandran, T. (2012). Optimization of process parameters on Eli-Twist Yarn. International Journal of Engineering Inventions, Volume 1, Issue 1, pp: 24-31.*
14. *Martindale, J.G. (1945). A new method of measuring the irregularity of yarn with some observations on the origin of irregularities in worsted sliver and yarns. Journal of the Textile Institute Transactions, Vol. 36, Issue 3, T35-T47.*
15. *Moučková E., Ursíny P., Jirásková P. and Kim, Y.(2015). Influence of drafting on mass irregularity of cotton ring yarns. Vlakna a Textil, Vol. 2015, Issue 1, pp. 49-52.*

THEORY OF MASS IRREGULARITY CHANGES IN THE OE- ROTOR SPINNING SYSTEM

Petr Ursíny

Technical University of Liberec, Faculty of Textile Engineering, Department of Textile Technologies, Liberec, Czech Republic, Studentská 2, 461 17 Liberec 1, The Czech Republic,
Telephone: +420 48 535 3274; Fax: +420 48 535 3120, petr.ursiny@tul.cz

Abstract:

In the work a theory of yarn mass irregularity changes in the OE-rotor spinning technology is presented. Three various approaches are described. In the first we assume the OE-rotor spinning system as a dynamic system and use the random mass function of short section of sliver and yarn as a function of time and we construct so called modulus of the transfer function. In the second approach we analyse the mass irregularity formation on the basis of the laws of variation phenomena in random processes. We express the total square mass irregularity by means of individual components which are influenced by technological process of final yarn formation. In the last approach we solved influence of OE-rotor spinning system on the yarn mass irregularity formation depending on the yarn fineness. We theoretically derive ratio of changes of draft of opening system and number of cyclic doubling as a function of OE-rotor yarn fineness. This ratio increases with decreasing value of yarn linear density. Increase in ratio corresponds with increase in mass irregularity. The described analysis is applicable for research of optimal technological conditions for OE-rotor spun yarn production.

Key words:

Yarn mass irregularity, partial square mass irregularity, OE-rotor spun yarn, OE-rotor spinning system, total square mass irregularity, cyclic doubling.

1. Introduction

Resulting mass irregularity of yarn depends not only on quality of raw material (fibre fineness and its variation, variation of fibre length) but also on the processing variables of several technological stages (for example draft, doubling…) while main influence has the finite technological stage – a spinning machine. During technological process of OE-rotor yarn production the mass irregularity of carded sliver is gradually transformed into the irregularity of final yarn. In the rotor spinning machine the feed sliver is opened into individual fibres by means of combing (opening) roller and consequently fibres are transported into the rotor by air stream. For this a very high draft is necessary. Fibres are collected in rotor groove (collecting surface) and thin fibres bundle is created by so called cyclic-doubling. For yarn manufacturing it is necessary to insert end of yarn into the rotor. Due to rotation of the rotor and high centrifugal forces the end of yarn starts to rotate around its axis and continuously to twists-in the fibres laying in the collection surface [1], [2]. It is known that the formation of yarn irregularity is mainly influenced by draft, which has negative effect and doubling, which has positive effect on mass irregularity [3]. In the literature the impact of cyclic-doubling on the change of structure of mass irregularity of fibrous product was theoretically described by so called modulus of relative transfer function of given system [1]. Generally, the modulus of relative transfer function is a ratio of amplitudes of corresponding harmonic components of output and input signal related to the respective mean value [4] (for example mean value of fineness of output and input fibrous product). The function expressing the course of mass of short length sections of corresponding fibrous products in

dependence on the length of these products is considered as an output (input) signal. Impact of general spinning system on total yarn mass irregularity can be also theoretically expressed assuming that the overall variance in the mass of short lengths of the end product in yarn manufacture can be regarded as the sum of the dispersions (variances) of the individual components of the mass irregularity [3], [5], [6].

The main aim of this article is to present the theory of yarn mass irregularity changes in the OE-rotor spinning system by various approaches. In the first method we assume the OE-rotor spinning system as a dynamic system and use the random mass function of short sections of sliver and yarn as a function of time and we construct experimental modulus of the transfer function. In the second approach we theoretically analyse the mass irregularity formation on the basis of the laws of variation phenomena in random processes. We express the total square mass irregularity by means of individual components which are influenced by technological process of final yarn formation. In the last method we solve influence of change of draft in the opening system and cyclic-doubling of OE-rotor spinning system on the yarn mass irregularity formation depending on the yarn fineness.

2. Influence of OE-rotor spinning system on the yarn mass irregularity

2.1 OE-rotor spinning system as a dynamic system, structure of spinning system

The basic concept of the mass irregularity transformation from the OE-rotor spinning system, as a dynamic system, consequents from the concept of the random mass function (fineness) of short parts of longitudinal textile (sliver, fiber flow, yarn) as a function of time or length. We use the function of time and the modulus of the transfer function of the specific dynamic system we express:

$$\left|F_{OE}(\lambda)\right| = \frac{A(\lambda)}{A_0\left(\frac{\lambda}{P_C}\right)} \qquad (1)$$

where $\left|F_{OE}(\lambda)\right|$ is modulus of the relative transfer function of a spinning system as a function of the wave length λ of harmonics component of the yarn mass irregularity; $A(\lambda)$ is relative amplitude of harmonics component (from mass irregularity of yarn) with the wave length λ; $A_0\left(\frac{\lambda}{Pc}\right)$ is relative amplitude of harmonics component of sliver mass irregularity with the wave length $\frac{\lambda}{Pc}$; P_c is total draft of technological system (OE-rotor spinning system); λ is the wave length of a harmonic component of mass irregularity of yarn [m].

The modulus of the relative transfer function from the equation (1) is possible to determinate experimentally using spectrograms of output and input (supply) fibrous product obtained as a results of mass irregularity measurement employing the Uster Tester 4-SX. To determine the modulus mentioned above we use CV values, which correspond to relevant harmonic components of the yarn and sliver mass irregularity. Similar method was applied for construction of experimental modulus of relative transfer function of drafting system of a ring spinning machine in the work [11]. The course of the experimental modulus of relative transfer function of the OE-rotor spinning system[1] is shown in the Figure 2. Drawn slivers of fineness 4.6 ktex and rotor spun yarn of count 23 tex produced from 100% Tencel fibres (1.3 dtex, 38 mm) were used for experiment. Measurements of yarn and sliver mass

[1] The experimental work was carried out and processed by Eva Moučková (Department of Textile Technologies).

irregularity were realized under these conditions - sliver: speed of measurement: 25 m/min, time of measurement: 5 min and yarn: speed of measurement: 400 m/min, time of measurement: 2.5 min. Examples of spectrograms are presented in the Figure 1a and 1b.

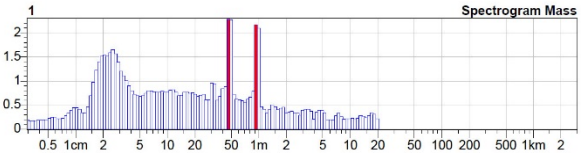

Figure 1a: Spectrogram of sliver mass irregularity

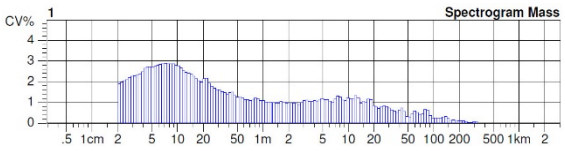

Figure 1b: Spectrogram of yarn mass irregularity

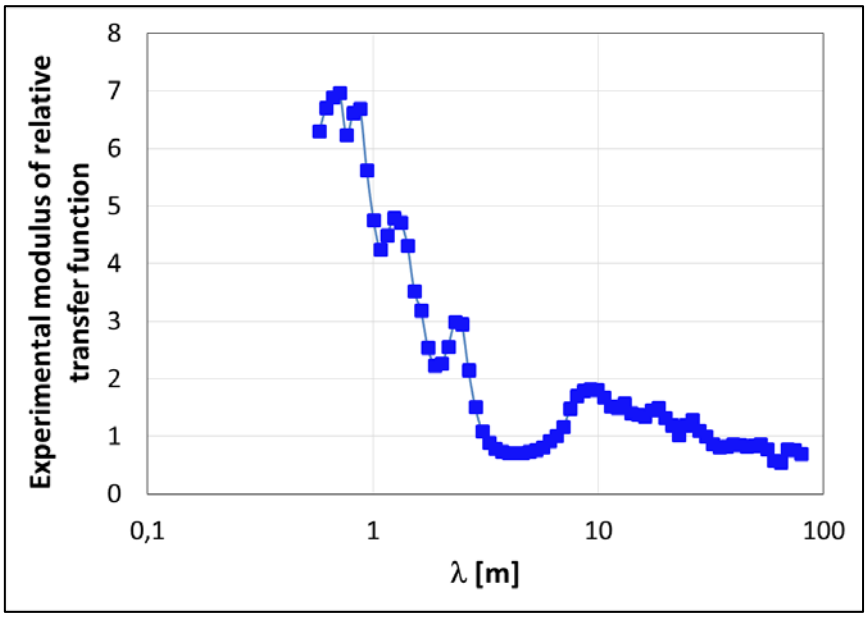

Figure 2: Experimental modulus of relative transfer function of OE-rotor spinning system

From the course of experimental modulus of relative transfer function it is obvious that the rotor spinning system deepens mass irregularity from the wavelength of yarn ca 25 m towards shorter wavelength. This increasing in values of experimental modulus of relative transfer function can be caused by higher draft between feed roller and rotor collecting groove. Components with longer wavelengths are not markedly affected by the high draft and furthermore effect of cyclic doubling suppresses also components with wave-lengths at the order of tens meters in the case of yarn.

The expression of characteristics of particular dynamic systems

For the expansion of analyses to the whole spinning system, as a dynamic system, it is necessary to calculate with the inner structure. The inner structure, how it is evident from the Figure 3 is divided in two basic partial systems, which have fundamental effect on the transformation of the mass irregularity – combing (opening) system and system of cyclic doubling. We rate the change of mass separation between fiber ribbon and the final yarn as relatively small. Fiber ribbon and the yarn correspond each other in aspect of mass distribution.

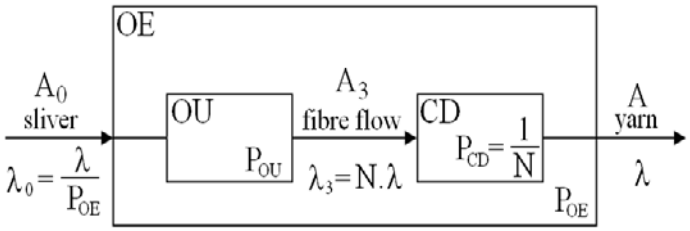

Figure 3: Block schema of OE-rotor spinning system
(*N* is cyclic doubling rate ; *Pou* is draft of combing (opening) system; P_{OE} is total draft of rotor spinning system; *OE* is rotor spinning system; *OU* is combing (separating) system; *CD* is system of cyclic doubling; λ_0, λ_3, λ are wave lengths of harmonic components of mass irregularity sliver (amplitude A_0), fiber flow (amplitude A_3) and yarn (amplitude *A*)).

Modulus of relative transfer function of total rotor spinning system is possible to express as follows:

$$|F_{OE}(\lambda)| = |F_{OU}(\lambda)|.|F_{CD}(\lambda)| \tag{2}$$

where $|F_{CD}(\lambda)|$ is modulus of relative transfer function of cyclic doubling system as function of wave length λ of harmonic components of yarn mass irregularity and $|F_{OU}(\lambda)|$ is modulus of relative transfer function of opening system as function of wave length λ of harmonic components of mass irregularity of yarn.

From equation (2) results the possibility to determine modulus of relative transfer function of opening system under application of modulus of relative transfer function of cyclic doubling system [7], [8] (see formula (3) and (4)).

$$|F_{CD}(\lambda)| = \frac{A(\lambda)}{A_3(N.\lambda)} \tag{3}$$

$$|F_{OU}(\lambda)| = \frac{\dfrac{A(\lambda)}{A_0\left(\dfrac{\lambda}{P_{OE}}\right)}}{\dfrac{A(\lambda)}{A_3(N.\lambda)}} = \frac{A_3(N.\lambda)}{A_0\left(\dfrac{\lambda}{P_{OE}}\right)} \tag{4}$$

where $A_3(N.\lambda)$ is relative amplitude of harmonic component mass of irregularity of fiber flow with wave length $\lambda_3 = N.\lambda$.

2.2. Analysis of the rotor spun yarn square mass irregularity formation in the spinning system

The overall dispersion (variance) in the mass of short lengths of the end product in yarn manufacture can be regarded as the sum of the dispersions (variances) of the individual components of the mass irregularity [3], [5].

$$CV^2 = \sum_{i=1}^{k} CV_i^2 \tag{5}$$

The individual components CV_i of the mass irregularity are independent on each other. As overall rate of variation in the mass of yarn short lengths CV we can use the parameter CV_{mass} determined by apparatus for measuring yarn mass irregularity based on capacitance principle (for example Uster Tester). It is yarn total square mass irregularity [3].

Further analysis is based on CV [%] i.e. square mass irregularity on the short sections. During yarn formation on the OE-rotor spinning system we can distinguish these linear fibrous assemblies: supplied sliver, fibre flow, fibre ribbon (yarn). Square mass irregularity of fibre ribbon (or resulting rotor spun yarn) CV_p we can express as:

$$CV_p^2 = CV_{\lim p}^2 + CV_{sp}^2 \tag{6}$$

Where $CV_{lim\,p}$ is square limiting irregularity of OE – rotor yarn; CV_{SP} is systematic square irregularity of OE – rotor yarn.

Square mass irregularity of fibre flow on the collecting surface CV_3 we can express as:

$$CV_3^2 = CV_{\lim 3}^2 + CV_{S3}^2 \tag{7}$$

Where CV_{lim3} is square limiting irregularity of fibre flow and CV_{S3} is systematic square irregularity of fibre flow which we can express as:

$$CV_{S3}^2 = CV_{S0}^2 + CV_{P03}^2 + CV_{VS03}^2 \tag{7a}$$

Where CV_{S0} is systematic square irregularity of supplied sliver; CV_{P03} is additional square irregularity induced in the opening process and CV_{VS03} is systematic developed square irregularity induced by draft in the opening process.

Square mass irregularity of supplied sliver CV_0 can be expressed as:

$$CV_0^2 = CV_{\lim 0}^2 + CV_{S0}^2 \tag{8}$$

Where CV_{lim0} is square limiting irregularity of supplied sliver and P_{03} is draft of the opening system.

When we convert the equations (6) ÷ (8) with use of technological patterns of doubling and drawing influence, we obtain formulas (9) ÷ (11):

$$CV_3^2 = CV_{\lim 0}^2 . P_{03} + CV_{P03}^2 + CV_{VS03}^2 + CV_{S0}^2 \tag{9}$$

$$CV_P^2 = CV_{\lim p}^2 + \frac{CV_{S3}^2}{N} \tag{10}$$

$$CV_0^2 = CV_{\lim 0}^2 + CV_{S0}^2 \tag{11}$$

Where N is number of cyclic doubling.

Influence of spinning process on final yarn square mass irregularity we can express by so called machine square irregularity CV_{OE} which is generally defined by formula (12) [9].

$$CV_{OE}^2 = \left(CV_P^2 - CV_{\lim P}^2\right) - \left(CV_0^2 - CV_{\lim 0}^2\right) \tag{12}$$

After substituting the formulas (10), (11) into (12) we obtain:

$$CV_{OE}^2 = \frac{CV_{P03}^2 + CV_{VS03}^2}{N} - CV_{S0}^2 \frac{N-1}{N} \quad (13)$$

Machine square irregularity CV_{OE} express the degree of equalizing effect of given spinning system on the final yarn mass irregularity. Opening system forms the mass irregularity and consequently mass irregularity decreases due to cyclic doubling system. In that way the formation of additional rotor yarn mass irregularity takes place. Next component of rotor yarn mass irregularity is given by the systematic square mass irregularity of supplied sliver.

The effect of changes of draft and cyclic doubling depending on the fineness of the fibrous product is possible to mathematically calculate according to following analysis.

2.3 Influence of the rotor spinning system on the yarn mass irregularity as a function of yarn fineness

Below we explain the influence of rotor spun yarn fineness on the internal level of draft of opening system and number of cyclic doubling. It follows, to certain extent, a limitation to produce rotor yarn with higher fineness. Total draft of OE- rotor spinning system P_c we can express by formula (14a) as well as by formula (14b):

$$P_c = P_{03} . \frac{1}{N} . \eta \quad (14a)$$

$$P_c = \frac{T_0}{T} \quad (14b)$$

Where: P_{03} is draft of the opening system, T_0 is fineness of the supplied sliver [tex], T is fineness of the final rotor yarn [tex], η is take – up coefficient (linear contraction of ribbon in consequence of twist) an N is number of cyclic doubling which can be calculated using diameter of the collecting surface d_3 [m] and machine twist Z [m^{-1}] according to formula (15):

$$N = \pi . d_3 . Z . \eta \quad (15)$$

When we express draft of the opening system P_{03} from the relation (14a) and substitute relation (14b) and (15) we obtain the formula (16).

$$P_{03} = \frac{T_0}{T} . \pi . d_3 . Z \quad (16)$$

Afterwards we express draft of the opening system and number of the cyclic doubling as a function of the final yarn fineness [10] and we will analyse this function. By using the relation for OE-rotor yarn twist as a fineness function with constant twist coefficient we obtain the relations for draft of the opening system P_{03} and number of cyclic doubling in the following form:

$$P_{03} = T_0 . \frac{K}{T^{5/3}} \quad (17)$$

$$N = \frac{K . \eta}{T^{2/3}} \quad (18)$$

Magnitude K is equal to: $K = \pi . d_3 . am . 100$ and am is twist coefficient (Phrix) [$ktex^{2/3}m^{-1}$].

The changes of draft P_{03} and number of cyclic doubling N as a function of OE-rotor yarn fineness T (derivation of a function P_{03} and N by course of fineness T as a function of yarn fineness T) are:

$$p(T) = -\frac{5}{3} K.T_0 . \frac{1}{T^{8/3}} \tag{19}$$

$$n(T) = -\frac{2}{3} K.\eta \frac{1}{T^{5/3}} \tag{20}$$

Where $p(T)$ is change of draft of opening system in relation to change of OE-rotor yarn fineness as a function of yarn fineness and $n(T)$ is change of number of cyclic doubling in relation to change of OE-rotor yarn fineness as a function of yarn fineness

Ratio $R(T)$:

$$R(T) = \frac{p(T)}{n(T)} \tag{21}$$

A graph in Figure 4 shows the course of the ratio $R(T)$, calculated for various yarn count. Individual curves respect the sliver fineness ($T0$) used for yarn production. For group of finer yarn count is recommended to use finer sliver [12]. Increase in ratio $R(T)$ corresponds with increase of mass irregularity. In the area of higher fineness of rotor yarns (T = 20 ÷ 12 tex) there are very high value of ratio $R(T)$ – see Figure 4. It means that influence of draft in opening system plays a more significant role on formation of yarn mass irregularity compared with cyclic doubling system. For this instance it is necessary to supply a sliver with higher quality in the case of adequate sliver fineness.

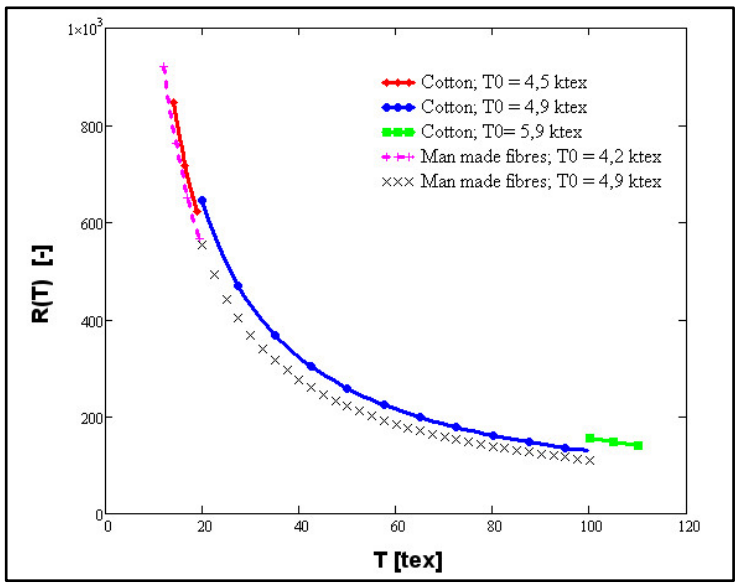

Figure 4: Courses of ratio $R(T)$ in dependence of yarn fineness T - calculated for various sliver fineness ($T0$)

3. CONCLUSION

This work presented theoretical relations of mass irregularity formation in the OE - rotor spinning technology. The analysis of OE-rotor spun yarn mass irregularity is focused on the three approaches:

- Transformation of irregularity by rotor spinning system expressed by means of experimental modulus of relative transfer function of OE-rotor spinning system;
- Analysis the total mass irregularity using the component parts, because structure of the mass irregularity of fibre product contains particular components such as limiting square irregularity, systematic square mass irregularity, additional square mass irregularity and induced systematic square mass irregularity. We theoretical expressed amount of yarn irregularity caused by the OE-rotor spinning machine;
- Analysis of influence of OE-rotor spinning system on the yarn mass irregularity formation depending on the yarn fineness in the area of higher yarn fineness (smaller linear mass).

From mentioned analysis implies a requirement on the supplied fibrous product (sliver). The obtained piece of knowledge about structure of yarn mass irregularity can be used for the research of the shorter spinning technology. New knowledge are applicable as well in the area of OE-rotor spinning machine with high productivity from point of view of the impact on the mass irregularity of final OE-rotor yarn.

References:

1. *Rohlena, V., et. al (1975): Open-end spinning. Elsevier Scientific publishing company, Amsterdam.*
2. *Heinz, E. (2014): The Rieter Manual of Spinning – Volume 5 – Rotor Spinning. Rieter Machine Works, LTd. Winterthur.*
3. *Bowles, A. H., Davies, L. (1978). The influence of drawing and doubling process on the evenness of spun yarn I. The Textile Institute and Industry, 11, 371-374.*
4. *Balda, M., Bošek, M., Dráb, Z. (1968). Basic of automation. SNTL Prague. In Czech.*
5. *Ursíny, P. (2003). Mass irregularity changes in spinning technology. Vlákna a textil (Fibres and Textiles), 10 (2),62-65.*
6. *Ursíny, P., Mägel, M. (1999). Short drawing set for ring - spinning. Melliand Textilberichte, 80 (4),242-243.*
7. *Krause, H. W., Soliman, H. A. (1971). Stőrungsausgleich durch Rűckdublierung in der Offen-End-Turbine Textil Industrie, 73 (4), 216-219.*
8. *Ursíny,P., Hedánek, O. (2005). Simulation of the mass irregularity transformation for OE-rotor spinning system, 5th World Textile Conference Autex 2005, Portorož, Slovenija. Proceedings Book pp. 924-928, University of Maribor.*
9. *ČSN 80 0706: Evaluation of material irregularity of threds, rovings and slivers. The office for Standards and Measurement, Prague. 1992.*
10. *Ursíny,P. (1988). New knowledge in the theory of OE-rotor spinning. Textiltechnik 38 (2), 71 – 73.*
11. *Moučková, E., Ursíny,P., Jirásková,P., Kim, Y. (2015). Influence of drafting on mass irregularity of cotton ring yarns. Vlákna a Textil (Fibres and textiles). 2015 (1), 49-52.*
12. *Rieter Machine works Ltd. (2008) Spinning documentation, Documentary for designing a short staple fibre spinning mill. Winterthur.*

EVALUATION OF USED NOZZLE TYPE ON YARN QUALITY IN OPEN END SPINNING

Michal Richtr [1, 2], Gabriela Krupincová [1], Karel Boněk [2]

[1] Technical University of Liberec Faculty of Textile Engineering, Liberec, Czech Republic,
Studentská 2, 461 17, 485353424, gabriela.krupincova@tul.cz,
[2] Rieter CZ s.r.o., Ústí nad Orlicí, Czech Republic, Moravská 519, 562 01

Abstract:

The draw off nozzle is one of the most important spinning unit exchangeable components of the open end spinning system. It is generally accepted, that it's using influences the quality of yarn and thanks to yarn breakage also production of spinning technology. There are number of comparative articles, where various draw of nozzle for various row fiber materials and yarn kinds are published. Results of these studies are not easily comparable due to less information about details of experiment realization. Main aim of this article is better understanding of this phenomena for selected fiber material, kind of yarn in terms of its end use while ensuring constant technological conditions.
First step is bibliography search including summarization of assumptions compiled on the basis of published results and earlier experience. Design of experiment, its realization including data treatment and results discussion follow. The set of 100% carded cotton 29,5 tex (Ne 20) yarns produced in two levels of Phrix twist coefficient (optimal for weaving and optimal for knitting) were produced. The BT 923 Rieter Open End machine and six types of draw off nozzle were used for spinning of yarn samples from the same sliver under same technical machine settings, which meets the all combination of selected analyzed factors (end use of yarn, type of draw off nozzle). Structural and mechanical parameters of yarns were determined in terms of yarn unevenness, cumulative yarn hairiness, number of faults, summation hairiness criteria, relative yarn strength and yarn elongation.
The results confirmed that the geometry of used draw of nozzle and setting of spinning process influence the fiber arrangement only in surfaces layers of yarn, which leads to significant difference in structural parameters and the mechanical ones is not affected.

Key words:

Draw of nozzle, open end spinning, yarn elongation, yarn hairiness, yarn IPI, yarn unevenness, yarn tenacity.

1. Introduction

Rotor spinning technology is very variable and using different machine parts or small change in settings allow production of qualitatively different yarns. In rotor spinning, not only characteristics of row material but also its preparation for spinning together with selection of machine type and its parts play very important roll. The effect of used draw off nozzle on yarn quality is investigated in this article. The verification of earlier results presented by various authors and discussion of obtained results with details of technology setting should give an idea in wider context. These outputs can be used for precision of components or machine manufacturer's recommendation for spinning mills. It can help with selection of draw of nozzle for demanded quality of yarns with respect to their end use.
In recent years, the 100% cotton yarns is still important segment at international markets and therefore also the experiment in this study is realized for one component cotton yarns. The experiment was designed in view of weaving and knitting product portfolio. The quality of yarn is evaluated considering six types of draw off nozzles and two levels of yarn twist coefficients. Results of realized experiment

based on production and analysis should allow better understanding of effect given by the geometry of draw off nozzle.

1.1 *Open end spinning*

Rotor spinning, commonly called open-end spinning and its principle is known since 1958, when the CZ patent No. 87947 was officially published [1] and improving or innovating by other scientific teams and other patent followed. The KS 200 rotor spinning machine was introduced in 1965 and new version under Rieter Company was presented in 1968 [2]. The successive progress and innovation of this technology was very huge and nowadays is adopted worldwide as one of the most economic spinning techniques to date.

Open end spinning generally consists of a drafting mechanism, a consolidation mechanism, and a winding mechanism. The drawn sliver is in this technology directly feed to the spinning process and the linkage between twisting and winding is braked. This fact enables higher production in comparison with classical ring spinning system. The sliver is open and individual fibers are fed by an air stream and guided to the rotor inner sliding wall surface. Twist is inserted by the rotation of the rotor making a yarn. The yarn withdrawal passage is shown on figure 1.

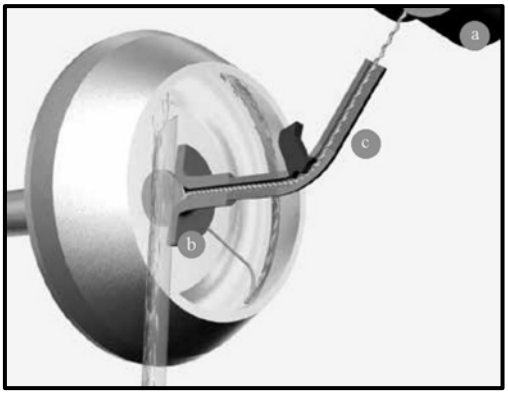

Figure 1 The yarn withdrawal passage in open end spinning [3]
a) draw off rollers of winding system, b) draw off nozzle c) draw off tube with twist stop

To obtain a good spinning stability, the yarn must have sufficient twist at the peeling point where the yarn leaves the rotor groove. The rotation of the yarn around the functional wall/ area of draw off nozzle creates an additional false twist on the yarn between the rotor groove and the yarn draw off tube. The schematic geometry of rotor and draw off nozzle is in detail shown on figure 2.

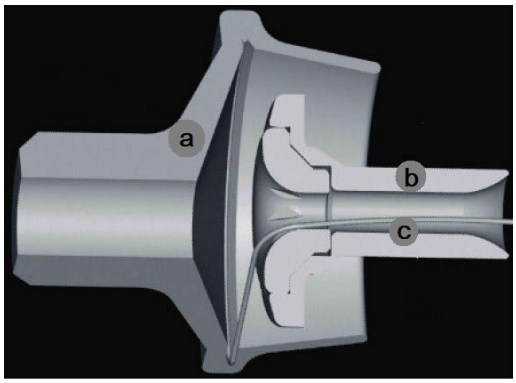

Figure 2 The schema of rotor and draw of nozzle position [4]
a) rotor b) draw of nozzle c) yarn

The lack of tension differential in rotor spinning reduces yarn strength because of the low fiber migration and low actual torque needful to twist the fibers. False twist insertion is caused by friction between the yarn surface and draw off nozzle, when the yarn is taken from the rotor groove at 90°turn inside the draw off nozzle. It is preferable to reduced torque friction moments and increase sliding friction moments

by the geometrical irregularity formation of draw off nozzle [5]. Over-twisting and yarn ruptures can occur, when smooth nozzles is used together with the higher rotor speeds. Higher rotor speed leads to increase the false twist effect, which caused the tension breaks. Therefore, grooves are cut or pressed into the nozzle, which briefly lift the yarn off the nozzle surface. Specific shapes of notches or specific end inserts of draw off nozzle excites the vibration, which facilitate the twist propagation into rotor groove [3] - [6]. The effect of false twist is fundamental for increasing of yarn strength and allows the yarn production by normal twist coefficient in combination with higher delivery speed. Without the effect of inserting false twist, the minimum required twist coefficient will achieved very high values [6] and [5]. The geometry, surface and other quality of draw off nozzle together with twist stop help the spinning stability and influence the quality of produced yarn. The insufficient torque at the point of yarn formation requires more fibers in yarn cross-section and due to this phenomena the open end spinning technology is recommended for production of medium fine and coarser yarns. Suitable selection of technological parameters, spinning unit components and its setting allow production of various yarn. Mainly suitable selection of draw off nozzle with yarn stop [3], [5], [6] and [7]. Theoretical bases of twist propagation in rotor spinning with using smooth draw of nozzle is introduced in studies [8] and [9]. Dynamic mechanical model is built for yarn forming process. The twist propagation in different yarn regions are appointed by using dimensional less variables. The equilibrium of all forces and moments are expressed in differential equations together with assumptions and boundary conditions. The numerical simulation of yarn tension and twist distribution under selected spinning condition are presented. The results valid for selected range of variables (torque factor, contact surface factor, yarn speed factor, air drag effect, draw off nozzle geometry in terms of wrap angel, yarn speed factor) and smooth drawn of nozzle indicated that the twist distribution is highly affected by torque factor and yarn tension is influenced by level of wrap angle, see more in [8] and [9].

1.2 ***Bibliography search***

There was published a lot of comparative studies based on comparison of qualitative criteria of various yarns (various fiber materials, various yarn parameters and various end use of yarns) produced by different machine types and their setting using various draw off nozzles [5] - [18]. The selection of machine components mainly rotor, draw off nozzle, twist stop and overall machine setting is multi-criteria decision problem. The one or multiple way analysis of variance (ANOVA) [5], [12] and [14] - [18], factorial analysis (FA) in combination with correlation analysis [13] or multi criteria decision making methods (MCDM) [6], [11] and [12] are usually used for evaluation and comparison of possible alternatives and finding the optimal suggestion.

The comparative studies are published in [5], [14] - [18]. The influence of used draw off nozzle and other selected factor is assessed and one way ANOVA is used to verify the significance of selected factors. The influence of five types of draw off nozzles for *Ne* 20 cotton yarns is presented in [5]. The effect of draw of nozzle and rotor groove type on physical and mechanical properties of 20 tex (*Ne* 29,5) viscose rotor yarns is investigated in [17]. Similar approach in experiment is used also in case of [18] and the set of 49 tex (*Ne* 12) cotton waste yarn was evaluated. The contribution of draw off nozzle profile to quality of blended acrylic / cotton yarn is evaluated in [15] and the significance of used draw off nozzle, yarn count and twist coefficient was observed. The set of blended rotor yarns of 50 nylon / 50 cotton was used to verify the significance of used draw off nozzle type on selected yarn quality characteristics in [17]. In case of [16], the four type of used draw of nozzle only on yarn hairiness is studied for the set of blended polyester / cotton.

The full FA is applied for investigation of significance of draw off nozzle type, rotor speed and sliver linear density on yarn strength of cotton rotor yarns in four level of yarn counts produced by Quickspin system [13]. The optimum setting for selected factors (draw of nozzle type, rotor speed and sliver linear density) is recommended.

In the study [12] the influence of distances between the draw off nozzle and rotor, type of draw off nozzle and the draw off tube on set of *Ne* 30 cotton rotor yarns for weft knitted fabric is observed by MCDM

cold TOPSIS. Four type of draw of nozzle were included to the analysis and the sixteen variants was realized. The results show that the spiral draw of nozzle, a take of tube without a torque stop and closer setting between the nozzle and the rotor can be suggested for this kind of application. The similar approach is apply in case of [11] only for 20 tex (*Ne* 29,5) spun from cotton yarns produced in combination of five types of draw of nozzle. The MCDM method ELECTRE III is introduced in [6] and the valuable assistance in reaching acceptable solutions in order to select the appropriate draw off nozzle for Ne 12 cotton waste rotor yarns spun to weave denim fabric is studied. Ten type of draw off nozzle is used and spiral ceramic draw off nozzle and smooth steel draw off nozzle is suggested for this kind of application as optimal. Yarn properties as a function of draw off nozzle design are presented in figure as an output.

Several studies were carried out about effects of rotor machine parameters on yarn quality and different methods were used to optimize those parameters. The bibliography search shows that only comparative study [15] also investigate the significance of applied twist coefficient level and used draw of nozzle on blended 50 cotton / 50 acrylic yarns quality. Two levels of yarn count (29,5 tex – *Ne* 20 and 49,2 tex – *Ne* 11,9), three levels of nominal twist (533,3 tpm, 586 tpm, 646,1 tpm) and two types of draw of nozzle (notched, spiral) were used in experiment realization [15]. The end use of yarn is not mentioned but the level of twist seems to be for weaving. Other publications focus only on the yarns for weaving or for knitting. In some cases the end use of yarns is not mentioned or is not taken in to consideration because it is the experimental study only.

Results of these studies are not easily comparable due to less information about details of experiment realization especially with regard to various technology settings (various machine, various technological parts and its setting), various design of the experiment (full or partial experiment, various fiber and yarn parameters, various tested qualitative characteristics, various testing instruments and its setting) and various way of data treatment.

2. Experimental part

The scope of experiment was designed in accordance with selected analyzed factors (used draw off nozzle and area of final use of yarn) and experiment was focused in respect to the informative value of obtained results, which should be applicable in practice by customers of Rieter CZ Company e.g. in form of application recommendations for various draw off nozzle selection. The common fiber material, middle level of yarn count, two levels of Phrix twist coefficient (optimal for weaving and knitting final application) and typical common setting of BT 923 Rieter Open End spinning machine were used. All laboratory measurement were realized consistently by International standards.

2.1. Materials

Rotor yarns nominal count 29,5 tex (*Ne* 20) spun form the same sliver under same condition from 100% cotton fibers 25,6 mm (25,34; 25,87) mean length *L(w)* measured by AFIS tester and middle level of fineness. Yarns were produced in two levels of Phrix twist coefficients *am* (optimal for weaving *am* = 65 $ktex^{2/3}m^{-1}$ and optimal for knitting *am* = 80 $ktex^{2/3}m^{-1}$). Mechanical parameters of BT 923 Rieter Open End spinning machine was set to meet all combinations of analyzed factors, which allow to eliminate the potential influence of additional factors or its interaction on yarn quality. The nozzles selected and used in presented study represent most frequent components which cover biggest yarn character variation requested by yarn market. Six types of drawn off nozzle commonly commercially used by yarn producers were selected and minimally ten bobbins with 5000 m length of package for each yarn sample were spun. The technological parameters of yarn samples and details about machine settings are given in table 1a. For more information about specification of draw of nozzle please see table 1b.

Table 1.a Mechanical spinning machine setting for BT 923 Rieter Open End and technological parameters of yarns for experiment

Machine settings	
open end spinning machine	BT 923 Rieter
number of spinning units	10
rotor type	C533/U-D
opening roller	C40D-PP
adapter	C5
used draw off nozzle	CR7R
	CR7RS
	CR7CS
	CKSNX
	CK4K
	CK6KF

Technological parameters		
material	100% cotton	
nominal yarn count *T*	29,5	[tex]
sliver count	5600	[tex]
draft	190	[-]
Prix twist coefficient *a*	65 / 80	[ktex$^{2/3}$m^{-1}]
twist	680 / 837	[m^{-1}]
rotor speed	100000	[rpm]
opening roller speed	9000	[rpm]
take up speed	150 / 120	[m.min^{-1}]
length of yarn package	5000	[m]
technological suction	6000	[Pa]

Table 1.b Specification of draw off nozzle

Type	Drawing	Specification	Raw material	End use
CR7R		ceramics, smooth surface	cotton, wool	high twist yarns
CR7RS		ceramics, sharp spiral	universal	knitting and weaving
CR7CS		ceramics, smooth spiral	universal	knitting and weaving
CKSNX		ceramics, smooth spiral with eddy insert in nozzle	cotton	knitting and weaving
CK4K		ceramics, 4 notches	cotton, viscose, polyester / acrylic, polyester / cotton, regenerate	knitting and weaving
CK6KF		ceramics, 6 notches and small nozzle radius	PES and it's blends	knitting and weaving

2.2. Methods

Yarn analysis included the verification of yarn count *T* together with evaluation of typical set of yarn qualitative structure and mechanical indicators. Yarn unevenness *CVm*, number of faults in terms of *IPI small* and *IPI big*, cumulative yarn hairiness index *H*, sum criteria of yarn hairiness S_{12}, S_3, relative yarn strength *R* and yarn elongation ε_p were determined. Yarn unevenness *CVm* was evaluated on short staple length 1 cm and 10 m.

All yarn samples were standard atmosphere conditioned (temperature 20 ± 2°C, humidity 65 ± 2 %) in accordance with International standards ČSN EN 12751 [19]. The selection of yarn samples was realized in respect to typical selection procedure given by International standards EN ISO 139 [20]. Compliance of nominal yarn count T_n and experimental yarn count *T* was realized in respect to International standards ČSN EN ISO 2060 [21] (testing length 1000 m, repeating of measurements 10, total tested length for one yarn sample 1 km). The definition of Phrix twist coefficient *am* is given as follows:

$$am = ZT^{2/3}. \quad (1)$$

The analysis of yarn unevenness *CVm*, number of faults in terms of *IPI small* and *IPI big* and cumulative hairiness index *H* were evaluated by Uster ® Tester 5 (testing speed 400 mmin^{-1}, testing length for each bobbin 1 km, repeating 10 times, total tested length for one yarn sample 10 km). In this case, the *IPI small* includes the number of faults in terms of Thin (- 30 %), Thick (+ 35 %), Neps (+ 140 %) and *IPI big* summarizes the number of faults in terms of Thin (- 50 %), Thick (+ 50 %), Neps (+ 280 %).

Absolute occurrence of hairs in given distances from yarn surface were analyzed by using Uster ® Zweigle HL tester 400 (testing speed 400 mmin^{-1}, testing length for each bobbin 400 m, repeating 10 times, total tested length for one yarn sample 4 km). The sum criteria of yarn hairiness S_{12} and S_3 are calculated according to equations (2), where the n_i is absolute occurence of hairs in given length catherory i = 1, 2, ... k per 100 m of tested length.

$$S_{12} = \sum_{i=1}^{i=2} n_i, \quad S_3 = \sum_{i=3}^{k} n_i. \quad (2 \text{ a, b})$$

The mechanical parameters in terms of relative yarn strength *R* and yarn elongation ε_p were measured by Uster ® Tensorapid 3 (testing speed 5 mmin^{-1}, testing length 500 mm, measurement repeating 30 for each yarn bobbin, total number of measurement for one yarn sample 300).

2.3. Assumptions based on previous experience and published results

The following text summarizes findings from bibliography search (see chapter 1) and earlier experience and try to find connections among them. The dynamic mechanical model published in [8] and [9] assumed as important factors for the case of application of smooth steel draw of nozzle torque factor ξ, draw of nozzle surface factor together with wrap angle ϕ and its geometry factor r_0 / r_m, where the r_0 is radius of the circular generatrix of the draw of nozzle surface and r_m is inner radius of the yarn doffing tube. The torque factor ξ significantly affected twist blockage. The twist blockage becomes larger with either increasing coefficient of friction or wrap angle ϕ, as well as the draw off nozzle geometry factor r_0 / r_m [8] and [9].

The available parameters of ceramics draw of nozzle used in our experiment was compared and at a certain level of simplification it is possible to say: Wrap angle ϕ of smooth draw off nozzle CR7R is comparable with all spiral draw of nozzles (CR7RS, CR7CS, CKSNX) and also with four notches draw off nozzle (CK4K). Slightly lower wrap angle ϕ has six notches draw off nozzle (CK6KF). All of draw off nozzles used in our experiment are comparable each other from the point of view of geometry factor r_0 / r_m. In respect to dynamic mechanical model, the higher torque factor ξ should have spiral and notched draw of nozzles. The twist propagation and minimal twist blockage can be expected in spiral draw off nozzles due to point contact between yarn and nozzle surface and its spiral geometry which supports torque effect. On the other hand the higher diversity in quality of yarn spun by notched draw off nozzles is expected due to high frequency vibration caused by number and geometry of notches on draw of nozzle surface, which leads to change of wrap angle.

Based the earlier studies published in [5] - [18] it can be expected, that yarns spun with smooth draw off nozzle CR7R and both spiral nozzles (CR7RS, CR7CS) will have similar quality. Draw of nozzle CR7RS differ from draw off nozzle CR7CS in radius of curvature of the spiral and in case of draw of nozzle CR7RS is slightly lower. The length of contact surface between yarn and both spiral draw off nozzles (CR7RS, CR7CS) is in comparison with smooth draw off nozzle CR7R and therefore the twist blockage will be probably lower. It is possible, that the difference among qualitative characteristics of yarn spun by using of smooth draw of nozzle CR7R will be similar with yarns produced with selected spiral draw of nozzle (CR7RS, CR7CS) in all of measured parameters or differences will be relatively small. The high frequency vibration caused by number and geometry of notches on draw of nozzle surface (CK4K, CK6KF) can lead to changes in yarn structure on the surface level. Changes in fiber arrangement will

probably cause the diversity in yarn unevenness, number of faults and yarn hairiness. The level of mechanical parameters can remain similar with yarn produced by using smooth draw of nozzle CR7R. The CKSNX is spiral draw of nozzle with insert and therefore the combination of both phenomena (geometry of spiral and number of used notches) is combined. The stronger significance of spiral geometry is more relevant to earlier experience because of high frequency vibration is realized only in yarn take of tube, which doesn't lead to change of wrap angle.

The higher twist coefficient leads to more compact yarn structure and can reduced yarn unevenness, number of faults, yarn hairiness and variability of yarn quality indicators [2], [4], [12] and [15]. The range of twist coefficient applied in this study is possible in extreme case used for both end applications of yarn and therefore the expected diversity among verified yarn characteristics is relatively small.

3. Results and discussion

The experimental data was statistically processed. Homogeneity, normality and independence were verified. The typical statistical parameters were calculated (mean, standard deviation, variation coefficient, 95 % confidence intervals). The graphical comparison of data was done in figures 3 – 6 to obtain the idea about the basic tendencies from the point of view of observed factors (end use of yarn, type of draw off nozzle). The mean values of evaluated characteristics are presented together with 95 % confidence interval bounds.

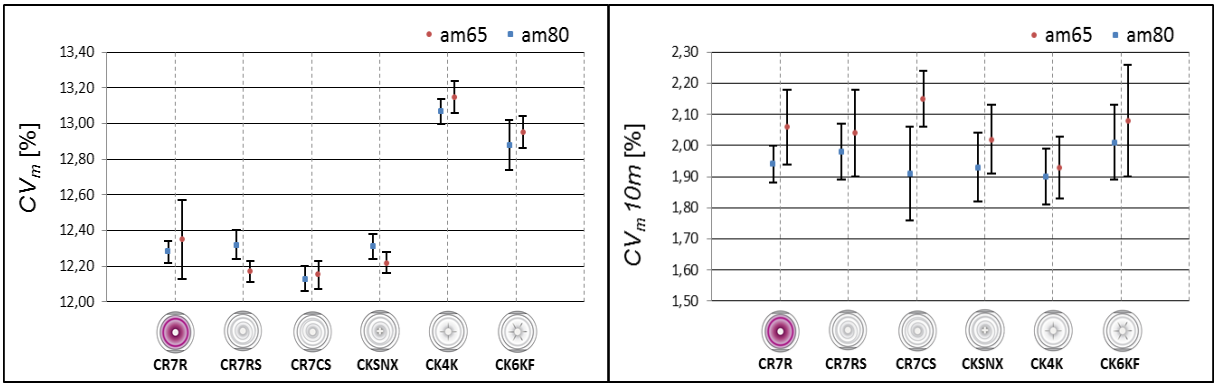

Figure 3 a, b Yarn unevenness *CVm* on short staple length 1 cm and 10 m

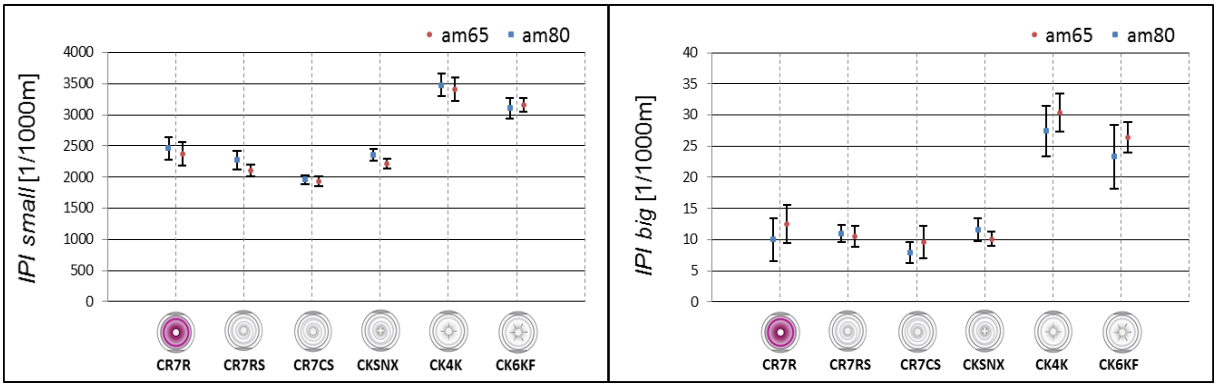

Figure 4 a, b Number of yarn faults *IPI big* and *IPI small*

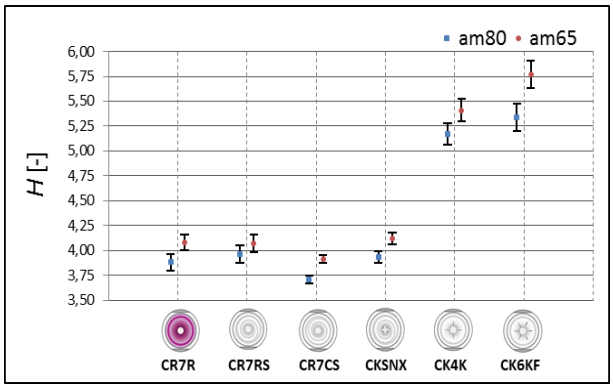

Figure 5 a Cumulative hairiness index *H*

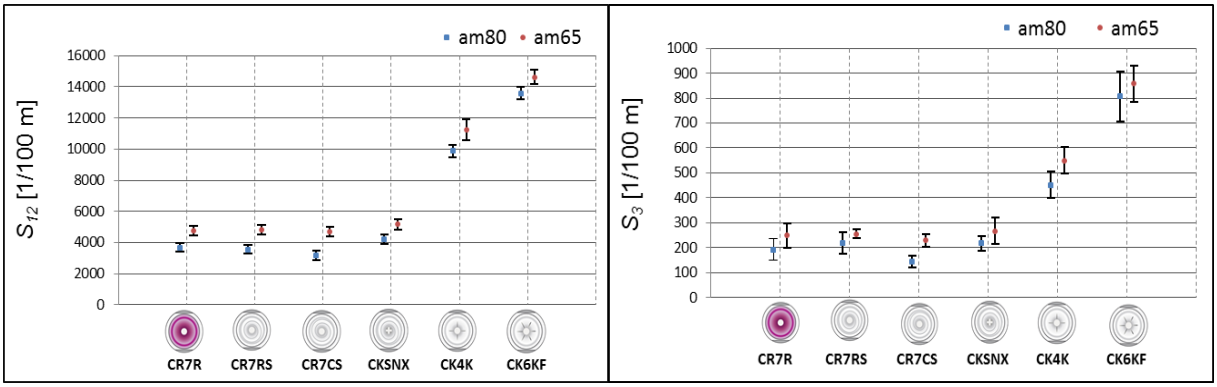

Figure 5 b, c Sum criteria of yarn hairiness S_{12} and S_3

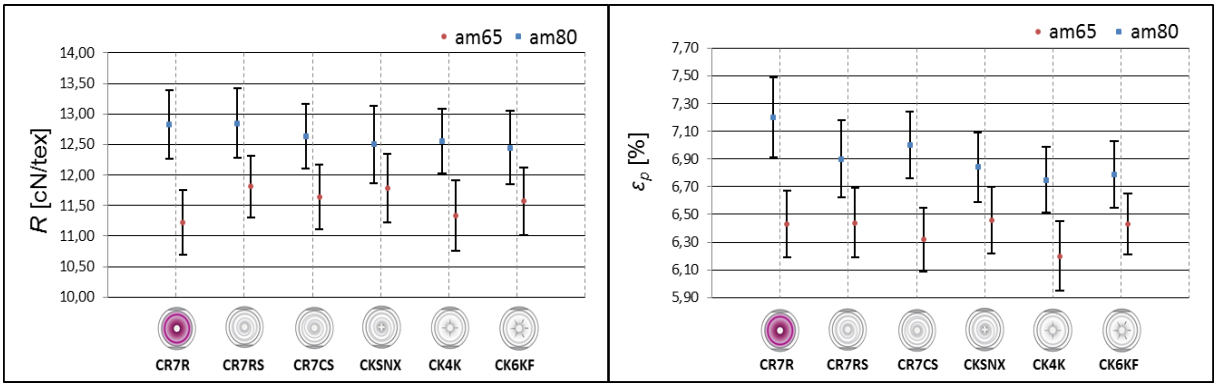

Figure 6 a, b Relative yarn strength *R* and yarn elongation ε_p

As can be seen in figure 3a, the level of yarn unevenness on short staple length is statistically comparable from the point of view of used draw of nozzles and applied twist coefficient for the rotor yarns produced by using smooth (CR7R), spiral (CR7RS, CR7CS) and spiral draw off nozzle with insert (CKSNX). Only rotor yarns spun by notched draw of nozzles (CK4K, CK6KF) have significantly higher level of yarn unevenness. The results of imperfection (in terms of *IPI small* and *IPI big*) and quantification of yarn hairiness (in terms of cumulative hairiness index *H* and summation criteria S_{12} and S_3) show similar trends as *CVm* on short staple length, see figure 4 and 5. Different outputs are clearly seen in figure 3b and 6, where all the yarn qualitative characteristics (*CVm* for 10m, *R*, ε_p) are statically comparable in most of cases from the point of view of used draw of nozzle and level of Phrix twist coefficient.

Yarn samples spun with higher twist coefficient show slightly lower *CVm* on 10m length, slightly lower yarn hairiness (*H*, S_{12}, S_3,) and slightly higher mechanical parameters (*R*, ε_p). The differences between rotor yarns prepared by the same draw of nozzle and various level of Phrix twist coefficient are in most cases statistically insignificant and the confidence bounds of obtained results are overlapped.

The significance of selected fixed-effect factors (end use of yarn – two levels, type of draw off nozzle – six levels) on yarn quality (in terms of *CVm, IPI small, IPI big, H*, S_{12}, S_3, *R*, ε_p) was verified by the two way ANOVA analysis at level of significance α = 5 %. Obtained results of F test including also *F* criterion *p* value together with critical quantile for factor 1 – type of used drawn of nozzle and factor 2 – level of Phrix twist coefficient *am* is summarized in table 2. All statistically significant outputs are marked bold.

Table 2. Results of two way ANOVA analysis

sources of variability	sum of squares	mean square	std. deviation	*F*- criterion	critical quantile	*p*- value	sum of squares	mean square	std. deviation	*F*- criterion	critical quantile	*p*- value
	***CVm* [%]**						***H* [-]**					
factor 1	**1,66**	**0,33**	**0,58**	**70,2**	**5,05**	**1,3E-04**	**5,85**	**1,17**	**1,08**	**202,26**	**5,05**	**9,2E-06**
factor 2	0,00	0,00	0,00	0,0	6,61	1,0E+00	**0,16**	**0,16**	**0,40**	**27,02**	**6,61**	3,5E-03
interaction	0,72	0,72	0,15	-4,1	7,71	1,0E+00	0,02	0,02	0,17	7,43	7,71	5,3E-02
residues	-0,69	-0,17					0,01	0,00	0,05			
summary	1,68	0,22					6,04	0,55	0,74			
	***IPI small* [1/1000m]**						***IPI big* [1/1000m]**					
factor 1	**3427586**	**685517**	**827,96**	**230,43**	**5,05**	**6,6E-06**	**747,74**	**149,55**	**12,23**	**79,68**	**5,05**	**9,2E-05**
factor 2	17003	17003	130,39	5,72	6,61	6,2E-02	5,74	5,74	2,40	3,06	6,61	1,4E-01
interaction	2956	2956	121,96	0,99	7,71	3,8E-01	3,78	3,78	3,06	2,70	7,71	1,8E-01
residues	11919	2980	54,59				5,60	1,40	1,18			
summary	3459464	314497	560,80				762,87	69,35	8,33			
	S_{12} [1/100m]						**S_3 [1/100m]**					
factor 1	**187134133**	**37426827**	**6117,75**	**1637,40**	**5,05**	**5,0E-08**	**642161**	**128432**	**358,37**	**478,51**	**5,05**	**1,1E-06**
factor 2	4398352	4398352	2097,22	192,43	6,61	3,5E-05	11907	11907	109,12	44,36	6,61	1,2E-03
interaction	4121	4121	338,06	0,15	7,71	7,2E-01	3	3	36,63	0,01	7,71	9,3E-01
residues	110167	27542	165,96				1339	335	18,30			
summary	19164677	17422434	4174,02				655410	59583	244,10			
	***R* [cN/tex]**						**ε_p [%]**					
factor 1	0,19	0,04	0,19	0,76	5,05	**6,1E-01**	0,12	0,02	0,15	1,75	5,05	**2,8E-01**
factor 2	**3,48**	**3,48**	**1,86**	**71,65**	**6,61**	**3,8E-04**	**0,85**	**0,85**	**0,92**	**62,41**	**6,61**	**5,2E-04**
interaction	0,03	0,03	0,49	0,52	7,71	5,1E-01	0,02	0,02	0,26	1,17	7,71	3,4E-01
residues	0,21	0,05	0,23				0,05	0,01	0,11			
summary	3,91	0,36	0,60				1,04	0,09	0,31			

The two way ANOVA confirmed that the factor 1 - type of used draw off nozzle influenced significantly the structural characteristics of yarn (in terms of yarn unevenness *CVm* on short staple length 1 cm, cumulative hairiness index *H*, summation criteria of hairiness S_{12} and S_3 and number of faults *IPI big* and *IPI small*). The factor 2 – level of Phrix twist coefficient *am* affected significantly only yarn hairiness (in terms of cumulative hairiness index *H*, sum criteria of hairiness S_{12} and S_3) and mechanical parameters (in terms of relative yarn strength *R*, yarn elongation ε_p). The interaction between factors is nonsignificant.

The obtained results are in good accordance with bibliography search [2] - [18], mainly with results presented by figure 7 published in [4] and by figure 8 published in [6]. Bröll company developed the new series of traditional draw off nozzle (KS, KG, K4, K8) cold SPIRIT based the extensive and comparative studies. The geometry of these draw of nozzles is improved e.g. in terms of shape of notches and radius.

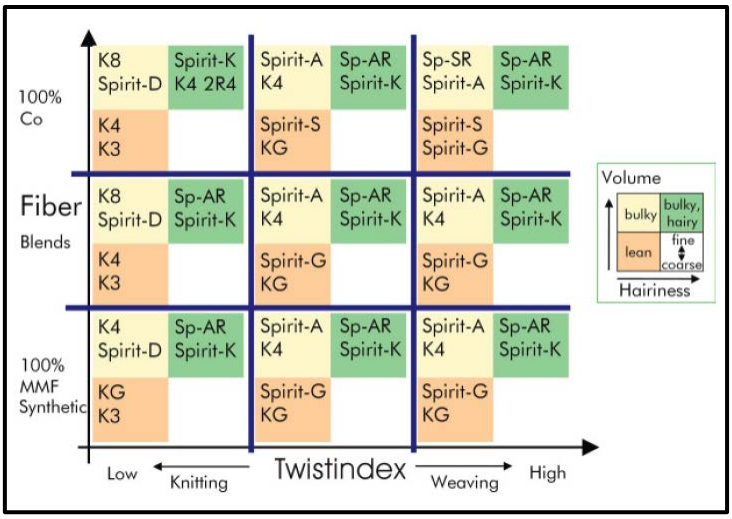

Figure 7 Selection diagram: Optimal navels as a function of twist coefficient and fiber type [4] (K3 3 notches, K4 4 notches, K42R4 4 notches with long whirl insert, K8 8 notches, KG smooth, Spirit A 6 notches, Spirit D 5 notches, Spirit K 5 notches, Spirit S spiral, Spirit G smooth, Spirit AR 6 notches with insert, Spirit SR spiral with insert)

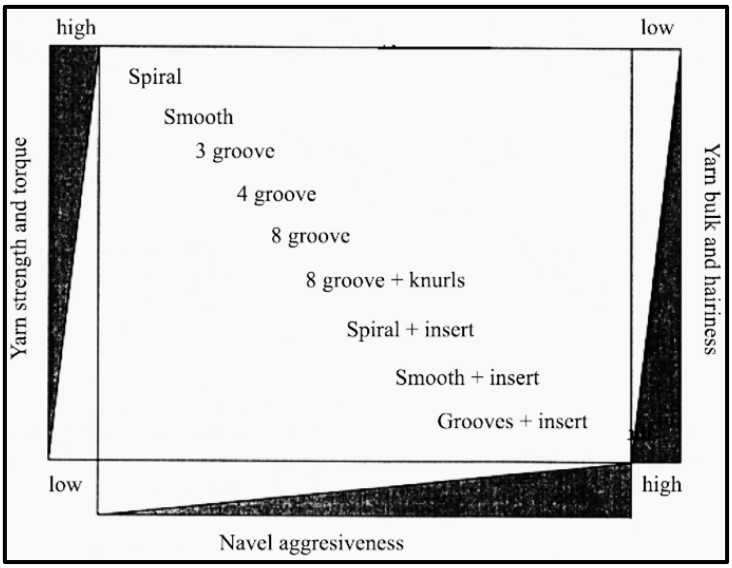

Figure 8 Yarn properties as a function of navel design [6]

4. CONCLUSIONS

Draw off nozzle is one of the basic technological components in rotor spinning technology, which can control the yarn structure and its quality. The selection of optimal draw off nozzle allow producing various quality of yarns in terms of yarn hairiness and bulkiness without the effect on process ability in weaving or knitting in terms of mechanical parameters. The geometry of draw of nozzle together with the overall setting of spinning machine influence dynamic of spinning process and utilization of false twist effect. These phenomena lead to different fiber arrangement in yarn structure mainly in surface layers of yarn. Main aim of this article is better understanding of these phenomena for selected fiber material, kind of yarn in terms of its end use while ensuring constant technological conditions.

Bibliography search including summarization of assumptions compiled on the basis of published results and earlier experience is followed by design and realization of experiment. The set of 100% cotton 29,5 tex yarns were spun. Yarn samples for analysis were produced in real industry conditions by the BT 923 Rieter Open End machine. The nozzles selected and used in presented study represent most frequent components which cover biggest yarn character variation requested by yarn market. Six types

of geometrically comparable ceramics draw off nozzle were used together with two levels of Phrix twist coefficient. Yarn samples were spun from the same sliver under same technical machine settings, which meets the all combination of selected analyzed factors (end use of yarn, type of draw off nozzle). Structural and mechanical parameters of yarns were determined in terms of yarn unevenness, number of faults, cumulative yarn hairiness index, summation hairiness criteria, relative yarn strength and yarn elongation.

The outcomes are in good accordance with bibliography search and earlier experience. The obtained results confirmed also our expectations. The used draw off nozzle and level of twist coefficient influence significantly the arrangement of fibers in surface layers of yarn and the internal structure of yarn is not affected meaningly. Therefore diversities of yarns are visible and verified only in case of yarn unevenness *CVm* on short length, yarn diameter variability determined by number of faults (*IPI small* and *IPI big*) and quantitative yarn hairiness parameters (H, S_{12}, S_3). Mechanical characteristics (R, ε_p) together with yarn unevenness *CVm* evaluated on 10m remain similar and their values are comparable from the point of view of used draw off nozzle and applied Phrix twist coefficient. Smooth and spiral draw of nozzles are effectively applied when the closed and compact yarn structure is demanded. Notched draw of nozzles are recommended for using when the bulkier yarn structure is advantageous for final application. This study represent only a small part of draw of nozzle type but on the other hand this article is a good base for future analysis of different raw material and also new coming nozzle type.

ACKNOWLEDGEMENTS

This study was supported by Rieter CZ Company.

References

1. Svatý V., Hula K. (1956) Equipment for the continuous production of yarn. *CZ Patent No. 87947 CZ*, Czech Industrial Property Office (only in Czech language).
2. Carl A Lawrence (2010) *Advances in Yarn Spinning Technology* pp. 261–273, Woodhead Publishing, Oxford ISBN 978-1-84569-444-9.
3. Heinz, E. (2014) *The Rieter Manual of Spinning.* Winterthur: Rieter Machine Works Ltd..
4. Sonntag E., Bolze J. (2003) Design of a navel and its influence on yarn structure. *Dornbirn: Bröll Textile Systems*, 3 (2003).
5. Coruh E., Celik N. (2013) Influence of nozzle type on yarn quality in open end spinning. *Fibers & Textiles in Eastern Europe*, 21, 2 (98), 38 – 42.
6. Kaplan S., Araz Ceyhun, Göktepe Ö. (2006) A multi-criteria decision aid approach on navel selection problem for rotor spinning. *Textile Research Journal*, 76 (12), 896 - 904.
7. Klein, W. (1993) *The Technology of Short Staple Spinning - Manual of Textile Technology.* The Textile Institute, England.
8. Guo B., Tao Xiaoming and Lo T. (2000) A mechanical model of yarn twist blockage in rotor spinning. *Textile Research Journal,* 70 (1), 11 – 17.
9. Xu B. G., Tao X. M. (2003) Integrated approach to dynamic analysis of yarn twist distribution in rotor spinning. Part I. Steady State. *Textile Research Journal*, 73 (1), 79 – 89.
10. Balasubramanian N. (2013) *Rotor Spinning: Effect of rotor, navel parameters, winding tension*. Bombay Textile Research Association.
11. Moghassem A. R. (2010) Application of TOPSIS Approach on Parameters Selection Problem for Rotor Spinning Machine. *Fibers and Polymers*, 11 (4), 669 - 675.
12. Moghassem A. R., Bahramzadeh H. (2010) Application of multi-criteria analysis for parameters selection problem in rotor spinning machine. *Textile Research Journal*, 80 (20), 2176 - 2187.
13. Cheng, Y. S. J. a Cheng, K. P. S. (2004) Selecting Processing Parameters that Influence of Rotor Spun Yarn Formed on SDL Quickspin System. *Textile Research Journal*, 74 (9), 792 - 796.

14. Roudbari B. Y. and Eskandarnejad S. (2013) Effect of Some Navels on Properties of Cotton/Nylon66 Blend (1:1) Rotor Spun Yarn and Wrapper Formation: A Comparison between Rotor and Ring Spun Yarn. *Journal of Textiles*, 2013 (ID 262635), 6 pages.
15. Tyagi K., Choudhary A. K. and Varshney R. K. (1996) Contribution of draw-off nozzle profile to certain characteristics of acrylic-cotton rotor-spun yarns. *Indian Journal of Fibre & Textile Research*, 21 (12), 261 - 264.
16. Erbil Y., Babaarslan O. a Baykal P. D. (2008) Influence of Navel Type on Hairiness of Rotor Spun Blend Yarns. *Fibres and Textiles in Eastern Europe*. 16 – 2 (67).
17. Esfahani, R. T. a Shanbeh, M. (2014) Effect of Navel and Rotor Type o on Physical. *Fibres & Textiles in Eastern Europe.* 22 – 3 (105).
18. Kaplan S. Göktepe O. (2006) Investigation into navel selction for totor spinning machine using cotton waste. *Fibres & Textiles in Eastern Europe*. 14 – 3 (57).
19. Mejzlíková V. (2000) ČSN EN 12751 *Textiles. Sampling for fibers, threads for testing.* Czech Standard Institute.
20. Mejzlíková V. (1996) ČSN EN ISO 2060 *Textiles. Yarn from packages. Determination of linear density (mass per unit length) by the skein method*. Czech Standard Institute.
21. Klimešová A. (2005) EN ISO 139 *Textiles - Standard atmospheres for conditioning and testing*. Czech Standard Institute.

A STUDY ON THE IMPROVMENT OF FABRIC COVER ON A SHUTTLELESS WEAVING MACHINE

Kasthuri Rajagopala Venkatesh, Rajesh Mishra, Mohanapriya Venkataraman.

Department of Material Engineering, Faculty of Textile Engineering, Technical University of Liberec, Czech Republic
Corresponding author Email: kasthuri.rajagopala.venkatesh@tul.cz

Abstract:

An investigation on effect of weaving conditions on the cover of fabric woven on a Projectile weaving machine is reported with the aid of Box and Behnken design of experiment. The individual effect and interactive effect of machine variables: shed timings, back rest roller and cloth fell support positions on cloth cover and fabric properties have been studied. It has been observed from the results that shed timing and back rest position have a significant effect on the air permeability of the fabric. The theoretically predicted results also have very good correlation with the experimental results.

Key words:

Cover, Box and Behnken, Back rest, Front rest, Shed timing, Projectile weaving machine.

1. Introduction

Cover factor indicates the extent to which the area of a woven fabric is covered by one set of threads. Significant effect of vertical displacement of the back rest and the shed timing on woven fabric cover has been well established and documented. But it should be pointed out; all the studies reported have been carried out in shuttle looms. [1] Three levels of variables have been used to study the individual effect and interactive effect of the three parameters, namely shed timings, back rest and cloth fell support positions on cloth cover and fabric properties that are influenced by fabric cover. It is possible to attain a closer pick spacing (i.e., a tighter packing of the picks) if the backrest is raised above its normal position [2-5]. By doing so, the top layer slacks and the bottom layer becomes tight. When the back rest is raised above its 'normal' position, upper shed becomes shorter, therefore at less tension than the lower shed. Upper shed becomes slack and lower one is tight. The pick inserted is forced downwards, since the ends that pass over it are now in the bottom shed and therefore tight. The preceding pick is forced upwards. These vertically displaced picks are clearly closer together than would be possible if placed in a horizontal plane.

In this work an attempt has been made to investigate the effect of these two process parameters i.e, back rest position and shed timing on cover of the fabric in a projectile weaving machine. It has been reported in the machine manual that adjustment of cloth fell support position will also affect the cover of the fabric, which is considered as the third parameter.

2. Experimental

2.1. Material

Rotor spun cotton yarn of count 20Ne as warp and 16Ne as weft was used for weaving fabric samples with 108 ends/inch and 40 picks/inch, plain weave.

2.2 Methods

Three process variables, back rest roller height, cloth support height and shed crossing were employed for the experimental design in order to optimise results and to reduce the number of experiments. Table 1 gives the 3 variables at 3 levels applied in the Box and Behnken design of experiments. Sulzer Ruti Projectile Weaving Machine of width 162inches was used to produce samples. To study the effect of machine parameters on the improvement of fabric cover, experiments were designed as per Box and Behnken factorial design for three variables at three levels.

Table 1. Three Variables at three levels for study

Parameters	**Level 1 (+1)**	**Level 2 (0)**	**Level 3 (-1)**
Back Rest Position (cm)	+10	0	-10
Cloth Fell Height (mm)	+2	0	-2
Shed Timing (degree)	15°	5°	355°

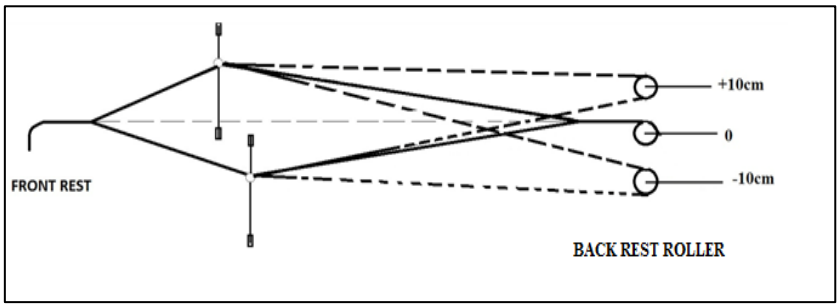

Figure 1. Position of the backrest roller

The physical properties of fabric samples were tested with standard testing equipments. Instron Tensile tester was used to determine the strength of fabric samples by ravelled strip method using CRE principle; Shirley Air Permeability tester was used to measure air permeability; weighing machine was used to measure fabric areal density.

Experimental Verification

Samples were produced to verify the response surface equation obtained from Box and Behnken design. For validation, four samples were prepared, two within the range of Box and Behnken design of experiments chosen for this study (1 and 2) and the other beyond the range (3 and 4). Table 2 gives the coded level and actual value for the three chosen variable. These samples were also tested for their tensile strength and air permeability. Tests were carried out to determine the actual tensile strength and air permeability of samples.

Table 2. Samples for experimental verification

Parameter	**Level 1 Back Rest Position (cm)**	**Level 2 Cloth Fell Height (mm)**	**Level 3 Shed Timing (degree)**
1	**7.5**	**49**	**10**
2	**5**	**49**	**7**
3	**15**	**50**	**350**
4	**17**	**50**	**17**

X1 - Back Rest Position (cm); X2 - Cloth Fell Height (mm); X3- Shed Timing (degree)

Table 3. Physical properties of woven fabric samples

Sample Code	Air Permeability (cm3/cm2/sec)	Tensile Strength (Warpwise) Load (N)	Tensile Strength (weftwise) Load (N)	Areal Density
1	22.25	749.5	245.8	210
2	22.36	707.3	258.7	211
3	22.48	755.9	248.3	210
4	19.42	734.8	272.5	214
5	21.41	748.4	264.6	211
6	22.13	756.9	251.3	205
7	26.50	770.8	260.2	206
8	28.89	733.6	265.1	201
9	21.78	712.5	252.1	208
10	28.32	723.2	268.0	212
11	20.36	731.7	270.3	207
12	25.13	693.1	266.8	213
13	21.5	756.8	254.5	206
14	20.66	749.1	280.9	207
15	22.68	705.2	221.0	206

3. Results and discussions

The various impacts of machine parameters on the fabric properties such as air permeability, tensile strength both in warpwise and weftwise and fabric weight.

Table 4. Regression equation for various properties.

Response Surface Equation	Property	R2
Y=21.61+ 0.05X1-0.93X2+2.88X3+0.439X12-0.425X22+2.679X32-0.792X1X2 + 0.417X1X3-0.412X2X3	Air Permeability	0.95
Y=737.033+0.65X1-9.276X2-3.598X3+18.572X12-18.73X22-3.18X32+5.275X1X2-11.425X1X3-12.322X2X3	Tensile Strength (Warpwise)	0.66
Y=253.133+1.026X1+6.77X2+2.756X3+0.084X12+4.122X22+8.044X32+2.84X1X2+4.512X1X3-4.85X2X3	Tensile strength (Weftwise)	0.32
Y=2.063+0.0025X1+0.011X2+0.026X3+0.0254X12+0.017X22+0.0002X32+6.103E-18X1X2+0.035X1X3-0.0125X2X3	Fabric Weight (Grams sq.meter)	0.87

Influence of process parameters on air permeability of fabric

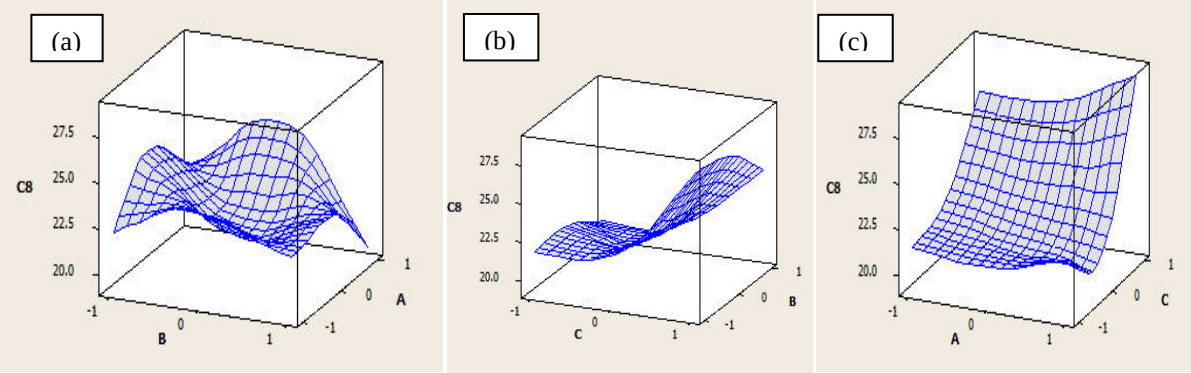

Figure 2. Influence of (a) cloth support height B and back rest roller position A, (b) shed timing C and back rest position A and (c) cloth support height B and the shed timing C on the Air permeability property of the fabric.

The effect of cloth support height and the back rest roller on air permeability of fabric can be studied from Figure 2 (a) it is observed from the graph, there is no effect when backrest roller is raised or lowered. But with respect to the cloth fell height, there is better effect. When the position of cloth fell height is raised, there is low air permeability and thus better fabric cover. The same is observed in all surface plots with all levels of C (shed crossing angle) such as -1, 0, and 1. (b) shows how the machine settings, cloth fell height and shed timing affects the air permeability of the sample fabric. It is evident from the figure that with alteration in cloth fell height there is no change in air permeability. But at early shed levelling (-1 position of C) there is low air permeability resulting in better fabric cover. In (c) with early shedding the permeability is low which indicates better fabric cover than at usual degrees (0° or 5°) of shed crossing and this may be due to retention of inserted weft from receding along with the reed.

Table 5. Experimental results and predicted values for air permeability test.

Sample Code	Air Permeability		
	Predicted	**Experimental**	**Abs Error%**
1	25.13	24.71	1.69
2	23.26	23.25	0.04
3	11.37	20.72	45.12
4	31.11	24.79	25.49

From table 5, the error percentage of predicted and experimental values is lower in case of sample code 1 and 2 which is within the range of the Box and Behnken design of experiments in this study. Prediction out of the range of the design shows higher error percentage. However, within the range is predictable.

Table 6. Experimental results and predicted values for tensile strength (Warpwise)

Sample Code	Tensile Strength Warpwise (N)		
	Predicted	**Experimental**	**Abs Error%**
16	746.36	701.72	6.36
17	763.85	695.5	7.77
18	818.05	732.68	11.65
19	759.60	716.76	5.97

Tensile Strength (Weftwise) Actual Vs Predicted Results

Sample code 18 has high error percentage and this may be due to the shed timing that was set at 350° which is earlier to early shedding (355°) itself.

Table 7. Experimental results and predicted values for tensile strength (Weftwise)

Sample Code	Tensile Strength Weftwise (N)		
	Predicted	**Experimental**	**Abs Error%**
16	254.76	266.49	4.60
17	252.07	261.78	3.85
18	222.47	245.7	10.44
19	279.2	262.6	5.94

Fabric weight Actual Vs Predicted results.

In Table 8, predicted and experimental results of areal density are tabulated.

Table 8 Experimental results and predicted values for GSM

Sample Code	Areal Density (GSM)		
	Predicted	Experimental	Abs Error%
16	2.09	2.12	1.43
17	2.07	2.11	1.93
18	2.02	2.08	2.97
19	2.24	2.11	5.80

4. CONCLUSION

4.1 Air permeability

From the results in previous chapter, it is pretty conclusive that shed timing has significant effect on cover of the fabric. With early shedding, (355°) there is high cover which is due to retention of newly inserted weft thread from receding along with the reed, which agrees with paper by B M D Dauda & M P U Bandara. The probable reason for no significant effect of backrest roller in a shuttleless weaving machine than that in a shuttle weaving machine may be due to,

High tension in warp yarn than in shuttle weaving machine.

Overall width of the machine operations is bigger than the conventional shuttle weaving machine.

4.2 Tensile strength of fabric

There is no significant effect of the machine parameters on fabric tensile, both warpwise and weftwise. There is no decrease in tensile strength with raising and lowering of the backrest roller which may be due to low tension applied on warp yarn. This is contradicting to the finding of L. F. Pickup.

4.3 Areal density of fabric

There is a change in areal density of fabric samples obtained at various machine settings. This is the reason behind improvement in cover of fabric. This may be due to tight packing of warp and weft threads at various machine settings.

References

1. *Dauda B M D & M P U Bandara, "Effect of Loom Setting on Fabric Cover and Beat-up Force", Indian Journal of Fibre & Textile Research -September 2004 Vol. 29,pp. 339-342*
2. *Eask Fernando, "Mathematical Model for Warp Tension with Various Back Rest Settings and Relationship with Technological Parameters", International Journal of General Engineering And Technology (IJGET) Mar 2014 Vol. 3, Issue 2, pp.17-26.*
3. *Pickup L.F., "Strength of Plain Cotton Cloth Woven from Folded Yarns", The Textile Institute, pp. 1948 T258-273.*
4. *Spencer H.C., "Methods of Obtaining Cover at the Loom", ATI. The Textile Manufacturer, July 1955 pp.356.*
5. *Uzma Syed, "Influence of Warp Yarn Tension on Cotton Woven Fabric Structures", Research Journal Of Engineering And Technology, Jan 2013 Vol. 32.*

3D PREFORM ARCHITECTURES IN TECHNICAL TEXTILE APPLICATIONS: SHORT REVIEW BASED ON CASE STUDIES

Kadir Bilisik

Erciyes University, Faculty of Engineering, Department of Textile Engineering 38039 Talas-Kayseri, Turkey, Tel: +90352 437 49 37, Fax: +90352 437 57 84, E-mail: kadirbilisik@gmail.com

Abstract

In this study, 3D preform architectures are summarized including author's last 28 years research contributions in the field. Multiaxis 3D woven preform is five yarn sets in which two of them bias sets are oriented in-plane of the structure, whereas remaining sets are orthogonal to each other. 3D fully interlaced woven preform has three sets of yarns in which warp yarns are interlaced with weft yarns at each layer based on the weave pattern in the in-plane principal directions, whereas z-yarns are interlaced with warp yarns at each layer based on weave pattern in the out-of-plane principal directions. Z-crimps in the 3D fully-interlaced woven preform structure are introduced. Multiaxial 3D braided preform has ±bias yarns placed in-plane, and warp (axial), radial (z-yarns) and ±braider yarns placed out-of-plane. The braider yarns are intertwined with the axial yarns whereas ±bias yarns are oriented at the surface of the structure and are locked by the radial yarns to the other yarn sets. In this architecture, the properties of the multi-axial 3D braided structure in the transverse direction can be enhanced and the non-uniformity in the directional poisson's ratios can be decreased. Multi-stitched 3D preform is made by stitching 2D fabric layers together at the warp (0°), weft (90°) and ±bias directions in the structure thickness. On the other hand, multiaxis non-interlaced 3D preform has four fiber sets oriented at 0°/90°/±45˚ directions. The fiber sets are all wound around each other to form the preform structure. The yarns are all positioned in the in-plane directions of the preform structure without any interlacement with each other. All these 3D fabric architecture can be used in various industrial applications as beams, shells, seats and chassis; ballistic applications as soft vest and rigid plates; space and aerospace as well as transportation including marine applications as various structural components as exit cones, cylinders and rods; medical applications such as tissue engineering scaffolds as to repair or regenerate tissues through combinations of implanted cells-biomaterial scaffolds-biologically active molecules.

Key words

3D woven preform, 3D braided preform, Multiaxis 3D woven preform, Multiaxis 3D braided preform, Non-interlaced fabric, Multi-stitched 3D preform, Fiber volume fraction, Z-crimp.

1. Introduction

At the beginning of the 21st century, textile structural composites have become attractive to various industrial applications. Fabrication of textile preform is generally made by weaving, braiding, knitting, stitching and nonwoven techniques, and recently nano electorsppinning. Multiaxis 3D flat and circular weaving are a newly developed concept, since it includes also bias yarn sets introduced to the orthogonally-structured preform and multiaxis 3D preforms may enhance in-plane properties [1, 3, 4, 11, 16, 15]. Three-dimensional woven lattice structures have three sets of yarns. These are the warp, weft and z-yarn (binder). These are interlaced with each other based on a plain weave pattern. The weft yarns in the lateral direction interlace around each warp yarn, which occupies the longitudinal direction, and the binder yarns in the vertical direction also interlace around each warp yarn [10, 14, 7]. 3D braided preforms are fabricated by traditional maypole braiding (slotted horn-gear matrix) or

innovative four-step and two-step braiding (track and column) or, more recently, by 3D rotary braiding and multi-step braiding. Multi-step braiding is a relatively new concept and, with this technique, it is possible to make multidirectional 3D braided preform by orienting the yarn in various directions in the preform [2, 8, 9, 17, 18]. Stitching technique is another method to make textile structural 3D preform for composites. The stitching is generally made by hand stitching, lock stitching and chain stitching are made by employing sewing machine, and recently, tufted stitching is employed by using the tufting carpet technique or embroidery techniques. It was reported that the stitched composites showed high damage tolerance properties [5, 13, 19]. On the other hand, it was demonetrated that shuttle winder is another method to make multiaxis 3D non-interlaced preform. Yarns are looped around the guide pins depending upon yarn orientation and layer sequence. It was reported that preforms fabricated with a shuttle winder possess better fiber alignment and lower fiber damage than conventionally stitched preforms [6, 11-2, 20].

2. Experimental

2.1. Materials and Methods

Multiaxis 3D woven preform

Multiaxis 3D woven preform has five yarn sets as ±bias, warp (axial), filling and z-yarns. Warp yarns are arranged in a matrix of rows and columns within the required crosssection. It looks a spares network for laying the fibers in between adjacent warp fibers. Filling fibers are laid down between each adjacent warp fiber row. They are double ended and deposited through the preform length. ± Bias yarns have two sets in which each set has half of the warp yarn ends in each row. They are positioned on both surfaces of the preform. They are oriented preform surface at an angle. Z-yarn ends are positioned between each warp row through the preform thickness. They lock all other yarn sets to provide structural integrity of the preform. The unit cell of the multiaxis woven preform is shown schematically in Figure 1(a). In addition, multiaxis 3D circular woven preform has five yarn sets as ±bias, axial, circumferential and radial yarns. Axial yarns are arranged in a matrix of circular rows and radial columns within the required circular cross-section. It looks a spares network for laying the fibers in between adjacent axial fibers. Circumferential fibers are laid between each adjacent axial fiber row. They are single ended and are deposited through the preform length. ± Bias yarns have two sets. They are positioned both surfaces of the preform. The first pair of bias yarns is placed on the outer surface and the second on the inner surface of the circular preform, but there is a circumferential yarn between +bias and –bias yarns. They are oriented preform surface at an angle. Radial ends are positioned between each axial row through the preform thickness. They lock all other yarn sets to provide structural integrity of the preform. The unit cell of the multiaxis woven preform is shown schematically in Figure 1(b). The machine to make multiaxis 3D woven preform is not explained in detailed here due to the out of scope of this proceeding.

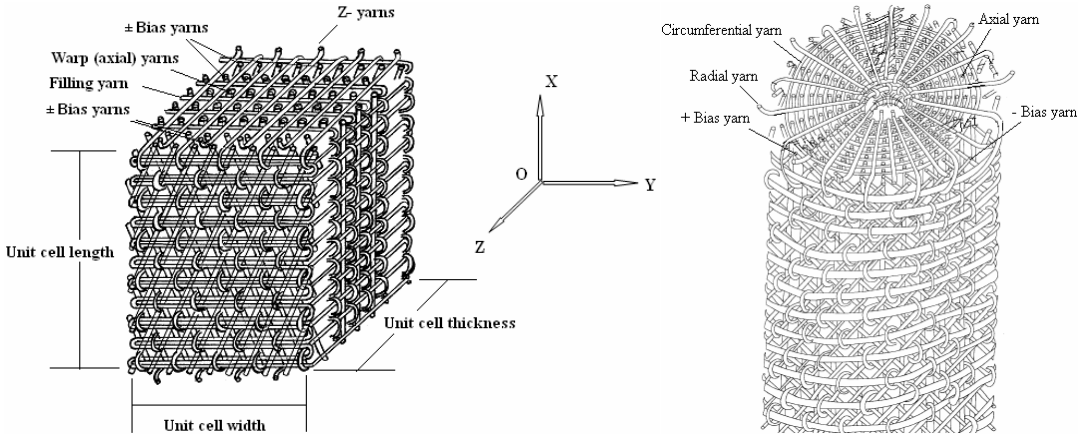

Figure 1. Perspective views of the unit cell of the multiaxis 3D flat woven preform (a), perspective views of the unit cell of the multiaxis 3D circular woven preform (b).

3D fully interlaced woven preform

3D fully interlaced woven preform is composed of three yarn sets as warp, filling and z-yarns. They are interlaced based on plain, twill and satin weave patterns in the plane and out-of-plane directions. The 3D plain, twill and satin woven preforms can be defined as warp–filling and warp–z-yarns that are interlaced based on plain, twill and satin weave patterns. Using the same analogy, the semi-interlaced woven preform can be defined as warp–filling that is interlaced based on a plain or twill or satin weave pattern, whereas warp–z-yarn is interlaced based on an orthogonal weave pattern. In order to make the 3D plain woven preform, the warp must be arranged in a matrix of rows and columns, as shown in Figure 2(a1). The first step is the one-step sequential movement of an even number of warp layers in the column direction (a2). The second step is filling insertion between each warp layer in the row direction (a3). The third step is the one step sequential movement of an even number of warp layers in the row direction (a4). The fourth step is z-yarn insertion between each warp layer in the column direction (a5). After the steps (a2–a5) are repeated, the 3D plain woven preform structure is achieved (a6). These steps are repeated depending on preform length requirements. The 3D plain-z-yarn orthogonal woven pattern is also shown in Figure 2 in steps b1–b6, where the z-yarn insertion is fulfilled without any interlacement in the preform structure (b4–b6). The number of warp layers can be expanded in the row and column directions depending upon preform dimensions.

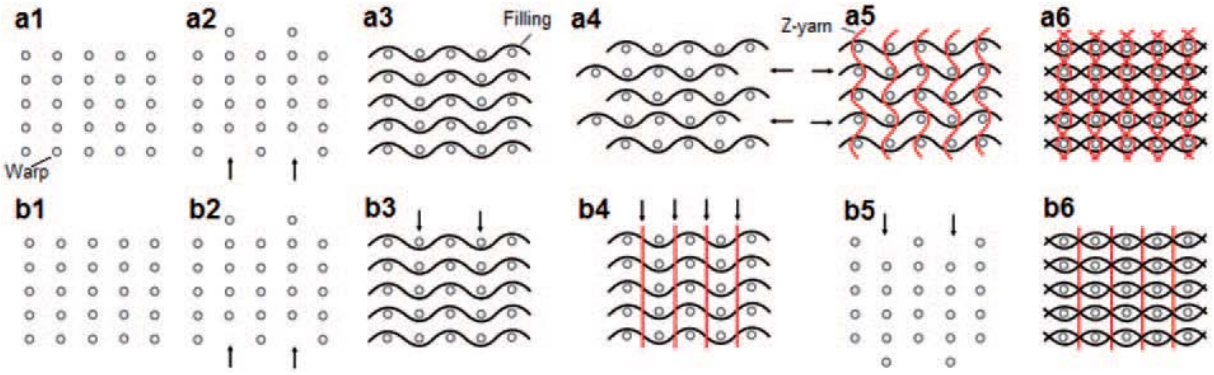

Figure 2. Three-dimensional (3D) weaving method to make representative fully interlaced woven preforms; 3D plain woven preform (a1–a6), 3D plain-z-yarn orthogonal woven preform (b1–b6).

Multiaxial 3D braided preform

Multiaxial 3D braided preform produced by the six-step method has ±bias yarns placed in the in-plane direction of the structure, and warp (axial), radial (Z-yarns) and ±braider yarns placed in the out-of-plane direction of the structure. The braider yarns are intertwined with the axial yarns, whereas ±bias yarns are oriented at the surface of the structure and are locked by the radial yarns to the other yarn sets. Figure 3 shows the multiaxial cylindrical and conical para-aramid 3D braided structure produced by the six-step method. The properties of the multiaxial 3D braided structure in the transverse direction could be enhanced and the non-uniformity in the directional poisson's ratios of the structure could be decreased. In this process, there are six distinct steps in each cycle. In Steps 1 and 2, ±braider yarns are intertwined around the axial yarns as in the four-step method. In Step 3, ±bias yarns are laid down on the surface of the structure. In Step 4, the radial yarns move in the thickness direction of the structure and lock the ±bias yarns to the ±braider and axial yarns. In Steps 5 and 6, the ±braider yarns are intertwined around the axial yarns as in the four-step method.

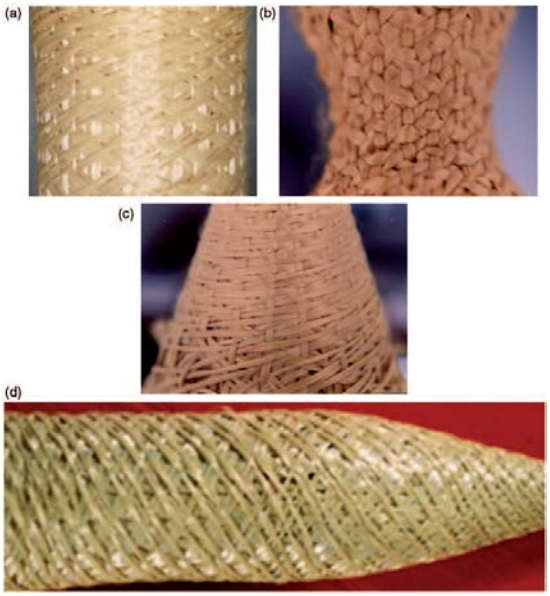

Figure 3. Multiaxis three-dimensional braided para-aramid preform. Cylindrical para-aramid (kevlar) preform (a), tightly braided neck part of the conical para-aramid (kevlar) preform (b), conical part of the para-aramid (kevlar) preform (c) and cylinder-conical para-aramid (kevlar) preform (d).

Multi-stitched 3D preform

Multi-stitched 3D preform structure is a layered fabric $[(0°/90°)]_4$, four-directionally stitched in the warp (0°), weft (90°), and ±bias directions. Figures 4 and 5 show multi-stitched 3D woven preforms, and schematic views of the multistitched 3D structure, respectively. In machine stitching, lock stitching is used, and the stitching density is varied at 2 and 6 step/cm. The distance between the adjacent stitching lines is 1 cm. The stitching yarns are also varied using fully nylon 6.6 (bobbin and needle yarn) and para-aramid (kevlar 129) as the bobbin-stitching yarn and polyamide (nylon 6.6) as the needle stitching yarn. The stitching machine is produced by Brother Industries Ltd., DB2-B736-3TR, Japan.

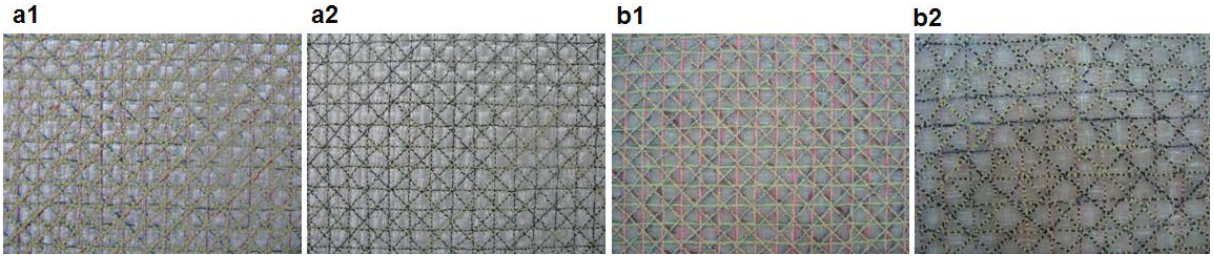

Figure 4. Views of multi-stitched 3D woven E-glass/polyester/nano silica preforms and composites. Front face preform (a1); back face preform (a2); front face composite (b1); back face composite (b2).

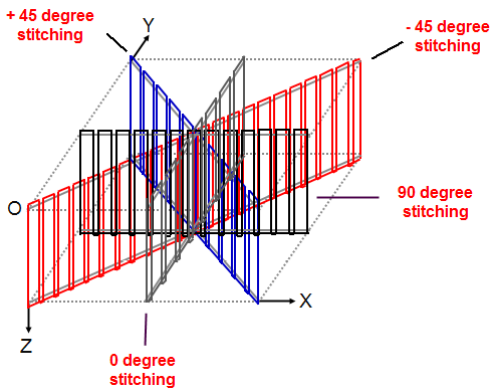

Figure 5. Schematic view of 3D multi-stitching at 0°,90° and ±45° directions.

Multiaxis non-interlaced 3D preform

Multiaxis non-interlaced 3D preform is developed. The manufacturing parameters considered are yarn orientation, number of layers, preform packing density and yarn linear density. Figure 6 shows the schematic views of the preform structures. A uniaxial preform has one fiber set oriented at 0°and has 10 layers, whereas biaxial preforms have two fiber sets oriented at 0°/90° and have a total of two and 10 layers. A multiaxis preform has four fiber sets oriented at 0°/90°/ ±45° and has a total of four layers. The fiber sets are all wound around each other to form the preform structure as shown schematically in Figure 7. The winding procedure is carried out once to make the structures. The yarns are all positioned in the in-plane direction of the preform structure without any interlacement with each other. After each layer is wound, an adhesive plaster is used to hold all the yarn ends around the structure during fabrication with a manually driven prototype flat winder. This provides structural integrity to the preform structure during the consolidation process as shown in Figure 7(d).

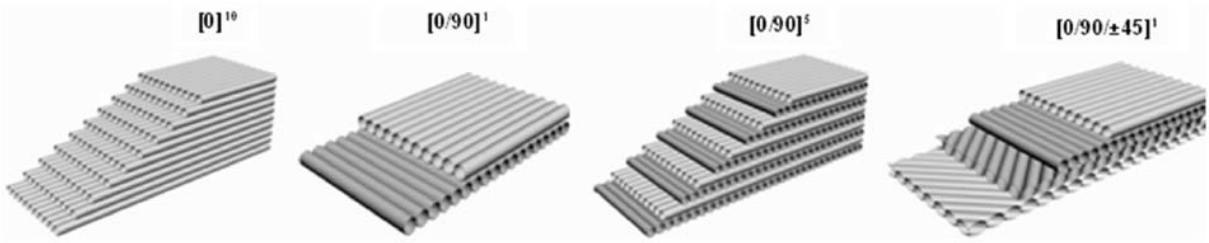

Figure 6. Schematic views of the 3D uniaxial $[0°]_{10}$, biaxial $[0°/90°]_1$, 3D biaxial $[0°/90°]_5$ and multiaxis $[0°/90°/±45°]_1$ non-interlaced 3D preform unit cell, respectively.

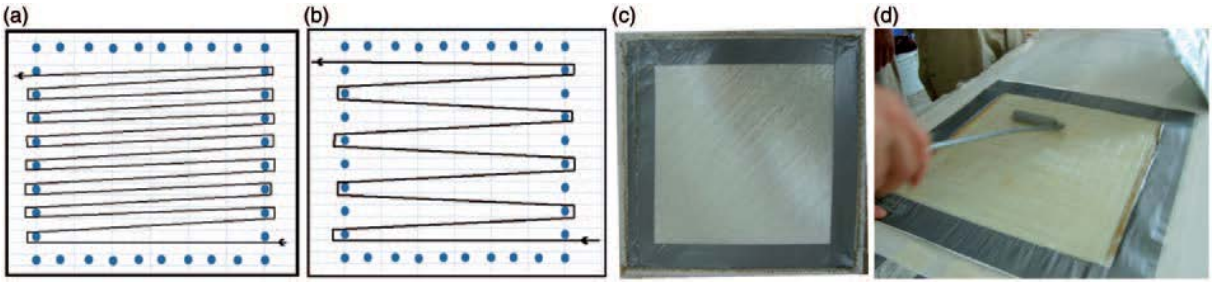

Figure 7. Schematic views of flat winder; tightly wound yarn path (a), loosely wound yarn path (b), E-glass multiaxis $[0°/90°/±45°]_1$ preform structure secured by adhesive plaster on the flat winder (c), E glass multiaxis $[0°/90°/45°]_1$ preform structure during hand lay-up consolidation (d).

3. Results and discussion

3.1. Multiaxis 3D woven preform

Figure 8 shows the multiaxis 3D prototype weaving. The multiaxis weaving has tube-carrier for ±bias yarn orientations, warp-filling-±bias-z-yarn feeding units, filling and Z-yarn insertion systems, take-up and selvage units.

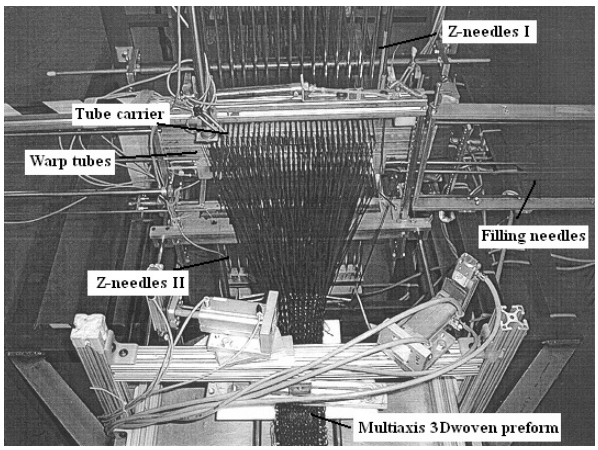

Figure 8. Multiaxis 3D weaving to form multiaxis 3D woven preform for composites [4].

Bias Orientation

After the initial trial, the bias tube-carrier moves smoothly in its place according to the required angle in the structure. Therefore, the edge yarn in the preform exchanges during the tube-carrier movement in the structure. The braider carriers feed the yarn to the tube-carrier as +bias and –bias yarns. The important part of the feeding is the yarn tension, which is changed during the edge exchange. It is sensible to form a 3D woven structure. High tensions in the braider carriers make it difficult to insert the other yarn sets, in particular z-yarns, and formation requires a high beat-up force to pack the 3D structure. On the other hand, a high beat-up force could break the brittle carbon filament during weaving, which reduces the properties of the structure.

Width Ratio

The width ratio is the characteristic parameter of the multiaxis 3D tube-carrier weaving, which describes the weaving zone width to the preform width (width ratio=preform width/weaving zone width). It is the main processing parameter to influence the preform fabrication during weaving.

Filling Insertion

After filling insertion is completed and is retracted from the weaving zone, excessive yarn length must be removed from inside the structure. This may be solved by using the negative tension control system. The excessive yarn length occurs because the preform width/tube rapier width ratio is not 1. It is almost 1/3. In this case, the filling length during insertion is 3 units, but when it returns to its starting position, 1 unit length remains in the preform. So, 2 unit lengths must be retracted to avoid a wavy structure.

Z-yarn Insertion

The z-yarn insertion system works properly and shed opening is determined through the trial and error method. It is observed that this is of particular importance during required spacing for filling insertion during z-needle staying in the weaving zone. In addition, there is a certain relation between the filling shed and the z-needle length. They must be determined properly to avoid excessive z-yarn length. A proper tensioning system in the z-yarn may be required in order to avoid unnecessary excessive pressure on the filling yarns, which causes local yarn distortions in the preform structure and it becomes an important processing parameter.

Beat-up

After the initial trail, it is realized that the weaving zone is a trapezoidal shape, and the bar arrangement in the beatup unit does not match with the weaving zone. The one side open reed moves to pact the inserted filling toward the weaving zone, but it opened the warp fibers and very high frictional pressure was exerted between the reed–warp, reed–bias and reed–filling. This caused filament breakages in the warp and bias yarns and created wavy filling in the preform and tangle in the z-yarns. Many weaving cycles later, it was understood that the beat-up unit must be modified for continuous weaving. For this reason, finger type blades are used and blades are arranged in the beat-up unit so that they change position during movement in the weaving zone, and the distance between blades becomes less when they move in the trapezoidal weaving zone toward the preform formation line. In the preform formation line blades beat the filling to the preform formation line and pack the preform.

Selvage

The basic function of the selvage is to secure the filling loop when it returns to its original position. There are two selvages for each edge of the preform. After an experimental trial, it is realized that one selvage rod without a latch needle is required to be positioned just opposite the side of the filling insertion side. However, the fabric width to weaving zone ratio is almost 1/3 and this causes a large filling yarn length to remain in the edge. As a result, the filling yarn in the structure surface becomes wavy. This problem has been solved by adding the additional selvage rod.

Take Up

The take-up unit is used to deliver the preform from the preform formation line in order to continue the weaving. In addition, the take-up unit controls the filling and z-yarns densities, as well as the warp density. Therefore, the directional volume fraction of the preform can be tailored based on end use requirements.

3.2. 3D fully interlaced woven preform

Preform space

Yarn-to-yarn spaces in all the 3D fully interlaced woven preform structures will affect the directional fiber volume fraction and they eventually affect the total volume fraction of the 3D woven preforms. The basic processing parameters for the yarn-to-yarn spaces is beat-up and take-up rate, which mainly affect the filling-to-filling and the z-yarn-to-z-yarn spaces. These spaces in the preform could also affect matrix infiltration during composite fabrication, for instance, directional porosity distribution in the preform, infiltration time and fiber alignment during consolidation.

Preform density

The filling and z-yarn densities of all the 3D fully interlaced woven preforms in the xz-plane mainly depended on take-up rate, which influences the directional volume fraction of the 3D woven preform. When the yarn sets in the 3D structure were interlaced, the warp and z-yarn densities in the yz-plane is slightly irregular, which eventually affects the local properties of the 3D preform structures. However, depending on soft or rigid requirements, the warp and filling, and the z-yarn densities in both the xz-plane and the yz-plane could be tailored based on the processing parameters.

Preform yarn length

The z-yarn length in all the 3D woven preform structures is identified as the most critical yarn length due to the placement of the 3D woven preform thickness. When all the yarn sets in the 3D woven preform are interlaced fully, the z-yarn arc length increases. On the other hand, weave pattern types slightly affects the z-yarn arc length. In addition, when the number of layers increases, the z-yarn arc length remaines the same. The z-yarn length in thickness depends on the number of layers and the yarn interlacements. In general, yarn interlacement and the number of layers influence all the yarn lengths in 3D woven preform structures.

Preform crimp

Geometrical properties of the 3D fully interlaced woven preforms are analyzed. Crimps in the 3D fully-interlaced and semi-interlaced representative woven preform structure are calculated based on the structure dimensions and the uncrimped representative yarn lengths. The following relations can be used:

$$cw(\%) = (lw - Sl) \times 100/Sl \quad (1)$$
$$cf(\%) = (lf - Sw) \times 100/Sw \quad (2)$$
$$cz(\%) = (lzt - St \times 100)/St \quad (3)$$

where, *cw* is the warp crimp (%), *lw* is the uncrimped warp length (cm), *Sl* is the structure length (cm), *cf* is the filling crimp (%), *lf* is the uncrimped filling length (cm), *Sw* is the structure width (cm), *cz* is the z-yarn crimp (%), *lzt* is the uncrimped total z-yarn length (cm) and *St* is the structure thickness. In addition, crimps in the 3D fully-interlaced circular woven preform structure are calculated based on the structure dimensions and the uncrimped yarn lengths. The following relations can be used:

$$Ca(\%) = (la - Sl) \times 100/Sl \quad (4)$$
$$Cc(\%) = (lc - Ssl) \times 100/Ssl \quad (5)$$
$$Cr(\%) = (lrt - St \times 100)/St \quad (6)$$

Where, *Ca* is the axial crimp (%), *la* is the uncrimped axial length (cm), *Sl* is the structures length (cm), *Cc* is the circumferential crimp (%), *lc* is the uncrimped circumferential length (cm), *Ssl* is the structures outside surface length (cm), *Cr* is the radial crimp (%), *lrt* is the uncrimped total radial length (cm) and *St* is the structures wall thickness.

The 3D fully interlaced woven structures has warp crimp, filling crimp and z-yarn crimp, whereas the 3D semi-interlaced woven structure had warp crimp and filling crimp. On the other hand, the traditional 3D woven structures had no directional crimps. It was found that the directional crimps of the 3D woven structures slightly depended on the types of weave pattern. The z-yarn crimp was also reversely affected by the number of layers.

3.3. Multiaxis 3D braided structure

Multiaxis 3D braided structure is successfully formed and Table 1 presents the specification of the structure. Axial yarn sets are interlocked by ±braid yarn sets but ±bias yarn sets are interconnected by radial yarn sets. The main problem is that radial insertion in the braided structure due to technical difficulties in the flat bed in which the braider carriers are rotated.

Table 1. Multiaxis 3D braided para-aramid preform.

Fiber	Kevlar® 29(K29), Kevlar® 129(K129)
Axial yarn	1100 dtex (3 ply), K29
±Bias yarn	1100 dtex (4 ply), K29
Radial yarn	1100 dtex (1 ply), K129
±Braider yarn	1100 dtex (4 ply), K29
Structure	Multiaxis 6-step 3D braided preform
Axial yarn	2 (circumferential layers × 18 radial rows)
+Bias yarn	1 layer × 18 radial rows
–Bias yarn	1 layer × 18 radial rows
Radial	18 ends (one radial for every axial row)
Cross- section	Cylinder
Dimensions	100 (outside diameter) × 5 (wall thickness) × 250 (length) mm
Preform tightness	Very high
Fiber	Kevlar® 49
Axial yarn	3400 dtex (3 ply)
±Bias yarn	3400 dtex (2 ply)
Radial yarn	3400 dtex (3 ply)

±Braider yarn	3400 dtex (2 ply)
Structure	Multiaxis 8- step 3D braided preform
Axial yarn	2 (circumferential layers × 18 radial rows)
+Bias yarn	1 layer × 18 radial rows
-Bias yarn	1 layer × 18 radial rows
Radial	18 ends (one radial for every axial row)
Cross- section	Conical
Dimensions	140 (large diameter) × 55 (small diameter) × 5 (wall thickness) × 210 (length) mm
Preform tightness	Medium

3.4. Multi-stitched 3D preform

The multi-stitched 3D preform and rigid forms is analysed. The fiber volume fraction results indicated that stitching caused local misalignment and uneven fiber placement in the structure. In addition, when the stitching directions in the structure increased, the stitching yarn volume fraction increased depending on the stitching density and yarn types. However, the total volume fraction of the structures did not increase proportionally due to the stitching process. The void content results indicated that stitching caused local micro misalignment and uneven fiber placement during needle piercing in the preform. Generally, the void content increases when the stitching direction increases. It can be considered that the stitching parameters in the developed multi-stitched 3D structures are stitching direction, stitching density, stitching yarn type, and stitching type.

3.5. Multiaxis non-interlaced 3D preform

Multiaxis non-interlaced 3D preform and production methods are evaluated. It was observed that flat winding is a simple and fast method to make multilayered and multiaxis part preform structures. In addition, each yarn sets in the structure are straight and there are not any considireable local misalanment in each yarn at structure plane.

4. CONCLUSIONS

Multiaxis 3D woven flat and circular preform architecture and new methods are developed. The fabrics and methods are evaluated. The preliminary results showed that structures and weaving methods were feasible compared to the state of the art techniques for their versatility and simplicity.

We found that the yarn-to-yarn spaces in 3D fully interlaced and semi-interlaced structures were high compared to those of the traditional 3D woven structures due to the directional interlacement where the directional fiber volume fraction can be affected. It was also observed that the interlacement in 3D woven structure caused slight irregular warp and z-yarn densities in fabric width. The interlacement on three yarn sets results in warp crimp, filling crimp and z-yarn crimp. Probably, the unique feature of this research was the z-yarn crimp in the 3D woven preform. In addition, it was found that the directional crimps of the 3D fully interlaced and semi-interlaced woven structures slightly depended on the types of weave pattern and the number of layers.

Multiaxis 3D braided fabrics have multiple layers and no delamination, and their in-plane properties are enhanced due to the ±bias yarn layers. However, the multiaxis 3D braiding technique is at an early stage of development. Multi-stitched 3D preform is simple to make and it could be used in the technical textile application due to enhance the properties as fracture toughness. It was observed that multiaxis non-interlaced 3D preform is simple structure, and its method is a convenient and fast in order to produce non-interlaced 3D multilayered and multiaxis preform structures for part manufacturing. However, this method must be integrated with the consolidation process as a future research subject.

ACKNOWLEDGEMENTS

This work is the product of Author's continued research efforts at the various textile material research centers and labs at the University of Leeds, North Carolina State University at Raleigh, Ege University and Erciyes University since 1988.

References

1. *Bilisik, K. (2012). Multiaxis Three Dimensional Weaving for Composites: A Review. Textile Research Journal, 82(7), 725–743.*
2. *Bilisik, K. (2013). Three Dimensional Braiding for Composites: A Review. Textile Research Journal, 83(13), 1414-1436.*
3. *Bilisik, K. (2010). Multiaxis 3D woven preform and properties of multiaxis 3D woven and 3D orthogonal woven carbon/ epoxy composites. Journal of Reinforced Plastics Composites, 29(8), 1173–1186.*
4. *Bilisik, K., Mohamed, M.H. (2010). Multiaxis Three Dimensional (3D) Flat Woven Preform-Tube Carrier Weaving. Textile Research Journal, 80(8), 696-711.*
5. *Bilisik, K., Yolacan, G. (2014). Experimental Characterization of Multistitched Two Dimensional (2D) Woven E-Glass/Polyester Composites under Low Velocity Impact Load. Journal of Composite Materials, 48(17), 2145-2162.*
6. *Bilisik, K., Yilmaz, B. (2012). Multiaxis Multilayered Non-interlaced/Non-Z E-Glass/Polyester Preform and Analysis of Tensile Properties of Composite Structures by Statistical Model. Textile Research Journal, 82(4), 336-351.*
7. *Bilisik, K, Sahbaz, N., Bilisik, N.E., Bilisik, H.E. (2013). Three Dimensional (3D) Fully Interlaced Woven Preforms for Composites. Textile Research Journal, 83(19), 2060-2084.*
8. *Brown, R.T. (1985). Through-the-thickness braiding technology. In: 30th national SAMPE symposium, Tokyo, Japan.*
9. *Florentine, R.A. (1983). Magnaweave process-From Fundamentals to applications. Textile Research Journal, 53, 620–623.*
10. *Fukuta, K., Onooka, R., Aoiki, E., et al. (1982). Three dimensionally latticed flexible structure composites. U State Patent No 4336296, USA.*
11. *Hearle, J. W. S. (1994). Textiles for Composites. Textile Horizon, 11, 11–15.*
12. *Kamiya, R., Cheeseman, B. A., Popper, P., and Chou, T. W. (2000). Some Recent Advances in the Fabrication and Design of Three Dimensional Textile Preforms: a Review. Composite Science and Technology, 60, 33–47.*
13. *Kang, T.J., Lee, S.H. (1994). Effect of stitching on the mechanical and impact properties of woven laminate composite. Journal of Composite Materials, 28, 1574-1587.*
14. *Khokar N. (2002). Noobing: a nonwoven 3D fabric-forming process explained. Journal of Textile Institute, 93, 52–74.*
15. *Mohamed, M. H. (1990). Three Dimensional Textiles. American Scientist, 78, 637–647.*
16. *Mohamed M.H., Bilisik, A. (1995). Multilayered 3D fabric and method for producing. US Patent No 5465760.*
17. *Popper, P., McConnell, R. A. (1987). New 3D braid for integrated parts manufacture and improved delamination resistance- the 2-step process. In: proceedings of 32nd international SAMPE symposium and exhibition, Anaheim, CA, USA.*
18. *Schneider, M., Pickett, A.K., Wulfhorst, B. A. (2000). New rotary braiding machine and CAE procedures to produce efficient 3D braided textiles for composites. In: 45th international SAMPE symposium, Long Beach, CA, USA.*
19. *Wu, E., Wang, J. (1995). Behavior of stitched laminates under in-plane tensile and transverse impact loading. Journal of Composite Materials, 29, 2254-2279.*
20. *Yasui, Y., Hori, F., Amano, M., Takeuchi, J. (1998). Method and apparatus for production of three dimensional fabric. US Patent No 5772821.*

ANALYSIS OF WATERPROOF AND THERMAL PROPERTIES FOR MULTI-LAYERED BREATHABLE FABRICS

Abdur Razzaque, Pavla Tesinova

Technical University of Liberec, Faculty of Textile Engineering, Department of Textile Evaluation,
Studentska 2, 46117 Liberec, Czech Republic, Tel : +420-776148252,
E-mail: araztm29@yahoo.com

Abstract:

Waterproof breathable layered fabrics allow water vapor passing through, but resist liquid water to pass. This ability of the fabrics to protect rain and snow water while allowing sweat vapor to evaporate from inside to outside atmosphere, leads them to be used as outdoor sportswear or protective clothing. On the other hand, thermal properties of these fabrics, i.e., thermal conductivity or thermal resistance should also be maintained properly for the comfort of wearers. This paper presents a study that aims to analyze the hydrostatic resistance and thermal properties of waterproof breathable fabrics considering their water vapor permeability as well. For this purpose, four different types of layered fabrics were used in the experiment. The effect of material composition and layered structure of fabrics on the mentioned properties has been analyzed. It has been found a significant influence of structure and construction of fabrics on their waterproof and thermal properties from the test results.

Key words:

Waterproof, breathability, layered structure, hydrostatic resistance, water vapor permeability, thermal conductivity

1. Introduction

Breathability of a fabric is the ability of clothing to allow moisture vapor transmission from inside to outside atmosphere and hence facilitate evaporative cooling. It is determined by water vapor permeability [1] and diffusion of water vapor through fabric is the determining factor of breathability. On the contrary, waterproofing is a term that can be described as the impermeability to water. Waterproof fabric which requires the filling of pores is resistant to the penetration of water under pressure. Resistance of a fabric to water depends on the nature of the fabric surface, the porosity of the fabric and the dynamic force behind the impacting water spray [2].

There are significant uses of waterproof breathable fabrics in the fields of protective clothing, sportswear and construction industries [3]. They have two contradicting properties at the same time – they are waterproof, but yet water vapor permeable. Hence, it is the biggest challenge for the manufacturers to produce waterproof breathable fabric maintaining these two properties properly. However, different types of breathable fabrics can be classified as like as : closely woven fabrics, micro-porous membranes and coating, hydrophilic membranes and coating, combination of micro-porous and hydrophilic membranes and coating, use of retroreflective microbeads, smart breathable fabrics and fabrics based on biomimetics [4].

Again, beside the above mentioned two properties, thermal property, i.e., thermal conductivity or thermal resistance of the waterproof breathable fabrics should be also maintained properly as these are the important parameters for thermo-physiological comfort. In the experiment, hydrostatic resistance, water vapor permeability, thermal conductivity and thermal resistance of different laminated multi-layered breathable fabrics were measured. Then the results have been analyzed. It has been found that the effects of material construction and layered structure of the fabrics on the waterproof and thermal properties are quite significant.

2. Experimental

2.1. Materials

Four different types of waterproof breathable layered fabrics were used in the experiment. All of them were three-layered and laminated by ploytetrafluoroethylene (PTFE) micro-porous membrane as shown in Table-1.

Table 1. Characteristics of laminated fabrics

Sample Nr.	Fabric structure [order : outer part to inner part]	Cover factor for outer woven part of fabric	Stitch density for inner knitted part of fabric [stitches/cm^2]	Areal density of fabric [g/m^2]	Thickness of fabric [mm]	Fabric density [kg/m^3]
S-1	PES plain + PTFE membrane + PES knit	17	273	89	0.21	423.81
S-2	PES plain + PTFE membrane + PES knit	33	925	167	0.35	477.14
S-3	PES plain + PTFE membrane +Rayon knitted fleece	25	180	451	1.25	360.80
S-4	PES plain + PTFE membrane + PES knitted fleece	27	192	314	1.20	261.67

Here, layers of each fabric sample are shown from outer part to inner part order. All the measurements were carried out at standard atmospheric condition.

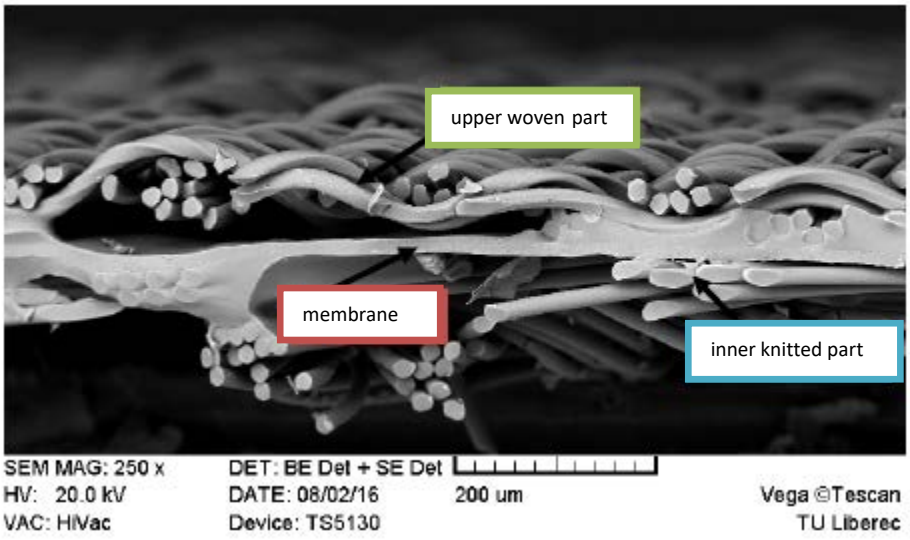

Figure 1. SEM image of a three-layered laminated fabric sample

2.2. Methods

All the different parameters of the laminated fabrics, like, cover factor of upper woven fabric, stitch density of inner knitted fabric, areal density of fabric, thickness of fabric and fabric density were measured according to standardized procedures.

Hydrostatic resistance tests were carried out by SDL ATLAS Hydrostatic Head Tester Model MO18 according to AATCC 127 [5] or ČSN EN 20811 (800818) [6] at 20±2ºC whereas the rate of increase of

water pressure was 60±3 cmH_2O/min. Water pressure was recorded at the point when water penetrated from outer layer to inner layer. The unit was expressed as cmH_2O.

PERMETEST instrument was used to measure the water vapor permeability of the samples according to ISO 11092 standard. This instrument is able to measure relative water vapor permeability [%] and water vapor resistance, Ret [m^2Pa/W] and works on a similar skin model principle [7].

Thermal conductivity and thermal resistance were measured by ALAMBETA which is a computer controlled instrument for measuring the basic static and dynamic thermal characteristics of textiles. The values of thermal conductivity and thermal resistance of the fabrics under a 200 Pa contact pressure were determined. Measurement of thermal properties by ALAMBETA is standardized in the Internal Standard of Textile Faculty of Technical University of Liberec [8].

3. Results and discussion

Hydrostatic resistance, water vapor permeability, thermal conductivity and thermal resistance of four different samples are different due to many factors related to structure and construction of the laminated fabrics. These properties are shown in Table-2. All the results are analyzed statistically and upper limit (UL) and lower limit (LL) for the properties of each sample are shown here in the table.

Table 2. Different properties of laminated fabrics

Sample Nr.	Hydrostatic resistance [cmH_2O]	Water vapor resistance, Ret [m^2Pa/W]	Thermal conductivity [(10^{-3}) W/mK]	Thermal resistance [(10^{-3}) Km^2/W]
S-1	1464 <UL:1467; LL:1460>	6.44 <UL:6.58; LL:6.30>	43.08 <UL:43.23; LL:42.93>	5.78 <UL:5.88; LL:5.68>
S-2	1522 <UL:1524; LL:1520>	8.42 <UL:8.54; LL:8.30>	39.12 <UL:39.22; LL:39.02>	8.50 <UL:8.62; LL:8.38>
S-3	1114 <UL:1117; LL:1112>	7.50 <UL:7.56; LL:7.44>	37.68 <UL:37.93; LL:37.43>	35.66 <UL:35.92; LL:35.40>
S-4	1087 <UL:1091; LL:1083>	15.38 <UL:15.51; LL:15.25>	38.98 <UL:39.11; LL:38.85>	30.46 <UL:30.73; LL:30.19>

Hydrostatic resistance and water vapor permeability

From the following graph, it is clear that there is a positive correlation between fabric density of laminated fabrics and hydrostatic resistance. S-2 fabric has the highest hydrostatic resistance among

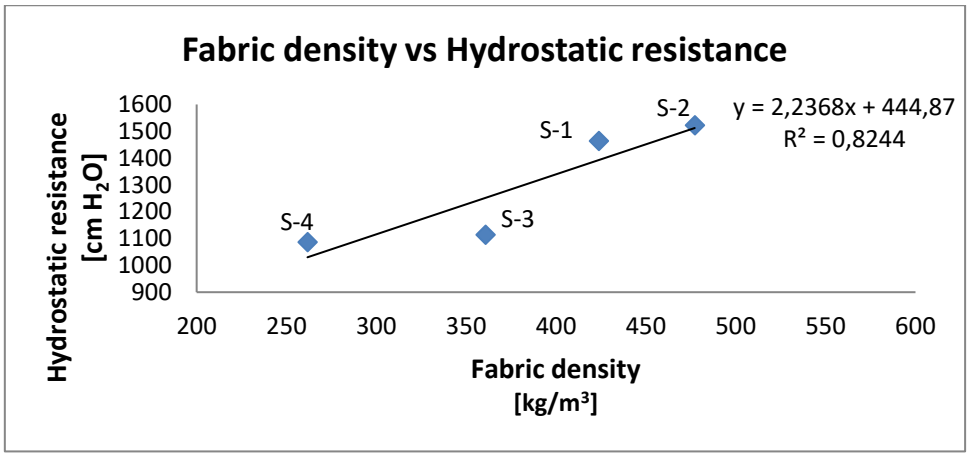

Figure 2. Hydrostatic resistance

all the samples, as it has the highest fabric density. Moreover, its cover factor of upper woven part and stitch density is also higher than any other sample. Hydrostatic resistance is lower for S-3 and S-4 due to their lower fabric density and fleece hairy inner knitted part which cannot resist water pressure properly.

Again, there is also a correlation when comparison with fabric density and water vapor resistance of the samples. But some other factors also influence on water vapor resistance. In case of S-1 and S-2

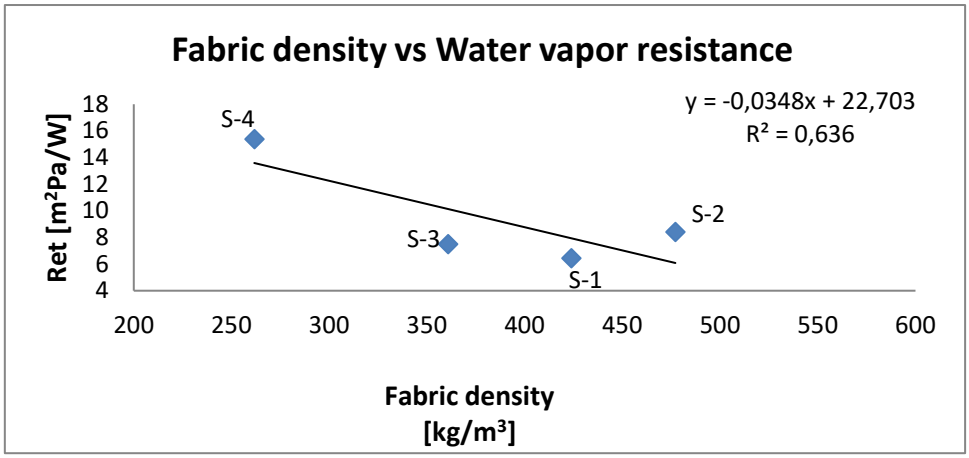

Figure 3. Water vapor resistance (Ret)

samples, water vapor resistance of S-1 is lower than S-2, due to its less fabric density as well as less cover factor of upper woven part and less stitch density of inner knitted part. On the other hand, both S-3 and S-4 samples have inner fleece hairy knitted part. But, S-4 Fabric has higher water vapor resistance though it has less fabric density than S-3. This is due to its polyester fleece knit structure as rayon fleece is more hygroscopic than polyester fleece knit and it influences on water vapor resistance or water vapor permeability.

Thermal conductivity and thermal resistance

There is a strong positive correlation between fabric thickness and thermal resistance. Thermal resistance is higher for higher thickness of fabric. S-1 has lowest thickness as well as lowest thermal resistance and S-3 has the highest thermal resistance due to its highest thickness property among all

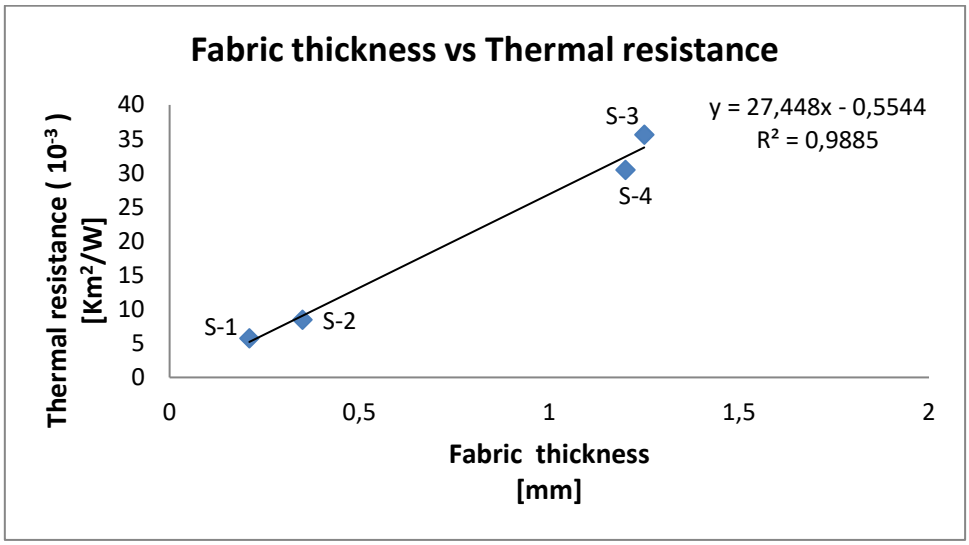

Figure 4. Thermal resistance

samples. Again thermal resistance is much higher for S-3 and S-4 than S-1 and S-2. This is due to their much higher thickness property and also their inner hairy knitted fleece structure for which air entrapping is occurred that causes higher thermal resistance.

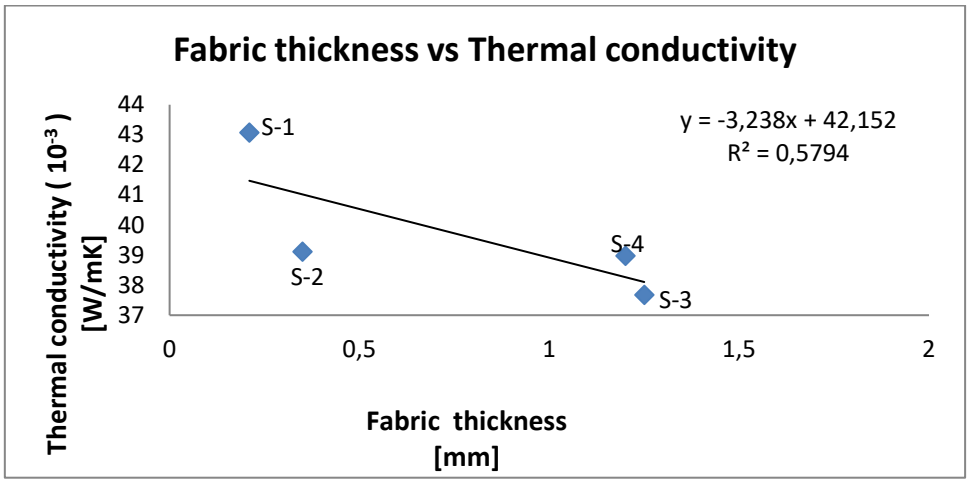

Figure 5. Thermal conductivity

Thermal conductivity is higher for the sample of less thickness property that is clear from the Figure-5. S-1 has the highest thermal conductivity due to its lowest thickness property and S-3 has the lowest thermal conductivity among all samples due to its highest thickness property.

4. CONCLUSIONS

In the experiment, hydrostatic resistance and thermo-physiological comfort of waterproof breathable fabrics have been discussed. It has been found that laminated fabrics have significant effects of their fabric density, thickness and other structures, like, cover factor of woven fabric part, knitted fabric composition, stitch density or fleece or non-fleece structure on hydrostatic resistance, water vapor permeability and thermal properties. Fabric density influences a lot on hydrostatic properties, whereas, water vapor permeability is influenced by fabric density as well as other fabric properties, like, hygroscopic nature of fibers. However, there is a great influence of thickness of laminated fabric on its thermal conductivity and thermal insulation properties.

ACKNOWLEDGEMENTS

This study is supported by the development program of Student Grant Competition SGC 2016 Nr. 21148.

References

1. *Das, B., Das, A., Kothari, V., Fanguiero, R., Araujo, M.D. (2009). Moisture flow through blended fabrics- effect of hydrophilicity. Journal of Engineered Fibers and Fabrics, 4(4), 20-28.*
2. *Chinta, Dr.S.K., Satish, Darbastwar. (2014). Studies in waterproof breathable textiles. International Journal of Recent Development in Engineering and Technology, 3(2), 16-20.*
3. *Kang, Y.K., Park, C.H., Kim, J., Kang, T.J. (2007). Application of electrospun polyurethane web to breathable waterproof fabrics. Fibers and Polymers, 8(5), 564-570.*

4. *Mukhopadhyay, A., Midha, V. (2008). A review on designing the waterproof breathable fabrics Part I: Fundamental principles and designing aspects of breathable fabrics. Journal of Industrial Textiles, 37, 225-262.*
5. *AATCC 127, Water resistance : Hydrostatic pressure test. (1989)*
6. *ČSN EN 20811 (800818) Textiles, Determination of water penetration resistance. Testing with water pressure. Date of announcement 1994-10-01. 8 pages. based on ISO 811:1981.*
7. *Hes, L., Dolezal, I. (2003). A new computer-controlled skin model for fast determination of water vapor and thermal resistance of fabrics. In: 7th Asian Textile Conference, New Delhi.*
8. *International Standard No. 23-204-02/01. (2004). Measurement of the thermal properties by Alambeta device, Technical University of Liberec.*

DEVELOPMENT OF A MULTILAYERED BANDAGE

Daniel Karthik[1], Dr. Vijaykumar Baheti[1], Prof. Jiri Militky[1], Prof. A.I. Wasif[2]

[1]Department of Materials Engineering,Faculty of Textile,Technical University of Liberec,Czech Republic.Mobile No: +420 704 121 175, e-mail: danielkarthiktex10@gmail.com
[2] Department of Textile Chemistry, DKTE Society's Textile & Engineering Institute, Ichalkaranji Maharashtra – 416115

Abstract:

Textiles materials play an important and crucial role in designing appropriate medical devices for health care and medical industries. Wound healing is a natural process, dressings and medication enhance it. Bandages and dressings are designed to produce a whole variety of special functions depending upon the type of wound and medical requirements. In this research work an attempt has been made to develop a suitable multi-layered nonwoven bandage comprising of a patch and a bandage roll that possess the ideal characteristics required to aid the process of wound healing. The patch was coated with four suitable commercial antibiotics ointments i.e., Neosporin, Soframycin, T-Bact and Betadine along with paste of hydrocolloids (CMC, gelatin and PVA).All the above used antibiotic agents showed good antibacterial inhibition. having CMC – 27.5gpl, Gelatin – 22.5gpl, PVA – 49.5gpl, and Mineral Oil - 10gpl and of viscosity 2239 centipoise shows better results in terms of ease of application and anti-microbial activity. The bandage roll shows good breathability with a MVTR value of 560 g/m^2/day and good tensile properties with breaking load in the range of 5-8 lb and 25-30% tensile strain. The bandage roll was used to hold the patch in place.

Keywords:

Wound care, Nonwoven, bandage, antibiotic ointment, patch, hydrocolloids, breathability.

1. Introduction

Wound care and management has always been a major concern and has led to the development of newer advanced and more suitable products to meet its requirements. For centuries wounds have been dressed in order to protect the wound from the harmful external environment. The act of covering a wound mimics the function of the epidermis. The variety of wound types has resulted in a wide range of wound dressings with new products frequently introduced to target different aspects of the wound healing process. Successful wound care involves optimizing patient local and systemic conditions in conjunction with an ideal wound healing environment. Many different products have been developed to influence this wound environment to provide a pathogen-free, protected, and moist area for healing to occur. The ideal dressing should achieve rapid healing at reasonable cost with minimal inconvenience to the patient.

The last two decades have witnessed the introduction of many dressings, with new ones becoming available each year. Dressings should be easy to apply, painless on removal, conducive and create an optimal environment for wound healing and should require fewer dressing change in turn contributing to the psycho-physiological comfort of the patient. From hospitals to first-aid kits at homes, bandages and dressings find their applications making them a vital ingredient in the management of a wound. The present scenario offers a wide spectrum of products ranging from common wound management dressings like gauze bandages, lint and band aids to sophisticated multifunctional systems and emerging technologies including/such as dressings and novel polymers used for the delivery of drugs to acute, chronic and other types of wound for achieving improved wound healing. These include hydrocolloids, alginates, hydrogels, polyurethane, collagen, chitosan, pectin and hyaluronic acid. Pharmacological agents such as antibiotics, vitamins, minerals, growth

factors and other wound healing accelerators that take active part in the healing process by combating infections are also available. [2,3,4]

Major Constraints to be considered

- **Moisture Balance**: Maintenance of a moist wound bed reduces pain, tenderness, tissue fibrosis, and risk of infection. Over drying a wound results in dressing adhesion to the wound bed, prolonging wound healing and leading to scarring. On the other hand, wounds that are over hydrated can experience maceration, a process in which new skin tissue breaks down and sloughs.
- **Antimicrobial Properties**: Infection is one of the biggest inhibitors of proper wound healing.
- **Non-toxic and non-allergenic**: It is necessary that the material and its components be non-toxic and non-allergenic because it could damage the tissue and elicit a serious immune response.
- **Physical Barrier impermeable to bacteria**: The most fundamental purpose of a wound dressing is to serve as a physical barrier to infection. A dressing that is permeable to bacteria simply encourages colonization and drastically increases the risk of infection.
- **Conformable and Comfortable**: Wounds can occur anywhere on the skin, thus it is essential that the wound dressing be capable of conforming to any surface on the body, and to a degree, allow unhindered movement.
- **Cytotoxicity**: The proposed solution must not kill any mammalian cells. It is essential that the design allows for the proliferation of mammalian cells, otherwise this will inhibit the healing process. [10]

2. Materials And Methods

2.1 Patch

The patch was made up of the following three layers

- **First layer (top contact layer)** – 100% Polyester apertured spunlace nonwoven
- **Second layer (middle layer)** – 100% Viscose needle-punched nonwoven
- **Third layer (bottom layer)** – 100% Polyester apertured spunlace nonwoven

Table 1: Fabric particulars of top/bottom and middle layers of the patch

Fabric particulars	100% Polyester apertured spunlace nonwoven	100% Viscose needle-punched nonwoven
Fabric thickness (mm)	0.40	1.22
GSM	30	100
Air-permeability ($cm^3/cm^2/s$)	112.55	139.38

i. **Fabrication of the Patch**: The patch was made in two forms

- Standard Patch form of size 5 x 5 cm and 10 x 10 cm – the three layers were stitched together at the edges.
  Specifications:
  - Stitch type – single needle lockstitch
  - Stitch density – 4 spi
  - Stitch thread – 2-ply polyester thread
- Continuous Roll form of preferred size - The three layers were joined together by introducing LMP (low melt polyester: melting point-110^0C) fibers twice between the layers of and passing it through a curing chamber to melt and set.
  - LMP – 5 gm for a sample size of 10x10 cm

2.2 Antibiotic Coating

The contact layer of the patch was coated with topical antibiotic agents mixed in a uniform paste of hydrocolloid materials. (antibiotic ointment + hydrocolloids)

i. **Preparation of Hydrocolloid paste**:

Recipe:

Table 2: Recipe for the four formulations of the hydrocolloid paste

Sl. No	Formulation No.	Chemicals (in gm/litr)				Viscosity (Centipoise)
		CMC	Gelatin	PVA	Mineral Oil	
1	Formulation 1 (F1)	54	45	99	20	84000
2	Formulation 2 (F2)	36	30	66	13.3	51200
3	Formulation 3 (F3)	27.5	22.5	49.5	10	2238
4	Formulation 4 (F4)	10.8	18	40.25	8	837

Note: Solvent/water used: de-mineralized water

The materials were mixed together as per the recipe mentioned above and mechanically stirred at high speed for three hours to obtain a uniform paste. The prepared paste was stored in beakers in a refrigerator.

The viscosities of the four formulations mentioned in the above table were tested on a “Brookfield Viscometer”.

ii. **Preparation of Coating paste:**

Following are the commercially available and more commonly preferred antibiotics and antiseptics (therapeutic agents) that were used:

- **Soframycin** (Framycetin Sulfate) – ointment
- **Bactroban/T-Bact** (Group - Mupirocin) – ointment
- **Neosporin** (Triple Antibiotic Ointment - bacitracin, neomycin, polymyxin B) - ointment
- **Betadine** (Povidone-iodine) – ointment

The Antibiotic ointment of various concentrations was mixed with 1gm of each of the formulations of the hydrocolloid paste that was prepared earlier in the following manner:

Table 3: Preparation of coating paste

Sl.No	*HP(1gm) + *AB	Concentration of *AB (mg)
1.	Formulation 1+Soframycin	200,300,400,600,800,1000
2.	Formulation 2+Soframycin	200,300,400,600,800,1000
3.	Formulation 3+Soframycin	200,300,400,600,800,1000
4.	Formulation 4+Soframycin	200,300,400,600,800,1000

***HP – Hydrocolloid paste**

***AB – Antibiotic Ointment**

Similarly as mentioned above 1gm of the hydrocolloid paste of four formulations were mixed with T-bact, Neosporin and Betadine ointments.

2.3 ***Method of application of coating paste***

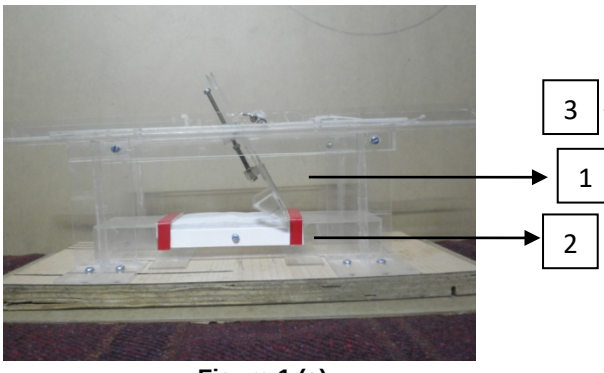

Figure 1 (a)

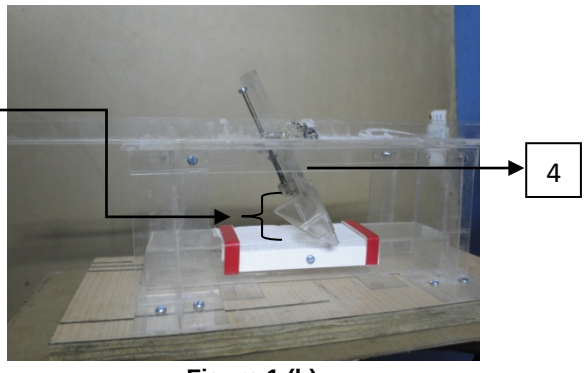

Figure 1 (b)

1) **Applicator** – applies the coating paste onto the fabric under a certain constant pressure (applied by the spring (4)) and is inclined at an angle of 45^0.
2) **Reservoir** – holds the coating paste that is to be applied with a total volume of approx.18 cm^3
3) **Fabric sample** – the fabric sample available for coating of size 5x10cm is firmly clamped.
4) **Spring** – compression spring was used to apply constant pressure.

i. **Procedure for application of coating paste:**

Fabric sample of 7x12cm was taken and clamped at both ends as shown in the figure. The fabric available for coating was 5x10cm (working area). The applicator was placed at one end of the fabric sample and the slit was adjusted at the bottom of the applicator as per the thickness of the paste. The prepared coating paste was filled into the reservoir and the paste was allowed to flow down through the slit. The applicator was made to slide along the track provided at an appropriate pace so as to allow the paste to flow down and get applied uniformly onto the fabric. The spring mounted on the applicator was adjusted so as to apply the desired pressure on the fabric during coating. The applicator was made to slide to the other end of the fabric at a constant rate so as to ensure complete coating of the entire area available (working area). Appropriate sliding rate was maintained to ensure complete transfer of coating paste from reservoir onto the fabric. If necessary, in case of extra paste remaining in the reservoir, the applicator was brought back to the beginning of the sample by lifting and placing it and carry out the same procedure again.

2.4 Bandage roll

This is the outer most layer covering the patch and holding the same in place.

The roll is made up of the following material:

- **First layer** – Polyester / Viscose blended spunlace nonwoven (3 blend ratios)

Table 4: Fabric particulars of the P/V blended fabric

Fabric particulars	Polyester/Viscose fabric		
Blend ratios	30/70	50/50	90/10
Fabric thickness (mm)	0.350	0358	0.348
GSM	30	40	40

- **Second layer** – Poly-urethane breathable membrane (film)
  - Thermoplastic monolithic film impermeable to water and air, permeable to water vapour
  - thickness – 0.102, GSM – 20, 6000mm water column pressure

The above two layers were laminated on the LACOM laminating machine (ATIRA) at temperature of 110^0C.

- **Adhesive** – PUR (poly-urethane reactive) holt-melt adhesive (Jowatherm).

3. Results and discussion

3.1 Introduction

The bandage system that was developed as per the plan of work mentioned in the previous chapter and was subjected to various tests to analyze their physical properties, anti-microbial efficiency and characterization. The results are tabulated and discussed in this chapter.

3.2 Properties of the Patch and Bandage Roll

Table 5 shows the physical properties of the multilayered patch comprising of spunlace polyester fabric as the top and bottom layers and needle punched viscose fabric as the middle absorbent layer joint together using LMP fibers. It can be seen that the thickness of the multilayered patch is 3.25 mm and the GSM is of 167. It can be observed that the air permeability of the multilayered patch is 67.51 $cm^3/cm^2/s$ which is a property required for the permeability of the oxygen and exchange of gases

necessary for the ideal functioning of the wound dressing. It is also observed that the water vapor permeability of the patch is 754.3 g/m^2/day which may be majorly due to the presence of viscose which is hygroscopic in nature and of high moisture regain absorbs the moisture and eventually releases it through the layers of the patch. The optimum release of moisture vapor is necessary for maintaining a suitable environment at the wound site. The absorption properties of the multi layered patch were tested and tabulated in table 3.1. The absorption capacity of the multilayered patch is 1008 % to original weight, retention capacity of 815 % to original weight and drop absorbency of less than one second are the important properties that a wound dressing should possess to absorb blood exudates, perspiration and other undesired fluids intern contribution to keep the wound clean and hygiene as this is necessary for a quick and scar fee healing process. It can be observed from the table that the thermal conductivity of the patch is 0.30 mk/W which is an important factor affecting the physio-psychological comfort of the patient.

Table 5: Properties of the Patch

Particulars	Patch
Fabric thickness (mm)	3.25
Air-permeability (cm^3/cm^2/s)	67.51
GSM	167
WVP (g/m^2/day)	754.3
Drop absorbency (secs)	< 1 sec
Absorption capacity (% on original wt)	1008
Retention capacity (% on original wt)	815
Thermal conductivity (mk/W)	0.30

3.3 Properties of the coated patch

3.3.1 Air and Water vapour permeability of the patch samples

The figures 2 (a) and 2 (b) and table 6 show the air-permeability and water vapour permeability test results of the patch samples coated with a paste containing antibiotics along with a blend of hydrocolloids in comparison to the uncoated patch. It can be observed that the air-permeability and water vapour permeability has considerably reduced after the coating paste has been applied which may be attributed to the formation of a layer on the surface of the patch. The layer formed after coating may cover the pores available for the movement of air, thereby reducing the porosity of the patch. The reduction in water vapour permeability of the coated samples may be due to some amount of water vapour being absorbed by the hydrocolloids present in the paste. Although the patch is coated with a paste, it still possesses the permeability of air and water vapour which is necessary for the patch to function as an optimum wound dressing.

Table 6: Air-permeability and Water vapour permeability of the patch samples

Sl. No.	Patch samples	Absorption capacity (% to original wt.)	Retention capacity (% to original wt.)	Drop absorbency (secs)
1	**Untreated-P1**	1008	815	< 1
2	**Sof-300-F3**	1083	856	2
3	**Tb-300-F3**	1096	893	3
4	**Neo-300-F3**	1126	875	2
5	**Beta-300-F3**	1083	901	2

6	**Sof-1000-F3**	1119	885	3
7	**Tb-1000-F3**	1090	892	2
8	**Neo-1000-F3**	1121	837	2
9	**Beta-1000-F3**	1113	857	2

3.4 Properties of the Bandage roll

Table 8: Properties of bandage roll

Particulars			**P/V fabric Laminated with PU**		
Blend ratio			**30/70**	**50/50**	**90/10**
Fabric thickness (mm)			0.455	0.500	0.510
GSM			73	81	82
Tensile properties	**Breaking load (lb)**		5.29	6.26	8.38
	Tensile Strain (%)		31.00	24.33	19.83
Wicking height	**Machine direction (cm)**	**5mins**	4.2	5.5	6.1
		10mins	5	6.2	6.4
		15mins	5.4	6.8	6.8
		20mins	5.7	7	7.1
	Cross direction (cm)	**5mins**	2.5	2.8	3.5
		10mins	2.7	3.1	4
		15mins	2.8	3.3	4.3
		20mins	2.8	3.4	4.5
MVTR (g/m^2/day)			476	340	238

Table 8 shows the properties of the bandage roll comprising of a spunlace polyester/viscose (P/V) nonwoven fabric laminated with polyurethane (PU) breathable membrane on one side of the fabric. Three different blend ratios of 30/70, 50/50 and 90/10 of polyester/viscose fabrics were considered for the preparation of three bandage rolls respectively. It can be seen that the breaking load of bandage roll increase with increase in polyester percentage in the blend, as polyester has a very good load bearing capacity of 3.5 to 7 gpd. This is an important factor for the bandage roll as its foremost application is to hold the patch in place and to apply the decide amount of pressure contributed to wound healing. It can be observed that the wickability of the bandage roll increases with the increase in polyester percentage which may be attributed to polyester being hydrophobic in nature has very good wicking property as compared to viscose in the blend ratio. Wicking is an essential property for a bandage to absorb and wick away the fluids which are not retained by the patch and thereby help the wound to remain clean.

It can also be observed from the table that the moisture vapour transmission rate values of the three bandage rolls increases with the increase in the viscose content as this may be due to ciscoes being hygroscopic in nature and tends to retain high amount of moisture. The bandage roll with 90/10 composition shows better result in terms of strength and wick ability which are essential properties of a roll, it can also be observed that the lower moisture vapour transmission rate value of 90/10 blend composition compared to the other two blend compositions may be due to the bandage roll retaining lesser amount of moisture.

3.5 SEM characterization – Surface morphology

The scanning electron microscopy (SEM) images of the coated and uncoated fabric surfaces of the top contact layer of the patch (100% polyester spunlace nonwoven fabric) were captured and analyzed.

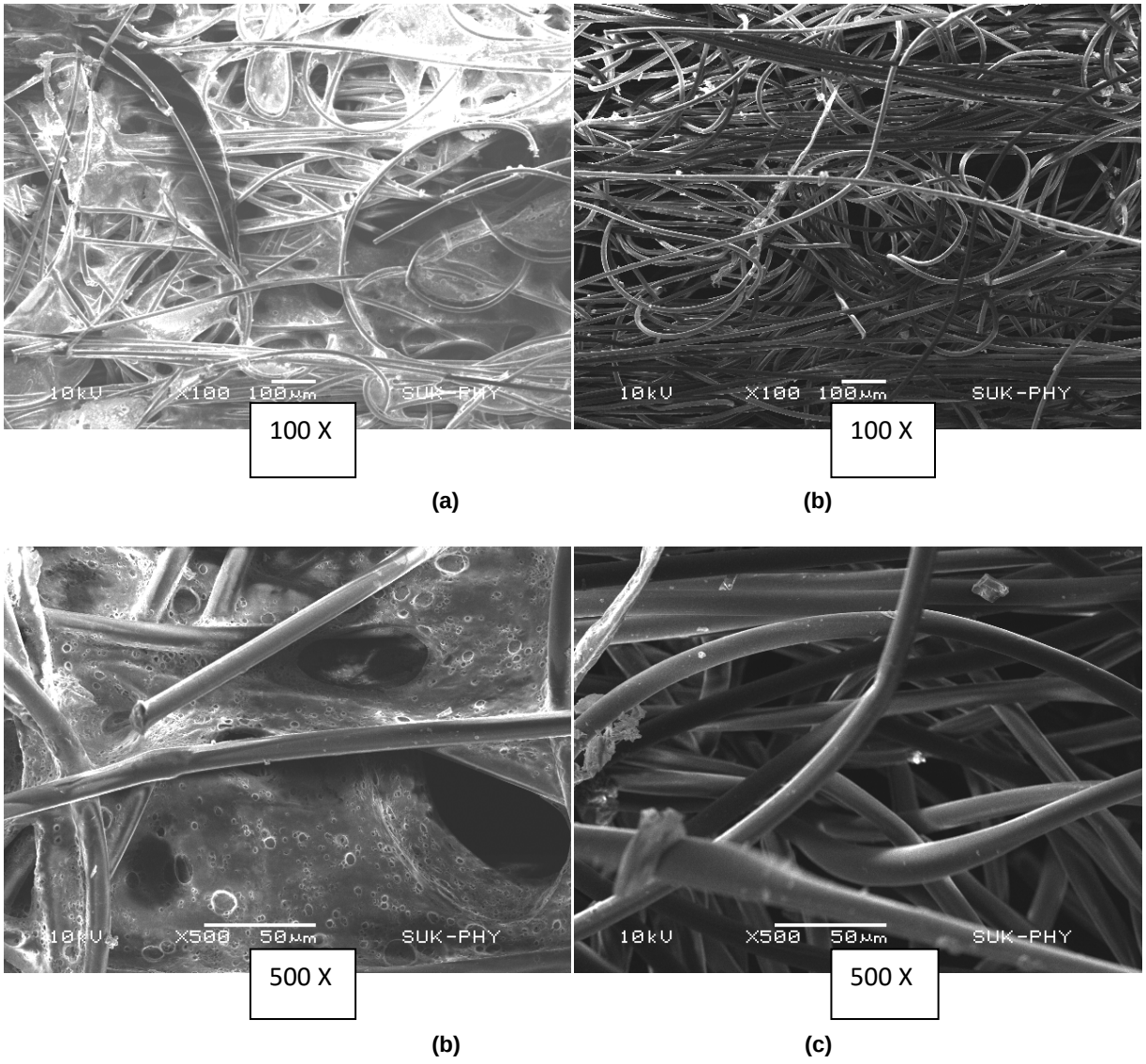

Figure 9. (a), (b), (c), & (d): SEM Images

It can be clearly observed from the SEM images shown above that the coated paste has been applied onto the surface of the fabric surface in comparison to the untreated fabric surface. The images clearly distinguish the coated and uncoated surfaces of the fabric. Coating has majorly been found on the outermost surface of the fabric and has partially penetrated within the structure. Coating is not found to be uniform throughout the material. Impregnation of the coating material is seen within the structure but, due to higher viscosity and better adhesion of the coating paste to the fiber surface there are void spaces between the hydrocolloid coated areas. It also reveals that due to interlacing of fibers and adsorption of coating material onto the surface has created more number of point contacts. A wide distribution of small air sacks or bubbles has been found throughout the coating material, this might be due to the colloidal particles present in the paste and might also due to the high speed stirring or whipping of the paste during preparation of the same.

4. CONCLUSIONS

The developed bandage product was tested and analyzed. From the test results and thorough discussions the following conclusions were drawn: In case of the multilayered coated patch, air permeability (36-39 $cm^3/cm^2/s$), water permeability (640-680 $g/m^2/day$), absorbency (1083-1126%) were observed which are the essential requirements for exchange of gases, optimum supply of oxygen and absorption of exudates, perspiration and other fluids contributing to a desired wound healing process. Bandage roll with 90/10 polyester/viscose blend composition shows good wicking properties as compared to the other blend compositions of 30/70 and 50/50 polyester/viscose which are essential requirements for absorption of fluids which are not retained by the patch and thereby help the wound to remain clean. The 90/10 P/V blend bandage roll shows good result in terms of strength, wickabilty and retaining least amount of moisture required to maintain an optimum and hygienic environment at the site of the wound. Out of the four hydrocolloid formulations prepared, formulation 3 having CMC – 27.5gpl, Gelatin – 22.5gpl, PVA – 49.5gpl, and Mineral Oil - 10gpl and of viscosity 2239 centipoise shows better results in terms of ease of application and anti-microbial activity. Similarly for all the four antibiotics used good antimicrobial activity is observed with for formulation 3. The results obtained were statistically analyzed using two-way ANOVA and it was found that that there exists a significant effect of concentration and viscosity of the coating paste on the anti-microbial efficiency.

References

1. *Patrick S. Murphy and Gregory R. D. Evans, Advances in Wound Healing: A Review of Current Wound Healing Products, Hindawi Publishing Corporation, Plastic Surgery International, , Article ID 190436, 8 pages, Jan 2012*
2. *Joshua S. Boateng et al, Wound Healing Dressings and Drug Delivery Systems: A Review, Journal Of Pharmaceutical Sciences, Vol. 97, No. 8, Wiley Interscience, DOI 10.1002/Jps.21210, August 2008.*
3. *Horrocks A.R. and Anand S.C, "Handbook of technical textiles", Wood Head Publishing Ltd, Vol 12, 2000 P 407-423.*
4. *Thamotharan G, "An analysis of medical textiles", http://www.fibre2fashion.com/industry-article/8/780/an-analysis-of-medical-textiles3.asp*
5. *A B Santamaria et al., Hydrocolloid Dressings in Small and Medium Split-Thickness Skin Graft Donor Sites, Annals of the MBC - vol. 5 - n2 - June 1992.*
6. *Priyadarshini, Nonwovens as medical textiles, Fibre2fashion, Published on Tuesday, October 07, 2008.*
7. *Nabanita Saha et al, Polymeric Biomaterial Based Hydrogels for Biomedical Applications, Journal of Biomaterials and Nanobiotechnology, 2, 85-90, Jan 2011.*
8. *Elbadawy A. Kamoun et al, Poly (vinyl alcohol)-alginate physically crosslinked hydrogel membranes for wound dressing applications: Characterization and bio-evaluation, Arabian Journal of Chemistry, 2013.*
9. *Abhilasha Mishra*, Nisha Chaudhary, Study of Povidone Iodine Loaded Hydrogels as Wound Dressing Material, Trends Biomater. Artif. Organs, Vol 23(3), pp 122-128, 2010.*
10. *B. Goekbora et al, A Hydrogel Wound Dressing with Bi-Layer Crosslinking and Silver/Copper Nanoparticles for the Treatment of Severe Burns, Drexel University of Biomedical Engineering and Health Sciences, Final Progress Report May 14, 2013.*
11. *Bonnie Grambow Campbell, Dressings, Bandages, and Splints for Wound Management, Elsevier, vet clin small anim 36, 759-791, 2006.*

INVESTIGATION OF THE CREEP AND DYNAMIC MECHANICAL PROPERTIES OF JUTE/GREEN EPOXY COMPOSITES INCORPORATED WITH CHEMICALLY TREATED PULVERIZED NANO/MICRO JUTE FIBERS

Abdul Jabbar, Jiří Militký

Department of Material Engineering, Technical University of Liberec, Studentská 2, 461 17 Liberec, Czech Republic
Email: abduljabbarntu@gmail.com

Abstract:

The cellulose based stiff fillers have attained considerable attention in the last few decades for use as a reinforcement in polymer composites. The creep and dynamic mechanical properties of alkali treated jute/green epoxy composites incorporated with 1, 5 and 10 wt % of chemically treated pulverized jute fibers (PJF) are presented in this work. The incorporation of PJF is found to significantly improve the creep resistance and strain rate of composites. Burger's model was used to model the creep behavior in this study. Dynamic mechanical thermal analysis (DMTA) results revealed the increase in storage modulus, glass transition temperature and reduction in the tangent delta peak height of composites with higher loading of PJF.

Key words:

Polymer composites, Creep, Compression molding, Pulverization

1. Introduction

Natural fiber polymer composites (NFPC) are increasingly used nowadays in industrial applications as a substitute of polymer composites made with mostly used synthetic fibers such as glass and carbon etc. due to their environmental and economic benefits. Polymer composites used in engineering applications are often subjected to stress for a long time and at high temperatures. Creep (a progressive deformation of a material at constant stress) is very important end-use property for material applications requiring long term durability and reliability [1]. Considerable studies can be found in literature on the creep behavior of natural fiber polymer composites [2-7]. Researchers have also tried to study the creep behavior of polymer composites by addition of different kinds of fillers in matrices [8-10]. To the author's best knowledge, there is no study available in open literature on the creep behavior of alkali treated jute reinforced green epoxy composites incorporated with chemically treated pulverized jute fibers as reinforcing fillers. Therefore, the objective of the present study is to investigate the incorporation of pulverized nano/micro jute fibers prepared from waste jute on the creep behavior under the conditions of different temperatures and dynamic mechanical behavior of alkali treated woven jute/green epoxy composites.

2. Experimental

2.1. Materials

Jute woven fabric produced from tossa jute (*C. olitorius*) fibers having an areal density of 600 gm^{-2} with 5-end satin weave design was produced on a shuttle loom. Warp and weft densities of the fabric were 6.3 threads per cm and 7.9 threads per cm respectively. Waste jute fibers, sourced from a jute mill, were used for pulverization. Green epoxy resin CHS-Epoxy G520 and hardener TELALIT 0600 were supplied by Spolchemie, Czech Republic. Sodium hydroxide (NaOH) was supplied by Lach-Ner, Czech Republic.

Sodium sulfate (Na_2SO_4) and sodium hypochlorite (NaOCl) were supplied by Sigma-Aldrich, Czech Republic.

2.2. Methods

The untreated fabric was first washed with 2 wt% non-ionic detergent solution at 70 °C for 1.0 h prior to surface treatments. The jute fabric and waste jute fibers were then immersed separately in 2% NaOH solution for 1 h at 80 °C maintaining a liquor ratio of 15:1. Alkali treated waste jute fibers were further treated with 7 g/l NaOCl solution at room temperature for 2 hours under pH 10-11 and subsequently antichlored with 0.1 % Na_2SO_4 at 50°C for 20 min. Both fabric and waste fibers, after chemical pretreatment, were then washed with fresh water several times until the final pH was maintained at 7.0 and then allowed to dry at room temperature for 48 h and at 100°C in an oven for 2 h.

Pulverization of chemically treated waste jute fibers was carried out using a high-energy planetary ball mill of Fritsch pulverisette 7. The sintered corundum container of 80 ml capacity and zirconium balls of 10 mm diameter were chosen for 1 hour of pulverization. The ball to material ratio (BMR) was kept at 10:1 and the speed was kept at 850 rpm.

The composites were prepared by hand layup method and compression moulding technique. The resin and hardener were mixed in a ratio of 100:32 (by weight) according to manufacturer recommendations before layup and then weighed amounts of pulverized jute fibers (PJF) under 1, 5 and 10 wt % were mechanically mixed with epoxy resin at room temperature until a homogeneous mixture was obtained. The prepared composite samples were designated as U (untreated), A-0% (alkali treated jute fabric with 0 wt% of PJF), 1%, 5% and 10% (alkali treated jute fabric with 1, 5, 10 wt% of PJF) respectively.

2.3. Testing

Particle size distribution of pulverized jute particles was studied on Malvern Zetasizer nano series based on dynamic light scattering principle of Brownian motion of particles. Deionized water was used as dispersion medium and it was ultrasonicated for 5 min with BANDELIN ultrasonic probe SONOPLUS before characterization. Refractive index of 1.52 was used to calculate particle size of pulverized jute. In addition, morphologies of pulverized jute fibers were observed with Vega-Tescan TS5130 Scanning Electron Microscope at 30 KV accelerating voltage. The surface of fibers was gold coated prior to SEM inspection.

Short-term creep tests were performed in three point bending mode at temperatures 40°C, 70°C and 100°C using Q800 Dynamic mechanical thermal analysis (DMTA) instrument of TA instruments (New Castle DL, USA) for 30 minutes. The static stress of 2.0 MPa was applied at the center point of long side of the sample through the sample thickness for 30 min after equilibrating at the desired temperature and creep strain was measured as a function of time. The dynamic mechanical properties of composites were measured in 3-point bending mode using the above same instrument. The testing conditions were controlled in the temperature range of 35–200°C, with a heating rate of 3°C/min, fixed frequency of 1 Hz, preload of 0.1 N, amplitude of 20 µm, and force track of 125%. The samples having a thickness of 4.5–5 mm, width of 12 mm and span length of 50 mm were used for both creep and DMTA testing. Two replicate samples were tested for each test condition and average values are reported.

3. Results and discussion

The jute fibers were pulverized to particles with an average size of 1480 nm in wider particle size distribution as shown in Fig. 1a. Fig. 1b shows the shape and surface morphology of pulverized jute fibers. The PJF can be seen in irregular shape and size with certain aspect ratio as well.

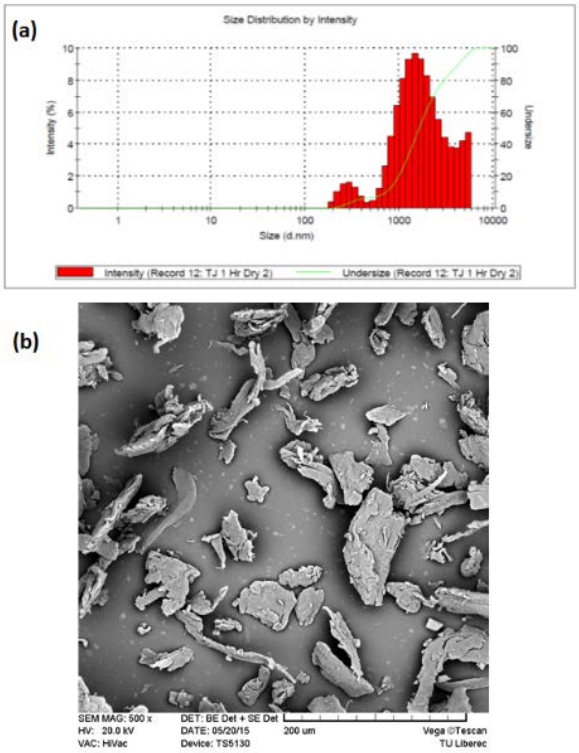

Figure 1. (a) Particle size distribution and (b) SEM image of jute fibers after pulverization

3.1. Creep behavior

Four parameters (or the Burger's) model is one of the mostly used physical models to give the relationship between the morphology of polymer composites and their creep behavior. The total strain as a function of time can be represented by the following equation:

$$\varepsilon(t) = \frac{\sigma_0}{E_M} + \frac{\sigma_0}{E_K}\left(1 - e^{-E_K t/\eta_K}\right) + \frac{\sigma_0}{\eta_M} t \qquad (1)$$

Figure 2 shows the creep strains for jute composites as a function of time with 0, 1, 5, 10 wt% of PJF content at three different temperature conditions. It is visibly apparent that the composites have low instantaneous deformation ε_M and creep strain at 40°C due to higher stiffness of composites but this deformation increases at higher temperatures due to decrease in composites stiffness. The creep strain of all composites also increased at higher temperatures but the untreated jute composites was affected more than the others. The creep strain of alkali treated with 0% PJF composite is less than untreated one. This may be explained due to increase in surface roughness of jute fabric after alkali treatment and decrease in frictional slippage of matrix polymer chains at the fiber/matrix interface resulting in less creep deformation than untreated composite.

The least creep strain is shown by composite incorporated with 10% PJF at all temperatures followed by 5% and 1% PJF incorporated composites. At 100 °C, 5% and 10% PJF composites have almost same instantaneous elastic deformation but 10% composite has less viscous deformation over time. This may be attributed to greater inhibition of slippage and reorientation of polymer chain with increasing contents of PJF. The Burger's model curves show a satisfactory agreement with the experimental data (Fig. 3). The four parameters E_M, E_K, η_M, η_K of Burger's model, used to fit the Eq. 1 to the experimental data, are summarized in Table 1. All four parameters were found to decrease for all composites as temperature increased (Table 1). E_M corresponds to the elasticity of the crystallized zones in a semicrystallized polymer. Compared to the amorphous regions, the crystallized zones are subjected to immediate stress due to their higher stiffness. The instantaneous elastic modulus is recovered immediately once the stress is removed. E_K is also coupled with the stiffness of material. The decrease in parameters E_M, E_K resulted from the increase in the instantaneous and the viscoelastic deformations as temperature increased. The viscosity η_M corresponds to damage in the crystallized zones and irreversible deformation in the amorphous regions and the viscosity η_K is associated with the

viscosity of the amorphous regions in the semicrystallized polymer (Militký and Jabbar, 2015). The decrease in viscosity parameters η_M, η_K propose an improvement in the mobility of molecular chains at higher temperature. The parameters for untreated and alkali treated with 0% PJF composites have undergone a largest decrease, resulting in higher creep strain. The composites incorporated with PJF, especially 5 and 10%, have comparatively better values of parameters particularly η_M which is related to the long term creep strain and validates less temperature dependence of these composites (Fig. 2). The viscosity η_M increases with the increase in PJF% and permanent deformation decreases.

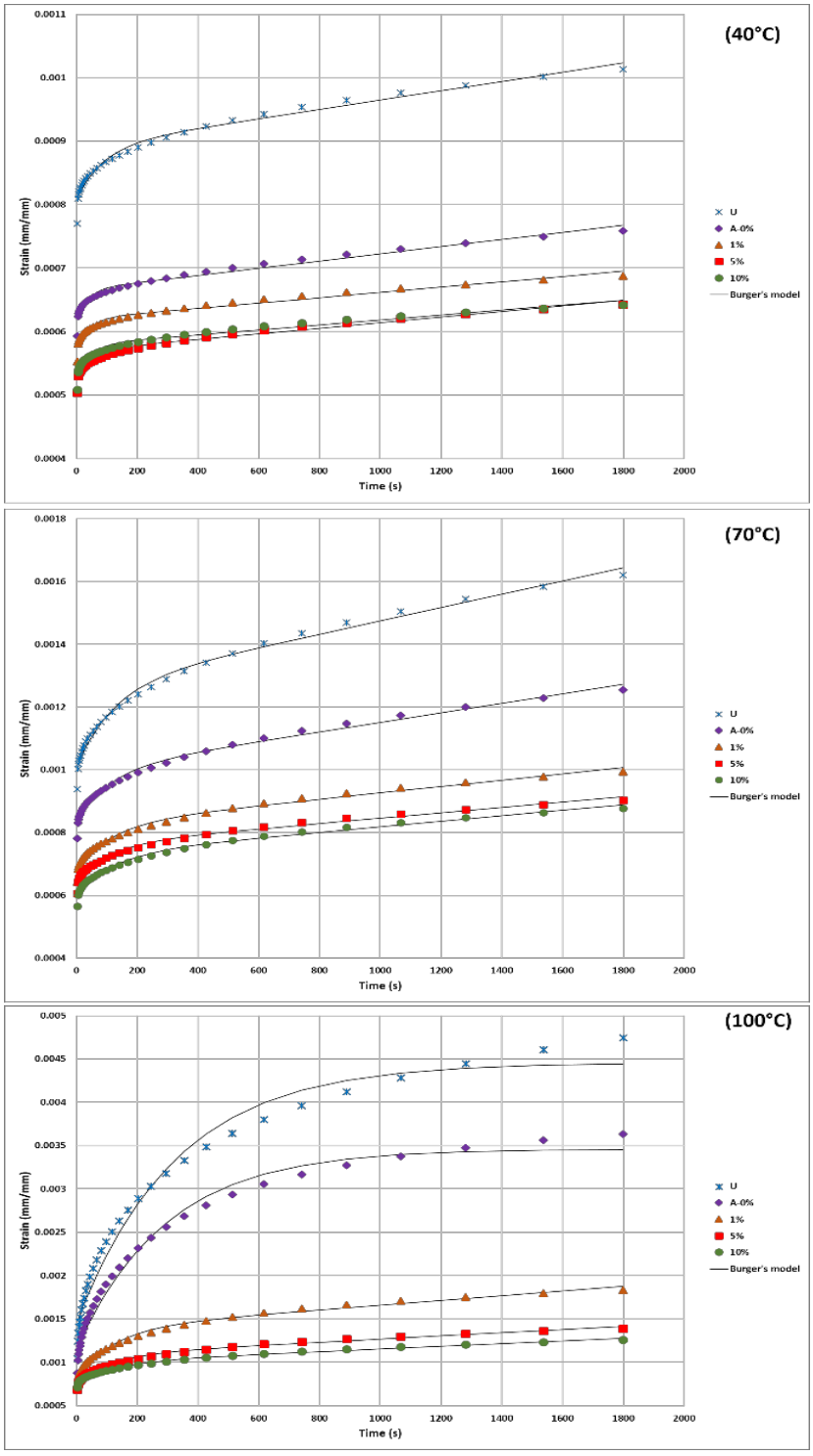

Figure 2. Creep curves of composites incorporated with different loadings of PJF at different temperatures.

Table 1. Simulated four parameters in Burger's model for short term creep of the composites.

Temperature	Parameters	Composite types				
		Untreated	**Alkali-0%**	**1%**	**5%**	**10%**
40°C	E_m (MPa)	2477.24± 78.3	3259.41±138.0	3492.53±133.8	3810.53±133.6	3774.75±149.1
	E_k (MPa)	23876.27±10854.5	38244.62±19726.9	42496.38±21110.6	44220.12±21281.1	40549.80±19016.6
	η_m (Pa.s)	2.72E7±1.33E7	3.54E7±1.22E7	4.77E7±2.04E7	4.54E7±1.97E7	5.11E7±2.47E7
	η_k (Pa.s)	2.11E6±2.38E6	1.37E6±2.09E6	1.73E6±2.5E6	2.53E6±3.49E6	1.90E6±2.62E6
	SS*	2.65033E-9	1.29037E-9	1.04302E-9	9.92292E-10	1.08146E-9
	Adj. R^2	0.97524	0.97061	0.96424	0.96929	0.96304
70°C	E_m (MPa)	1985.89±91.9	2403.61±102.7	2921.19±118.5	3116.67±118.6	3323.10±131.9
	E_k (MPa)	7790.84±2752.5	11972.90±4497.3	14228.47±5360.3	16946.57±6037.4	15615.45±5726.5
	η_m (Pa.s)	9.48E6±3.81E6	1.32E7±5.14E6	1.98E7±9.71E6	2.33E7±1.08E7	2.27E7±1.13E7
	η_k (Pa.s)	956179.43±6.90E5	1.32E6±1.09E6	1.71E6±1.34E6	1.81E6±1.45E6	1.94E6±1.44E6
	SS*	1.08937E-8	5.93037E-9	3.81543E-9	2.74811E-9	2.87718E-9
	Adj. R^2	0.98881	0.98689	0.9851	0.9847	0.98596
100°C	E_m (MPa)	1380.05±294.3	1743.43±306.1	2417.83±218.3	2653.56±183.6	2616.45±123.7
	E_k (MPa)	665.35±117.7	865.63±121.6	3543.54±958.0	6087.72±1783.7	8457.41±2683.5
	η_m (Pa.s)	-4.13E20±0.0	-6.00E32±0.0	7.44E6±3.92E6	1.08E7±5.26E6	1.31E7±5.97E6
	η_k (Pa.s)	219089.75±1.03E5	255733.51±9.91E4	457813.67±2.43E5	705184.01±4.39E5	1.11E6±6.84E5
	SS*	8.30033E-7	3.37586E-7	2.87859E-8	1.31777E-8	6.79893E-9
	Adj. R^2	0.97565	0.98358	0.99023	0.98826	0.98971

3.2. *Dynamic mechanical thermal properties*

Dynamic mechanical thermal analysis can characterize the viscoelastic properties of the materials and determine the information of storage modulus, loss modulus (the energy dissipation associated with the motion of polymer chains) and loss factor (tan delta) of polymer composites within the measured temperature range (Wang et al., 2015). The variation of storage modulus (*E'*) of composites incorporated with different content of PJF as a function of temperature at frequency of 1 Hz is shown in Fig. 3.

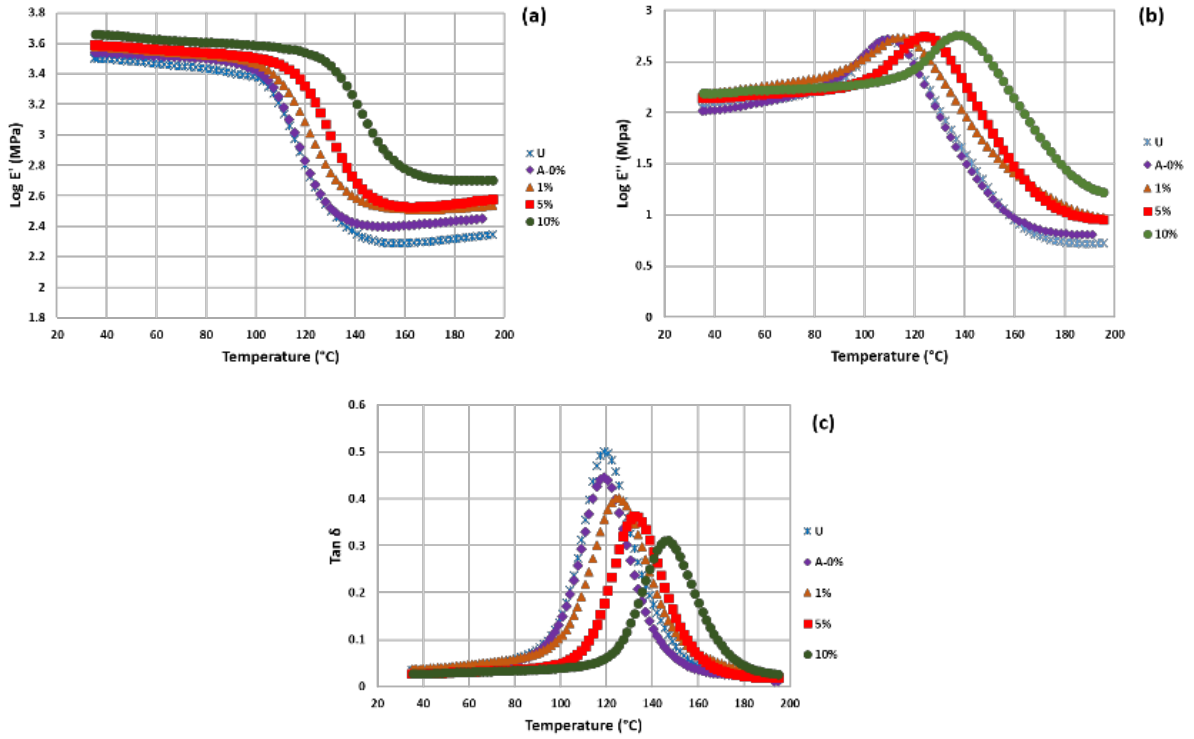

Figure 3. Dynamic mechanical properties composites incorporated with different loadings of PJF; (a) storage modulus, (b) loss modulus, (c) tan delta.

It can be seen from Fig. 3a that there is a gradual fall in the storage moduli with temperature, which should be related with an energy dissipation phenomenon involving cooperative motions of the polymer chains with temperature. The increase in storage modulus over the whole temperature range was observed for composites incorporated with different loadings of PJF, for example, addition of 1, 5 and 10% PJF causes a significant increase of ~18%, 22% and 43% in the storage modulus respectively at 35°C. Moreover, the storage modulus curves of composites have been shifted to higher temperatures after addition of the PJF, particularly 5 and 10% loading. This significant improvement in storage modulus is due to better reinforcing effect of PJF leading to increased stiffness and the mobility restriction of polymer chains. The change in loss factor (tan δ, the ratio of loss modulus to corresponding storage modulus) of composites with different loading of PJF as a function of temperature is shown in Fig. 3c. Untreated composite displayed a higher tanδ peak value than others. This may be attributed to more energy dissipation due to frictional damping at the weaker untreated fiber/matrix interface. The temperature at which tanδ attains a maximum value can be referred to as the glass transition temperature (T_g). A positive shift in T_g can be observed for all composites incorporated with PJF compared to untreated composite The lower tanδ peak height is shown by composite incorporated with 10% PJF followed by 5% and 1% PJF composites, exhibiting a strong fiber/matrix interfacial interactions which can restrict the segmental movement of the polymer chains leading to the increased T_g.

4. CONCLUSIONS

Creep behavior of alkali treated woven jute/green epoxy composites incorporated with different loadings of chemically treated pulverized jute fibers (PJF) was presented at various environment temperatures. The creep deformation was found to increase with temperature. The creep resistance of composites was found to improve significantly with the incorporation of PJF. The modeling of creep data was satisfactorily conducted by using Burger's model. The Burger's model fitted well the short-term creep data. Dynamic mechanical test results revealed the increase in storage modulus, glass transition temperature and reduction in the tangent delta peak height of PJF incorporated composites. Based on the analysis of results, the improved creep resistance of the composites were likely attributed to the inhibited mobility of polymer matrix molecular chains initiated by large interfacial contact area of PJF as well as their interfacial interaction with the polymer matrix.

ACKNOWLEDGEMENTS

This work was supported under the student grant scheme (SGS-21158) by Technical University of Liberec, Czech Republic. One of the authors is thankful to doc. Ing.Antonín Potěšil and Ing. Petr Hornik for providing DMA testing facilities.

References

1. *Krempl, E., Khan, F., (2003). Rate (time)-dependent deformation behavior: an overview of some properties of metals and solid polymers. International Journal of Plasticity, 19, 1069-1095.*
2. *Acha, B.A., Reboredo, M.M., Marcovich, N.E., (2007). Creep and dynamic mechanical behavior of PP–jute composites: Effect of the interfacial adhesion. Composites Part A: Applied Science & Manufacturing 38, 1507-1516.*
3. *Bledzki, A.K., Faruk, O., (2004). Creep and impact properties of wood fibre–polypropylene composites: influence of temperature and moisture content. Composites Science & Technology 64, 693-700.*
4. *Hao, A., Chen, Y., Chen, J.Y., (2014). Creep and recovery behavior of kenaf/polypropylene nonwoven composites. Journal of Applied Polmer Science, 131.*
5. *Jia, Y., Peng, K., Gong, X.-l., Zhang, Z., (2011). Creep and recovery of polypropylene/carbon nanotube composites. International Journal of Plasticity, 27, 1239-1251.*

6. *Marcovich, N.E., Villar, M.A., (2003). Thermal and mechanical characterization of linear low-density polyethylene/wood flour composites. Journal of Applied Polmer Science, 90, 2775-2784.*
7. *Xu, Y., Wu, Q., Lei, Y., Yao, F., (2010). Creep behavior of bagasse fiber reinforced polymer composites. Bioresource Technology, 101, 3280-3286.*
8. *Shen, L., Phang, I.Y., Chen, L., Liu, T., Zeng, K., (2004). Nanoindentation and morphological studies on nylon 66 nanocomposites. I. Effect of clay loading. Polymer, 45, 3341-3349.*
9. *Yang, J.-L., Zhang, Z., Schlarb, A.K., Friedrich, K., (2006a). On the characterization of tensile creep resistance of polyamide 66 nanocomposites. Part I. Experimental results and general discussions. Polymer, 47, 2791-2801.*
10. *Yang, J.-L., Zhang, Z., Schlarb, A.K., Friedrich, K., (2006b). On the characterization of tensile creep resistance of polyamide 66 nanocomposites. Part II: Modeling and prediction of long-term performance. Polymer, 47, 6745-6758.*

USE OF REINFORCING FABRIC FOR PREPARATION OF MORE RESISTANCE ION EXCHANGE MEMBRANE

Eliška Stránská, David Neděla

MemBrain s.r.o., Pod Vinici 87, Straz pod Ralskem, 471 27, Czech Republic,
Eliska.Stranska@membrain.cz, tel. +420 725 358 422

Abstract:

Mechanical characteristics are one of the important properties of ion exchange membranes. These parameters are required for next operation and for an application in an electrodialysis (as tightness of stack).

The most important properties of fabric in this application are thickness (diameter of used fibers), free area related to warp and weft, mechanical strength, material and of course price. Between less relevant parameters of a reinforcing fabric belong a type of fabric (monofilament or multifilament), a type of bond (plain or twill weave, a knit), shrinkage and for example purity.

As a reinforcing fabric in ion exchange membranes can be used a weave fabric, a knit or a nonwoven fabric. Ion exchange membranes have different parameters which are connected with parameters of a reinforcing fabric. The goal of this article is comparison of influence of different reinforcing fabric on the properties of ion exchange membranes. Electrochemical, physical and mechanical properties of ion exchange membranes compared to different reinforcing fabric were studied.

Key words:

Reinforcing fabric, ion exchange membrane, weave fabric, knit, nonwoven fabric.

1. Introduction

Coated fabrics used since the 18th century, when the fabric was soaked in linseed oil for the production of waterproof cloth. Since then coated fabrics started to use extensively for a variety of applications and created composite materials. The most widely used fabric coated on one or both sides of a polymer. Properties of the resulting layers are dependent on many parameters, such as the types of bonding fabric, the fiber density in the fabric sett or orientation. Other important parameters fabrics are:

- good mechanical properties (elongation, modulus, strength),
- fiber type,
- dimensional stability,
- adhesion, absorption of the polymer matrix and textile,
- temperature resistance,
- the homogeneity of the fabric [4, 10].

Due to the parameters of fibers, material or a type of bond on the resulting properties of textiles is covered by many authors [2, 6, 8, 11, 12].

Heterogeneous ion exchange membranes are also layered systems. They contain a polymer matrix having ion exchange function groups which are reinforced with the reinforcing fabric. Ion exchange membranes (IEMs) are separation membranes which separate cations and anions form solution if electric field is applied. Thanks to the fact that the IEM contains fixed ionic functional groups free counter-ions can be transported through IEMs but transport of co-ions is limited [7]. Figure 1 shows

the scheme and simple principle of IEMs. An IEM can be anion exchange membrane (AEM) or cation exchange membrane (CEM) depending on the counter-ion which can be transported through IEM.

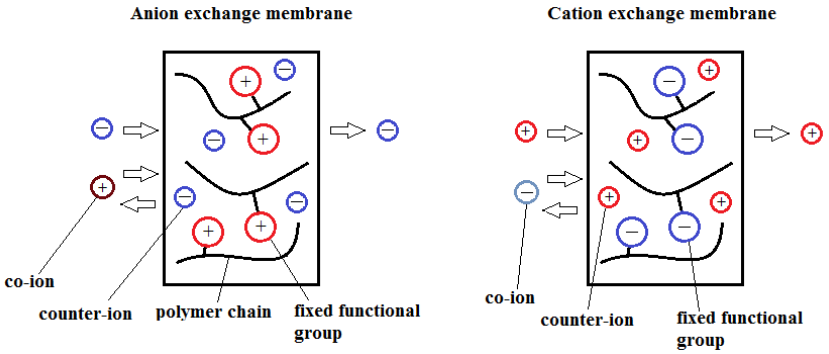

Figure 1. Scheme of IEMs

IEMs are used for electrodialysis (ED), electrodeionization (EDI), membrane electrolysis, electrophoresis (EF) or in power sources as fuel cells [1, 7, 9]. IEMs are the most frequently utilized in desalination of brackish and surface water, purification of waste water, water desalination after tertiary biological treatment, purification of organic substances, stabilization of wine, demineralization of whey, separation of inorganic and organic solutions, purification of organic substances.
The goal of this article is comparison of influence of different reinforcing fabric on the properties of ion exchange membranes. Electrochemical, physical and mechanical properties of ion exchange membranes compared to different reinforcing fabric were studied. For a characterization of IEMs were chosen six type of IEMs with the nonwoven fabric, the monofilament knit, the multifilament knit, the monofilament weave fabric, the multifilament weave fabric and for comparison non-reinforcing IEMs.

2. Experimental

2.1. Materials

IEMs preparation and used materials were described in the literature [13]. Five kinds of reinforcing fabrics were used; Ulester, Uzel, Zora, Wora (Silk & Progress) and Novolin (Polytex). Their properties are described in the Table 1 and Figure 2. Zora and Wora are the knits, Ulester and Uzel are the woven fabrics and Novolin is a nonwoven fabric. The structure of individual reinforcing fabrics is shown in the scans from scanning electron microscope (SEM), Figure 3. Observe and reverse side of knit Wora is presented on the SEM scans.

Table 1. Properties of used reinforcing fabrics

Reinforcing fabric	Material	Thickness µm	Warp/weft[1] 1/cm	Free area %	Shrinkage[2] %	Ultimate force[3] N	Ultimate strain[3] %	Threads
Zora	PES	180	11,5/28,0	59,0	2,5	124/78	31/73	multifilament
Wora	PAD	180	11,5/22,5	74,0	8,0	120/37	27/97	monofilament
Ulester	PES	100	32,0/35,0	66,8	0,1	220/238	28/28	monofilament
Uzel	PES	80	40,0/43,0	28,1	0,9	280/260	35/35	multifilament
Novolin	PP	100 - 110	-	not determined	3,6	15/24	97/80	-

[1]Number of yarns of reinforcing fabric applied to 1 centimetre.
[2]Shrinkage was determined at 160 °C for all fabrics except to Novolin PP than temperature was only 120 °C.
[3]Ultimate strain and force in warp/weft direction (MD/TD).

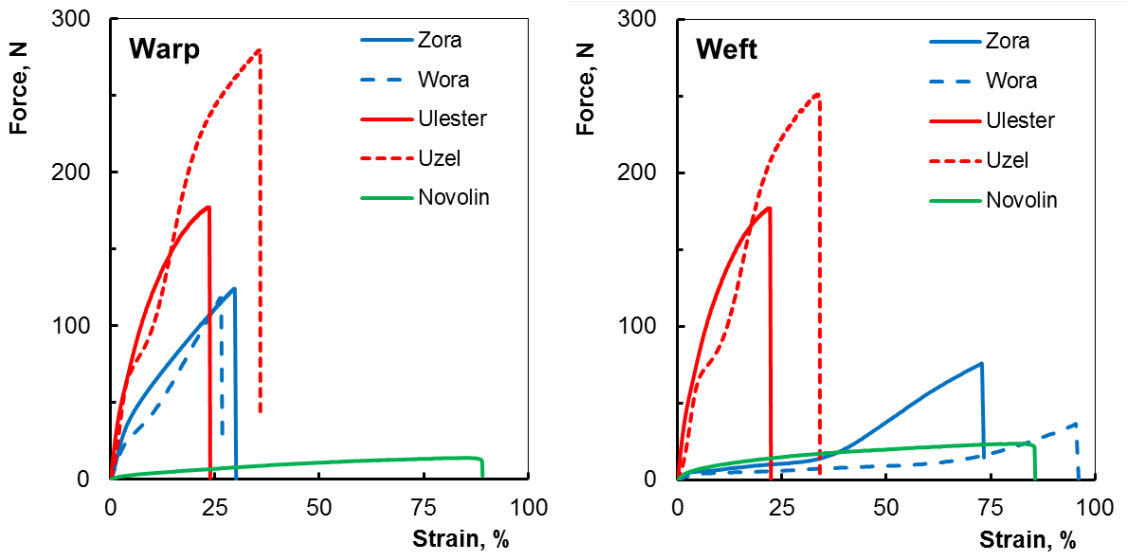

Figure 2. Tensile curves for the reinforcing fabrics (warp and weft direction, MD/TD)

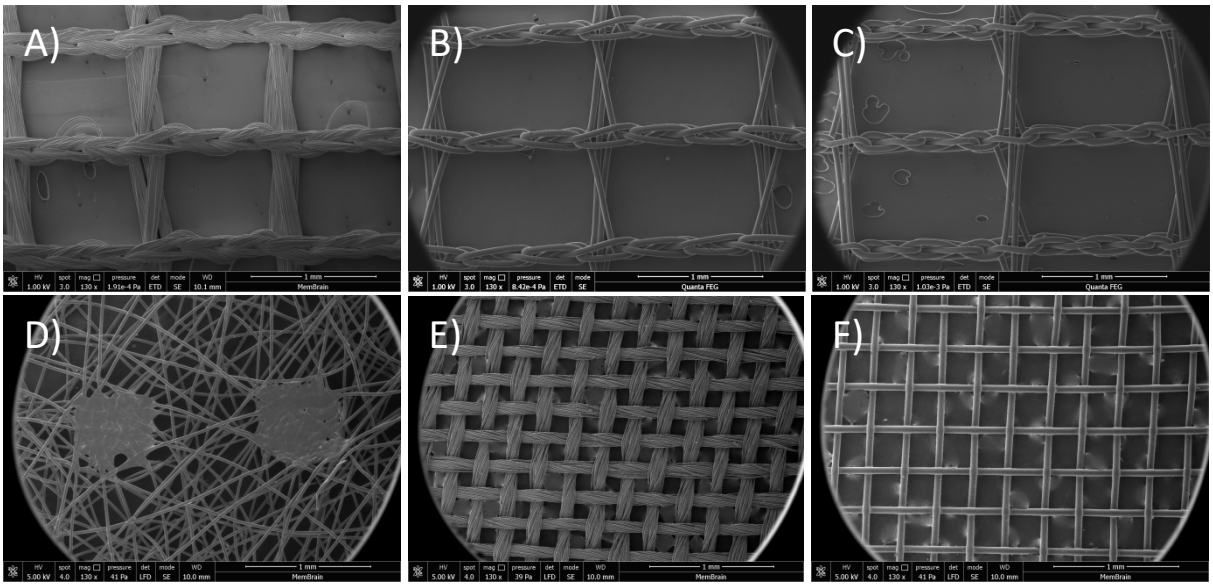

Figure 3. SEM for reinforcing fabric; A) obverse side of Zora, B) obverse and C) reverse side of Wora, D) nonwoven fabric Novolin, E) Uzel and F) Ulester 32S

2.2. Methods

Electrochemical, physical and mechanical properties of ion exchange membranes compared to different reinforcing fabric were studied. Measurements of permselectivity, specific and areal resistivity, relative water content with other physical properties (relative change of thickness, length and width after swelling in demineralized water) are published in the literature [13]. Mechanical properties are described in the [14].

2.2.1. Relative water content and other physical properties

The relative water content and other physical properties such as relative change of thickness, length and width after swelling in demineralized water were determined in the following way. IEMs were dried in an oven at 75°C to constant weight and weighed in the dry form. Length, width and thickness were

determined. Subsequently IEMs were swelled in demineralized water at room temperature for 24 h and dabbed with a filter paper to remove excess water. The weight, length, width and thickness of IEMs in the wet form were measured. Then physical properties were determined using this formula [3]:

$$physical\ properties = \frac{wet\ state - dry\ state}{dry\ state} \cdot 100\ \%$$

2.2.2. Specific resistance

IEMs for measurement of resistance had to be swollen in demineralized water at room temperature. The next operation was the same as in the IEC measurement (membranes' conditioning). IEMs were equilibrated in 0.5 M NaCl for 24 h. Electric resistance was measured in 0.5 M NaCl solution at room temperature in a special experimental cell using a compensation method. The experimental cell consisted from two parts separated from each other. The appropriate solution was mixed in experimental cell. Electric resistance was measured between reference electrodes and then the direct current was applied between platinum electrodes. Electric resistance was determined by two measurements of potential difference. The first measurement was performed without the IEM (only solution) and the second with the IEM between the two parts [1, 5]. The active area of IEM was 0.785 cm^2.

2.2.3. Permselectivity

Permselectivity of IEMs was determined by Henderson's method in the same measuring cell as electric resistance but with the following KCl solution pair 0.1 – 0.5 M in separated part and without applied direct current. IEMs were equilibrated in 0.5 M KCl for 24 h before the measurement [3].

2.2.4. Mechanical properties

Mechanical properties of membrane specimens were measured with samples of dimensions of 25 mm × 50 mm (clamping length) according to the ČSN EN ISO 527-3 standard using an H5K-T (Tinius Olsen) tensile testing machine with a speed of 5 $mm \cdot min^{-1}$. Ultimate force and ultimate strain were determined. Before measurement CEMs are swollen in demineralized water for 24 h.

2.2.5. Morphology

The morphology of the membrane surface was investigated using a FEI Quanta 250 FEG scanning electron microscope. The conditions for measurement on SEM were 5 kV voltage, high vacuum (4.5 x 10-3 Pa pressure) and ETD (Everhart Thornley detector) or in low vacuum (40 Pa) with LFD (large field detector) for secondary electrons. Samples of reinforcing fabrics were sputtered by 10 nm thick layer of chromium before measurement by the Quorum Technologies Q150T S/E/ES. The second microscope was chosen optical microscope Intracomicro.

3. Results and discussion

The thickness, free area of reinforcing fabric and the stability bond are the most important technical parameters which fabric has to fulfill. Minimum thickness of prepared IEM is treble of used reinforcing fabric. So the thinner the reinforcing fabric and the smaller is the resulting IEM. Bigger value of free area ensures the lower resistance of IEM but this must not be at the expense of stability bond. Stability bond is important for manufacture of IEM. During lamination of reinforcing fabric to IEM must not lead to deformation of the fabric, for example narrowing. Other parameters which play the role in manufacture of IEM are mechanical durability, the material of the fabric, diameter and the type of threads, the type of bond, temperature and chemical stability or the purity of the fabric.
Electrochemical and physical properties of CEMs are published in the Table 2. Permselectivity is higher than 90 % that is important for the best function of IEMs. Permselectivity is parameter of CEMs which indicates the number of counter ions transferred across CEMs to co-ions. Counter ions have the

same polarity as the function groups in the IEMs and co-ions have the opposite polarity than the function group. Ideally the permselectivity is equal 100 %. So used reinforcing fabric has the influence, positive impact, on the permselectivity of CEMs. Reinforcing fabric disallows the polymeric materials absorb so much demineralized water and the structure of CEMs is more compact. Any holes and cracks do not create which cause the decrease of permselectivity.
CEM Novolin has the biggest value of specific and areal resistance. Non-reinforcing CEM and CEM Uzel show low values of areal resistance but thickness of these CEMs is relatively small so the specific resistance which is not dependent on the thickness is higher than for other CEMs. The lowest resistance has CEM Ulester. Resistance of CEMs is dependent on many parameters of reinforcing fabric. For example is open area or thickness of fabric. The woven fabric Uzel has the smallest value of open area and in the opposite side is the knit Wora but CEMs with these fabrics do not have significantly different electrochemical properties.

Table 2. Properties of six types of CEMs

IEMs	Thickness of wet CEM μm	Relative change of			Relative water content %	Areal resistance Ω.cm^2	Specific resistance Ω.cm	Permselectivity %
		thickness %	length %	width %				
CEM non-reinforcing	370	27,3	17,5	12,2	72,0	4,24	113,7	90,0
CEM Zora	534	58,4	2,5	4,0	51,3	5,10	95,5	95,0
CEM Wora	468	44,4	5,0	3,0	54,2	4,53	96,8	94,9
CEM Ulester	497	56,9	2,0	2,9	53,5	4,45	89,6	94,4
CEM Uzel	407	56,4	1,0	3,0	49,9	4,81	118,2	93,8
CEM Novolin	438	38,4	11,1	11,6	51,7	8,48	193,6	90,6

The type of reinforcing fabric has the influence on the relative change of thickness, length and width and relative water content. Relative water content for reinforcing CEMs is about 50 – 55 % but non-reinforcing CEM swells by more than 20 %. CEMs with woven fabrics and knits have the bigger relative change of thickness after swelling compared to relative change of length and width. For non-reinforcing CEM and CEM Novolin applies the reverse trend. Stable physical properties of IEMs are very important for used of IEMs in a specific electrodialysis application. Due to the high dimensional changes of IEMs may be reduced tightness of ED unit, be plugged inlets of solution which in turn may cause stop of electrodialysis process.
Tensile curves for CEMs are in the Figure 4. Non-reinforcing CEMs have very low mechanical strength, but it is not problem to protract their structure. This is due to the fact that in the structure any reinforcing fabric is not present which causes increase of mechanical strength and it does not allow so high elongation of polymeric structure.
High value of elongation is not so important for final use of CEMs. Using the nonwoven fabric Novolin is not improved mechanical strength, moreover CEMs Novolin has a lower percentage elongation than non-reinforcing CEMs. The knits have distinctly bigger value of elongation and lower value of strength in the weft direction than in the warp direction that it is due to manufacture of the knit. These trends are same for CEM Zora and CEM Wora. The woven fabrics Ulester and Uzel have the similar value of elongation and ultimate force in both direction and the same trend applies for CEMs. CEM Ulester has the biggest value of ultimate force and the lowest value of elongation. Using woven fabrics or knits improves mechanical strength and durability. These parameters are important for next application of CEMs in electrodialysis process.

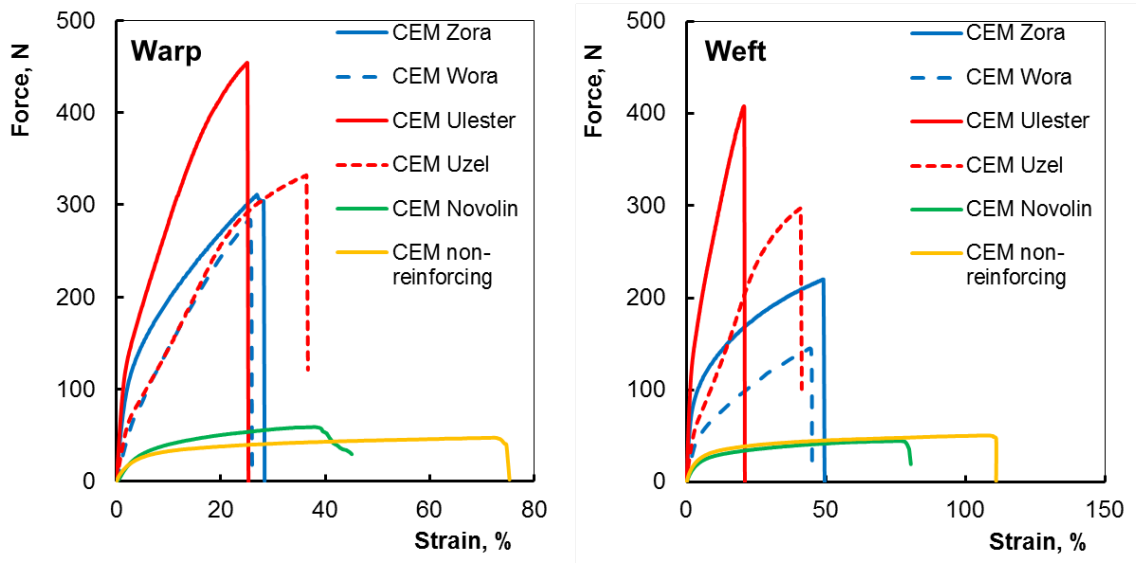

Figure 4. Tensile curves for CEMs (warp and weft direction, MD/TD)

The quality of lamination incorporating the fabric into the polymer binder is so important for application of IEMs in the electrodialysis. The quality of lamination shows Figure 5. Only binding points are evident on the surface of CEM Ulester but other CEMs with Uzel, Zora or Novolin have worse quality of lamination. For CEM Zora and Uzel this is due to the fact that the reinforcing fabrics are composed of multifilament. For CEM Novolin it is caused by heterogeneity of fibers in the structure of non-woven fabrics. Thickness of Novolin is not constant and moving around 100 – 110 μm.

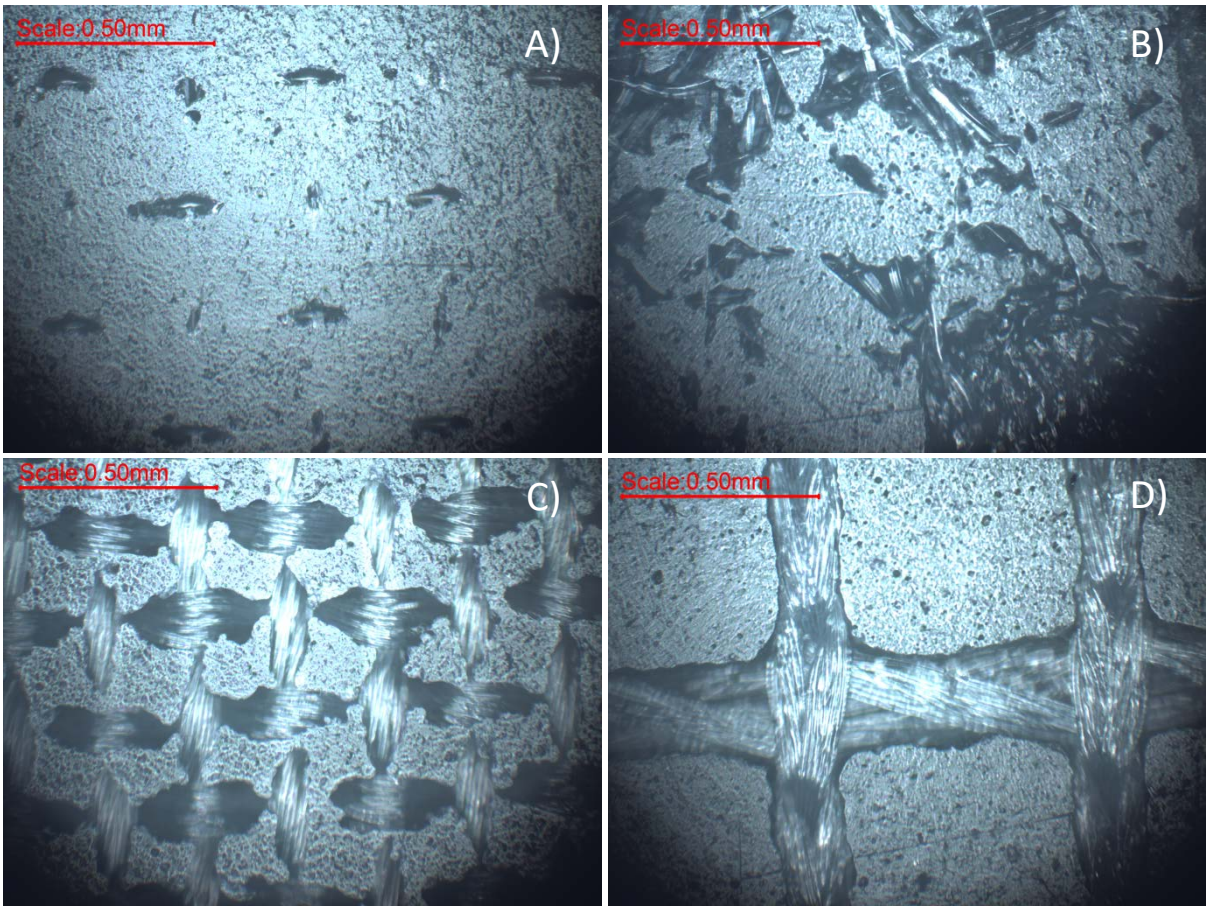

Figure 5. Quality of lamination of CEMs; A) CEM Ulester, B) CEM Novolin, C) CEM Uzel and D) CM Zora

4. CONCLUSIONS

As a reinforcing fabric in CEMs were used two woven fabrics Ulester and Uzel, two knits Zora a Wora and the nonwoven fabric Novolin. CEMs have different parameters which are connected with parameters of the reinforcing fabric. The goal of this article was compared to electrochemical, physical and mechanical properties of CEMs with different reinforcing fabric.

- Non-reinforcing CEMs have lower mechanical strength, but the best elongation. These CEMs have big relative dimension change after swelling in demineralized water. Areal resistance of these CEMs is the best.
- Nonwoven fabric causes decrease of dimension change but mechanical durability of CEMs is still lower.
- CEMs with woven fabrics and knits have good mechanical durability, lower swelling dimension changes. But using the fabric increase the areal resistance which has influence on the flow solution in the electrodialysis stack.
- The cheapest variant of CEMs is CEM with non-woven fabric or do not used any reinforcing fabric because non-woven fabric increases resistance and mechanical strength is still low.
- In terms of quality of lamination and other electrochemical, physical and mechanical parameters is the best CEM Ulester after comparison with other CEMs.

ACKNOWLEDGEMENTS

The work was carried out within the framework of the project No. LO1418 "Progressive development of Membrane Innovation Centre" supported by the program NPU I Ministry of Education Youth and Sports of the Czech Republic, using the infrastructure Membrane Innovation Centre.

References

1. *Agel, E., Bouet, J., Fauvarque, J. F. (2001). Characterization and use of anionic membranes for alkaline fuel cells. J. Power Sources 101, 267-274.*
2. *Bilisik, A. K., Turhan, Y. (2009). Multidirectional Stitched Layered Aramid Woven Fabric Structures and their Experimental Characterization of Ballistic Performance. Text. Res. J., 79 (14), 1331–1343.*
3. Cui, W., Kerres, J., Eigenberger, G. (1998). Development and characterization of ion-exchange polymer blend membranes. Sep. Purif. Technol. 14, 145–154.
4. *Dubrovski, P. D.(Ed.). (2010). Woven Fabric Engineering. (1st ed.). Sciyo (India).*
5. Gohil, G. S., Shahi, V. K., Rangarajan R. (2004). Comparative studies on electrochemical characterization of homogeneous and heterogeneous type of ion-exchange membranes. J. Membr. Sci. 240, 211-219.
6. *Içten, B. M., Karakuzu, R. (2008). Effects of Weaving Density and Curing Pressure on Impact Behavior of Woven Composite Plates. J. Reinf. Plast. Compos., 27 (10), 1083–1092.*
7. *Křivčík, J., et al. (2010). The effect of an organic ion-exchange resin on properties of heterogeneous ion-exchange membranes. Desal. Wat. Treat. 14,179-184.*
8. *Mehta, H. U., Gupta, K. C., Bhatt, V. R., Somashekar, T. H., Modi, C. A., Malatesh, S. (1978). Effect of Construction and Weave on Some Mechanical Properties of Untreated and Resin-Treated Cotton Fabrics. Text. Res. J., 48 (9), 512–517.*
9. *Oren, Y., Freger, V., Linder, C. (2004). Highly conductive ordered heterogeneous ion-exchange membranes. J. Membr. Sci. 239, 17-26.*
10. *Saiman, M. P., Wahab, M. S., Wahit, M. U. (2014). The Effect of Fabric Weave on Tensile Strength of Woven Kenaf Reinforced Unsaturated Polyester Composite. International Colloquium on Textile Engineering, Fashion, Apparel & Design.*

11. *Seyam, A., El-Shiekh, A. (1995). Mechanics of Woven Fabrics: Part V: Impact of Weavability Limit Parameters on Properties of Fabrics from Yarns with Thickness Variation. Text. Res. J., 65 (1), 14–25.*
12. *Shahpurwala, A., Schwartz, P. (1989). Modeling Woven Fabric Tensile Strength Using Statistical Bundle Theory. Text. Res. J., 59 (1), 26–32.*
13. *Stránská, E. (2014). Relationships between transport and physical-mechanical properties of ion exchange membranes. Desalination and Water Treatment. Retreaved Nov 11, 2014.*
14. *Stránská, E., Weinertová, K., Křivčík, J., Neděla, D. (2015).Vlastnosti kationvýměnné membrány v závislosti na počtu vláken dostavy armující textilie. CHISA (Seč).*

NATURAL FIBRE COMPOSITES FOR PROTECTION AGAINST ENVIRONMENTAL ELEMENTS

Khubab Shaker, Yasir Nawab, Munir Ashraf, Madeha Jabbar, Muhammad Umair

Textile Composite Materials Research Group, Faculty of Engineering and Technology, National Textile University, Faisalabad, Pakistan

Abstract

The current study aims to fabricate the composite parts that provide protection against environmental elements like moisture and microorganisms. The ZnO nanoparticles were immobilized in the composite material to impart bio-functionality, while moisture absorption was lowered by caustic treatment of the reinforcement. The ZnO nanoparticles were synthesized by sol-gel method and added in different fractions to unsaturated polyester resin before impregnation of reinforcement. The composites were fabricated by vacuum bag molding technique. All the composites had different concentration of nanoparticles. Similarly, the reinforcement was treated with different concentrations of caustic soda.
The protection of these composites for bacterial attack against both gram positive (S. Aureus) and gram negative (E. Coli) bacteria was tested according to AATCC 147. The composites without ZnO nanoparticles did not restrict the growth of bacteria, while the lowest amount of ZnO nanoparticles (0.02% by weight) imparted antimicrobial activity to the composites. Moisture regain of treated reinforcement and the subsequent composite materials was investigated. The caustic treatment of natural fibers resulted in a decreased value of moisture absorption. The developed composites will absorb less moisture, restricting the growth of bacteria and lowering the risks of fiber degradation. Such composite materials will have enhanced service life.

Key words

Nanoparticles, Sol-gel method, Mercerization, Moisture, Antibacterial activity

1. Introduction

The natural fibre reinforced composites (NFRC) are widely researched now a dsys owing to increased environmental concerns and decreasing non-renewable resources [1]. The NFRC were originally develoepd as a replacement of glass fibre reinforced composites, and now offer massive opportunities in furniture industry as replacement of wood. The flax fibre reinforced composites have automobile and structural applications as door and instrument panels, package trays, glove boxes, arm rests, seat backs, etc. Shah et al. [2] manufactured and compared the mechanical properties of a small wind turbine blade built from flax/polyester and E-glass/polyester. The lower density of flax fibre helped in weight reduction of the blade (10% lighter), satisfying the design and structural integrity requirements for turbine.

With advancements and to meet diverse customer needs, the focus is to fabricate materials having functional properties like electrical, magnetic, optical, antimicrobial, etc. These properties can be achieved by adding nano-fillers (at least one dimension in the nanometer range, i.e. 1–100 nm) to the composite material [3]. The nano-fillers are incorporated in very small amounts (less than 10 wt.%) into the polymer matrix to get functional property [4]. Nanoparticles have reduced size associated with high surface area/volume ratio, which increases as the size of nanoparticles decreases. With decrease in particle size, a large number of constituting atoms can be found on the surface of the particle, which make the particle highly reactive [5]. The selection of nanoparticles depends on the desired thermal, mechanical, antibacterial, electrical properties required in composite [6]. The addition of nano-sized

fillers into the polymer matrices will result into a composite material exhibiting distinct properties, depending on the nano-filler added.

The main factors limiting the bulk scale manufacturing of natural fibre composites are the low strength and water absorption of natural fibres from environment [7].The absorption of water causes swelling of natural fibres and enhances its susceptibility to microorganisms attack which leads to deterioration of mechanical properties. The composites degrades faster, losing half of its tensile strength in the time it takes for a glass composite to lose only 10 % [8]. A lot of research has been made on the treatment of natural fibres to increase hydrophobicity of fibres and improve the fibre matrix interface, enhancing mechanical properties of the composite. Natural fibres are not immune to microorganisms, like synthetic fibres, and provide excellent environment for microorganisms to grow owing to their ability to retain moisture. These microorganisms pose a significant danger not only to human health by means of contact transmission but also deteriorate the mechanical properties of composites by degradation of fibres.

The aim of current study was to fabricate the composite parts that provide protection against environmental elements like moisture and microorganisms. The ZnO nanoparticles were immobilized in the composite material to impart bio-functionality, while moisture absorption was lowered by caustic treatment of the reinforcement. The ZnO nanoparticles were synthesized by sol-gel method and added in different fractions to unsaturated polyester resin before impregnation of reinforcement. The composites were fabricated by vacuum bag molding technique. All the composites had different concentration of nanoparticles. Similarly, the reinforcement was treated with different concentrations of caustic soda.

2. Experimental

2.1. Materials

The materials used in this study include flax woven fabric (areal density 150 g/m^2), ZnO nanoparticles, NaOH and unsaturated polyester resin.

2.2. Methods

The study was completed in two steps. First step was to get protection against microorganisms, while second step deals with the mositure protection of the flax fiber composite materials. The list of experiments is given in Table 1. The mercerization of reinforcement was obtained by treating it with three different concentrations of caustic soda (i.e. 5%, 10% and 15%). The treated and untreated reinforcement was used for composite fabrication.

The composites plates were fabricated using the vacuum bag moulding technique. The resin (unsaturated polyester) was mixed with the ZnO nanoparticles solution in methanol (different concentrations for different samples) during composite fabrication, stirring continuously at a low rate to evaporate the methanol from the solution. Eight layers of woven flax plies having a stacking sequence of [(0/90)2]S were used to form the laminated composite, with fibre volume fraction of 40%.The curing was done at room temperature for 12 hours, followed by post curing at 120°C for 3 hours.

Table 1. List of samples produced for the study

Sample ID	Reinforcement	Amount of Zno NP (%)
S1	Untreated	0.0
S2	Untreated	0.02
S3	Untreated	0.04
S4	Untreated	0.08
S5	5% NaOH treated	0.0
S6	10% NaOH treated	0.0
S7	15% NaOH treated	0.0
S8	X% NaOH treated	Y%

Where, X and Y represnet the %age of NaOH and ZnO NP, giving optimum results.

3. Results and discussion

The tensile properties of these composite materials were tested using ASTM D3039 to ensure that the addition of nanoparticles have not deteriorated the mechanical properties of the composite. The bioactivity of the developed composites was tested by the zone of inhibition test(AATCC 147)[9]. The zone of inhibition is a clear area of interrupted growth underneath and along sides of the test material; and it indicates the bioactivity of specimen. It is a qualitative test for the bacteriostatic activity by the diffusion of antibacterial agent through agar.

3.1. Mechanical Properties

The tensile properties of composites was investigated, with three repetitions for each sample. The results are shown in Figure 1. It can be noted that the addition of ZnO nanoparticles has no significant effect on the tensile strength of woven flax fabric composites due to very small amount of nanoparticles present in the composite. Contrary to that, the tensile modulus of composite samples is increasing consistently with the increase in the content of the ZnO nanoparticles. This may be attributed to the formation of nanocomposite comprising of ZnO particles and matrix in the resin rich areas resulting into improvement in mechanical properties[10].

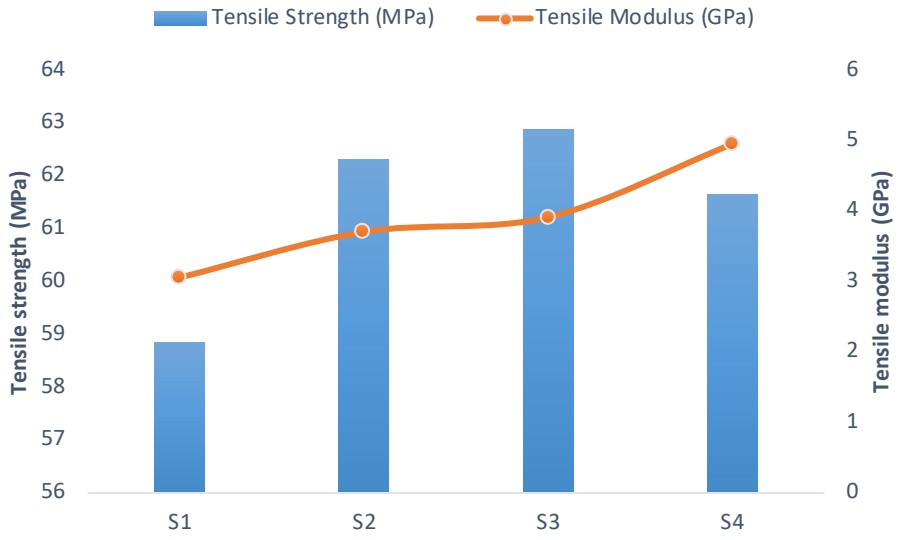

Figure 1. Mechanical properties of composite materials

3.2. Protection against microorganism

The composite protection against microorganisms was investigated in terms of antibacterial activity. The zones of inhibition around composite samples was observed and the results are shown in Figure 2 after 24 hours of incubation in dark at 37 °C. The unique properties of nanoparticles arise from a variety of attributes, including the similar size of nanoparticles and bio-molecules such as proteins and poly-nucleic acids [11]. In this study, the antibacterial activity of ZnO nanoparticles is better explained in terms of chemical mechanism. According to this mechanism, the ZnO NP generate reactive oxygen species like •OH, H_2O_2 and O_2^{-2}. The bacteria carry negative surface charge, therefore, the penetration of O_2^{-2} seems impossible but hydroxyl radical and hydrogen peroxide can penetrate into the cell membrane which leads to the death of bacteria. Another reason for bacterial growth inhibition can be the release of Zn++ ions in the bacterial culture. As the bacteria have negative charge on their surface, the Zn++ ions adhere on them and modify the membrane structure. With the increase in nanoparticles

concentration, the generation of ROS and/or Zn++ also increase which leads to production of bigger zones of inhibition and they continue to grow bigger.

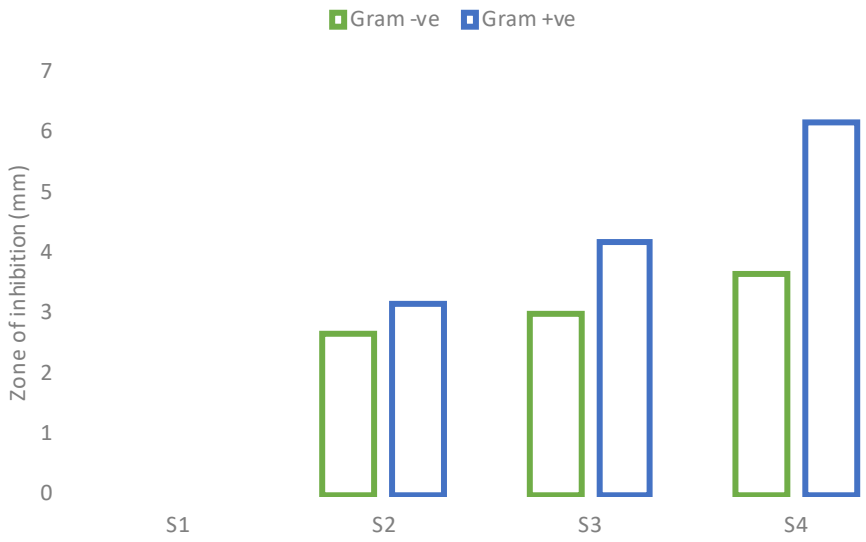

Figure 2. Antibacterial properties of composite materials

3.3. Protection against moisture

The moisture regain of reinforcement (untreated and mercerised) was carried out according to standard test method ASTM D2495. While, the moisture regain tests were carried out on composites according to ASTM D5229. This part of study is currently in progress. It is expected that the mercerization of reinforcement will result in moisture reduction of both reinforcement and subsequent composite.

4. CONCLUSIONS

The current study was aimed to develop the composite parts that provide protection against environmental elements like moisture and microorganisms. It was achieved by embedding ZnO nanoparticles in the composite material to impart bio-functionality, while moisture absorption was lowered by caustic treatment of the reinforcement. It was observed that these composites have antibacterial activity against both gram positive and gram negative bacteria. The lowest amount of ZnO NP (0.02%) gives desired results, while increased amount of NP increases the zone of inhibition of composites. The bioactivity is advantageous for the protection of natural fibre reinforcement against bacterial attack. Therefore, the developed composites have better protection against environmental elements and are expected to have an enhanced service life.

References

1. *S. Chabba, "Composites get greener," Mater. Today, no. April, pp. 22–29, 2003.*
2. *D. U. Shah, P. J. Schubel, and M. J. Clifford, "Can flax replace E-glass in structural composites? A small wind turbine blade case study," Compos. Part B Eng., vol. 52, pp. 172–181, Sep. 2013.*
3. *F. Xie, E. Pollet, P. J. Halley, and L. Avérous, "Starch-based nano-biocomposites," Prog. Polym. Sci., vol. 38, no. 10–11, pp. 1590–1628, Oct. 2013.*
4. *P. Bordes, E. Pollet, and L. Averous, "Nano-biocomposites: biodegradable polyester/nanoclay systems," Prog. Polym. Sci., vol. 34, no. 2, pp. 125–155, Feb. 2009.*
5. *A. Umar and Y. B. Hahn, Eds., Metal Oxide Nanostructures and Their Applications, vol. 5. New York: American Scientific Publishers, 2010.*
6. *L. Wang, Y. Ding, Y. Shen, Z. Cai, H. Zhang, and L. Xu, "Study on properties of modified nano-TiO2 and its application on antibacterial finishing of textiles," J. Ind. Text., vol. 44, pp. 351–372, 2013.*

7. *M. P. Westman, S. G. Laddha, L. S. Fifield, T. A. Kafentzis, and K. L. Simmons, "Natural fiber composites: a review," Washington, 2010.*
8. *Z. Dominkovics, L. Dányádi, and B. Pukánszky, "Surface modification of wood flour and its effect on the properties of PP/wood composites," Compos. Part A Appl. Sci. Manuf., vol. 38, no. 8, pp. 1893–1901, Aug. 2007.*
9. *"AATCC Test Method 147-2011 Antibacterial Activity Assessment of Textile Materials: Parallel Streak Method," in AATCC Technical Manual, American Association of Textile Chemists and Colorists.*
10. *S. Y. Fu, X. Q. Feng, B. Lauke, and Y. W. Mai, "Effects of particle size, particle/matrix interface adhesion and particle loading on mechanical properties of particulate-polymer composites," Compos. Part B Eng., vol. 39, no. 6, pp. 933–961, 2008.*
11. *M. Zheng, F. Davidson, and X. Huang, "Ethylene glycol monolayer protected nanoparticles for eliminating nonspecific binding with biological molecules.," J. Am. Chem. Soc., vol. 125, no. 26, pp. 7790–1, Jul. 2003.*

GEOPOLYMER/FLY ASH CONCRETE COMPOSITE MATERIALS

Promoda Behera, Daniel Karthik, Salman Naeem, Vijay Baheti, Jiri Militky

Faculty of Textile Engineering, Dept. of Material Engineering, Studentská 2, Technical University of Liberec 461 17 Czech Republic
Corresponding author: promodabehera@gmail.com

1. Introduction

Portland cement is the most widely used construction materials for decades due to its excellent thermal performance, mechanical properties and durability [1-3]. The production of cement is increasing about 3 % annually. However, the cement industry is the second largest producer of the greenhouse gas. Among the greenhouse gases, CO_2 contributes about 65% of global warming. The cement production and resulting emissions are expected to increase by 100 % from the current level by 2020. Beside the emission of CO_2, cement industry launches SO_3 and NO_x which can cause the greenhouse effect and acid rain [4-7]. This is particularly serious in the current context of climate change caused by CO_2 emissions worldwide, causing a rise in sea level and the occurrence of natural disasters and being responsible for future meltdown in the world economy. As a result, there is a growing debate in environmental circle on the tremendous energy consumption and emission of carbon dioxide during cement production. With the mounting pressure to reduce energy consumption and pollution in all industrial processes in global manufacturing, the pursuit of alternative cement material with less energy consumption and pollution has become an important objective of many recent research studies.

Geopolymers are new class of synthetic alumino-silicate materials formed due to reaction between alumino-silicates and oxides with alkaline media [8]. Due to easy, energy efficient, ecofriendly processing and excellent mechanical properties, geopolymers are fast emerging materials of choice for a range of construction and building materials, fire resistance ceramics, composites, matrix for immobilization of toxic wastes, precursor for monolithic and many others. A large number of naturally occurring and industrially produced aluminosilicate solids are used for geopolymer synthesis. The three most widely used materials for geopolymer as supplementary cementitious materials are calcined clay, blast furnace slag and fly ash [9]. Recently there has been a growing trend to use fly ash in geopolymers due to their easy availability, good workability during processing and improved durability in final product.

Fly ash is the residue of power plants generated during combustion of coal [10]. Fly ash is comprised of fine spherical particles, mostly amorphous, in addition to unburnt carbon, crystalline mullite, quartz and hematite [11, 12]. The generated quantity of the fly ash is between 10 % and 30 % of the original volume of burned coal. However, the utilization rate of the fly ash is rather low, approximately 15% of the generated amount. Fly ash consist mostly of SiO_2, Al_2O_3 and Fe_2O_3 [10]. On the basis of silica, alumina and iron oxide content, ASTM C-618 categorizes coal combustion fly ash into two classes: Class F (low lime) and Class C (high lime) (ASTM C618). The burning of harder, older anthracite and bituminous coal typically produces Class F fly-ash, which generally contains less than 10% CaO [13-15]. Fly-ash produced from the burning of younger lignite or sub-bituminus coal is of Class C, which typically contains CaO in excess of 10 % up to 40 % [13-15]. Alkali and sulfate (SO_4) contents are generally higher in Class C than Class F fly-ash. Class C fly ashes participate in both cementitious and pozzolanic reactions, whereas Class F fly ashes predominately participate in pozzolanic reaction during the hydration process [14, 15]. Therefore, Class C fly ashes are classified as cementitious and pozzolanic admixtures/additives and Class F fly ashes as normal pozzolans for use in concrete. It was

found that the Class C fly ash has a greater delay in setting time than Class F fly ash, due to its higher sulphate contents.

The major chemical components of fly ash are SiO_2, Al_2O_3, and Fe_2O_3, which can react with $Ca(OH)_2$ to form calcium silicate hydrate (CSH) and calcium aluminate hydrate (CAH) and improve many properties of concrete and mortar such as increase ultimate compressive strength, increase sulfate resistance, and reduce water permeability [16-18]. The use of fly ash as a cement replacement in concrete results in significant enhancement of the basic characteristics of concrete both in its fresh and hardened states. Use of fly ash as a fine aggregate improved the mechanical properties and a reduction in water absorption, with good compatibility between sand and ash [19, 20]. Fly ash improves the workability of fresh mortar and the resulting concrete shows excellent surface finish. The small size of spherical fly ash particles also contributes to a better packing of the aggregate materials, which reduces porosity and hinders the penetration of aggressive agents, thus considerably improving the chemical resistance of concrete [21-23]. Also, recently, researchers have shown that alkali activated-thermal cured fly ash based concrete could be produced with a compressive strength of about 60 MPa. The advantages of fly ash based concrete are:

- Improved long-term strength and performance and durability
- Reduced heat of hydration
- Reduced water required for equal workability
- Minimised risk of alkali silica reaction

The limiting factor which has hindered the development of fly ash based geopolymers is its low reactivity [24-25]. The reactivity of fly ash largely depends on its amorphous content which undergoes faster dissolution in alkali solution, whereas the crystalline fraction takes a longer time [26-30]. Most of the research effort on improving the reactivity is directed towards addition of calcium bearing substance such as $Ca(OH)_2$, limestone and blast furnace slag [30-36]. However the modification of precursor chemistry often leads to additional reaction paths which are not desirable. The aim of the present research was to improve the reactivity of fly ash via mechanical activation in ball milling and to elucidate the effects on the mechanical properties of ambient temperature cured geopolymer samples synthesized from calcined kaolin and shale clay residues with Si/Al ratio of 2.0. The size and surface of fly ash are important factors to decide the interfacial properties. The size of filler is important factor to govern the size of interface, whereas surface of filler decides the strength of interface. The surface of fly ash is usually modified based on silane or non-silane (i.e. stearic acid, titanate, etc) coupling agents. Mechanical activation through ball milling offers the possibility to alter the reactivity of solids through physicochemical changes in bulk and surface but without altering the overall chemistry of the material. Ball milling results into the modification of the fly ash by transforming the micro sized fly ash into nanostructured fly ash. The smooth, glassy and inert surface of the fly ash altered to a rough and more reactive surface after ball milling.

2. Materials and methods

The fly ash used in the study was collected from source in Plzeň, Czech Republic. Mechanical activation of fly ash was carried out using a high-energy planetary ball mill of Fritsch Pulverisette 7 in a sintered corundum container of 80 ml capacity using zirconia balls of 3 mm Ø under wet condition in distilled water for 1, 2, 3, 4, and 5 hours. The ball mill was loaded with ball to powder weight ratio of 10:1. The rotation speed of the planet carrier was 850 rpm. In this mechanical treatment, powder particles are subjected to a severe plastic deformation due to the repetitive compressive loads arising from the impacts between the balls and the powder. The milled sample powder was taken out at a regular interval of every 1 hour of milling to test for particle size distribution on Malvern Zetasizer Nano based on dynamic light scattering principle. The dispersion medium was deionised water. The dispersion was ultrasonicated for 5 min with Bandelin ultrasonic probe before characterisation.

Refractive index of 1.55 used for fly ash to calculate particle size. Later the size and dimensions of fresh as well as ball milled fly ash were examined by means of Scanning Electron Microscope TS5130-Tescan SEM at 30 kV accelerated voltage.

Geopolymer binders were prepared by mixing of alkali activator containing Na_2SiO_3/K_2SiO_3 and NaOH/KOH with ratio 1.50:1.95. At first, the geopolymer resin was prepared by mixing the alkaline activator with the raw materials. The liquid and solid components were mixed about 10 minutes at room temperature until the solution homogenized. Next, the geopolymer resin mixture was mixed with fly ash in two ways. On one way wet milled dispersion of fly ash in water was directly mixed with geopolymer resin without evaporating the excess water in dispersion. While on other way the excess water from wet milled dispersion of fly ash was evaporated first and then the dried nano particles of fly ash were mixed with geopolymer resin. The mixing was done in an air conditioned room at approximately 20 ^oC until the well homogenized mixture (about 5 minutes). Directly after mixing, the fresh mortar was poured in the moulds and vibrated for 2 minutes on the vibration table to remove air voids. These samples were cured at room temperature for 3 days after casting. Next, the samples were removed from the moulds and left in laboratory ambient conditions till 7, 14, and 28 days. Figure 1 shows the detail procedure of geopolymer preparation. Compressive strength testing of mortar was performed as per AS 1012.9 using (Ø50 x 100) mm diameter cylindrical moulds. The uncertainty in the measurement was taken as the standard deviation of the compressive strength of three samples. Data that deviated more than 10 % were eliminated.

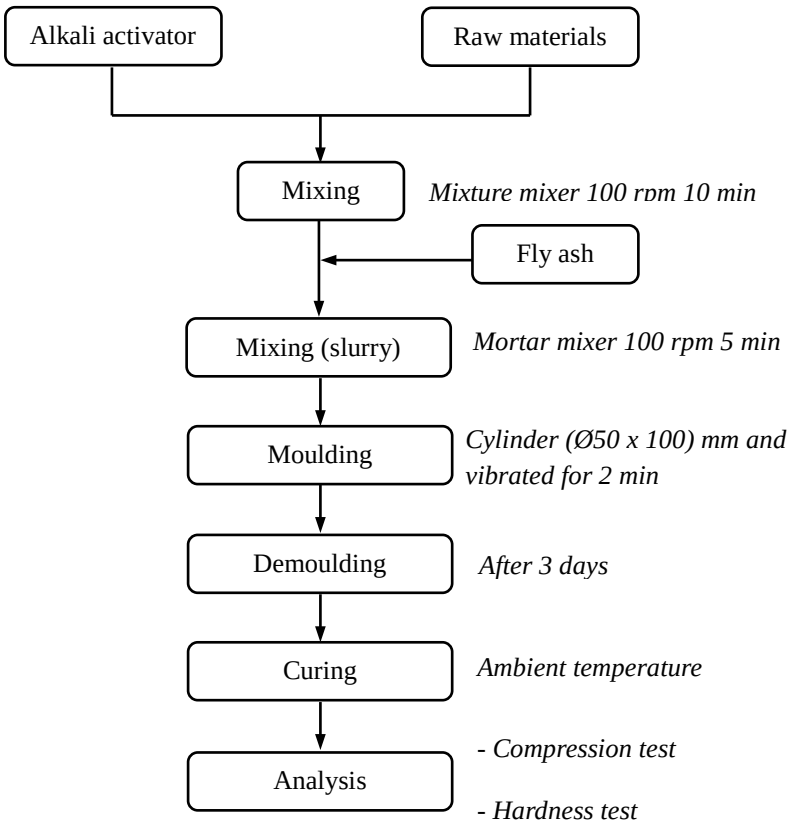

Figure 1. Geopolymer preparation Procedure

3. RESULTS AND DISCUSSIONS

3.1 Morphology and elemental analysis of original fly ash

Fly ash particles are generally spherical in shape and range in size from 1 µm to 10 µm as shown in the Figure 2. The chemical analysis of the fly ash determined by EDX analysis is also given in Table 1 and Figure 3.

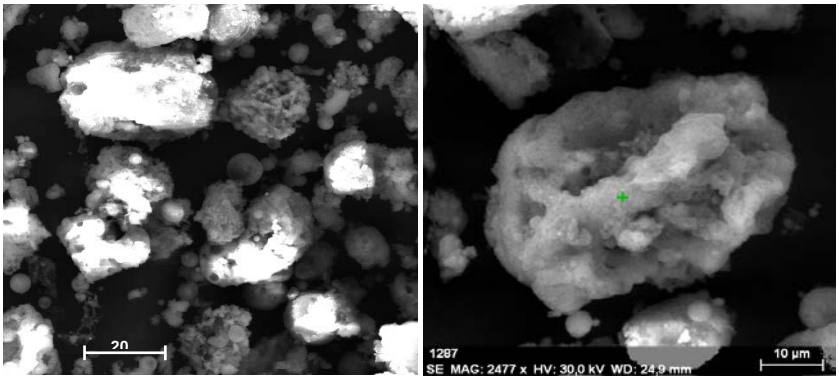

(a) (b)

Figure 2. SEM images of fly ash particles

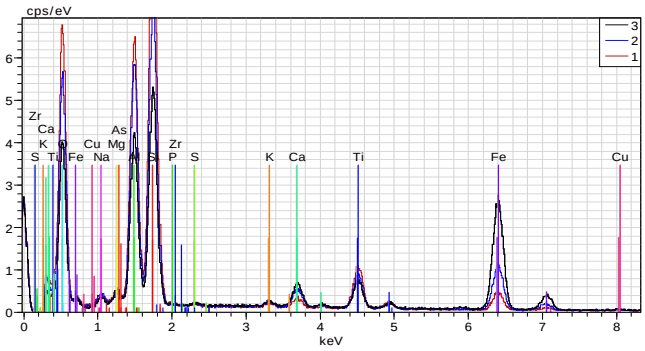

Figure 3: Quantitative elemental analysis of unmilled fly ash

Table 1. Quantitative elemental analysis data of fly ash

Element	O	Na	Mg	Al	Si	P	S	K	Ca	Ti	Fe	Cu	As	Zr
Atomic [%]	53.80	1.84	1.06	14.27	20.25	0.09	0.19	0.25	0.94	1.95	4.72	0.16	0.15	0.34
Standard deviation	1.13	0.22	0.26	0.65	1.87	0.02	0.01	0.04	0.31	0.22	2.32	0.02	0.01	0.04

3.2 Effect of ball milling on particle size distribution

Figure 4 (a) shows the particle size distribution curves of the unmilled and milled fly ash for different time 1, 2, 3,4 and 5 hr. The rate of particle size reduction was greatest during the initial 1hr of milling during which the characteristic particle diameter Z-average reduced from 3547 nm to 989 nm. The particle size gradually decreased with milling time and reached to 493 nm after 5 hrs of wet milling as shown in Figure 4 (b) and (c). This shows that the main influence of the mechanical activation of fly ash is to decrease particle size rather than change mineralogical content.

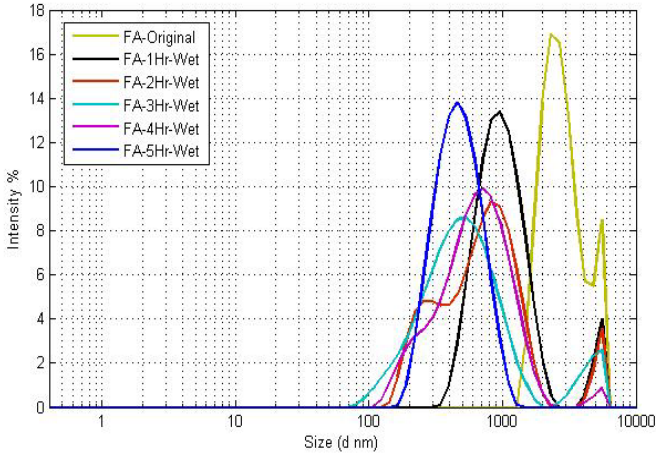

(a) Unmilled and milled fly ash

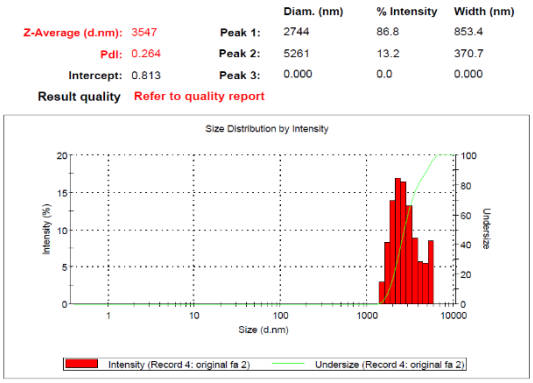

(b) Unmilled fly ash

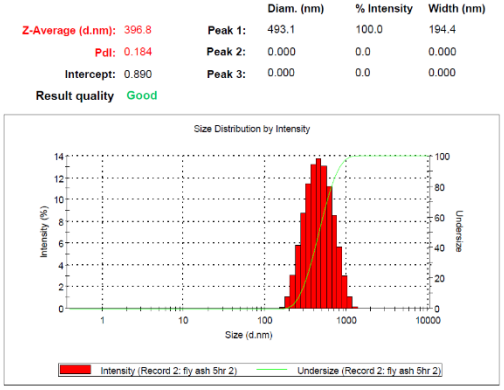

(c) Milled fly ash after 5 hr

Figure 4. Particle size distributions of unmilled and milled fly ash

Figure 5 (a) and Figure 5 (b) shows SEM image of unmilled and milled fly ash particles. It clearly shows that milling destroys a large proportion of the spherical morphology of the unmilled original fly ash. However, the spherical morphology of the unmilled fly ash was not fully destroyed and there is some agglomeration of the fine grained particles.

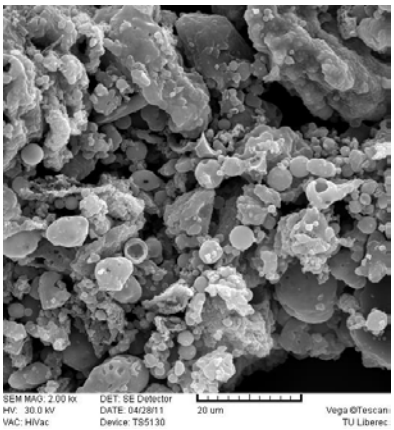

Figure 5 (a). Unmilled original fly ash

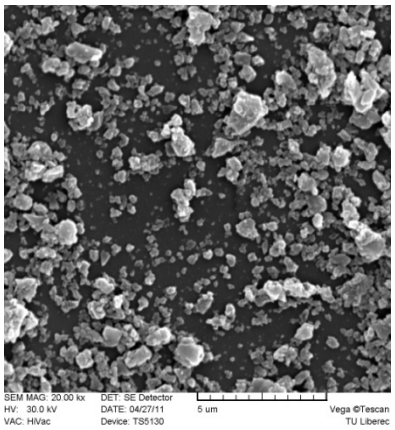

Figure 5 (b). Milled fly ash

3.3 Effect of mechanical activation on physical properties of geopolymer

The physical properties of the geopolymers were tested for unmilled fly ash and milled fly ash both in dispersion and powder form and shown in Table 2. The 10 MPa increase in compression strength was

observed for the geopolymers made from nanoparticles of wet milled fly ash in all 7, 14 and 28 days of ambient curing as compared to the geopolymers made from microparticles of unmilled fly ash. Whereas significant loss of 30-35 MPa in compression strength was observed for the geopolymers made from water dispersion of wet milled fly ash as compared to those of unmilled fly ash. The same trend was observed in case of density for all types of geopolymers. However, lower value of hardness was observed for mechanically activated fly ash than unmilled fly ash geopolymers.

T**able 2.** The properties of 10% fly ash (FA) (without milling and with milling) based geopolymer mortar curing at room temperature

Properties	**Time [days]**	**FA without milling**	**FA water dispersion after wet milling**	**FA powder after wet milling**
Compressive strength [MPa]	7	44.41 ± 3.2	28.59 ± 1.1	53.56 ± 7.1
	14	48.42 ± 4.4	24.88 ± 1.9	58.61 ± 9.1
	28	50.72 ± 3.2	13.69 ± 6.2	62.80 ± 10.3
Hardness [HV]	7	291 ± 2.0	229 ± 2.0	284 ± 4.0
	14	307 ± 2.0	197 ± 5.0	304 ± 3.0
	28	325 ± 4.0	168 ± 8.0	320 ± 4.0
Density [g/cm^3]	7	1.73	1.61	1.77
	14	1.72	1.57	1.77
	28	1.71	1.55	1.76
Grain size [nm]		3547	298.4	298.4

3.4 Effect of mechanical activation on compression strength of geopolymer

Figure 6 shows significant improvement in compression strength of geopolymers made from wet milled fly ash which was dried before mixing with geopolymer resin as compared to unmilled fly ash. One of the reasons for improved compressive strength in mechanically activated fly ash mixtures is the high rate of geopolymerisation in the sample. Mechanical activation increases the reactivity of the fly ash causing faster dissolution of the fly ash and rapid setting. Fast setting is the result of improved dissolution of the fly ash into alkaline liquid; leading to improved polymerisation and hardening of the gel phase and thus developing compact structure within the geopolymer.

On the other hand sharp reduction in compression strength was observed for the geopolymers made from wet milled fly ash which was not dried before mixing with geopolymer resin as compared to unmilled fly ash geopolymer. The loss of compression strength is due to the excess water present in wet milled fly ash dispersion, which reduces the concentration of sodium hydroxide. The less concentration of sodium hydroxide leads to lower dissolution of the starting materials and consequently reduced geopolymerisation reaction and thus lower compressive strength.

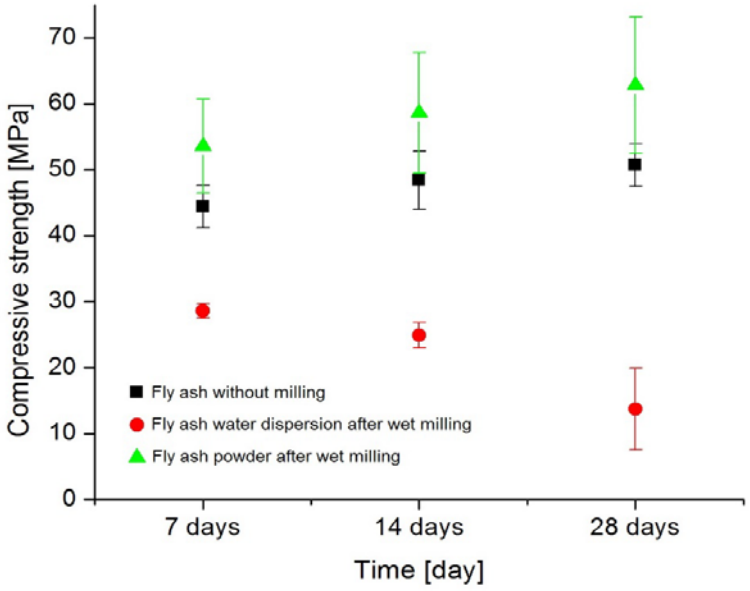

Figure 6. Effect of mechanical activation of fly ash on compression strength of geopolymer

4. CONCLUSION

Mechanical activation of fly ash in a planetary ball mill with milling media to powder ratio of 10:1 leads to a reduction of particle size and change in particle shape but little change in mineralogical composition. Geopolymer paste made with mechanically activated fly ash cured at ambient temperature leads to an increase in compressive strength of 10 MPa when compared with geopolymer made from unmilled fly ash. The main contribution to increased compressive strength of the geopolymer is attributed to reduction of particle size and change in morphology allowing a higher dissolution rate of the fly ash particles. Mechanically activation of fly ash can be seriously considered as a viable method to achieve ambient temperature curing of geopolymers.

References

1. *Böke N et al., New synthesis method for the production of coal fly ash-based foamed Geopolymers, Construction and Building Materials 2015; 75: 189–199.*
2. *Misran H et al., Processing of mesoporous silica materials (MCM-41) from coal fly ash / Journal of Materials Processing Technology, 2007; 186: 8–13.*
3. *Pavel Padevět, Petr Bittna, Influence of fly ash content in cement paste on size of creep, Procedia Engineering, 2012; 48: 520 – 524.*
4. *Bilir T et al. Properties of mortars with fly ash as fine aggregate / Construction and Building Materials, 2015; 93: 782-789.*
5. *Manisha Basu, Potential fly-ash utilization in agriculture: A global review, Progress in Natural Science 2009; 19 (10): 1173–1186.*
6. *Kupaei RH et al., Mix design for fly ash based oil palm shell geopolymer lightweight concrete Construction and Building Materials 2013; 43: 490–496.*
7. *Alaa M. Rashad, A comprehensive overview about the influence of different admixtures and additives on the properties of alkali-activated fly ash, Materials and Design, 2014; 53: 1005–1025.*
8. *Zapata Ordúz LE et al., Weibull statistical analysis of splitting tensile strength of concretes containing class F fly ash, micro/nano-SiO_2, Ceramics International 2014; 40: 7373–7388.*
9. *Kuder K et al. Mechanical properties of self-consolidating concrete blended with high volumes of fly ash and slag, Construction and Building Materials 2012; 34: 285–295*
10. *Baheti V, Militky J, Mishra R, Behera BK, Thermomechanical properties of glass fabric/epoxy composites filled with fly ash, Composites Part B (2015), doi: 10.1016/ j.compositesb.2015.09.049.*

11. *Amnadnua K et al. Strength, water permeability, and heat evolution of high strength concrete made from the mixture of calcium carbide residue and fly ash, Materials and Design 2013; 51: 894–901.*
12. *García-Lodeiro I et al., Variation in hybrid cements over time. Alkaline activation of fly ash–portland cement blends, Cement and Concrete Research2013; 52: 112–122.*
13. *Hai-yan Zhang et al., Fiber Reinforced Geopolymers for Fire Resistance Applications, Procedia Engineering 2014; 71: 153–158.*
14. *Tarun R. Naik, Shiw S. Singh, Fly Ash Generation and Utilization - An Overview, Recent Trend in Fly Ash Utilization, June 1993.*
15. *Crouch L K et al., High Volume Fly Ash Concrete, World of coal ash (WOCA) Conference, May 2007.*
16. *Ravina D, Mehta P, Properties of fresh concrete containing large amounts of fly ash, Cement and Concrete Research 1986; 16 (2): 227-238.*
17. *Ahmaruzzaman M, A review on the utilization of fly ash, Progress in Energy and Combustion Science 2010; 36 (3): 327–363.*
18. *Kou S C, Poon C S, Construction and Building Materials 2013; 41: 146–151.*
19. *Saafi M et al., Enhanced properties of graphene/fly ash geopolymeric composite cement, Cement and Concrete Research 2015; 67: 292–299.*
20. *Zhang Z et al., Fly ash based geopolymers: The relationship between composition, pore structure and efflorescence, Cement and Concrete Research 2014; 64: 30–41.*
21. *Mohammed A E et al., Strength development of concrete containing coal fly ash under different curing temperature conditions, World of coal ash (WOCA) Conference, May 2009.*
22. *Grzeszczyk S, Lipowski G, Effect Of Content And Particle Size Distribution Of High-Calcium Fly Ash On The Rheological Properties Of Cement Pastes, Cement and Concrete Research 1997; 27 (6): 907-916.*
23. *Hu C, Microstructure and mechanical properties of fly ash blended cement pastes, Construction and Building Materials 2014; 73: 618–625.*
24. *Ryu G S et al., The mechanical properties of fly ash-based geopolymer concrete with alkaline activators, Construction and Building Materials 2013; 47: 409–418.*
25. *Lima C et al., Physical properties and mechanical behaviour of concrete made with recycled aggregates and fly ash, Construction and Building Materials 2013; 47: 547–559.*
26. *Yoshitake I et al., Tensile properties of high volume fly-ash (HVFA) concrete with limestone aggregate, Construction and Building Materials 2013; 49: 101–109*
27. *Yoshitake I, Zhang W, Mimura Y, Saito T. Uniaxial tensile strength and tensile Young's modulus of fly-ash concrete at early age, Construction and Building Materials 2013; 40: 514–521.*
28. *Phoo-ngernkham T et al., The effect of adding nano-SiO_2 and nano-Al_2O_3 on properties of high calcium fly ash geopolymer cured at ambient temperature, Materials and Design 2014; 55: 58–65.*
29. *Michael Thomas, Optimising the use of fly ash in concrete, Concrete, PCA-Portland Cement Association, 2007.*
30. *Adak D et al., Effect of nano-silica on strength and durability of fly ash based geopolymer mortar/ Construction and Building Materials 2014; 70: 453–459.*
31. *Shaikh F U A et al., A study on the effect of nano silica on compressive strength of high volume fly ash mortars and concretes, Materials and Design 2014; 60: 433–442.*
32. *Celik et al., Characterization of Fly Ash and its effects on the Compressive strength properties of Portland cement, Indian Journal of Engineering & Material Sciences, 2008; 15: 430-440.*
33. *Tarun R. Naik, Shiw S. Singh, and Bruce W. Ramme, Durability Of Fly Ash Concrete System Incorporating High-Calcium Fly Ash - A Review, Center for By-Products Utilization, Report No. CBU-1997-23, November 1997.*
34. *Li G, Properties of high-volume fly ash concrete incorporating nano-SiO2, Cement and Concrete Research 2004; 34: 1043–1049.*
35. *Ibrahim R K et al., Fire resistance of high-volume fly ash mortars with nanosilica addition, Construction and Building Materials 2012; 36: 779–786.*
36. *Bumjoo Kim et al., Geotechnical Properties of Fly and Bottom Ash Mixtures for Use in Highway Embankments Journal of Geotechnical and Geo-environmental Engineering 2005; 131(7): 914–924.*

A STUDY ON THE PERFORATED POLY-URETHANE FOAM FOR THE CAR SEAT

Funda Buyuk Mazari, Antonin Havelka, Michal Chotěbor, Jakub Wiener, Adnan Mazari

Technical University of Liberec, Studetnska 2, Husova, 46117, Czech Republic
fundabuyuk@hotmail.com

Abstract:

Poly Urethane (PU) foams are the most essential part of the car seat cushion. The PU foams are durable and easily moldable according to the shape of car seat but they are poor permeable to moisture. This impermeability of PU foam causes the wetness of microclimate between person and the car seat and makes it uncomfortable. In this research PU foams with two different thickness and three different holes sizes are obtained from industry by molding process. The foams are tested for moisture permeability by standard cup method to determine the effect of size of hole on the overall moisture permeability. The foams are further tested with 11 most common top layer fabrics to check the effect of top fabric layer on overall moisture permeability of car seat. All the top layers are first tested by sweating guarded hot plate (SGHP) to measure the water vapor resistance (Ret) and then 4 materials with the minimum Ret values are tested with the most permeable foam. The results shows that the perforation of PU foam causes a significant increase in moisture permeability whereas the top layer with minimum Ret value decreases the overall moisture permeability and a maximum of 40g/m^2 of moisture per hour is obtained with the most permeable foam with the least Ret value of top layer. The research work is initial work on replacing the car seat with perforated PU-foams.

Key words:

Car seat, comfort, poly-urethane, moisture permeability.

1. Introduction

Comfort is the basic and universal necessity of human being. Though, it is very complicated and challenging to define. Slater[1] defined comfort as pleasant state of psychological, neurophysiological and physical harmony between environment and human being. According to him comfort can be defined in following ways [2].

i. Absence of discomfort or unpleasant feeling
ii. Physiological response of the wearer
iii. Temperature regulation of human body
iv. Condition of pleasant physical, physiological, psychological and harmony between a human being and surrounding environment

Normal internal body temperature of human beings is 37 ^{o}C (98.6 ^{o}F) with tolerance of $\pm$ 0.5 ^{o}C under different climatic conditions. Any variation from of body temperature from 37 ^{o}C may create changes in rate of heat production or rate of heat losses to bring the body temperature back to 37 ^{o}C. Metabolic activity or oxidation of foods causes production of heat and can be partially adjusted by controlling metabolic rate [2-4].

At present, the thermophysiological comfort of car seats can be acquired by set of laboratory test apparatus. It is now probable to improve and calculate thermophysiological characteristics of car seats at development stage by using skin model and seat comfort tester [5-7].

It was initially observed that strong discomfort sensation arise due to small quantity of water in microclimate between person and the car seat [8]. It has been confirmed in numerous researches that either moisture from sweating or additional moisture creates clothing contact sensations.

2. Experimental

There are two common thickness of car seat PU foams which are used according to the seat requirement. Each foam with 3 different holes size are obtained from industry by molding process. The foams are not drilled nor cut from top or bottom in laboratory so that the real surface property of the foams should be kept, as molded surface are very different then the cut foams.

The original foam was firstly observed under the X-ray micro tomography, the method is very beneficial to observe the internal structure of the material.

Table1. Properties for PU foam used for the experiment

	Foam thickness	Number of holes	Hole diameter	Total area of foam sample	Area of holes	Area of solid foam
	mm		mm	mm^2	mm^2	mm^2
A	60	0	0	16505	0	16505
A1	60	7	10	16505	550	15955
A2	60	7	15	16505	1236	15268
A3	60	7	20	16505	2198	14307
B	85	0	0	16505	0	16505
B1	85	7	10	16505	550	15955
B2	85	7	15	16505	1236	15268
B3	85	7	20	16505	2198	14307

The Figure 1 shows the real picture of the perforated foams

Figure 1. PU foam samples

All the foams are tested with upright cup method (ASTM E 96-66) for water vapor permeability. Any other technique of moisture permeability measurement is not possible as the foams are thick and it's not possible to use such thick samples. The testing is performed in a climate chamber with controlled condition to avoid condensation of moisture in the sample. The testing is performed for 3 hours and measurements are obtained after every 1 hours.
Eleven most common top layer fabric are obtained from car industry and tested firstly for the water vapor resistance (Ret) on sweating guarded hot plate (SGHP) the 4 samples with minimum Ret value are selected to test for moisture permeability as combined layer with the perforated foams.

Table 2. Properties of top layer of car seat cover

		Fleece		3D Spacer			Face Fabric			
	Mass per unit area [g/m²]	Thickness [mm]	Material Composition	Mass per unit area [g/m²]	Thickness [mm]	Material Composition	Technology	Warp direction details	Weft direction details	Material Composition
26989	100	2	100% PES	250	3	100% PES	warp knitted	14 wale/cm	29 course/cm	100% PES
25976	230	5	70% PES, 30%WO				warp knitted	13 wale/cm	24 course/cm	100% PES
25979	230	5	70% PES, 30%WO	335	5	100% PES	warp knitted	13 wale/cm	24 course/cm	100% PES
26728	230	5	70% PES, 30%WO	335	5	100% PES	woven	33 end/cm	18pick/cm	100% PES
26977	100	2	100% PES	250	3	100% PES	woven	32end/cm	18 pick/cm	100% PES
26200	230	5	70% PES, 30%WO	335	5	100% PES	warp knitted	15 wale/cm	25 course/cm	100% PES
26195	100	2	100% PES	250	3	100% PES	warp knitted	15 wale/cm	25 course/cm	100% PES
25962	100	2	100% PES	250	3	100% PES	woven	34 end/cm	18 pick/cm	100% PES
25967	230	5	70% PES, 30%WO	335	5	100% PES	woven	36 end/cm	16pick/cm	100% PES
29086	230	5	70% PES, 30%WO				warp knitted	14wale/cm	28course/cm	100% PES
29084	230	5	70% PES, 30%WO				woven	36 end/cm	16 pick/cm	100% PES

3. Results and discussion

All the PU foams are tested for the moisture permeability tested with upright cup method (ASTM E 96-66) for water vapor permeability; the test is performed for 3 hours and measurement are obtained after every 1 hours.

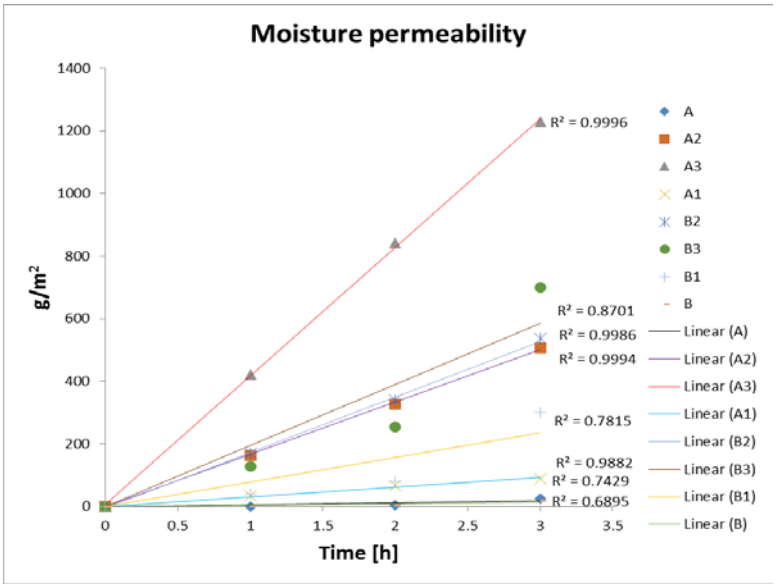

Figure 2. Moisture permeability through PU-foam

It is observed from figure 2 that the non-perforated foams A and B are almost impermeable to moisture and bigger size of the porosity is causing higher breathability of the foam, the foam A3 and B3 have

the maximum air area (area of the holes) in the sample and shows a significant increase in the moisture permeability of the sample. A3 sample shows more permeability then the B3 which is due to the thickness difference of the sample and moisture permeability is dependent on the thickness of the sample.

As the results of the perforated foams came very reasonable regarding the moisture permeability so different top layers combination are used to test the overall permeability of the car seat sandwich structure. All the top layers are tested first for the air permeability by ISO standard 9237, as shown in table 3 to determine the air permeability of the top layers. The air permeability and moisture permeability are not comparable when the material is thick and there is possibility of the axial airflow. So the top layers are also tested for moisture vapor resistance by standard ISO 11092. Four of the samples are chosen according to low resistance to moisture and better air permeability, and sandwiched later with the perforated foam.

Table 3. Air and moisture permeability of car seat's top layers

no.	Ret [m2Pa/W]	Air permeability DIN EN ISO 9237 [l/min/100cm²]
26989	14.2318	500
25976	12.405	275
25979	16.1789	263
26728	16.9876	195

As shown in table 3, the four top samples are sandwiched with the highest permeable foam A3 and again tested for the moisture permeability tested with upright cup method (ASTM E 96-66) for water vapor permeability.

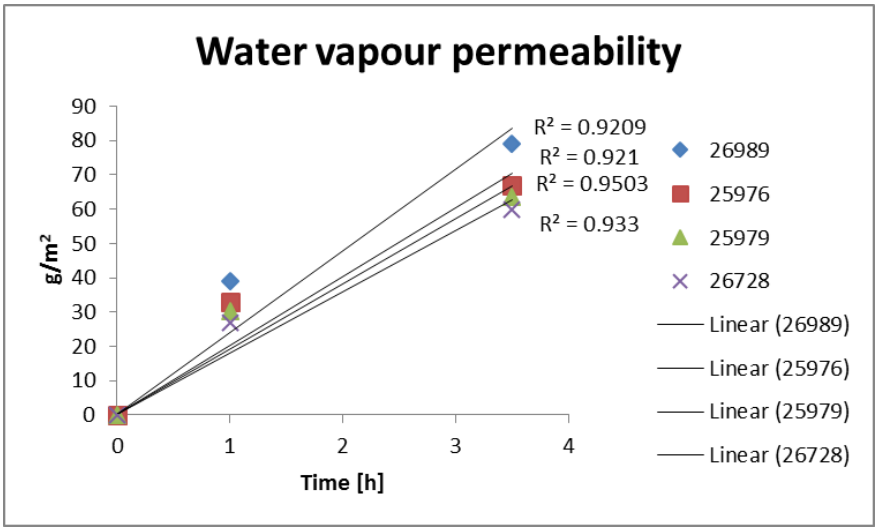

Figure 3. Water vapor permeability of sandwich car seat cushion.

4. CONCLUSIONS

The breathability of car seat is a serious issue and in this research a unique concept of perforated molded PU-foams is used instead of classical foams, the results shows that the perforation plays a significant role in the moisture transfer. An average human perspire 20-40g per hour during driving and classical foams are impermeable and causes a discomfort for the driver, on the other hand perforated foam and the top layer together works efficiently to transfer nearly 40g/hour of moisture.

The top layers of the fabric also plays an important role and it is observed that the layers with 3d spacer fabric and wool percentage causes better transportation of moisture from the PU-foam below. The top layer will be studied further in future research as different layers are sandwich together with the flame or chemical adhesion which further reduces the breathability, but in this research some of the most common top layers are taken to just investigate the overall performance with the perforated foams. The perforated foams can be future replacement for the classical foams. Different design of grooves and shapes of holes can also be introduced to increase the porosity of the foams. This is novel and initial work and further research will be done regarding the life time of the perforated foams.

ACKNOWLEDGEMENTS

The research work is funded by project SGS 21146

References

1. *Slater K. Comfort properties of textiles. Text. Prog.1977; 9(4): 1–42*
2. *Slater K. The assessment of comfort. J. Text. Inst. 1986; 77: 157–171*
3. *Das A and Alagirusamy R. Science in clothing comfort. India: Woodhead Publishing, 2010.*
4. *Li Y. The science of clothing comfort. Textile progress. 2001; 1(2)*
5. *Zhang et al. Thermoregulatory responses to different moisture-transfer rates of clothing materials during exercise. J. Text. Inst. 2001; 92 (1): 372-378.*
6. *K. H Umbach, Parameters for the physiological comfort on car seats, 38th International Man-Made Fibres Congress, Dornbirn, Austria. (1999).*
7. *K. H Umbach, Physiologischer Sitzkomfort im Kfz', Kettenwirk-Praxis, 34 (2000a) 34–40.*
8. *Hollies, N.R.S. Psycological Scaling in Comfort Assessment, Ch. 8 in Clothing Comfort. Ann Arbor: Ann Arbor Science, 1977.*

DESIGNING AND PATTERNMAKING WITH STRETCH FABRICS

[1]Nareerut Jariyapunya, [2]Jelka Geršak, [3]Blažena Musilová, [4]Smita Boob

[1,3,4]Technical University of Liberec – Faculty of Textile Engineering, Department of Clothing, Studentská 2, Liberec, Czech Republic
[2]University of Maribor – Faculty of Mechanical Engineering, Research and Innovation Centre for Design and Clothing Science, Smetanova 17, SI-2000 Maribor, Slovenia
+420 773591414. nareerut.jariyapunya@tul.cz

Abstract

The pattern construction for woven fabric is considered to be very ordinary when comparing with the patterns construction for tight-fitting clothing characterized by its stretched fabric. Fabric elasticity is an important parameter, which plays a key role particularly when constructing patterns for tight-fitting clothing, in respect of changing pattern-piece size, resp. adapting the garment to the contours of a body in motion. The purpose of this research is to design 3D pattern construction with stretch fabric for women tight-fitting sportswear using OptiTex software to represent the tension properties of fabric generated on the surface of the simulation model. Moreover, the study on mechanical properties of stretch fabric and its result have illustrated that OptiTex could be used to simulate the tension map options so as to inspect its colored map depicting amounts of tension between clothing and model. It is certainly obvious that tension map area could be adjusted in accordance to the pattern design suitable for tight-fitting clothing wearing. Subsequently, the final pattern of 3D simulation would be compared with the actual clothing worn by rigid mannequin and also to be measured by PicoPress pressure tester.

Key words

Stretch fabric, 3D pattern construction, Tension distribution, Tight-fitting, Pressure comfort

1. Introduction

3D virtual pattern construction representation of garment provides high potential for design clothing and development. Clothing industry rapidly turns to virtual simulation which not only presents realistic 3D view of garment but also simulates mechanical behaviour of materials. Elastic garments for sportswear has been providing comfortable movement, minimizing the risk of injury or muscle fatigue, and reducing friction between body and clothing [1]. Patterns construction for tight-fitting garments which very closely contour the human body. The moment the physical movement is made, the comfort performance level changes and different parts of the body stretch very differently, and the amount of stretch will vary differently in each direction [2]. J. Geršak [3] report that adjustment adapting an initial pattern of a tight-fitting garment is often done by decreasing the pattern-pieces. The garment pattern-pieces are often, in practice, reduced by subjectively evaluating fabric elasticity, using only a manual elongation test. A simple and ordinary body movement expands the skin by about 10–50% [4]. Pressure garments are defined as custom made elastic garments that exert pressure on the body by virtueof the fact that they are made smaller than the body they are designed to fit [5, 6].

Accounting for garment pressure and comfort sensations at the waist, they have observed that in the lower garment pressure range (0–15 gf/cm^2) no sense of discomfort is there. In the medium range of

garment pressure (15–25 gf/cm^2) negligible or only slight discomfort is perceived. But in higher pressure range, i.e. when the garment pressure exceeds 25 gf/cm^2, extreme discomfort is perceived [7]. The Reduction Factor method reduces all of the size measurements by a standard amount, typically between 10 and 20% [5, 6], regardless of the fabric used. Krzywinski et al [8] evaluate elastic properties of a fabric, wearing tests will determine the necessary load to match adequate garment fit with required comfort during wear. Investigations have shown that the feeling of comfort when wearing tight garments is reached at fabric elongation occurring at a load of 1.5 or 2.0 N (5 cm) $^{-1}$. The Laplace Law method uses the Laplace equation to calculate the reduction factor for each circumferential measurement in order to deliver a specific pressure [8]. However, the Laplace Law method takes account of the fabric tension when calculating garment dimensions while the Reduction Factor method does not [9]. The compression tester PicoPress was used by Vinckx et al [10] estimating the pressure perturbation when PicoPress sensor is used to measure the interface pressure applied to a cylinder, which is used in the apparatus, as no other mathematical model is currently available to estimate this perturbation. The estimated value of perturbation was, then, used to apply a correction factor to the pressure values measured by PicoPress.

2. Experimental

The research has been using stretch fabric to construct tight sportswear and its pattern by reducing its size in accordance with its pressure simulated by Optitex software. Simulation of tension map has shown different levels of physical tensions distribution on the sportswear model. Then the last suitable pattern adjusted by Optitex would be compared by Pico Press pressure measurement device.

2.1. Materials

Two different types of stretch knitted fabrics were used: (a) the fabric containing 65% Polyamide (PA), 35% elastane with 183 g/m^2 and (b) fabric from 38% Outlast, 52% Polyester (PES) and 10% Spandex with 151 g/m^2. The experiment using Fabric Assurance by Simple Testing (FAST) system and Kawabata Evaluation System for Fabrics (KES FB-Auto) to determine the parameter requirements with OptiTex 3D simulation. The experiment preparation, pre-conditioning and testing were carried out under standard atmospheric conditions of 20 ± 2 °C temperatures and 65 ± 5% relative humidity.

2.2. Methods

The properties of stretch fabrics requirment from Optitex simulator software for input parameters measure by The FAST-1 compression meter provides a direct measure of fabric thickness at 2 gf/cm^2 (196 Pa) and 100 gf/cm^2 (9.81 kPa). The FAST-2 bending meter provides a direct measure of fabric bending length in either the wale or course direction. Bending rigidity is calculated from the bending length and fabric mass per unit area. The FAST-3 Extension meter provides a direct measure of fabric extension under selected loads with wale and course directions. Shear rigidity is using extension on the bias at 5 gf/cm. Extensibility using measure of fabric extension under selected loads at 100 gf/cm with wale and course directions by KES FB-Auto system because the fabric speciments were every hightly extension with loading at E100 (100 gf/cm) from FAST Extension meter. KES FB-Auto determind the strain at 100 gf/cm and samples are clamped between 2 jaws with an effective test area of 5 cm x 5 cm.

Simulation method

The OptiTex software simulate the model of human body by input parameter of the model which determind the model medium size from European standard size 38 with 88 cm. bust circumference. The figure 1 illustrates the pattern construction for aerobic sportswear of ladies which reduced all of the size measurements 10% and designing 2D pattern from computer-aided program shows in the figure 1(a) and the figure 1(b) illustrates 3D simulation of human body surface for visual model.

(a) (b)

Figure 1. Pattern construction for aerobic sportswear: (a) 2D pattern construction, and (b) 3D pattern contour on model and setting measuring points for measuring pressure.

Evalulation method

PicoPress used to measure the pressure the relation between time and pressure (mmHg) by setting the important parts on the body for measuring which have risked or the highly extension when covering with rigid mannequin. In figure 1(b), it could been seen that the critical points pressure on the visual mannequin had been measured by PicoPress pressure measurement system; however, these pressure results in the right side could be resembling the left side values as well.

3. Results and discussion

The result of stretch fabrics properties could input parameters from Optitex simulator software had been used to determine the tension map on the virtual mannequin are as follows: The figure 2 shows the results of mechanical properties which were measured by FAST system. The value of extensibility marked (20.6%*) in figure 2 mean the tested fabric had very high extensibility due to the limitation of equipment measurement performance which could only measure 20.6%. Whereas, we use to simulate the value of tensile properties obtained by using the KES-FB system.

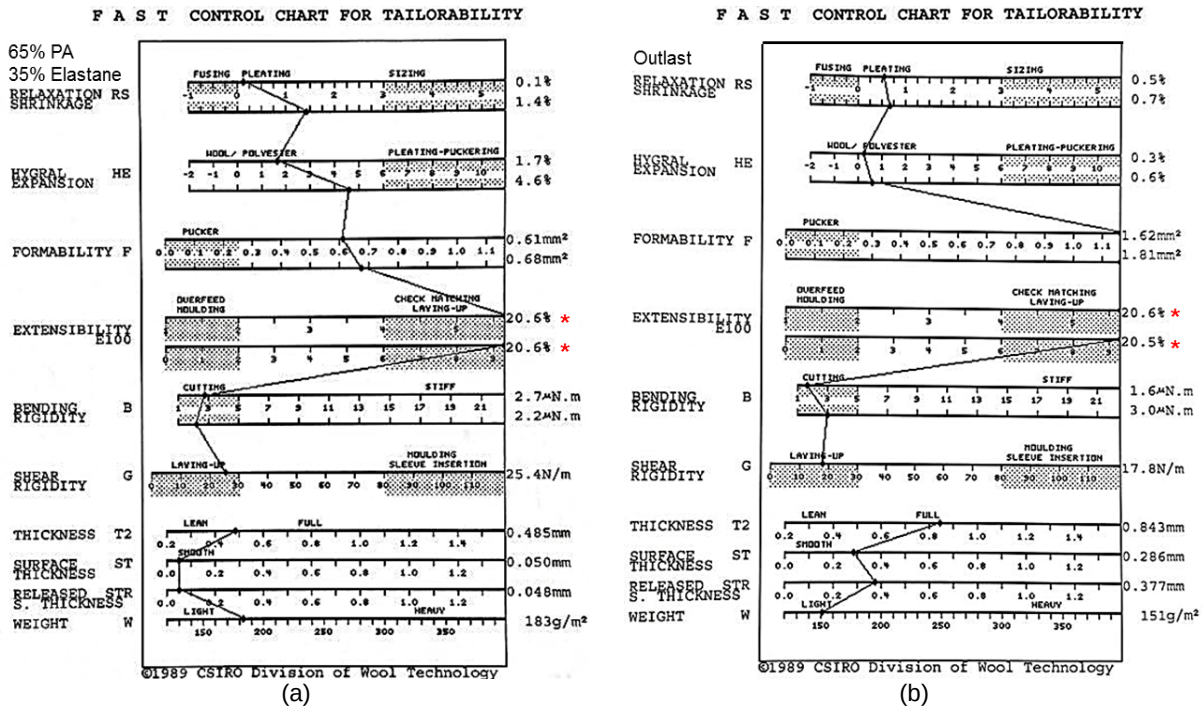

(a) (b)

Figure 2. FAST system control chart.
(a) 65% PA, 35% Elastane and (b) 38% Outlast, 52% PES, 10% Spendex

The results of stretch fabric properties as shown in the Table 1 illustrated the parameters and functions of fabric editor from OptiTex. The editor function would be used to convert fabric physical attributes from FAST parameter to OptiTex parameter in oder to evaluate the tension of clothing when draping with the 3D model.

Table 1. Elastic knitted properties from FAST system convert parameter to OptiTex parameter.

Parameter of fabric	65% PA, 35% Elastane		38% Outlast, 52% PES, 10% Spendex	
	FAST	OptiTex	FAST	OptiTex
Bending X (Wale) Y (Coures)	2.70 µN.m 2.20 µN.m	245 dyn.cm	1.60 µN.m 3.00 µN.m	230 dyn.cm
Stretch X (Wale) Y (Course)	31.61 % 21.84 %	121.68 g/cm 176.11 g/cm	63.60 % 38.89 %	60.47 g/cm 98.89 g/cm
Shear	25.40 N/m	762 dyn.cm	17.80 N/m	534 dyn*cm
Friction	0.19	0.19	0.27	0.27
Surface Thickness	0.05 mm.	0.005 cm.	0.286 mm.	0.0286 cm.
Weight	183 g/m^2	183 g/m^2	151 g/m^2	151 g/m^2

The figure 3, results from these 3D simulation had shown maximum tension value at the upper right corner of figure as well as tension gradient map of the stretch fabrics. In figure 3(a) 65% PA, 35% Elastane clothing had given higher tension value of 26.98 fg/cm more than 15.00 fg/cm maximum tension value of 38% Outlast, 52% PES and 10% Spandex clothing illustrated in figure 3(b). After observing 3D tesion gradient map, the colour distribution value on clothing from figure 3(a) and 3(b) are quite similar. In fact, the red areas in both figures had show differences in term of tension value. Besides, critical points should be determined in order to find out extension values of clothing from eight given points on the 3D simulated model.

(a) (b)

Figure 3. 3D simulation tension map gradient.
(a) 65% PA, 35% Elastane and (b) 38% Outlast, 52% PES, 10% Spendex

Tension value of two types of stretch fabrics at 8 different points of the body as shown in figure 1(b) had been compared in the figure 4. The values of tension in the figure 4(a) are evaluated by OptiTex software. The tension values of 65% PA, 35% Elastane fabric are approximately 46.30% higher than 38% Outlast, 52% PES and 10% Spandex fabric. At specific point 1 and 2 of shoulder positions in the figure 4(a), low values of tension have been illustrated.

In the figure 4(b), pressure volume graph shows how PicoPress is used to determine pressure values from eight specific points on two different types of clothing worn on the rigid mannequin. Referring from the pressure testing, the results show that the value of pressure from fabric 65% PA, 35% Elastane are higher than the fabric 38% Outlast, 52% PES and 10% Spendex. Located at the back of the waist, specific point 7 shows the lowest value of pressure due to the fact that surface of rigid mannequin and the prototype had air gaps.

Obviously, the third point at bust position had respectively shown the highest tension value and pressure value of 26.98 fg/cm and 9 mmHg measuring on fabric 65%PA, 35% Elastane clothing.

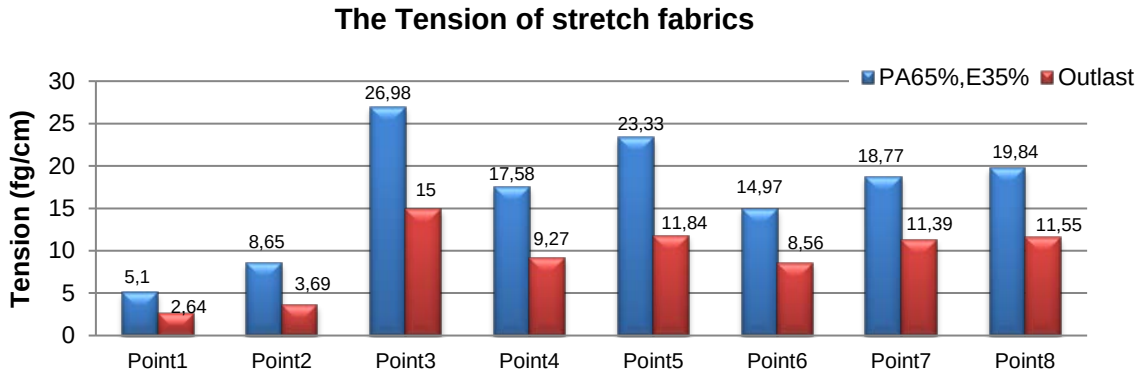

(a)

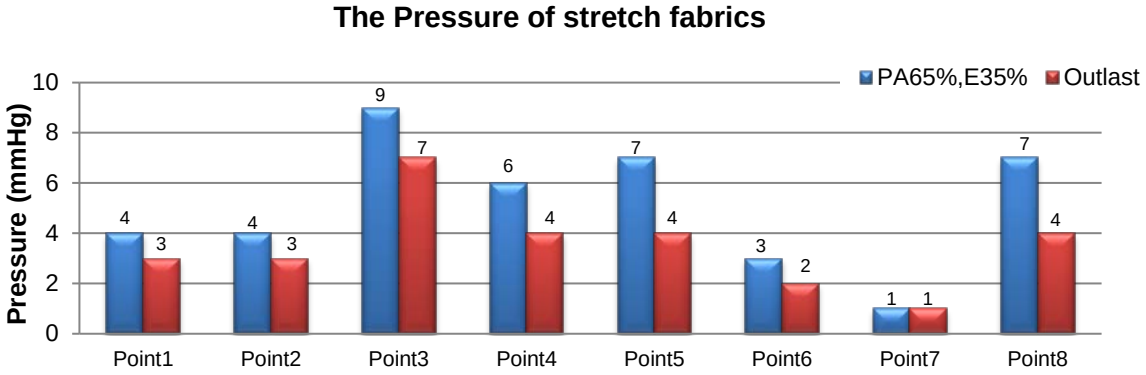

(b)

Figure 4. Comparison the value of tension and pressure between two stretch fabrics. (a) 8 critical points in the tension graph and (b) 8 critical points in the pressure graph.

4. CONCLUSIONS

The results of the simulation has shown on the pattern construction 3D and the virtual mannequin that evaluated amend the tension map gradient results. The colour of tension map when simulated the distribution of 2 types of stretch fabrics had shared similar gradients. However, the results of the value of tension were different by the value of extensibility. The values of fabric elasticity in wale and course direction have an influence on values of tension and the value of the pressure. Obviously, the results of tension simulated by OptiTex were compared with the pressure of prototypes worn by rigid mannequin measured by PicoPress pressure tester. The extensibility values of stretch fabric from 65% PA, 35% Elastane of 31.61 % in wale direction and 21.84 % in course direction. Whereas, tension value of 26.98 fg/cm and pressure value of 9 mmHg at the bust point have no sense of discomfort in the lower garment pressure range (0 – 15 gf/cm^2 or 0 - 11.03 mmHg) accounting for garment pressure and comfort sensations. This could be concluded that the lower the extensibility value is, the higher pressure and tension will be and vice versa. It is certain that the extensibility of fabric tension could be evaluated by OpiTitex to adjusted in accordance to the pattern design suitable for tight-fitting clothing.

ACKNOWLEDGEMENTS

The authors would like to extend sincere appreciation to the Research and Innovation Centre for Design and Clothing Science, Faculty of Mechanical Engineering, University of Maribor and Department of Clothing, Faculty of Textile Engineering, Technical University of Liberec and This work was supported by "SGS 21147". as well as Dr. Danijela Klemenčič from LISCA company in Slovenia.

References

1. *Taya, Y. Shibuya, A., Nakajima, T. (1995). Evaluation method of Clothing Fitness with Body – Part 4: Evaluation by Waveform Spacing between Body and Clothing Journal Textile Machinery Society of Japan 48 (11), 261 – 269.*
2. *Voyce, J. Dafniotis, P. and Towlson, S. (2005). Elastic Textiles, Textiles in Sport, Wood Head Publications, Cambridge, UK.*
3. *Geršak, J. (2013). Design of clothing manufacturing processes, Woodhead publishing series in textile, 125*
4. *Voyce, J.,Dafniotis, P. and Towlson, S. (2005). Elastic Textiles, In: Shishoo,R. (ed.),Textiles in Sport, WoodHead Publications, Cambridge, UK, 205.*
5. *Macintyre L, Baird M. (2006). Pressure garments for use in the treatment of hypertrophic scars – a review of the problems associated with their use, 32, 10-15.*
6. *Macintyre L, Baird M. (2005). Pressure garments for use in the treatment of hypertrophic scars – an evaluation of current construction techniques in NHS hospitals. BURNS, 31(1), 11-14.*
7. *Makabe H., Momota H., Mitsuno T. and Ueda K. (1993). Effect of covered area at the waist on clothing pressure, Sen-iGakkaishi 4109, 513–521.*
8. *Krzywinski, S., Tran Thi, N. and Röder, H. (2002). Schnittgestaltung für körpernahe Bekleidung aus Maschenwarenmit Elastangarnen, Maschen-Industrie, 6, 36 – 39.*
9. *Macintyre L. (2007). Designing pressure garments capable of exerting specific pressures on limbs. Burns, 33(5), 579-86.*
10. *Vinckx, L., Boeckx, W. and Berghmans, J. (1990). Analysis of the pressure perturbation due to the introduction of a measuring probe under an elastic garment, Medical and Biological Engineering and Computing, 28(2), 133-138.*

ARTIFICIAL TURFS AND THEIR TESTING

Hana Pařilová, Michael Perun

Hana Pařilová, Technical univerzity of Liberec, Liberec, ČR, hana.parilova@tul.cz, tel. 485353162
Michael Perun, Lohman&Rauscher, Nová Paka, ČR michael.perun@gmail.com

Abstract:

Artificial turfs of 4.th generation for soccer field requries strong parameters from FIFA. One of problematics moments is unwanted wave-deformation of the surface. The diploma work of Michael Perun from 2013 solves the problem and gives us the solution how to prevent from this issue.

Key words:

infill, artificial turf, monofilament, warp, tufting, rating

1. Technological procedure of artificial turf production

The production of artificial turf sustains of number of technological procedures. At the beginning of production is the manufacturing of monofil, which produces the turfs strings. At the next step, the monofils wraped or textured. Into turfs, produced from fibrilated tape, are implemented bendings, which eases the further processing. Coils with monofils are hangt onto creels. The monofils are then guided into pneumatical sewing machine. In the sewing machine are the monofils sewed in the turf strings. This string is not fixed in the primary underlay textile layer. Therefore coating is then the final procedure. By the coating procedure is on the reverse side implemented an SBR latex layer. This secures, after the desiccation and curing, the fixation so stiff, that the string can not be tear out from the underlay textile.

2. Types of Artificial turfs

The artificial turfs are subjects of ongoing development. First turf types were filled up with silicon sand with seed diametre up to 1mm. Second and third turf generation used as filling material sand and granulate, co called infil. By the fourth turf generation (see figure 1) is the infil not used anymore. In this turf type were identified some problems caused by climatic issues. The turf began to undulate and because of that, it did not fulfill the specifications requested by FIFA. This problematics is solved in disertation work by Mr. Michael Perun (2008). Turfs up from fifth generation are produced in cassets 1,2 x 2,4 m which can be easy connected togedher by Hook and loop fasteners (so called Velcro) [1]. This turf types are not the subject of this article. The scope of this article are the 3rd. and 4th.. turf generaitons.

Figure 1. Cut in 4th generation turf

Turf by name Active is the first turf of 4th generation which company Juta, a.s. developed and introduced on market. Turf Active is formed by underlayer fabric in canvas binding, woved from polypropylene straps. Underlayer fabric is simmilar to underlayer fabric by 3th generation turf by name Champion. Turf string is instead of Champion turf formed by two types of monofil. See figure 1. First stripe type is a monofil with lenticular cross, second stripe is formed by textured monofil.

You can tell from the picture, that the turf stripes are formed not only with narow monofils, but also by shorter monofils, which are draped by texturing technology.

3. Underlayer fabric

Underlayer fabric from dutch company Tencate is used for production of 4t generation of artificial soccer turfs. This type of underlayer fabric is used also in construction of 3rd. generation turf Champion 60/140. On this underlayer fabric will be measured the ductility values. It will be also used for testing in climate chamber, where the hypothesis of warpage caused by thermal load will be investigated.

Underlayer fabric Tencate Thiobac Glass Reinforced

Underlayer fabric was selected for the testing in order to determine, if usage of this fabric solves the current issue with unerlayer fabric Tencate Thiobac Multi Layer, which construction is created by polypropylene fabric in canvas binding. The construction of underlayer fabric Tencate Thiobac Glass Reinforced consist of polypropylene fabric in canvas binding. This fabric is on the verso side stiffen with fabric in gauze binding from glass monofil. This should ensure dimensional stability and by this solve the problem with fabric warpage of precious type.

Table 1. Technical parameters of underlayer fabric Tencate Thiobac Glass Reinforced

WEFT:	63 / 10 cm
WARP:	60 / 10 cm
WEIGHING:	303 g/m^2
WEIGHING INCLISIVE COATING:	904g/m^2

Underlayer fabric Tencate Thiobac Multi Layer

Underlayer fabric from dutch company Tencate is used for production of 4t. generation of artificial soccer turfs. On this underlayer fabric will be measured the ductility values. It will be also used for testing in climate chamber, where the hypothesis of warpage caused by thermal load will be investigated.

Table 2. Technical parameters of underlayer fabric Tencate Thiobac Multi Layer

WEFT:	51/10 cm
WARP:	60/10 cm
WEIGHING:	270 g/m^2
WEIGHING INCLISIVE COATING:	600 g/m^2

4. FIFA Requirements

In the experiment are compared Champion and Active turfs, according to field and machanical-physical tests and standards given by International football association - FIFA. The criterias, which needed to be achieved, are set by document: *The FIFA Quality Concept Handbook of Requirements.*. This documents sets up the requirements, which needs to be acomplished by artificial turfs. Testing. By both of tested turfs were ested followed parameters: ball rebound, impact absorbtion, vetŕtical deformation, ball behaving during rolling, simulated wear-off and resistance against rotation.

Table 3. Some requirements for testing given by FIFA [2]

test	**testing method**	**testing parameters**			**requirements**	
		editing	**temperature**	**status**	**FIFA 1 Star**	**FIFA 2 Stars**
ball rebound	FIFA 01 & FIFA 09	before load	23°C	dry	0,6m - 0,85m	0,6m - 1m
				wett		
		simulated load 5200 cycle		dry	0,6m - 0,85m	N/A
		simulated load 20200 cycle		dry	N/A	0,6m - 1m
ball rolling	FIFA 03	before load	23°C	dry	4m-8m	4m-10m
				wett		
schock absorption	FIFA 04a & FIFA 09	before load	23°C	dry	60-70%	55-70%
				wett		
		simulated load 5200 cycle		dry	60-70%	N/A
		simulated load 20200 cycle		dry	N/A	55-70%
		before load	40°C	dry	60-70%	55-70%
	FIFA 04a 1st. Impact	-	-5°C	wett	60-70%	55-70%
vertical deformation	FIFA 05a & FIFA 09	before load	23°C	dry	4mm-10mm	4mm-11mm
		before load		wett		
		simulated load 5200 cycle		dry	4mm-10mm	N/A
		simulated load 20200		dry	N/A	4mm-

		cycle				11mm
resist against rotation movement	FIFA 04a & FIFA 09	before load	23°C	dry	30Nm-45Nm	25Nm-50Nm
				wett		
		simulated load 5200 cycle		dry	30Nm-45Nm	N/A
		simulated load 20200 cycle		dry	N/A	25Nm-50Nm

Ball rebound

The testing method is set up in standard ČSN EN 12235 [3]. The principle of the test, is to set up the ball rebound, after the ball hits the tested surface following the vertical drop. They are two principles how to record ball rebounce. Acustic and visual. The rebound high is measurred and calculated as a percentage rebound, corresponding to the drop high. [3]

Figure 2. Device used for rebound test [2]

Ball behaviour by rolling

The ball, located on top of testing ramp, is let to roll down from the ramp onto tested surface. Even the distance carired by the ball, oll the velocity differential are measured. [4]

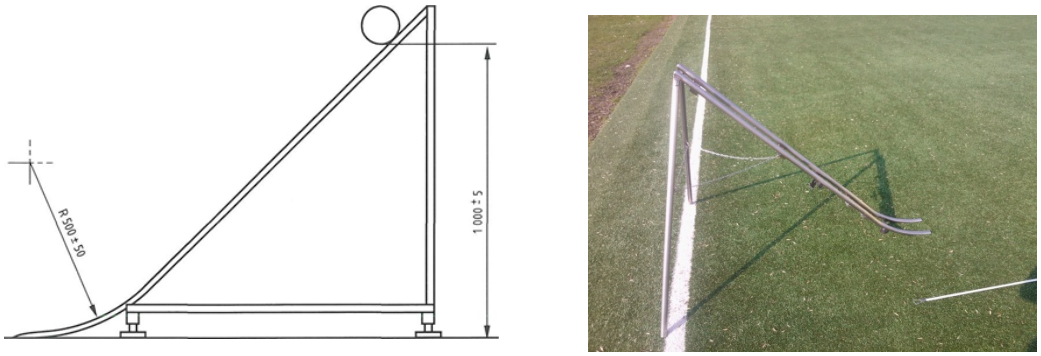

Figure 3. Device used fot ball rolling test [2]

Impact absorption

During this test is the specified weight droped onto spring, which is located on tested surface. Maximal applied force is recorded. The difference between this force and force measured on surface is called force reduction [5].

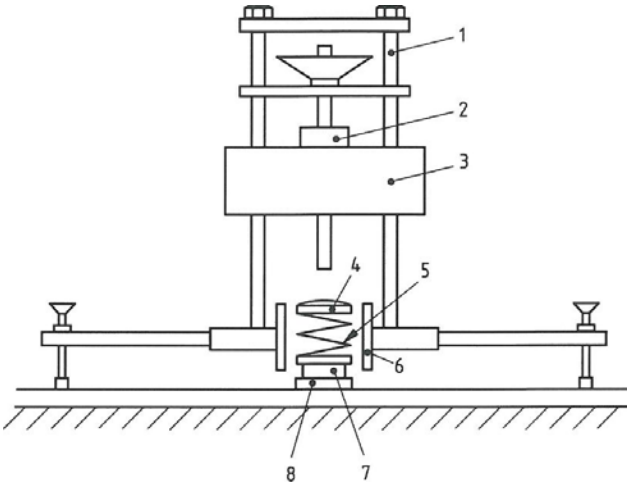

1. guiding frame for weight
2. electromagnet
3. weight
4. top plate
5. spring
6. guidint pipe
7. force recording device
8. bottom plate

Figure 4. - Device Triple A [5].

Vertical deformation

Vertical deformation is set up according to ČSN EN 14809 [6]. The weight is let to fall on spring on tested surface. The maximal surface deformation is recorded.

Simulated wear-off

Testing device consist of two cylinders. Each with length of minimal 300mm and with diameter of 118±5 mm. One of the cylinders is rotating 40 ±2 % faster the other one. Testing sole is mounted onto cylinders according to product specification. On normalized testing sole must be 145 ± 5 plugs. Plugs are made from plastic material with hardness of 96 ± 2ShoreA. The cylinder weight, including frame and plugs, must be 31 000 ± 500 g by cylinder length 300 mm. If using longer cylinders, the weight must also increase. The plugs must not be mounted to cylinders lineary. It must be mounted so, that their movement will produce sinusoid waves on the surface. [7] This ensures, that the tested surface will be weared-off uniformed.

Figure *5.* *Device for turf wear-off simulation (Lisport)* [2]

This test rates the total result of simulated wear-off. All changes on fibres, deformation, damaging, infill changes, fibres abrasion etc. Cycle number is counted and recorded.

5. Experiment

In order to achieve the requiered test results is necessary, that the turf is stable and will not move/drift in play field. The task of the experiment is to solve the unwanted wave motion of the 4.th generation turf Active with underlayer fabric Tencate Thiobac Multi Layer.

Technical parameters measured by the underlying fabric

Underlayer fabric Tencate Thiobac Glass Reinforced is replacing previous older type Tencate Thiobac Multi Layer, The construction of underlayer fabric Tencate Thiobac Glass Reinforced consist of polypropylene fabric in canvas binding. This fabric is on the verso side stiffen with fabric in gauze binding from glass monofil. The glass fibre matrix is damaged due to implementation process of turf hair. Older type (Multi Layer) complies the in-sawing assembly, however, it starts to wave-deforming on field because of weather influence.

Technical parameters of both underlayer fabrics were measured in Institute for textile technology, Technical university of Liberec. It was found out, that both are according to technical datasheet from company Tencate. Weft and weighing were figured out. Both types of underlayer fabric were tested in clima chamber in Institute. The reason for testing, was to figure out, if older type Tencate Thiobac Multi Layer will react under thermal influence by weave- deforming such as on test field assembled by company Juta, a.s. in Dvůr Králové nad Labem.

Tested fabrics were tested in clima chamber without weight load for 20 minutes by 60°C, 70 °C, 80 °C a 90°C.

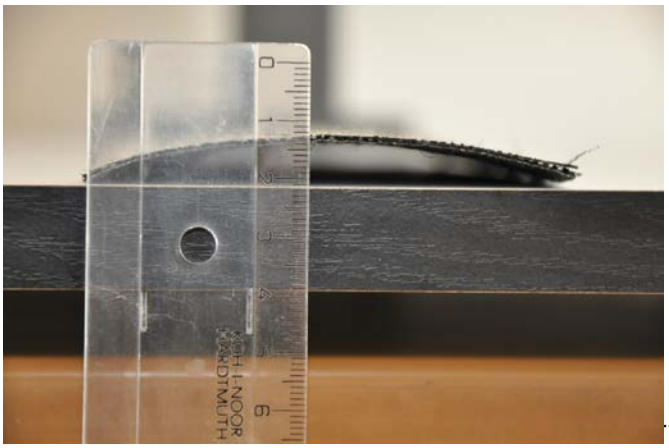

Figure 6. Unwanted effect of waving after clima chamber test by 80°C without weight load [2]

Underlayer fabric Tencate Thiobac Multi Layer was stabilized in clima chamber in order to find out the cause of wave-deformation. Prepared sample with dimensions 29 x 31 cm was layed down onto supported plate. On this sample lays another metal plate, which covered the complete sample (see figure 7) On this tom plate was inserted weight load with 6,6kg. This served as contact pressure for fabric. The calculated pressure in complete surface is 772 Pa. Temperature for heat stabilization was set to 100°C. The sample was fixed in chamber for 20 minutes. [2]

Figure 7. Tested underlayer fabric with weight [2]

The result of heat stabilized sample of Tencate Thiobac Multi Layer was flat surface even after the trial.

6. CONCLUSIONS

The task of experiment was to prevent inwanted turf wave-deformation on soccer field. The problem is silved with heat stabilization of underlayer fabric Tencate Thiobac Multi Layer. The wave-deformation is caused by the fact, that the underlayer fabric is after weaving not heat stabilized, it is directly stored on the roll and send to custommer. Storage of the rolls under different temperatures causes the inner pressure in the fabric. From testing of heat stabilization of the underlayer fabric is obivious that the thesis about absence of heat treatment confirms itself. Heat stabilization solves the problem of wave-deformation of 4.th generation Active turfs. The way, in which was the heat stabilization performed is not possible to implement in serial production. In serial production can be used the strain frame. It is a device, which strainting up and heating up the fabric continously during the manufacturing process.

Artificial turf of 4.th Generation Active is a product of company Juta, a.s. It was tested in soccer field of High School in Dvůr Králové nad Labem. The purpose of 4.th generation turfs is to replace previous generation, which needs to be filled by sand or granulate, which is a high cost for the investors. The proposed heat stabilisation for this typ of turf is a solution for quality improvement and long term usage of this product.

References

1. *Zahálková Helena. Umělý trávník 5. Generace [cit. 26. 5. 2016] Dostupné z: http://www.ceskestavby.cz/clanky/umely-travnik-5-generace-4617.html*
2. *Perun, Michael. Zhodnocení funkčnosti umělého trávníku 4. Generace. Artificial turf for football. Diplomová práce TUL, 2013*
3. *ČSN EN 12235. Povrchy pro sportoviště: Stanovení výšky odrazu míče. 2. doplněné vydání. Praha: ČESKÝ NORMALIZAČNÍ INSTITUT, 2005*
4. *ČSN EN 12234. Povrchy pro sportoviště: Stanovení chování míče při valení. Praha: ČESKÝ NORMALIZAČNÍ INSTITUT, 2003.*
5. *ČSN EN 14808. Povrchy pro sportoviště: Stanovení absorpce nárazu. Praha: ČESKÝ NORMALIZAČNÍ INSTITUT, 2006.*
6. *ČSN EN 14809. Povrchy pro sportoviště: Stanovení vertikální deformace. Praha: ČESKÝ NORMALIZAČNÍ INSTITUT, 2006.*
7. *ČSN EN 15306. Povrchy pro sportoviště: Vystavení syntetické trávy simulovanému opotřebení. Praha: ČESKÝ NORMALIZAČNÍ INSTITUT, 2007.*

MECHANICAL PROPERTIES OF POLYPROPYLENE/HALLOYSITE COMPOSITE FIBRES

Jozef Ryba[1], Mária Petková[2], Šimon Polák[2], Anna Ujhelyiová[2], Marcela Hricová[2], and Tomáš Mackuľak[3]

Slovak University of Technology in Bratislava, Faculty of Chemical and Food Technology
[1]Department of Polymer Processing, [2]Department of Plastics, Rubber and Fibres,
[3]Department of Environmental Engineering
Radlinského 9, 812 37 Bratislava, Slovak Republic
jozef.ryba@stuba.sk

Abstract:

Polypropylene (PP) is an important commercial polymer widely used to produce technical and textile composite fibres due to its well-balanced physical and mechanical properties and easy processability at a relatively low cost. The application of PP in various industrial sectors can be further expanded once its mechanical performances have been highly upgraded. Therefore, PP has been a popular matrix used in association with all kinds of nanofillers such as carbon nanotubes (CNTs), layered silicates (clays such as montmorillonite) and nanoparticles such as silica, graphite and calcium carbonate, even though the nanofiller dispersion is challenging in that case and often remains an issue. Halloysite nanotubes (HNTs) have recently become the subject of research attention as a new type of additive for enhancing the mechanical, thermal and fire-retardant performance of polymers. Halloysite is mainly composed of aluminosilicate and has a predominantly hollow tubular structure with the chemical composition $Al_2(OH)_4Si_2O_5(2H_2O)$. Common halloysites can be found in form of fine, tubular structures with a length of 300~ 1500 nm, and with inner and outer diameters of 15–100 nm and 40–120 nm, respectively.

The aim of this paper is the presentation of properties of PP fibres modified by Halloysite nanotubes. Therefore results of modification of polypropylene fibres will be presented. Mechanical properties of nonmodified and modified fibres will be evaluated.

Keywords:

polypropylene, halloysite nanofiller, dispersant, composite fibres

1. Introduction

Polymer nanocomposites are new class of materials. They are filled with nanoadditives and usually have much better some properties like thermal and mechanical in comparison with conventional polymer composites at much lower additive loadings [1–4].Improvements in mechanical properties, such as stiffness and toughness, dimensional stability, barrier and thermal properties as well as better fire retardant properties are usual observed [1–4]. The interfacial interactions between polymer matrix and nanoadditive and the degree of dispersion of additives are key problems for determination of the performance of prepared nanocomposites [5–8]. Polypropylene (PP) is very important commercial plastic used to produce household goods and automotive parts, electronics, packaging due to its well-balanced physical and mechanical properties and easy processability at a relatively low cost. The application of PP in various industrial sectors can be further investigated. Polypropylene is a popular

matrix used with many kinds of nanoadditives such as carbon nanotubes (CNTs) [9], layered silicates (montmorillonite etc.) [10] and silica, graphite and calcium carbonate [11].

Halloysite nanotubes (HNTs -$Al_2Si_2O_5(OH)_4.2H_2O$) recently are the subject of research attention as a new type of additive for improving of the mechanical, thermal and fire-retardant properties of polymers [12-13]. Halloysite is tubule aluminosilicate clay with external diameter of 50–80 nm, lumen of 10–15 nm and length of about 1000 nm. Chemically, halloysite is similar towell-known and commonly used platy clay kaolin but its aluminosilicate sheets are rolled into tubes [14]. Due to the tubular shape and less abundant surface hydroxylgroups, halloysite is readily dispersed in polymers withoutneed for the exfoliation, contrary to the case of platy clays – kaolin and montmorillonite.

Compared with other nanoparticles such as fumed silica, montmorillonite and carbon nanotubes, halloysite nanotubes are more easily dispersed in polymer matrix by shearing due to their rod-like geometry and limited inter tubular contact area [15]. Therefore, the aggregation induced by the intertubular hydrogen bonding is susceptible to the shearing force. In fact, morphology study for many polymer/HNTs composites has shown single-tube dispersed halloysites in the matrix [16]. HNTs are readily obtainable, are much cheaper than other nanofillers such as carbon nanotubes and they are biocompatible [17].Tubular halloysite clay is “green” material, which is not hazardous for the environment and these clay nanotubes are available inexpensively in thousands of tons from natural deposits[18].

2. Experimental

2.1 Materials

The isotactic Ziegler-Natta polypropylene TATREN HT 2511 (PP), Slovnaft Petrochemicals Co., Slovakia, MFI = 25g/10 min, halloysite nanotubes (HNTs) with chemical formula $Al_2Si_2O_5(OH)_4.2H_2O$, pore size 1.26-1.34 mL/g, surface area 64 m^2/g (Applied Minerals, Inc., USA supplied by Aldrich Chemistry) as nanofiller and non-reactive hydrophobic non-ionic dispersant was used for preparation of the dispersion of HNTs in the PP matrix. Commercially available dispersant Tegopren 5885 (TEG) based on polyethersiloxane, produced and donated by Evonik Industries AG., Germany.

2.2 Masterbatches preparation

The masterbatches of PP with HNTs, and PP with HNTs and dispersants were prepared on co-rotating twin screw extruder from Labtech Scientific (Thailand) with parameters L/D=40 and D=16mm. Temperature profile from hopper to head of extruder was from 190°C to 220°C and speed of screws was 120rpm.Pure PP was also passed through extruder under the same conditions to serve as a reference sample.

2.3 Fibre preparation

The undrawn composite fibres were prepared by classical procedure of spinning from chips of blends using laboratory pilot plant with the screw ϕ = 16 mm at a temperature of 240°C. Metering of melt via spinneret nozzle with 13 orifices (ϕ = 0.5 mm) was 13$g.min^{-1}$and take-up speed at the spinning was 2.5 ms^{-1}. The prepared undrawn fibres were drawn at vertical laboratory drawing machine at four different drawing ratios for following of changes during drawing procedure at temperature of 120°C. Maximum drawing ratio was chosen with aim to investigate ability of prepared fibres reach highest possible tensile properties. This drawing ratio is different for all mentioned samples.

2.4 Methods used

Mechanical properties
The Instron 3343 equipment was used for evaluation of the mechanical properties (tenacity and elongation at break, Young's modulus) of PP and modified PP fibres. The mechanical characteristics of the PP and modified PP fibres were determined in accordance with STN EN ISO 139, STN EN ISO 2060, STN EN ISO 2062.

3. Results

The fineness and mechanical properties of PP/HNTs composite fibres with and without content of non-reactive non-ionic dispersant TEG was evaluated. Prepared fibres were drawn at four different drawing ratios. The fineness of the composite fibres is mainly influenced by increase of drawing ratio. Content of HNTs and dispersant was at low level and outstanding increase of this parameter wasn't observed. Fineness is also influenced by feeding of chips into spinning extruder which is automatically regulated via pressure sensor in spinneret nozzle. According to results (Fig. 1.) fineness of composite fibres is decreasing with higher drawing ratio for all samples. This is generally observed tendency.
The tenacity of composite PP/HNTs fibres is influenced mainly by the morphological structure of elements formed by nanoadditive and by changes which occurs during drawing process [19]. Content of solid particles in micro or nanoscale incorporated into polymer matrix lead to decreasing of orientation of an anisotropic system of fibre [20].From point of view of tenacity is clear that optimal amount of HNTs in fibre is 1 wt. % for maximal drawing ratio because at that value tenacity reach maximum at level of nonmodified PP fibres and next addition of nanoadditive into oriented system of fibre lead to decreasing of tenacity (Fig.2). Addition of non-reactive dispersant TEG cause increase of tenacity value for fibres with content of 3 wt. % HNTs in comparison with modified fibres with same content of HNTs without added dispersant. Its evidence of better dispersion of HNTs particles in PP matrix and lower level of irregularity in morphological structure of modified PP/HNTs fibres during drawing process.

The elongation at break of undrawn composite PP/HNTs fibres is influenced by addition of nanoadditive and non-reactive dispersant TEG into blends. With increasing drawing ratio elongation at break decreasing because of orientation of composite fibres is still higher (Fig.3).

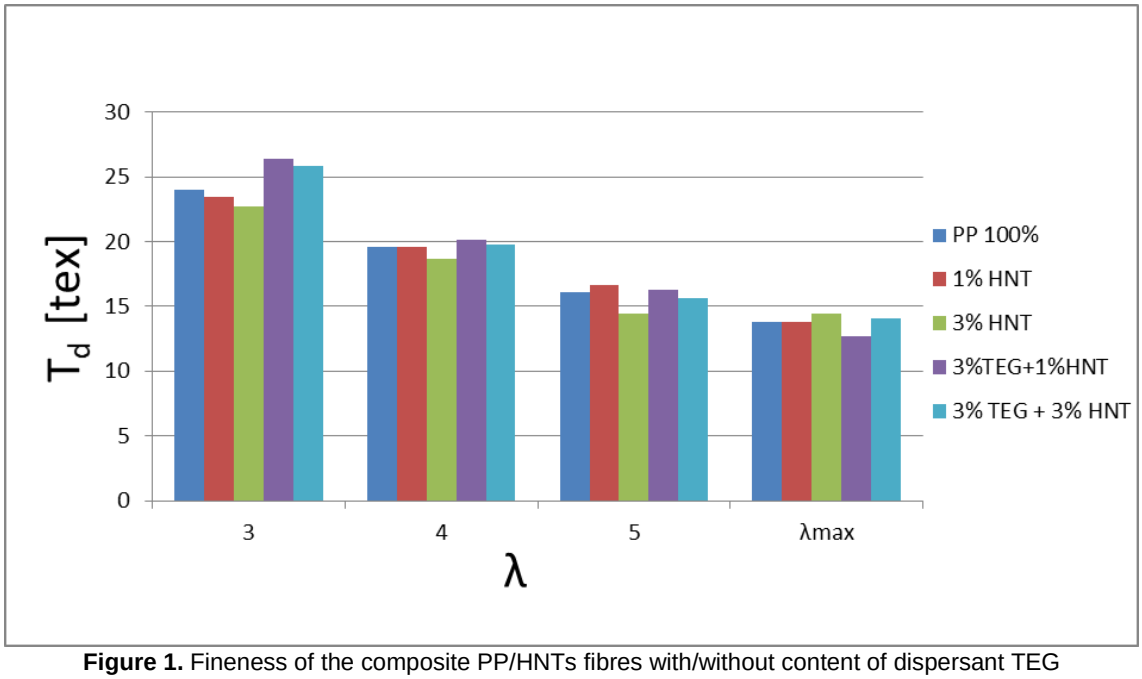

Figure 1. Fineness of the composite PP/HNTs fibres with/without content of dispersant TEG

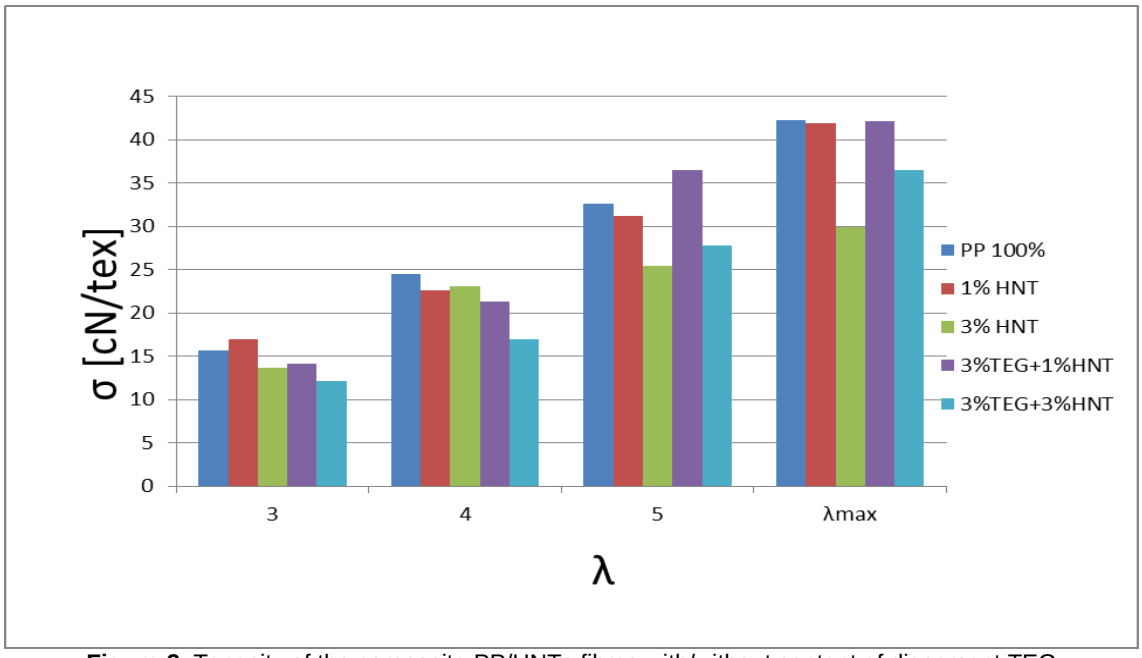

Figure 2. Tenacity of the composite PP/HNTs fibres with/without content of dispersant TEG

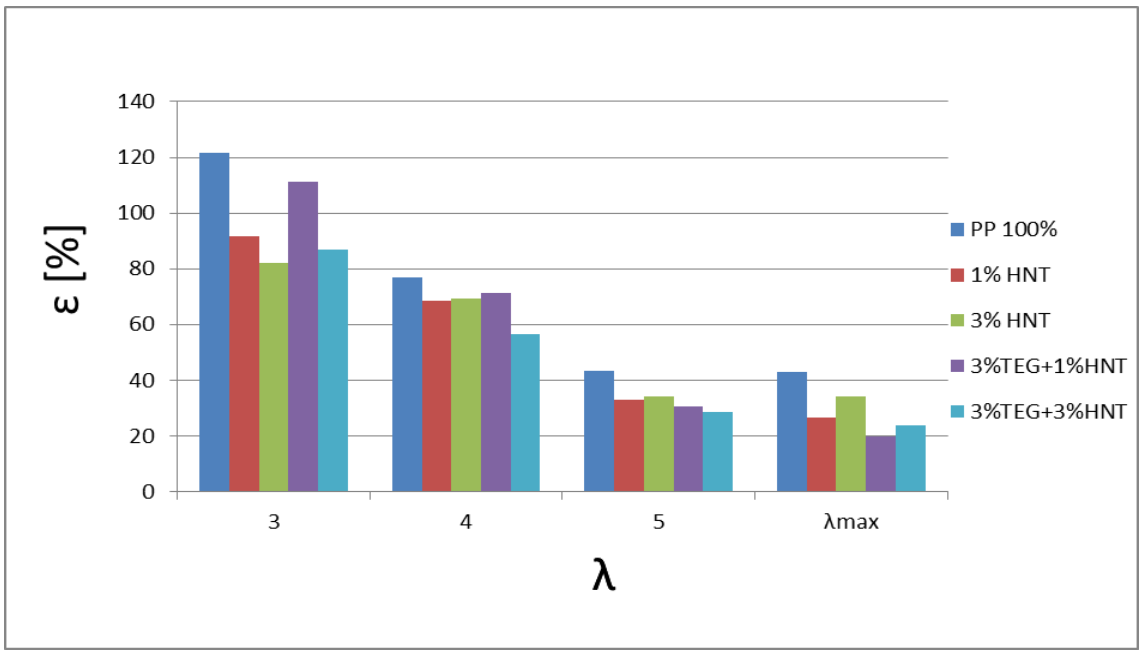

Figure 3. Elongation at break of the composite PP/HNTs fibres with/without content of dispersant TEG

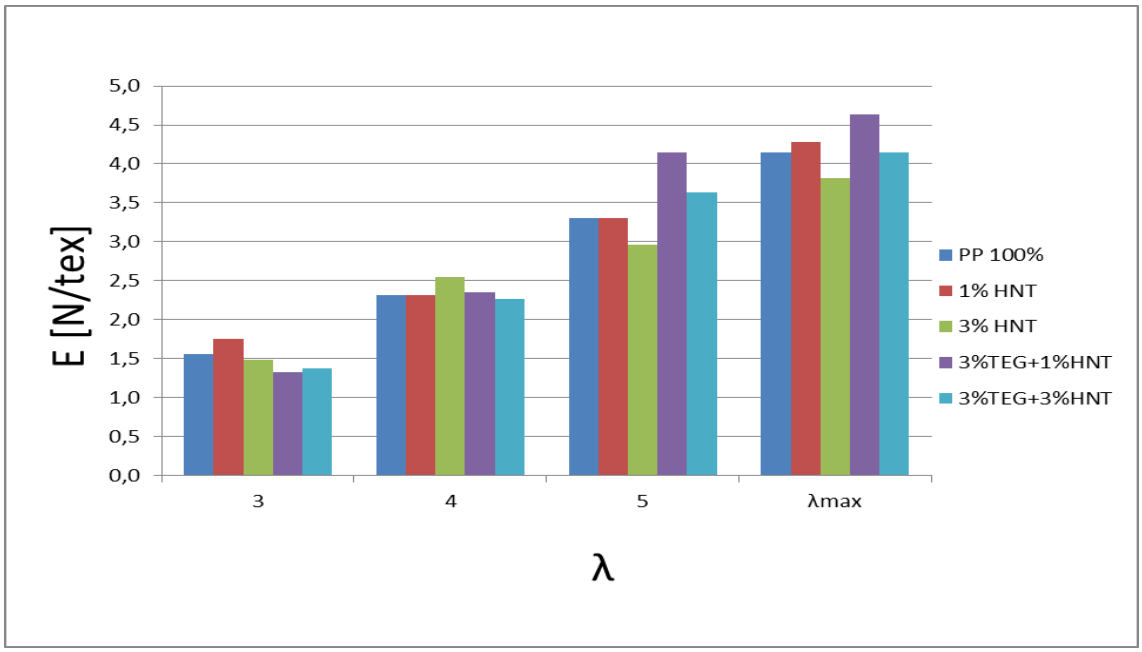

Figure 4. Young´s modulus of the composite PP/HNTs fibres with/without content dispersant TEG

The reinforcing effect of nanoadditives onto thermoplastic matrix is very well known from literature for "low" oriented system prepared by common procedures of extrusion or injection moulding. In highly oriented systems like fibres are is situation different. Particles of nanoadditive during drawing process cause irregularity and nonuniformity in structure of fibre. This phenomenon can be followed on values of tenacity (Fig. 2.) and Young´s modulus (Fig. 4). Drawing caused increase of values of Young´s modulus for all prepared nonmodified and modified PP/HNTs fibres. At content of 1 wt. % of HNTs with content of 3 wt. % non-reactive dispersant TEG in composite PP/HNTs fibres is Young´s modulus the highest for maximal drawing ratio. As was mentioned at tenacity discussion, addition of non-reactive dispersant TEG into blends have positive influence on values of Young's modulus at maximum drawing onto modified PP/HNTs fibres with higher content of nanofiller (3 wt. %) in comparison with modified PP/HNTs fibres without addition of this dispersant.

4. CONCLUSIONS

Polypropylene composites and modified fibres due to their unique properties are still interesting aim of scientific research. HNTs have unique properties (zero cytotoxicity, hollow nanotubular structure, etc.) Those properties predict this type of nanoadditive for wide applications with/without previous pretreatment. In this work was studied influence of content of HNTs and non-reactive dispersant TEG onto mechanical properties of prepared composite fibres.

1. Content of nanoadditive and non-reactive dispersant TEG has no negative influence on spinning process of prepared blends. Fineness of prepared drawn fibres decreasing with higher drawing ratio of prepared fibres.

2. Elongation at break decreased with increasing drawing ratio. Main differences in elongation at break took place at low level drawn fibres (λ=3) where we can observe an influence of nanoadditive onto stiffness of polymer matrix. Increasing of drawing ratio caused that differences in elongation at break are smaller.

3. Composite PP/HNTs fibres with content of 1 wt.% of HNTs and 3 wt.% of nonreactive dispersant TEG reach higher values of tenacity in comparison with nonmodified PP fibres and modified PP/HNTs fibres without content of nonreactive dispersant TEG at maximum drawing ratio. It is evident that this content of HNTs is suitable for modification of this type of PP matrix. Higher content of nanoadditive cause irregularity and nonuniformity of composite fibres during drawing process. That has negative influence onto level of tenacity of modified PP/HNTs. According to expectations the presence of nonreactive dispersant TEG has positive influence onto dispersion of filler particles in PP matrix. These expectations were indirectly confirmed via higher values of tenacity of modified PP/HNTs fibres with content of 3 wt. % of nanofiller and dispersant in comparison with values of tenacity of PP/HNTs fibres without content of this dispersant. Similar results were observed for Young´s modulus evaluation.

ACKNOWLEDGEMENTS

This work was supported by the Slovak Research and Development Agency under contract No. APVV-14-0175.

References

1. *Alexandre*, M., Dubois, P. (2000). Polymer-layered silicate nanocomposites: preparation, properties and uses of a new class of materials. *Material Science and Engineering: Reports*, Vol.28, pp. 1–63, ISSN 0927-796X
2. *Prashantha, K., Soulestin, J., Lacrampe, M. F., Krawczak,P. (2009). Present status and key challenges of carbon nanotubes reinforced polyolefins: a review on nano- composites manufacturing and performance issues. Polymers and Polymer Composites, Vol.17, pp. 205–245, ISSN 1478-2391*
3. *Prashantha, K., Lacrampe, M.F., Krawczak, P. (2011). Processing and characterization of halloysite nanotubes filled polypropylene nanocomposites based on a masterbatch route: effect of halloysites treatment on structural and mechanical properties, eXPRESS Polymer Letters, Vol.5, No.4., pp. 295–307, ISSN 1788-618X*
4. *Shi, Z., Gao, X., Song, D., Zhou, Y., Yan, D. (2007). Preparation of poly(caprolactone) grafted titanate nanotubes. Polymer, Vol. 48, pp. 7516–7522, ISSN 0032-3861*
5. *Auras, R., Harte, B., Selke, S. (2004). An overview of polylactides as packaging materials. Macromolecular Bioscience, Vol. 4, pp. 835–864,ISSN: 1616-5195*
6. *Kale, G., Auras, R., Singh, S. P., Narayan, R. (2007). Biodegradability of polylactide bottles in real and simulated composting conditions. Polymer Testing, Vol. 26, pp.1049–1061, ISSN0142-9418*
7. *Bao, S. P., Tjong, S. C. (2008). Mechanical behaviors o fpolypropylene/carbon nanotube nanocomposites: the effects of loading rate and temperature. Material Science and Engineering: A, Vol. 485, pp. 508–516, ISSN 0921-5093*
8. *Hári, J., Dominkovics, Z., Fekete, E., Pukánszky, B. (2009). Kinetics of structure formation in PP/layered silicate nanocomposites. Express Polymer Letters, Vol.3, pp. 692–702, ISSN 1788-618X*
9. *Papageorgiou, G. Z., Achilias, D. S., Bikiaris, D. N.,Karayannidis, G. P. (2005). Crystallization kinetics and nucleation activity of filler in polypropylene/surface-treatedSiO2nanocomposites. Thermochimica Acta, Vol. 427, pp.117–128, ISSN 0040-6031*
10. *Marney, D. C. O., Russell, L. J., Wu, D. Y., Nguyen, T.,Cramm, D., Rigopoulos, N., Wright, N., Greaves,M. (2008). The suitability of halloysite nanotubes as a fire retardant for nylon 6. Polymer Degradation and Stability, Vol. 93, pp. 1971–1978, ISSN 0141-3910*

11. *Hedicke-Höchstötter, K., Lim G. T., Altstädt, V. (2009). Novel polyamide nanocomposites based on silicate nanotubes of the mineral halloysite. Composites Science and Technology, Vol. 69, pp. 330–334 ISSN 0266-3538*
12. *Du, M., Guo, B., Lei Y., Jia,D. (2007). Thermal decomposition and oxidation ageing behaviour of polypropylene/halloysite nanotube nanocomposites. Polymers and Polymer Composites, Vol.15, pp. 321–328, ISSN 1478-2391*
13. *Du, M., Guo, B., Jia,D. (2010). Newly emerging applications of halloysite nanotubes: A review. Polymer International, Vol. 59, pp. 574–582, ISSN 1097-0126.*
14. *Liu, M. X., Guo, B. C., Du, M. L, Cai, X. J., Jia, D. M. (2007). Properties of halloysite nanotube-epoxy resin hybrids and the interfacial reactions in the systems. Nanotechnology, Vol. 18, pp. 455703, ISSN 1361-6528*
15. *Vergaro, V., Abdullayev, E., Lvov, Y. M., Zeitoun, A., Cingolani, R., Rinaldi, R., Leporatti, St. (2010). Cytocompatibility and uptake of halloysite clay nanotubes. Biomacromolecules,Vol.11, pp. 820–826, ISSN 1526-4602*
16. *Abdullayev, E, Lvov, Y. (2011). Clay nanotubes for controlled release of protective agents – a review. Journal of Nanoscience and Nanotechnology, Vol.11, pp.10007–26, ISSN1533-4899*
17. *Abdullayev, E, Price, R, Shchukin, D, Lvov, Y. (2009). Halloysite tubes as nanocontainers for anticorrosion coating with benzotriazole. Applied Materials and Interfaces,Vol.2, pp. 1437–42, ISSN 1944-8252*
18. *Abdullayev, E, Lvov,Y. (2013). Halloysite clay nanotubes as a ceramic "skeleton" for functional biopolymer composites with sustained drug release. Journal of Materials Chemistry B, Vol.1, pp.2894–90, ISSN 2050-7518*
19. *Kristofic, M.,Vassova, I.,Ujhelyiova, A.,, Ryba, J. (2011). Functionalisation of polypropylene. Part I. Mechanical, electric and sorptive properties of PP fibres modified with concentrates consisting of copolyamides and nanoclay. Fibres & Textiles in Eastern Europe, Vol. 19, pp. 18–22, ISSN 1230-3666*
20. *Ujhelyiova, A.,Slobodova, M.,Ryba, J.,Borsig E.,Vencelova, P. (2012). The effect of inorganic nanoadditives on the thermal, mechanical and UV radiation barrier properties of polypropylene fibres. Open Journal of Organic Polymer Material, Vol. 2, pp. 29–37, ISSN 2164-5736*

MECHANICAL AND THERMAL PROPERTIES OF BIODEGRADABLE FIBRES

Veronika Hrabovská, Marcela Hricová, Jozef Ryba and Anna Ujhelyiová

Faculty of Chemical and Food Technology, Slovak University of Technology in Bratislava,
Department of Plastics, Rubber and Fibres, Institute of Natural and Synthetic Polymers,
Radlinského 9, 812 37 Bratislava
veronika.hrabovska@stuba.sk

Abstract:

The aim of this paper is preparing biodegradable fibres from renewable resources. For preparation of fibres was used pure poly (lacticacid) (PLA) and PLA combine with plasticizers and fluorescent pigment, which can be used as a new material with multifunctional properties produced from renewable and biodegradable materials.The effect of various plasticizers in poly(lactic acid) and various conditions of preparing is presented. Mechanical properties (tenacity and elongation at break, Young's modulus), thermo-mechanical and thermal properties of prepared fibres were evaluated and discussed.

Key words:

biodegradable fibres, poly (lacticacid), plasticizers, fluorescent pigment, thermal properties, mechanical properties

1. Introduction

In present time, increase the global production of polymer waste and a large part cannot be recycled [1]. A big problem is also the gradual depletion of oil resources for the production of synthetic polymers. A suitable alternative are ecological biodegradable polymers - biodegradable polymers or polymers from renewable resources [1, 2]. Their physical or mechanical properties are lower compared to synthetic polymers, which can be improved by the addition of suitable additives or creating blends with other biodegradable polymers [2].

Poly (lacticacid) (PLA) is biodegradable polymer and also the polymer from renewable resources.Fibres from pure PLA have inadequate properties, so the addition of plasticizers to the mixture increases plasticity and resistance to external effects. For a research materials made of PLA have a huge potential bioplasticizers based on citric acid. The most famous is acetyltributylcitrate (ATBC) and 1,2,3-triacetoxypropane (TAC) [3].

The PLA fibers containing fluorescent pigments can be used as a new material with multifunctional properties produce from renewable and biodegradable materials.
The effect of various plasticizers and various concentration of fluorescent pigment in poly (lactic acid) is presented. Mechanical properties (tenacity and elongation at break, Young's modulus), thermo-mechanical and thermal properties were evaluated and discussed.

2. Experimental

2.1. Materials

For preparing fibres poly (lactic acid) 6201D PLA (Ingeo™ biopolymer) (produced by Nature Works LLC), plasticizer Acetyltributylcitrate – ATBC (citrofol B II) (produced by Junbunzlauer Ladenburg GmtH, Germany) and fluorescent pigment EA-15 (produced by RADGLO® EA) were used.
PLA fibres with plasticizer and fluorescent pigment were prepared by spinning of blend to obtain the final concentration of pigment in the fibres.The concentration of plasticizer was 7.5 wt% for all fibres

and the concentrations of fluorescent pigment in fibres were 0.1; 0.3; 0.5 and 0.8 wt%. The spinning temperature was 190°C with the take-up speed 150 $m.min^{-1}$.Fibres were drawn using a laboratory drawing machine at maximal draw ratios λ_{max} at a drawn temperature of 60, 70 and 100°C.

2.2. Methods

Mechanical properties
The mechanical properties (tenacity and elongation at break, Young's modulus) of PLA and modified PLA fibres were evaluated by the Instron 3343 equipment and the mechanical characteristics were determined with according to ISO 2062:1993 from 10 measurements. The initial length of fibres was 125 mm.

Thermo-mechanical properties
Thermo-mechanical characteristics of PLA and modified PLA fibres were measured by equipment Schimadzu TMA-50. There were measured the deformation (extension or shrinkage) of fibres at constant load in the temperature range 30-100°C (heating speed 5°C/min). The length of fibresample was 9.8 mm.

Thermal properties
Thermal properties were measured by DSC 1/750 with ceramic sensor FRS5 with software SW STARe by company Metler Toledo. Conditions used for measurement were: 1. heating 30-190°C, cooling 190-30°C, 2. heating 30-190°C. The speed of heating or cooling was 10°C/min. The measurements were made in inert nitrogen atmosphere. There were determined the glass temperature (T_g), cold crystallization temperature (T_{cc}), cold crystallization enthalpy (ΔH_{cc}),melting temperature (T_m) and melting enthalpy (ΔH_m).

3. Results and discussion

Mechanical properties of PLA and PLA/ATBC fibres with fluorescent pigment
All prepared undrawn fibres were drawn at maximum drawn ratio λ_{max}. Drawn temperature for PLA fibres with fluorescent pigment (PLA/P)was 100°C, for PLA/ATBC fibres was decreased on value 70°C and addition of fluorescent pigment to PLA/ATBC fibres was decreased this value on 60°C. Drawn ratio PLA/P fibres decreases with content of pigment until 0.3 wt%, so we can state that the fluorescent pigment has positive effect for fibres from PLA. Above 0.5 wt% drawn ratio increases. It can be result of effect the higher concentration of pigment, which in this case has the same effect as plasticizers. Drawn ratio modified PLA/ATBC/P fibres with increasing concentration of fluorescent pigment decreased on value 2.9.

Table 1: Drawn ratio for PLA and modified PLA fibres

fibre	T_D [°C]	λ_{max}	fibre	T_D [°C]	λ_{max}
PLA 6201	100	3.1	**PLA + 7.5% ATBC**	70	3.8
PLA + 0.1% pig.	100	2.9	**PLA + 7.5% ATBC + 0.1% pig.**	60	3.0
PLA + 0.3% pig.	100	2.8	**PLA + 7.5% ATBC + 0.3% pig.**	60	3.3
PLA + 0.5% pig.	100	3.2	**PLA + 7.5% ATBC + 0.5% pig.**	60	2.8
PLA + 0.8% pig.	100	3.3	**PLA + 7.5% ATBC + 0.8% pig.**	60	2.9

T_D – drawn temperature

The tenacity at break and Young's modulus of the PLA decrease with content of pigment until 0.3 wt% and the minimum is around 0.1 wt%. Above 0.5 wt%, the tenacity at break and Young's modulus increase again (Figures 1 a,1c). The fibres from PLA with higher concentration of pigment have tenacity at break as well as fibres with addition of plasticizer. The tenacity at break and Young's modulus of the PLA increase with content of pigment until 0.3 wt% and the maximum is in fibres

without fluorescent pigment. Above 0.5 wt%, the tenacity at break and Young's modulus decrease (Figures 1a, 1c).

On Figure 1 b, it can be seen the elongation at break of PLA and PLA/ATBC fibres. The elongation at break of the PLA fibres decreases with content of fluorescent pigment. The elongation at break of the PLA fibres has increasing character with content of fluorescent pigment (Figure 1b).

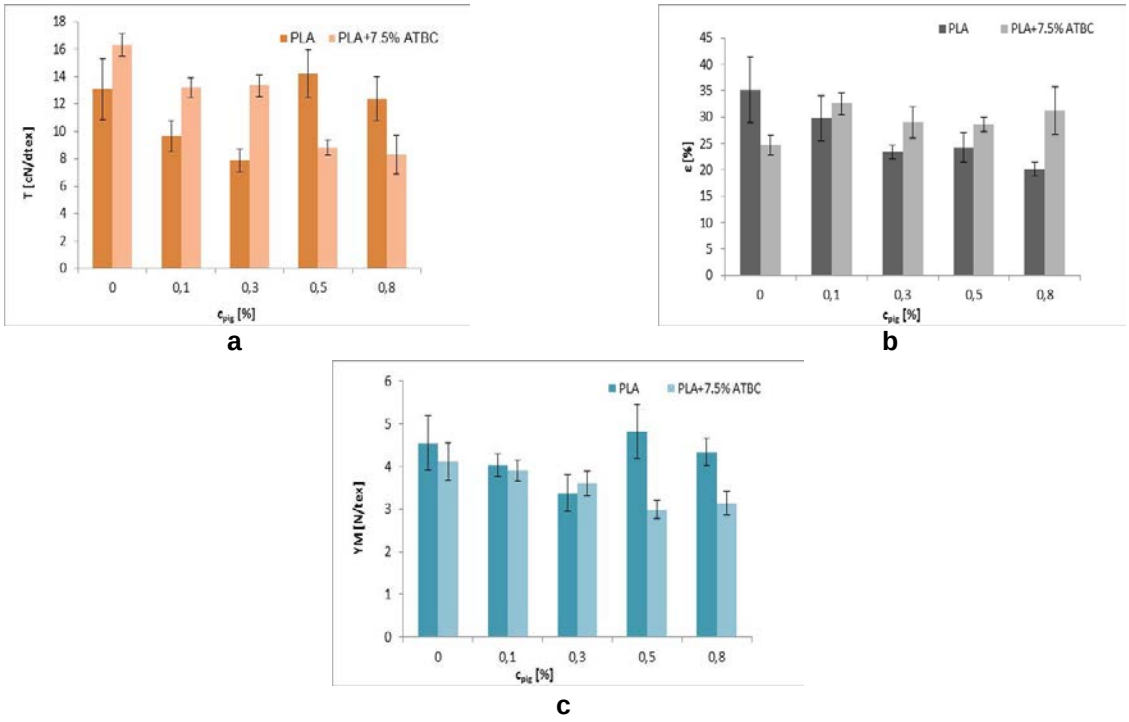

Figure 1: Dependence oftenacity at break (**a**), elongation at break (**b**),Young's modulus (**c**) of PLA/P and modified PLA/ATBC fibres on concentration of fluorescent pigment

Thermo-mechanical properties of PLA and PLA/ATBC fibres with fluorescent pigment

The graphical presentation of dimensional stability (deformation) and temperature of deformation for PLA/P and PLA/ATBC/P fibres and effect of content of fluorescent pigment on deformation of these fibres in dependence on temperature in defined temperature mode can be seen on Figures 2, 3.

The deformation of PLA/P fibres decrease with content of pigment until 0.3 wt% and the value is almost the same. Above 0.5 wt%, the deformation increases with increasing concentration of fluorescent pigment, which has the same effect as plasticizer. For the PLA/ATBC/P fibres is trend of deformation the same, but values of deformation are two times higher (Figure 2). It can be result of effect of plasticizer, which allows movement of the macromolecular chain and this leads to worsening of dimensional stability.

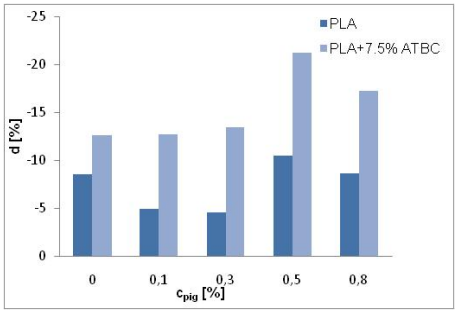

Figure 2: Dependence of deformation (shrinkage) of PLA and modified PLA fibres on concentration of fluorescent pigment

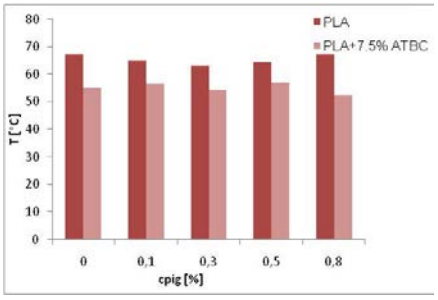

Figure 3: Dependence of temperature of deformation of PLA and modified PLA fibres on concentration of fluorescent pigment

From the graphical presentation on Figure 3 we can show that concentration of fluorescent pigment does not significantly effect on the temperature of deformation PLA/P and PLA/ATBC/P fibres drawn at λ_{max}. PLA/P fibres have higher temperature of deformation in comparison with PLA/ATBC/P fibres.

Thermal properties of PLA/P and PLA/ATBC/P fibres

The glass temperature (Tg) of PLA/P fibres is almost equal. Addition of plasticizer ATBC decreases the T_g. The additions of plasticizer ATBC and fluorescent pigment to the PLA fibers have no effect on melting temperature T_m of fibres (Tables 2, 3). Addition of plasticizer ATBC has no effect on the melting enthalpy ΔH_m. The concentration of 0,1 and 0,3 wt% of pigment and 0,5 and 0,8 wt % of pigment with plasticizer ATBC acts as nucleating agent, which can be seen from higher melting temperature Tm and melting enthalpy ΔHm.

Table 2: Glass temperature Tg, melting temperature Tm, melting enthalpy ΔHm and cold crystallization of PLA/P fibres

fibre	1st heathing			cold crystallization	
	T_g[°C]	T_m [°C]	ΔH_m[J.g^{-1}]	T_{cc} [°C]	ΔH_{cc}[J.g^{-1}]
PLA 6201	59,57	160,04	-41,04	103,69	20,76
PLA + 0.1% pig.	51,59	165,20	-42,97	90,29	20,44
PLA + 0.3% pig.	60,78	164,68	-43,15	103,50	23,51
PLA + 0.5% pig.	59,58	159,68	-41,85	104,69	24,23
PLA + 0.8% pig.	59,58	159,75	-41,73	105,70	22,82

Table 3: Glass temperature Tg, melting temperature Tm, melting enthalpy ΔHm and cold crystallization of PLA/P fibres

fibre	1stheathing			cold crystallization	
	T_g[°C]	T_m [°C]	ΔH_m[J.g^{-1}]	T_c[°C]	ΔH_c[J.g^{-1}]
PLA + 7.5% ATBC	50,09	151,75	-39,36	90,11	8,46
PLA + 7.5% ATBC + 0.1% pig.	49,96	150,97	-39,21	98,23	10,12
PLA + 7.5% ATBC + 0.3% pig.	48,90	149,63	-39,32	92,36	8,66
PLA + 7.5% ATBC + 0.5% pig.	51,24	165,46	-41,36	91,98	13,78
PLA + 7.5% ATBC + 0.8% pig.	60,61	164,80	-43,50	103,66	23,57

4. CONCLUSIONS

The work was aimed at the preparation of PLA fibres with contain of plasticizer from biodegradable a renewable materials. The results obtained by experimental work have confirmed that it is possible to prepare the PLA fibres and modified PLA fibres with plasticizer and fluorescent pigment for the multifunctional fibres for application as safety materials.

The properties of PLA fibres and modified PLA fibres may be refined in future by other types of PLA, plasticizers and optimization of the processing conditions.

ACKNOWLEDGEMENTS

This work was supported by the Slovak Research and Development Agency under the contract No: APVV-14-0175.

References

1. *Auras, R. et al: Poly (lactic acid): Synthesis, Structures, Properties, Processing and Applications, Wiley 2010, ISBN: 978-0-470-29366-9*
2. *Sin, T.L. et al: Polylactic Acid; PLA Biopolymer Technology and Applications, GB 2013, ISBN: 978-1-43-77-4459-0*
3. *Avinc, O. et al: Investigation of the influence of different commercial softeners on the stability of poly(lactic acid) fabrics during storage, Polymer Degradation and Stability, 95 (2010), pp. 214-224, ISSN: 0141-3910*

EFFECT OF PROCESS CONDITIONS ON PROPERTIES OF MODIFIED POLYPROPYLENE FIBRES

Anna Ujhelyiová, Mária Petková, Jana Johanidesová, Leona Omaníková

Faculty of Chemical and Food Technology, Slovak University of Technology in Bratislava, Institute of Natural and Synthetic Polymers, Department of Plastics, Rubber and Fibres, Radlinského 9, 812 37 Bratislava, anna.ujhelyiova@stuba.sk

Abstract:

Physical modification of polypropylene (PP) fibres by inorganic additives insures more intense anchoring of PP fibres in constructional composites, what leads to expressive improve of functional of PP fibres in relation to transmission and absorption of deformation energy to form and load composites. This work focuses on the preparation of PP fibres modified with inorganic nanoadditive halloysite for constructional composites. It is investigated the effect of conditions of drawing and stabilization on the thermomechanical and mechanical properties of prepared modified PP fibres. The drawing temperature and stabilization change of properties observed of modified PP fibres with halloysite.

Key words:

polypropylene fibres, drawing temperature, stabilization, inorganic nanoadditive, structure and properties of modified PP fibres

1. Introduction

Unmodified short and long polypropylene (PP) fibres are standard used in constructional composites. The PP fibres used as reinforcement in construction composites induce to the reduction of cracks propagation, increase of flexural and bending strength, improve of impact resistance. Their advance is very good chemical resistance and low sensitivity to moisture. [1] But, its unpolar hydrophobic physical and chemical inactive polyolephinic character does not provide to create the chemical as well as physical intermolecular bonds between concrete matrix and fibres a low affinity of PP fibre to the cement matrix resulted from. One from disadvantages is mainly the decreasing of absorption ability of deformation energy during the load of the concrete composite in flexure and bending strength and the increasing of the release of fibre from the composite instead the deformation of fibres as the composite component is became [2].

One from possible modification of PP fibres for improvement of the chemical and physical interaction between of fibre and the concrete matrix is a modification with nanoparticles of inorganic fillers. If the particles incorporated in the fibre surface then the interactions between the inorganic particles in fibre surface and inorganic concrete matrix would cause the increase of significantly stronger bonds. Some knowledge from application of PP fibres in concrete composites with nano-SiO_2 particles is interested. It was presented that physical and chemical effects of nanoparticles are helping to the reduction of water film around PP fibre and nanofillers decrease porosity at the interface fibre/matrix. Results also showed that nano-SiO_2 improves the mechanical parameters of fibre-concrete composite [3].

PP is relative high brittleness and addition of inorganic nanoadditives ($CaCO_3$, SiO_2,TiO_2 and halloysite) also eliminates this property. The high agglomeration ability and worse dispersion of nanoparticles into PP matrix is caused by the high surface energy of nanoparticles and because the

improvement of their mechanical properties is very difficult. Therefore, the specific methods to the preparation of nanoparticles/polymer composites are used [4]. It was ascertained that yet small amount of nanoparticles results an effective increase of flexural and bending strength, elastic module and rigidity [5, 6].
Halloysite belongs to a class of clay minerals with nanotubular structure. The various conditions of crystallization and geological formation caused the occurrence of several morphologies - tubular, plate-shaped and spherical, of which the most common and the most important is the tubular structure. The halloysite is very suitable filler for polymers for its relatively low cost, convenient tubular structure, as well as bearings widespread throughout the world [7].
This work focuses on the preparation of PP fibres modified with inorganic nanoadditive halloysite in presence of dispersant Tegopren (TEG) for constructional composites. It is investigated the effect of conditions of drawing and stabilization on the supermolecular structure and thermomechanical and mechanical properties of prepared modified PP fibres. The drawing temperature and stabilization change of properties observed of modified PP fibres with halloysite.

2. Experimental

2.1. Materials

Isotactic polypropylene (PP, TATREN HT2511) with MFR = 25 g/10 min (produced by Slovnaft Company, Slovakia), halloysite (HNT) as nanoadditive (Aldrich Chemistry, product of USA) and different dispersants - tegopren 6875 (TEG) (organomodified siloxane, produced by Evonik Industies) were used for the preparation of fibers.

Fibre preparation

At first, PP concentrates are consisting of pure PP, inorganic nanoadditive of halloysite (1% wt.) and dispersant Tegopren (3% wt.) were mixed and subsequently they were melting using the twin screw extruder. PP fibres and modified PP fibres (PP/HNT/TEG) with nanoadditive of halloysite were prepared using the pilot continual line by the spinning of masterbatches at the temperature 240°C with the take-up speed 150 $m.min^{-1}$ at the spinning. The undrawn fibres were drawn at the maximum drawing ratios λ_{max} at the various drawing temperatures – 90-120 °C. The prepared modified PP/HNT/TEG fibres were stabilised at the temperature 90; 110 and 130 °C during 3 min.

2.2. Methods

Mechanical properties

Tenacity at break and elongation at break and Young's modulus represent the mechanical properties. The mechanical properties of PP and modified PP fibers were evaluated by the Instron 3343 equipment (USA). Measuring conditions were the length of fiber 125 mm and rate of clamp 500 mm/min. The mechanical characteristics of the PP and modified PP/HNT/TEG fibres were determined in accordance with standard (Standard ISO 2062:1993).

Thermo-mechanical properties

Thermo-mechanical characteristics of PP and modified PP/HNT/TEG fibres were measured by equipment Schimadzu TMA-50 (Japan). There were measured the deformation (extension or shrinkage) and the temperature of first deformation of fibre. Conditions of measurement were following: in the temperature range from room temperature to 383K, at the heating rate 5 K/min, and fiber length 9.8 mm.

3. Results and discussion

On the previous works there were prepared of undrawn modified PP/HNT/TEG fibres containing 1 % of HNT and 3% of TEG. These fibres were drawn at the maximum drawn ratio λ_{max} at the various drawing temperatures. It was observed the effect of drawing temperatures on the mechanical and thermomechanical properties (Figs 1 and 2).

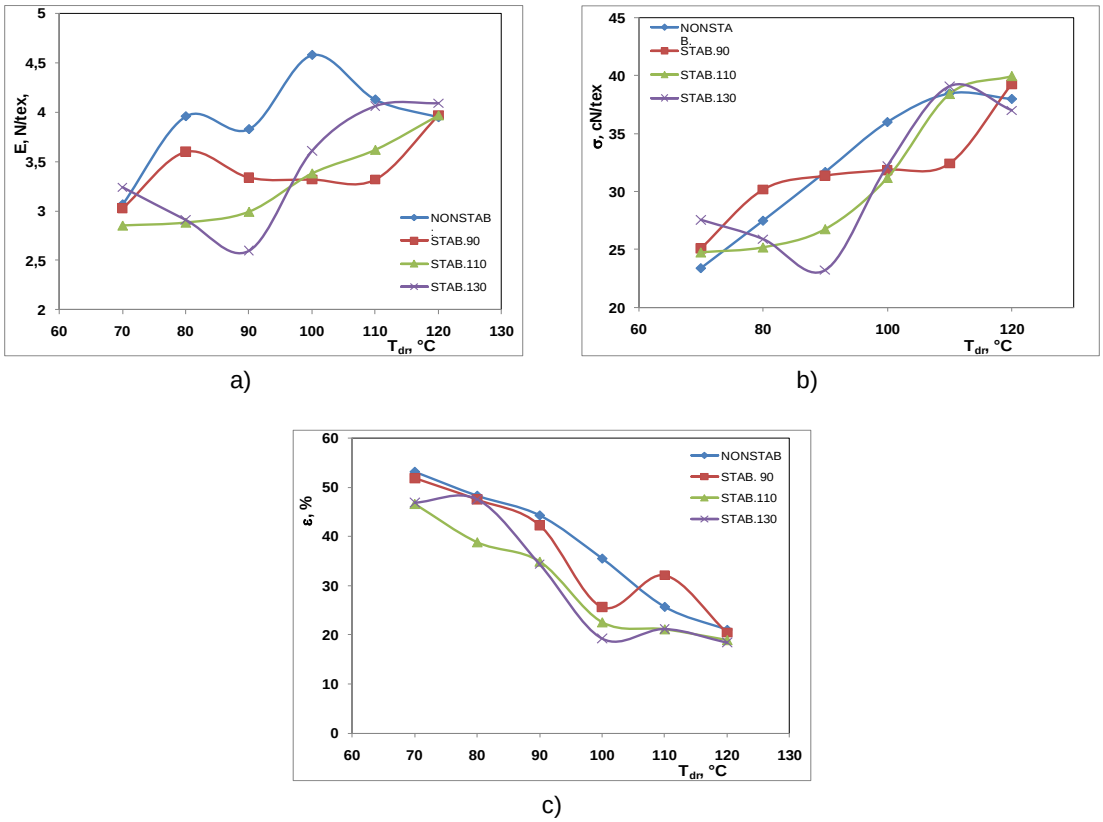

Figure 1. Dependence of Young′s modulus (a), tenacity at the break (b) and elongation at the break (c) of nonstabilized and stabilized modified PP/HNT/TEG fibres on drawing temperatures at their preparation

The Young′s modulus and tenacity at the break of modified PP/HNT/TEG fibres nonstabilized as well as stabilized at all temperature increase with the increase of drawing temperature (Fig. 1a, b). The increase of drawing temperature at the preparation of modified PP/HNT/TEG fibres decreases the final elongation at the break of these fibres (Fig. 1c). At the higher drawn temperatures forms the more stabilized structure with the higher Young′s modulus and tenacity at the break and lower the elongation at the break. The stabilization processes due to the decrease of all mechanical properties in comparison with the nonstabilized PP/HNT/TEG fibres.

The results of the thermomechanical analysis, dimensional stability (d) and temperature of first deformation (T_D) of the modified PP/HNT/TEG fibres drawn at the various drawing temperature are in Fig. 2. The drawing temperature does not influence the thermomechanical parameters of nonstabilized and stabilized modified PP/HNT/TEG fibres. The more influence on the change of themomechanical parameters was observed for modified PP/HNT/TEG fibres stabilized at the various temperature. At the higher temperature of stabilization an internal stresses embedded during the monoaxial orientation of fibres in the spinning and drawing relax and stabilize the created supermolecular structure. Because the improved dimensional stability and higher temperature of first deformation of PP/HNT/TEG fibres stabilized at the higher temperature (110 and 120 °C) are results of the more stable structure of these fibres.

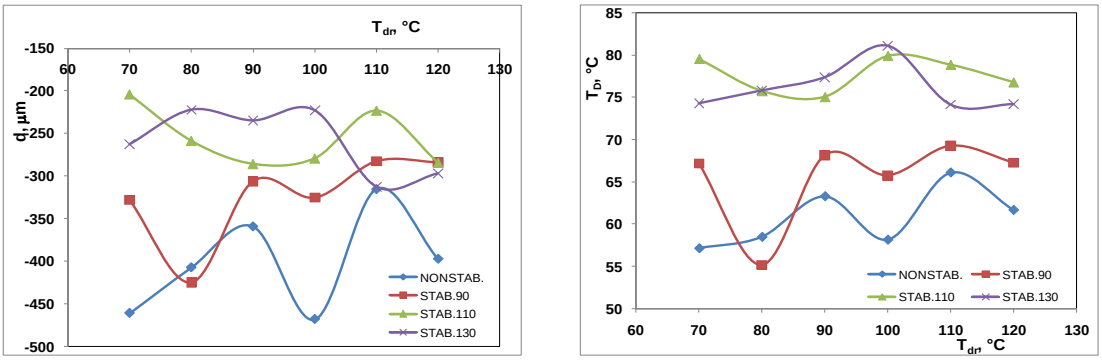

a) b)

Figure 2. Dependencies of deformation (shrinkage – d, μm, a) and temperature of first deformation (T_D, b) of nonstabilized and stabilized modified PP/HNT/TEG fibres at their preparation

4. CONCLUSIONS

The work was aimed at the evaluation of effect of the drawing temperature and the stabilization conditions on the mechanical and thermomechanical properties of modified PP/HNT/TEG fibres. The results obtained by experimental work show that the mechanical properties of observed modified PP/HNT/TEG fibres are influenced by drawing temperature as well as stabilization conditions. The thermomechanical properties of these fibres are influenced only the stabilization conditions.

ACKNOWLEDGEMENTS

This work was supported by the Slovak Research and Development Agency under the contract No: APVV-14-0175.

References

1. *Kim, S. B., et al. (2010). Cement & Concrete Composites,* ***32,*** *232–240.*
2. *Zollo, R. F., (1997). Cement and Concrete Compositer,* ***19,*** *107-122.*
3. *Lane, J.M., Hourston, D.J. (1993) Surface treatments of polyolefins. Progress in Organic Coatings,* ***21,*** *269-284.*
4. *Wang, W., et al. (2006). Progress of the Surface Modification of PP Fiber Used in Concrete. Polymer-Plastics Technology and Engineering,* ***45,*** *29-34.*
5. *Naik, T.R., et al. (1996). Use of post-consumer waste plastics in cement-based composites. Cement and Concrete Research,* ***26****, 1489-1492.*
6. *Koh, S.K., et al. (2002). Altering a polymer surface chemical structure by an ion-assisted reaction. Journal of Adhesion Science and Technology,* ***16,*** *129-142.*
7. *Du, M., Guo, B., Jia, D. (2010). Newly emerging applications of halloysite nanotubes: a review. Polymer International, 59, 574-582.*

DEVELOPING SURFACE CHARACTERIZATION OF JUTE FIBERS VIA HYDROPHOBIC MODIFICATION FOR POLYMERIC DOPED MATERIALS

Yasemin SEKİ, Aysun AKŞİT

Department of Textile Engineering, Dokuz Eylul University, Tınaztepe Campus, 35397, Buca, Izmir, TURKEY

Abstract:

The effects of surface modification on jute characterization were investigated in this current study. For this purpose, Jute were modified with stearic acid (StJ), silicone oil (ScJ), tetra ethoxy silane (SiJ) and laccase enzyme with tween 20 (LaJ) as a mediator. Unmodified and modified jute were investigated by fourier transform infrared spectroscopy (FTIR), thermogravimetric analysis (TGA), determining moisture content scanning electron microscopy (SEM). Silane, silicone oil and stearic acid modifications decreased hydrogen bond index and moisture content of the jute. However, J and LaJ presented similar chemical properties. Morphological observations confirmed the structure of the jute as a bundle of fiber cells after modification but also a layer covering fiber surface after silicone oil treatment. According to the findings of the analyses, silicone oil modification can be a good alternative for surface modification for cellulose based fibers for polymeric composite materials. The highest improvement in thermal stability of the jute was achieved with silicone oil modification.

Key words:

Jute, modification, silicone oil, polymeric, composite

1. Introduction

Usability of cellulose based natural fibers as an additive material for polymeric composites have attracted attention due to their light weight, non-toxicity, easily availability in nature, less health hazards, absorbing CO_2 during their growth and relatively high specific modulus in comparison with other conventional fibers (Hossain et al., 2010). In spite of their advantageous properties, their high moisture absorption tendency, low surface wettability and high amount of non-cellulosic components on surface of the jute fibers restricted their utilization in composites. In order to improve the compatibility between non-polar polymers and cellulosic fibers, their surface should be modified (Bulut and Akşit, 2013; Liu et al., 2016).

In this study, jute fibers which are commoly used in fiber reinforced composite materials were modified with were modified with laccase enzyme/tween 20 mediator (LaJ), tetra ethoxy silane (SiJ), stearic acid (StJ) and silicone oil (ScJ). The changes in jute characteristics were analyzed with fourier transform infrared spectroscopy (FTIR), determining moisture content scanning electron microscopy (SEM).

2. Experimental

2.1. Materials

Jute yarns were supplied from a local company. Stearic acid ($CH_3(CH_2)_{16}COOH$), tetra ethoxy silane ($C_8H_{20}O_4Si$) and silicone oil which are used for modification processes were supplied from Setaş Kimya, Turkey. Laccase enzyme was locally provided and tween 20 ($C_{58}H_{114}O_{26}$) as a mediator was supplied from Sigma-Aldrich.

2.2. Methods

Jute yarns were ground to obtain jute fibers as in particle form. Firstly, jute yarns were ground with Retsch Cutting Mill SM 100 grinder using a sieve having holes of 250 µm. Then, jute fibers in powder form were also ground in Fritsch Pulverisette 7 (Oberstein, Germany) grinder at the speed of 850 rpm for 20 min to decrease the size of the jute particles.

1 g of jute particles were continuously stirred in 80/20 v/v 0.2M acetate buffer/ethanol solution with 1.0U/mL laccase and 5mM tween 20 at 50oC for 4h. After treatment, jute particles were washed with distilled water at 80oC twice and then extracted in acetone. The treated jute particles were dried at ambient temperature (Dong et al., 2014). Jute particles were modified with 1 % v/v stearic acid in ethanol solution at 20oC for 10 min. After treatment, fibers were oven-dried at 80oC for 45 min (Spoljaric et al., 2009). For silicone oil modification, the procedure of the stearic acid treatment was applied. Prior to silane treatment, 5 wt% tetra ethoxy silane was hydrolyzed in 80/20 (v/v) ethanol/water solution for 2h. After modification, jute particles were treated in hydrolyzed silane solution at 80oC for 2h. Then, the jute particles were washed with 80/20 (v/v) ethanol/water solution for three times and dried for 2 days at ambient temperature (Rachini et al., 2012).

The effects of modification on jute were assessed with FTIR, TGA, SEM and determination of moisture content.

3. Results and discussion

FTIR spectra of the unmodified and modified jute particles are presented in Figure 1. As a first, it is clearly seen in Figure 1 that FTIR spectrum of J and LaJ are very similar. This may be because of that treatment with laccase enzyme slightly changed the jute. The absorption band in the range of 1,636-1,643cm^{-1} indicates COO- stretching and absorbed water in crystalline cellulose (Dong et al., 2014). The peak in this band could not be seen after the modifications with stearic acid, silicone oil, and silane. Although the peaks at 1,051 cm^{-1} and 1,105 cm^{-1} absorption bands indicating C-O-C glicosidic ether bands and C-OH stretching vibrations disappeared after silicone oil modification, new peaks at 2,963 cm^{-1} (Si-O), 1,259 cm^{-1} (Si-O), 864 cm^{-1} (Si-O-Si) and 795 cm^{-1} (Si-C) were obtained in the spectrum of ScJ (Matrajit et al., 2005; Jahagirgar and Tiwari, 2004).

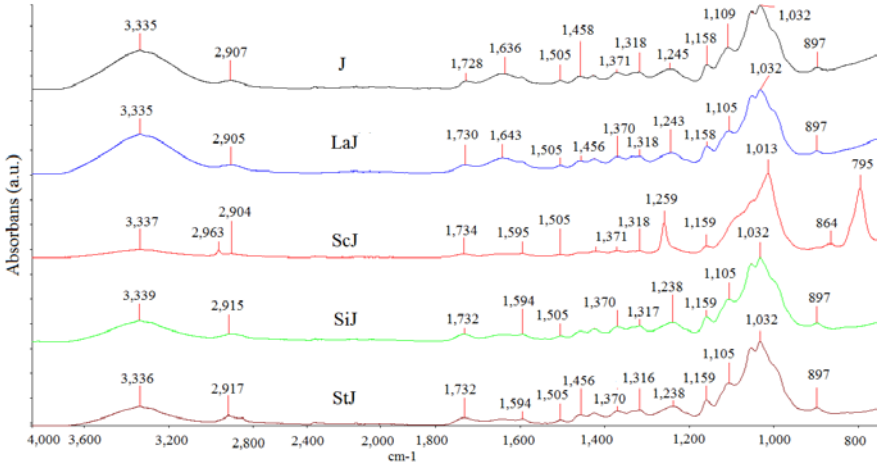

Figure 1. FTIR spectra of the jute

Figure 2 presents the moisture content of the unmodified and modified jute. It is clearly observed that the modification processes influenced the moisture content of the jute. Laccase/tween 20 treatment increased moisture content of J by 38% whereas silane, stearic acid and silicone oil modifications reduced moisture content of J by 57, 67 and 74%, respectively. Treatment with coupling agents and

surface agents such as stearic acid and silicone oil may result in reduction in moisture content of the jute. In case of laccase enzyme treatment, cleaning effect on the surface of the fiber may have increased the moisture content of J.

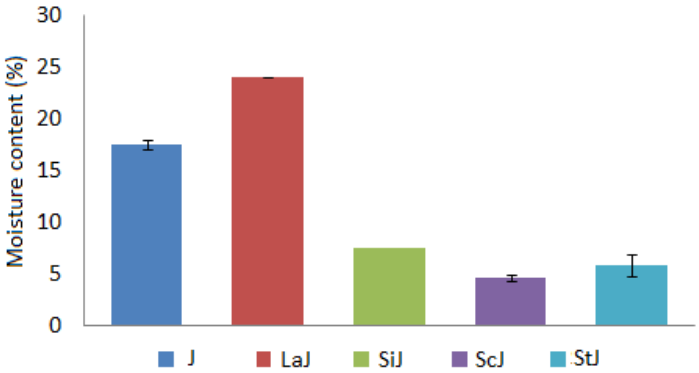

Figure 2. Moisture content of the jute

TGA analysis was performed to evaluate effect of surface modification on thermal stability of the jute. DTG-TGA graphics of the jute are depicted in Figure 3 and the results are listed in Table 1. T_i, T_m and $T_{50\%}$ correspond to initial degradation temperature, maximum degradation temperature and the temperature at which 50% weight loss occurs, respectively. It is clearly understood in Table 1 that all modification processes improved the Ti of the jute. As can be seen from DTG curves of the jute, a shoulder around 300ºC can be noticed. This may mainly correspond to the thermal depolymerization of hemicellulose and the cleavage of glycosidic linkages of cellulose (De Rosa et al., 2010). In order to investigate the values in details, although the Tm of the modified jute are similar, the lowest related weight loss is obtained for ScJ. Additionally, the highest $T_{50\%}$ was also obtained for ScJ. Weight loss corresponding until 600ºC for all of the jute changes between 78 and 81%. This step is mainly due to decomposition of α-cellulose available in the jute (Seki et al., 2014). As a conclusion, the highest improvement in thermal stability of the jute was achieved with silicone oil modification.

Table 1. TGA parameters of the unmodified and modified jute

	T_i (ºC)	T_m (ºC)	$T_{50\%}$ (ºC)	Weight loss at T_m (%)	Weight loss at 600ºC (%)
J	230.0	368.2	340.8	57.4	79
LaJ	232.0	375.8	360.0	64.5	81
SiJ	235.0	373.5	370.4	54.4	79
StJ	236.0	378.2	374.4	55.2	78
ScJ	241.0	378.9	385.6	43.1	79

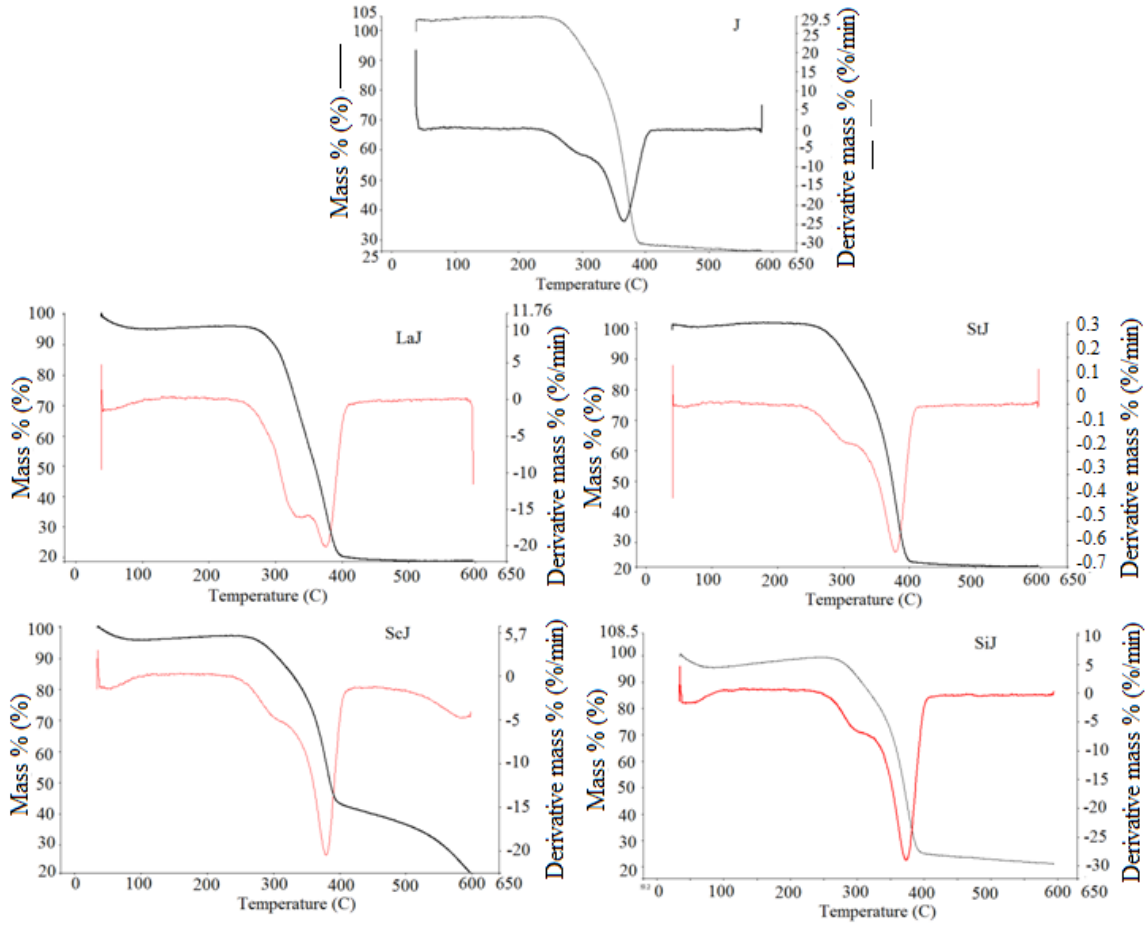

Figure 3. DTG-TGA graphics of the jute

Figure 4 shows SEM images of the jute. In Figure 4 both of the jute exist as a bundle of fibers which are composed of individual fiber cells and also covered with surface impurities. In the case of ScJ, silicone oil particles in different sizes dispersed can be observed on surface of the jute.

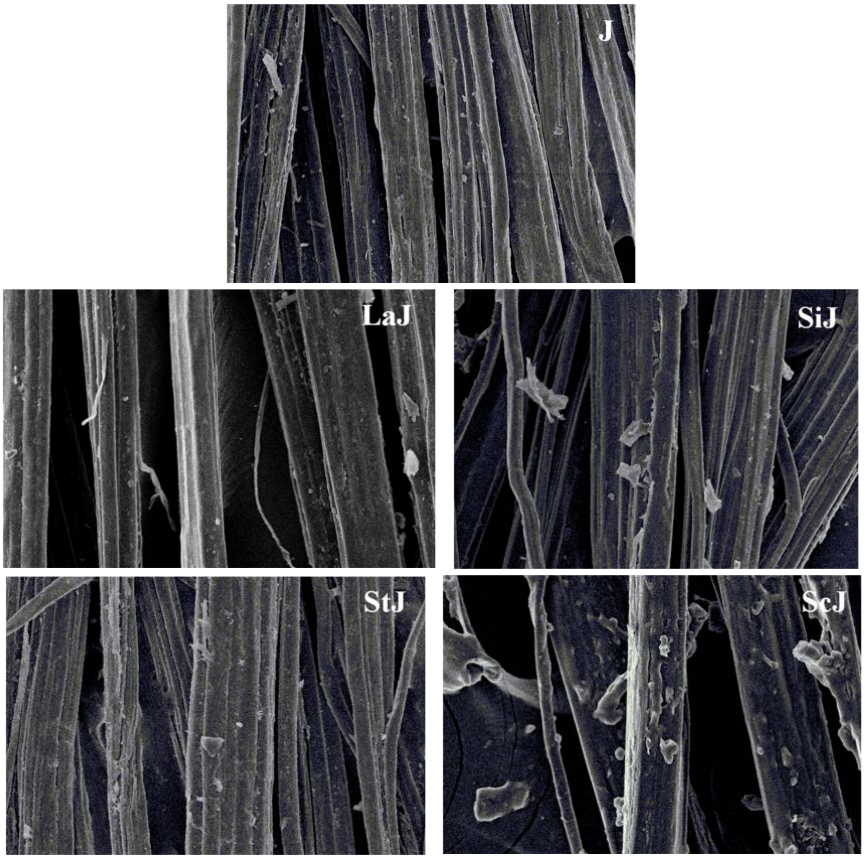

Figure 3. SEM images of the jute (x500)

4. CONCLUSIONS

In this study, the effects of laccase/tween 20, silane, stearic acid and silicone oil modifications on jute fiber were investigated. The modified jutes were characterized with FTIR, SEM and determination of moisture content. With the application of silicone oil, a new absorption peaks are determined which can be attributed to Si-O, Si-C and Si-O-Si bands on jute fiber. The addition of silane coupling agent, silicone oil and stearic acid significantly hydrophilicity related to moisture absorption of the unmodified jute. Additionally, SEM images are similar for the jute fibers, but silicone layer is observable on the surface of the ScJ. Consequently, silicone oil modification is thought to be a good alternative for cellulose based fibers for polymeric composite manufacturing.

References

1. *Hossain M.K., Dewan, M.W., Hosur, M., Jeelani, S., (2010). Surface modification and performance analysis of jute based nanophased green composites. NSTI-Naotech 1, 697-700 .*
2. *Bulut, Y., Akşit, A., (2013). A comparative study on chemical treatment of jute fiber: potassium dichromate, potassium permanganate and sodium perborate trihydrate. Cellulose, 20, 3155-3164,*
3. *Liu, R., Dong, A., Fan, X., Yu, Y., Yuan, J., Wang, P., Wang, Q., Cavaco-Paulo, A., (2016) Enzymatic hydrophobic modification of jute fibers via grafting to reinforce composites. Applied Biochemistry and Biotechnology, DOI 10.1007/s12010-015-1971-x.*
4. *Dong, A., Yuan, J., Wang, Q., Fan, X., (2014) Modification of jute fabric via laccase/t-BHP-mediated graft polymerization with acrylamide. Journal of Applied Polymer Science, 131,1-6*
5. *Spoljaric, S., Genovese, A., Shanks, R.A., (2009) Polypropylene–microcrystalline cellulose composites with enhanced compatibility and properties. Composites Part A, 40, 791-799.*
6. *Rachini, A., Le Troedec, M., Peyratout, C., Smith, A., (2012). Chemical modification of hemp fibers by silane coupling agents. Journal of Applied Polymer Science, 123, 601-610*
7. *Matrajit, G., Munoz Caro, G.M., Dratois, E., d'Hendecourt, L., Deboffle, D., Borg, J., (2005). FTIR analysis of the organics in IDPs: Comparison with the IR spectra of the diffuse interstellar medium. Astron Astrophys, 433, 979-95.*
8. *Jahagirdar, C.J., Tiwari, L.B., (2004). Effect of dichlorodimethylsilane on plasma treated cotton fabric. Journal of Physics, 62,1099-1109.*
9. *De Rosa, I.M., Kenny, J.M., Puglia, D., Santulli, C., Sarasini, F., (2010). Morphological, thermal and mechanical characterization of okra (Abelmoschus esculentus) fibres as potential reinforcement in polymer composites. Composites Science and Technology, 70, 116–122*
10. *Seki, Y., Seki, Y., Sarikanat, M., Sever, K., Durmuşkahya, C., Bozaci, E., (2014). Evaluation of linden fibre as a potential reinforcement material for polymer composites. Journal of Industrial Textiles DOI: 10.1177/1528083714557055.*

BANANA PLANT WASTE AS RAW MATERIAL FOR CELLULOSE EXTRACTION

Umit Halis Erdogan , Figen Selli*, Hicran Duran

Dokuz Eylul University, Department of Textile Engineering, Tinaztepe Campus, 35160, Buca, Izmir, Turkey
*Corresponding author: Figen Selli, figenselli@gmail.com

Abstract

Renewable raw materials and sustainability has a widespread significance for all types of industry. Cellulose, which has a great potential as a raw material for various branch of industry including textile, is the main component of most vegetable fibers. Cellulose from different vegetable resources can be isolated using chemical and mechanical treatments. Chemical treatments are effective for delignification. Based on this, the aim of our study is extraction of sustainable cellulose from ligno-cellulosic banana plant waste using chemical treatment. First, the waste banana plants were supplied as resource of cellulose considering the previous works about this topic and preliminary experimental studies. After that, the composition of the extract was determined in order to confirm the high cellulose content. At the next stage of this study, organic acid extraction method was used to extract cellulose from banana plant wastes. The cellulose content of banana plant was determined as 57 % and 24 % of hemicellulose. The cellulose was successfully extracted from banana plant wastes. Characterization results suggest that cellulose, an important raw material for textile, pulp and paper, composite and defense industries, can be effectively regained from banana plant wastes.

Key words

Cellulose, extraction, banana plant wastes, pulping

1. Introduction

Recently, research has focused on sustainability, renewable materials and recycling in the textile sector in conjunction with the other branches of industry. Cellulose is the most abundant natural polymer that can be used as a raw material in various industries such as paper, food and composite materials. Vegetable fibers are one of the raw materials of textile and they content various amounts of cellulose. Vegetable fiber wastes in the forms of cotton linter, fiber, yarn and fabric are being produced during production processes. Cellulose can be extracted from banana plant with mechanical, chemical treatments and also by combining these two types of treatment [2]. Banana is one of the most important fruit and vegetable crop plants. Banana pseudo stem is known as a potential cellulose source, though usually discarded as agricultural waste in many countries [1, 3]. Turkey has a high production capacity for banana plants with 206,346 tons in 2012 [7]. Based on this high production capacity in Turkey we aimed to recycle cellulose from banana plant wastes (Fig.1).

Figure 1. Waste Banana Plants-Fibers

2. Experimental

2.1. Materials

Banana waste plants were obtained from Anamur/Turkey. The chemical treatment materials used in this work were: Formic Acid (98-100 %), Hydrogen Peroxide (35 %), Ethanol, Benzene, Ethylenediaminetetraacetic acid (EDTA) and Hydrochloric acid (37 %). All chemicals are purchased from Sigma Aldrich.

2.2. Methods

2.2.1. Determination of Chemical Composition

Chemical composition of the samples was determined using China Textile Industry Standard process steps from the article 'Evaluation of liquid ammonia treatment on surface characteristics of hemp fiber' [6]. In the first step, banana waste plants are dried for 12 hours at 100 °C in order to achieve to dry weight of samples. Pectin composition of samples was determined with 0.5 % EDTA (ethylene diamine tetra acetic acid) solution. Hydrochloric acid (HCl) was used to determine the hemicellulose content and sulphuric acid (H_2SO_4) was used to determine both the cellulose and lignin content of the samples.

2.2.2. Pre-cleaning of Banana Waste Plants

In our study; at first cleaning of waste jute fibers with hot distilled water were carried out. Banana waste plants are cut into 1-2 cm small pieces and washed for 3 hours at boiling temperature. Afterwards, they are dried in an oven for 12 hours at 105 °C. Materials after hot wash pre-cleaning is given in (Figure 2).

Figure 2. Material after Hot Wash Cleaning

Figure 3. Materials after Dewaxing

Following the hot wash cleaning treatment, banana waste plants are washed with Ethanol/Benzene 1:2 v/v solution in order to perform dewaxing. Dewaxing treatment is carried out for 4 hours in a Soxhlet apparatus at boiling temparature. Banana waste plants after dewaxing is given in Figure 3.

2.2.3. Extraction of Cellulose

Extraction of cellulose and fractionating the non-cellulosic materials were performed by organic acid pulping. Organic acid pulping method is chosen due to preliminary tests and literature (5). Firstly an organic acid, formic acid (CH_2O_2) 90% concentration, was used to treat banana plant wastes as initial removal of the non-cellulosic materials. Banana plant wastes are washed with formic acid for 150 minutes at 80° C and then dried. Material during formic acid treatment and after the treatment is given in Figure 4 and 5.

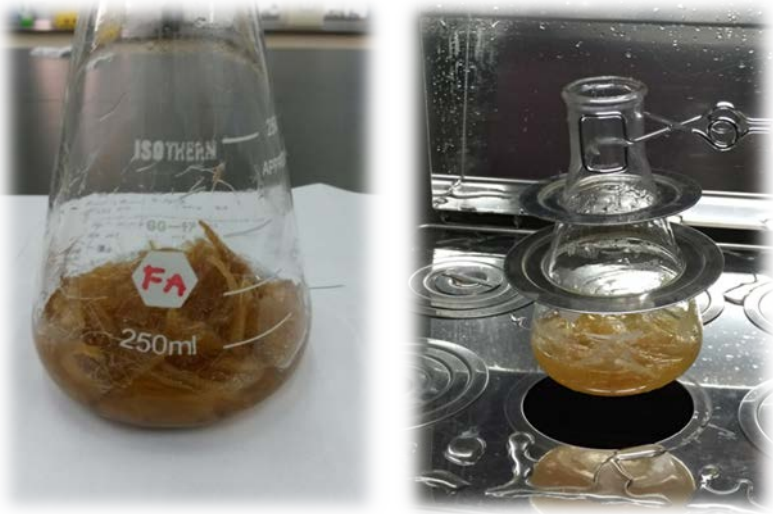

Figure 4. Formic Acid Treatment

Figure 5. Material after Formic Acid Treatment

Following the formic acid treatment, peroxoacidic treatment was carried out to improve delignification. Peroxoacid was synthesized via combining formic acid with hydrogen peroxide 35 % concentration. Samples are washed with peroxoformic acid for 150 minutes at 80°C and dried. Material after peroxoacid treatment is given in **Figure 6.** Finally, bleaching of obtained pulp was performed with hydrogen peroxide (H_2O_2) for 75 minutes at 65°C. A bleaching stage was applied to improve the brightness of obtained pulp [4]. Material bleached with hydrogen peroxide is given in Figure 7.

Figure 6. Material after Peroxoacid Treatment

Figure 7. Material Bleached with Hydrogen Peroxide

2.2.4. Characterization

The purity and chemical structure of extracted cellulose were compared with α-cellulose (Sigma Aldrich) which has a lab grade purity. X-Ray Diffraction (XRD) and Fourier Infrared Spectroscopy (FTIR) methods are used to analyze the internal structure of obtained cellulose.

2.2.4.1. *FTIR (Fourier Infrared Spectroscopy) Analysis*

The extracted cellulose obtained with formic acid-peroxoformic acid pulping method and α-cellulose purchased from Sigma Aldrich were analyzed using FTIR method. Infrared spectral measurements were made using Perkin Elmer Spectrum BX instrument , wavelength 400–4000cm^{-1}, 2cm^{-1} resolution (% absorbance).

2.2.4.2. *XRD (X-Ray Diffraction) Analysis*

XRD analyses of extracted cellulose and α-cellulose purchased from Sigma Aldrich were performed by Rigaku D/MAX200 X-Ray diffractometer using CuKα radiation and operating at 40 kV and 36 mA.

3. Results and Discussion

3.1. Chemical Composition Results

The percentages of pectin, hemicellulose, lignin, and cellulose are summarized in Table 1. The high cellulose content of banana plant wastes with *57 %* enhances the variety of utilization and sustainability. Organic acid extraction method was effective for the extraction of cellulose from banana plant waste.

Table 1. Lignocellulosic content of banana plant waste

	wt
Pectin	7
Hemicellulose	24
Lignin	12
Cellulose	57

3.2. Elementary Analysis Results (FTIR)

FTIR results which were performed to analyze and compare the functional groups and bond energies of extracted cellulose and α-cellulose, is given in Figure 8.

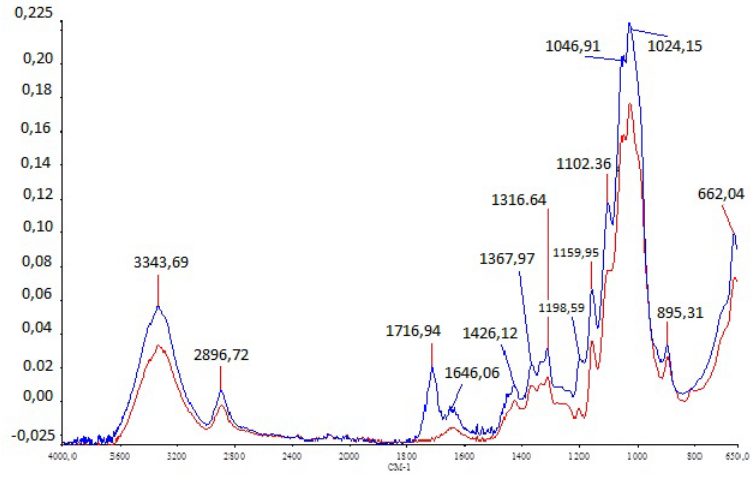

Figure 8. FTIR spectra of the extracted cellulose and α- cellulose.

FTIR spectra of the α-cellulose (purchased from Sigma Aldrich) and the cellulose extracted from banana plant waste are very similar. The peak in the absorption band of 1716cm^{-1} in the spectra of cellulose extracted from banana plant waste may indicate the residual of the hemicellulose.

3.3. Structural Analysis Results (XRD)

The diffraction intensities of the α-cellulose and extracted cellulose were recorded between 3◦ and 90◦ (2θ). XRD patterns of α-cellulose and cellulose extracted from banana plant waste are shown in Figure 9.

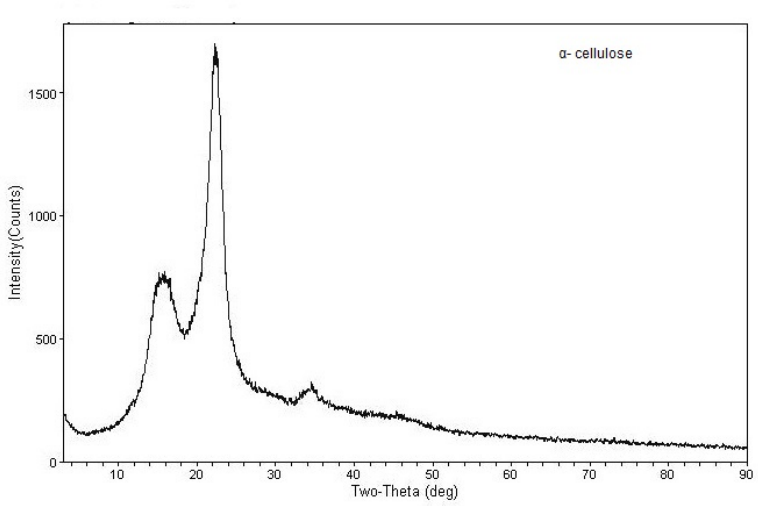

Figure 9. XRD patterns of the α- cellulose and cellulose extracted from banana plant waste

The diffraction peaks at 2θ = 22–23◦ and 2θ = 18-19◦ indicate the typical diffractions of cellulose. The crystallinity indexes of cellulose samples were calculated as 67 and 61,9 % respectively. According to

XRD patterns of the α-cellulose (purchased from Sigma Aldrich) and the cellulose extracted from banana plant waste , samples show the same intensity peaks at the same diffraction angles.

CONCLUSION

Our results suggest that, material which is a waste product after harvesting the banana plant can be used as a potential source for cellulose. Cellulose extracted from banana plant wastes can be used in the production of regenerated cellulose fibers and composite materials and also in the paper and food in*dustry. Moreover, microcrystalline and nano crystalline cellulose may be produced by acid hydrolysis of* extracted cellulose. The thermal properties of extracted cellulose will be further investigated by using analytic methods. For a further study, cellulose extraction from banana plant wastes will be also investigated by using different chemical and mechanical treatments and their combination.

ACKNOWLEDGEMENTS

The authors gratefully acknowledge the funding by Scientific and Technological Research Council of Turkey (TÜBİTAK) under grant 115M736.

References

1. *Blackburn R. S., (2009), "Sustainable Textiles; Life Cycle and Environmental Impact", Woodhead Publishing, UK.*
2. *Kumar, M., Kumar, D. (2011), "Comparative Study of Pulping of Banana Stem", International Journal of Fiber and Textile Research, 1(1): 1-5.*
3. *Klemm, D., Heublein, B., Fink, H-P., Bohn, A. (2005), "Cellulose: Fascinating Biopolymer and Sustainable Raw Material", Angewandte Chemie International Edition, 44(22), 3358–3393.*
4. *Khan, M., Z., H., Sarkar, M. A. R, Al Imam, Md. Forhad Ibne, Malinen, O., R., (2013), Fiber morphology and Pulping study of Banana Pseudo-stem, International Journal of Fiber and Textile Research, 3(1), 31-35.*
5. *Kumar, M., Kumar, D., (2011), 'Comparative study of pulping of banana stem', International Journal of Fiber and Textile Research, 1(1), 1-5.*
6. *Zhang J., Zhang H., Zhang J. (2014), 'Evaluation of Liquid Ammonia Treatment on Surface Characteristics of Hemp Fiber', Cellulose, 21/1, 569-579.*
7. *www.fao.org, Food and Agricultural Organization of the United Nations.*

CENTRIFUGAL FIBER FORMING FROM BLENDS OF POLYMER SOLUTIONS

Jana Hlavatá, Eva Kuželová Košťáková

Technical University of Liberec, Faculty of Textile Engineering, Department of Nonwovens and Nanofibrous Materials, Liberec, Czech Republic, jana.hlavata1@tul.cz

Abstract:

This paper presents centrifugal fiber forming from blends of polymer solutions. The process of centrifugal spinning was executed on two different types of spinning machine in needle-less and needle way. Processing parameters such as linear velocity and type of spinneret unit were analyzed. For this research, polymer materials poly(ε-caprolactone), poly(vinyl butyral) and copolymer of lactic acid and ε-caprolactone were chosen. Mixtures with different proportions of the polymer components were prepared. Solubility of polymers in solvents, defects generated in fiber layers and distribution of two polymers in blend fibers were characterized. Needle and needle-less centrifugal spinning related to changing process and material conditions and their effects on fiber morphology were studied. Morphology of produced fibers and distribution of two polymers in blend fibers were observed using scanning electron microscopy and image analysis software.

Key words:

Centrifugal spinning, poly(ε-caprolactone), poly(vinyl butyral), blends of polymer solutions, solubility of polymers in solvents, distribution of two polymers in blend fibers

1. Introduction

Centrifugal Spinning, also called Forcespinning or Rotary Jet Spinning, is relatively new technology, which uses only centrifugal forces for fiber formation. This technology is very productive and relatively simple. Fibers are formed due to high-speed rotation of spinneret unit. As soon as the critical angular velocity of spinneret is reached, polymer jets are ejected from the orifices of the spinneret unit, stretched and elongated into fibers and deposited on the collector. Any voltage is not required for this method [3]. There are two different ways, needle [2] and needle-less [4], which differs in shape of spinneret unit.

A wide range of conductive and nonconductive materials in the form of solutions or melts could be spun. Fibers with a wide distribution of diameters from nanofibers to microfibers are produced. Homogenous fibrous layers could be used for many applications, e.g. biomedical applications, tissue engineering, scaffolds, drug delivery systems, filtration, etc. [3].

2. Experimental

Two polymer materials, poly(ε-caprolactone) and poly(vinyl butyral), were chosen based on earlier experiments. These mixtures with different proportions of the polymer components were prepared. Furthermore, copolymer of lactic acid and ε-caprolactone was spun for the comparison of productivity and fiber morphology of prepared copolymer and polymer blend.

Two ways of centrifugal spinning, needle and needle-less, were used for fiber forming. Both technologies were compared on base of productions and results. They were studied the spinning ability, fiber diameters, morphology of the fibers and amount of defects in fibrous layers.

The aim of this research was to find suitable polymer blends and their spinning, making structural and material analysis on the created fibers and their evaluation. The distribution of polymer materials in the final fibers was also detected by washout one component of the polymer blend. The result of this research is the determination how the changing process and material parameters, how they affect the quality of the spinning process, produced fibers and impact assessment of individual washout procedures on the polymer distribution in blend fibers.

2.1. Materials

Fibers were made from following materials: Poly(ε-caprolactone) (PCL, Mn = 45 000 g/mol) was purchased from Sigma Aldrich, USA. Poly(vinyl butyral) (PVB, Mn = 60 000 g/mol) was donated by Kuraray, Japan. This type of PVB contains 18–21 wt.% of poly(vinyl alcohol) (PVA) and 1–4 wt.% of poly(vinyl acetate) (PVAc). Copolymer Purasorb PLC 7015 containing 70 % of lactic acid and 30 % of ε-caprolactone was purchased from Purac, USA. As a solvent system for all of the materials were used chloroform (Penta, Czech Republic) and ethanol (Tereos TTD, Czech Republic) in the ratio 9:1.

Series of six polymer solutions (concentration 14 wt.%) having ratios of components PCL/PVB 95/5, 90/10, 80/20, 70/30, 60/40, 50/50 were utilized. Two polymer solutions containing only one component, i.e. 100% PCL and 100% PVB were also applied for comparison of results. PLC solution with concentration 10 wt.% was used for comparison with blends and copolymers fibers.

2.2. Centrifugal spinning

The whole process of centrifugal spinning was made at two different devices. One of them was the needle device Fiberlab L-1000 M (FibeRio® Technology Corporation, Texas, USA) in the company Pardam, s.r.o., Roudnice nad Labem, Czech Republic (see Fig. 1a). In the Fig. 1b, there is shown detail of spinneret unit (1), which was consisted of reservoir of polymer solution (2) and two spinning needles (3). Size of spinneret unit was 16 cm in diameter and size of collector was 38 cm Needle way of centrifugal spinning process was carried out at three linear velocities, 33 m/s, 50 m/s, 67 m/s.

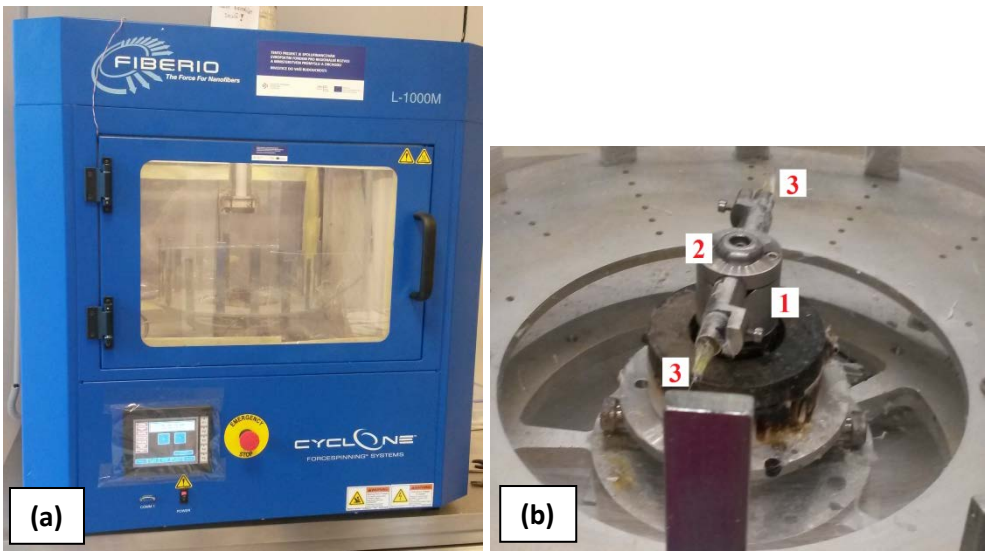

Figure 1. Needle device Fiberlab L-1000 M (FibeRio® Technology Corporation) in the company Pardam, s.r.o., Roudnice nad Labem, Czech Republic; (a) overview of the needle device; (b) detail of the spinneret unit (1) consisted of reservoir of polymer solution (2) and two spinning needles (3).

The second one was the needle-less laboratory device at Department of Nonwovens and Nanofibrous Materials, Technical University of Liberec, Czech Republic (Fig. 2). The spinneret unit (1) was circle shaped disk. Size of spinneret unit was 5 cm in diameter and size of collector (2) was 26 cm. Because of lower output of motor unit (3) needle-less way of centrifugal spinning process was realized only at two linear velocities, 33 m/s, 50 m/s.

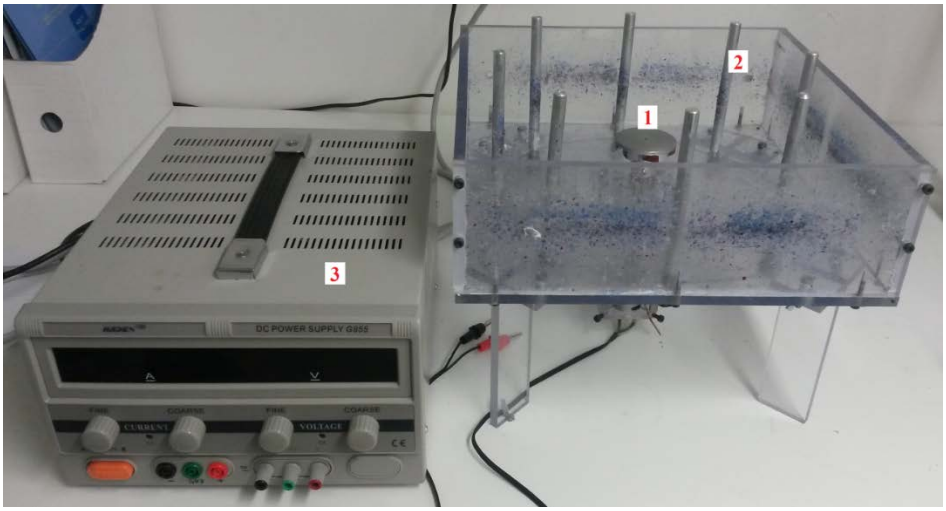

Figure 2. Needle-less laboratory device at Department of Nonwovens and Nanofibrous Materials, Technical University of Liberec, Czech Republic consisted of circle shaped disk (1), collector (2) and motor unit (3).

2.3. Solubility of PCL and PVB

Solvent system chloroform:ethanol 9:1 (w/w) was chosen for preparation of polymer solutions. It was important to know solubility of polymer materials PCL and PVB in this solvent system. Solubility could be predicted according to three Hansen solubility parameters (δ_d, δ_p, δ_h) and radius of interaction R. 2D or 3D chart could be compiled based on this parameters. Polymer material is represented by center point of solubility sphere. Radius of interaction indicates line of solubility. Then three types of solvents could be differ: i) solvents placed around the center point are called good solvents; ii) solvents occurred near the solubility line are called bad solvents; iii) behind the solubility line are non-solvents [1].

2.4. Distribution of two polymers in blend fibers

Distribution of two polymer materials in the blend fibers was analyzed by washout PVB component by ethanol through magnetic stirrer with higher temperature, ultrasonic bath or shakers at different time and temperature.

2.5. Scanning Electron Microscopy

Scanning electron microscope (SEM) Tescan, Vega3 SB Easy Probe, Czech Republic was used for analysis of fiber morphology. Before SEM observation, all fibrous samples were coated with 7 nm gold layer via sputter coater Quorum Q150R ES, United Kingdom. Fiber diameters were measured using image analysis software NIS-Elements AR 4.30.00 (LIM s.r.o., Czech Republic).

3. Results and discussion

3.1. Centrifugal spinning of polymer blends

In the case of needle centrifugal spinning was possible to spin a larger variety of polymer solutions. Although, these fiber diameters were approximately four times smaller than fibers made by needle-less spinning (see Fig. 3 and Fig. 4), fibrous layers contain a large number of drop-shaped defects. Only the PLC fibers showed the same diameter values in both technologies. It follows that, the process conditions are not important for some types of materials. It suppose the increasing contain of PVB in polymer mixture should raise fiber diameters but it was not confirmed. Experiments showed that mixture compositions and fiber diameters have not any dependency. That could be caused by many reasons, e.g. unsuitable choice of solvent system, dosage of polymer solutions, imperfections of device, etc.

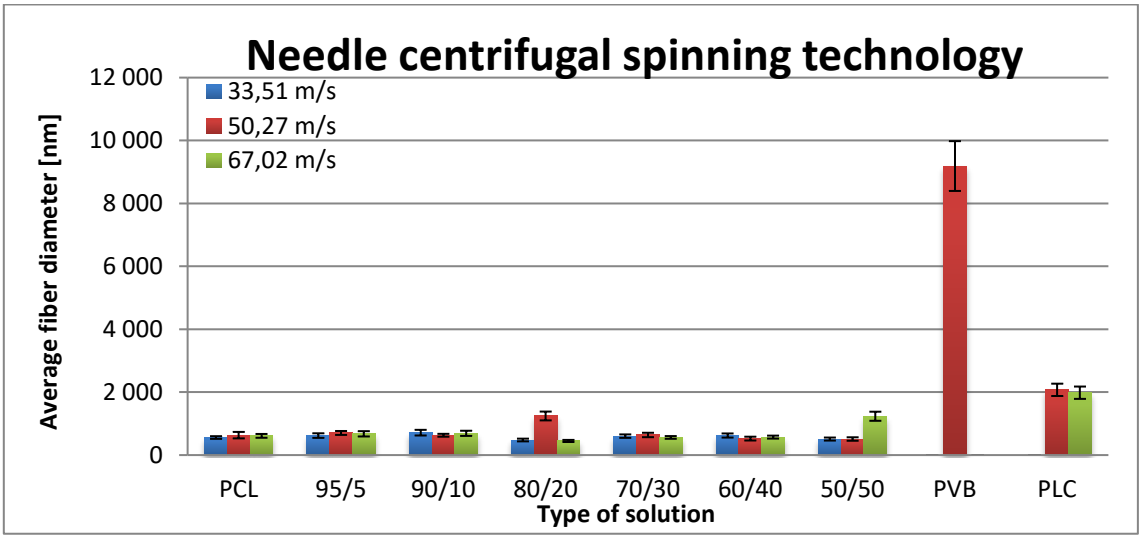

Figure 3. Average fiber diameter from needle centrifugal spinning technology depending on the velocity and solution composition. Average values are calculated from 100 fibers.

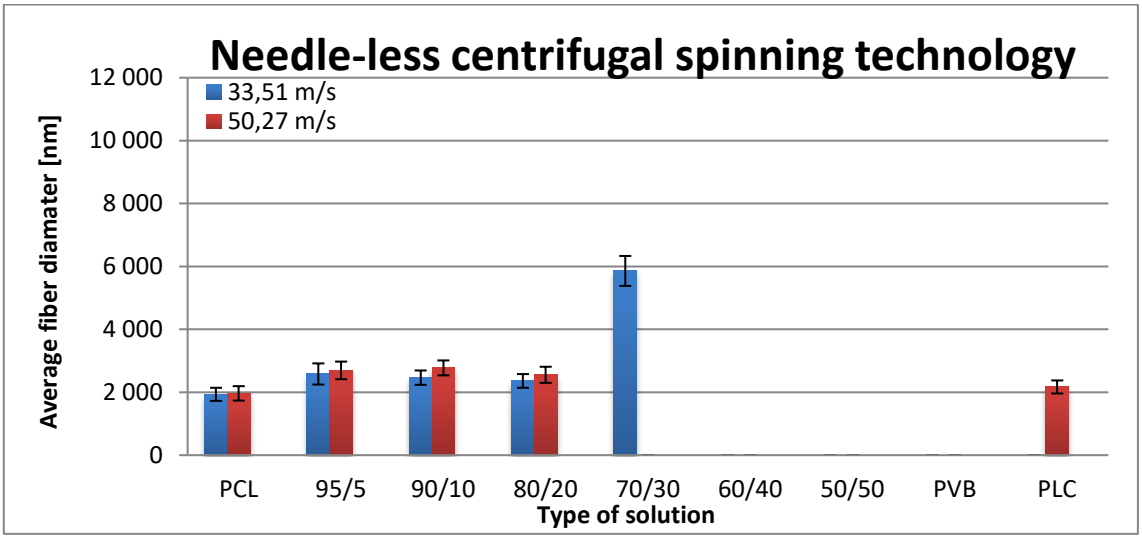

Figure 4. Average fiber diameter from needle-less centrifugal spinning technology depending on the velocity and solution composition. Average values are calculated from 100 fibers.

3.2. Solubility of PCL and PVB

From literature [1] Hansen solubility parameters and radius of interaction for chloroform, ethanol and PVB were found out. Unfortunately, there was not any information about PCL. Figure 5 illustrates 2D graph of solubility made only for PVB.

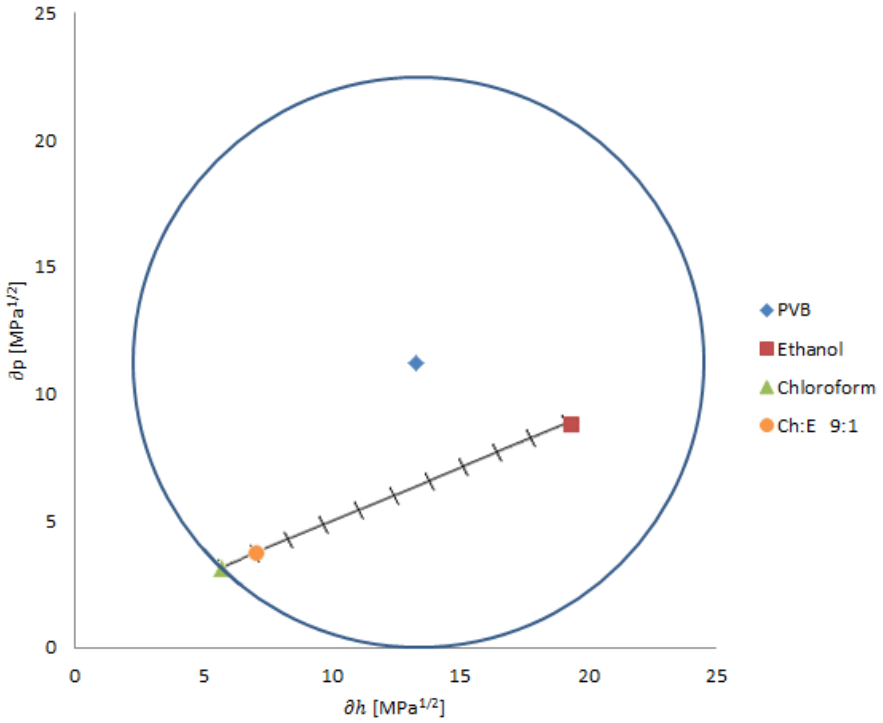

Figure 5. 2D graph of solubility PVB in chosen solvents chloroform, ethanol and solvent system compiled based on Hansen solubility parameters and radius of interaction.

It is obvious that ethanol was situated near center point of solubility sphere and it represented good solvent for PVB. However, chloroform was placed behind solubility line and for PVB was non-solvent. For that reason solvent system chloroform:ethanol 9:1 (w/w) belonged to bad solvent systems. That mean PVB was in this system soluble, but not so readily.

3.3. Distribution of two polymers in blend fibers

Washout PVB component of blend fibers by ethanol was made by several methods, namely by magnetic stirrer with higher temperature, ultrasonic bath or shakers at different time and temperature. In the case of fibers from the needle or needle-less centrifugal spinning any trend between wash conditions has not been found. It was shown that the polymers in the fibers are not uniformly distributed (see Fig. 6). Centrifugal spinning divides them into sections, after washout PVB only sections of PCL were formed, and fibrous layer was split.

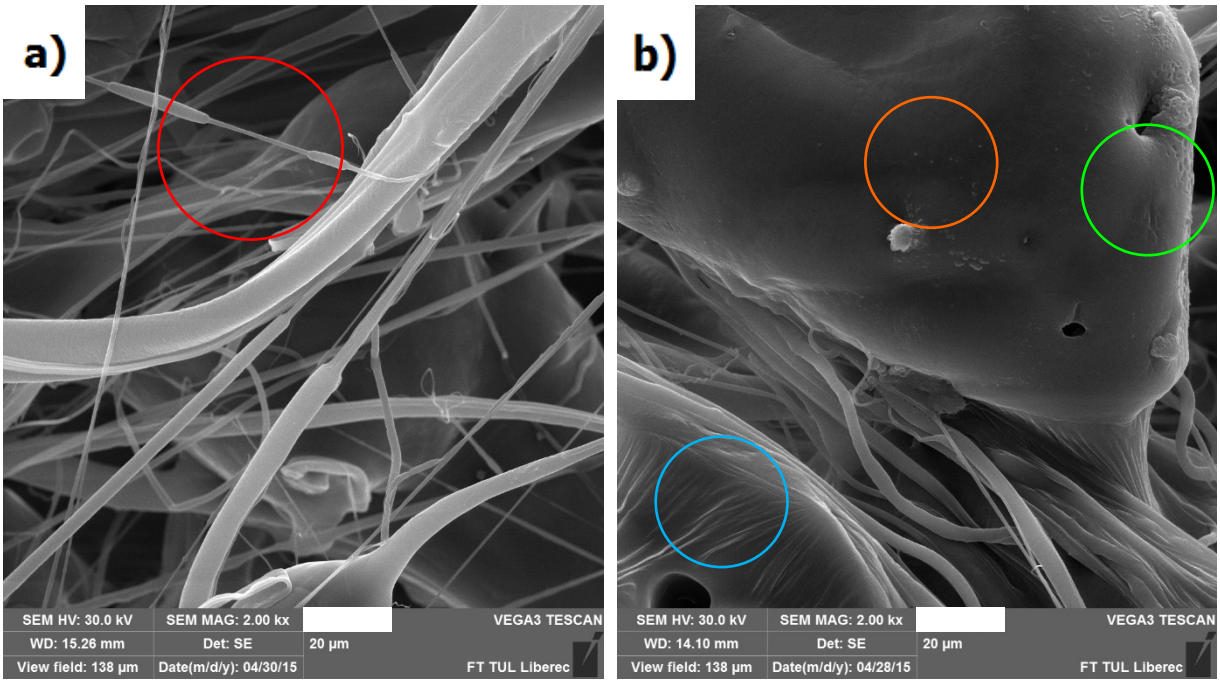

Figure 6. Defects created on the fibers from needle and needle-less centrifugal spinning technologies after washout PVB component of blend fibers.

4. CONCLUSIONS

In this study, we focused on centrifugal spinning from blends of polymer solutions. Two ways of centrifugal spinning were used for fiber formations, namely needle and needle-less. Fibers were made from mixtures contained different proportions of PVB and PCL components, and from PLC copolymer. The work does not lead to the production of material for some application. It should primarily show types of problems, which may be occurred during spinning a mixture of two polymer materials. Materials PVB and PCL are not clearly compatible, but they have relatively similar molecular weights, compared to spinning of PLC copolymer. It would be useful to find an appropriate solvent system for further research, which would be completely soluble for both of polymer materials. There are also great amounts of other analyses that have not been done and could be recommended for further testing.

References

1. *Hansen, Ch. M., (2007). Hansen Solubility Parameters: A User's Handbook. (2nd ed.).CRC Press (New York).*
2. *Mellado, P., McIlwee, H. A., Badrossamay, M. R., Goss, J. A., Mahadevan, L., Parker, K. K. (2011). A simple model for nanofiber formation by rotary jet-spinning. Applied Physics Letters, 99, 203107. Retrieved May 15, 2016, AIP Scitation.*
3. *Sarkar, K., Gomez, C., Zambrano, S., Ramirez, M., Hoyos, E., Vasquez, H., Lozano, K., (2010). Electrospinning to Forcespinning™. Materials Today, 13, 12-14. Retrieved May 20, 2016, from ScienceDirect.*
4. *Weitz, R. T., Harnau, L., Rauschenbach, S., Burghard, M., Kern. K., (2008). Polymer Nanofibers via Nozzle-Free Centrifugal Spinning. Nano Letters, 8, 1187-1191. Retrieved May 15, 2016, from ACS Publications.*

INFLUENCE OF LOW-TEMPERATURE PLASMA UNDER ATMOSPHERIC PRESSURE ON THE NANOCOATING OF THE TEXTILE MATERIALS

D. Rástočná Illová[1], Z. Špitálsky [2], M. Maľovaníková[3], K. Drozdová [3], J. Ligas[3]

[1] Research Institute for Textile Chemistry (VÚTCH)-CHEMITEX, Ltd., Rybníky 954, 011 68 Žilina, Slovak Republic, rastocna-illova@vutch.sk
[2] Polymer Institute, Slovak Academy of Sciences.,Dúbravská cesta 9, 845 41 Bratislava45, Slovak Republic, Zdeno.Spitalsky@savba.sk
[3]Research Institute for Textile Chemistry (VÚTCH)-CHEMITEX, Ltd., Rybníky 954, 011 68 Žilina, Slovak Republic, chemitex@vutch.sk

Abstract:

In the presentation there are presented results of research solution focused on innovative technologies of nanocaoting of polypropylene textile materials for improvement of functional properties. Results of the application of sol-gel technology on the formation of various nanosol types (hydrophilic, electroconductive) and their application in nanostructuralization of textile surfaces are presented. Besides, results of change of performance characteristics and functional properties of the textile materials with achieved effect of hydrophilic finish and highly effective reduction of electrostatic charging of textile materials prepared from PP fibres.

The paper futher presented the results of the impact of the low-temperature plasma generated by DCSBD (Diffuse Coplanar Surface Barrier Discharge) under atmospheric pressure to increase the afinity of nanocoating to textile surfaces and ensure permanence of nanocoating. The research solution of influence of application of low-temperature plasma under atmospheric pressure in the afinity of nanocoating is oriented on investigation of influence of various time of textile surface activation by plasma. There are presented results from used methods for evaluation of the concentration of free radicals on the surface PP woven fabric after plasma treatment.

Key words:

Low-Temperature Plasma by Atmospheric Pressure, functionalisation of textile materials, Nanocoating, surface activation, concentration of free radicals

1. Introduction

Conventional finishing methods such as pad-dry-cure process, used at present to apply antimicrobial, self-cleaning and flame-retardant finishes, have the disadvantage that hand and drape of a fabric is impaired, they are often accompanied by significant increase of weight, insufficient fastness to washing, loss of mechanical strength and, what is very important, they have negative influence on the wearing comfort. Protective clothing made from such special fabrics restrains in many cases performance of a man. Besides, there is a number of safety risks, associated with application and disposal of chemicals used in finishes at present. Therefore, alternative cost-effective permanent means and technologies are being sought, which do not present danger to health and environment, do not impair wearing comfort and provide at the same time optimum protection.

Methods of functional coating are a flexible alternative to conventional finishing methods as they are independent on fabric type, require small quantities of additives and permit combinations of various functional properties. These technologies include immobilization of enzymes on textile substrates, layered structures, nano-coatings and plasma technologies used to apply functional

groups and molecules on textile surfaces. These technologies differ from the conventional finishing methods as they impart special functional properties to textile surfaces via modification on a level of micro-dimensions and nano-dimensions without influencing bulk properties of the textile materials. The conventional finishing methods, such as pad-dry-cure process, used at present to apply antimicrobial, self-cleaning and flame-retardant finishes, have the disadvantage that hand and drape of a fabric is impaired, they are often accompanied by significant increase of weight, insufficient fastness to washing, loss of mechanical strength and, what is very important, they have negative influence on the wearing comfort [1].

Nano-coating is deposition of a layer of nano-particles (with a thickness of 10-100 nm) with the aim to create a nano-composite and/or nano-structured material. Nanostructured surfaces are point of considerable interest as they have big surface area which could impart significant functionality to materials finished this way. There are various coating techniques used to apply nano-particles e.g. deposition of chemical vapours, plasma technologies, „self-assembly"of thin functional layers of nano-particles, successive deposition of several layers, dip coating, sol-gel method. Solvent coating is based on application of molecules of a precursor or nano-particles to form a layer. Electrostatic interaction, hydrogen bonds and covalent bonds facilitate adhesion between the coating and the coated material [2].

Theme of plasma application used to modify textile surfaces is known already for more than 40 years, however introduction of the technology into industrial operation is very slow [3]. The reason for this is that majority of plasma processes, developed in the past, was based on methods realized under low pressure, permitting processing of specific lots (batches) only, so-called „off-line" application, which is practically infeasible in textile industry. New plazma systems performed under atmospheric pressure permit already continuous textile processing, so-called „in-line" application [4]. Plasma polymerization is able to impart various functional characteristics, e.g. hydrophobic, hydrophilic, electroconductive properties, it can improve dyeability, conductivity and biocompability via modification of textile and fibre surfaces on a level of nano-dimensions. An advantage in comparison with conventional wet chemical processes is very low consumption of raw materials and energy and ecological acceptability. Besides, these coatings applied using plasma are much more durable than coatings deposited by other methods of surface modification, e.g. wet processes or radiation, because polymeric coatings on a level of nano-dimensions, deposited by plasma, are bonded with textile surfaces by covalent bonds [5, 6].

2. Experimental

Our research focuses on investigation of surface changes in macrostructure of textile materials made from polypropylene, initiated by low-temperature plasma under atmospheric pressure (DCSBD – Diffuse Coplanar Surface Barrier Discharge), study of free radical formation on textile surfaces from a viewpoint of chemical composition and from viewpoint of various conditions of surface activation by low-temperature plasma (time of plasma activation, output of plasma electrodes, distance of plasma electrodes) with the aim to increase adhesion of the nano-coating. Unique textile finishing device ZUP 400 designed for application of low-temperature plasma under atmospheric pressure of the company VÚTCH-CHEMITEX, spol. s r.o. was used for plasma activation of textile surfaces. The device ZUP 400 is integrated into innovated pilot scale line SAAG designed for double-sided continuous finishing of textile materials. It permits to combine activation of textile surfaces using low-temperature plasma under atmospheric pressure with subsequent chemical finish.

Surface activation of polypropylene structure using low-temperature atmospheric plasma was performed under conditions as follows:

- output of plasma electrodes: 350 W
- time of surface activation using plasma: 5s, 10s, 20s, 60s, 100s, 150s

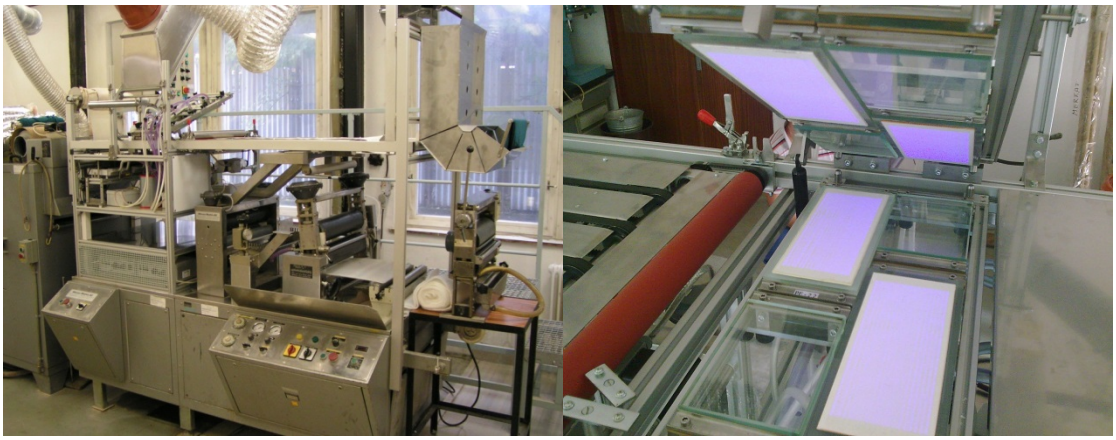

a b

Figure 1: a) Innovated SAAG finishing equipment integrating ZUP 400 device, b) Plasma sources of ZUP 400 device installed in operational mode

Available nanosols, developed in the frame of previous research projects, were applied on the plasma activated surface in order to achieve nano-coated surface with special functional properties:

- hydrophilic (HFIL) nanosol, prepared by sol-gel method based on hydrolysis of precursors on the base of organosilanes with amino groups in alkaline medium;
- electroconductive (EVN) nanosol, prepared by sol-gel method using acidic and/or alkaline hydrolysis of organosiloxane precursors (triethoxysilane – TEOS and vinyltriethoxysilane – VTEOS) incorporating carbon nanotubes (CNT).

2.1.1. Materials

Hydrophilic (HFIL) nanosol Techazil H20 in concentration of 30 g/l was applied on plasma activated surface of a fabric made from polypropylene in the frame of the experimental part.
Conditions of HFIL nanosol application:

- 15 min. action of the bath with HFIL nanosol;
- drying in SAAG Werner Mathis device at 120 ˚C;
- setting in SAAG Werner Mathis device at 120 ˚C.

Besides, electroconductive nanosol Techazil EVN3-PEG in concentration of 10 g/l was applied on plasma activated surface of a fabric made from polyproylene. Application conditions were as follows:

- 15 min. sonification (ultrasonic cleaner PS 10000A);
- squeezing of the sample in laboratory padder, type VFM, Werner-Mathis AG, pressure: 100;
- drying in SAAG Werner Mathis device at 100 ˚C / 2 min.;
- setting in SAAG Werner Mathis device at 120 ˚C / 3 min.

The nanosols were applied also on woven fabrics made from polypropylene without activation of their surface structure by plasma in order to compare influence of low-temperature plasma on enhancement of efficiency of functional properties of the nano-coated material made from polypropylene.
To evaluate influence of plasma on enhancement of affinity of the nano-layer to the surface of polypropylene textile material and/or permanency of the nano-coating, samples of the woven fabric were washed and dried. Subsequently, maximum number of washing and drying cycles was specified. The nano-coated samples were washed and dried in accordance with the standard STN EN ISO 105-C06, method A2S under following conditions:

- washing temperature: 40 ˚C / 15 min
- washing agent, c = 1 g/l
- rinsing after washing 1 min / 40 ˚C distilled water
- drying temperature: air-drying at a temperature not exceeding air temperature of 60 ˚C.

Subsequently, new functional properties of the nano-coated samples of textile materials prepared this way relating to hydrophility and electroconductivity were evaluated. Efficiency of the nanosols itselves,

efficiency of nano-coating as well as influence of plasma on permanency of the nano-coating was evaluated.

Table 1. Characteristics of samples

Samples	Description of preparation of samples for experiments
PP standard	Woven fabric from 100% polypropylene
PP/0s/ HFIL	Woven fabric from 100% polypropylene, with application of hydrophilic nanosol, without plasma pre-treatment
PP/5s /HFIL	Woven fabric from 100% polypropylene, with surface pre-treatment using low-temperature plasma under atmospheric pressure, with time of plasma activation 5s and subsequent application of the hydrophilic nanosol
PP/10s/ HFIL	Woven fabric from 100% polypropylene, with surface pre-treatment using low-temperature plasma under atmospheric pressure, with time of plasma activation 10s and subsequent application of the hydrophilic nanosol
PP/20s/ HFIL	Woven fabric from 100% polypropylene, with surface pre-treatment using low-temperature plasma under atmospheric pressure, with time of plasma activation 20s and subsequent application of the hydrophilic nanosol
PP/60s/ HFIL	Woven fabric from 100% polypropylene, with surface pre-treatment using low-temperature plasma under atmospheric pressure, with time of plasma activation 60s and subsequent application of the hydrophilic nanosol
PP/100s /HFIL	Woven fabric from 100% polypropylene, with surface pre-treatment using low-temperature plasma under atmospheric pressure,with time of plasma activation 100s and subsequent application of the hydrophilic nanosol
PP/150s /HFIL	Woven fabric from 100% polypropylene, with surface pre-treatment using low-temperature plasma under atmospheric pressure, with time of plasma activation 150s and subsequent application of the hydrophilic nanosol
PP/0s/ EVN	Woven fabric from 100% polypropylene, with application of the electroconductive nanosol without plasma pre-treatment
PP/5s /EVN	Woven fabric from 100% polypropylene, with surface pre-treatment using low-temperature plasma under atmospheric pressure, with time of plasma activation 5s and subsequent application of the electroconductive nanosol
PP/10s/ EVN	Woven fabric from 100% polypropylene with surface pre-treatment using low-temperature plasma under atmospheric pressure, with time of plasma activation 10s and subsequent application of the electroconductive nanosol
PP/20s/ EVN	Woven fabric from 100% polypropylene with surface pre-treatment using low-temperature plasma under atmospheric pressure, with time of plasma activation 20s and subsequent application of the electroconductive nanosol
PP/60s/ EVN	Woven fabric from 100% polypropylene, with surface pre-treatment using low-temperature plasma under atmospheric pressure, with time of plasma activation 60s and subsequent application of the electroconductive nanosol
PP/100s /EVN	Woven fabric from 100% polypropylene, with surface pre-treatment using low-temperature plasma under atmopheric pressure, with time of plasma activation 100s and subsequent application of the electroconductive nanosol
PP/150s /EVN	Woven fabric from 100% polypropylene, with surface pre-treatment using low-temperature plasma under atmospheric pressure, with time of plasma activation 150s and subsequent application of the electroconductive nanosol

2.2. Measurements and evaluation methodology

Formation of reaction sites and/or free radicals and their concentration on the activated surface was evaluated using *UV spectroscopic* method in order to assess permanency of the nano-coating and define the most suitable conditions of plasma activation of the surface. The method consists in determination of the amount of peroxides and hydroperoxides formed on the modified textile surface after plasma activation and after oxygen bonding to the formed free radicals. Decrease of peroxide

concentration in dependence on „ageing“ of the plasma activated textile surface was observed. UV spectroscopic method, based on determination of iodine formed by oxidation of iodide ions, was used to determine the low concentrations of hydroperoxides. The unstable peroxides and hydroperoxides transform into more stable carbonyl functional groups whose concentration on the plasma treated textile surface was determined by UV spectroscopy. Determination of concentration of hydrazones formed by reaction of oxidized polymer with 2,4-dinitrophenylhydrazine is involved.

Static contact angle (SCA) was determined on the samples of polypropylene woven fabric with hydrophilic nano-coating before washing and drying and after washing and drying. The static contact angles were measured by Drop Shape Analysis System DSA 30 designed for measurement of contact angles. Every value of contact angle is average from 10 measurements. Maximum error of measurement was 6 %.

Surface resistance of the textile samples made from 100 % polypropylene with electroconductive nano-coating was evaluated using Tera-ohmmeter TO6 according to the standard STN EN 1149-1 (IPS 31583814/114/274) „Protective clothing. Electrostatic properties. Part 1: Surface resistivity. Test methods and requirements“.

3. Results and discussion

Results from study of free radical formation on plasma activated textile surface from polypropylene achieved by evaluation of concentration of amount of formed peroxides and hydroperoxides bonded to the formed free radicals are given in Figure 2. It can be seen from the graphical relationship that concentration of free radicals has exponential trend in dependence on time of plasma activation. Concentration of free radicals on plasma activated surface increases with time of plasma activation. Relationship between ageing of the plasma activated polypropylene textile surface and concentration of free radicals was studied as well (Figure 3). Graphical relationship in Figure 3 shows exponentially decreasing trend; namely concentration of free radicals decreases with time of ageing of the plasma activated surface.

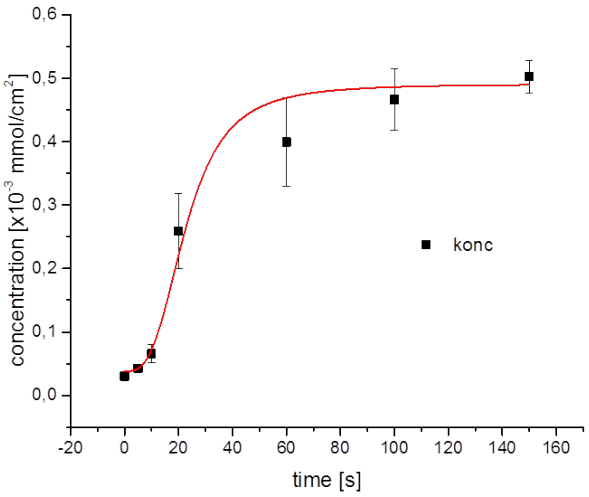

Figure 2. Concentration of peroxides and hydroperoxides bonded to free radicals in dependence on activation time of the surface of polypropylene woven fabric using low-temperature plasma.

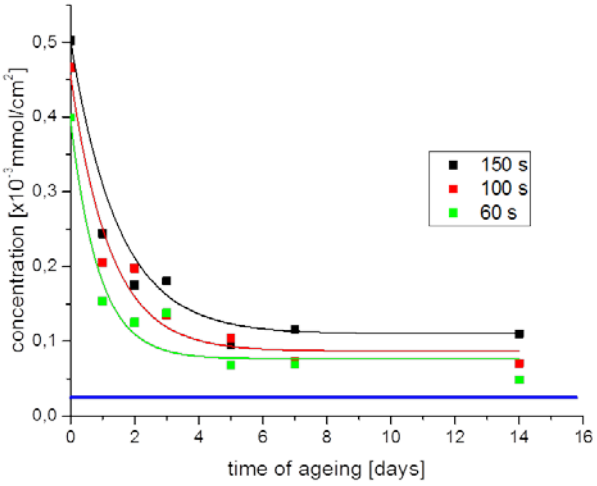

Figure 3. Concentration of peroxides and hydroperoxides bonded to free radicals in dependence on time of ageing of the surface of polypropylene woven fabric activated using low-temperature plasma

Results from evaluation of static contact angle of the hydrophilically nano-coated textile material are given in Table 2.

Table 2. Static contact angle of the materials from 100% polypropylene with HFIL nanosol without/with surface activation using low-temperature plasma

	Static contact angle SCA [°]							
Care (washing drying)	PP stan-dard	PP/0s/ HFIL	PP/5s /HFIL	PP/10s/ HFIL	PP/20s/ HFIL	PP/60s/ HFIL	PP/100s /HFIL	PP/150s /HFIL
without care	134,27	128,8	127,62	93,79	81,19	69,18	60,84	immeasurable water drop soaks
1x cycle	134,27	129,86	128,54	127,88	119,32	110,61	62,5	54,9
5x cycle	134,27	130,73	129,91	129,25	122,36	98,8	93,2	70,6
6x cycle	134,27	-	-	-	-	-	86,87	79,8
7x cycle	134,27	-	-	-	-	-	87,38	86,6

Results given in Table 2 show positive influence of pre-treatment of polypropylene woven fabric using low-temperature plasma before application of the hydrophilic nanosol. Values of static contact angle (SCA) decrease on samples pre-treated by plasma in comparison with application of HFIL nanosol without plasma pre-treatment. Values of SCA decrease with time of activation of polypropylene surface using low-temperature plasma. From 10s time of surface activation using plasma water drop soaks completely due to longer effect on the surface and at 150 s time of polypropylene surface activation using plasma before application of HFIL nanosol it was not possible to measure SCA as the polypropylene textile material was completely hydrophilic.

Results achieved on samples with plasma activated surface hydrophilic nano-coating and performed care – washing and drying show positive influence of low-temperature plasma. Surface activation of polypropylene woven fabric using plasma before application of HFIL nanosol increases permanency of the nano-coating. Lower values of SCA (<90˚) are achieved in comparison with nano-coated woven fabric without plasma application.

Electroconductive nanosol was applied on the surface of polypropylene woven fabric without plasma pre-treatment and after plasma-treatment in further experiments. Surface resistance of the textile samples without pre-treatment and with pre-treatment using plasma was evaluated by Tera-ohmmeter TO6 according to the standard STN EN 1149-1 (IPS 31583814/114/274) „Protective clothing. Electrostatic properties. Part 1: Surface resistivity. Test methods and requirements“.

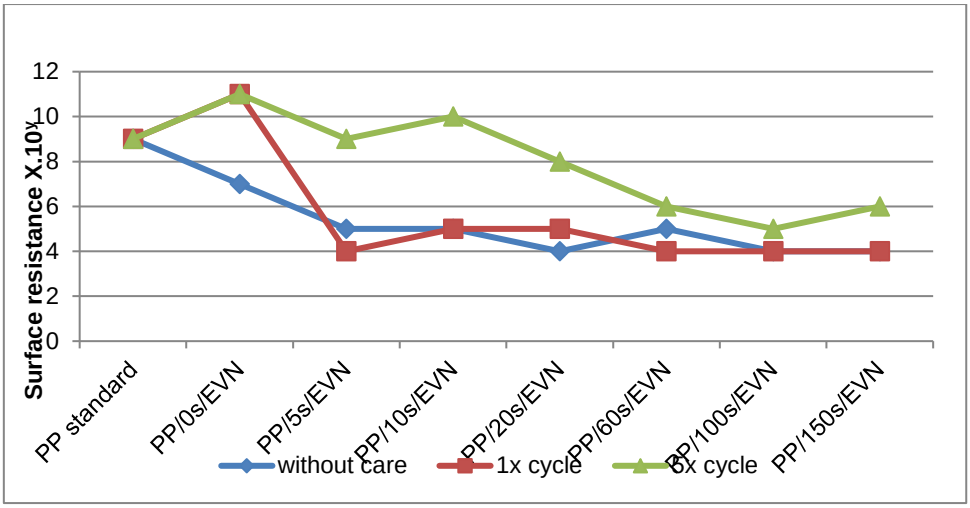

Figure 4. Surface resistance of electroconductively nano-coated polypropylene woven fabrics in dependence on time of plasma activation

It is possible to state on the base of results given in Figure 4 that application of the electroconductive nanosol reduces surface resistance of polypropylene woven fabric on a level of 10^7 Ω in comparison with a standard polypropylene woven fabric without electroconductive nano-coating, which is 10^9 Ω. Surface activation of polypropylene woven fabric using plasma under atmospheric pressure before application of the electroconductive nanosol decreases surface resistance on a level of 10^5 Ω - 10^4 Ω in comparison with surface resistance of polypropylene woven fabric with electroconductive nano-coating without pre-treatment using low-temperature plasma, which is on a level of 10^7 Ω, whereby positive influence of plasma on achievement of electroconductive properties was demonstrated. Higher times of surface activation of polypropylene woven fabric using low-temperature plasma (100s, 150s) result in surface resistance on a level of 10^4 Ω.

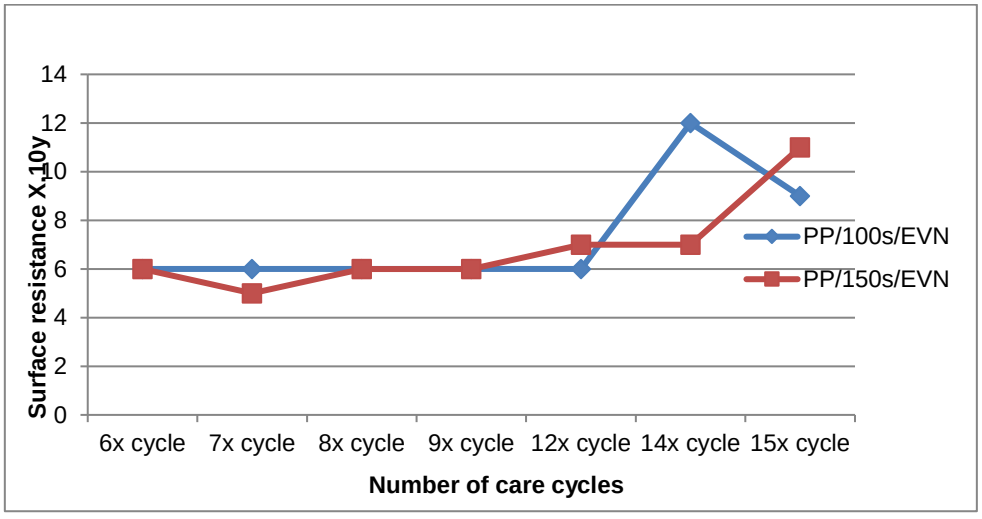

Figure 5. Surface resistance of polypropylene woven fabrics nano-coated with electroconductive nanosol in dependence on number of care cycles

Positive influence of plasma on affinity of the nano-coating and its permanency was demonstrated by washing and drying of the nano-coated polypropylene woven samples. Surface resistance on a level

of 10^5 Ω - 10^4 Ω was achieved at higher times of surface activation of polypropylene woven fabric using low-temperature plasma (100s, 150s).

Surface resistance of the nano-coated woven fabric after multiple care cycles was evaluated in order to assess affinity of the nano-coating to the textile material and/or permanency of the nano-coating. Results of surface resistance of the electroconductively nano-coated polypropylene fabrics in dependence on number of care cycles show that the electroconductively nano-coated polypropylene woven fabric with higher times of activation using low temperature plasma (100s, 150s) preserved surface resistance on a level of 10^6 Ω - 10^7 Ω even after 12 care cycles. The polypropylene nano-coated woven fabric with 150s time of activation preserved very good electroconductive properties even after 14 washing and drying cycles; its value of surface resistance was on a level of 10^7 Ω.

4. CONCLUSION

Surface activation of polypropylene textile material using low-temperature plasma causes formation of free radicals and concentration of the free radicals on polypropylene surface increases with time of plasma activation. Concentration of free radicals on plasma activated polypropylene textile surface decreases with aging time of the plasma activated surface.

Textile materials with hydrophilic nano-coating were prepared by application of hydrophilic nanosol Techazil H20 on plasma activated surface of polypropylene woven fabric. Evaluation of static contact angle demonstrated enhanced hydrophility of the prepared nano-coated textile materials; SCA on a level of <90° was achieved. Positive influence of plasma on permanency of the nano-coating was demonstrated mainly at higher times of plasma activation (100s, 150s), when static contact angle on a level of <90° was achieved even after 7 care cycles; these results point to very good hydrophilic properties.

Application of electroconductive nanosol Techazil EVN3-PEG on the surface of polypropylene woven fabric decreased surface resistance on a level of 10^7 Ω. Further decrease of surface resistance of the nano-coated fabrics was achieved by surface activation using low-temperature plasma before application of the electroconductive nanosol. Values on a level of 10^5 Ω - 10^4 Ω were obtained on woven fabrics prepared this way. Positive influence of low-temperature plasma on affinity of electroconductive nano-coating to surface of textile material was demontrated mainly at higher times of plasma activation (100s, 150s) when surface resistance on a level of 10^7 Ω - 10^6 Ω was achieved even after 12 care cycles involving washing and drying. Surface resistance on a level of 10^7 Ω was achieved even after 14 care cycles involving washing and drying with 150s time of surface activation using low-temperature plasma before application of electroconductive nanosol on the polypropylene fabric.

ACKNOWLEDGEMENTS

This paper was worked out in the frame of the scientific/technical project APVV-14-0518 „Research of the impact of low-temperature PLASma on increase the surface treatment permanence of TEXtile materials using NANOsols – PLAZ-NANO-TEX“ supported by the Slovak Research and Development Agency Bratislava, Slovak Republic.

References

1. *Li Land Hu, J.: Nanotechnology in Textiles. Textile Asia, p 29–34, November 2003*
2. *Roe, B.: Duarble Hydrophobic Textile Fabric Finishing Using Silica Nanoparticles and Mixed Silanes. Textile Research Journal, Vol. 79, No. 12, p. 1115-1122, August 2009*
3. *Herbert, T.: Atmospheric-Pressure Cold Plasma Processing Technology. Plasma Technologies for Textile, Woodhead Pubklishing, Cambridge, p. 79, UK, 2007,*
4. *Malkov, G., S., Fisher, E.R.: Plasma Processes Polym, Vol. 7, p. 695, 2010*
5. *Shishoo, R(Ed): Plasma Technology for Textiles. Woodhead Publishing Ltd. Cambridge (UK), 2007*
6. *Kang. J., Yand Sarmadi, M.: AATCC Review, Vol. 10, p 28, 2004*

DEVELOPMENT AND TESTING OF COTTON COATING WITH ANTIFUNGAL PROPERTIES

Hana Křížová[1], Lucie Palánková[2], Alice Krumova[1], Jakub Wiener[1]

[1] Technical University of Liberec, Faculty of Textile Engineering, Department of Material Engineering, Studentská 2, Liberec, Czech Republic
[2] National Library of The Czech Republic, Development and Research Laboratories, Sodomkova 2, Prague, Czech Republic
corresponding author: hana.krizova@tul.cz

Abstract:

The purpose of this work was the preparation and testing of the selected range of chemicals with a potential antifungal effect that could be added as additives to coating materials in the production of bookbinding canvases. The specific setup (cardboard - dispersion bonding material based on PVA - cotton canvas - acrylic coating) simulated a typical surface layer on a cover of archived or newly restored books. This system was exposed to the direct contact with a suspension of several fungi species at the room temperature and at the elevated humidity. The influence of selected additives in different concentrations in acrylic coating on mold growth was observed. Compared was also the effect of fungicides added to the cotton fabric coating in contact with the malt agar. The most effective chemicals in coatings were evaluated. Their advantages and disadvantages for the use as additives to bookbinding fabric coatings are also discussed with respect to the behavior of these substances after the simulated aging in the climatic chamber.

Key words:

Mold, fungi, antifungal, coating, canvas, book archives, library collections, book protection.

1. Introduction

Bookbinding canvases are used for cardboard packaging forming the boards of books during the conservation of library collections, especially the books after the year 1800. [1] Ideally, they should meet several functions: mechanical resistance and strength, sufficient flexibility, resistance to water / humidity, wash ability, non-inflammability, compatibility with adhesives and dyes used in subsequent bookbinding technological process, resistance to pests (insects, molds), and general antibiotic effect (resistance against bacteria and fungi). Currently for this purpose are mainly used fabrics woven in the plain weave (canvas) with a special treatment – the coating. The fabric is used as a base for the coating, which provides further mechanical, visual and useful characteristics to the book canvas.

Molds (filamentous fungi) that range from unicellular to multicellular eukaryotic organisms form the fibrous layers within or on the surface of substrates. The basic structural unit is the fiber (*hypha*), their framework is called *mycelium*. The hypha germinates from spores in suitable conditions and branches further. This creates a substrate (vegetative) mycelium that is used to feed the mold. The aerial mycelium grows on the substrate surface and has a reproductive function. The mycelium can be formed by one cell (genus *Mucor*) but it is more often multicellular with partitions (*septa*) that have the openings in the centre, which allow the passage of protoplasm, nuclei and organelles from the cell to cell. Fungal cell wall consists mainly of polysaccharides (chitin, chitosan, glucans, mannans,

sometimes glucose and lignin). Furthermore, it contains proteins, lipids and waxes that cause low wet ability of hyphae. Fungal cells usually contain one or more haploid nuclei. Molds proliferate by the vegetative growth of the hyphae or with the aid of *conidia* (asexually generated spores), or sexually via the fusion of sexual spores at the stage of *teleomorph*. [2]

Families of molds most commonly found in book archives are: *Penicillium, Aspergillus, Cladosporium, Chaetomium,* additional families are *Fusarium, Alternaria, Trichoderma, Botrytis, Stachybotrys, Ulocladium, Scopulariopsis.* [3, 4, 5]

Penicillium chrysogenum is a very common mold of the class *Ascomycetes* that grows abundantly on various plant and animal substrates. It reproduces asexually by the conidia. The branched conidiophores with smooth shanks grow out of hyphae.) The elliptical smooth conidia of size 2.5 - 4 microns grow in the form of chains from hyphae end portions (fialides). (Fig.1).

Aspergillus niger belongs to the same class as *Penicillium*. It creates fast-growing black colonies and reproduces asexually through the conidia. It can be found all over the world on various substrates, especially in warmer areas, because the optimum temperature for its growth is around 35 – 37 °C.

Cladosporium sphaerospermum is a saprophyte growing on a plant or animal substrate, very common on the wet building material (e.g. gypsum board, acrylic painted walls, wood, wallpaper, carpet and mattress dust). It can also reproduce by the sexual way at the stage of teleomorph.

Chaetomium globosum from the class *Sordariomycetes* is a saprophytic fungus that primarily resides on plants, soil, straw, and dung. It assists in cellulose decomposition of plant cells using the hyphal cellulase activity. It could be a human allergen and opportunistic agent of the ungual mycosis and neurological infections. The ascospores are produced sexually; they are contained in the *ascus*. The fruiting body (*ascocarp*) consists of a very tightly interwoven *hyphae* and may contain millions of asci, each of which typically contains four to eight ascospores. Clusters of ascospores are released from the spherical dark *perithecia* with unbrached radiating hairs (Fig.2).

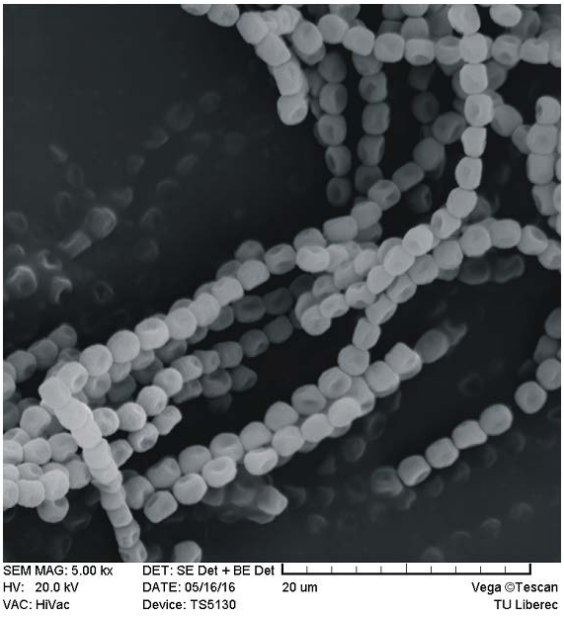

Figure 1. Conidia of *Penicillium chrysogenum*

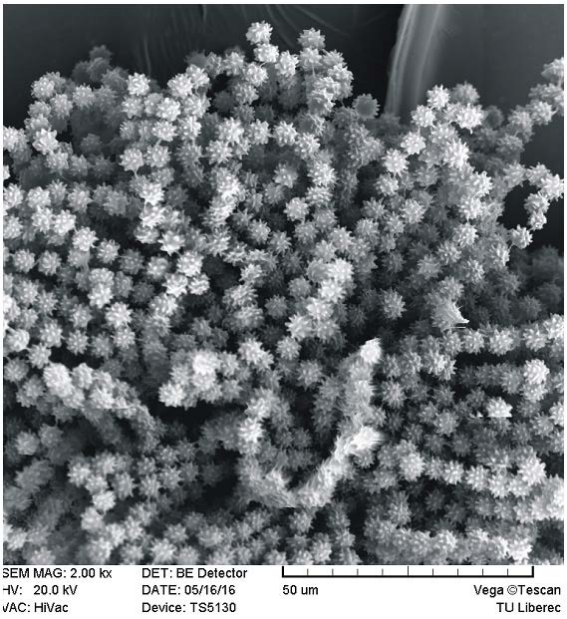

Figure 2. Ascospores of *Chaetomium globosum*

Omnipresent mold spores often represent a serious problem for the book archives, because the molds themselves are usually very undemanding. Under ideal conditions (relative air humidity above 65 %, temperature 12-35 °C with temperature optimum between 18-22 °C), they grow readily on a nutrient poor substrate such as paper, fabric, wood or parchment. The slightly acidic environment (pH 5.6 - 6)

usually suits them and their spores can survive for a long time even in adverse conditions. Molds are damaging book and museum collections not only visually (spots), mechanically (decomposition of the substrate and the subsequent disintegration of the material), but they also represent a health risk to the staff working in the environment of book archives (allergens, spores, mycotoxins). [6, 7]

The molds from *Aspergillus* genus have a rich enzymatic apparatus that produces different mycotoxins. *Aspergillus fumigatus* and *Aspergillus flavus* produce the toxin and carcinogen aflatoxin which can contaminate food. The most common species causing allergic disease are *Aspergillus fumigatus* and *Aspergillus clavatus*. The *Aspergillus fumigatus*, as well as the mycotoxin ochratoxin A, produced by an opportunistic pathogen *Aspergillus ochraceus*, can cause bronchial *aspergillosis* in the form of the chronic pulmonary aspergillosis, aspergilloma or allergic bronchopulmonary aspergillosis. [8, 9] Over 40 mycotoxins chaetoglobosins were isolated and characterized from the *Chaetomium globosum* species present on the cellulose surface of gypsum boards. Many of them demonstrated acute toxicity to mammals and a strong cytotoxicity to cells. [10] Also *Penicillium* produces chemical compounds that were reported to be strong allergens. They may cause hypersensitivity pneumonitis and allergic alveolitis. [11, 12] The mycelium of *Cladosporium* causes allergic reactions or asthma symptoms due to the production of mycotoxins such as asperentin and cladosporic acid. [13]

The preventive protections against fungi are appropriate storage conditions, primarily elimination of the air humidity, as well as active mechanical, physical and chemical protection of books [14, 15, 16] against fungi (for example, mechanical cleaning, freezing, gamma radiation, fungicides in the form of solutions, fumigation agents, aerosols, etc.).

2. Experimental

2.1. Materials

Cotton fabric Sara (Licolor), area weight 135 gm^{-2}, fabric thickness 0.37 mm
Water soluble glue Planaxol (Planatol Wetzel, Germany) based on PVA
Cardboard, area weight 200 gm^{-2}
Acronal S 996 S (BASF SE, Germany) - aqueous polymer dispersion based on ester of acrylic acid and styrene, viskosity 2 Nsm^{-2}
Suspension of four kinds of fungi in water - concentration 10^8 CFU/ml: *Penicillium chrysogenum* (CCM F-362), *Aspergillus niger* (CCM 8189*)* and concentration 10^5 CFU/ml: *Cladosporium sphaerospermum (*CCM F-351*), Chaetomium globosum* (CCM 8156)
Kuprikol (commercial antifungal product, copper oxychloride), (AgroBio Opava, Czech Rep.)
Biostat (commercial antifungal product containing biogenic silver), (ANSIL, Slovakia)
Zinc nitrate ($Zn(NO_3)_2$), salicylic acid, boric acid (LachNer, Czech Rep.)
Ketoconazole ((±)-*cis*-1-Acetyl-4-(4-[(2-[2,4-dichlorophenyl]-2-[1H-imidazol-1-ylmethyl]-1,3-dioxolan-4-yl)-methoxy]phenyl)piperazine), (Sigma Aldrich)
Malt agar (Čaderský-Envitek), Rice agar (Biovendor)

2.2. Methods

Chemicals at concentrations of 5 - 2.5 – 1 – 0.5 and 0.05 weight percentage were added to the acrylic paste, (concentrations used for all test chemicals except ketoconazole, which was used at concentrations of 1 – 0.1 – 0.01 and 0.001 weight percentage). The coating mixture was applied to the fabric on a printing machine by using pressure of the rolling steel rod with weight of 555 g with the magnetic pressure stage 2 and feed rate of the rod 2 m min^{-1}. After drying at 80 °C the samples of 2x3 cm were cut from the coated canvas and glued with Planatol, and subsequently secured by stitching with cotton thread to cards from the printing carton with dimensions 8x15 cm. Half of the prepared coatings was exposed to the simulated humidity aging in the climate chamber under conditions of 80

°C and 65% humidity content, for duration of 144 hours. [17] From these canvases were also prepared samples on the cardboard for application of the fungi suspension. The suspension of fungi was applied to the cards with samples using a pipette in an amount of about 2 ml of suspension per card. These samples were stored in the desiccator box at the room temperature and continuously moistened using a spray. The growth of molds was observed during six weeks.

Four samples from each canvas, area of 1 cm^2, with maximum concentrations of chemicals (5%) (including canvases that passed through simulated aging) were taken for the control test. These samples were placed on Petri dishes with a malt or rise agar and there was applied 30 microlitres of *Aspergillus niger* or 30 microlitres of suspension containing a mixture of the three other fungi on each sample, at concentrations 10^8 or 10^5 CFU/ml. This controlled cultivation was carried out at 23 ± 3 °C for 2 weeks.

3. Results and discussion

Figure 3 shows an overview of all types of tested substances with a potential antifungal effect in the highest concentration (5%) used in the coating in interaction with the *Aspergillus niger* on the malt agar after 5 days of cultivation. The best antifungal effect is evident on samples with the zinc nitrate, partial effect is observed also on samples with Kuprikol (copper oxychloride). The lower half of the Petri dishes contains the samples after simulated wet aging. The concentration range of the zinc nitrate in interaction with the *Aspergillus niger* on the malt agar is in Figure 4, where it is seen that the stronger antifungal effect of zinc nitrate is manifested only at its highest concentration used (5 %).

Figure 6 shows a relatively good inhibitory effect of the cotton canvas with acrylic and starch coating with the addition of the 15 % boric acid. These samples glued on the cardboard exhibited a good inhibitory effect against the molds mixture, in comparison with the uncoated cotton and the cotton coated only with a starch even after 5 weeks of cultivation in humid conditions.

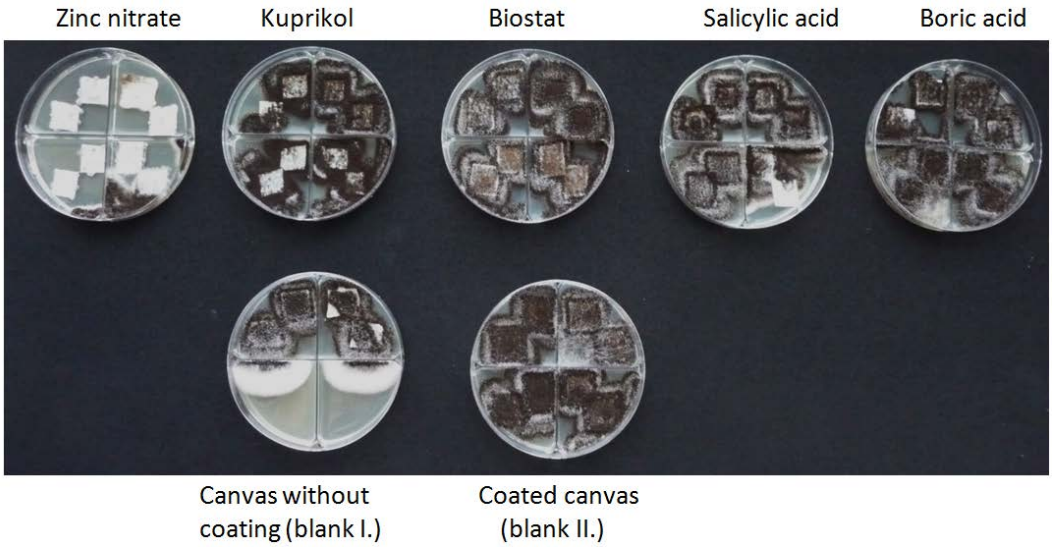

Figure 3. The growth of Aspergillus niger colonies on the cotton coatings with the highest concentration of antifungal additives (5%) after 5 days of cultivation

Figure 4. The growth of Aspergillus niger colonies on the cotton coatings with a different ratio of Zn(NO3)2 after 5 days of cultivation

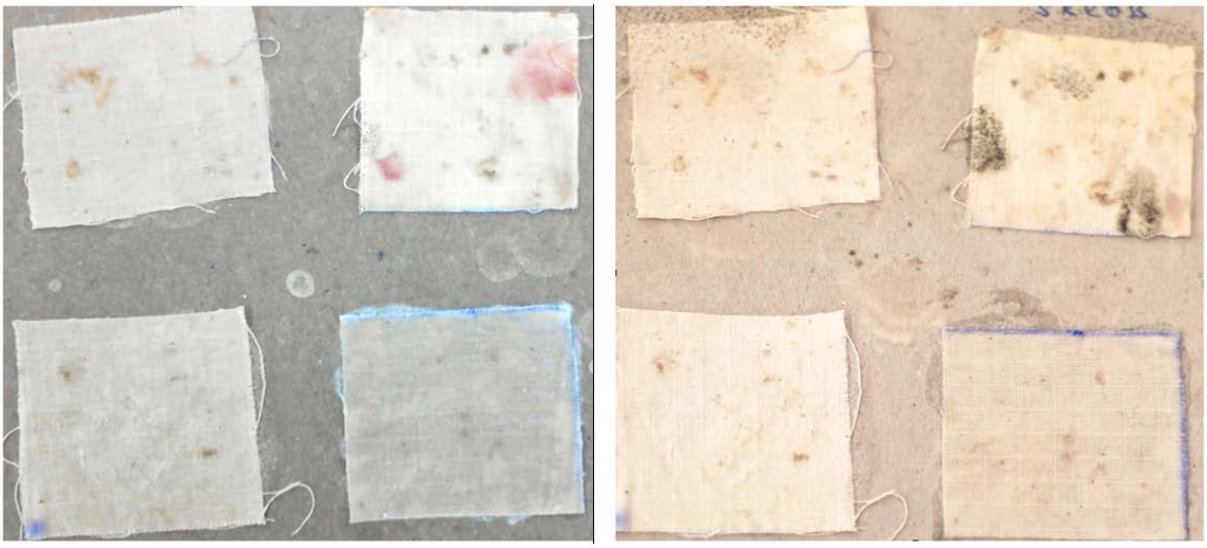

Figure 5. Testing of 15 % boric acid antifungal properties on coated cotton glued to the cardboard.
Left: after 2 weeks, right: after 5 weeks of cultivation.
Placing of the samples: cotton fabric – blank (top left), cotton fabric with starch coating (top right), cotton fabric with starch coating and 15 % of borid acid (bottom left), cotton fabric with acrylate coating and 15 % of boric acid (bottom right)

Table 1. Antifungal effectiveness of the test substances on coated cotton glued to the cardboard

Chemicals	Concentration [wt %]						Antifungal effectiveness
	0.05	0.5	1.0	2.5	5.0	15.0	
Zinc nitrate	○	○	◔	◑	●		
Kupricol	○	◔	◑	◕	●		
Biostat	○	○	◔	◑	◕		
Salicylic acid	○	○	○	○	○		
Boric acid	○	○	○	○	○	◔	
	0.001	0.01	0.1	1.0	-	-	
Ketoconazole	○	◕	●	●			

Note: ○ 0 % ◔ 25 % ◑ 50 % ◕ 75 % ● 100 %

The process of simulated wet aging or weathering (80 °C, 65 % RH, 144 days) had no significant effect on the antifungal activity of tested substances, but it pointed out the problem that some of tested substances changed color during their aging. All tested substances were initially white or colorless (with the exception of green copper oxychloride that dyed the coated fabric to a color near to the so-called sea foam (or sea green) and due to the simulated aging it has changed to olive green hue). Due to the aging, temperature and oxidation processes the ketoconazole significantly reddened (coral red), silver turned to gray and black, that was not even camouflaged by a presence of the white titanium dioxide in the product used (Biostat), zinc nitrate became slightly ocher (Fig.6). All these hue changes of coated canvas can be very undesirable, especially when using the lighter shades of book canvases.

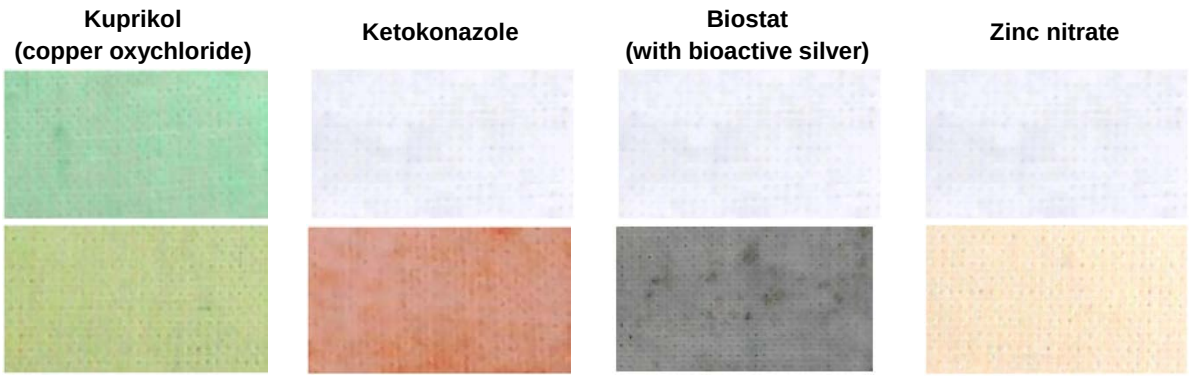

Figure 6. Color changes of white coated cotton fabric with antifungal additives of 5% concentration before (up) and after simulated wet aging (down)

Another disadvantage of some of the substances is their ability to change the ester of acrylic acid viscosity and effectively liquefy the initially viscous coating that complicates the entire technological process of the coated canvas production. Mainly zinc salts (zinc nitrate, zinc chloride, zinc sulfate) have this ability. Due to good antifungal activity of zinc ions and not very significant hue changes of the coating during aging, this disadvantage can be bypassed by changing of the technological process of coating application on the canvas (eg. a deposition from a bath or spraying), or by selecting another form of zinc (zinc oxide, organic zinc substances).

4. CONCLUSIONS

The best antifungal effect against the mixture of molds (*Penicillium chrysogenum*, *Aspergillus niger, Cladosporium sphaerospermum and Chaetomium globosum)* of tested chemicals showed ketoconazole and zinc salt (zinc nitrate) present as additives in the acrylates coating cloth, both when tested on agar, and in the setup simulated a typical surface layer on the cover of archived books (cotton canvas with acrylic coating bonded on cardboard by dispersion bonding material based on PVA). Also, products containing silver or copper (specifically the copper oxychloride) added to the acrylate coating relatively well prevent growth of fungi, usually at a concentration of 5% or more. Other tested compounds did not stop the growth of molds very much, the boric acid showed some inhibitory effect on the growth of molds at a high concentration of 15%.
With regard to the color changes of coatings and various antifungal efficacies of the tested chemicals, the zinc nitrate was evaluated preferably as the best antifungal additive. The zinc nitrate as an additive in coating, prevented the growth of different molds on the surface of coated cotton fabric at the concentration of 2.5 % with moderate efficiency, and of 5% of the wet coating weight with good efficiency, while the color changes during simulated aging were not as significant, and it would be

almost not noticeable when using a colored fabric. However, the problem with liquefying of acrylic coating, that zinc nitrate causes already early at low concentrations, still has to be resolved.

ACKNOWLEDGEMENTS

This work was supported by the project No. DF13P01OVV004 Exploration, conservation and care of modern library collections - materials and technologies provided by the Ministry of Culture within the Program of applied research and development of national and cultural identity (NAKI).
Special thanks to Mrs. Grabmüllerová.

References

1. *Guerreau, A., & Nguyen, T. P. (2003). La restauration des cartonnages d'éditeur romantiques en percaline gaufrée. Coré: conservation et restauration du patrimoine culturel, (14), 36-41.*
2. *An, Z. (2004). Handbook of Industrial Mycology. Marcel Dekker Inc. ISBN: 9780824756550*
3. *Konkol, N. R. et al. (2012). Early detection of fungal biomass on library materials. Journal of Cultural heritage, 13(2), 115-119.*
4. *Zyska, B. (1997). Fungi isolated from library materials: a review of the literature. International Biodeterioration & Biodegradation, 40(1), 43-51.*
5. *Mesquita, N. et al. (2009). Fungal diversity in ancient documents. A case study on the Archive of the University of Coimbra. International Biodeterioration & Biodegradation, 63(5), 626-629.*
6. *Frisvad, J. C., Thrane, U., Samson, R. A., & Hoekstra, E. S. (2004). Mycotoxin production by common filamentous fungi. Introduction to food-and airborne fungi, (Ed. 7), 321-331.*
7. *Schuster, E., Dunn-Coleman, N., Frisvad, J. C., & Van Dijck, P. (2002). On the safety of Aspergillus niger–a review. Applied microbiology and biotechnology, 59(4-5), 426-435.*
8. *Mourya, S., & Jauhri, K. S. (2000). Production of citric acid from starch-hydrolysate by Aspergillus niger. Microbiological research, 155(1), 37-44.*
9. *Latgé, J. P. (1999). Aspergillus fumigatus and aspergillosis. Clinical microbiology reviews, 12(2), 310-350.*
10. *Fogle, M. R., Douglas, D. R., Jumper, C. A., & Straus, D. C. (2007). Growth and mycotoxin production by Chaetomium globosum. Mycopathologia, 164(1), 49-56.*
11. *Van Assendelft, A. H., Raitio, M., & Turkia, V. (1985). Fuel chip-induced hypersensitivity pneumonitis caused by penicillium species. CHEST Journal, 87(3), 394-396.*
12. *Fergusson, R. J., Milne, L. J., & Crompton, G. K. (1984). Penicillium allergic alveolitis: faulty installation of central heating. Thorax, 39(4), 294-298.*
13. *Bush, R. K., & Portnoy, J. M. (2001). The role and abatement of fungal allergens in allergic diseases. Journal of Allergy and Clinical Immunology, 107(3), S430-S440.*
14. *Emam, H. E., Saleh, N. H., Nagy, K. S., & Zahran, M. K. (2015). Functionalization of medical cotton by direct incorporation of silver nanoparticles. International Journal od Biological Macromolecules, 78, 249-256*
15. *Ogar, A., Tylko, G., & Turnau, K. (2015). Antifungal properties of silver nanoparticles against indoor mould growth. Science of the Total Environment, 521-522, 305-314.*
16. *Kartal, S. N., Green, F., & Clausen, C. A. (2009). Do the unique properties of nanometals affect leachability or efficacy against fungi and termites? International Biodeterioration & Biodegradation, 63(4), 490-495.*
17. *ISO 5630/3 (1956). Paper and board – Accelerated ageing – Part 3: Moist heat treatment at 80 and 65 % relative humidity.*

MOISTURE MANAGEMENT FOR DIFFERENT AIR CONDITIONS

Tereza Heinisch, Pavla Těšinová, Lucie Pološčuková

Technical University of Liberec, Faculty of Textile Engineering, Department of Textile Evaluation, Studentská 2, Liberec, Czech Republic, tereza.heinisch@tul.cz, +420485353179

Abstract:

Paper deals with evaluation of moisture management of textiles. It comprises management types and evaluates fabrics comfort in the terms of liquid moisture transport, drying speed and management resistivity. Because methods has got some limitations and cares with presumptions it is discussed here necessary interpretation of results, especially for smart fabrics.

Key words:

moisture management, drying rates, hydrostatic resistance, woven fabrics

1. Introduction

We can meet concept of fast-drying clothes. Majority of apparel producers label clothes and final products by this term on textiles made from synthetic fibres which have got lower wettability itself in comparison to natural fibres. Testing is necessary instrument for exact determination of newly invented types and constructions of fabrics same as profiles of fibres. Unfortunately existing methods do not provide sufficient manual how to test the drying speed objectively. Important factors are mostly neglected which are influences of flow speed or heating of human skin.

This paper summarises important standards dealing with moisture management and determines way of textiles testing.

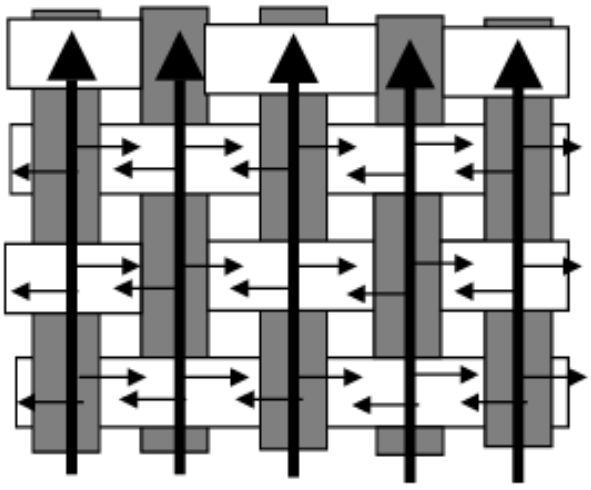

Figure 1. Transport of liquid in textiles during suction – net model where arrows represent main fluid of humidity including side branches [8]

Related standard AATCC Test Method 195-2009: Liquid Moisture Management Properties of Textile Fabrics is based on kind of wetting resistivity in relation to textile geometry and fabric parameters when sample is placed between two electronic sensors to be possible to apply liquid in the middle of sample. Electric resistance is detected in dynamic way of the process in plane of both surfaces and through the material [1].

Nonofficial techniques were already published in 2008 as Technical attachment of AATCC / ASTM for textile gods. Official standard [2] AATCC Test Method 199-2011: Drying Time of Textiles: Moisture Analyzer Method was published later on. Testing method is based on gravimetric principle when wetting is defined. Wetting of sample is absorption in deionised water for 1 minute. Decreasing of weight is detected in the real time conditions. End state of measurement is when weight of sample is only 4% higher than completely dry state. Method is limited for high absorbing materials such as first layer of sports clothes higher then 30s [3] and is suitable for suction materials according to definition at (AATCC TM 79 – suction of textiles).

Important BMI method (from set of standards from 2015 TNI CEN/TR 16422: Buffering capacity of liquid sweat and sweat transport) uses small skin model to evaluate water vapour resistance and thermal resistance. Skin heat temperature and air fluid are testing parameters on the instruments following ISO 11092. Advantage of this method is simulation of human skin by wet polyester fabric which absorbed 15 cm^3 humidity in temperature 35°C. Testing lasts 15 minutes and difference is detected by gravimetric method. This method is not sensitive for drying process and state of dry material [4].

Standard for exact value of moisture drying rate with drying characteristics is ISO 17616: Textiles: Determination of moisture drying rate and is useful to determine speed of drying of textile. It is as well based on gravimetric principle in stationary state of air without heating effect. Testing lasts 60 minutes or at least to the 10% of initial humidity weight [5]. Same principle is used for Asian countries in JIS L 1096: 1999 – Drying speed [6].

Laing in Determining the Drying Time of Apparel Fabrics comparises two types of drying evaluation. The first method is based on standard AATCC Test Method 195-2009 without air fluid. Second method is based on BPI method with principle of wetted sample faced right side up to the 90° angle to the air flow 1±0,05$m.s^{-1}$ and in contact with heated plate (according to standard ISO 11092). Stable state and end of measurement is defined when temperature is stabile at 35±0,1°C. It respects real conditions the best from existing methods still does not detect drying process [7].

2. Experimental

Experimental material is defined at first for its moisture management properties with set of methods as capillary action test, Moisture Management Test by instrument MMT SDL Atlas and droplet test. After determination of moisture management it is possible to define reverse process – drying, especially for samples with good moisture management or samples with very good humidity transport through the thickness of the sample. Such a material can be defined as fast-drying and complex drying characteristics including skin heating and air flow in the time is necessary to be determined.

2.1. Materials

It was tested number of samples from fibres PES, PAD in plain, twill and satin weaves provided by Department of Textile Technologies FT TUL.

It was chosen PES material for abstract in plain, twill (3/1), satin (7/1) weaves when warp set is 42 [1/cm], fineness of warp yarn 78 [dtex], fineness of weft yarn165 [dtex].

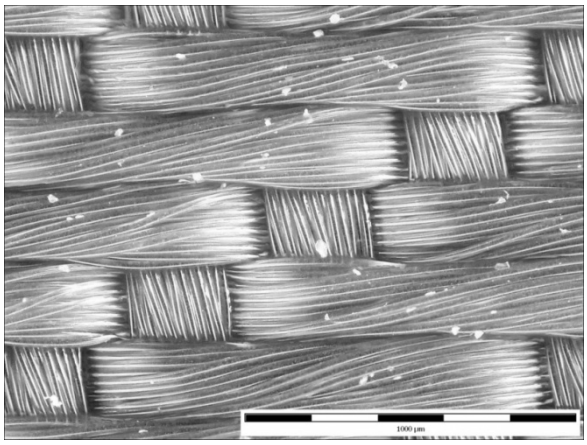

Figure 2. Microphotography of tested sample, twill weave of multifilament yarns, magnification 10x

Table 1. Material identification for set of PES fabrics

Weave	Plain					Twill (3/1)					Satin (7/1)				
Weft set [1/cm]	21	23	25	27	29	25	27	29	31	33	29	31	33	35	37
Area density [g/m^2]	80	79	95	94	96	95	96	95	105	108	101	103	106	109	118
Porosity [%]	47.4	45.8	44.2	42.6	41.0	44.2	42.6	41.0	39.4	37.8	41.0	39.4	37.8	36.2	34.6

3. Results and discussion

It was tested suction and moisture management including its theoretical computation build on the model of Lucas–Washburn Equation [9]. Linear model was used and independent variable was theoretical suction. As visible from Figure 3, the closest prediction fits to the plain weave. Calculation is not sensitive for fabric weave in this case. Our task is to find models with satisfactory prediction for two other basic weaves too. After that it will be possible to evaluate better also draying process same as moisture management.

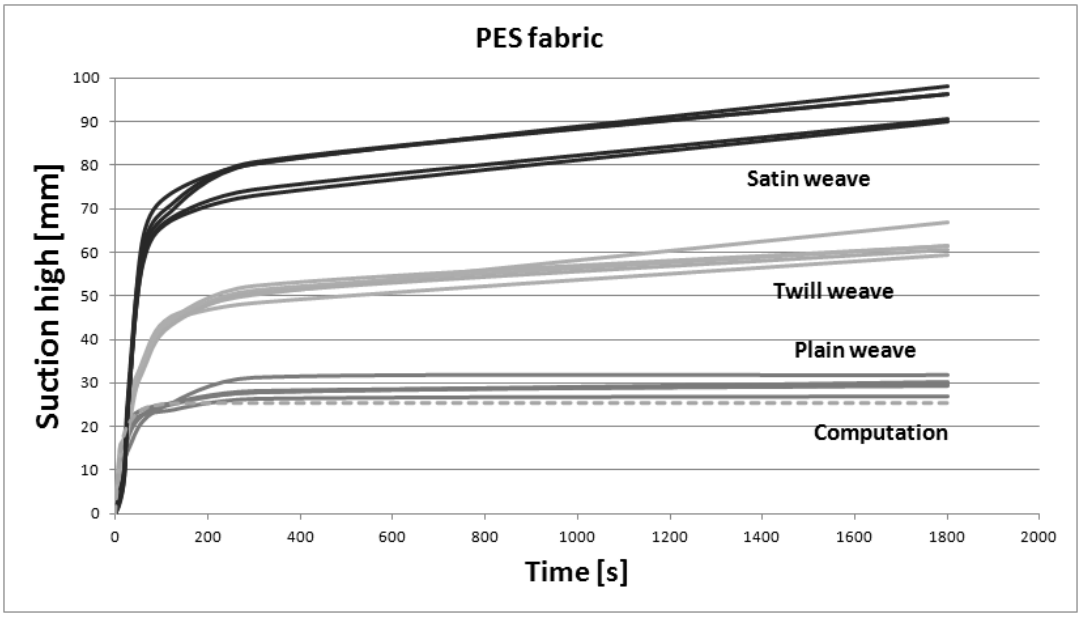

Figure 3. Suction high in time relation for PES fabric with visible difference in weaves, warp direction

Drying properties of woven PES were tested on prototype instrument which is constructed from two main parts, see figure 4. The first part is channel where can be defined exact laminar air flow. This air flow can be set up according to standard needs. Air flow blows tested sample in the whole sample area.

Second part is testing device when tested sample is placed horizontally. Testing device is composed from analytical scales (a), aluminum ribs (b) and plates (c). Rib with plate are blown by more ventilators to provide isothermal drying conditions. With help of clamping means of the frame (e) sample is fixed on the plate. Sample is placed whole to the channel. The instrument is possible to be placed in the air conditioning chamber.

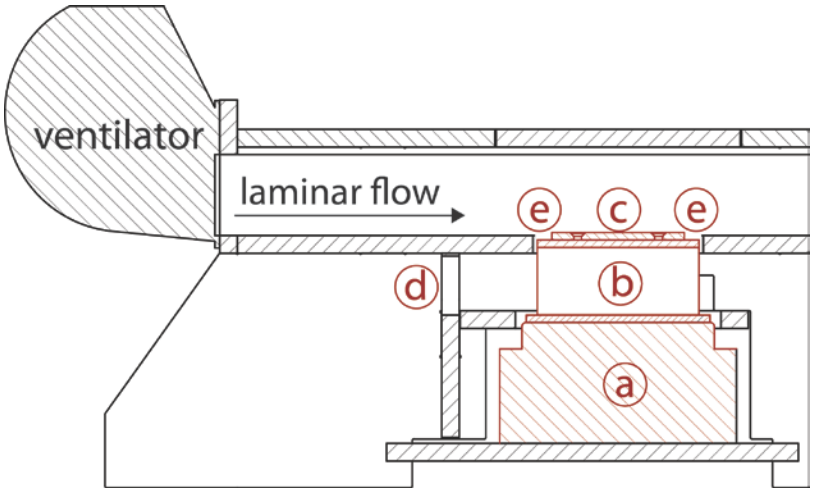

Figure 4. New instrument: analytical scales (a), aluminum ribs (b), plates (c), 3 ventilators (d), clamping means of the frame (e)

The instrument is connected with PC when weight of tested sample is recorded in the minute intervals. Every minute ventilator is stopped for 7 seconds and SW records current weight of sample.

Our experiment run in temperature 18°C and relative humidity 65 %. Sample size was in size 11 x 8 cm. All samples were air-conditioned in laboratory environment for 24 and weighted on analytical scales of tested instrument in dry state to define standard weight of sample. Tested samples were dipped into distilled water in temperature 18°C for 60 minutes. Every sample was left to drain away on the absorbent paper for one minute after that and placed to the instrument on the plate. Testing begun after ventilator started in speed 5 $m.s^{-1}$. Testing parameters were temperature 18°C and relative humidity 65 %. See drying results on following Graphs.

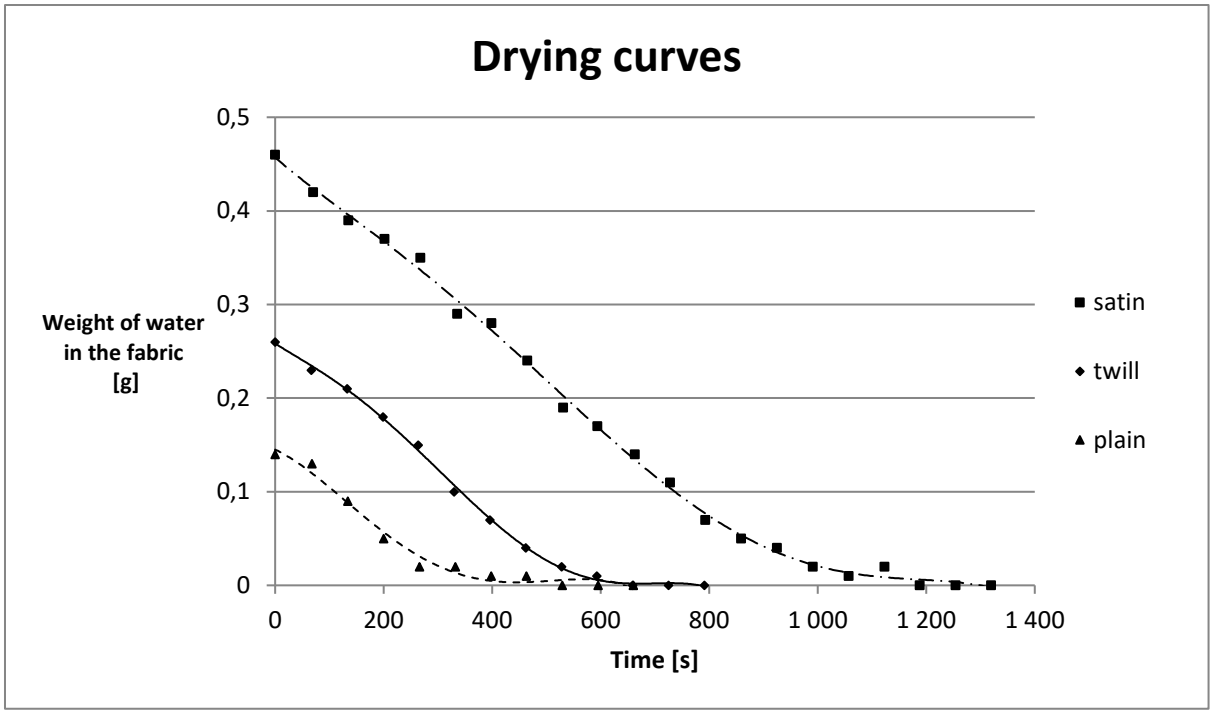

Figure 5. Drying curves in maximum water content (suction ability of samples)

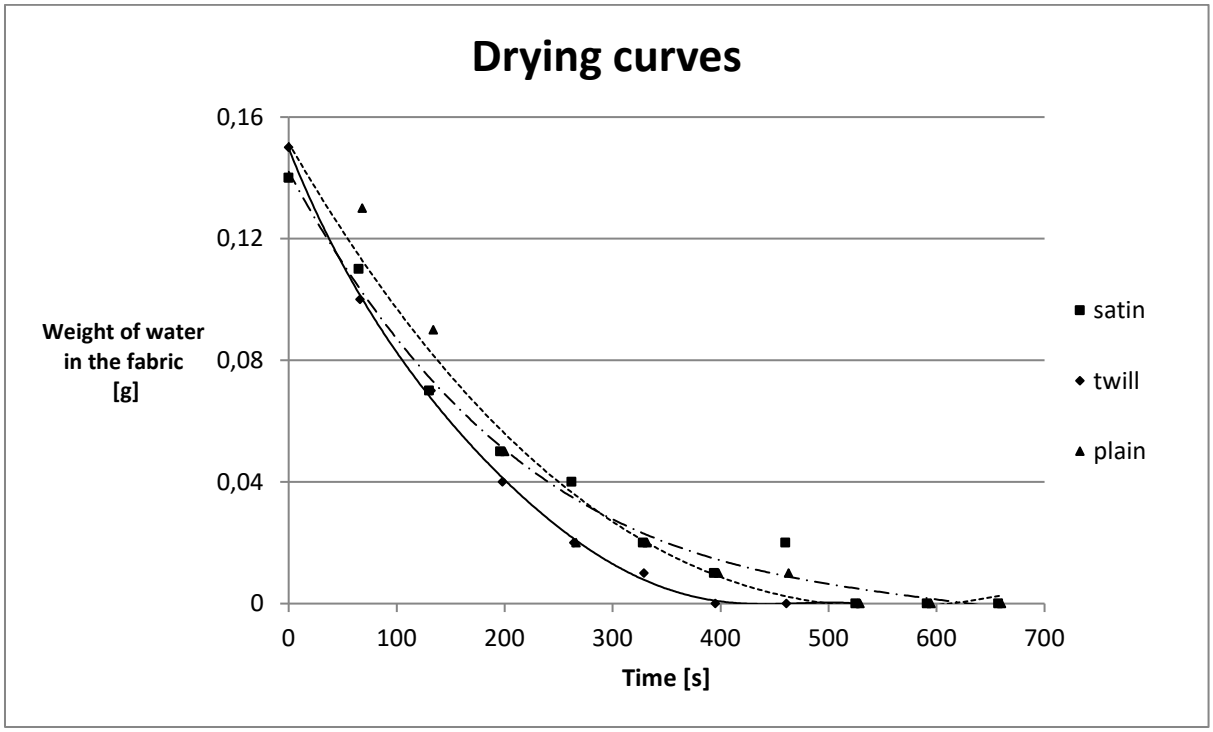

Figure 6. Drying curves for the same level of absolute water content of samples

Maximum absorbed water content is for satin weave 51%, twill 35% and plain 23% of dry state in testing visualised in Figure 5. It is obvious then drying curves begin on different start point of absolute weight of water in the tested fabric. Suction of PES fibres itself is small. Tested sample in this example is dependent on the different porosity of samples (size of macro pores vary in selected weaves types). Decrease of humidity is in very close trends for all samples.

Graph in figure 6 shows drying process in case of absolute water content same for all tested samples. When fabrics are same content of humidity in the means of plain weave maximum water suction ability drying speed does not affect on the weave type as in previous test. Drying curves are very close together.

4. CONCLUSIONS

Changes in moisture management transport can be seen in the terms of weave of fabrics. Correlation of suction high test is dependent in warp direction mostly. Satin weave samples have got significant difference with weft weave and plain weave in time. Plain weave as a structure with the highest curvature in structure and tightness between yarns embody the smallest suction and moisture management. On the other hand satin weave with its flotation has got high suction on the warp direction – flotation affected moisture management. After detection of drying time it will be possible to define relationship with fabric parameters, for example suction high in time range.

Though results are not that clear in the reverse process. Drying speed and trend in humidity decrease are very close together for various weaves from this the very first testing with new instrument. Test ability was that what was tested and results are important for next steps which will be testing in various air velocity, broad sample set, various environment conditions etc. New instrument is precise in testing, clear in data interpretation and relevant to continue with.

ACKNOWLEDGEMENTS

This paper was financially supported by the Department of Textile Evaluation FT TUL and supported by the development program of Student Grant Competition SGC 2016 Nr. 21148 granted financial aid for Specific Undergraduate Research.

References

1. *AATCC Test Method 195-2009: Liquid Moisture Management Properties of Textile Fabrics. USA: AATCC Committee RA63, 2009.*
2. *AATCC Test Method 199-2011. Drying Time of Textiles: Moisture Analyzer Method. USA: AATCC Committee RA63, 2011.*
3. *AATCC Test Method 79-2003. Absorbency of Textile. USA: AATCC Committee RA63, 2003*
4. *TNI CEN/TR 16422: Klasifikace termoregulačních vlastností. Praha: Úřad pro technickou normalizaci, metrologii a státní zkušebnictví, 2015*
5. *ISO 17616, 2014: Textiles: Determination of moisture drying rate. Switzerland: International organization for standardization, 2014*
6. *JIS L 1096: 1999. Testings methods for wowen fabrics: Drying speed. Tokyo: Japanese Standards Association, 1999.*
7. *Laing, R. M., Wilson, CH. A., Gore, S. E., Carr, D. J., Niven, B. E. Determining the Drying Time of Apparel Fabrics. Textile Research Journal [online]. 2007-08-01, issue 77, no. 8, p. 583-590 [cit. 2013-03-13]. ISSN 0040-5175.*
   Avalaible from: http://trj.sagepub.com/cgi/doi/10.1177/0040517507078232.
8. *WIENER, J. Vzlínání kapaliny do plošné textilie. 10/2013. VCT CENTRUM TEXTIL*
9. *HAMRAOUI, A. a T. NYLANDER. Analytical Approach for the Lucas–Washburn Equation. Journal of Colloid and Interface Science [online]. 2002, 250(2), 415-421 [cit. 2016-05-01]. DOI: 10.1006/jcis.2002.8288. ISSN 00219797. Available at: http://linkinghub.elsevier.com/retrieve/pii/S0021979702982883*

STUDY ON MOISTURE TRANSPORT OF SOCKS

Petra Komárková, Viera Glombíková

Technical University of Liberec, Faculty of Textile Engineering, Department of Clothing Technology, Liberec, Czech Republic, Studentska 1402/2, +485353500, petra.komarkova@tul.cz

Abstract:

Investigating the liquid moisture transport and thermal properties is essential for understanding physiological comfort of clothes. This study reports on an experimental investigation of moisture management transport on the physiological comfort of commercially available socks. There are subjective evaluation and objective measurements. Subjective evaluation of the physiological comfort of socks is based on individual sensory perception of probands during and after physical exertion. Objective measurements were performed according to standardized methods using Moisture Management tester for measuring the humidity parameters. The obtained values of liquid moisture transport characteristics were related to the material composition and structure of the tested socks. In summary, these results show that objective measurement corresponds with probands feelings.

Key words:

Physiological comfort, knitting, socks, moisture management

1. Introduction

The most important feature of functional clothing is to create a stable microclimate next to the skin in order to support body's thermoregulatory system, even if the external environment and physical activity change completely [1, 2]. Socks belong to group of first layer clothing products that should protect skin in warm or cold weather conditions and should safe good thermo-physiological comfort. Till date, a lot of research work has been devoted to comfort of socks. Van Amber et al. analysed effect of fabric thickness on thermal and moisture transfer properties of socks [3]. The study was aimed to determine the relative effects of fiber type, yarn type, and fabric structure on thermal resistance, water vapour resistance, thermal conductance, water vapour permeability, liquid absorption capacity, and regain of sock fabrics. In study of Čiukas the influence of different fibres of the socks on the thermal conductivity coefficient of plain knits and plated plane knits with textured polyamide or elastane wrapped with textured polyamide thread was investigated [4]. In the past few years, different advanced experimental techniques have been used to characterize liquid water transport and thermal transport in fabrics or socks. Leisen et al. applied magnetic resonance to study the moisture transport in different textiles [5]. Neutron radiography was used for measurement measurements of moisture distribution in multilayer clothing systems by Weder [6]. Rossi used X-ray tomography to analyse the transplanar and in-plane water transport in different sock materials when two defined pressures were applied [7]. This method enables quantify the three-dimensional water transport properties in textile structures, which is especially relevant for fabrics with asymmetrical capillary transport properties like the sock materials. Researchers have reached the conclusion that fibre type, yarn properties, fabric structure, finishing treatments and clothing conditions are the main factors affecting thermo-physiological comfort of socks wearing. But, it is very difficult to uncover how to set afore mentioned parameters of socks material to production suitable socks for winter or summer conditions. Till date, performance of socks was mainly determined by objective measurement. Therefore, our study is focus on analysation of results from both objective and subjective evaluation of physiological properties of socks.

2. Experimental

The experiment was divided to two steps. In the first step the subjective physiological feelings of probands during wearing of socks were recorded. In second step the objective parameters of moisture management of socks were tested. In the end the results from both part of experiment were compared.

2.1. Materials

Commercially available sport and everyday wear socks differing in fiber content, structure, weight and thickness were selected for this research. Table 1 shows the characteristics of the socks used in this experiment. Socks were divided in three characteristic classes according to material composition. Basic series comprises the socks from the nearly one hundred-percent share of raw materials. Classic series includes socks for leisure activities from blended materials with nearly the same share of basic raw materials – cotton. And functional series is designed for sports activities and is made from yarns with functional properties.

Table 1. Specification of tested socks.

Sample code	Fiber content	Pattern	Wearing purpose (by manufacturer)
Basic series			
B1	100% cotton	Welt: turned welt with inlaid rubber thread, Leg: plain jersey	Everyday wearing, No special treatment
B2	100% polypropylene	Welt: turned welt Leg: plain jersey Foot: float fabric, single jersey jacquard Heel, toe: plating fabric	Everyday wearing, Summer sport combined structure Instep part – good moisture transport, good air permeability
B3	98% polyester 2% Lycra	Welt: turned welt Leg, foot: plain jersey with inlaid rubber thread (2:1), single jersey jacquard Heel, toe: plating fabric	Casual activity, combined structure for good close-fitting (tight)
Classic series			
C1	65% cotton 30% polypropylene – Siltex 5% Lycra	Welt: turned welt Leg: plain jersey with inlaid rubber thread (3:1) Heel, toe: plating fabric	Antibacterial effect (Siltex), Instep part – fixing strip
C2	68% cotton 30% polyester 2% Lycra	Welt: turned welt Leg, heel, toe: plating fabric	Healing and soothing effects -extract from the Aloe Vera
C3	67% cotton 31% polyamide 2% Lycra	Welt: turned welt Leg: plain jersey with inlaid rubber thread (3:1) Foot, bottom part –plush fabric Heel, toe: plating fabric	Instep part – fixing strip, Bottom part - loop fabric for shock, absorption during walking
Functional series			
F1	50% CoolMax 30% cotton 10% PP – Siltex 7% polyamide 3% Lycra	Welt: turned welt with inlaid rubber thread Leg: plain jersey Foot: plain jersey with inlaid rubber thread (3:1) Heel, toe: plating fabric	For outdoor sports, Wicking sweat away from the skin, Suppression of unpleasant odors
F2	75% Merino wool 20% polypropylene – Siltex 5% Lycra	Welt: turned welt Leg: plain jersey Foot: float fabric, single jersey jacquard Heel, toe: plating fabric	For professional outdoor and indoor sports, Instep part - special structure for ventilation (for the best thermal comfort), Antibacterial effect (Siltex), Suppression of unpleasant odors,
F3	45% Outlast 25% polypropylene 20% wool 5% Lycra	Welt: turned welt Leg, foot, heel, toe: plush fabric	For e.g. winter mountain hiking, padded zones against the bruising, anatomically shaped for left / right, excellent thermoregulation (due to the material composition)

2.2. Methods

The performance of socks was investigated by two ways: *subjective evaluation and objective measurements.* Before being tested, the socks had been conditioned for 24 hours. The testing and measurement were carried out in an air-conditioned room under constant relative humidity of 55 % and the temperature of 21° C.

Subjective evaluation of physiological comfort

Subjective physiological feelings were tested by a group of 7 probands within their 30 minutes physical activity on stationary bike. A special questionnaire to collect information from probands was created. This questionnaire included information about physiological feelings of proband before physical activity, during (after 15 minutes from start of physical activity), immediately after and 15 minutes after physical activity. Proband were inquired about feelings of cold / heat, moist, fitting of socks, irritation of socks, overall comfort of socks. Questions had a closed character in the form of opposing terms (bipolar adjectives), divided into five-point scale (from 1 to 5, where 1 means the best and 5 the worst value). After 30 minutes of physical activity the socks were weighted and compare with weigh before test in order to investigate the over weight of sweat.

Objective evaluation of liquid moisture transport by Moisture management tester

Objective evaluation of liquid moisture transport was tested by standardized measurement with laboratory equipment Moisture management tester (MMT). MMT was developed to quantify dynamic liquid transport properties of knitted and woven fabrics through three dimensions: absorption rate – time for absorption of moisture on fabric's face and back surfaces, one-way transportation capability – one-way transfer from the fabric's back surface to its face surface, spreading/drying rate – the speed at which liquid moisture spreads across the fabric's back and face surfaces. [8]

3. Results and discussion

3.1. Subjective evaluation of physiological comfort

Data from all probands for all socks were averaged and processed into graphs.

Table 2. Location of places with the biggest wet. Visual evaluation.

Sock code	Grafic map of wet places	Sock code	Grafic map of wet places	Sock code	Grafic map of wet places
B1	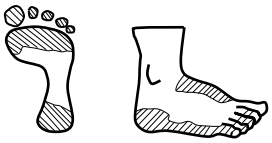	C1	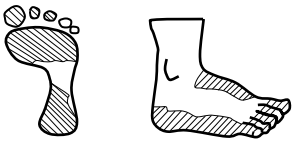	F1	
B2	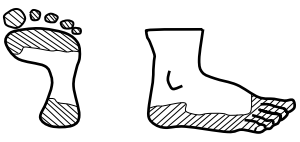	C2	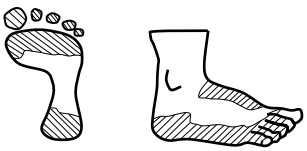	F2	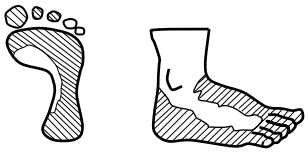
B3	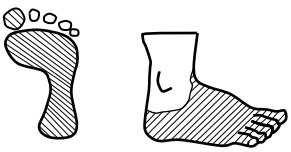	C3	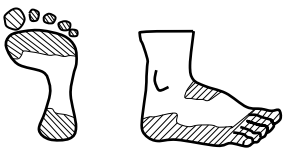	F3	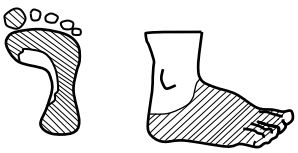

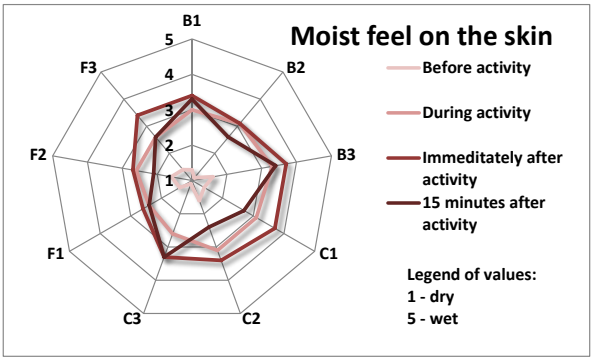

Figure 1. Graph based on the average of seven tested probands for moist feeling on the skin

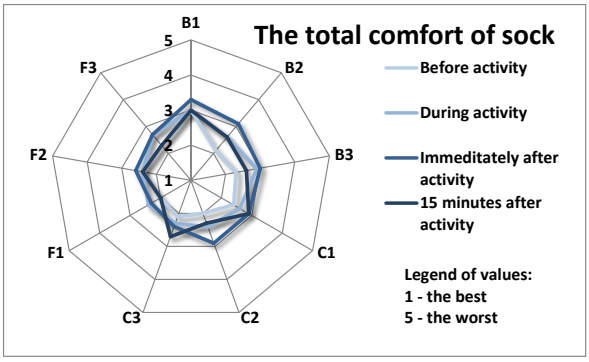

Figure 2. Graph based on the average of seven tested probands for total comfort feeling

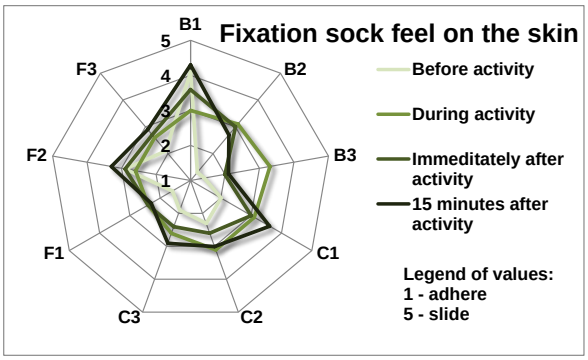

Figure 3. Graph based on the average of seven tested probands for feeling of sock fixation

Table 3. Weigh over of tested socks

Tested socks	B1	B2	B3	C1	C2	C3	F1	F2	F3
Average of weigh over of sweat [g]	1,236	0,393	0,776	0,406	0,661	0,616	0,604	0,747	3,108

Overall, these results indicate that the socks B1 (100% cotton) are evaluated as the worst from all tested socks. Questionnaires reported very bad fitting (shape adaption), very bad ability of drying out during and after sport activity. Socks F1 (Coolmax / cotton / polypropylene) were evaluated as the best. Questionnaires felt minimal amount of moisture, their feet were heated within sport activity and after activity provided optimal state of comfort.

3.2. Objective evaluation of liquid moisture transport by Moisture management tester

Average values of moisture transport investigated by MMT are shown in Fig.4. Comparison of tree important parameters between all tested socks is presented in Fig. 5., Fig. 6. and Fig. 7.

	Degree
Wetting time [s]	Top
	Bottom
Absorption rate [%/s]	Top
	Bottom
Max wetted radius [mm]	Top
	Bottom
Spreading speed [mm/s]	Top
	Bottom
OWTC	
OMMC	

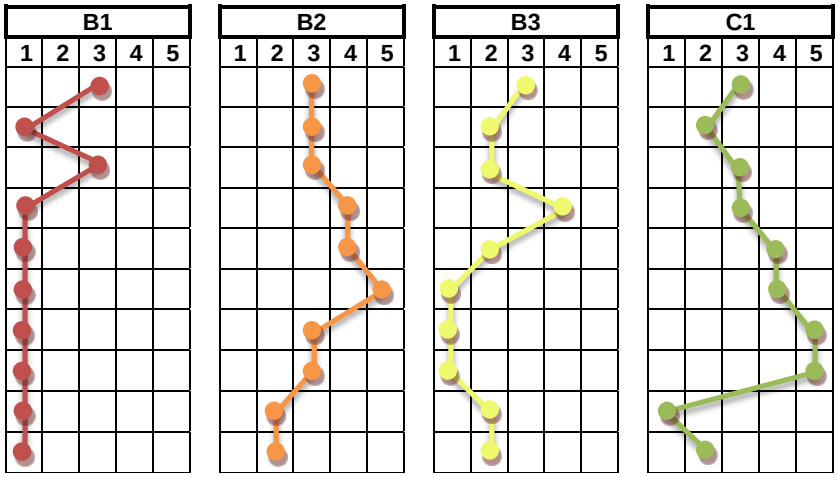

Note: OWTC - Cumulative one-way transport capacity
OMMC - Overall moisture management capacity

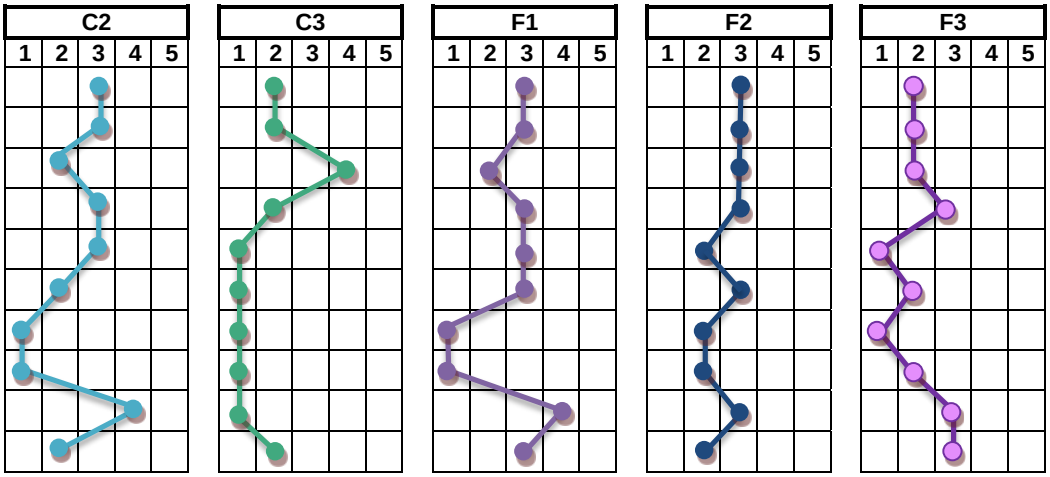

Figure 4. The graphs of liquid moisture transport parameters investigated by MMT

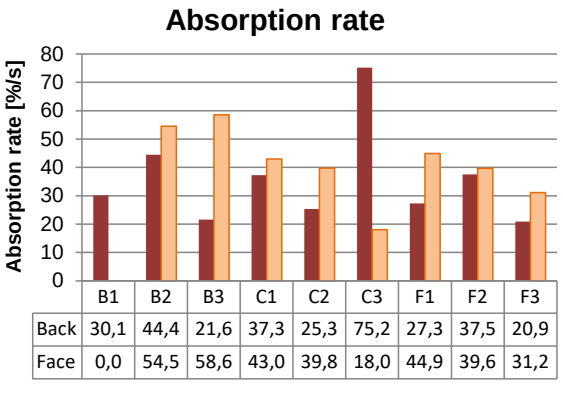

Figure 3. The graphs of absorption rate of tested socks investigated by MMT

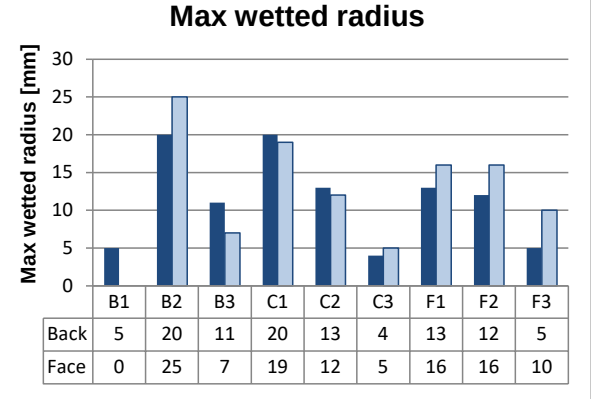

Figure 6. The graphs of maximal wetted radius investigated by MMT

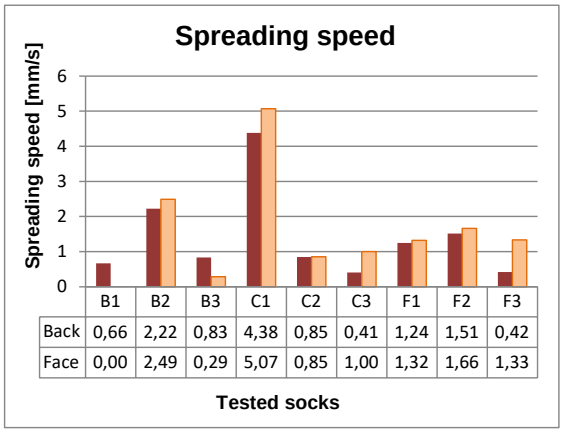

Figure 7. The graphs of moisture spreading speed in tested socks investigated by MMT

Lower values of absorption rate in face side indicated smale or none transport of moisture between sides (surfaces) of sock (moisture content in back side was significantly higher than in face side).

The graph of maximal wetted radius shows that the 100% cotton sock B1 has the smallest wetted surface. This parameter is indicator of bad draying out ability. Speed of drying out is inversely depended on a wetted radius size. On the contrary the sample of 100% polypropylene sock had the large wetted surface.

The Figure 5 presents the spreading speed in tested socks. From the graph, it can be seen that the smallest speed was measured in case of 100% cotton sock B1. This result shows that a material of sock didn´t absorb the moisture (sweat) into the weave structure. It can be assumed that the material of this sock has no effect on this property.

Table 4. Fabric classification of tested socks by MMT

Sample code	Type name	Properties
B1	Water proof fabric (despite the fact that no special finishing) 	Very slow absorption (in spite of 100% cotton), slow spreading, no one-way transport, no penetration
B2	Fast absorbing and quick drying fabric 	Medium to fast wetting, Medium to fast absorption, large spreading area of ellipse shape (better spreading in wale direction), slow spreading, poor one-way transport
B3	Slow absorbing and slow drying fabric	Slow absorption, slow spreading, poor one-way transport
C1	Fast absorbing and medium drying fabric	Medium to fast wetting, medium to fast absorption, medium spreading area, fast spreading, poor one-way transport
C2	Fast absorbing and slow drying fabric	Medium to fast wetting, medium to fast absorption, small spreading area, slow spreading, medium one-way transport
C3	Slow absorbing and slow drying fabric	Slow absorption, slow spreading, poor one-way transport

F1	Fast absorbing and slow drying fabric (one measurement – water proof fabric)	Medium to fast wetting, medium to fast absorption, middle spreading area, slow spreading, good one-way transport
F2	Fast absorbing and slow drying fabric	Medium to fast wetting, medium to fast absorption, small to middle spreading area, slow spreading, good one-way transport
F3	Slow absorbing and slow drying fabric	Slow absorption, slow spreading, good one-way transport

Overall, the results from MMT do not confirmed the fact that the socks from "Functional Series" achieve the best transport of liquid moisture how the manufacturers declare. The results show slow or middle the wetting time for all samples of socks, absorption rate is very small in keys of sock B1 (100% cotton) and spreading speed is the worst. This sock has the smallest max wetted radius too; it means that this sock has very bad drying ability. OWTC (Cumulative one-way transport capacity) parametrs shows negative values for socks B1, C1, C3 which demonstrate that water content of fabric´s face surface is lower than its back one. This indicates that the liquid introduced onto the back surface of the fabric transfers to the face surface not so fast.

4. CONCLUSIONS

The results of both subjective and objective evaluation have shown that the pattern of sock, porosity, and further fiber content and surface finishes have the greatest influence on transport of liquid moisture transport. It is ideal that the sock is quick-absorbing and quick-drying. Only one type from all tested socks reached this key idea parameter – namely B2 (100% polypropylene). These socks are knitted from several patterns (mainly plain jersey and plain jersey with bottom loom and insert thread). It is essential that the socks transport the sweat outside to the surrounding environment during physical activity. Subjective evaluation of probands confirms the results of MMT that socks B2 have good drying ability.

From the results it is evident that the socks from 100% natural fibers e.g. cotton has good absorption properties, however the results of subjective evaluation probands mentioned that they felt discomfort after 30 minute of sport activity due to slow moisture transport. This was confirmed by objective evaluation by MMT. Results of objective measurement correspond with probands feelings.

Further research should be undertaken to investigate the influence of maintenance on physiological comfort of socks. It would be interesting to determine the 100% cotton sock behaviour after several cycles of maintenance.

ACKNOWLEDGEMENTS

This research work was supported by Technology Agency of the Czech Republic Project No. TA04011273 and we also thank the student Tereza Pešanová, who cooperated on experimental part of this paper.

References

1. *Das B., Das A., Kothari V. K., Fanguiero R., Araújo M. (2008). Effect of Fibre Diameter and Cross-sectional Shape on Moisture Transmission through Fabrics. Fibers and Polymers, Vol.9 (2), pp. 225-231.*
2. *Nemcokova, R., Glombikova, V., Komarkova, P., (2015). Study on moisture liquide transport of knitting fabrics by means of MMT, termography and microtomography systems. AUTEX Research Journal, Vol. 15(4), pp. 233-242,*
3. *Van Amber, R. R., Wilson, Ch. A., Laing, R.M., Lowe, B.J., Niven, B.E., (2015). Thermal and moisture transfer properties of sock fabrics differing in fiber type, yarn, and fabric structure. Textile Research Journal, Vol. 85(12), pp. 1269–1280*
4. *Čiukas R., Abramavičiūtė J., Kerpauskas P.; (2010). Investigation of the Thermal Properties of Socks Knitted from Yarns with Peculiar Properties. Part I. Thermal Conductivity Coefficient of Socks Knitted from Natural and Synthetic Textured Yarns. Fibres & Textiles in Eastern Europe, Vol. 18, No. 3 (80), pp. 89-93.*
5. *Leisen J, Schauss G, Stanley C and Beckham HW. (2008). Magnetic resonance imaging applications in textile and fiber engineering: Fabrics and diapers. AATCC Rev, Vol. 8 (5), pp. 32–36*
6. *Weder, M., Bruhwiler, P.A., Herzig, U., Huber, R., Frei, G., Lehmann, E., (2004). Neutron radiography moisture distribution in multilayer clothing systems. Textile Research Journal, Vol. 74, pp 695–700*
7. *Rossi M. R., Stämpfli R., Psikuta A., Rechsteiner I. and Brühwiler P. A. (2011). Transplanar and in-plane Wicking Effects in Sock Materials Under Pressure. Textile Research Journal, Vol. 81 (15), pp. 1549-1558*
8. *Hu, J., Li, Y., Wong, A. S. W. and Xu, W. (2005). Moisture Management tester: A Method to Characterize Fabric Liquid Moisture Management. Textile Research Journal. Vol. 75 (1), pp. 57-62*

TEXTILE WATER ABSORPTION PARAMETERS AND HUMAN WETNESS PERCEPTION

Margherita Raccuglia, Simon Hodder and George Havenith

Environmental Ergonomics Research Centre, Loughborough University Design School, LE113TU, Loughborough, Leicestershire, UK, +44 (0) 1509 228485, m.raccuglia2@lboro.ac.uk

Abstract

Moisture in clothing induces skin-wetness-perception which greatly affects thermal and sensorial discomfort [6,8]. Following on from studies investigating sensory modalities underpinning skin-wetness-perception [3,9,4,5], in this study we looked at two different methodologies to study skin wetness perception of fabrics [11]. Twenty-four fabrics, varying in thickness, fibre-type and absorption capacity were studied. Using twelve participants (males/females), the skin-wetness-perception induced was studied in 2 wetness states of the fabrics [11]: 1:ABS, all having the same absolute water content of 2400µl per sample (= 0.024µl.mm^{-2}); 2:REL: wetted with water corresponding to the 50% of their individual absorption capacity. As total absorption capacity was highly correlated (r = 0.99) to fabric thickness, condition 2 was approximately equivalent to having the same water content per volume of textile, i.e. 0.4µl.mm^{-3}. Samples were applied to the upper back statically to avoid impact of surface roughness/friction.

Skin-wetness-perception was correlated to the total fabric water content (r^2 = 0.87), mainly influenced by fabric thickness. Fabric thickness thus was considered a valid predictor of skin-wetness-perception under static-skin-contact (r^2 = 0.82). No effect of fibre-type was observed.

In REL, with equal µl.mm^{-3}, skin-wetness-perception showed a positive correlation to total fabric water-content-per-area (µl.mm^{-2}), and thus also to thickness. In ABS on the other hand, with equal µl.mm^{-2}, and thus with relative water content (µl.mm^{-3}) inversely proportional to thickness, skin-wetness-perception was also inversely proportional to thickness. Thus skin-wetness-perception showed opposing responses depending on the wetting type, indicating that the methodology of manipulating fabric water content should be selected in relation to the product end-use [11] in order to understand fabric properties correctly for the application.

Key words

Fabric thickness, fibre type, absorption capacity, water content, human wetness perception.

1. Introduction

The study of human wetness perception has attracted many researchers over the years [2,6,1,3]. It has been indicated that, in absence of skin moisture receptors, wetness is perceived through the central integration of cold-sensation and mechano-sensation [4,5]. With regard to textile factors contributing to wetness perception, recently, Tang et al. [12] highlighted the critical role of fabric thickness in determining wetness perception, indicating that thinner materials are perceived significantly wetter than thicker ones. In this experiment, given that the same absolute per sample water amount was added to the experimental fabrics, thinner samples presented higher relative water amount to textile volume-ratios compared to the thicker samples and the latter could have been the reason for thinner fabrics being perceived wetter. However, in conditions in which profuse sweat production occurs, both thinner and thicker materials might get saturated. In this scenario fabrics could

present same relative to fabric volume water content and Tang's et al. [12] may not be applicable. As such, the aim of this study was to compare wetness perception outcomes between two wet states, i.e. absolute per sample ($\mu l.mm^{-2}$) versus relative to volume ($\mu l.mm^{-3}$).

2. Experimental

2.1. Materials

Twenty-four knitted fabric samples (100 x100 mm) selected for different structure, thickness and fibre type were included in this experiment. Both single jersey and double jersey materials were included in the study. The thickness range of the experimental samples was 0.3 to 4.5 mm, Furthermore, in order to observe the effect of fibre type on wetness perception cotton, polyester, polyester blend, Nylon and wool materials were used.

Twelve young (23.4± 2.4) males (7) and females (5) of Western European Origin volunteered to participate in this study.

2.2. Methods

The experimental fabric samples were assessed in two separate trials, which differed in the amount of water applied:

REL = 50% of the individual fabric absorption capacity;

ABS = same absolute water content (2400 µl per sample).

Fabric water absorption capacity was determined according to the 'water absorption capacity test' described by Tang et al. [7]. For the test a fabric sample (100 x 100 mm) was put into a tank of water and 5 min was allowed for it to sink completely into water. Following from this, the fabric was taken out by tweezers and hung onto a rod vertically until there was no water dripping within a 30 seconds interval. The water gain was calculated according to:

$$\text{Water absorbed } (\mu\text{L}) = (\text{wetF} - \text{dryF}) * 1000$$

Where,

wetF, is the weight of the saturated fabric (g);

dryF, is the weight of the dry fabric (g).

The experimental samples were placed on each participant's upper back in counter balanced order. After each sample application, participants were asked to report their wetness perception, thermal sensation and thermal comfort on ordinal scales. A 30 points ordinal, unipolar scale, with high level of resolution, was developed to assess fabric wetness perception. The scale ranged from 0 (extremely dry) to 30 (extremely wet). To assess fabric thermal sensation an ordinal, bipolar, unbalanced, scale was designed. The scale presented a central neutral point (0) with 10 positive points (from 1 to 10) associated to warm sensation, above and 15 negative points (from -1 to -15), associated to cool and cold sensation, below. Finally, the increase in thermal discomfort, associated to the application of the wet samples, was assessed using a seven points ordinal, unipolar scale, ranging from 1 (comfortable) to 7 (very uncomfortable).

3. Results and discussion

A strong relationship was observed between absorption capacity and fabric thickness (r^2 0.98), with no effect of fibre type.

In the 50REL condition, a relationship (second order polynomial fit) was found between wetness perception and sample water content ($r^2 = 0.87$, $p < 0.001$).

Rank analyses indicated that two different, or even opposite wetness perception scores, are obtained for the same fabric when adopting two different methodologies to manipulate fabric water content, i.e. REL ($\mu l.mm^{-3}$) versus ABS (µl per sample). In particular, in the REL condition wetness perception increased with the increase in fabric thickness. In fact, by applying the same relative water content, fabric samples presented different total water amounts according to their volume, therefore thicker fabrics contained more water in absolute terms. On the other hand, in line with Tang's et al. results [7], in ABS wetness perception decreased with the increase in fabric thickness, given that thicker fabrics had lower relative amount of water to volume-ratio compared to thinner fabrics (i.e. in thicker fabrics the same absolute amount of water was spread over a larger volume).

4. CONCLUSION

Fabric thickness was indicated as the major parameter determining fabric absorption capacity and considered a valid predictor of fabric wetness perception under static skin contact. Furthermore, because of thickness/volume related differences in fabric wetness perception, we suggest that the methodology used to manipulate fabric water content should be considered in relation to the product end-use.

References

1. *Ackerley R., Olausson H., Wessberg J., McGlone F. Wetness perception across body sites. Neuroscience Letters. 2012; 522:73–77.*
2. *Bentley I.M. The Synthetic Experiment The American Journal of Psychology. 1990; Vol. 11, No. 3, pp. 405-425.*
3. *Bergmann Tiest W.M., Kosters N.D., Kappers A.M.L., Daanen HAM. Haptic perception of wetness. Acta psychologica. 2012;141(2):159–63.*
4. *Filingeri D., Fournet D., Hodder S., Havenith G. Why wet feels wet? A neurophysiological model of human cutaneous wetness sensitivity. Journal of neurophysiology. 2014; 112(6):1457–69.*
5. *Filingeri D., Havenith G. Human skin wetness perception: psychophysical and neurophysiological bases. Temperature. 2015; 3;2(1):86–104.*
6. *Fukazawa T., Havenith G. Differences in comfort perception in relation to local and whole body skin wettedness. European journal of applied physiology. 2009;106(1):15–24.*
7. *Li Y., Holcombe B V., Apcar F. Moisture Buffering Behavior of Hygroscopic Fabric During Wear. Textile Research Journal. 1992; 62:619–627.*
8. *Li Y. Perceptions of temperature, moisture and comfort in clothing during environmental transients. Ergonomics. 2005; 22;48(3):234–48.*
9. *Niedermann R., Rossi R.M. Objective and subjective evaluation of the human thermal sensation of wet fabrics. Textile Research Journal. 2012; 21;82(4):374–84.*
10. *Plante A.M., Holcombe B.V., Stephens L.G. Fiber Hygroscopicity and Perceptions of Dampness: Part I: Subjective Trials. Textile Research Journal. 1995; 65:293–298.*
11. *Raccuglia M., Hodder S., Havenith G. Fabric water absorption and wetness perception. 7th European Conference on Protective Clothing. 23-25 May 2016, Izmir, Turkey.*
12. *Tang KPM, Kan CW, Fan JT (2014) Assessing and predicting the subjective wetness sensation of textiles: subjective and objective evaluation. Textile Research Journal 85:838–849.*

INFLUENCE OF INTERCONNECTION OF CONDUCTIVE FIBRES ON TRANMISSION CHARACTERISTICS OF ELECTRIC SIGNAL

Ján Barabáš[1], Ľudmila Balogová[2], Michal Gála[1], Branko Babušiak[1]

[1] Department of Theoretical Electrical Engineering and Biomedical Engineering, Faculty of Electrical Engineering, University of Žilina in Žilina, Univerzitná 1, 011 26 Žilina, Slovak Republic, jan.barabas@fel.uniza.sk, michal.gala@fel.uniza.sk, branko.babusiak@fel.uniza.sk
[2] VÚTCH-CHEMITEX, spol. s r.o., Rybníky 954, 011 68 Žilina, Slovak Republic, balogova@vutch.sk

Abstract:

Smart clothing containing electroconductive fibres, integrated into construction of textile material, are an alternative for continuous long-term monitoring of human biomedical signals. Operational elements located in the smart clothing are interconnected by conductive paths enabling transmission of data gained via textile sensors to a control and communication unit from where they are transferred to mobile or PC using wireless technology. Method of interconnection of the conductive paths with operational elements of the clothing depends mainly on character of materials used (electroconductive fibre – metal/plastic/textile material). Emphasis is placed on establishment of a stable connection with required transmission characteristics. The paper present results of measuring transmission characteristics of the conductive paths, embroidered with electroconductive thread on a non-conductive textile material, terminated with metal press fasteners. Electrical resistance of the conductive paths for the whole uninterrupted conductive path length, specific segments (right and left) of the conductive path with the metal press fastener and the both segments connected with the metal press fastener was evaluated. Transmission characteristics of harmonic signal (sin) and non-harmonic rectangular signal for frequency ranging from 1 Hz up to 300 kHz with input voltage of 1 V and 3 V (TTL logic) were evaluated on a solid joint made by closure of the metal press fasteners. Results of the measurement confirmed trouble-free transmission of the harmonic and non-harmonic signal using proposed conductive paths and satisfactory quality of the output signal without any deformations.

Key words:

smart clothing, electroconductive sewing thread, conductive path, metal press fasteners, electric resistance, harmonic signal, non-harmonic signal

1. Introduction

Monitoring of human physiological signals using intelligent clothing is based on a concept of so-called Body Sensor Networks (BNS) with an emphasis placed on sensing systems, autonomous primary data processing, miniaturization and last but not least also on reliable interconnection of specific BNS components. The sensors have analog outputs, representing physiological parameters, from which a picture about health condition of a patient is established. Conductive paths (Wired Body Area Network) or wireless interconnections (Wireless Body Area Network) are used in the system for power supply, signal transmission to the sensors and data transmission to a data bus. Analog data are converted to digital form in the data bus and they are transmitted to a local central unit e.g. smartphone (PDA). They can be further wirelessly transmitted from the local central unit e.g. to a healthcare system (Remote System). [1]

Major task of the conductive paths is transmission of electrical biosignals, sensed from textile electrodes (e.g. ECG sensors), which are manifestation of electrical activity in a living organism. The biosignals are based on electrical properties of muscle and neural tissue. Electrocardiography (ECG), using electrodes

placed on the human body, measures difference of voltage as manifestation of propagation of action potential in myocardium. The active electrodes act as sensors, detecting electrical signals, generated by the heart and conducted through the heart tissue. Electrocardiography (ECG) is a process of recording electrical activity of the heart in a form of electrocardiogram, i.e. recording time change of electrical potential caused by heart's electrical activity in a form of ECG curves. [2] Other applications include heart-rate variability assessments from long-term recordings, wherein the subject is monitored freely during his/her daily activities [3] or special photoplethysmography measurements, wherein data acquired by the photodiodes is transmitted to the processing unit by means of conductive fibres and then wirelessly transmitted to other processing modalities [4].

Quality of the output electrical biosignals transmitted by means of conductive paths is influenced by properties of materials used to prepare the conductive paths, by way of incorporation of the conductive paths into the structure of textile material and by stability of interconnection of the conductive paths with functional components of the intelligent clothing. Basically, the conductive paths consist of electroconductive fibres made from 100 % metal (e.g. copper, silver) or polymer containing conductive particles (e.g. carbon) and/or fibres with conductive surface treatment (core/shell structured bicomponent fibres – e.g. polyamide/silver). A possibility how to create conductive paths is embroidering electrical circuit on a textile substrate with an electroconductive sewing thread incorporating electroconductive fibres, enabling electrical signal transmission. This embroidering technology substitutes an uncomfortable system of cables common on traditional ECG monitoring methods. Particular attention should be given to a method of interconnection of the conductive paths with functional components of the clothing. Emphasis should be placed on establishment of a stable interconnection with required transmission characteristics. A necessary condition is to ensure resistance of the connection to mechanical stress and propose an appropriate configuration responding to the required application. All of the above prerequisites were partially studied in our previous experimental endeavors [5,6].

Additionally, the quality of the output biosignal can be characterized and evaluated by transmission characteristics such as e.g. harmonic and square signal for specific heart rate at particular input voltage. Periodic, indefinite, cyclic signals serving as a medium for information transfer are involved. Graphical evaluation of the transmission characteristics is a way how to confirm functionality of the electrical circuit in a form of conductive paths and biosignal transmission.

2. Experimental

Technology of conductive paths prepared from electroconductive sewing thread with metal accessories attached at the end of the conductive path for stable interconnection of the conductive paths and functional components of the intelligent clothing is described in the experimental part. Besides, method for measurement of transmission characteristics of the conductive paths used for evaluation of quality of the output signal is described as well.

2.1. Materials

The conductive paths were prepared from electroconductive sewing thread containing Elitex®, commercially available conductive multifilament fibre, using embroidering technology. Core of the Elitex® conductive fibre is polyamide covered by a thin layer of pure silver. Electrical resistance of the sewing thread was on a level of cca 17 Ω/m.

The embroidering technology was used to achieve flexible interconnection of the functional modules/components of the electronic circuit. The conductive path consisted of a series of stitches created by interlocking upper and bottom electroconductive sewing thread. Each conductive path consisted of two independent segments (right and left segment) with a length of 10 cm. A system of metal textile accessories was proposed to connect two segments into one conductive path. Respective part of the metal textile accessories (metal button and/or metal snap fastener) was attached at one end

of each segment. Strong bond and electrical contact was established by interlocking the conductive segments. A conductive path unbroken by metal accessories with a length of 20 cm was prepared as well. It was used to evaluate influence of interconnection of the conductive paths (fibres) with metal accessories on transmission characteristics of the electrical signal. Preparation of the conductive paths is described in Table 1 and samples of the conductive paths are shown in Figure 1a -1d.

Table 1. Characteristics of the prepared conductive paths

Designation of the conductive path	Description of preparation of the conductive path
VC1	Conductive path with a length of 20 cm.
VC2	Conductive path consists of two independent segments of conductive paths with a length of 10 cm. At one end of the conductive path of each segment there is a conductive area with dimensions of 0,5 x 0,5 cm, created by irregular stitching with conductive sewing thread, to which respective part of a metal button was attached mechanically by riveting. The other end of the conductive path of each segment is finished by free end of the electroconductive sewing thread. A strong bond and interconnection of the both segments to one conductive path is established by interlocking the both parts of the metal button.
VC3	Conductive path consists of two independent segments of conductive paths with a length of 10 cm. At one end of the conductive path of each segment there is respective part of a metal snap fastener (spring socket and stud) sewn by free end of the electroconductive sewing thread used to prepare the conductive path. The other end of each segment is finished by free end of the electroconductive sewing thread. A strong bond and interconnection of the both segments to one conductive path is established by interlocking the both parts of the metal snap fastener.
VC4	Conductive path consists of two independent segments of conductive paths with a length of 10 cm. At one end of the conductive path of each segment there is a conductive area with dimensions of 0,5 x 0,5 cm, created by manual stitching with conductive sewing thread, on which respective part of metal snap fastener (spring socket and stud) was sewn. The other end of conductive part of each segment is finished by free end of the electroconductive sewing thread. A strong bond and interconnection of the both segments to one conductive path is established by interlocking the both parts of the metal snap fastener.

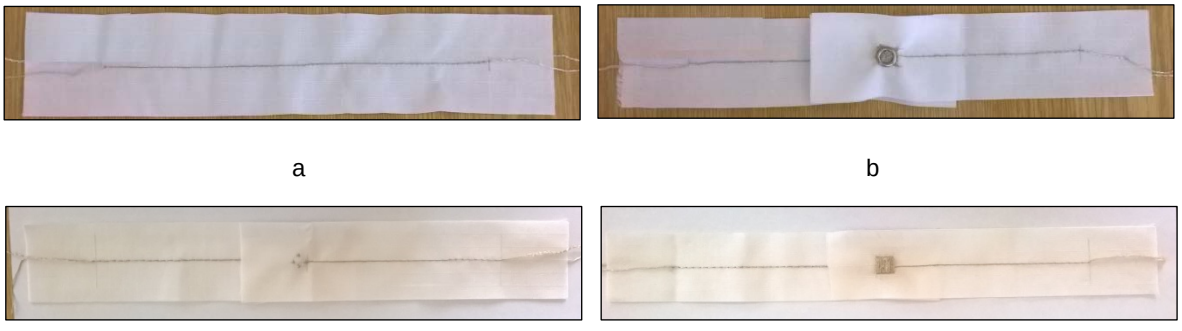

a b

c d

Figure 1. Conductive paths: VC1 (a), VC2 (b), VC3 (c), VC4 (d)

Electrical resistance and transmission characteristics were evaluated on samples prepared using the above methods.

2.2. Measurements and evaluation methodology

The transmission characteristics of the conductive threads and interconnection of left and right segments (sample VC2, VC3 and VC4) were evaluated by measuring the electrical resistance [Ω] and quality of signal transmission (amplitude measurements and visual inspection of the wave form).

The first phase included a simple evaluation of the electrical resistance measured using the Agilent 34404A laboratory precision multimeter from defined points of measurement. The average value from three measurements was calculated and is listed in the corresponding table of results – left segment, right segment and interconnected segments, from which we calculated the resistance of the snap fastener interconnection itself. Sample VC1 only includes the total impedance of the electro conductive thread since no snap fastener interconnection is present.

The second phase included the testing of harmonic signal transmission. The harmonic signal was generated using the Rigol DG4162 signal generator within the 1 Hz to 300 kHz range, with a peak-to-peak amplitude of 1 V and transmitted over the electro conductive threads.

The third phase of measurements included the testing of square signal transmission – to mimic the 3V TTL logic used in subsequent application of the electro conductive threads in our intelligent clothing prototype. Square signal with frequencies from 1 Hz to 300 kHz was evaluated and transmitted over the electro conductive threads.

For phase 2 and phase 3 we evaluated the amplitude of the transmitted signal and also visually inspected the waveforms – comparing the original and transmitted signal using the KEYSIGHT MSO-X 3012A oscilloscope.

3. Results and discussion

Phase one results are listed in Tables 2 - 4. They include the measured impedance of individual left and right segments (VC2, VC3, VC4), the total impedance of both connected segments and the calculated impedance of the snap fastener interconnection. The lowest impedance was obtained from VC3 wherein the snap fastener was sewed in 4 positions (see Figure 1c) – thus we opted to use this method of connecting the electro conductive threads with snap fasteners in all future designs instead of mechanical pressing method (Figure 1b, VC2). The additional area created under the snap fastener by sewing the electro conductive thread also increased the impedance of the interconnection (Figure 1d, VC4) and significantly increased the impedance of the right segment.

Table 2. Measured impedance values for VC2 – mechanically pressed snap fastener

	Meas. n.1	***Meas n.2***	***Meas n.3***	***Average***	***Snap fastener***
Left segment impedance	8,1 Ω	8,0 Ω	8,3 Ω	**8,1 Ω**	**-**
Right segment impedance	7,0 Ω	7,3 Ω	7,1 Ω	**7,1 Ω**	**-**
Total impedance	24,2 Ω	23,8 Ω	22,5 Ω	**23,5 Ω**	**8,3 Ω**

Table 3. Measured impedance values for VC3 – 4 point sewed snap fastener

	Meas. n.1	***Meas. n.2***	***Meas. n.3***	***Average***	***Snap fastener***
Left segment impedance	3,6 Ω	3,5 Ω	3,6 Ω	**3,6 Ω**	**-**
Right segment impedance	3,7 Ω	3,8 Ω	3,4 Ω	**3,6 Ω**	**-**
Total impedance	8,2 Ω	9,1 Ω	8,1 Ω	**8,5 Ω**	**1,3 Ω**

Table 4. Measured impedance values for VC4 – area sewed under snap fastener

	Meas. n.1	***Meas. n.2***	***Meas. n.3***	***Average***	***Snap fastener***
Left segment impedance	5,5 Ω	5,7 Ω	6,1 Ω	**5,8 Ω**	**-**
Right segment impedance	12,0 Ω	11,8 Ω	12,3 Ω	**12,0 Ω**	**-**
Total impedance	18,1 Ω	19,6 Ω	19,8 Ω	**19,2 Ω**	**1,4 Ω**

Phase two results have confirmed excellent transmission of the harmonic signal in all samples, see Figure 1 for amplitude plot results using VC1 and Figure 2 for amplitude plot results using VC2. The input waveform is transmitted undistorted with appropriate amplitude for all tested samples, regardless of the presence of the snap fastener interconnection.

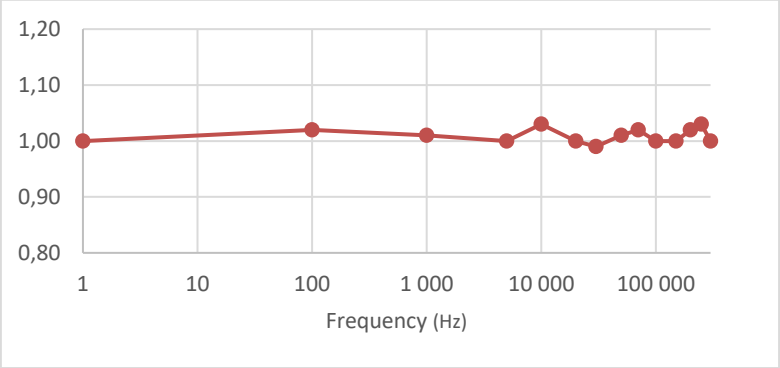

Figure 2. Transfer characteristic of textile without snap fastener (VC1) - sine wave - input amplitude 1V

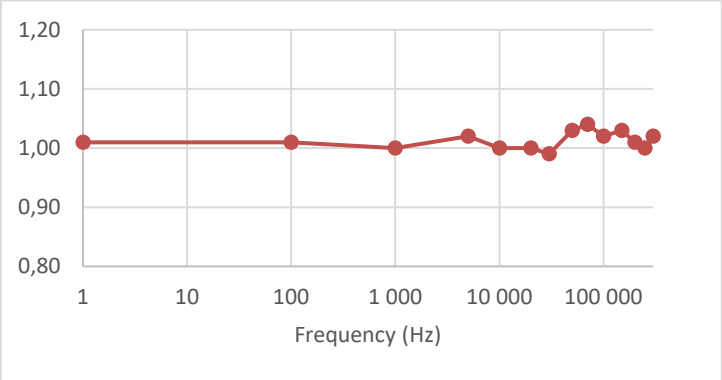

Figure 3. Transfer characteristic of textile with snap fastener (VC2) - sine wave - input amplitude 1V

Phase three results are more interesting. Due to the nature of the square signal a transient effect is visible at the rise and fall slopes of the waveform, especially for higher frequencies (beyond 20 kHz) – see Figure 4. However, the average amplitude is well within the expected TTL levels and the transmitted signal can be processed without any errors. We verified this by transmission of a real digital signal over the I^2C bus – see Figure 5. The TMP275 IC from Texas Instruments was powered by a pair of electro conductive threads and the digital temperature output was transmitted using another pair. The PCB with the electric components (pictured left, disconnected for more detail) was connected with the electro conductive fibers using four snap fasteners, as was the receiving side connector (pictured right, connected).

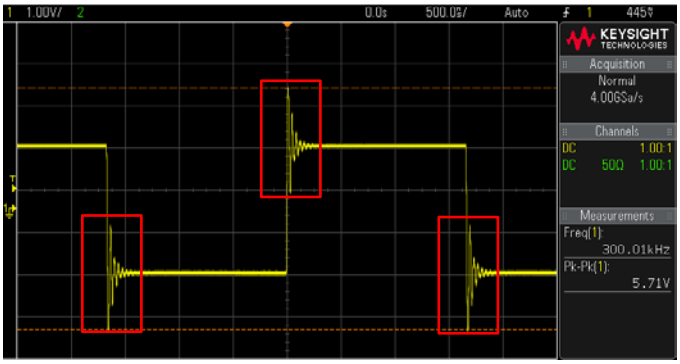

Figure 4. Visible transient effects beyond 20 kHz, rise and fall slopes of square signal, 3V TTL

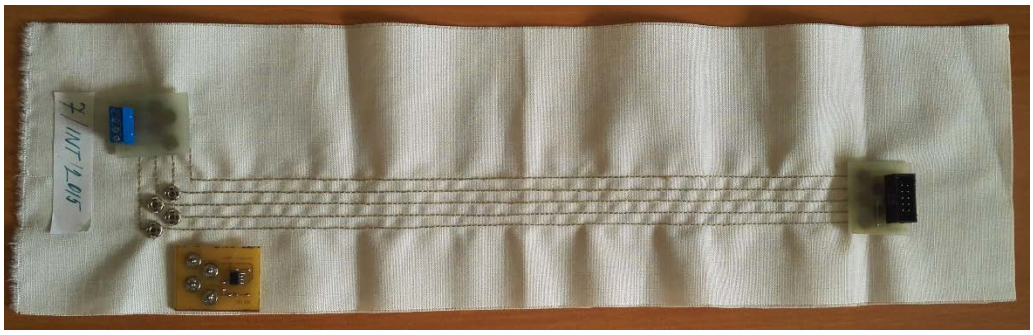

Figure 5. Sample I²C bus digital signal transmission – PCB with TMP275 IC, snap fasteners, electro conductive threads

Figures 6 and 7 show the average amplitudes of the transmitted square signal, confirming our above findings.

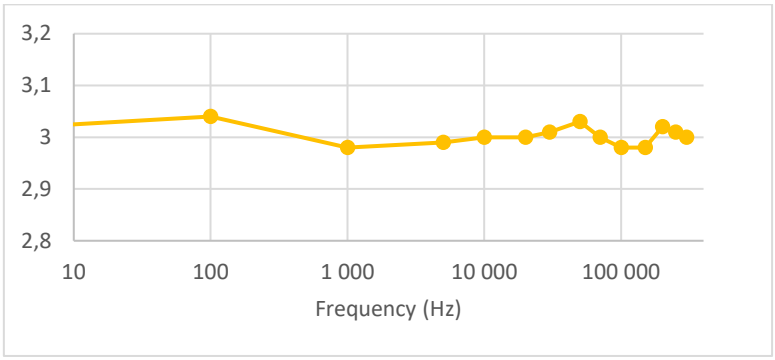

Figure 6. Transfer characteristic of textile without snap fastener (VC1) – square signal - input amplitude 3V

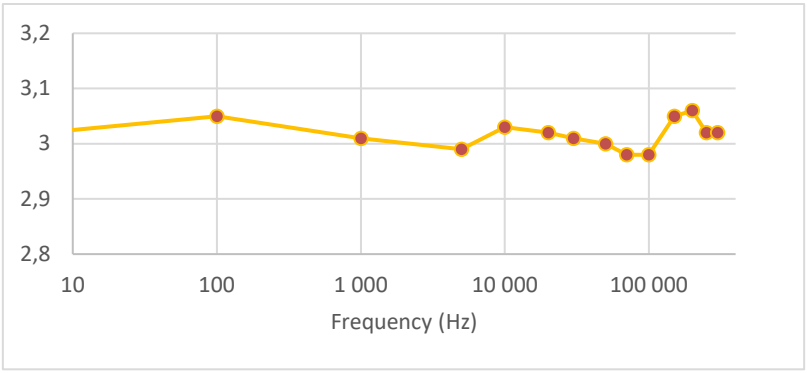

Figure 7. Transfer characteristic of textile with snap fastener (VC2) – square signal - input amplitude 3V

Similar transfer characteristics were obtained for VC3 and VC4 samples and are thus not pictured in this article.

4. CONCLUSION

Electro conductive threads are an important component of so-called intelligent textiles. Instead of using traditional wires which can be bulky and uncomfortable, all electrical connections are created using electro conductive threads which are sewn within the clothing itself. These are then used not only to power the necessary electronic components but also for signal harnessing and transmission thereof within the body signal network system.

Based on our results from phase 1 we can conclude that the interconnection of conductive threads using snap fasteners is possible and feasible. The lowest impedance was observed when the snap fasteners were sewed using the electro conductive thread in 4 locations. This method of attaching also lowered and equalized the right and left segment impedance values – especially when comparing samples VC3 and VC4. Additionally, phase 2 and phase 3 results have confirmed proper signal transmission over the electro conductive threads – both for harmonic and non-harmonic signals in a wide frequency range. The transient effects present in non-harmonic signal transmission do not influence signal quality when using 3V TTL logic as was verified by transferring a real-life digital signal over the I^2C bus.

The obtained results and methods have been further employed in the development of a wearable intelligent clothing prototype pictured in Figure 8 and will be subject to further testing of not only electrical but also mechanical properties in order to assure a functional unit.

Figure 8. Developed intelligent clothing prototype with processing unit (white box, bottom left) attached using snap fasteners connected by sewed electro conductive threads

ACKNOWLEDGEMENTS

This work was supported by the Slovak Research and Development Agency on the base of Agreement No. APVV-14-0519"

References

1. *Kang, T., Merritt,C., Karaguzel, B., Wilson,J., Pourdeyhimi,B., Grant,E., Nagle, T.: Sensors on Textile Substrates for Home-Based Helthcare Monitoring. Proceedings of the 1st Distributed Diagnosis and Home Healthcare (D2H2) Conference Arlington, Virginia, USA, April 2-4, 2006, p. 5 – 7. ISBN 1-4244-0058-9.*
2. *Baum, O. V., Voloshin V. I.; Popov, L. A.: Biophysical models of the heart electrical activity. Biofyzika, 2006, November - December, Vol. 51, No. 6, p. 1069-1086. ISSN: 0006-3029.*
3. *Penhaker, M., Stula, T., Augustynek, M.: Long-term heart rate variability assessment. Proceedings of 5th Kuala Lumpur International Conference on Biomedical Engineering and IFMBE Proceedings volume 35 IFMBE, 2011, BIOMED 2011, Held in conjunction with the 8th Asian Pacific Conference on Medical and Biological Engineering, APCMBE 2011; Kuala Lumpur, 20-23 June 2011, ISSN 16800737, ISBN 978-364221728-9.*

4. *Borik, Š., Čáp, I.: Implementation of wireless data transfer to photoplethysmographic measurements. In Proceedings on 9th International Conference - 2012 ELEKTRO, IEEE Xplore, ISBN 978-1-4673-1179-3.*
5. *Ľ. Balogová, B. Babušiak and M. Gála: Biopotential sensing with electroconductive fabrics. In Fibres and Textiles (3) 2014, Special issue venue 4th International Conference TEXCO'14, August 2014, Ružomberok, Slovakia, ISSN 1335-0617.*
6. *Ľ. Balogová, B. Babušiak and M. Gála: Possibilities of application of electroconductive fabrics to prepare smart clothing designed for ECG monitoring. In Fibres and Textiles (4) 2014, December 2014, Slovakia, ISSN 1335-0617.*

TEXTRONICS UNDERWEAR WITH PANTILINERS FOR PROPHYLACTIC AND SUPPORT TREATMENT OF A LOWER URINARY TRACT INFLAMMATION

Emilia Frydrysiak[1], Krzysztof Śmigielski[1], Michał Frydrysiak[2]

[1]Lodz University of Technology, Institute of General Chemistry, Lodz, Poland, Stefanowskiego 4/10, 90-924, em.frydrysiak@gmail.com, tel. +48 42 631-34-10, fax +48 42 631-28-42

[2]Lodz University of Technology, Faculty of Material Technologies and Textile Design, Lodz, Poland, St. Zeromskiego 116, 90-924

Abstract:

Inflammation of a lower urinary tract is a very common problem which occurs particularly in women. The one of the treatment methods is having steam baths which are recommended by doctors. However it is not comfortable to use, even at home, so then the idea of a textronics system for prophylactic and support treatment of a lower urinary tract inflammation came to be. That system consists of a textronics pantiliner integrated with the underwear and a replaceable pantiliner with applied microcapsules with essential oils on it. Those essential oils includes active substances which help the treatment and also have an antibacterial activity to Escherichia coli sp. which causes 90% of those infections. The textronics system is safe for users and comfortable for using.

Key words:

Underwear, pantiliner, lower urinary tract inflammation, textronics, microcapsules

1. Introduction

Electroconductive textile products introduced into the market have opened a new era in textiles and created for them a wide range of applications. A new generation of textile products has been introduced in more and more areas of life, also in textronics, cosmetotextiles, video game avatars [1]. Moreover, these products can be used in clothing which supports the treatment of the lower urinary tract inflammations.

Inflammation of the lower urinary tract is a very common problem which occurs particularly in women. According to statistics, every fifth woman suffers from such inflammations at least once in her life. Typical disease symptoms are: pain or burning during urination, feeling the need of frequent urination and even blood in urine. Non-treated can cause kidney diseases which cause pain, high fever and vomiting [2, 3, 4, 5]. This type of bacteria accounts for 90% cases of inflammation of the lower urinary tract, which are 50 times more frequent in women than in men [5, 6, 7].

The treatment of inflammation of the lower urinary tract includes not only antibiotics, but also hip baths or steam baths [2, 3]. Some doctors recommend taking such baths several times a week to 2-3 times a day in the initial phase of treatment, for 15-20 minutes at a time. Hot water or steam increases blood flow, which helps the treatment. Essential oils (from *Matricaria chamomilla* or *Salvia officinalis*) are often added to the water in order to support healing and relieve discomfort. Those essential oils include biologically active compounds which have a medical effect on the inflammation of the lower

urinary tract [8, 9]. However, that treatment is not comfortable for using, even at home. That is why the idea of a textronics system for prophylactic and support treatment of the lower urinary tract inflammation which facilitates mobility came to be. That system would accelerate the therapy and return the patient to work. The described researches are in the initial phase and are a part of an entire system. Next researches will be described in other papers. The system is patented in Poland (P. 408106) and it was awarded in the 'Innovation is a woman' competition in Poland.

2. Experimental

It is a pro-medical textronics system in the form of therapeutic clothing (Figure 1) in which essential oils are encapsulated and applied onto pantiliners, from where the compounds of microcapsules are released under higher temperatures. The pantiliners maintain a constant temperature thanks to textronics heating systems. This innovative system provides mobility and seems to be a perfect solution for many women who have to do steam baths because of inflammation of the lower urinary tract [10].

A pantiliner (4) (Figure 2) consists of 4 layers: one of them (C) is a heating pad and it is an element of a heating system made of electroconductive textile materials. This layer is laid between two others (B, D) which are electrically insulating layers; layer B is additionally a good thermal conductor. These three layers are integrated with the clothing and they are washable. Layer C is connected to the regulating system (3) with a textile signal line (4). The last layer (A) is a replaceable outer layer, on which the microcapsules with active compounds are applied.

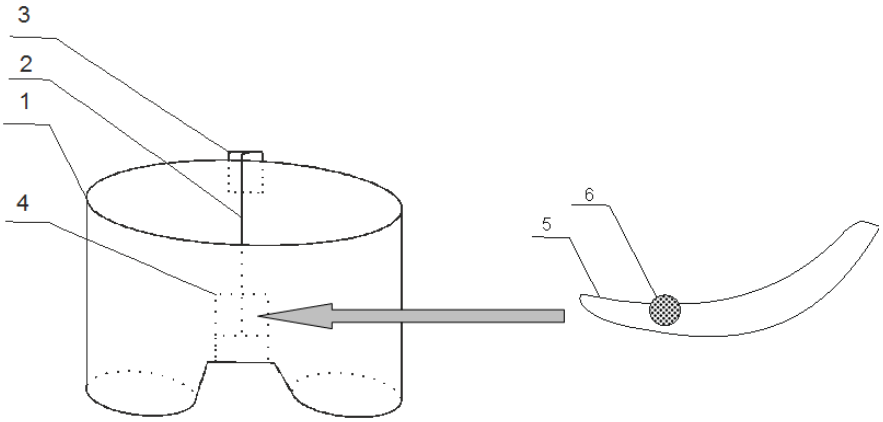

Figure 1. Scheme of the textronics system: 1 – prophylactic and support treatment underwear; 2- textile signal line connecting the control system with a heating textronics pad - 4; 3 –regulation system; 5 – panty liner with microcapsules- 6 [10]

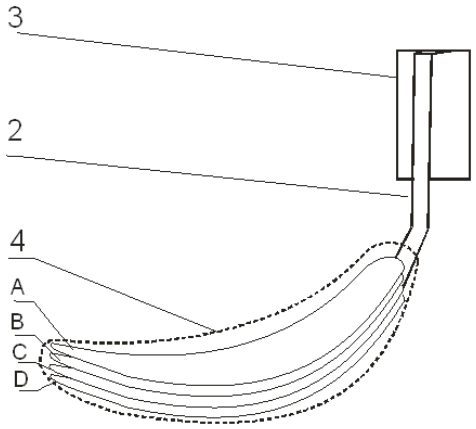

Figure 2. Scheme of a textronics pantiliner: 4 – heating pad (A – panty liner with microcapsules; B and D – electrical insulating layer; C –system heating element); 2 – textile signal line; 3 – regulation system [10]

The material for the core of microcapsules will be essential oils from *Salvia officinalis* L. and *Matricaria chamomilla* L. Both essential oils intensify themselves activity. So far there was performed quantitative and qualitative analysis of Matricaria chamomilla and Salvia officinalis essential oils and created a textronics pantiliner. The essential oils were obtained in hydrodistillaion with the use of modified Deryng apparatus. The identification of their components to confirm the active substances presence was investigated with the use of gas chromatography coupled with mass spectrometry (GC-MS). The research was carried out for to choose the essential oil which should be encapsulate.

Microcapsules will be prepared with the use of spray drying apparatus which schematic is presented in the Figure 3. Spray drying is the physico-mechanical method commonly used for microencapsulation where an active material is dissolved or suspended in a melt or polymer solution and becomes trapped in the dried particle. In this process an emulsion is created from the liquid product to be treated, a carrier substance and a filmogen solution. This emulsion is sprayed into small droplets in hot air. In high temperature, the solvent evaporates leading to a solid matrix around the dispersed second phase. It causes the small droplets of the product to be stored in the carrier substance and embedded in the filmogen [11].

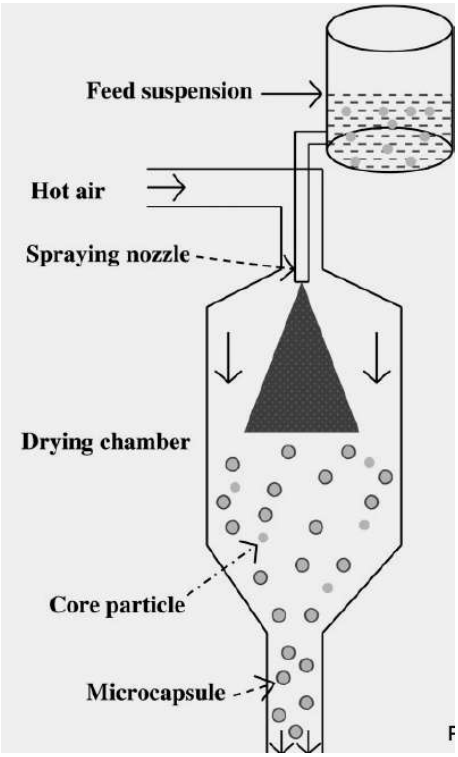

Figure 3. Spray drying apparatus [12]

3. Results and discussion

In essential oils there were identified compounds which help in treating of lower urinary tract inflammation such as alpha bisabolol A, bisabolol oxide and chamazulen in *Matricaria chamomilla* essential oil and alpha pinene in *Salvia officinalis* essential oil. An example of chromatogram of *Salvia officinalis* essential oil is presented in Figure 4. In *Matricaria chamomilla* essential oil there are more compounds with anti-inflamatory activity than in *Salvia officinalis* essential oil, however its producing is much less efficiency. The designed pantiliner conducts heat and is safe to use. The material for outer part of the pantiliner which is linen knitted fabric is presented in Figure 5. Textile heater which is a part of the inner part of it is made of silver nonwoven. Silver does not only conducts current but it is also bacteriostatic which is very important in that project.

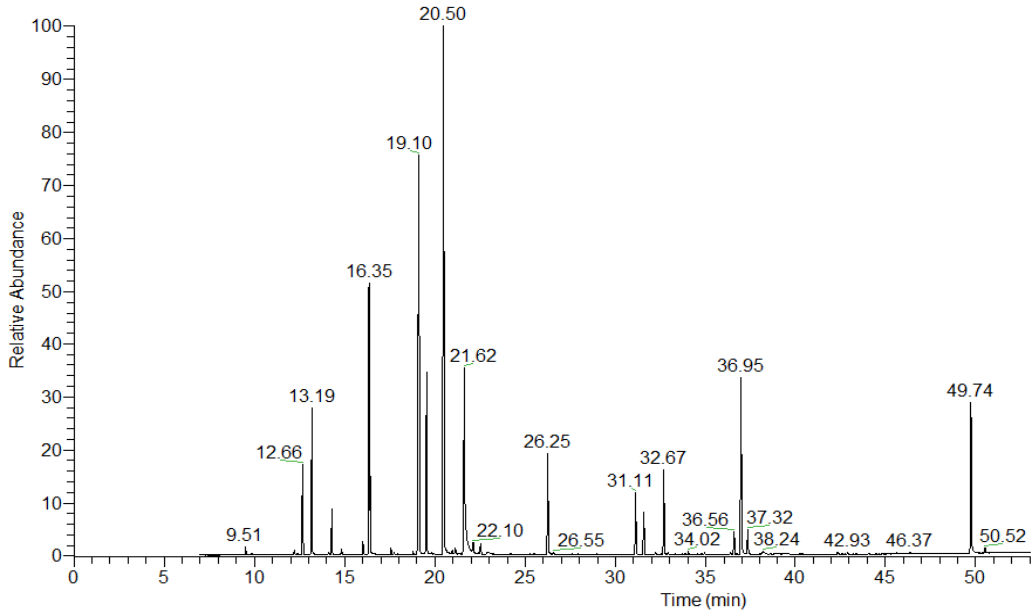

Figure 4. Example of a chromatogram of *Salvia officinalis* essential oil

Figure 5. Material for the outer part of a pantiliner – linen knitted fabric

It is planned to obtain microcapsules with the wall of maltodextrins and the core of essential oils. Obtained microcapsules should release their core under higher temperatures which will be safe for the user.

The next step in research is applying microcapsules with essential oils onto the pantiliners. The best method chosen from spraying, filling or sputtering will be defined. The pantiliner with microcapsules applied on it will be tested for its durability in time and releasing active substances in controlled temperature. It is planned to obtain textronics system for protection and support treatment of lower urinary tract inflammation that will be tested on patients.

4. CONCLUSIONS

A new generation of textile products has been introduced in more and more areas of life. Textronics systems combined with medicine and fashion help people with their diseases. The textronics system for prophylactic and support treatment of a lower urinary tract inflammation is one of such products. Its

aim is to help women with prophylactic and reducing the symptoms and duration of the disease. Microcapsules made with maltodextrins and essential oils from *Salvia officinalis* L. and *Matricaria chamomilla* L. that contain active substances can have a good impact on women' urinary tract. Those essential oils contain active substances which support healing process. Microcapsules will be applied on textronics pantiliners with various methods to choose the best one. The paintiliner with microcapsules should maintain its durability in time. There are more and more such products in our lives which make them better and easier.

References

1. *Loker, S. Ashdown S. (2008). Dress in the Third Dimension. Online Interactivity and Its New Horizons. Clothing & Textiles Research Journal, 26(2), 164-176.*
2. *Janicki, K. (1991). Choroby narządów wewnętrznych. [Diseases of internal organs]. DOMOWY poradnik medyczny. Państwowy Zakład Wydawnictw Lekarskich. Warsaw, Poland, 335-338.*
3. *Kunttu, K. (2010). URINARY tract infections in young women. YLIOPPILAIDEN terveydenhoitosäätiö.1-12.*
4. *Mashall, K. (2003). INTERSTITIAL Cystitis: Understanding the Syndrome. ALTERNATIVE Medicine Review. 8(4), 1-12.*
5. *Urinary Tract Infection (UTI). (2012). A GUIDE for Women, INTERNATIONAL Urogynecological Association. 1-2.*
6. *Cystitis. (August 22, 2014). http://www.womhealth.org.au*
7. *Meyrier, A. URINARY Tract Infection, Chapter 7, TUBULOINTERSTITIAL Disease, 1-18.*
8. *Nasiadówki proste formy leczenia naturalnego. [Sitz baths simple forms of natural healing]. (August 22, 2014). http://www.leczenienaturalne.com.pl.*
9. *Rumianek pospolity (Matricaria chamomilla). [Chamomile (Matricaria chamomilla)]. (August 22, 2014). http://www.zdrowie.gazeta.pl.*
10. *Adamowicz, E., Śmigielski, K., Frydrysiak, M. Tekstroniczny system do profilaktyki i wspomagania leczenia zapaleń dolnych dróg moczowych [Textronics system for prophylactic and support treatment of a lower urinary tract inflammation]. Patent Application (P. 408106). May 5, 2014.*
11. *Adamowicz, E., Śmigielski, K., Frydrysiak, M. (2015). Microencapsulation of active substances and fragrances in textile material applications. Tekstil. 64(3-4), 128-131.*
12. *Jyothi. N, Prasanna, M., Prabha, S., Seetha Ramaiah, P., Srawan, G., Sakarkar, S. (2008). Microencapsulation Techniques, Factors Influencing Encapsulation Efficiency: A Review. The Internet Journal of Nanotechnology. 3(1).*

EFFECT OF TEMPERATURE, HEATING RATE AND HOLDING TIME ON THE PROPERTIES OF CARBON WEB MADE FROM ACRYLIC WASTE

Salman Naeem[1], Saima Javed[2], Vijay Baheti[1], Jiri Militky[1], Zuhaib Ahmad[1], Promoda Behera[1]

[1] Department of Material Engineering, Faculty of Textile Engineering, Technical University of Liberec, Studentska 2, Liberec 46117, Czech Republic

[2] Department of Microbiology & Molecular genetics,University of the Pujab, Lahore 54590, Pakistan.

Corresponding author: salman.ntu@gmail.com

Abstract:

In this study carbon webs are prepared through controlled pyrolysis of web from acrylic waste using physical activation in high temperature furnace. The objective is to analyze the effect of three factors (effect of final temperature, holding time after carbonization and heating rate) on physical characteristics of carbon web. The effect of these factors on the yield (%), shrinkage, flexibility, surface area and electrical conductivity have been analyzed. The yield of carbon web decreases by increasing temperature, heating rate and holding time due to more decomposition of PAN. The surface area of carbon web is found to be maximum at optimum values of heating rate (300 ◦c hr^{-1}), higher temperature with no holding time. Higher heating rate causes sudden release of volatile matter, which is not good for getting good results. However there was not much difference in surface area when heating rate was decreased from 300 ◦c hr^{-1} to 150 ◦c hr^{-1}. The electrical conductivity is found to increase with increase of holding time, temperature and reduces with increasing of heating rate. At high temperature the basal planes in the carbon becomes more parallel oriented, hence electrical conductivity increases at high temperature.

Key words:

Acrylic fiber, Pyrolysis, Activated carbon, Heating rate.

1. Introduction

Activated carbon comprises on highly processed amorphous based materials. Activated carbon is not truly an amorphous material but comprises on microcrystalline structure with a highly developed porous structure, large internal surface area along with high surface reactivity due to different functional groups present on the surface of activated carbon [1]. Around 80% of total manufactured activated carbon is used in liquid phase application for removal of organic and inorganic dyes [1]. Activated carbon in the form of fibers have certain advantages over other forms of activated carbon like powder, granules etc. for higher adsorption capacity and higher rate of desorption [2-3]. These characteristics of activated carbon have made the development of new carbon materials for different applications like anti-bacterial wound dressing [4-5], gas masks [6] and polarizable electrodes [7]. Hence the demand for activated carbon is increasing day by day. Literature review shows that around 90% of carbon fibers are made from PAN based precursors due to less shrinkage, strength, reliability of structure, less ash content and greater carbon yield. Researchers are trying to reduce the cost of activated carbon by using different cheap and alternate materials. In this context, the idea of converting fibrous waste of acrylic into multi-functional activated carbon is a good option. The short acrylic fibers are suitable for converting into porous activated carbon because of low ash content and excellent natural structure.

In this study, acrylic fibrous waste is converted into acrylic web. This web was then physically activated via thermal treatment in high temperature furnace under the layer of charcoal. The activated carbon was prepared at different temperatures 800 ◦c, 1000 ◦c and 1200 ◦c at different heating rates (150, 300 and 450 ◦c hr^{-1}) with different holding time (0 to 60 min).

2. Experimental

2.1. Materials

The acrylic fibrous waste was obtained from GrundIndustries, Czech Republic in form of short lengths generated during mechanical processing of bath mats. The short acrylic fibers are suitable for porous activated carbon because of their excellent natural structure and low ash content. The acrylic fibrous wastes are anionic copolymers containing 85-89 % of acrylonitrile. The physical properties are mentioned in Table 1.

Table 1. Physical properties of acrylic short fiber wastes

Property	Value
Fineness (denier)	13
Tenacity (g/tex)	2.7
Shrinkage (%)	2.5

2.2. Methods

The short acrylic fibers were separated from bath mats by using mechanical cutting method. The acrylic fibers were then further opened at carding machine and transformed into compact structure of non-woven by using needle punching machine. From this web different samples were cut (10 inch × 12 inch) and washed with distilled water in order to remove impurities. Later the webs were dried in oven for 5 to 6 hours to make them completely dry.
In this study, activated carbon was prepared by multi stage pyrolysis. In the initial stage of pyrolysis, the precursor material was heat treated at low temperature under tension in the presence of oxidizing atmosphere and the resulting product became thermally stable and withstood with the futher high temperaure treatment .The temperature used for stabilization was 35 ◦c hr^{-1} up to 250 ◦c. The subsequent high temperature treatment after stabilization resulted in pore formation and pore enlargement.

3. Results and discussion

3.1. Effect of temperature

Pyrolysis experiments were performed at different temperatures in order to find the optimum values of temperature for getting good results in terms of electrical conductivity and surface area. From the figure 1, it is clear that electrical conductivity of carbon increased with increase of temperature.

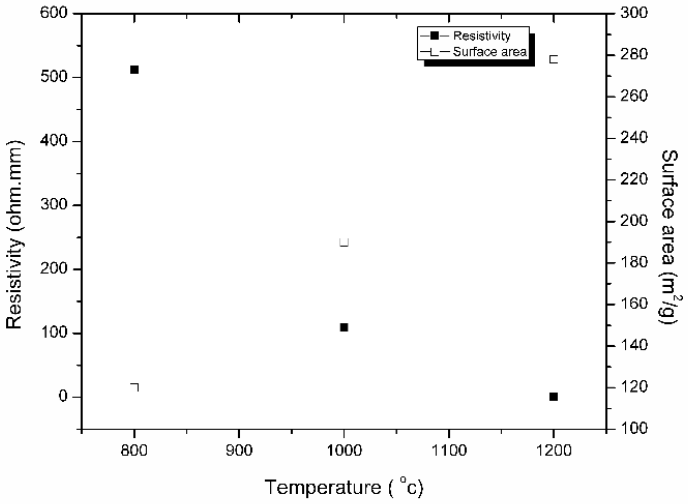

Figure 1. Impact of temperature on surface resistivity and surface area

The electrical conductivity sharply increased from 1000 ◦c to 1200 ◦c with heating rate of 300 ◦c hr^{-1} having no holding time because at higher temperature carbon basal planes kept on arranging parallel to each other.These parallel chains were more ordered at 1200 ◦c than 1000 ◦c and 800 ◦c due to which good results of electrical conductivity can be seen at higher temperature.

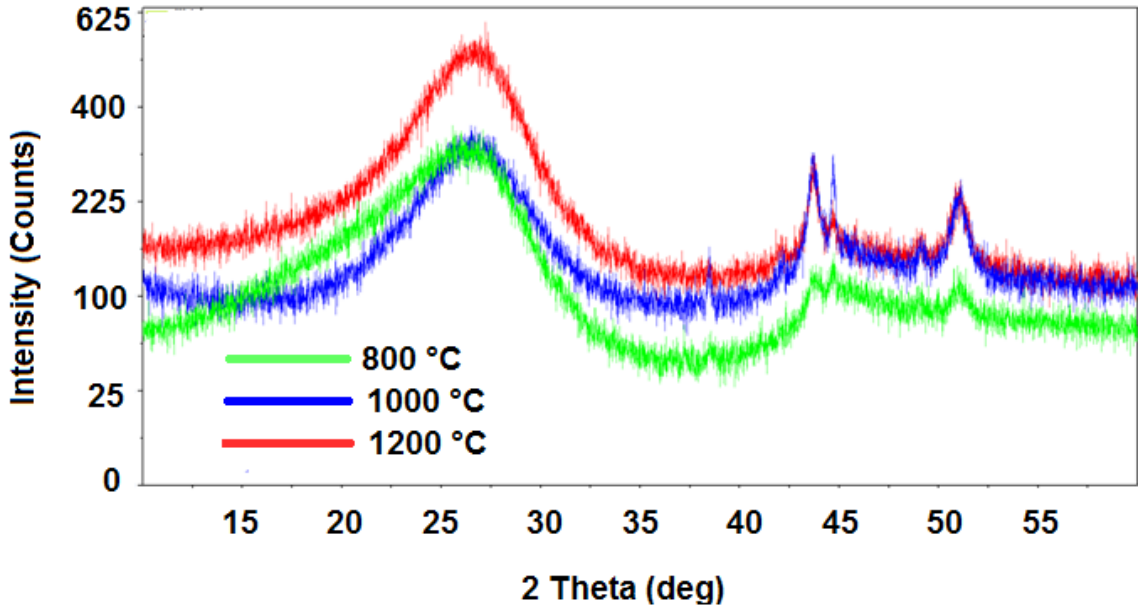

Figure 2. Effect of carbonization temperature on crystallinity of activated carbon web

The x-ray diffraction (XRD) pattern also shows that at higher temperature more crystalline structure was achieved as can be seen from figure 2, the intensity and sharpness of peak was found to increase with increase in carbonization temperature. This confirmed the development of higher crystallinity in activated carbon samples produced at higher temperature. The strongest diffraction peak was found at 25.5º, which confirmed the presence of hexagonal graphitic structure due to C (002) reflection. The other diffraction peaks found at 43º and 52.5º were associated with C (100) and C (004) diffraction of graphitic structure. The presence of sharp and intense peak for 1200 ◦C activated carbon sample showed more transformation of amorphous structure into graphitized structure. This was useful observation for increasing the electrical conductivity of activated carbon samples. The energy-dispersive x-ray spectroscopy (EDX) analysis of different samples is shown in table 2. The activated carbon web produced at 1200 ◦C exhibited 93.39 % increase in carbon content and 6.61 % reduction in oxygen content. This behavior was attributed to removal of hydrogen, sulfur, nitrogen and other elements due to decomposition at higher temperature.

Table 2. Effect of carbonization temperature on elemental composition of activated carbon web

Element	App conc.	Intensity	Weight [%]	Atomic [%]
800 ◦c				
C K	0.26	2.12	0.13	91.76
O K	0.01	0.761	0.01	8.24
1000 ◦c				
C K	0.37	2.12	0.18	91.87
O K	0.02	0.760	0.02	8.13
1200 ◦c				
C K	0.18	2.10	0.09	93.39
O K	0.01	0.744	0.01	6.61

Figure 3 shows the SEM image of carbon samples prepared at different temperatures (1000 ◦c and 1200 ◦c) showing the porous structure is developed in 1200 ◦c. These results are also validated by

Brunauer-Emmett-Teller test. The specific surface area of prepared activated carbon web was found to be increasing with increase in carbonization temperature. The activated carbon web prepared at 1200 ◦c, 1000 ◦c and 800 ◦c exhibited the specific surface area of 278 m^2/g, 190 m^2/g and 120 m^2/g respectively.

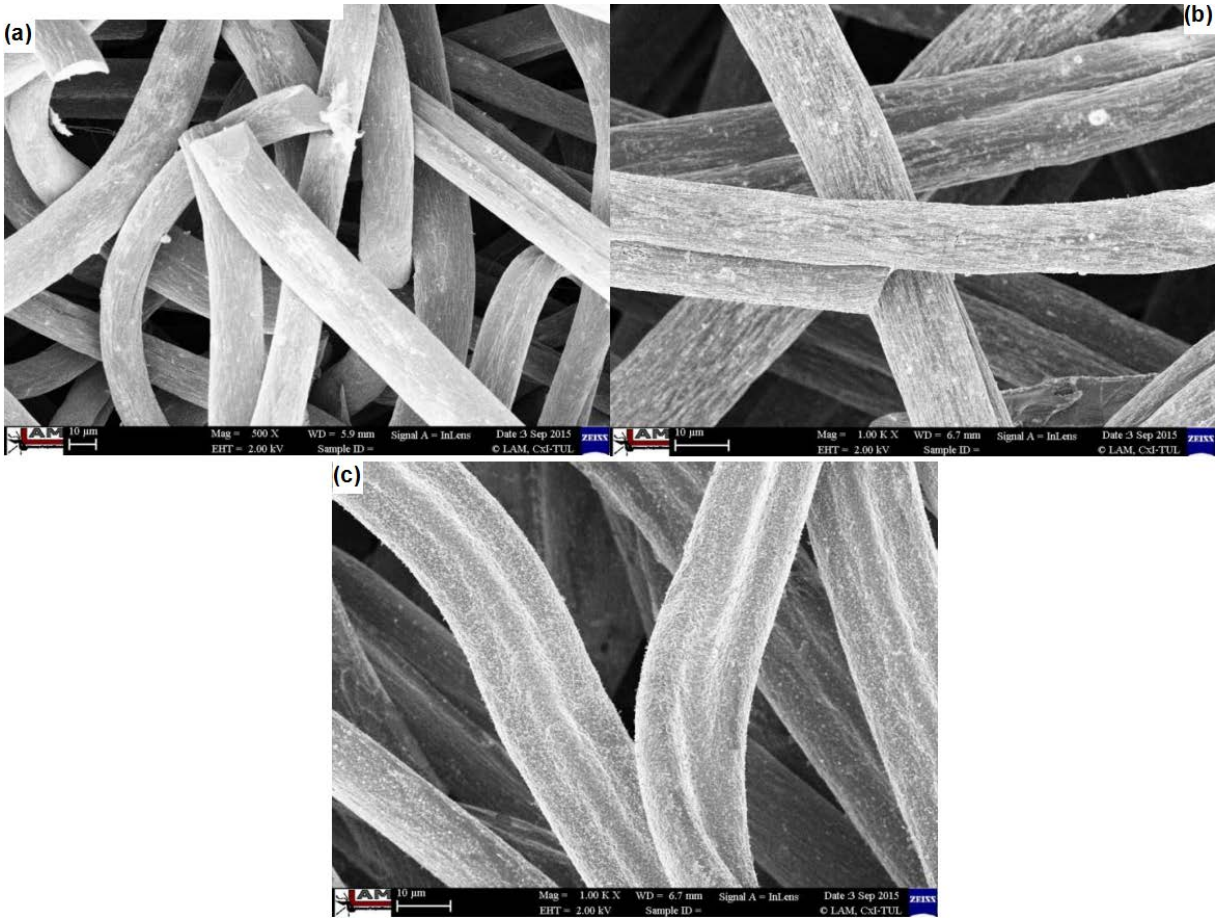

Figure 3. SEM image of ac web (a) at 800 ◦c (b) at 1000 ◦c (c) at 1200 ◦c

3.2. Effect of heating rate

In order to understand the impact of heating rate on electrical conductivity and surface area, heating rate was varied from 150 ◦c hr^{-1} to 450 ◦c hr^{-1} keeping final temperature (1200 ◦c with heating rate 300 ◦c $hr^{-1)}$ and holding time same. The impact of heating rate on electrical conductivity and surface area can be seen from the figure 4. It is clear from the figure 4 that there is not much difference in the electrical conductivity at different heating rates. As electrical conductivity is related to proper arrangement of basal sheets, which is also a measure of degree of crystallinity. Since crystallinity is more influenced by the final temperature hence little difference in the arrangement of sheets is responsible for almost similar values of electrical conductivity.

The escape of volatile material during carbonization is influenced by heating rate. Although there is not big difference of surface area when the heating rate is increased from 150 ◦c hr^{-1} to 300 ◦c hr^{-1} , however surface area is then reduced when heating rate was increased to 450 ◦c hr^{-1} due to sudden escape of volatile matter which caused bad impact on the surface area.

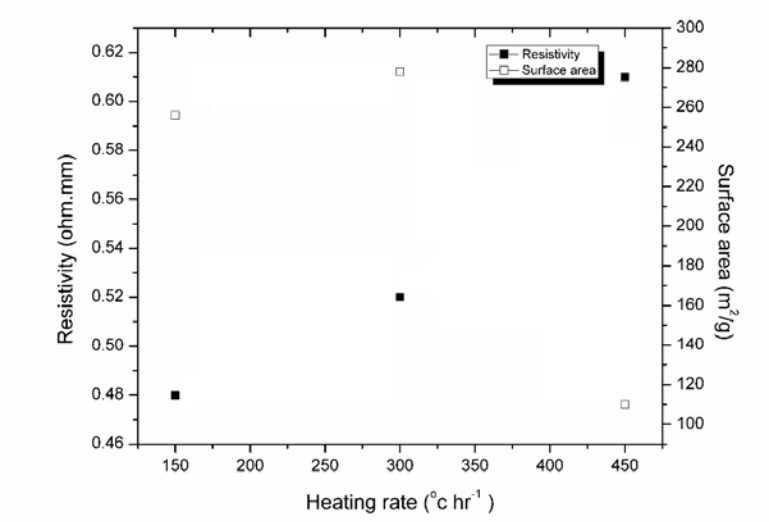

Figure 4. Impact of heating rate on surface resistivity and surface area

3.3. ***Effect of holding time***

In order to evaluate the impact of holding time on physical properties of carbon web, the heating rate and final temperature has been finalized on the basis of previous results. The holding time was varied from 0 minutes to 60 minutes after achieving 1200 ◦c at a heating rate of 300 ◦c. As far as electrical conductivity and surface area is concerned, the electrical conductivity kept on increasing as the holding time was increased from 0 to 60 minutes as can be seen from figure 5. This is because conductivity is related to orientation of basal planes in the carbon fibers. And more holding time means fibers in carbon web got more chances of orientation of sheets, due to which electrical conductivity increased. But surface area is decreased when holding time was increased. Because when the web was given more time at high temperature it causes the burning of pores and hence reducing the surface area of carbon web.

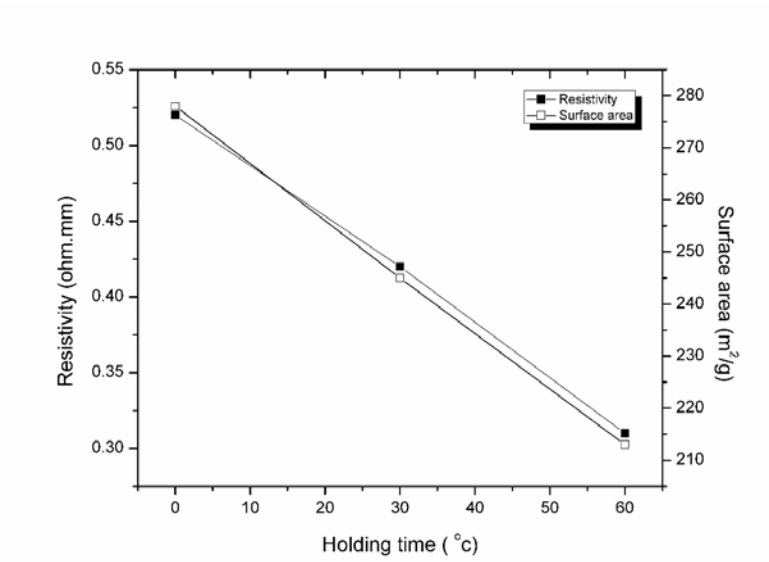

Figure 5. Impact of holding time on surface resistivity and surface area

4. CONCLUSIONS

The acrylic fibrous waste was successfully converted into activated carbon by physical activation in presence of air using controlled thermal treatment in high temperature furnace. The carbonization was performed under the layer of charcoal at 800 °c, 1000 °c and 1200 °c with the heating rate of 300 °c h^{-1} and without any holding time. Further, the influence of carbonization temperature on physical and morphological properties of activated carbon web was studied The multistage pyrolysis with 1200 °c of final pyrolysis temperature with heating rate 300 °c h^{-1} and no holding time resulted into activated carbon having higher specific surface area and higher electrical conductivity. The lower heating rate and shorter holding time are found to have significant effect on the development of porous morphology with higher surface area and better electrical conductivity. This behavior is attributed to gradual reaction of atmospheric oxygen with carbonized acrylic fibrous waste.

ACKNOWLEDGEMENTS

This work was supported by the SGS 2016 project of Technical University of Liberec, Czech Republic No. 21153.

References

1. *Goyal, M., Bansal, R. C. (2005). Activated carbon adsorpton, Taylor and Francis, USA.*
2. *Suzuki, M. et al. (1994). Activated carbon fiber: fundamentals and applications. Carbon, vol. 32, pp. 577-586.*
3. *Korai, Y., Shirahama, M., Kawano, S., Hada, T., Seo, Y., Yoshikawa, M., Yasutake, A., Mochida, I. et al. (2000). Removal of SO and NO over activated carbon fibers. Carbon, vol. 38, pp. 227-239.*
4. *Wang, Y., Wen, T., Wan, Y., et al. (1999). Effect of specific surface area and silver content on bacterial adsorption onto ACF (Ag). Carbon, vol. 37, pp. 351-358.*
5. *Wan, Y., Wang, J., Wang, Y., Jiang, X., Han, L., Li, C., et. al. (1998). Antibacterial pitch-based activated carbon fiber supporting silver. Carbon, vol. 36, pp. 61-65.*
6. *Casa-Lillo, M., Cazorla-Amoros, D., Linares-Solano, A., Alcaniz-Monge, J., et. al. (1997). Methane storage in activated carbon fibres. Carbon, vol. 35, pp. 291-297.*
7. *Tanahashi, I., Nishino, A., Yoshida, A., et. al.(1990). Effect of concentration of surface acidic functional groups on electric double-layer properties of activated carbon fibers. Carbon, vol. 28, pp. 611-615.*

INVESTIGATION OF CONVENTIONAL THERMAL TREATMENT AND LASER IRRADIATION OF ACRYLIC COATED GLASS FIBER NONWOVENS TO MAKE ELECTRICALLY CONDUCTIVE NONWOVEN SURFACE

Syed Qummer Zia Gilani, Jakub Wiener, Vijay Baheti, Hafiz Affan Abid, Jiri Militky

Department of Material engineering, Faculty of Textile Engineering, Technical University of Liberec, Liberec, Czech Republic
Email: qummerzia@gmail.com

Abstract

Research was done on thermal and laser irradiation of acrylic coated glass fiber nonwoven sheets. Glass fiber nonwoven sheets were padded in acrylic solution and dried. Conventional thermal treatment as well as Infrared laser irradiation of the coated nonwoven sheets was investigated for possible carbonization of acrylic to produce electrically conductive surface. It was found that laser irradiation produces electrically conductive surface of the material. The conductivity is increased when intensity of laser beam is increased and vice versa. Moreover the material exhibits even better electrical conductivity when it is stabilized by preheated at 300°C before laser exposure. It was also found that conventional thermal treatment is not suitable for carbonizing the surface of developed acrylic coated nonwoven sheets.

Key Words:

PAN, Carbonization, Conductive nonwoven

1. Introduction

Acrylic fibers also known as Polyacrylonitrile (PAN) is a common material used as a precursor in manufacturing of carbon fibers. Carbonization of acrylic produces carbon fibers. Nowadays about 90% of carbon fibers are manufactured by thermal conversion of PAN precursor [1]. Usually acrylic precursors are heat treated at various temperatures for converting them into carbon fiber. The conversion is done in three steps which are oxidative stabilization, high temperature carbonization and graphitization.

Oxidative stabilization is done in temperature range 180~300°C [2,3]. Some researchers found 270°C the best suitable temperature for oxidative stabilization [4] however some studies also recommended higher temperatures exceeding 300°C for stabilization process [5]. If the temperature is very high the fiber can fuse or burn, but at very low temperatures incomplete stabilization can be the result. Once the fiber is stabilized it will not melt again when exposed to high temperatures.

Carbonization is the step in which the fiber is exposed to temperature ranging from 800°C to 3000°C. This heating can produce upto 95% carbon content [6]. Heating around 1000°C can produce carbon fibers of high tensile strength but higher temperature is necessary to manufacture high modulus carbon fibers [7].

Graphitization is the step of heating the fiber in the temperature range 1600~3000°C. It means graphitization is a carbonization process at high temperature. When heating is done around 1600°C to 3000°C about 99% polymer is converted to carbon [8,9,10]. Carbon fibers manufactured by this process are high modulus carbon fiber and classified as type-1 carbon fiber.

In the recent years most PAN based carbon fibers are being used in composite manufacturing [11].

Besides other benefits presence of carbon or graphite imparts better electrical conductivity. Moreover better resistance to corrosion and lighter weight materials with good strength find applications to replace metals. Conductivity is also a desirable property in manufacturing of electromagnetic and radio frequency interference (EMI/RFI) shielding for electronic devices, moderate conductivity is necessary for electrostatic dissipation (ESD) [2]. Better physical and mechanical characteristics of PAN based composites have given them a good space in automotive and aerospace applications [12]. Finding solutions to challenges in aerospace applications can be done by optimization of the acrylic (PAN) fiber which can prove it the ideal fiber for aerospace applications [13,14]. In this study the acrylicfibers from waste are dissolved in solvent to make acrylic fiber solution (acrylic solution) and then this solution is applied on glass fiber nonwoven sheet to manufacture composite sheets. Subsequent thermal and laser treatment of the prepared samples is studied to impart electrical conductivity in the material.

2. Experimental

2.1 Materials

Acrylic fibers waste from Gurund Industries, Czech Republic. DMF (by RCI Labscan Limited).

Glass fiber non-woven sheet of 270 g/m^2 (provided by SEPAT Specialni Papirenske Technologie, Czech Republic).

2.2 Methods

Main purpose of the study was effective utilization of acrylic waste. Since acrylic fibers can be dissolved in dimethyl-formamide (DMF), acrylic fiber solution was prepared using DMF. The samples were produced by padding glass non-woven sheet in acrylic solution at 100% pickup. In this way the glass fibers in the nonwoven sheet were covered and coated with the acrylic solution.

3. Results and discussion

The acrylic coated samples were treated in oven at different temperatures to study the effect of heat treatment on their properties. Heat treatment was carried out between 200°C to 450^{o}C. Weight of each sample before and after heat treatment was determined using electronic balance. Based on these observations percent weight loss of each sample was determined. Table 1 shows the results of weight loss (%) of acrylic coated nonwoven sheets.

It is clear from the results summarized in Table 1, that increasing temperature increases weight loss. At 450^{o}C almost half of the samples weight is reduced which means that major amount of the applied acrylic polymer is evaporated of the sample. This implies that the conventional thermal pyrolysis process is not suitable to convert the coated acrylic polymer to carbon or graphite structure.

Table 1. Weight loss (%) of acrylic coated nonwoven after heat treatment.

Sample	Treatment Temperature	Initial Weight	Final weight	Difference	weight loss
Sr. no.	°C	(gm)	(gm)	(gm)	%
1	200	1.00	0.89	-0.11	-11
2	250	1.00	0.87	-0.13	-13
3	300	1.00	0.81	-0.19	-19
4	350	1.00	0.64	-0.36	-36
5	400	1.00	0.59	-0.41	-41
6	450	1.00	0.51	-0.49	-49

Since the ideal oxidative stabilization temperature of acrylic is 270~300 oC [4,5]. The samples heat treated at 300oC is selected for laser irradiation to study the effect of laser treatment.
Two set of experiments were performed in order to check the suitability of laser treatment for imparting electrical conductivity in the material. Firstly samples after drying and curing were directly exposed to laser at different marking speed. Secondly samples after curing were preheated at 300oC for one hour in an oven for stabilization [4], and were then exposed to laser
The figure 4 shows that samples preheated at 300oC before laser treatment shows very less electrical resistance (good electrical conductivity) after laser treatment as compared to that of non-preheated samples.
High energy laser beam is carbonizing the acrylic to impart electrical conductivity. This means electrical conductivity is imparted in the irradiated samples due to the presence of carbon or graphite structure [2] which is responsible for conductivity. Preheating the samples at 300oC stabilizes the acrylic [4] on the surface of the glass sheets hence after laser irradiation more carbon or graphite is responsible for better conductivity.

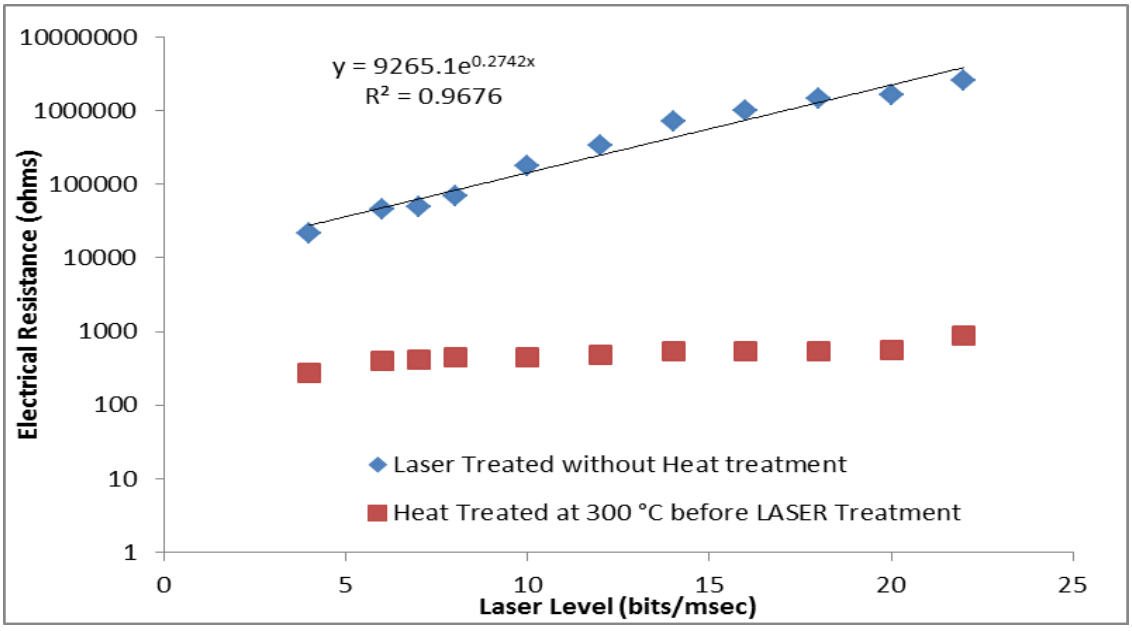

Figure 4. Electrical resistance of acrylic coated glass nonwovens at varying laser parameters.

More powerful laser irradiation at lower mark speed has shown less electrical resistance and good conductivity. However at very lower mark speeds more intensity of laser irradiation can altogether destroy the sample.

4. CONCLUSION

It is concluded that laser irradiation of acrylic coated glass fiber nonwoven sheets is capable of imparting electrical conductivity in the material. More is the powerful laser beam level, more is the electrical conductivity and vice versa. Hence using lower marking speed, but without destroying the sample, is necessary to get less electrical resistance and good conductivity.

References

1. *Cato Anthony D, Edie DD. Flow behavior of mesophase pitch. Carbon 2003; 41(7):1411-7.*
2. *Clingerman ML. Development and modelling of electrically conductive composite materials. PhD thesis, Michigan Technological University, USA, 2001.*
3. *Paiva MC, Kotasthane P, Edie DD, Ogale AA. UV stabilization route for melt-processible PAN-based carbon fibers. Carbon 2003; 41(7):1399-409.*
4. *Fitzer E, Frohs W, Heine M. Optimization of stabilization and carbonization of PAN fibers and structural characterization of the resulting carbon fibers. Carbon 1986; 24(4):387-95.*
5. *Gupta A, Harrison IR. New aspect in the oxidative stabilization of PAN based carbon fibers II. Carbon 1997; 35(6):809-18.*
6. *Ko TH. The Influence of pyrolysis on physical properties and microstructure of modified PAN fibers during carbonization. Appl Polym Sci 1991; 43(3):589-600.*
7. *Trinquecoste M, Carlier JL, Derrb A, Delhaes P, Chadeyron P. High temperature thermal and mechanical properties of high tensile carbon single filaments. Carbon 1996; 34(7):923-9.*
8. *Mittal J, Mathur RB, Bahl OP. Single step carbonization and graphitization of highly stabilized PAN fibers. Carbon 1997; 35(8):1196-7.*
9. *Kaburagi M, Bin Y, Zhu D, Xu C, Matsuo M. Small angle X-ray scattering from voids within fibers during the stabilization and carbonization stages. Carbon 2003; 41(5):925-6.*
10. *Mittal J, Mathur RB, Bahl OP, Inagaki M. Post spinning treatment of PAN fibers using succinic acid to produce high performance carbon fibers. Carbon 1998; 36(7e8):893-7.*
11. *Pamula E, Rouxhet GP. Bulk and surface chemical functionalities of type III PAN-based carbon fibers. Carbon 2003; 41(10):1905-15.*
12. *Wiles KB. Determination of reactivity ratios for acrylonitrile/methyl acrylate radical copolymerization via nonlinear methodologies using real time FTIR. MSc thesis, Faculty of the Virginia Polytechnic Institute and State University: Blacksburg, Virginia, 2002.*
13. *Fitzer E. PAN based carbon present state and trend of the technology from the viewpoint of possibilities and limit to influence to control the fiber properties by the process parameter. Carbon 1989; 27(5):621-45.*
14. *Chen JC, Harrison IR. Modification of polyacrylonitrile (PAN) carbon fiber precursor via post-spinning plasticization and stretching in dimethylformamide (DMF). Carbon 2002; 40(1):25-45.*

STUDY ON ACOUSTIC AND THERMAL PERFORMANCE OF STRUTO NONWOVENS

Tao Yang, Xiaoman Xiong, Mohanapriya Venkataraman, Kasthuri Venkatesh, Rajesh Mishra, Jan Novák[1] and Jiří Militký

Department of Material Engineering, Faculty of Textile Engineering, Technical University of Liberec, Liberec 46117, Czech Republic
[1]Department of Vehicles and Engines, Faculty of Mechanical Engineering, Technical University of Liberec, Liberec 46117, Czech Republic

Abstract:

This paper presents an experimental investigation on the sound absorption behaviour and thermal properties of struto nonwovens, the relationship between these properties were studied as well. Seven struto nonwoven fabrics were selected to examine sound absorption like noise reduction coefficient (NRC) and average values of sound absorption coefficients as well as thermal insulation properties including thermal conductivity and thermal resistance. It was also observed that sound absorption had insignificant correlation with thermal conductivity while they were strongly correlated with thermal resistance. And the correlation coefficient of NRC and thermal resistance was 0.98313, indicating that NRC was directly proportional to thermal resistance of struto nonwovens. It was concluded that a higher thermal resistance suggested a better sound absorption performance for a struto nonwoven fabric.

Key words:

struto nonwoven, sound absorption, thermal resistance, thermal conductivity

1. Introduction

Nonwovens have very high porosity, high specific surface area, economical price, light weight, good elasticity and a great flexibility in air permeability, they can be presented in a large number of kinds of fibre assemblies, above characteristics decide that nonwovens have been widely applied in thermal insulation and sound absorption field [1].

Thermal properties of nonwoven fabrics are extensively studied by researchers. Generally, the thermal insulation properties of nonwoven fabric have a strong correlation with its fabric dimensional and structural parameters [2]. Moreover, a lot of research and modelling effort devoted to understanding the noise control performance of nonwovens can be found in literature [3][4]. Struto, a nonwoven structure where all the fibres are orientated in the vertical plane, developed by the Technical University of Liberec (TUL), Czech Republic, is proved to be an excellent sound absorber used in noise control field especially in automotive industry [5][6].

Since the thermal and acoustic property of nonwoven both strongly depend on its structure parameters, for a specified nonwoven fabric there should be some relation between these two performances. However, there is very limited research devoted to understanding this relationship. In this paper, seven struto nonwovens were selected to measure sound absorption properties and thermal performance. The effect of fabric thickness and GSM on sound absorption and thermal insulation properties were investigated. The relationship between sound absorption and thermal properties were studied as well.

2. Experimental

2.1. Materials

Seven struto nonwoven fabrics made by TUL were selected to measure thermal and acoustic properties. The characteristics of the specimens are shown in Table 1.

Table1. Characteristics of struto nonwovens

Samples code	Content	GSM g/m2	Thickness mm
A	Polyester (PET) 45%-Staple PET 25%-Bicomponent PET 30%-Hollow PET	507.51	24.09
B		478.32	28.36
C		465.22	27.48
D	70%- PET 30%-Bicomponet PET	335.68	20.82
E		317.51	19.85
F		198.64	20.12
G		259.28	20.66

2.2. Measurement of sound absorption

Sound absorption of struto nonwovens were measured according to ASTM E 1050: Standard Test Method for Impedance and Absorption of Acoustical Properties Using a Tube, Two Microphones and a Digital Frequency Analysis System. The testing principle of this system is illustrated in Figure 1. A sound source is mounted at one end of the impedance tube and the material sample is placed at the other end. The loudspeaker generates broadband, stationary random sound waves. These incident sound signals propagate as plane waves in the tube and hit the sample surface. The reflected wave signals are picked up and compared to the incident sound wave [7].

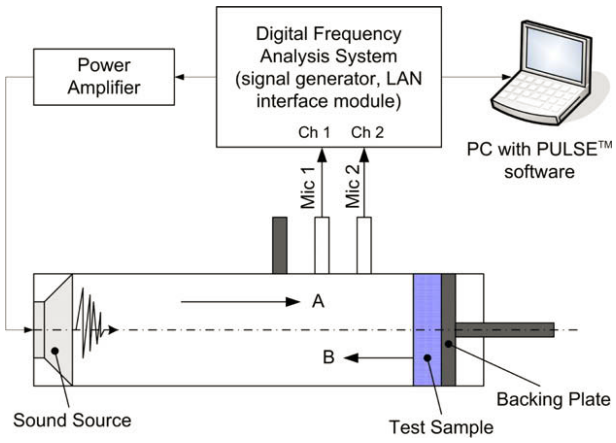

Figure 1. Measuring system configuration [7].

2.3. Measurement of thermal properties

Alambeta instrument was used to measure thermal conductivity and thermal resistance, according to EN 31092 standard. The measuring head of the Alambeta contains a copper block which is electrically heated to approximately 32℃ to simulate human skin temperature, this temperature is maintained by a thermometer connected to the regulator.

3. Results and discussion

3.1. Sound absorption

The normal incidence sound absorption coefficient (α) of struto nonwovens were determined as a function of the sound frequency (f), as shown in Figure 2.

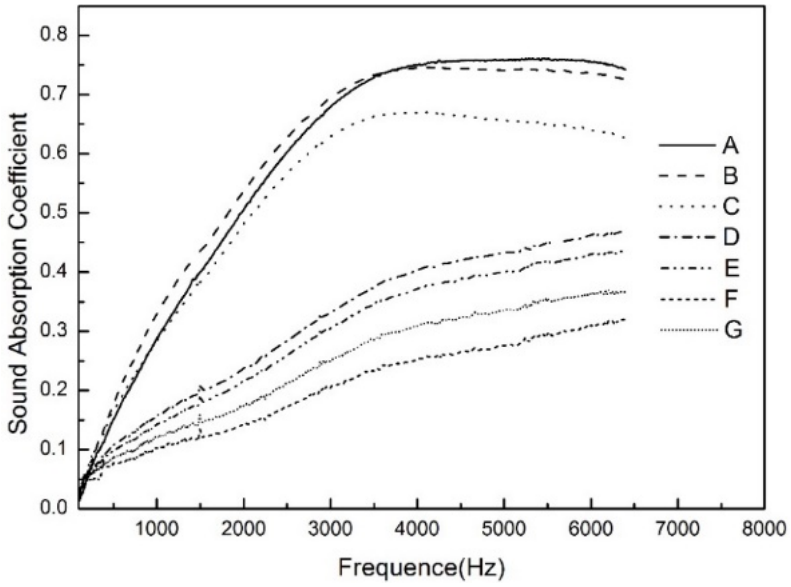

Figure 2. Sound absorption coefficient of struto nonwovens.

The noise reduction coefficient (NRC) and average values of sound absorption coefficients (SAC) for all the nonwovens were calculated. The NRC is the average value of Sabin alphas for 250, 500, 1000 and 2000 Hz, which exhibits a typical sound absorption behaviour of porous material. The NRC and average values of SAC ($\bar{\alpha}$) of struto nonwovens were calculated using the following equations:

$$NRC = \frac{\alpha_{250Hz} + \alpha_{500Hz} + \alpha_{1000Hz} + \alpha_{2000Hz}}{4} \quad (1)$$

$$\bar{\alpha} = \frac{\int_{F_1}^{F_2} \alpha(f)df}{F_2 - F_1} \quad (2)$$

where *F1* (100 Hz) is lower bound of sound frequency in testing and *F2* (6400 Hz) is upper bound of sound frequency in measurement [17]. The NRC and computed $\bar{\alpha}$ values between *F1* and *F2* for the struto nonwovens are listed in Table 2.

Table 2. NRC and means of SAC

Samples code	$\bar{\alpha}$	NRC
A	0.584	0.254
B	0.592	0.281
C	0.527	0.255
D	0.317	0.142
E	0.292	0.129
F	0.202	0.092
G	0.244	0.110

3.2. Thermal properties

Thermal conductivity and thermal resistance of struto nonwovens are presented in Table 3.

Table 3. Thermal properties of nonwovens

Sample code	Thermal conductivity 10-3 W·m-1·K-1	Thermal resistance 10-3 K·m2·W-1
A	55.84	431.80
B	61.70	460.60
C	60.04	458.20
D	63.30	329.06
E	63.42	313.03
F	71.10	283.11
G	67.00	308.34

3.3. The relationship between acoustic and thermal properties

Figure 3 illustrates the estimation correlation between thermal properties of struto nonwovens and sound absorption, NRC and average value of SAC ($\bar{\alpha}$). It is observed that both NRC and $\bar{\alpha}$ have insignificant correlation with thermal conductivity, the correlation coefficient are 0.60337 and 0.68975, respectively. The result also shows that sound absorption performance has a very strong correlation with thermal resistance, especially the correlation coefficient of NRC and thermal resistance is 0.98313, which indicates that NRC is directly proportional to thermal resistance of struto nonwovens.

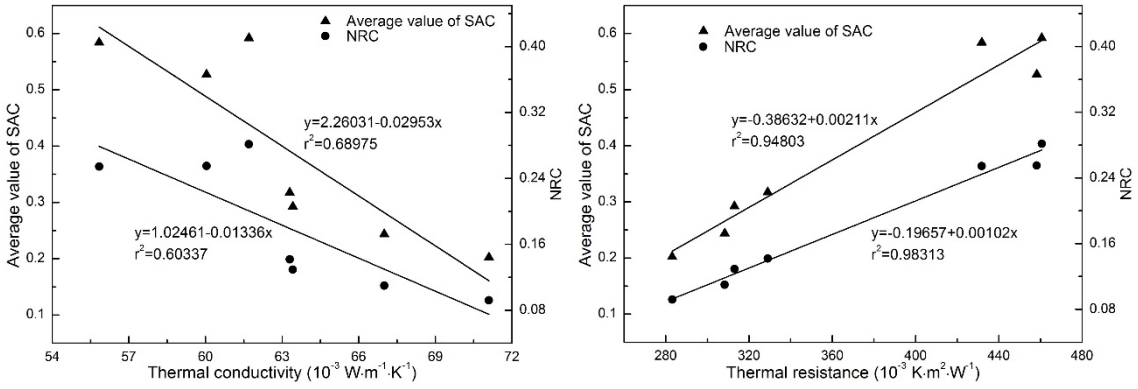

Figure 3. Estimation correlation between thermal properties (thermal conductivity and thermal resistance) and sound absorption (NRC and average value of SAC).

4. CONCLUSION

In this paper, seven struto nonwovens with varying thickness and GSM were selected to study their sound absorption and thermal properties as well as the relationship between these two performances.

It is observed that sound absorption, NRC and $\bar{\alpha}$, have insignificant correlation with thermal conductivity while they are strongly correlated with thermal resistance. Especially, the correlation coefficient of NRC and thermal resistance is 0.98313, which indicates that NRC is directly proportional to thermal resistance of struto nonwovens. Thus, a higher thermal resistance suggests a better sound absorption performance for a struto nonwoven fabric. This may provide a new method to evaluate sound absorption performance of struto nonwovens by measurements of their thermal insulation properties.

References

1. *Thilagavathi, G., Pradeep, E., Kannaian, T. and Sasikala, L. Development of Natural Fiber Nonwovens for Application as Car Interiors for Noise Control. Journal of Industrial Textiles 39, 267–278 (2010).*
2. *Xiaoman, X., Tao, Y., Juan, H., Rajesh, M., T, M, Kotresh., and Jiri, Militky. (2015). Heat transfer through thermal insulation materials Part I- Nonwoven fabrics. Recent developments in fibrous material science, VOL.II, 85-104 (2015).*
3. *Biot, M. A. Theory of propagation of elastic waves in a fluid-saturated porous solid. I. Low-frequency range. The Journal of the acoustical Society of america 28, 168–178 (1956).*
4. *Delany, M. E. and Bazley, E. N. Acoustical properties of fibrous absorbent materials. Applied Acoustics 3, 105–116 (1970*
5. *Struto International Inc., Struto® Nonwoven, http:/ / www.struto.com/, consulted in April 2016.*
6. *Parikh, D. V., Calamari, T. A., Goynes, W. R., Chen, Y. and Jirsak, O. Compressibility of Cotton Blend Perpendicular-Laid Nonwovens. Textile Research Journal 74, 7–12 (2004).*
7. *Jiang, N., Chen, J. Y. and Parikh, D. V. Acoustical evaluation of carbonized and activated cotton nonwovens. Bioresource Technology 100, 6533–6536 (2009).*

Theoretical models of tensile behavior of staple fiber yarns

Liberec
Strutex 2016

INTRODUCTION

1.One yarn is usually able to transfer much more higher tensile force then one textile fiber, however
2.one textile fiber can carry significantly higher tensile stress then a yarn (by a comparable conditions).

Why? It is because :

- Each fiber worked in a specific geometric situation of **yarn structure** (twist, radial migration, etc.).
- There are various **interactions** among fibers into a yarn (fiber-to-fiber friction, fiber-to-fiber slippage, etc.).

Note: We use the specific stresses in this contribution;

σ_f...for fiber, σ_Y...for yarns. *Dimension:* force /fineness (e.g. N/tex) or stress/mass density (e.g. Pa/(kg/m^3)

Scheme of stress-strain curves of fiber and yarn

σ_f, σ_Y ...specific stresses, $\varepsilon_f, \varepsilon_Y$ ...strains,

σ_f^*, σ_Y^* ...tenacities

a_f, a_Y ...breaking strains

Different tenacities - two influences:

$$\sigma_Y^* = \sigma_f^* - h_1 - h_2,$$

h_1 ...lower stress-strain curve of yarn

h_2 ...smaller braking strain of yarn

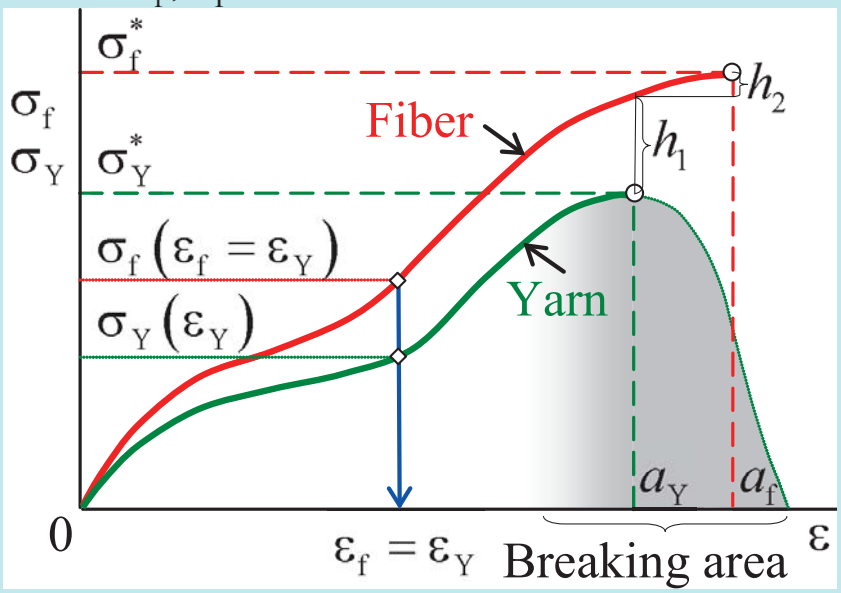

Two parts of stress-strain curve of (common) yarn:

First part – yarn elongation without significant breaks of fibers; "white".

Second part – significant breaking of fibers; "gray" (no precise border)

We are solving the first part, now

by using of fiber stress utilization:

$$\varphi(\varepsilon_Y) = \frac{\sigma_Y(\varepsilon_Y)}{\sigma_f(\varepsilon_f = \varepsilon_Y)}$$

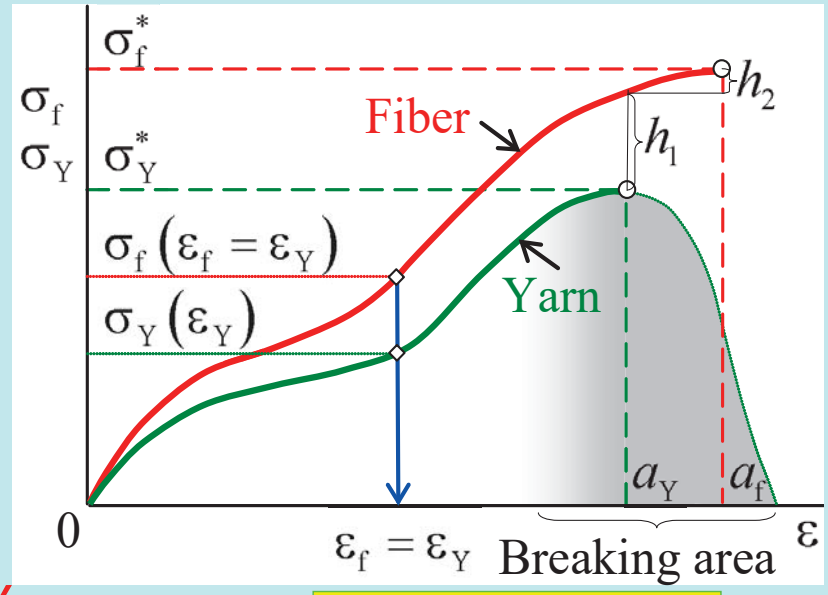

Common assumptions

D...yarn diameter, Z...yarn twist,
r...general radius of fiber

A) *Ideal helical models:*

1. All fibers creates helixes with same direction of rotation.
2. All helixes have one common axis (yarn axis).
3. Height of each coil is constant $1/Z$; slope angle β: $\tan\beta = 2\pi r Z$
4. Packing density $\mu = V/V_c$ is constant in all places into yarn. (V...fiber volume, V_c...total volume)

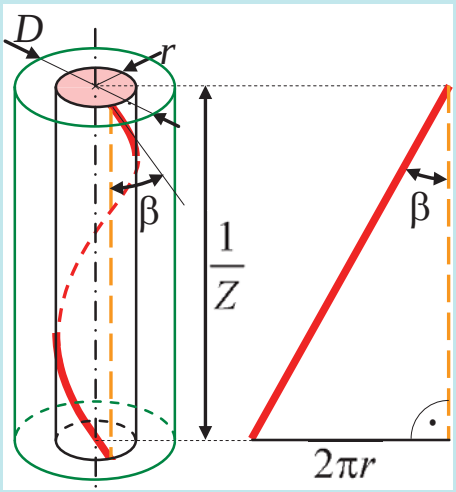

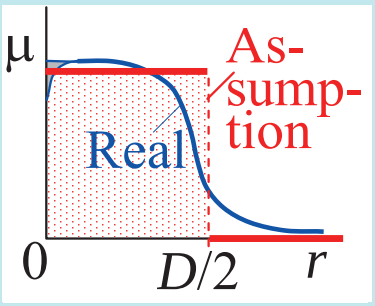

B) *Small strains:* Fiber element - before straining dl
- after straining dl'

Yarn strain $\varepsilon_Y = (d\zeta' - d\zeta)/d\zeta$

Fiber strain $\varepsilon_f = (dl' - dl)/dl$

Radial strain $\varepsilon_r = (r' - r)/r$

Contraction ratio $\eta = -\varepsilon_r/\varepsilon_Y$

By small yarn strain

$$\varepsilon_f = \varepsilon_Y\left(\cos^2\beta - \eta\sin^2\beta\right)$$

and $\cos\beta'/\cos\beta \to 1$

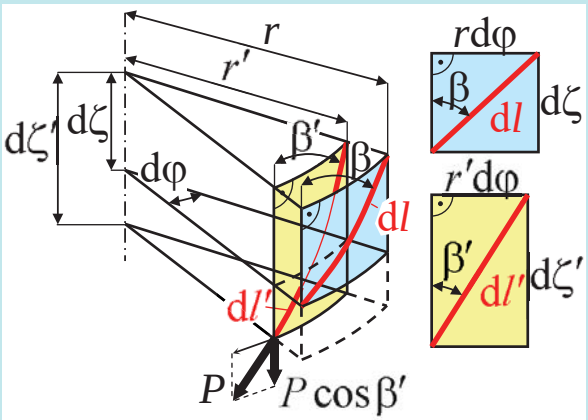

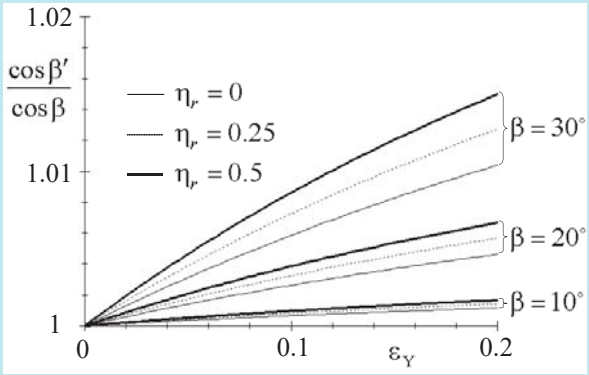

1. GEGAUFF'S THEORETICAL MODEL (1907)

Additionaly condition (simplification): Relationship between specific stress and strain in fiber is linear.

$$\sigma_f(\varepsilon_f) = K\varepsilon_f, \quad K = E/\rho \ldots \text{constant}$$

E...fiber (Young) modulus, ρ...fiber density.

Then the **resulting utilization of fiber stress** is

$$\varphi(\varepsilon_Y) = (1+\eta)\cos^2\beta_D + \eta\frac{\ln\cos^2\beta_D}{\tan^2\beta_D} \cdots\cdots \varphi_G$$

where $\tan\beta_D = 2\pi \underbrace{r}_{D/2} Z$, $\tan\beta_D = \pi DZ$ ...twist intensity.

Note: This Gegauff's utilization is independent to the yarn strain ε_Y .

Note: Gegauff's original work uses $\eta = 0, \Rightarrow \varphi(\varepsilon_Y) = \cos^2\beta_D$.

Utilization of fiber stress - graphical interpretation:

φ_G **decreases** with increasing of yarn twist (angle β_D). **Why**?

Slant of fiber (different resolution of forces)

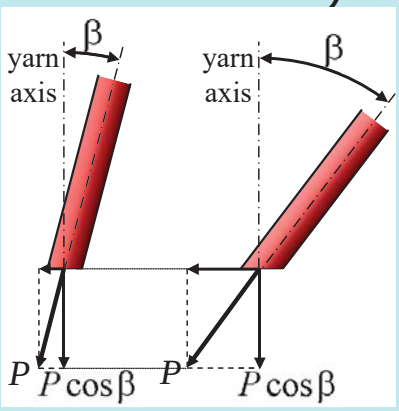

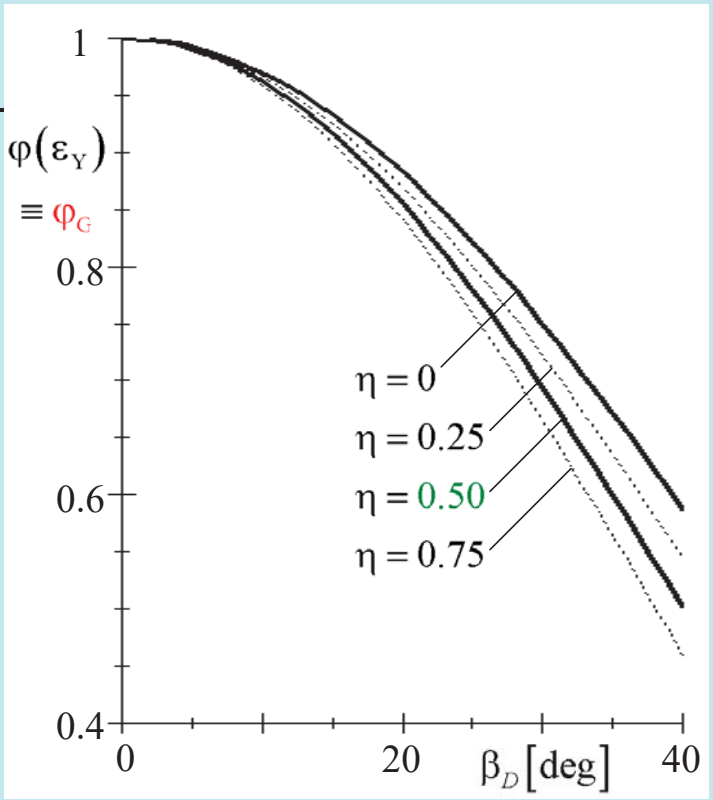

2. GENERALIZED GEGAUFF'S MODEL

Additional condition: The tensional stress-strain relation of fiber $\sigma_f(\varepsilon_f)$ is the real (mean) curve, determined experimentally (e.g. by a set of points).

Then the **resulting utilization of fiber stress** is

$$\varphi(\varepsilon_Y) = \frac{2\int_0^{\beta_D} \sigma_f(\varepsilon_f)\tan\beta\,d\beta}{\sigma_f(\varepsilon_Y)\tan^2\beta_D} \ldots\ldots \varphi_{C1}$$

$\sigma_f(\varepsilon_f)$…determined experimentally

$\varepsilon_f = \varepsilon_Y(\cos^2\beta - \eta\sin^2\beta)$…slide 6,

η…contraction ratio,

$\tan\beta_D = \pi DZ$…slide 7

Note: C1 means "calculated" and "simple integral".

Note: Numerical integration is necessary.

Utilization $\varphi(\varepsilon_Y) = \varphi_{C1}$ depends on ε_Y (and β_D) !

3. GENERALIZED GEGAUFF'S MODEL - EMPIRICAL CORRECTION

Because also another influences works on lower trend of stress-strain curve of yarn, it may be better to correct previous formula empirically by multiplication of a suitable parameter k.

Then the **resulting utilization of fiber stress** is

$$\varphi(\varepsilon_Y) = k\,\frac{2\int_0^{\beta_D} \sigma_f(\varepsilon_f)\tan\beta\,d\beta}{\sigma_f(\varepsilon_Y)\tan^2\beta_D} \ldots\ldots k\varphi_{C1}$$

where: $\varepsilon_f = \varepsilon_Y(\cos^2\beta - \eta\sin^2\beta)$…slide 6

η…contraction ratio, $\tan\beta_D = \pi DZ$…slide 7

$k < 1$…suitable parameter

4. GENERALIZED ASSUMPTIONS OF HELICAL MODEL

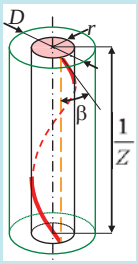

"Traditional" concept – all fibers on the same radius have always the same angle β (same slope).

Not right in the reality!

Generalized assumption:

1. Also fibers on the same radius have different angles ϑ – various slope. (Earlier helical β is a general ϑ, now.)
2. Modal value of angle ϑ on radius r corresponds to the "traditional" slope from the helical model ($\hat{\vartheta} = \beta$ where $\tan\beta = 2\pi r Z$ - slide 5)
3. Probability density function $u(\vartheta)$ of angle ϑ follows the unimodal distribution of fiber orientation in plane. (Same type of distribution, different modes $\hat{\vartheta} = \beta$ only.)

Probability density function:

$$u(\vartheta) = \frac{1}{\pi}\frac{C}{C^2 - (C^2-1)\cos^2(\vartheta+\beta)} + \frac{1}{\pi}\frac{C}{C^2 - (C^2-1)\cos^2(\vartheta-\beta)},$$

$C \geq 1 \ldots$ parameter of variability,

$\tan\beta = 2\pi r Z$

(Neckář,B. Das, D.: Theory of structure and mechanics of fibrous assemblies. WPI, New Delhi, Cambridge, 2012.)

Example by $\hat{\vartheta} = \beta = \pi/6$

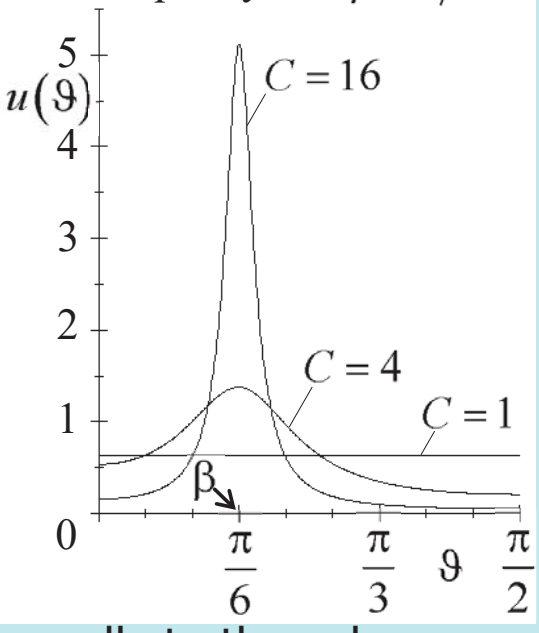

Note: A carded web corresponds usually to the value of parameter $C \in (1.6, 1.9)$.

TENSILE BEHAVIOR OF STAPLE FIBER YARNS

How to imagine it?

a) Let us think about a planar "strip" of fibers having the directional distribution $u(\vartheta)$ with modal value $\hat{\vartheta} = \beta$.

b) Let us have a cylinder on the radius $r = \tan\beta / (2\pi Z)$.

c) Let us wind this "strip" on the mentioned cylinder.

d) So, we obtain the differential layer of fibers into the yarn (on the radius r) having required distribution

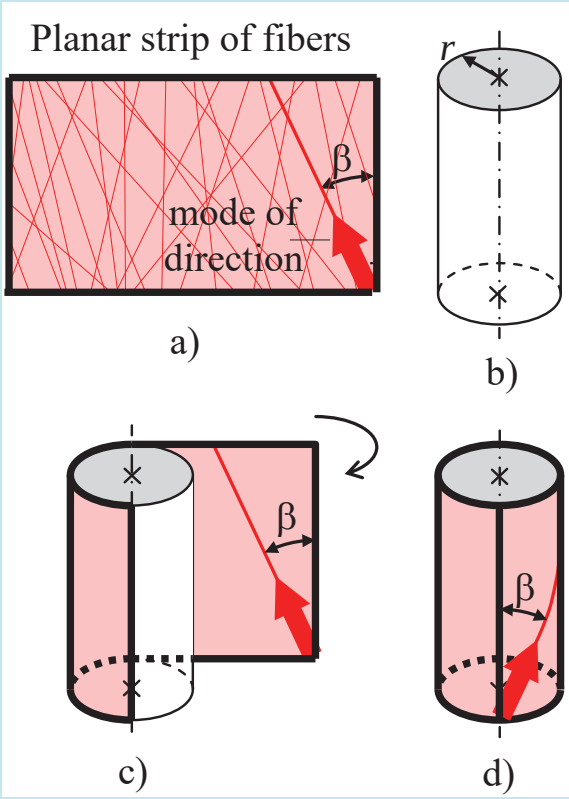

TENSILE BEHAVIOR OF STAPLE FIBER YARNS

Then the **resulting utilization of fiber stress** is

$$\varphi(\varepsilon_Y) = \frac{2\int_0^{\beta_D}\left[\int_0^{\arcsin\left(1/\sqrt{1+\eta}\right)} \sigma_f(\varepsilon_f)\cos^2\vartheta\, u(\vartheta)\,d\vartheta\right]\frac{\sin\beta}{\cos^3\beta}\,d\beta}{\sigma_f(\varepsilon_Y)\tan^2\beta_D} \cdots\cdots \varphi_{C2}$$

$\sigma_f(\varepsilon_f)$…determined experimentally,

$\varepsilon_f = \varepsilon_Y\left(\cos^2\vartheta - \eta\sin^2\vartheta\right)$…see slide 6, η…contraction ratio,

$u(\vartheta)$…see slide 11, C…a suitable constant,

$\tan\beta_D = \pi DZ$…see slide 7

Note: C2 means "calculated" and "double integral" .

Note: Numerical integration is necessary.

5. FULLY EXPERIMENTALLY DETERMINED UTILIZATION OF FIBER STRESS IN YARN

The utilization of fiber stress in yarn can be determined also **fully experimentally**.

Then we determine (from laboratory) :

$\sigma_f(\varepsilon_f)$ ...experimental stress-strain function of fiber (mean curve),

$\sigma_Y(\varepsilon_Y)$...experimental stress-strain function of yarn (mean curve).

The **resulting utilization of fiber stress** is then

$$\varphi(\varepsilon_Y) = \frac{\sigma_Y(\varepsilon_Y)}{\sigma_f(\varepsilon_f = \varepsilon_Y)} \cdots\cdots \varphi_E$$

COMPARISON OF EXPERIMENTAL AND THEORETICAL RESULTS - one example

Fiber material: Viscose fibers, 1.3 dtex, 38 mm.

Yarns: Common ring and rotor yarns, 20-50 tex.

Table of yarn parameters:

Technology	Nominal yarn count T[tex]	Actual yarn count T[tex]	Yarn twist Z[m^{-1}]	Yarn diameter D[mm]	Twist angle of surface fibres β_D[deg]
Ring	45	46.78	515	0.263	22
	29.5	32.45	650	0.210	21
	20	20.07	840	0.169	23
Rotor (Type BD)	50	52.15	550	0.294	27
	29.5	30.71	680	0.222	23
	20	20.03	900	0.177	27

TENSILE BEHAVIOR OF STAPLE FIBER YARNS

Mean experimental stress-strain curves

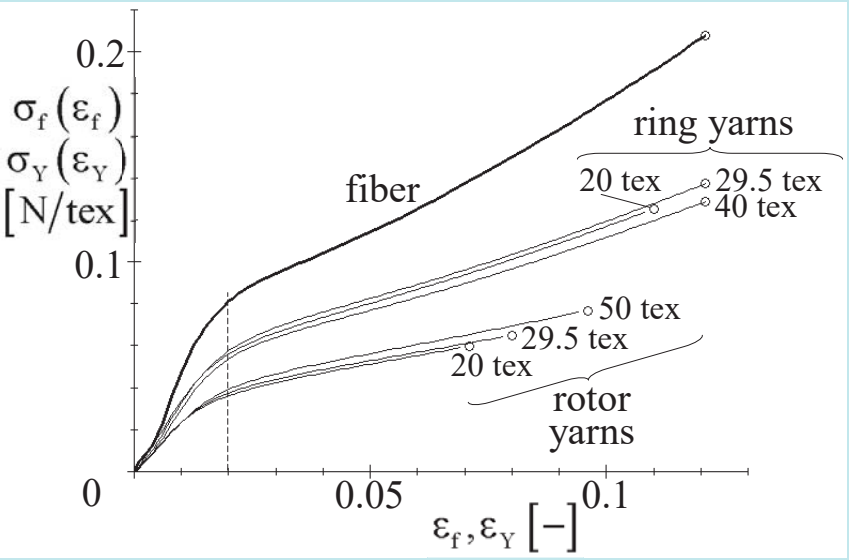

We don't evaluate:

1. (Gray) area near to yarn break (slide 3)
2. Area of very small strains (small values, big statistical discrepancy, pretension, etc.)

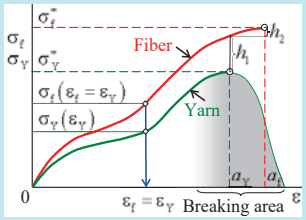

TENSILE BEHAVIOR OF STAPLE FIBER YARNS

Utilization of fiber stress by ring yarns

Common parameters of ring yarns:

$\eta = 0.5,$

$k = 0.79,$

$C = 4.9$

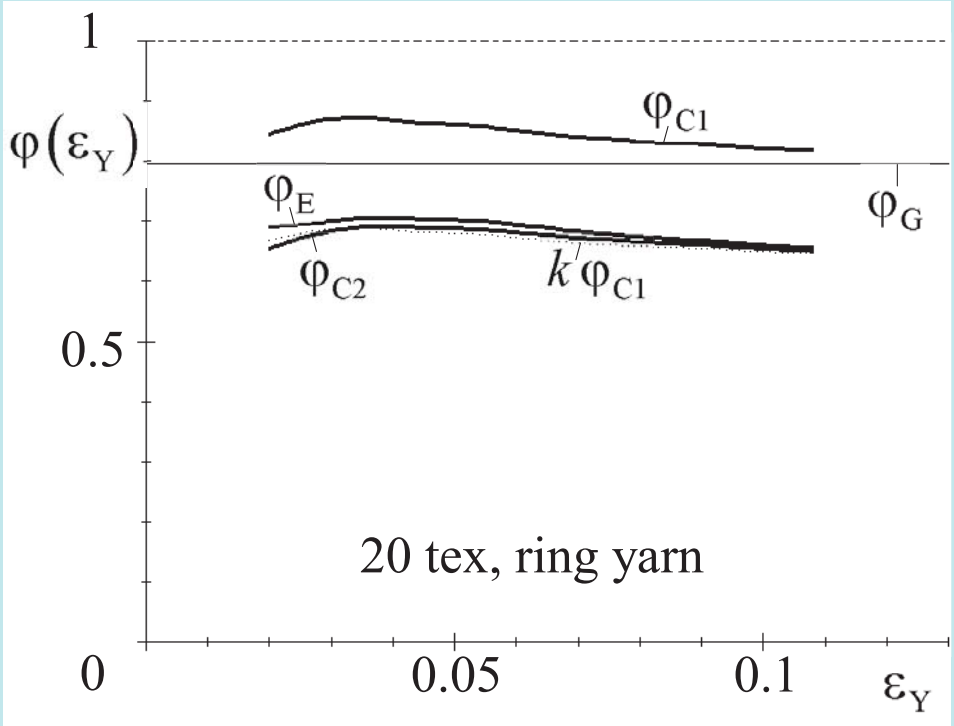

TENSILE BEHAVIOR OF STAPLE FIBER YARNS

Common parameters of ring yarns:

$\eta = 0.5,$

$k = 0.79,$

$C = 4.9$

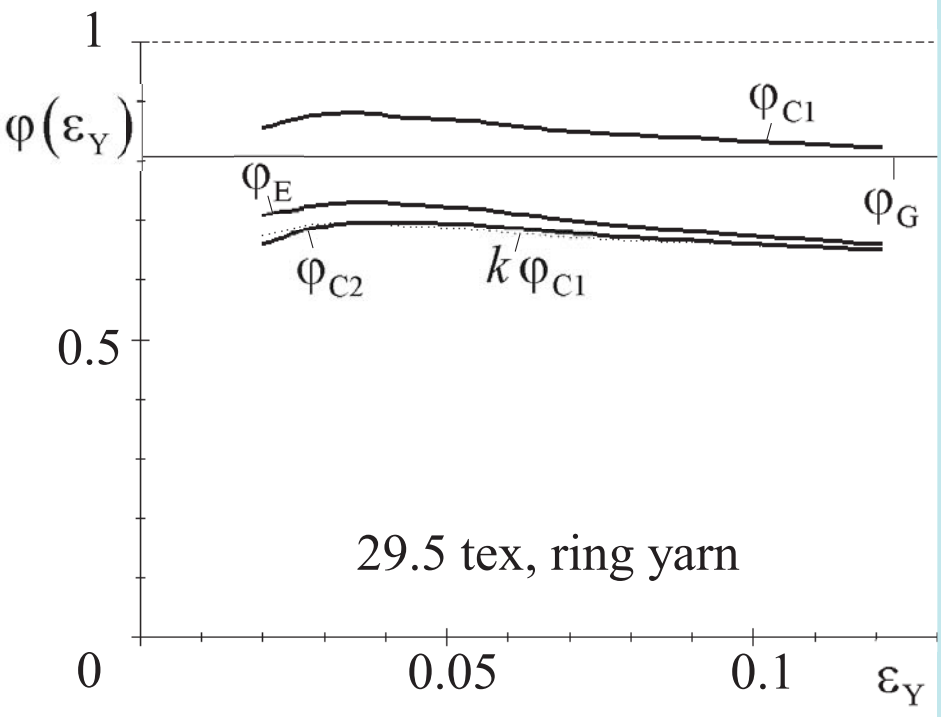

TENSILE BEHAVIOR OF STAPLE FIBER YARNS

Common parameters of ring yarns:

$\eta = 0.5,$

$k = 0.79,$

$C = 4.9$

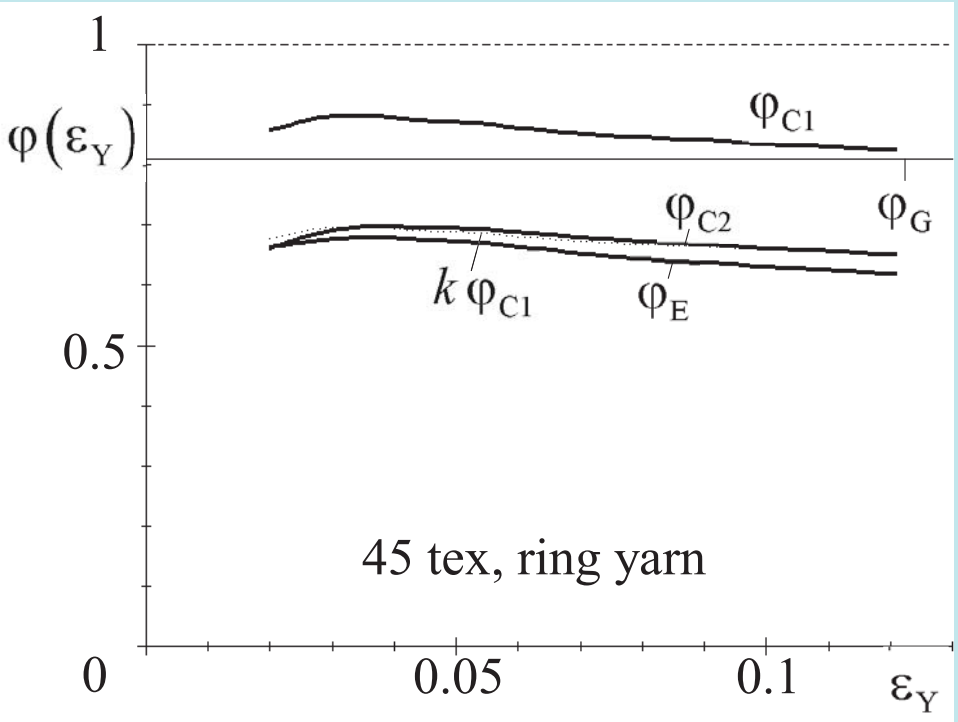

Utilization of fiber stress by rotor yarns

Common parameters of rotor yarns:

$\eta = 0.5,$

$k = 0.55,$

$C = 1.6$

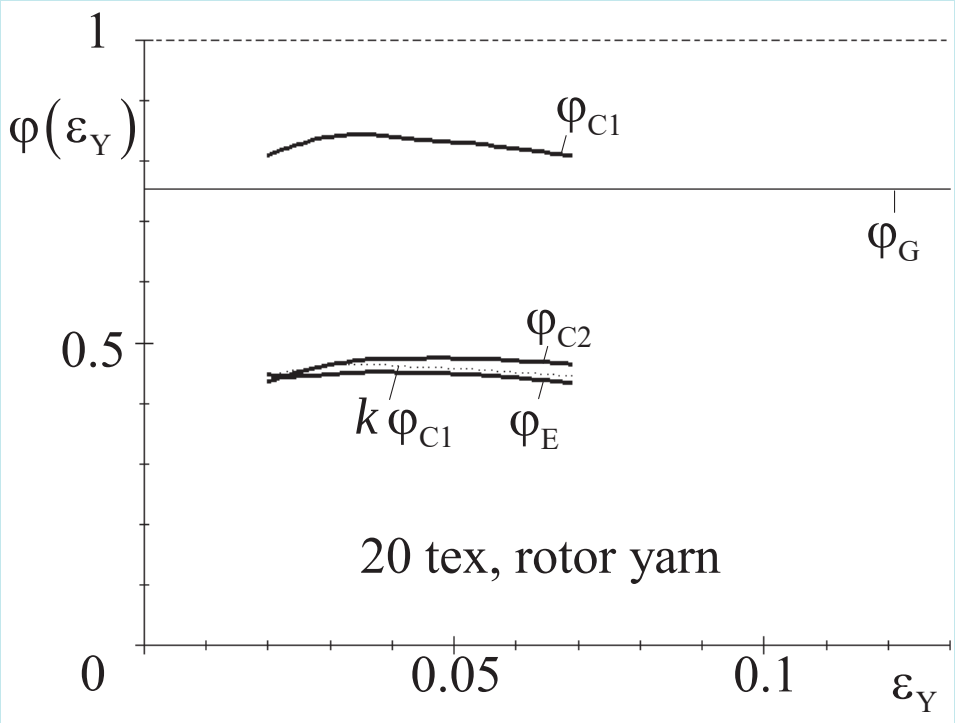

Common parameters of rotor yarns:

$\eta = 0.5,$

$k = 0.55,$

$C = 1.6$

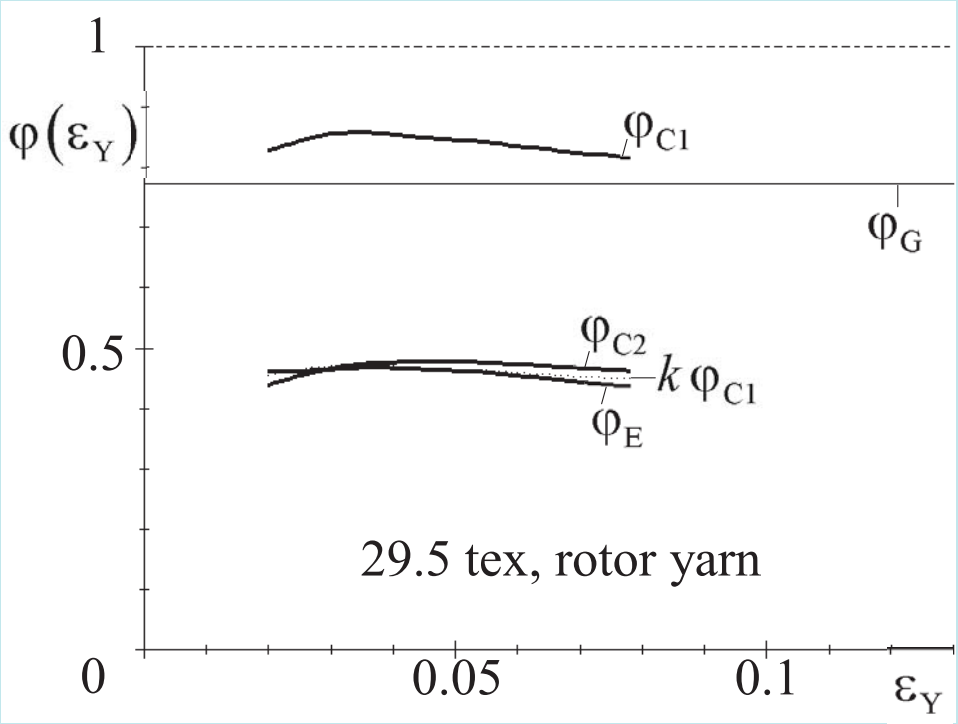

Common parameters of rotor yarns:

$\eta = 0.5,$

$k = 0.55,$

$C = 1.6$

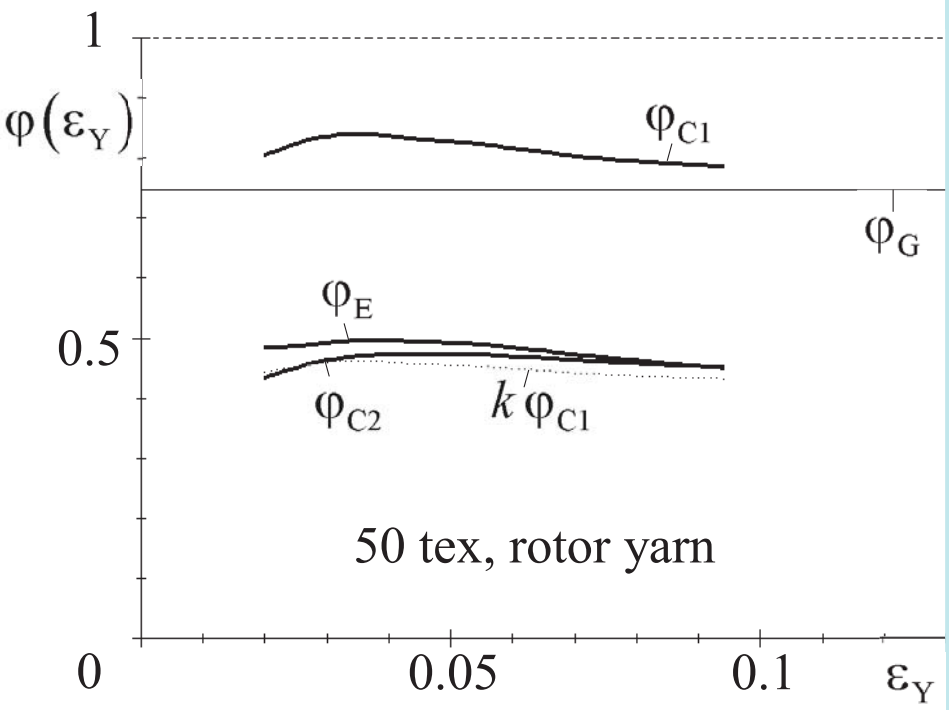

MAIN CONCLUSIONS

1. Gegauff's theoretical model φ_G, as well as the same concept with real stress-strain relation of fiber - $\varphi_{C,1}$, are far from experimental reality φ_E.

2. Theoretical model $\varphi_{C,1}$, empirically reduced by coefficient k, i.e. $k\varphi_{C,1}$, gives a good accordance with experimental results. Nevertheless, a logical sense of such reduction remains unknown.

3. Theoretical model $\varphi_{C,2}$, using variable slopes of fiber, gives also the good accordance with experimental results and shows that the significance of "unparallelity" of fibers (fiber portions) is high.

Note: Also another factors (fiber-to-fiber slippage, etc.) can partly influence the selected suitable parameter C.

More details, derivations, connections:

Neckář, B., Das, D. (2016): Tensile behavior of staple fiber yarn, part I: theoretical models.
J. Textil. Inst., DOI: 10.1080/00405000.2016.1204899.

Zubair, M., Neckář, B., Das, D. (2016): Tensile behavior of staple fiber yarn, part II: model validation.
J. Textil. Inst., DOI: 10.1080/00405000.2016.1204898.

Zubair, M., Eldeeb, M., Neckář, B. (2016): Tensile behavior of staple fiber yarn, part III: comparison of mathematical models.
J. Textil. Inst., DOI: 10.1080/00405000.20161237064.

Zubair, M., Neckář, B., Eldeeb, M., Gulzar, A.B. (2016): Tensile behavior of staple fiber yarn, part IV: experimental verification of predicted stress-strain curves.
J. Textil. Inst., DOI: 10.1080/00405000.2016.1243195.

Zubair, M., poster of this conference.

Thank you for your attention

Heat Transfer and Fluid Flow Laboratory
Brno University of Technology, Faculty of Mechanical Engineering

Application of polymer hollow-fibers to heat exchanger

Miroslav Raudenský

POLYMER HOLLOW FIBERS

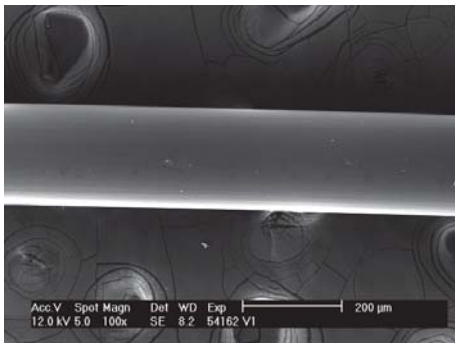

Polypropylene solid-wall hollow fiber

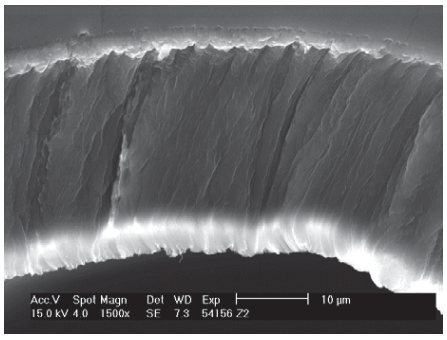

Crosscut of fiber

Motivation

To produce the above at least by 60% lighter and for half cost.

Material - Technical polymer

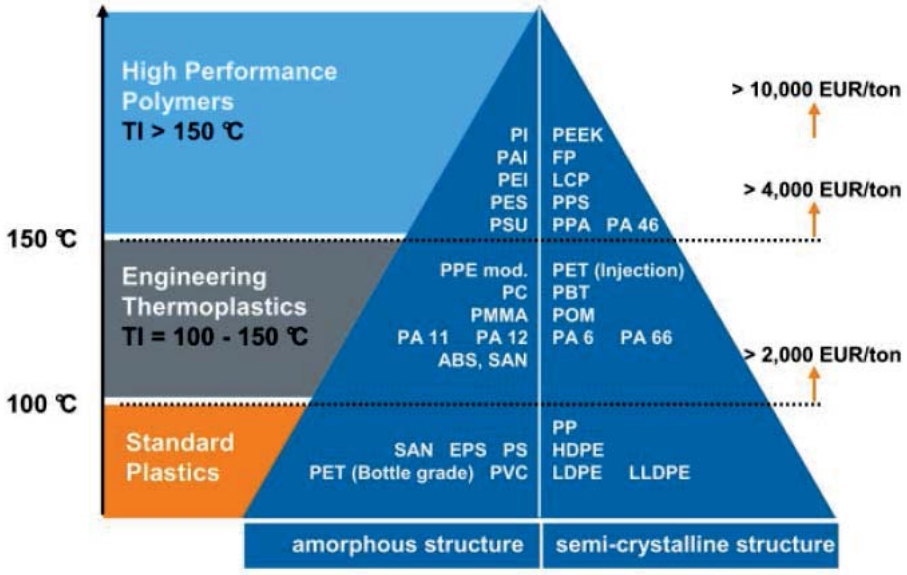

Source : PlasticsEurope Market Research (PERMG)

Polyphthalamide (aka. **PPA**, **High Performance Polyamide**) 30 EURO/kg, **Polypropylene PP,** 1.6 EURO/kg

Heat transfer – small diameter

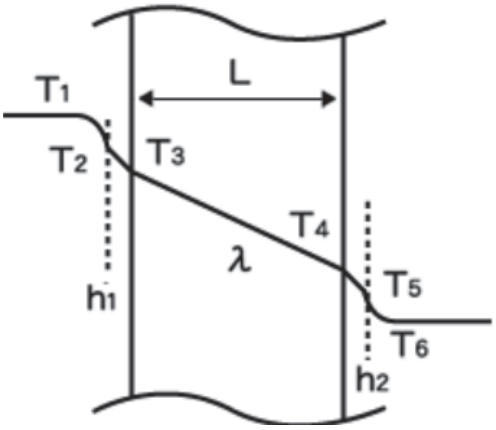

- To achieve high convective HTC values
- To have high compactness (high heat transfer surface in small volume)

Heat Ttransfer Coefficient - flow outside tube

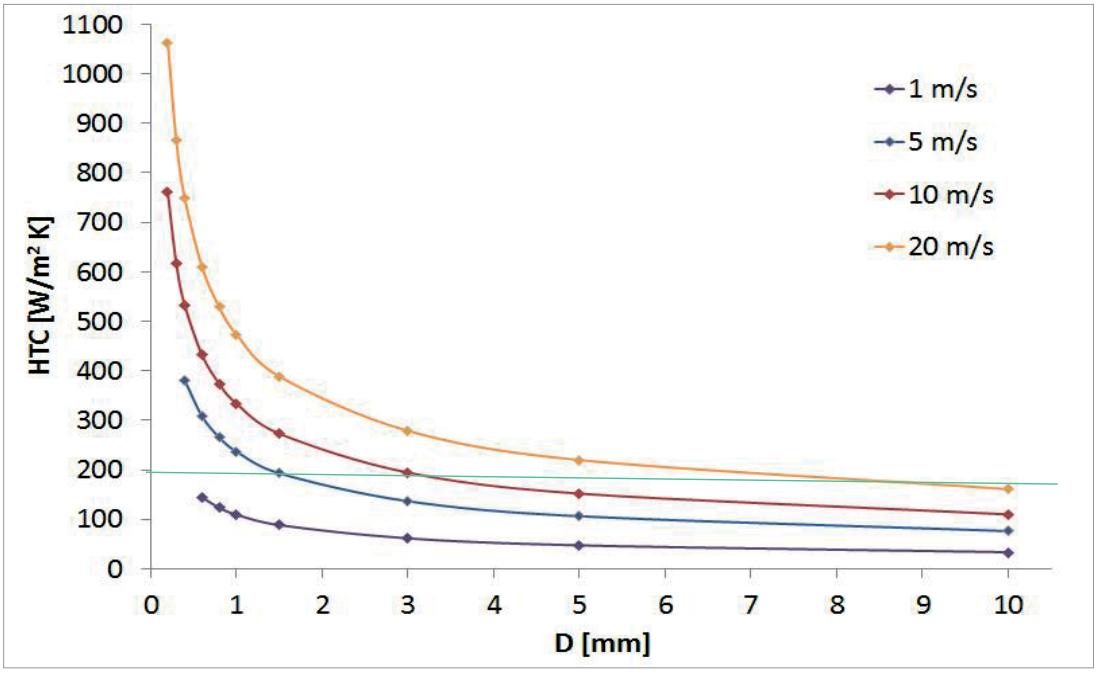

External flow of air (20° C) across circular fiber

Heat Ttransfer Coefficient: flow inside tube

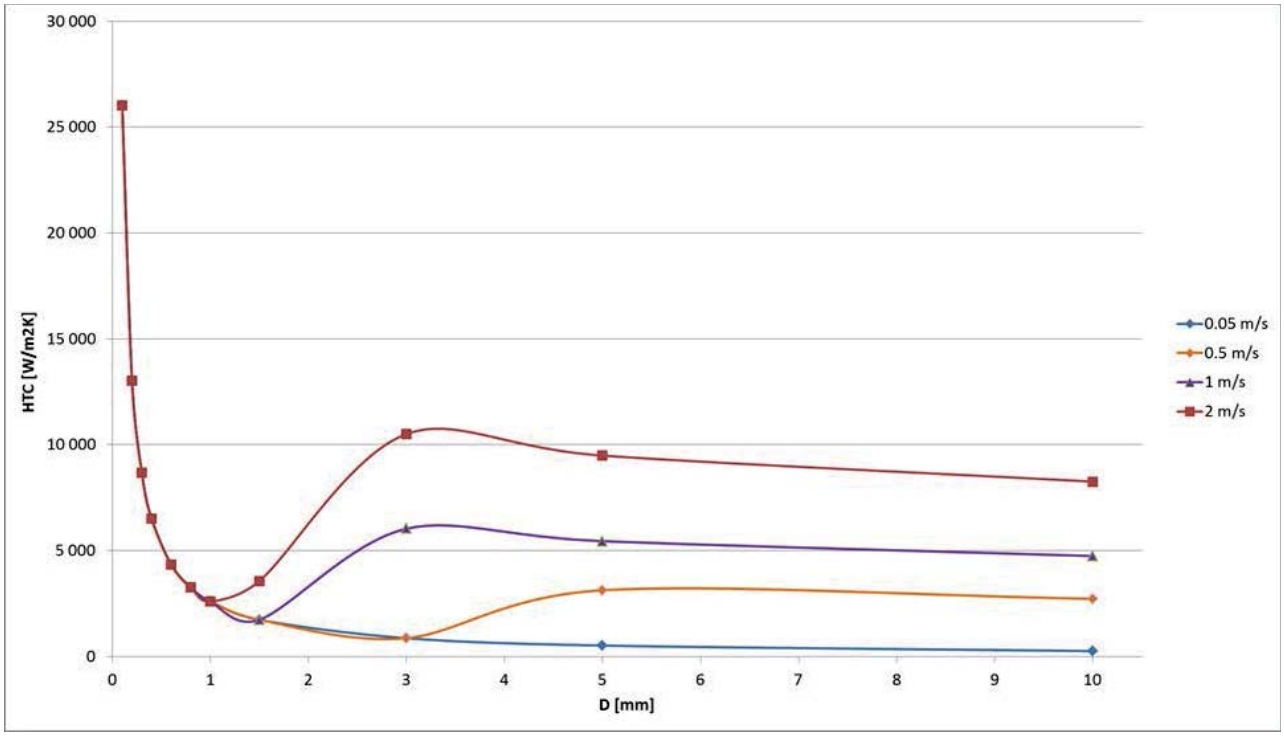

Internal flow of water (20 °C) within a tube. HTC values for different diameters (0.1-10 mm) and velocity (0.05-2 m/s)

Main heat transfer task

Separation

of polymer hollow fibers

Polypropylene Hollow-Fiber Bundle – chaotic structure

SEPARATION
chaotic structure

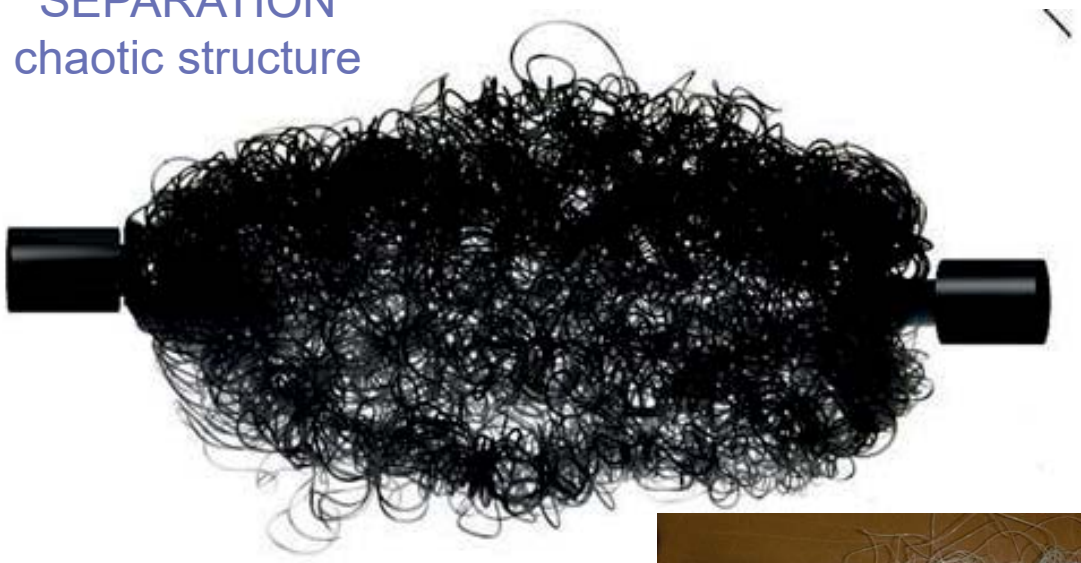

POLYMER HOLLOW-FIBER HEAT EXCHANGERS

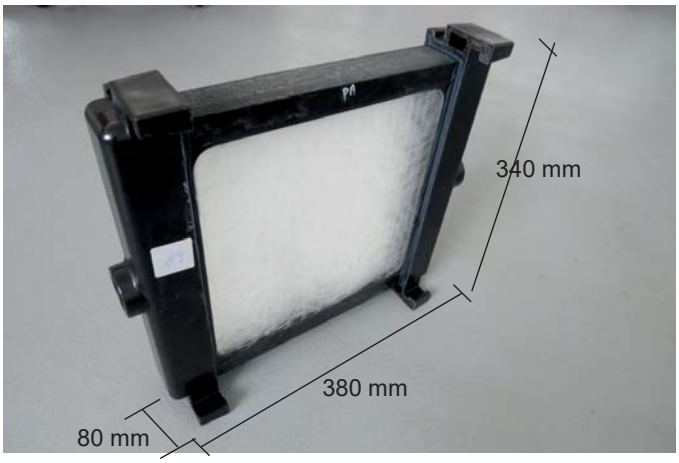

Prototypes of hollow
fiber heat exchangers

SEPARATION
Regular structure

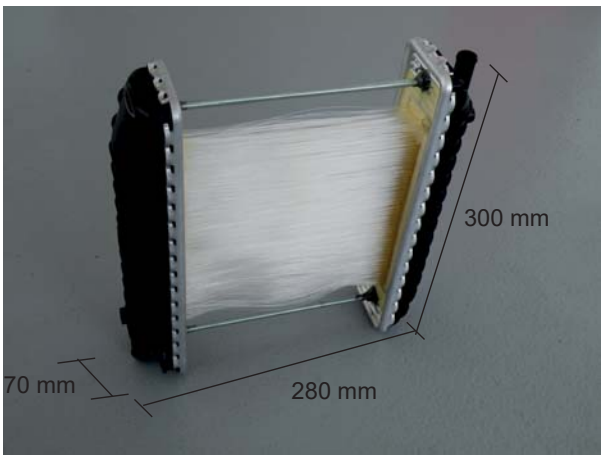

Woven heat transfer surfaces

Woven heat transfer surfaces

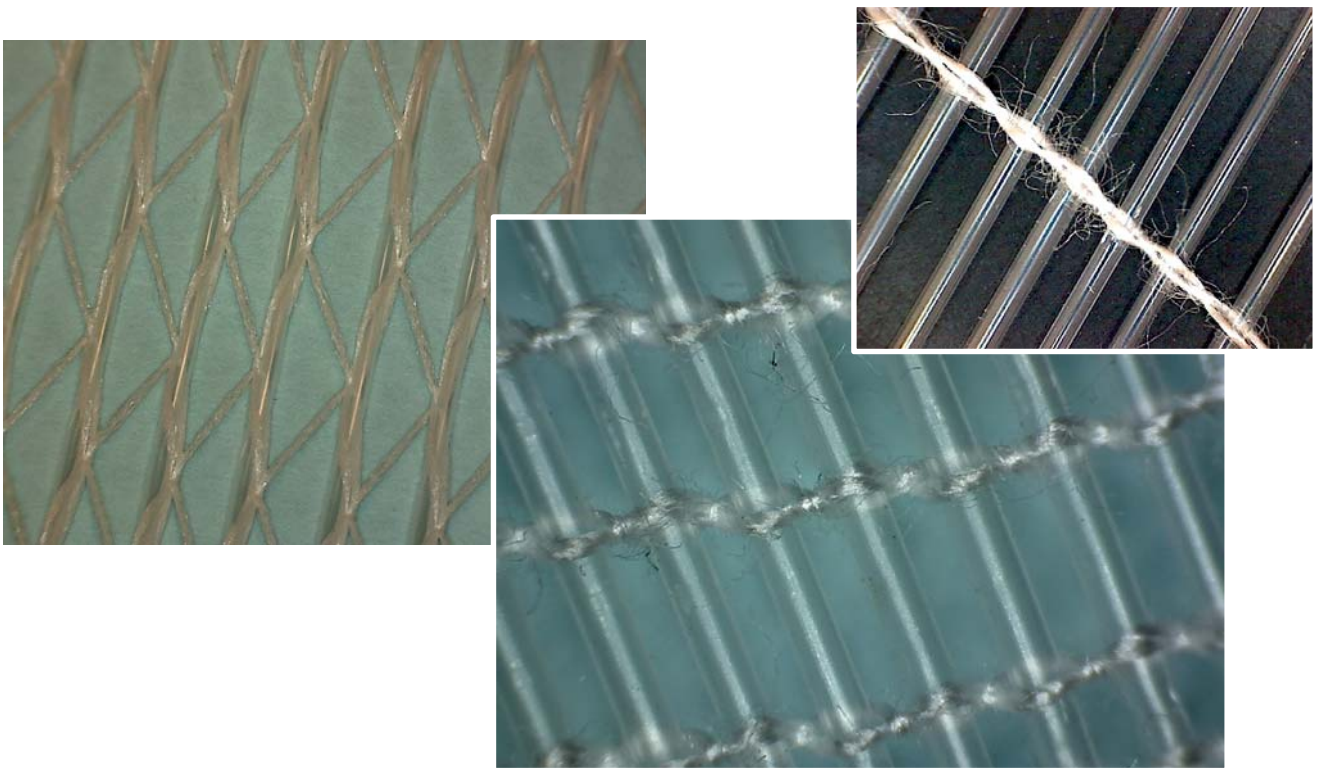

Woven heat transfer surfaces

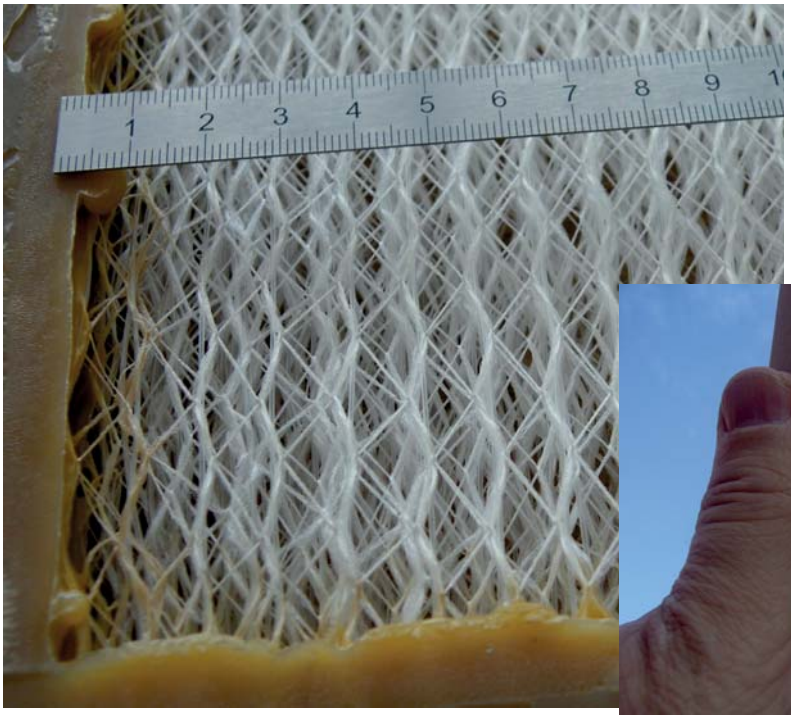

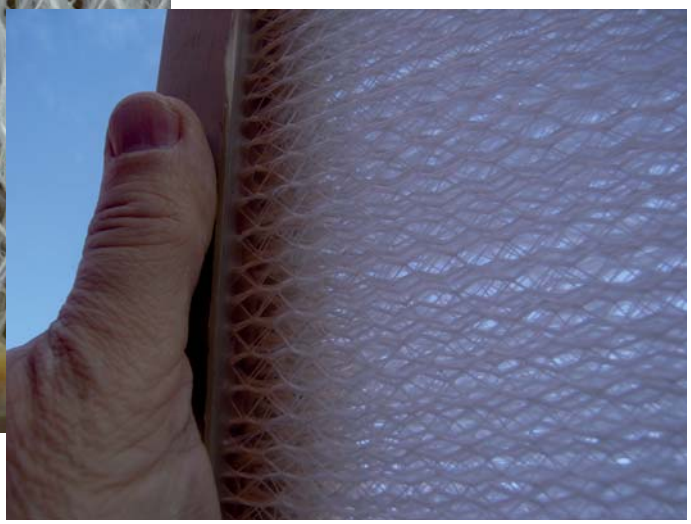

Use of fabric for formation of heat transfer surface

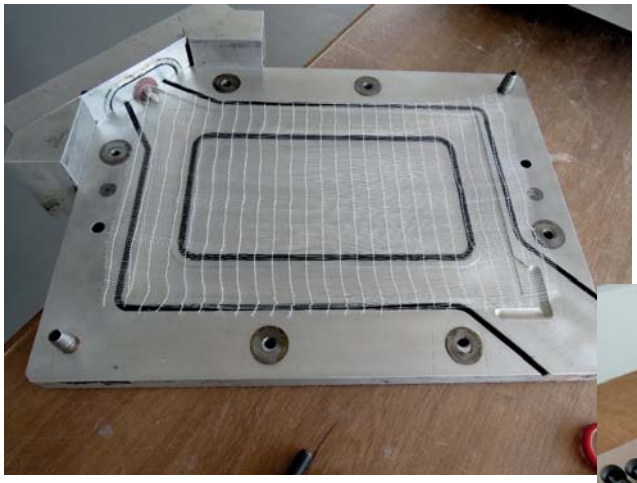

Use of fabric for formation of heat transfer surface

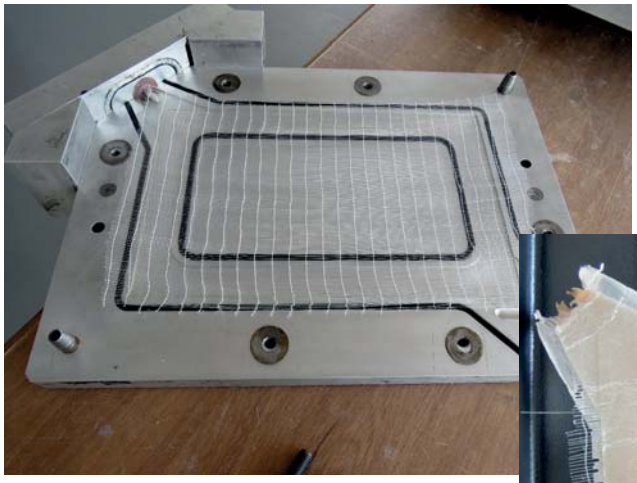

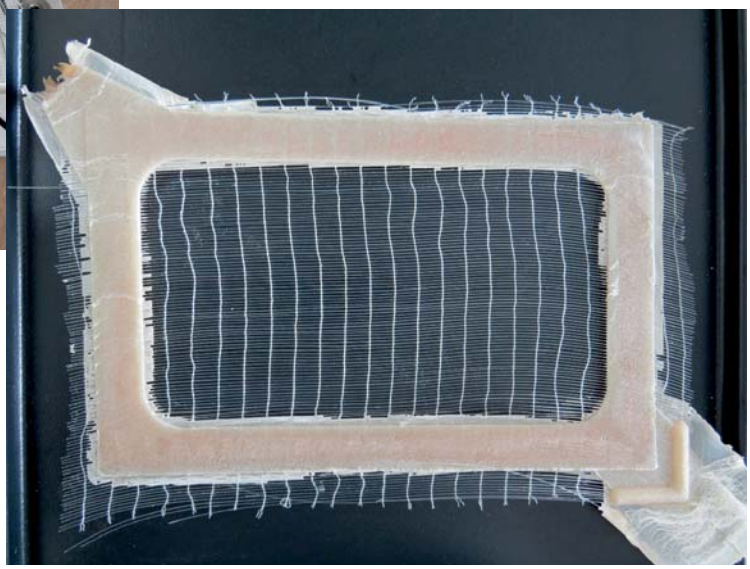

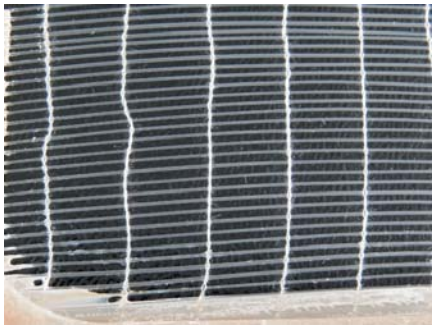

How to get in?

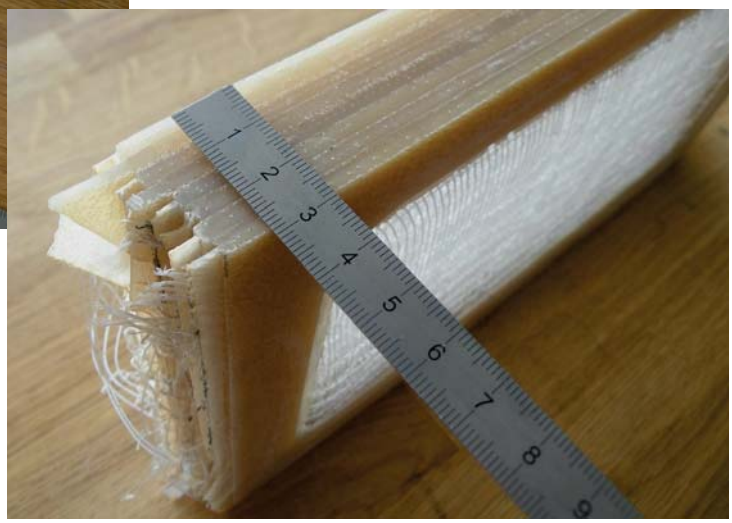

Use of fabric for formation of heat transfer surface

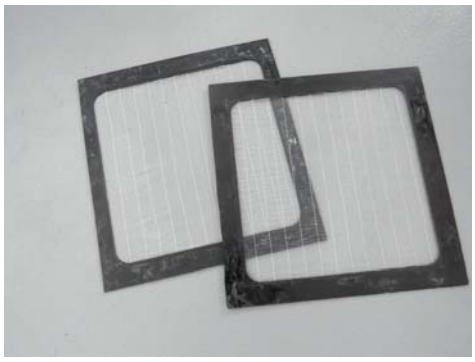

Use of fabric for formation of heat transfer surface – shell and tube

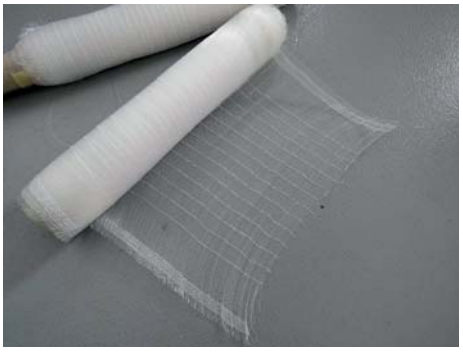

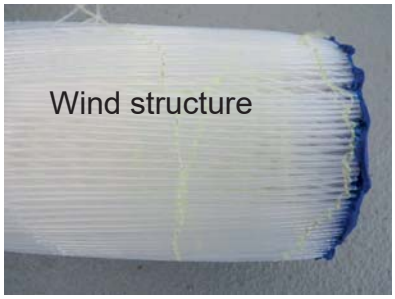

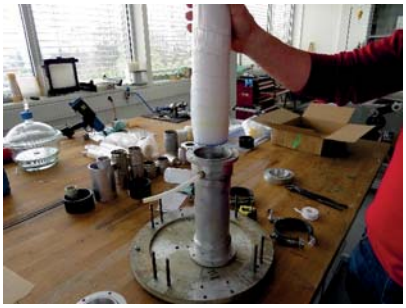

Thermal performance tests – high air velocity

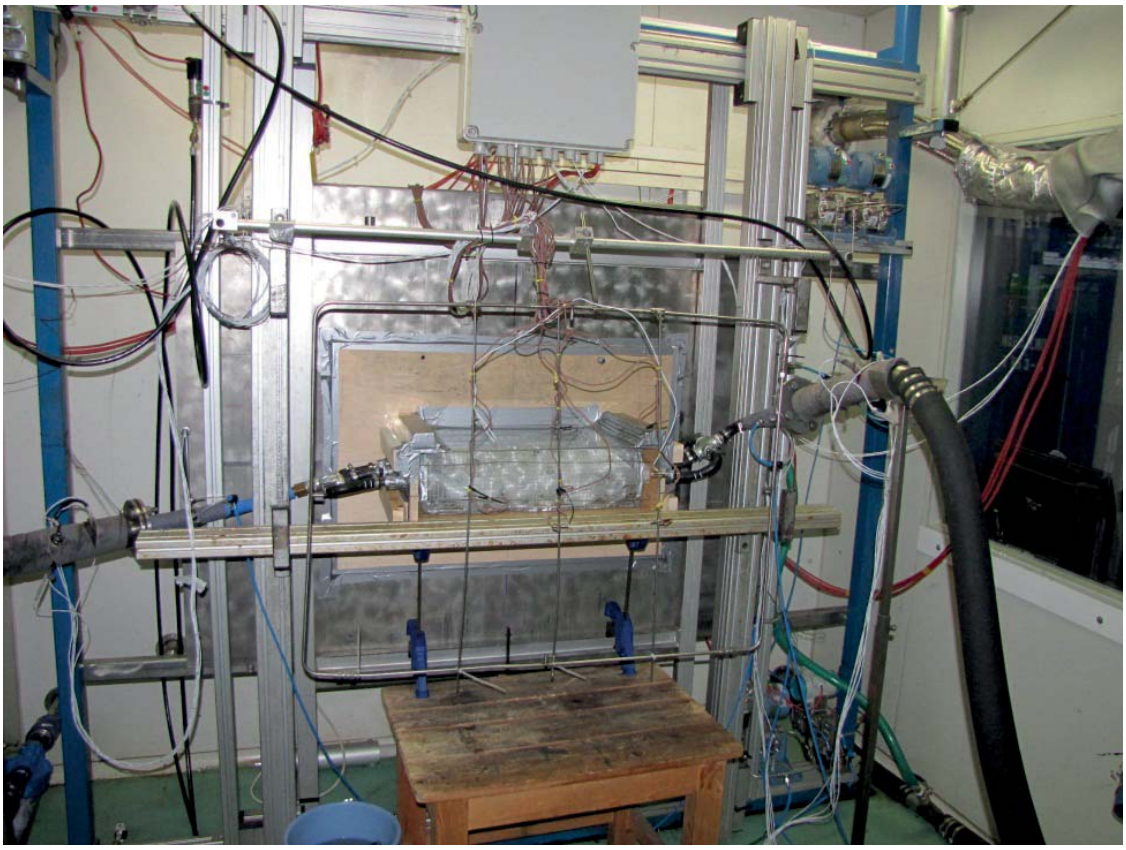

Calorimetric room

Calorimetric room

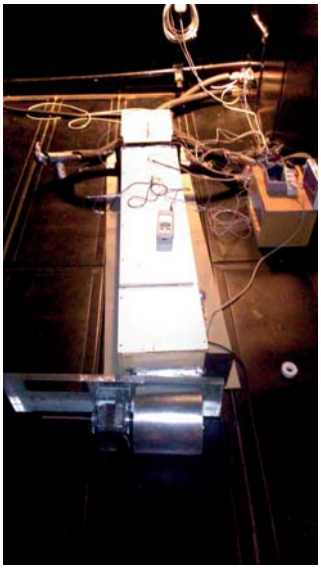

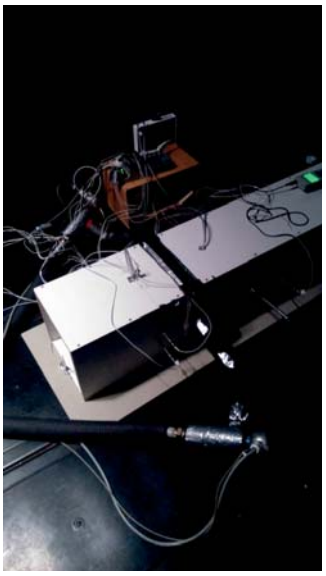

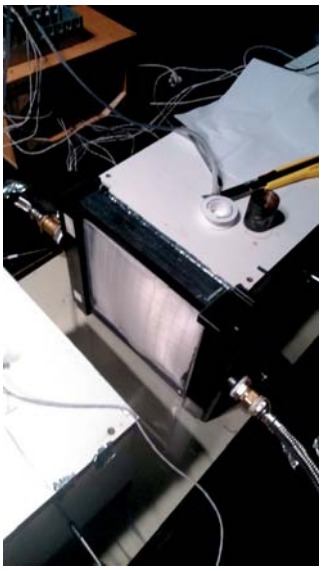

Twisted bundle heat exchanger – performance comparison

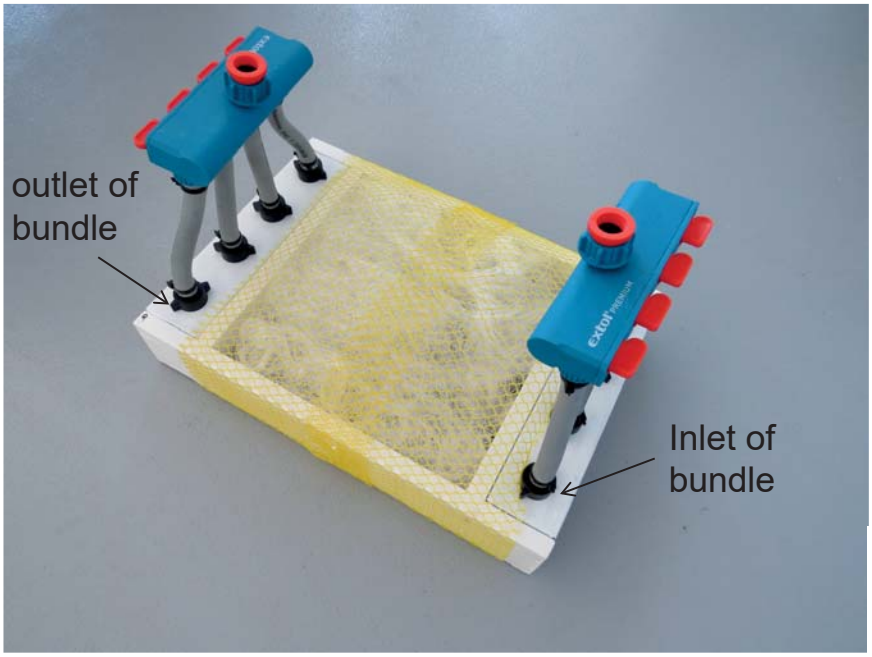

- 300x300x40 mm
- 1880 fibers
- Do = 0.7 mm
- Di = 0.6 mm
- L = 650 mm
- Ain = 2.30 m^2

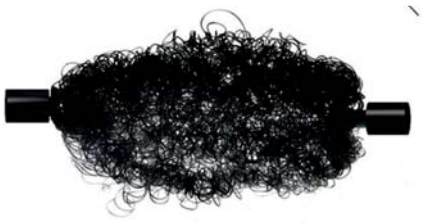

Fiber fabric heat exchangers

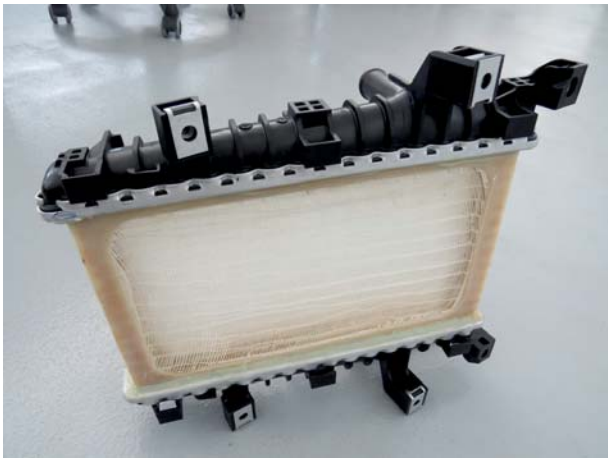

N2 Fibers along short side
732 fibers
Do = 0.7 mm
Di = 0.6 mm
L = 135 mm
Ain = 0.19 m^2

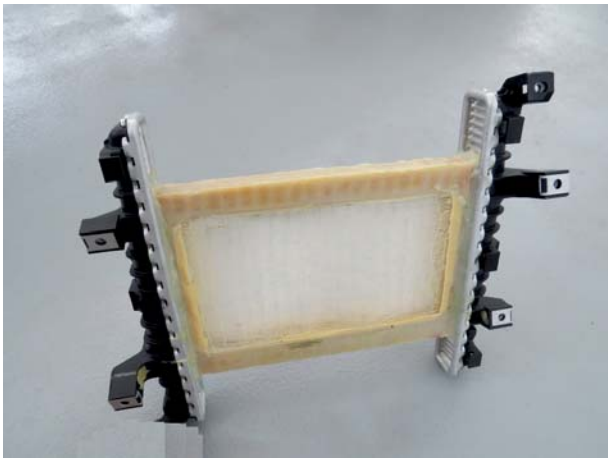

N3 Fibers along long side
490 fibers
Do = 0.55 mm
Di = 0.45 mm
L = 240 mm
Ain = 0.17 m^2

Experimental results: overall heat transfer coefficients

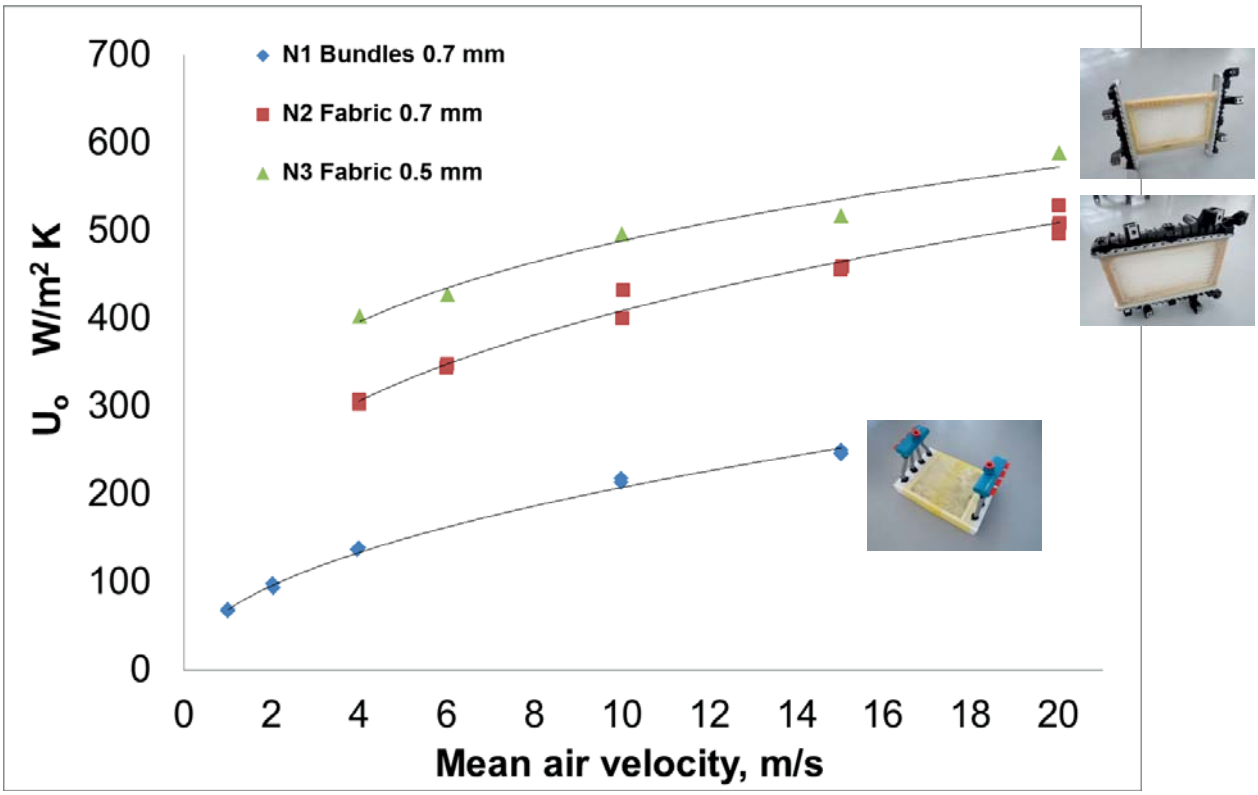

Codensation

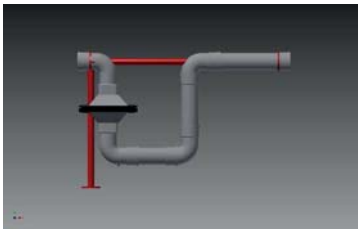

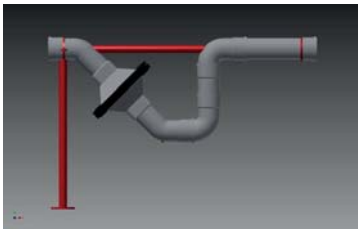

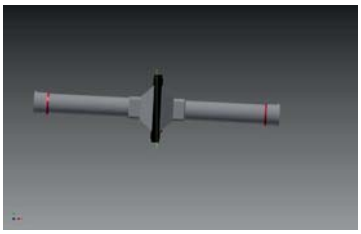

Comparison between conventional aluminium car radiator and PHF radiator

Heat exchange core of aluminium radiator for AUDI Q7 was compared with polymeric fiber core of heat exchanger. Testing conditions: coolant flow rate 18 l/min, inlet temperature 90° C; air velocity 10 m/s, inlet temperature 30° C

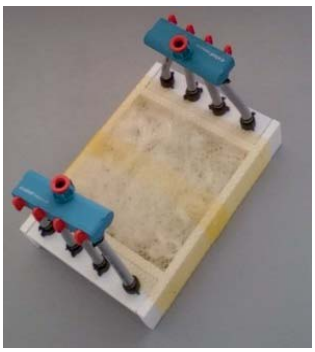

	Audi Q7 LTR radiator	heat exchanger N1
Dimensions	290x295x25	290x300x40
Weight	1.4 kg	0.4 kg
Heat transfer rate, kW	25 kW	22 kW

Comparison of Polymer and Metal Heat Exchangers

Weight of empty core (without coolant), full core weight and weight ratio:	
933 g, 1502 g, 100%	101 g, 396 g, 26%
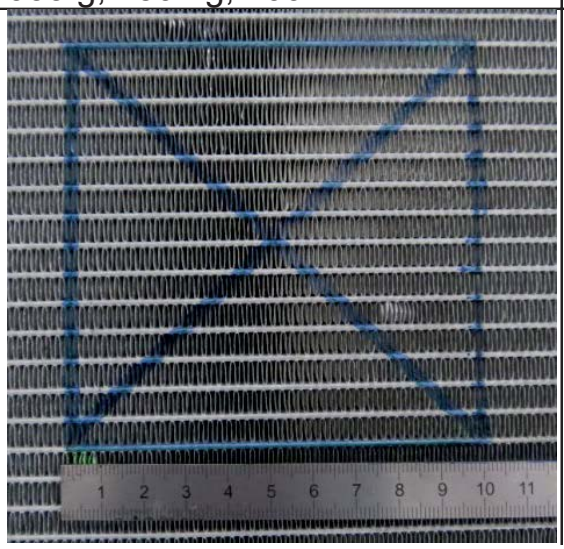	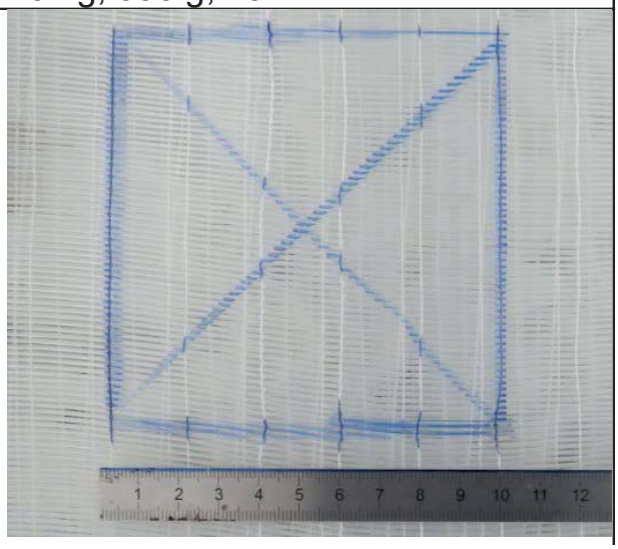

Pressure drops and surface-to-air HTC

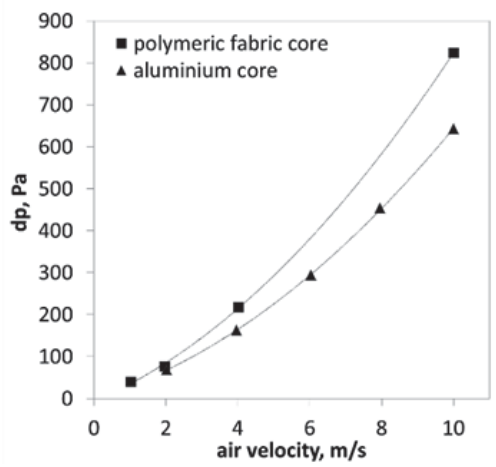

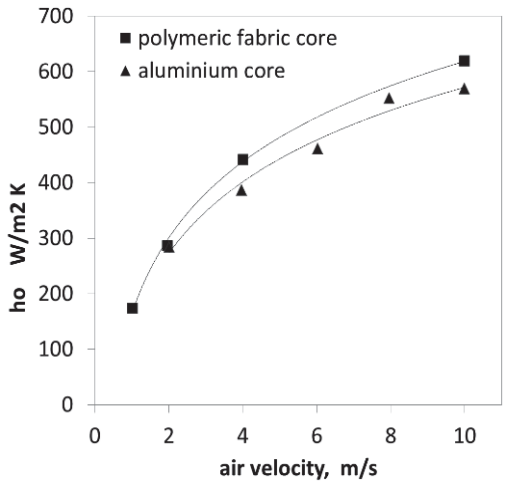

Weight comparison between conventional aluminium car radiator and PHF radiator

Al core mass = 993 g
coolant mass = 509 g

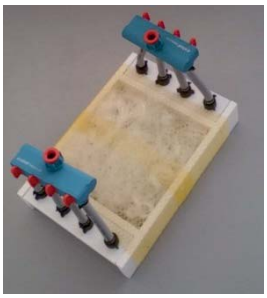

PP mass = 112 g
coolant mass = 346 g

PP mass = 60 g
coolant mass = 170 g

PP mass = 40 g
coolant mass = 148 g

Weight comparison between conventional aluminium car radiator and PHF radiator - SUMMARY

	Core material	Core weight, g	Coolant weight in the core, g	Total weight, g	Relative weight, %
	Al	993 (100%)	509	1502	100%
	PP	112 (12%)	346	458	30%
	PP	60 (6%)	170	230	15%
	PP	40 (4%)	148	188	13%

Development of liquid-to-gas prototypes for application as fan-coil heat exchangers

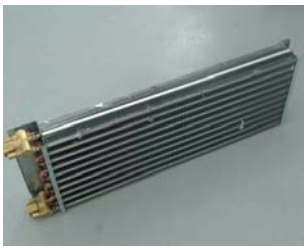

Original copper finned tube heat exchanger for CH 216 fancoil

weight empty = 3955 g
coolant weight = 1425 g

Module 1: Heat exchanger based on hollow fiber fabric

16 layers of fabric
2400 PP fibers total
1.35 m^2 area

weight empty = 1215 g
coolant weight = 640 g

Module 2: Heat exchanger based on hollow fiber fabric

15 layers of fabric
2100 PP fibers total
0.91 m^2 area

weight empty = 1650 g
coolant weight = 625 g

Module 3: Heat exchanger based on fibers

22 layers of fibers
2640 PC fibers total
1.25 m^2 area

weight empty = 961 g
coolant weight = 270 g

Weight comparison between conventional copper finned tube heat exchanger and PHFs - SUMMARY

	Heat exchanger weight, g	Coolant weight in the core, g	Total weight, g	Relative core weight, %
 **CH 216**	**3955**	1425	5380	**100**
 **Module 1**	**1215**	640	1850	**31**
 **Module 2**	**1650**	625	2275	**42**
 **Module 3**	**961**	270	1231	**24**

Název/Title	21. konference STRUTEX (sborník) 21st conference STRUTEX (Proceedings)
Autor/Author	Kolektiv autorů/Team of Authors
Vydavatel/Publisher	Technická univerzita v Liberci Technical University of Liberec
Schváleno/Authorized	Rektorátem TU v Liberci dne 20.10.2016 čj. RE 37/16
Vyšlo/Date of issue	Prosinec / December 2016
Vydání/Edition	první/first
Tiskárna/Printed by	Vysokoškolský podnik Liberec, s.r.o., Hálkova 6, Liberec
Číslo publikace/Publication number	55-037-16

ISBN 978-80-7494-269-3

ISBN 978-80-7494-269-3